Dynamical Effects and Disorder in Ultracold Bosonic Matter

Dissertation

zur Erlangung des Doktorgrades
der Naturwissenschaften
vorgelegt beim Fachbereich der Physik
der Johann Wolfgang Goethe-Universität
in Frankfurt am Main

von
Dipl.-Phys. Ulf Bissbort
aus Freiburg im Breisgau

Frankfurt 2012

vom Fachbereich der Physik der Johann Wolfgang Goethe-Universität
als Dissertation angenommen.

Dekan:	Prof. Dr. Michael Huth
Gutachter:	Prof. Dr. Walter Hofstetter Prof. Dr. Roser Valenti

Datum der Disputation: 26.11.2012

Contents

1 Ultracold Atoms in Optical Lattices **5**

1.1 Bose-Einstein Condensation . . . 5

1.2 Cooling Techniques . . . 7

1.3 The AC-Stark Effect . . . 8

1.4 Optical Lattices . . . 10

1.5 Detection . . . 12

1.6 Interactions in Ultracold, Dilute Atomic Gases . . . 15

1.6.1 Interatomic Potentials . . . 15

2 The Bose-Hubbard Model **19**

2.1 Bloch States . . . 19

2.2 Bloch States in a $1D$ Optical Lattice . . . 22

2.3 Eigenstates in an Optical Lattice with a Trap . . . 24

2.4 Maximally Localized Wannier States . . . 26

2.4.1 Usual Definition . . . 26

2.4.2 Wannier Functions as Maximally Localized States . . . 27

2.5 Alternative Definition: Wannier States as Eigenstates of the Band Projected Position Operator . . . 28

2.6 Wannier Functions in Higher Dimensions . . . 32

2.7 Wannier States in Inhomogeneous Lattices . . . 33

2.8 The Lattice Hamiltonian in the Wannier Basis . . . 35

2.9 Interactions in the Wannier Basis . . . 37

2.10 Scaling of the Hubbard Parameters U and J . . . 38

2.11 The Bose-Hubbard Model . . . 39

3 Phases in the Bose-Hubbard Model & Theoretical Methods **41**

3.1 Static Bosonic Gutzwiller . . . 41

3.2 The Bose-Hubbard Phase Diagram within the Gutzwiller Approach . . . 44

3.3 Expressing any single particle Operator within the Gutzwiller approximation . . . 48

3.4 Time-Dependent Bosonic Gutzwiller . . . 49

3.5 The Projection Operator Approach . . . 50

4 The Extended Bose-Hubbard Model in the Lowest Dressed Band 57

4.1 Multi-Orbital vs. Dressed-Band Description . . . 58

4.2 Definition of the low-energy subspace . . . 61

4.3 Numerical Implementation . . . 63

4.4 Transformation into the new dressed band basis . . . 63

4.5 Application to the Bose-Hubbard model: Multi-body induced tunneling and interactions . . . 67

4.5.1 Single-particle tunneling term . . . 67

4.5.2 Two-particle correlated hopping . . . 69

4.5.3 Nearest neighbor interactions . . . 69

4.5.4 On-site terms . . . 69

4.6 Density-dependent parameter formulation of the Bose-Hubbard model . . . 71

4.6.1 Single-particle tunneling term . . . 72

4.6.2 Two-particle correlated hopping . . . 73

4.6.3 Nearest neighbor interactions . . . 73

4.6.4 On-site energies . . . 74

4.7 Correlations vs. Orbital Deformation . . . 75

4.8 Conclusions . . . 77

5 Honeycomb Optical Lattices 79

5.1 The ETH Honeycomb Lattice Potential . . . 79

5.2 Band Structure & Bloch States . . . 80

5.3 Wannier States . . . 82

5.3.1 Evaluation of the real-space coordinate operator matrix elements . . . 82

5.3.2 Determining the Wannier States . . . 83

5.3.3 Sublattice conjugate Wannier states for unit cells with reflectional symmetry 85

5.3.3.1 Symmetry properties of the c-coefficients . . . 86

5.3.4 Alternate representation of the conjugate Wannier states . . . 87

6 A Generalized Approach to Bogoliubov Theory 91

6.1 Derivation of Bogoliubov Theory on an Operator Level . . . 92

6.1.1 Homogeneous Case . . . 94

6.1.2 Transformation of Operators . . . 101

6.2 Gross-Pitaevskii Theory . . . 105

6.3 Derivation of Bogoliubov Theory from Classical Gross-Pitaevskii Theory . . . 109

6.3.1 Final step: quantizing the Gross-Pitaevskii energy functional . . . 116

6.3.2 Higher Order Decay and Interaction Processes . . . 116

6.3.3 Leggett's Number-Conserving Formulation of Bogoliubov Theory . . . 116

6.4 Deriving Bogoliubov Theory from the Heisenberg Equations of Motion for the Fluctuation Operators . . . 117

6.5 Comparison of the Derivations . . . 118

7 Quasi-Particle Theory for Strongly Interacting Lattice Bosons 121

7.0.1 Eigenvector Structure in the Condensate . . . 125

7.0.2 Eigenvector Structure in the Insulator . . . 126

7.1 Structure of the Quasi-Particle Transformation . . . 127

7.2 Time Evolution Close to Equilibrium . . . 129

7.3 Fluctuation Expansion of the Classical Energy . . . 130

7.3.1 Diagonalization of the Quasi-Particle Hamiltonian . . . 131

7.4 Quantization of the Theory . . . 132

7.4.1 The Quasi-Particle Hamiltonian . . . 133

7.5 Quasi-Particles in the Translationally Invariant System . . . 134

8 Diagonalization of the Fluctuation Hamiltonian above the Gutzwiller Ground State 143

8.1 Fluctuation Operators in the Gutzwiller Approach . . . 144

8.2 Expressing the Full Bose-Hubbard Hamiltonian in Terms of Fluctuation Operators σ 146

8.3 Homogeneous Case . . . 148

8.3.1 Determining the Quasi-Particle Mode Structure . . . 149

8.4 Completeness Relation . . . 151

8.5 Transformation Relations . . . 153

8.5.1 Condensate . . . 153

8.5.2 Insulator . . . 154

8.6 Jordan Normal Form of the Quasi-Particle Hamiltonian . . . 156

8.6.1 Condensate . . . 156

8.6.2 Insulator . . . 156

8.6.2.1 The Spurious Mode's Effective Mass . . . 157

8.6.2.2 The Quasi-Particle Ground State . . . 158

8.7 Expressing Operators in Quasi-Particle Operators . . . 158

8.8 Results . . . 160

8.8.1 Structure of the Excitations . . . 160

8.8.2 Spectral Functions . . . 166

8.8.3 Single-Particle Density of States . . . 168

8.8.4 Dynamic Structure Factor . . . 169

8.8.5 Single Particle Density Matrix . . . 169

8.8.6 The Quasi-Momentum Distribution . . . 171

8.9 Deviation of the Quasi-Particle Ground State from the Gutzwiller Ground State . . 172

8.10 Results for the Two-Species Case . . . 173

8.11 Conclusion . . . 174

9 Probing Strongly Interacting Lattice Bosons with Bragg Spectroscopy 177
9.1 Introduction to Bragg Spectroscopy . . . 177
9.2 Microscopic Derivation of the Bragg Operator . . . 178
9.3 The Bragg Operator in the Quasi-Momentum and Wannier Bases . . . 180
9.4 Linear Response Theory . . . 182
9.5 Beyond Linear Response: Exact Time Evolution in a Non-Interacting System . . . 183
9.5.1 The Lattice Hamiltonian in the Relevant Subspace . . . 184
9.6 Coupling to Quasi-Particles in the Interacting System . . . 186
9.6.1 Density Wave Operator . . . 186
9.6.2 The Bragg Operator in Terms of Quasi-Particle Operators . . . 187
9.7 Results for the Homogeneous Interacting System . . . 188
9.8 Comparison with Linear Response Theory . . . 192
9.9 Results for a Realistic Trapped System & Experimental Comparison . . . 193

10 Lattice Modulation Spectroscopy 199

11 Collapse and Revival of a Coherent Matter Field 205
11.1 Homogeneous Case . . . 205
11.2 Inhomogeneous Case . . . 207
11.3 Special Case: Harmonically Trapped System . . . 209
11.4 Validity of our predictions . . . 211

12 Stochastic Mean-Field Theory 213
12.1 Method . . . 215
12.1.1 Numerical solution . . . 217
12.2 Phases of the disordered BHM . . . 219
12.2.1 Phases at $T = 0$ . . . 219
12.2.2 Phases at $T > 0$ . . . 220
12.2.3 Deviations in Finite Size Systems . . . 221
12.3 Box Disorder . . . 221
12.4 Speckle Disorder . . . 227
12.4.1 Disorder-induced reentrant Superfluidity . . . 231
12.4.2 Hopping Disorder . . . 233
12.5 Incorporating experimental aspects . . . 236
12.5.1 Temperature estimation in an optical lattice . . . 236
12.5.2 LDA incorporating trap effects . . . 237
12.6 Conclusion & Outlook . . . 237

A Structure and Symmetries of the u-Functions 243

B Time-Dependent Perturbation Theory 245

C Wannier State Relations in Double-Welled Unit Cells 247

D Implementation of the Multiorbital Exact Diagonalization Procedure 251

E Aspects of Bosonic Gutzwiller Theory 253

E.1 Particle Number Conservation within the Dynamic Gutzwiller Approach 253

E.2 Efficient Method of Calculating the Momentum Distribution for Gutzwiller States . 254

E.3 Efficient Calculation of the Condensate Fraction for Gutzwiller States 254

F Equations of Motion for the Projection Operator Approach 257

G Orthogonality Relations for Bogoliubov de Gennes Eigenmodes 259

G.1 Orthogonality Relations for the GW Fluctuation Coefficients 259

G.1.1 Orthogonality Relation 1 and Realness of Eigenfrequencies 260

G.1.1.1 Realness of Eigenfrequencies 261

G.1.1.2 Orthogonality Relation 1 262

G.1.1.3 Orthogonality Relation 2 262

H Action for the Coherent State Bosonic Path Integral 265

I Formal independence of complex variables and their conjugates 267

J Unitary Fock Space Transformation Operator for Single-Particle Basis Transformations 269

K Properties of Generalized Unitary Transformation Matrices 271

K.1 Basis-Transformation for Generic Bosonic Quasi-Particle Hamiltonians 273

K.1.1 Eigenvector Properties 273

K.2 Construction of a Basis from Eigenvectors of ΣH_{QP} and Supplemental Vectors . . . 275

K.2.1 Completeness 276

L Green's Functions 279

L.1 Definition of Green's Functions 279

L.2 Spectral Function 281

L.3 Reconstructing the Green's Functions from the Spectral Functions 282

L.4 Single Particle Operator Expectation Values 283

L.5 Density of States 283

M Technical Details of the SMFT **285**

M.1 Multi-Grid discretization 285

M.2 Numerical calculation of the CDF $F(\psi|\eta)$ for box disorder 285

M.3 PDF for a product of random variables 286

M.4 Compressibility in the insulating phases 286

M.5 Local Green's functions and DOS 287

M.6 Method of incorporating thermal fluctuations explicitly into SMFT 288

N Dispersion of a Wave Packet for Various Dispersion Relations **291**

O Discrete Fourier Transform of a Quadratic Function **295**

Bibliography **301**

Index **315**

Introduction

Before the advent of quantum mechanics, it was believed that all fundamental processes in our universe could be understood within the prevalent realm of classical physics. Seemingly, the only remaining task for physicists was to tie up some loose ends. This view drastically changed in the first decades of the twentieth century with the discovery and development of the theory of relativity and the quantum mechanics. These two theories constitute the main pillars for the description of the universe at opposite ends of the spectrum. General relativity, describing the structure of space-time and gravity by relating its curvature to the distribution of mass, provides the relevant physical laws on a cosmic scale with remarkable accuracy. Quantum mechanics, on the other hand, describes how our world behaves on a shorter scale with startling precision. After several decades of experiments (in the broadest sense), not a single observation has been (verifiably) made, which is at variance with the fundamental theory. It may thus be stated that quantum mechanics is one of the best, if not the best, theories known to mankind – in the sense that it is capable of describing a vast range of observations within a large range of applicability – and lays the foundation to describe almost all phenomena relevant to our everyday life in our relatively small (i.e. non-cosmic) everyday world.

At first, this may sound like the answer to all problems and questions, but of course there is a caveat. Although fundamental laws are extremely well described by many-particle quantum theory, this does not imply that all phenomena resulting from the formulation of the theory are known or within reach. The challenge is ubiquitous to the theory of complex systems: even if the *microscopic* laws of the individual constituents, such as Newton's laws for classical particles or the behavior of an individual consumer in an economic model are well known, surprisingly rich collective phenomena may arise in a system if a large number of such interacting constituents are taken together. These collective phenomena are often well described by new *effective* laws governing a new set of relevant degrees of freedom, but their relation and derivation from the precise microscopic laws is often complicated, unclear or not even known. Anderson expressed this as "*More is different*" [7], an allusion to the concept of emergence.

Take for instance a non-integrable system of classical particles: Since the complexity of the numerical calculations grows linearly with the number of particles, such systems with a large number of particles ($\gtrsim 10^6$) are apt for numerical simulations. However, if the system is chaotic, an exponentially small change in the initial conditions may have huge influence on the state of the system at a later time. Thus, even in such classical systems, a precise prediction of the system's long-time behavior may become very hard or impossible, a problem well known from everyday life in the case of weather forecasts.

In the case of a many-particle quantum system, the difficulty of the task is exacerbated by the exponential growth of the Hilbert space with the particle number, rendering even a direct numerical approach to solving the microscopic equations impossible for any system consisting of more than a very small number of particles. Although a number of exactly solvable, theoretically idealized models exist, these remain the exception. For the majority of theoretical models and essentially for the simulation of almost all realistic systems, one relies on simplified theoretical methods, adapted to the description of the relevant degrees of freedom. Commonly, an analytic solution – unless very crude and unjustifiable approximations are made – is not possible, requiring a numerical implementation at some point to understand and describe the behavior of such systems. With the significant advances in computational power in recent years, numerical approaches have gained an ever increasing relevance and are essentially indispensable in most fields of theoretical physics today.

One may of course pose the question, whether further advances in the processing power will not eventually change this scenario and allow us directly simulate the microscopic equations of quantum systems. In contrast to classical systems, where this development in recent years has allowed for the simulation of significantly more complex systems, this is unfortunately not the case for quantum systems, due to the exponential growth of the computational complexity with system size. If we, for instance, consider the direct simulation of a spin-1/2 system, adding a single additional particle, in general doubles the size of the configuration space.

It is this aspect which drives the development of a quantum computer. Instead of simulating a quantum mechanical problem on a classical computer, where the equations of motion are mapped onto a discrete computation routine, usually formulated in terms of floating point variables, it was Richard Feynman's idea in 1982 to simulate a complex quantum system by using another quantum system described by the same model within the horizon of interest, but which can be experimentally well controlled [52]. This is the central idea of the analogue quantum computer. For example, analog quantum computers in the form of ultracold atoms in optical lattices, could play a significant role in future in simulating and understanding real materials [75]. Such quantum computers are somewhat different from the quantum computer, which usually appear in the context of quantum information theory: in this type of quantum computer, the classical bit is replaced by its quantum counterpart, allowing for superpositions of states. Certain algorithms can harness the power in performing computations with a various number superimposed classical states, which allows some problems to be performed within a different complexity class than algorithms on a classical computer.

The central challenge in constructing a quantum computer thus consists of finding and designing a system, where the microscopic quantum degrees of freedom can be well controlled, clearly measured and which provides sufficient flexibility to simulate the more complex system of interest or, alternatively, contain a sufficiently large number of qbits. Different promising experimental approaches exist, such as trapped ion systems, ultracold atoms in optical lattices and cavity QED resonators. These differ in various characteristics, such as coherence times, scalability and fidelity. With the goal of constructing a universal, scalable quantum computer, it is presently not clear which one, if any, will win the race. We will focus, in this thesis, on ultracold atoms in optical lattices, a field which has developed since the first creation of a Bose-Einstein condensate (BEC) in dilute gas of bosonic atoms.

A BEC is a quantum state of matter, which cannot be understood or pictured within the classical laws of physics, in which a macroscopic number of particles occupy one single-particle state. The quantum mechanical, wave-like properties of massive particles become particularly apparent in a BEC and directly visible at an unprecedented level modern cold atom experiments. A fundamentally different counting statistics for this class of quantum particles was first devised by Satyendra Nath Bose. In a lecture he wanted to show his students that constructing a theory using classical statistics for the quanta of light does not lead to predictions in accordance with experimental observation. Fortuitously, Bose made a mistake in derivation during the lecture and the result he obtained was very well in accordance with experiments. This mistake motivated him to consider using a fundamentally different form of counting statistics for photons. Having briefly met and translated Einstein's paper on general relativity into the English language, Bose sent the seminal manuscript to Einstein with the request of translation into German and: *'If you think the paper worth publication I shall be grateful if you arrange for its publication in Zeitschrift für Physik'.* The manuscript *'Plancks Gesetz und Lichtquantenhypothese'* [21] was published in 1924 and the work immediately captured Einstein's attention, who, within a few months, extended it to massive particles and predicted the phenomenon to become known as Bose-Einstein condensation [45].

After the rapid initial progress, many decades passed until the BEC was first observed in a weakly interacting gas of ultracold atoms in 1995. Since the density of the atomic vapor needs to be kept extremely low to prevent heating and losses, the required temperatures to achieve BEC in these systems are extremely low. The appropriate cooling techniques to reach these temperatures of a few μK first had to be developed, leading to a number of Nobel prizes in the field. The first BEC was created in the group of group of Eric Cornell and Carl Wiemann in 1995 in a gas of 2000 Rubidium atoms [6, 32], shortly followed by the group of Wolfgang Ketterle, where a BEC

was created with $2 \cdot 10^5$ Sodium atoms [38, 86]. In the idealized case of zero temperature, all particles of a non-interacting BEC would be in the same single particle state. Performing any measurement corresponding to a single-particle operator on the atomic cloud, such as the position or momentum of a particle, is essentially equivalent to performing an independent measurement for each particle in the given single-particle state individually. Hence, performing a measurement on a BEC containing a large number of particles, directly reflects the statistical distribution of the single-particle measurement outcomes and in this sense directly probes probes the properties of the single-particle BEC state on a macroscopic scale.

Since the very first experiments creating BECs with ultracold bosonic atoms, a lot of progress and development into a number of different subbranches has been made. In contrast to solid state systems, where after the choice or synthetization of a specific material the control of the microscopic parameters is very limited, trapped atomic gases feature a remarkably many options of tunability and customizability. By superimposing retroreflected laser beams, periodic potentials, known as optical lattices, can be created to additionally trap the atoms. The atoms couple to the time-averaged intensity of laser and feel this periodic lattice structure as a conservative potential, giving rise to physics analogous to solid state systems, where electrons are exposed to the electric potential created by the periodically arranged nuclei. It is this similarity, combined with the large degree of tunability, which allows ultracold atoms in optical lattices to be used as analog quantum computers for simulating solid state systems.

The versatility of different setups and the control over these systems that has been achieved in recent years is remarkable. By using different geometrical arrangements for the lasers, superimposing different laser beams and exploiting the additional freedom of their polarization, a number of different lattice geometries can be created and even adjusted dynamically during the experiment. By using Feshbach resonances in the low energy scattering of two atoms, the strength of the effective short-range interaction between atoms can be adjusted over several orders of magnitude. This allows for the realization of systems ranging continuously from the non-interacting to the strongly interacting regime, where quantum phase transitions, such as the Mott insulator transition have clearly been observed. Even systems with infinitely strong short-ranged interactions can be created in these systems, as in the recent experiment in the Zwierlein group, where the equation of state of a unitary Fermi gas was measured for the first time with high precision. Theoretically, this challenging problem was out of reach for a long time and only recently computed using a diagrammatic Monte-Carlo approach. This case is a prime example, where the experimental data from a highly complex system was used to benchmark and verify a theoretical method, which may thereafter also be applied in other contexts. Furthermore, making use of dipole interactions in certain elements or in molecules, long range interactions can also be realized in these systems.

However, cold atom systems are not only of interest as quantum simulators of other systems, but can also be used to realize novel physical systems, which are theoretically challenging and interesting in their own right. For instance, different atomic species, both bosonic or fermionic, with different hyperfine states can be used. This allows for the realization of systems with spin larger than the well-known spin-1/2 case known from electrons in solid state systems. For instance, the formation of different color-superfluid phases, involving the formation of cooper pairs between different hyperfine states, has been predicted, a mechanism which is also conjectured to be of relevance in neutron stars. Using circularly polarized light, which only couples to certain electronic transitions within each atom, the optical lattices can be made spin-dependent. This allows atoms in different hyperfine states to be operated upon differently, which is an important tool in the quest to construct an optical lattices based quantum computer.

Spatial potentials, other than typical lattice systems can also be engineered using different beam profiles. An important example is the creation of a disorder potential by using a laser passing through a speckle plate. This allows the study of the influence of disorder in a controlled manner, both in the presence and absence of an underlying optical lattice. Other examples of trapping geometries are double-well structures, lower dimensional pancake or tube structures with a strong trapping potential along one or two dimensions, or ring structures.

Since the particle number in these systems is also highly tunable, continuously ranging from 10^6 down to an arbitrarily low number, these systems are also suitable to study the crossover from

macroscopic, mesoscopic to microscopic systems. This is particularly interesting with the very recent invention of the quantum gas microscope, with which it has become possible to detect individual atoms in an in-situ imaging procedure with single site resolution in an optical lattice. This development has enabled not only the real-space measurement of certain correlation functions and the spreading of excitations throughout the lattice, but also for a very high resolution measurement of the energy.

Another prominent difference between cold atom systems and solid state systems are the typical time scales. Whereas the microscopic processes in a material on an absolute time scale occur extremely fast and are very difficult, if not impossible, to observe directly, this is easily possible in cold atom systems. This additional observable degree of freedom can often be used to gain significant insight into the structure and properties of many-body phases. Moreover, it allows for the experimental investigation of systems far away from equilibrium, a challenging and theoretically interesting field for interacting many-particle systems. It also allows for an additional comparison of time-dependent theoretical methods and experiments, which is usually not possible in solid state systems.

Outline of the Thesis

In this thesis, various aspects on the theoretical description of ultracold bosonic atoms in optical lattices are investigated. After giving a brief introduction to the fundamental concepts of BECs, atomic physics, interatomic interactions and experimental procedures in chapter (1), we derive the Bose-Hubbard model from first principles in chapter (2). In this chapter, we also introduce and discuss a technique to efficiently determine Wannier states, which, in contrast to current techniques, can also be extended to inhomogeneous systems. This technique is later extended to higher dimensional, non-separable lattices in chapter (5). The many-body physics and phases of the Bose-Hubbard is shortly presented in chapter (3) in conjunction with Gutzwiller mean-field theory, and the recently devised projection operator approach. We then return to the derivation of an improved microscopic many-body Hamiltonian, which contains higher band contributions in the presence of interactions in chapter (4). We then move on to many-particle theory. To demonstrate the conceptual relations required in the following chapter, we derive Bogoliubov theory in chapter (5.3.4) in three different ways and discuss the connections. Furthermore, this derivation goes beyond the usual version discussed in most textbooks and papers, as it accounts for the fact, that the quasi-particle Hamiltonian is not diagonalizable in the condensate and the eigenvectors have to be completed by additional vectors to form a basis. This leads to a qualitatively different quasi-particle Hamiltonian and more intricate transformation relations as a result. In the following two chapters (7, 8), we derive an extended quasi-particle theory, which goes beyond Bogoliubov theory and is not restricted to weak interactions or a large condensate fraction. This quasi-particle theory naturally contains additional modes, such as the amplitude mode in the strongly interacting condensate. Bragg spectroscopy, a momentum-resolved spectroscopic technique, is introduced and used for the first experimental detection of the amplitude mode at finite quasi-momentum in chapter (9). The closely related lattice modulation spectroscopy is discussed in chapter (10). The results of a time-dependent simulation agree with experimental data, suggesting that also the amplitude mode, and not the sound mode, was probed in these experiments. In chapter (11) the dynamics of strongly interacting bosons far from equilibrium in inhomogeneous potentials is explored. We introduce a procedure that, in conjunction with the collapse and revival of the condensate, can be used to create exotic condensates, while particularly focusing on the case of a quadratic trapping potential. Finally, in chapter (12), we turn towards the physics of disordered systems derive and discuss in detail the stochastic mean-field theory for the disordered Bose-Hubbard model.

1. Ultracold Atoms in Optical Lattices

1.1 Bose-Einstein Condensation

A fundamental difference between quantum and classical mechanics is the concept of indistinguishable particles. Even if one might imagine classical particles which are identical and cannot be distinguished from their outer appearance, the concept is much deeper in the true quantum description. When counting microstates in the classical world, we would formally consider a given state and another state, where two particles are exactly interchanged, to be different. We would include both these states in the microcanonical partition function within a statistical mechanics description. However this is not how the real world is. The concept of indistinguishability on a quantum mechanical level is defined, that out of all these microstates related by arbitrary permutation of particles, only a single one is counted in the partition function. In other words, we should think in terms of many-particle states from the beginning and we have to give up the concept of classical particles. To see that this alternative description has measurable implications for well known systems, we consider the ideal gas: to obtain the correct thermodynamic relations when describing the gas as N classical, distinguishable particles, it was found long before the discovery of quantum mechanics that an additional factor $1/N!$ was needed in the partition function. This factor cannot be explained from first principles within classical physics, but appears naturally from the quantum mechanical counting prescription described above, since for N particles there are exactly $N!$ different permutations of the particles, each of which would correspond to a distinct classical microstate.

For the complete formulation of many-particle quantum mechanics, one additional postulate is needed. If a particle permutation operator is applied to a many-body state, the state may still change in sign[1]. In principle, every permutation operator could lead to a different change in sign. It is a postulate that for any given species of identical particles appearing in our universe, the sign of the many-body state changes under every particle permutation (fermions) or remains equal under any particle permutation (bosons). This property applies to elementary particles, but composite particles can also be classified to be either bosons of fermions, provided that all internal degrees of freedom are frozen out.

For fermions the Pauli exclusion principle inherently emerges from this postulate: if any single particle state were occupied twice, an interchange of these two particles would lead to a change in sign. But equally well, we are dealing with the identical state, two properties which cannot be reconciled for any normalizable state, thus forbidding it.

For bosons on the other hand, there is no restriction to the number of particles occupying the same single particle state. In fact, a higher occupation of any given single particle state is even

[1] An arbitrary change in complex phase is not allowed, since a two-fold application has to yield the same state, i.e. a prefactor 1.

statistically enhanced, when compared to classical particles. Satyendra Nath Bose was the first to implicitly use this counting procedure in 1924 for photons to derive the Planck distribution without classical electrodynamics [21]. Albert Einstein, who translated Bose's manuscript into the German language, then extended upon this idea and postulated that it also applies to massive particles [45]. For non-interacting particles he found that below a critical temperature, a macroscopic (i.e. a number proportional to the total particle number in the thermodynamic limit) number of particles occupy one given single particle state, a phenomenon ubiquitous to bosons known as Bose-Einstein condensation. The specific single particle state the particles condense into depends on the details of the potential, the temperature of the cloud and interactions between the particles. In contrast to gaseous, liquid and solid phases of matter, which can be conceptually understood within a classical framework, this cannot be done for a Bose-Einstein condensate. As a thermodynamic phase, its existence is thus a macroscopic manifestation of quantum mechanics. In this quantum phase of matter, the wavelike properties of matter become particularly apparent, as particles in the same orbital behave collectively and quantum effects become macroscopically visible.

Up to now we have discussed a gas of non-interacting bosons, where all particles reside in the same single particle state at zero temperature and we say that the gas has completely condensed. For many types of particles, interactions are present and it is a relevant question to ask whether a BEC continues to exist and how the state is changed. However one first notices, that the definition of a BEC is no longer that simple when interactions are present. In contrast to the non-interacting case at zero temperature, the ground state of an interacting bosonic system is no longer a direct product of single particle states and the criterion for a BEC and the condensate fraction in such a system first has to be defined. The most general and best definition for a BEC was given by Penrose and Onsager[122] in 1956: for the system with a total particle number expectation value of N one calculates the single particle density matrix $\rho_{i,j} = \langle a_i^\dagger a_j \rangle$, where a_i is the bosonic annihilation operator to a single particle orbital $|i\rangle$ and the expectation value is evaluated with a pure quantum state or with respect to a density matrix for a statistical ensemble. If the largest eigenvalue λ_0 of the Hermitian matrix $\rho_{i,j}$ scales extensively with the system size (i.e. is macroscopic) and all other eigenvalues do not, the state many-body state is a BEC. λ_0 is the best possible measure for the number of particles in the condensate orbital and the ratio $f_c = \lambda_0/N$, referred to as the *condensate fraction*, is the order parameter of the transition. The corresponding eigenvector $v_i^{(0)}$ defines the condensate orbital $|\psi_{\mathrm{BEC}}\rangle = \sum_i v_i^{(0)} |i\rangle$. The definition is independent of the initial choice of the single particle basis $|i\rangle$, as the single particle density matrices evaluated in different single particle bases are related by unitary transformations.

This definition is superior to other criteria commonly used to identify a BEC, such as the concept of $U(1)$-symmetry breaking when the expectation value $\langle a_i \rangle$ takes on a non-vanishing value, or the concept of off-diagonal long range order introduced by Yang [176]. The $U(1)$-symmetry breaking approach clearly fails to describe a BEC in a system with an arbitrarily large, but fixed particle number, where $\langle a_i \rangle$ is always identically zero. This is particularly apparent in cold atom experiments, which contain a fixed number of particles. The concept of off-diagonal long range order follows from the Penrose and Onsager definition for repulsively interacting, homogeneous systems. It does however not generally extend to inhomogeneous systems, such as in the presence of a trap in cold atom experiments.

The occurrence of BEC is also commonly related to a sufficiently high density in the semi-classical phase space. In a non-interacting system, this is equivalent to the thermal deBroglie wavelength λ_{dB} of the particles becoming of the order of the interparticle spacing and condensation occurs at $\lambda_{\mathrm{dB}}^3 n \approx 2.612$ in free space, where n is the density. This is exactly the regime, where Bose statistics deviates strongly from Boltzmann statistics for classical particles. Since the deBroglie wavelength $\lambda_{\mathrm{dB}} = \sqrt{\frac{2\pi\hbar^2}{m k_B T}}$ is inversely related to the temperature T, the required temperature for condensation scales as $T_c \propto n^{2/3}$. To achieve condensation, one may thus either decrease the temperature or increase the density. However, the range in which clouds of cold atomic gases are stable is restricted by the density from above. Working at the usual densities we are used to in every day life, most elements would simply form a liquid or solid at very low temperature and not condense. Working with a ultracold atomic vapor, we are in an entirely different regime. This is a metastable state, which is only stable if the system has a sufficiently low density, such that

three-body collisions causing recombination and heating of the system can be neglected. In this regime, the gas typically has a density of 10^{14} to $10^{15}/cm^3$, which is about 10^5 times more dilute than air on the earth's surface. To reach condensation in these systems, the temperature has to be lowered drastically to the order of 1 μK and below to achieve condensation.

Ultracold atomic gases are however not the only systems in which BEC can be observed. It was already discovered in 1936 that ^{4}He looses its entire viscosity when cooled below the lambda-point of 2.17 K and becomes a superfluid. In fact, it is also a BEC, but is strongly affected and depleted[2] by the strong interatomic interactions (due to the high density), which makes it very hard to unambiguously identify it as a BEC. Its description requires a strong modification of Gross-Pitaevskii or Bogoliubov theory, which describe weakly or non-interacting condensates.

1.2 Cooling Techniques

The reason why Bose-Einstein condensation in cold atomic gases was observed for the first time only 71 years after its initial prediction, was the lack of cooling techniques to reach the required temperature as well as methods to trap the atomic vapor. Two different cooling techniques were required to reach the very low temperatures: laser cooling and evaporative cooling.

Laser Cooling

It may at first seem paradoxical, but atoms in the gaseous phase can be cooled to very low temperatures by illuminating them with a laser. In most experiments, hot atoms leave an oven and are illuminated with a laser beam with a frequency tuned below an electronic transition frequency of the atom. If the direction of the laser opposes the motion of the atom, the laser frequency in the atom's rest frame is shifted to a higher frequency. If this frequency lies within the line width of the electronically allowed transition, the atom may absorb a photon from the laser beam, which pushes it into an internally excited state. At the same time, it acquires a momentum kick in the opposite direction of its velocity as seen from the lab frame, thereby slowing it down. If the transition back into the ground state occurs via a spontaneous emission of a photon, the direction of this photon is random and the resulting recoil momentum the atom experiences averages out to zero over a large number of emissions. Thus by tuning the laser frequency, atoms in a specific velocity range can be addressed and cooled down. During the cooling process, the frequency of the cooling laser is continuously increased to adapt to the lower velocities of the atomic beam. This cooling procedure can be used to cool atoms down to the temperature associated with the velocity an atom gains from a single spontaneous emission event. This is called the Doppler limit and is of the order of 150μK for ^{87}Rb. Steven Chu, Claude Cohen-Tannoudji and William D. Phillips were awarded the physics Nobel prize in 1997 for the development of this technique.

Evaporative Cooling

After the laser cooling process, the atoms are usually confined in a magnetic trap. The next stage in the cooling process to reach the very low temperatures required for BEC is performed using evaporative cooling. This process is similar to one of the mechanisms cooling a hot coffee. The water molecules leaving the coffee lie inside the high energy tail of the velocity distribution. Only the ones with a sufficiently high velocity have enough energy to overcome the potential barrier and leave the system, thus lowering the mean velocity of the remaining molecules and hence reducing its temperature. An analogous mechanism is used to evaporatively cool the atomic gas, with the main difference that the potential barrier that has to be overcome does not mainly originate from the attractive interactions between the water molecules in the liquid, but from the external magnetic confining potential. Since this barrier height can be dynamically adjusted, the cooling process can be optimized to always just allow the atoms in the tail of the velocity distribution to escape, while the atoms remaining in the trap rethermalize. The rethermalization procedure is mediated by interatomic interactions, which poses a problem for cooling fermions. In

[2] The condensate fraction is only $\approx 10\%$, even when approaching the zero temperature limit.

the limit of low temperatures, the possible interactions reduce to two-body s-wave scattering, which vanishes identically for fermions due to the antisymmetry of the many-body state under particle permutation. One thus requires an additional (usually bosonic) species to *sympathetically* cool the fermionic cloud. Using this cooling technique, it has become possible to reach temperatures as low as 50 to 100 nanokelvin.

To experimentally observe further interesting phenomena in cold atom systems, such as effective spin ordering in lattice systems, even lower temperatures are required and further cooling methods are still being devised.

1.3 The AC-Stark Effect

Optical potentials play an important role in the trapping, addressing and manipulation of cold atoms. They rely on the optical dipole force, which is based on the AC-Stark effect.

The AC-Stark effect describes the interaction of an atom with a temporally oscillating electric field $\mathbf{E}(t) = E_0\,\mathbf{e}\,\cos(\omega t)$. This field induces a dipole moment $\mathbf{d}(\mathbf{t})$ in the atom, which oscillates periodically at the same frequency ω as the external field. Here we will follow the derivation by Pethick and Smith [124]. Within a linear response treatment, the magnitude and the shift in phase of the atom's polarization can be conveniently described by a complex polarization $\alpha(\omega)$, such that $\mathbf{d}(\mathbf{t}) = \alpha(\omega)\mathbf{E}(\mathbf{t})$.

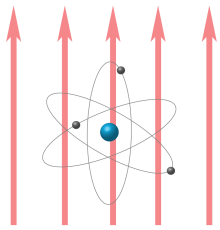

In analogy to a driven classical pendulum, the polarization of the atom will follow the electric field in phase if the driving frequency is much lower than the atom's resonance frequency, leading to an attractive potential.

This can be substantiated within a quantum mechanical picture for an alkaline atom, where we consider the electronic ground state $|g\rangle$ and a set of excited states $|e\rangle$ with energies E_g and E_e respectively. Using the ansatz

$$|\psi(t)\rangle = c_g(t)\,e^{-\frac{i}{\hbar}E_g t}\,|g\rangle + \sum_e c_e(t)\,e^{-\frac{i}{\hbar}E_e t}\,|e\rangle \tag{1.1}$$

for the time-dependent state with the coefficients $c_g(t)$ and $c_e(t)$ (corresponding to the state amplitudes in the interaction picture), the equations of motion are determined by the time-dependent Schrödinger equation

$$i\hbar\frac{\partial}{\partial t}|\psi\rangle = (H_0 + H_{\mathrm{dip}}(t))|\psi\rangle. \tag{1.2}$$

Here, H_0 is the unperturbed atomic Hamiltonian with the eigenstates $|g\rangle$ and $\{|e\rangle\}$, the Hamiltonian $H_{\mathrm{dip}}(t) = -\mathbf{d}\cdot\mathbf{E}$ describes the coupling to the classical electric field and $\mathbf{d}$ is the atomic dipole operator. Typically, the excited states $|e\rangle$ are energetically well separated and a two level description, considering only a single excited state, suffices to describe the polarization. To first order in the transitions, one obtains the time-dependent amplitude for the excited states

$$c_{e'} \approx \frac{E_0}{2\hbar}\langle e'|\mathbf{d}\cdot\mathbf{e}|g\rangle\left[\frac{e^{i(\omega_{e'g}+\omega)t}-1}{\omega_{e'g}+\omega} + \frac{e^{i(\omega_{e'g}-\omega)t}-1}{\omega_{e'g}-\omega}\right]. \tag{1.3}$$

The polarizability can be inferred from the energy reduction of the time-averaged state $\Delta E = -\frac{1}{2}\langle E^2(t)\rangle_t\,\alpha(\omega)$

$$\alpha = \frac{2(E_e - E_g)|\langle g|\mathbf{d}\cdot\mathbf{e}|e\rangle|^2}{(E_e-E_g)^2 - \hbar^2\omega^2}. \tag{1.4}$$

This result was obtained within the framework of a purely unitary time evolution of the two-state system in a classical electromagnetic field and does not contain spontaneous emission processes, which lead to a broadening of the imaginary part of α.

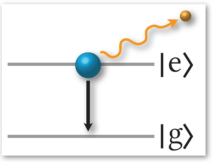

To incorporate spontaneous emission from first principles requires a quantization of the electromagnetic field; however this can also be included on a phenomenological level in the simpler treatment above by allowing for complex energies $E_e \mapsto E_e + \frac{i\hbar}{2}\Gamma_e$. Here, the real parameter Γ_e is the decay rate of the excited state $|e\rangle$ and within the rotating wave approximation[3], the polarizability takes on the form

$$\alpha(\omega) \approx \frac{|\langle e|\mathbf{d}\cdot\mathbf{e}|g\rangle|^2\,(E_e - E_g - \hbar\omega)}{(E_e - E_g - \hbar\omega)^2 + (\hbar\Gamma_e/2)^2} + i\,\frac{|\langle e|\mathbf{d}\cdot\mathbf{e}|g\rangle|^2\,\hbar\Gamma_e/2}{(E_e - E_g - \hbar\omega)^2 + (\hbar\Gamma_e/2)^2}. \tag{1.5}$$

Defining the detuning

$$\delta = \omega - \frac{E_e - E_g}{\hbar} \tag{1.6}$$

and the Rabi frequency

$$\Omega_R = E_0\,\frac{|\langle e|\mathbf{d}\cdot\mathbf{e}|g\rangle|}{2\,\hbar}, \tag{1.7}$$

the conservative potential, which is related to the real part of the polarizability and proportional to the electric field strength, can be written as

$$V_{\text{dip}} = -\frac{1}{2}\text{Re}(\alpha(\omega))\,\langle \mathbf{E}^2(\mathbf{r},t)\rangle_t = \frac{\hbar\,\Omega_R^2\,\delta}{\delta^2 + \Gamma_e^2/4}. \tag{1.8}$$

The rate at which atoms are lost from the ground state Γ_g shown in Fig. (1.1) is of Lorentzian form in the detuning

$$\Gamma_g = \frac{\text{Im}(\alpha(\omega))}{\hbar}\,\langle \mathbf{E}^2(\mathbf{r},t)\rangle_t = \frac{\Omega_R^2\,\Gamma_e}{\delta^2 + \Gamma_e^2/4}. \tag{1.9}$$

The dipole potential is attractive if the frequency ω is lower than the two-state resonance frequency (red detuned) and repulsive if $\delta > 0$ (blue detuned). For large detuning the potential falls off with the inverse of the detuning $|V_{\text{dip}}| \propto |\delta|^{-1}$, whereas the decay date from the ground state falls off with the square $\Gamma_g \propto |\delta|^{-2}$.

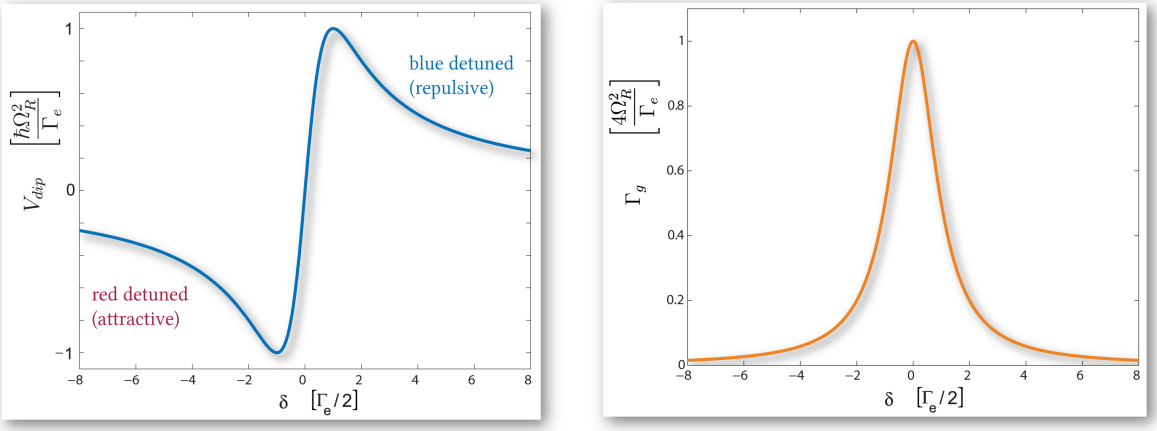

Figure 1.1: Left figure: Optical dipole potential strength (proportional to $\text{Re}(\alpha)$) as a function of the detuning at constant electric field intensity. The potential is attractive (repulsive) if the optical field is red detuned (blue detuned) and decays as $|\delta|^{-1}$ for large detuning. The extrema are located at $\pm\Gamma_e/2$. Right: The loss rate from the ground state Γ_g leads to heating of the atomic cloud and decays as $|\delta|^{-2}$ for large detuning.

Both quantities are directly proportional to the electric field intensity: to reduce the inelastic scattering Γ_g, which leads to a heating of the atomic cloud for a fixed potential strength, both the

[3]This approximation is applicable if the electromagnetic frequency ω is very close to the energy level difference $(E_e - E_g)/\hbar$ relative to the absolute frequency scale and entails neglecting the smaller of the two terms.

detuning and the laser intensity are to be chosen as large as possible. In experiments the heating rate is thus usually technically restricted by the intensity power of the lasers.

It is important to note that in this form the optical dipole potentials do not depend on the internal hyperfine state of the atoms and couple to all of these equally. The internal hyperfine state thus remains as an independent internal degree of freedom. However, using circularly polarized light, it is also possible to create optical potentials, which couple differently to the various internal states.

1.4 Optical Lattices

In this section we will shortly describe one of the major tools in the field of ultracold atoms, drawing the connection to condensed matter physics: the creation of optical lattices for neutral atoms. We first elucidate the concept in one dimension. Within a classical treatment, the electric field of a laser is very well described by a monochromatic wave $\mathbf{E}_1(\mathbf{r},t) = E_0\mathbf{e}\cos(\mathbf{k}\cdot\mathbf{r}-\omega t)$, where the lattice momentum $k_L = |\mathbf{k}|$ is related to the laser wave length λ_L by $k_L = 2\pi/\lambda_L$. In an optical lattice, the laser is either reflected by a mirror as shown in Fig. (1.2), or alternatively a second counterpropagating laser locked to the first one is used $\mathbf{E}_2(\mathbf{r},t) = E_0\mathbf{e}\cos(\mathbf{kr}+\omega t)$, which gives rise to a standing wave

$$\mathbf{E}(\mathbf{r},t) = \mathbf{E}_1(\mathbf{r},t) + \mathbf{E}_2(\mathbf{r},t) = 2E_0\mathbf{e}\cos(\omega t)\cos(\mathbf{k}\cdot\mathbf{r}). \tag{1.10}$$

Due to the AC-Stark effect, atoms feel a potential proportional to $|\mathbf{E}(\mathbf{r},t)|^2$ and are attracted to the intensity maxima (minima) for red (blue) detuned lattice lasers. Note that the lattice spacing a of the time-averaged intensity profile of the standing wave is half the laser wavelength $a = \lambda_L/2 = \pi/k_L$. In contrast to incoherent light with a broad spectral distribution where the intensities of various light sources can simply be superimposed, it is essential to superimpose the electric fields before determining the intensity from the square modulus in this case.

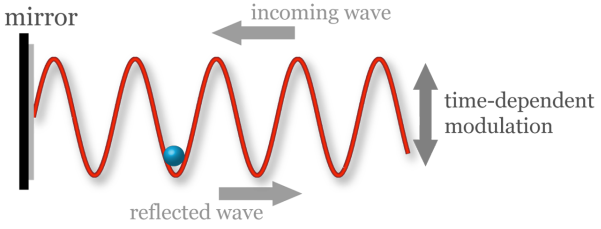

Figure 1.2: Creation of a standing wave by using a mirror to reflect a laser. The superposition of the incoming wave with the reflected wave leads to an intensity modulation at the optical frequency, which is far beyond the time scale of the atoms. These only feel the time-averaged intensity and are attracted to the antinodes (high average intensity) of the lattice for a red-detuned laser.

The optical potential (1.8) resulting from the electric field Eq. (1.10) is also a standing spatial wave, modulated in time with the frequency of the optical field ω. Since ω is typically 10 orders of magnitude larger than the inverse time scale of the atomic motion, the atoms only feel the time-averaged optical potential. For experiments in three spatial dimensions, a one-dimensional analysis is of course not sufficient. In order to reduce the dimensionality of the system, 1D experiments typically impose very strong confinement[4] in the two remaining spatial dimensions, such that any excitation beyond the single particle ground state along these dimensions is effectively frozen out.

[4]The trapping along the axial direction can be achieved either through additional deep optical lattices or other optical or magnetic traps.

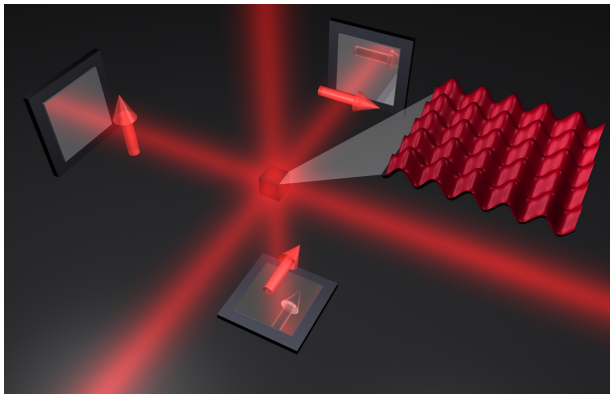

Figure 1.3: Each of the incoming laser beams is retroreflected by a mirror, forming a temporally modulated standing wave. If the polarizations of the three lasers beams, indicated by the respective arrows, are chosen orthogonally, the resulting potential is a hypercubic lattice, which is separable along each of the three dimensions. The potential is shown on a $2D$ slice within the central region, where all three beams are superimposed.

In this section we will focus on the three dimensional case, where three retroreflected coherent laser beams are superimposed at right angles. Since the polarization is always orthogonal to the direction of propagation, it is impossible to choose all three polarization vectors to be equal, but one possible choice is to set all mutually orthogonal, as shown in Fig. (1.3). For the case that the polarization in the z-direction is always orthogonal to the polarization in both other directions (as in both Fig. (1.3) and Fig. (1.4)), the potential in the x-y-plane can be written as

$$V(x,y) = -V_{\text{lat}}\left(\cos^2(k_L x) + \cos^2(k_L y) + 2\,\mathbf{e}_1 \cdot \mathbf{e}_2 \cos(k_L x)\,\cos(k_L y)\right) \tag{1.11}$$

and is respectively shown in both figures for the limiting cases of fully parallel and orthogonal polarizations $\mathbf{e}_1$ and $\mathbf{e}_2$.

On a historical side note, it is interesting that in early optical lattice experiments much effort was invested in calibrating the different polarizations of lattice vectors orthogonally to create separable hypercubic lattices. Only somewhat later was it realized, that tuning the lattice lasers to slightly different frequencies has exactly the same effect on the relevant atomic time scale and is a considerably easier task.

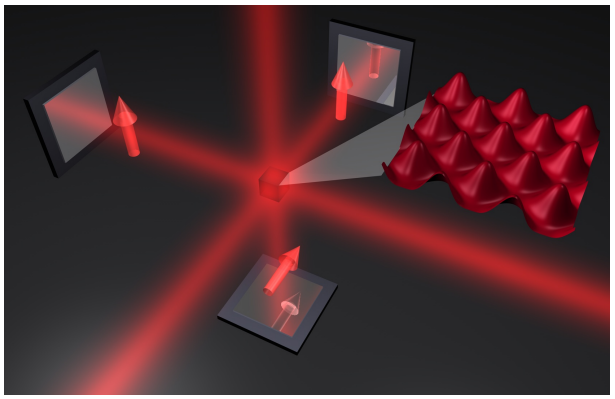

Figure 1.4: The lattice structure produced by two locked lasers with the same polarization is not separable in the x and y directions. It is impossible to choose the polarization of the remaining third laser to be along the same direction. Here it is chosen orthogonally, making the potential along the z-direction separable from the other two dimensions.

Clearly, the description of the laser light field as a plane wave is only an approximation and any beam has a finite extent perpendicular to the direction of propagation. For a laser in the lowest

transverse mode, the true intensity profile is a Gaussian beam waist, which is typically of the width $\approx 100\mu m$. Optical lattices can be made using either red or a blue detuned laser, where the atoms are attracted to the spatial regions with high or low intensity respectively. In the latter case, an additional trap is usually required, since it is otherwise energetically favorable for the atoms to entirely leave the repulsive optical beam. For red detuned lattices the atoms are thus automatically trapped in the cross section of the beam by a Gaussian trap potential, which is commonly approximated as an additional harmonic trapping potential (in quadratic order).

Using circularly polarized light, as described in the previous section, it is possible to engineer *spin*-dependent[5] optical lattices, which have been successfully used for the preparation of entangled states. These constitute a key tool in the engineering of a cold atom based scalable quantum computer.

A major advantage of optical lattices over lattices in solid state systems is their vast tunability, even during the experimental procedure. Since the time scale of optical and electronic devices is far beyond the time scale of the atomic motion, essentially all parameters of the optical trapping system, except for the mechanical setup, can be well controlled and adjusted as *external knobs* during the experimental run. These are

1. the intensity of the individual lattice beams
2. the polarization of the laser beams
3. the frequency of the laser beams, allowing for an effective acceleration of the lattice and shifting the positions of the lattice sites.

Additional laser beams can also be switched on at some stage in the experiment, the frequency difference between different beams can be well controlled and each of the above parameters can furthermore be modulated in time. These features are used in established probing techniques, such as Bragg and lattice modulation spectroscopy. Using different geometrical laser setups allows for a number of qualitatively different lattice geometries to be realized. Apart from the hypercubic lattice, which is the most common optical lattice geometry used to date, hexagonal [152, 151], triagonal[158], kagome [83] and honeycomb lattices have been successfully realized [162]. Recently, significant progress has furthermore been made in adding effective magnetic gauge fields to systems of neutral atom in optical lattices, of which several different approaches have been successfully experimentally implemented to date [3, 159].

1.5 Detection

The main technique to detect cold atoms is absorption imaging. The cloud is illuminated with a probing laser beam resonant to the electronic transition and the intensity is magnified and measured with a CCD-camera after passing through a cloud. Inside the cloud, the resonant light is scattered (spontaneous emission) by the atoms, which reduces the beam's intensity by an amount proportional to the atomic cloud density integrated along the direction of the imaging beam if the atomic density is not too high.

One may think that only a limited amount of information about the structure of the many-particle quantum state is accessible by measuring the density $n(\mathbf{r}) = \langle \psi^\dagger(\mathbf{r})\, \psi(\mathbf{r}) \rangle$ of the cloud, however from it a large range of properties may be inferred, of which some important examples are below.

[5] Depending on the internal hyperfine state of the atom.

Time of Flight Imaging

A very commonly used technique to approximately determine the momentum distribution $n(\mathbf{k}) = \langle a^\dagger(\mathbf{k})\, a(\mathbf{k})\rangle$ of the many-body state is time of flight imaging. In this method the trapping potential (and the optical lattice if present) is suddenly switched off and the cloud expands for a time interval t_{tof} before the density is imaged. During expansion, the density decreases and interactions play an ever smaller role. In the approximation that they are neglected altogether and that the initial cloud size is negligible in comparison to the size of the expanded cloud at the time of imaging, the measured real space density profile can be exactly related to the momentum profile at the time of release. Thus, time of flight measurements provide direct access to the momentum distribution of the many-particle state. This technique can be applied both to systems with and without a lattice (or any other potential), as shown in Fig. (1.5).

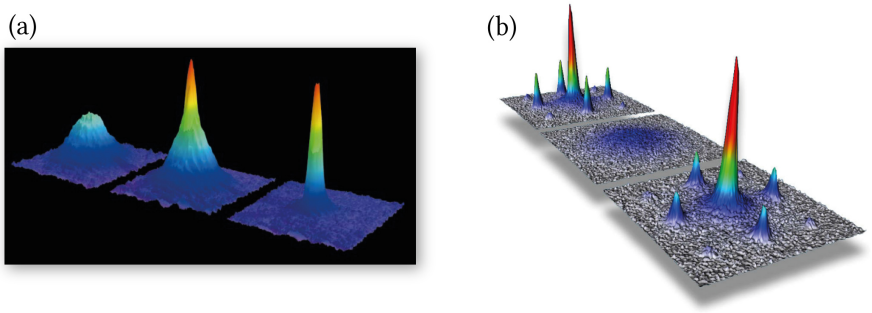

Figure 1.5: (a): One of the first time of flight images showing the formation of a BEC in a weakly interacting gas of cold atoms in the Ketterle group. Above the critical temperature T_c, the cloud is a broader Gaussian distribution of a thermal gas (left image). As the temperature is lowered beyond T_c (central image), a second narrow peak emerges, originating from the macroscopic occupation of a single orbital with a narrow momentum distribution. As the temperature is lowered further, more and more atoms leave the thermal component and reside in the condensate orbital. The image is taken from [86]. (b): Time of flight profiles of a bosonic cloud in an optical lattice during collapse and revival. The two outer images are the time of flight expansion profiles of a condensate in an optical lattice. Satellite peaks typically appear in a lattice BEC, where the single particle ground state is not only the momentum $\mathbf{k} = 0$ state, but contains admixtures of higher momentum components. The image is taken from [67].

In Situ Imaging

Using high resolution optics, it is also possible to directly measure the real space density distribution of the cloud (in situ). Using this technique, it was possible to directly measure the formation of vortices in BECs [2] and BCS superfluids [184]. Over the last two years this approach has been strongly improved for lattice systems, where this powerful and promising new technique has become known as the *quantum gas microscope*. It refers to a very high resolution optical setup operating close to the fundamental optical limit, with which it is possible to observe individual atoms with single site resolution in lattice systems with submicrometer lattice spacings. See for eaxmple Fig. (1.6), where the preparation of systems with selectively populated atomic distributions is also demonstrated.

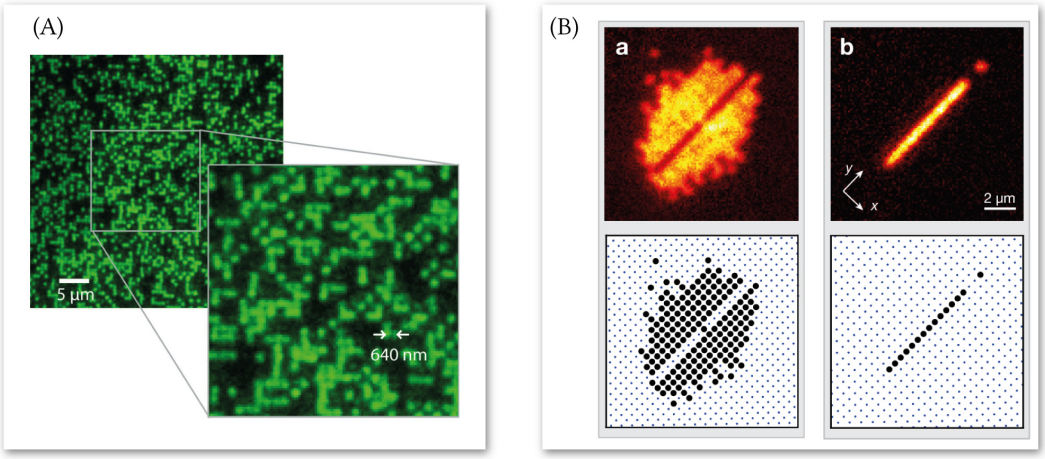

Figure 1.6: Images of ultracold atoms in a 2D optical lattice taken with quantum gas microscopes. With the high resolution optics it is possible to detect individual atoms with single site resolution. In the experiment by W. Bakr et al. [11] (subfigure A), it is possible to engineer a wide range of two-dimensional potentials. In the experiment by C. Weitenberg et al. [169] (subfigure B), the atoms are prepared in a single layer of a retroreflected optical lattice and using a highly focused addressing laser together with a microwave pulse, individual atoms can be removed. This allows for the preparation of arbitrary patterns of insulating states with one atom per site. The images (A) and (B) are taken from [11] and [169] respectively.

Spectroscopic Imaging

To gain insight into the excitation and internal structure of a many-body state, it is useful to perturb the system and bring it out of equilibrium before measuring the quantities described above. Depending on the perturbation that is used and the measured quantity, different correlation functions can be measured within linear response. A prominent example is Bragg spectroscopy, where collective excitations can be addressed with full momentum and energy resolution. Within linear response theory, the dynamic structure factor determines the transition rate into excited states. This method and its application to measure the amplitude mode of a system of strongly interacting lattice bosons is discussed in detail in chapter (9).

Similarly, Raman spectroscopy provides a momentum-resolved measurement, but the internal hyperfine state of the atom is changed during the two-photon process (in contrast to the Bragg spectroscopy, where the initial and final internal state of the atom are identical). The different hyperfine states can be spatially separated during the time of flight procedure using a Stern-Gerlach setup, thus allowing for a state-dependent detection. Within linear response theory, Raman spectroscopy measures the single particle spectral function of the many-particle system [37]. This method is analogous to angle resolved photoemission spectroscopy used in solid state physics [35].

Noise Correlation Measurement

Intrinsically, time of flight profiles contain noise in the sense that the images measured by a camera deviate from the mean density value at a given point. A part of this noise can be attributed to technical reasons, but the discrete nature of the counting statistics additionally contributes to the measured fluctuations on a fundamental level. It was first proposed by Altman et al. [4], that the shot to shot statistical fluctuations in these images contain information on the many-body state, originating from the bosonic counting statistics as found by Hanbury Brown and Twiss [24]. Using this technique, the density-density correlator $\mathcal{G}(\mathbf{r}, \mathbf{r}') = \langle \hat{n}(\mathbf{r})\, \hat{n}(\mathbf{r}') \rangle - \langle \hat{n}(\mathbf{r}) \rangle \langle \hat{n}(\mathbf{r}') \rangle$ can be measured, which was first done by Fölling et al. [57] for a bosonic Mott insulator, as shown in Fig. (1.7).

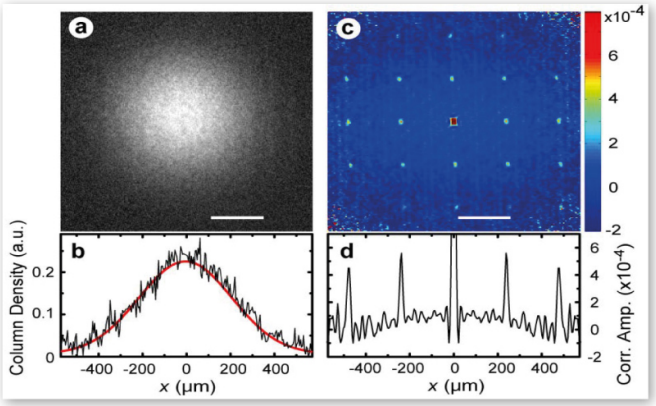

Figure 1.7: Left: a single time of flight profile of a gas initially in the Mott insulating phase does not contain the short-range correlation in the Mott insulator. Only when taking a large number of images and analyzing the correlations in the shot noise, these spatial correlations and the reciprocal lattice structure become visible, as shown in the right figure. The figure is taken from [57].

Phase Contrast Imaging

A non-destructive technique, which has successfully been used to probe BECs[9] and density differences of two spin species in a fermionic gas[148], is phase contrast imaging. The probing beam is tuned off resonance, such that the heating of the cloud is two orders of magnitude lower in comparison to absorption imaging and does not destroy the sample. Here the light scattered by the atoms acquires a phase shift, which can be detected by interference with the unscattered light. Using this technique, the temporal evolution an atomic cloud can be followed in real time for a single sample.

Imaging with an Electron Microscope

Shortly before the single site addressability with an optical setup was demonstrated by the experiment in the Greiner group [11], this was realized using scanning electron microscopy in the Ott group by Würtz et al. [175]. Here it was also possible to selectively remove atoms from the system with full spatial resolution.

1.6 Interactions in Ultracold, Dilute Atomic Gases

One of the great advantages of ultracold atomic gases in contrast to solid state systems, is the control over the effective inter-particle interactions. For atomic gases, this can be externally controlled by adjusting experimental parameters, such as the external magnetic field (addressing a Feshbach resonance) or the lattice depth, which can be varied over several orders of magnitude, even allowing for a change of sign of the effective interaction parameter g (corresponding to repulsive or attractive interactions). This is in strong contrast to the very limited control over the Coulomb interaction in solid state systems, where the interaction parameter depends on the compound at hand and can only be altered slightly by the exertion of great pressure. In this section, we shall shortly review and summarize the underlying principles leading to the effective short-range interaction between atoms.

1.6.1 Interatomic Potentials

The physical origin of the interaction between atoms in their ground state are the attractive van der Waals forces, reflected by the $1/r^6$ decaying tail of the molecular potentials. In this section, we

shortly review the principles through which the tunable effective short range interactions, which can be both attractive as well as repulsive, arise from the physical interactions in the low energy and low density limit.

It is important to remember throughout all further sections, that in the context of ultracold atomic gases, where the interactions are modeled by effective two-particle interactions for sufficiently dilute gases, we are never working in the true physical ground state of these systems. Even when one often talks about the *ground state* of the effective model Hamiltonians, this is not actually the true physical ground state of the system, but a highly excited metastable state. After all, the true ground state of alkaline atoms is a metal slab with a crystalline structure, as we know it from the chemistry lab!

To describe the interaction between two atoms located at $\mathbf{R}_1$ and $\mathbf{R}_2$, it is useful to change into the basis of the center of mass coordinate $\mathbf{R} = (\mathbf{R}_1 + \mathbf{R}_2)/2$ and relative coordinate $\mathbf{r} = \mathbf{R}_1 - \mathbf{R}_2$. If the two atoms are not exposed to any external potential, the total momentum is conserved and the energy only depends on the relative coordinate $\mathbf{r}$. One may approximately describe the complicated interactions between the many different internal states of the atoms by a molecular potential V_{mol}, which is strongly repulsive at short distances on the scale of a few Bohr radii due to the repulsion of overlapping electron shells. For larger distances and without considering potential dipole-dipole interactions, the potential becomes attractive and decays as $\propto r^6$, corresponding to the van der Waals interaction, i.e. mutually induced polarization of the electron clouds.

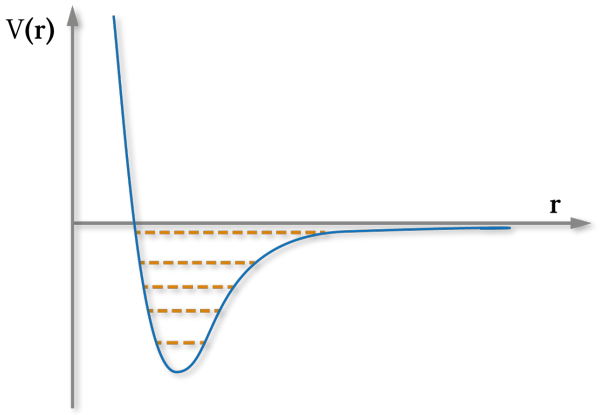

Figure 1.8: The molecular potential in the relative coordinate between two atoms. Several low energy, molecular bound states may exist. The substantial scattering properties in the unbound low energy limit, are determined by the state closest to zero energy.

Note that although the physical potential is attractive everywhere except at very close relative distances, this can given rise to both attractive, as well as repulsive effective interactions. For any but the simplest of atoms, the precise structure of the interatomic potential is not precisely known and can presently also not be calculated from first principles with the required level of precision. However, this detailed knowledge is not required to describe the relevant scattering properties in the low energy limit. In the partial wave expansion, low temperatures (which is well given for typical experiments) imply that the colliding atoms do not possess the energy to overcome the centrifugal barrier and hence only the lowest partial wave, which is the s-wave, contributes. The scattering process within the s-wave channel is described by a single quantity, which is the s-wave scattering length a_s. This defines the asymptotic properties of the scattering wave function, which one takes to be the only parameter to describe the scattering properties of dilute gases. This allows us to replace the exact multichannel potentials by an effective contact potential, which reproduces the same asymptotic scattering behavior. The simplest choice suitable for most theoretical models is the delta contact potential between two atoms of mass m at positions $\mathbf{r}$ and $\mathbf{r}'$

$$V(\mathbf{r} - \mathbf{r}') = \frac{4\pi\hbar^2 a_s}{m}\delta(\mathbf{r} - \mathbf{r}'). \tag{1.12}$$

This potential is subsequently used to determine the interaction constant for the many-particle lattice model.

2. The Bose-Hubbard Model

The Hubbard model, both in bosonic and fermionic form, lies at the heart of condensed matter physics. Being a minimalistic model that describes the tunneling of particles between different lattice sites together with local interactions, it gives rise to a surprisingly vast plethora of different phenomena. Whereas the Hubbard model is often a crude approximation for electrons in solid state systems, owing to the strong attraction between electrons and the complex structure of real materials, they can be almost perfectly realized systems of cold atoms in optical lattices. In this chapter we derive and discuss in detail the construction of the Bose- and Fermi-Hubbard model in optical lattice systems and relate the effective Hubbard parameters to the microscopic parameters, such as the laser intensity, wavelength, atomic scattering length, mass, etc..

We begin by reviewing the single particle physics in a periodic potential, i.e. the emergence of a band structure and Bloch states, and show explicit results for the case of a hypercubic optical lattice. Furthermore, we discuss the effect of an additional inhomogeneous trapping potential on the eigenvalue and eigenstate structure. Next, we discuss the construction of a localized basis within each band, i.e. the Wannier states. We first review the standard construction procedure, before building on an alternate definition of Wannier states by Kivelson in 1982 [89] to construct an alternate method to numerically determine Wannier states. We show that the calculation of the matrix elements of the band projected position operator can be reduced to a simple form, the evaluation of which is numerically very efficient. The power of this technique, in contrast to the usual symmetry-based and minimization of spatial variance approach, is its numerical efficiency, the uniqueness of the resulting Wannier states and the extendability to inhomogeneous systems. Moreover, it is also suited to efficiently determine Wannier states of inseparable potentials in higher dimensions, which will be illustrated for the specific case of a honeycomb lattice in chapter (5).

After this intermezzo, we discuss the behavior of tunneling matrix elements and introduce the tight-binding model. The last step consists of including interactions and expressing these in the Wannier basis, before combining these constituents to the Bose- and Fermi-Hubbard model.

2.1 Bloch States

In this section we review the structure of eigenvalues and eigenstates in a spatially periodic potential, i.e. the band structure. The derivation will be given for the general d-dimensional case, before we present results for the case of a cubic optical lattice, where the problem can be reduced to the one-dimensional case.

We consider a single particle of mass m, described by a Hamiltonian

$$\mathcal{H}_{\text{s.p.}} = \frac{\hat{p}^2}{2m} + \int d^3r \; V(\mathbf{r}) \; |\mathbf{r}\rangle\langle\mathbf{r}| \tag{2.1}$$

in a spatially periodic potential

$$V(\mathbf{r}) = V(\mathbf{r} + \mathbf{T}), \tag{2.2}$$

where $\mathbf{T} = \sum_i m_i \mathbf{a}_i$ is an arbitrary real space lattice vector, $\mathbf{a}_i$ are the primitive lattice vectors and m_i are integer values. Our goal is to determine and classify the eigenvalues and eigenstates (called *Bloch states*) of a general Hamiltonian of this form.

The discrete translational invariance of the potential is directly reflected in the symmetry of the Hamiltonian (2.1)

$$\tau^\dagger(\mathbf{T})\, H_{\text{s.p.}}\, \tau(\mathbf{T}) = H_{\text{s.p.}} \tag{2.3}$$

with $\tau(\mathbf{r}) = e^{-i\mathbf{r}\cdot\hat{\mathbf{p}}}$ denoting the spatial translation operator, written in terms of the generators of translations $\hat{p}_i$, i.e. the momentum operators. We now exploit this symmetry to infer a property of the eigenstates of $H_{\text{s.p.}}$. Let $|\theta\rangle$ be an eigenstate of $H_{\text{s.p.}}$ with the eigenvalue λ_θ and we will consider the translation along one specific primitive lattice vector $\tau = \tau(\mathbf{a}_j)$. According to Eq. (2.3), we have $H_{\text{s.p.}}\, \tau|\theta\rangle = \lambda_\theta \tau|\theta\rangle$. This is just the eigenvalue equation for $\tau|\theta\rangle$, which is also an eigenstate to the same eigenvalue λ_θ. If the spectrum of $H_{\text{s.p.}}$ is non-degenerate[1], this implies that $\tau|\theta\rangle$ is the same state as $|\theta\rangle$, up to a complex phase factor $e^{i\theta}$. Let us define the real-space representation of the state $\psi_\theta(\mathbf{r}) = \langle \mathbf{r}|\theta\rangle$, which are called *Bloch functions*. Using the property $\tau(\mathbf{a}_j)|\mathbf{r}\rangle = |\mathbf{r} + \mathbf{a}_j\rangle$ and the associativity of operators for the expression $\langle \mathbf{r}|[\tau(\mathbf{a}_j)]^l|\theta\rangle$ for an arbitrary integer l, one finds

$$\psi_\theta(\mathbf{r} - l\mathbf{a}_j) = e^{il\theta}\, \psi_\theta(\mathbf{r}). \tag{2.4}$$

The only ansatz which fulfills this requirement for all values of $\mathbf{r}$ and arbitrary l is

$$\psi_{\mathbf{k},\alpha}(\mathbf{r}) = \langle \mathbf{r}|\theta\rangle = e^{i\mathbf{k}\cdot\mathbf{r}}\, u_{\mathbf{k},\alpha}(\mathbf{r}), \tag{2.5}$$

where $u_{\mathbf{k},\alpha}(\mathbf{r})$ is a complex-valued function with the full periodicity of the original lattice

$$u_{\mathbf{k},\alpha}(\mathbf{r}) = u_{\mathbf{k},\alpha}(\mathbf{r} + \mathbf{T}). \tag{2.6}$$

Due to the structure of the Hamiltonian, a number of symmetry properties and relations follow for the u-functions, which are discussed is App. (A). Instead of labeling the state by the angle θ, we have introduced the *quasi-momentum* $\mathbf{k}$, which is a tuple of d quantum numbers, describing the change of the state's complex phase under translations in the various lattice directions. It is related to the phase factor by $\theta = -\mathbf{k}\cdot\mathbf{a}_j + 2\pi n$, where n is an arbitrary integer. However, there may generally be more than one state which transforms in the way described above under translations. We therefore introduced an additional quantum number α, such that each energy eigenstate is uniquely specified by the set $(\mathbf{k}, \alpha)$. As will become clear, α is the band index.

Note that due to the $2\pi i$-periodicity of the exponential function, the quasi-momentum $\mathbf{k}$ is not unique, i.e. there exist different $\mathbf{k}$, which lead to the same transformation behavior of the eigenstates. We now analyze in more detail which values of $\mathbf{k}$ correspond to the same transformation behavior, which will lead to the concept of the reciprocal lattice. We define the primitive reciprocal lattice vectors $\mathbf{b}_j$ implicitly by requiring

$$\mathbf{a}_i \cdot \mathbf{b}_j = 2\pi\delta_{i,j}. \tag{2.7}$$

For a given set of $\{\mathbf{a}_i\}$, these can easily be determined by the inversion of the matrix containing $\mathbf{a}_i$ as column vectors. The Bloch states (in different bands) for a given quasi-momentum $\mathbf{k}$ are identical to the Bloch states[2] for another quasi-momentum $\mathbf{k}' = \mathbf{k} + \mathbf{G}$, if the quasi-momenta are related through the translation by a reciprocal lattice vector $\mathbf{G} = \sum_j n_j\, \mathbf{b}_j$. Thus the infinitely many pairs $(\mathbf{k} + \mathbf{G}, \alpha)$ for fixed $\mathbf{k}$ and α, but varying $\mathbf{G}$ all refer to the same physical state. To uniquely denote a state, we may therefore implicitly require that the vector $\mathbf{k}$ has a smaller euclidean norm than any vector $\mathbf{k} + \mathbf{G}$. The set of all $\mathbf{k}$ referring to different physical Bloch states constitutes the first Brillouin zone.

[1] In case of degeneracy it can be shown that a suitable set of eigenstates can be chosen, such that the above relations are exactly fulfilled.

[2] Note however that the functions $u_{\mathbf{k},\alpha}(\mathbf{r}) = e^{i\mathbf{G}\cdot\mathbf{r}}\, u_{\mathbf{k}',\alpha}(\mathbf{r})$ are not identical, but related by a multiplicative exponential factor.

Determining the Bloch States

We can now use the knowledge of the Bloch functions' structure to describe an efficient method to determine these explicitly.

Inserting the ansatz (2.5) into the time-independent Schrödinger equation, one obtains an effective Schrödinger equation for the functions $u_{\mathbf{k},\alpha}(\mathbf{r})$

$$\left[-\frac{\hbar^2}{2m}\left(-i\,\nabla+\mathbf{k}\right)^2+V(\mathbf{r})\right]\,u_{\mathbf{k},\alpha}(\mathbf{r})=E_{\mathbf{k},\alpha}\,u_{\mathbf{k},\alpha}(\mathbf{r}). \tag{2.8}$$

Since both the potential and the u-functions possess the full discrete translational symmetry, they can be expressed as a Fourier series

$$u_{\mathbf{k},\alpha}(\mathbf{r})=\sum_{n_1,n_2,n_3} c^{(\mathbf{k},\alpha)}_{n_1,n_2,n_3}\;e^{i(n_1\,\mathbf{b}_1+n_2\,\mathbf{b}_2+n_3\,\mathbf{b}_3)\cdot\mathbf{r}} \tag{2.9}$$

$$V(\mathbf{r})=\sum_{n_1,n_2,n_3} V_{n_1,n_2,n_3}\;e^{i(n_1\,\mathbf{b}_1+n_2\,\mathbf{b}_2+n_3\,\mathbf{b}_3)\cdot\mathbf{r}}. \tag{2.10}$$

For a given periodic potential, the Fourier coefficients V_{n_1,n_2,n_3} can be directly determined from the inverse transformation, i.e. an integration over the unit cell. The task of explicitly finding the Bloch functions is then reduced to determining the coefficients $c^{(\mathbf{k},\alpha)}_{n_1,n_2,n_3}$. Inserting (2.9) and (2.10) into the effective Schrödinger equation (2.8) reduces the coupled differential equations into a set of linear, algebraic equations

$$E_r\left[\frac{\mathbf{k}+n_1\mathbf{b}_1+n_2\mathbf{b}_2+n_3\mathbf{b}_3}{k_L}\right]^2 c^{(\mathbf{k},\alpha)}_{n_1,n_2,n_3}\;+\sum_{n_1',n_2',n_3'} V_{n_1-n_1',n_2-n_2',n_3-n_3'}\;c^{(\mathbf{k},\alpha)}_{n_1',n_2',n_3'}=E_{\mathbf{k},\alpha}\;c^{(\mathbf{k},\alpha)}_{n_1,n_2,n_3}. \tag{2.11}$$

For sufficiently smooth potentials the Fourier coefficients V_{n_1,n_2,n_3} decay rapidly with increasing frequency components and so too will the coefficients $c^{(\mathbf{k},\alpha)}_{n_1,n_2,n_3}$ for sufficiently low energy states. One can thus safely truncate the high frequency space at some $\mathbf{n}_{\max}$ (analogously on the negative frequency side of the spectrum) and the equations (2.11) can be written as a finite-dimensional eigenvalue problem in matrix form

$$H^{(\mathbf{k})}\begin{pmatrix} c^{(\mathbf{k},\alpha)}_{-\mathbf{n}_{\max}}\\ \vdots\\ c^{(\mathbf{k},\alpha)}_{\mathbf{n}_{\max}}\end{pmatrix}=E_{\mathbf{k},\alpha}\begin{pmatrix} c^{(\mathbf{k},\alpha)}_{-\mathbf{n}_{\max}}\\ \vdots\\ c^{(\mathbf{k},\alpha)}_{\mathbf{n}_{\max}}\end{pmatrix}. \tag{2.12}$$

Written within the integer vectorial index notation $\mathbf{n}=(n_1,n_2,n_3)$, the matrix

$$H^{(\mathbf{k})}_{\mathbf{n},\mathbf{n}'}=\left(\mathbf{k}+n_1\mathbf{b}_1+n_2\mathbf{b}_2+n_3\mathbf{b}_3\right)^2\frac{E_r}{k_L^2}\,\delta_{\mathbf{n},\mathbf{n}'}+V_{\mathbf{n}-\mathbf{n}'} \tag{2.13}$$

contains all kinetic energy terms (i.e. resulting from the first term in (2.11)) on the diagonal. The off-diagonal Fourier components effectively couple different plane wave states, a behavior which is analogous to scattering. For a periodic potential, only momentum states related by reciprocal lattice vectors $\mathbf{G}$ are coupled, making the problem separable. For each $\mathbf{k}$ within the first Brillouin zone, the matrix $H_{\mathbf{k}}$ can be seen as the corresponding subblock of the full lattice Hamiltonian and the quasi-momentum $\mathbf{k}$ only enters parametrically.

For separable potentials, the problem can be reduced to separate diagonalizations in each dimension. For a suitable choice of basis, the matrix $H^{(\mathbf{k})}$ is the Kronecker product of the corresponding matrices in the individual dimensions. The diagonalization of $H^{(\mathbf{k})}$ can be performed numerically for each quasi-momentum $\mathbf{k}$, yielding the eigenenergies $E_{\mathbf{k},\alpha}$ for the different bands, as well as the coefficients $c^{(\mathbf{k},\alpha)}_{n_1,n_2,n_3}$ of the corresponding Bloch states.

Note that the u-functions are of the same units (length)$^{-d/2}$ as the Bloch functions in d dimensions. We will use the normalization convention

$$\sum_{n_1,n_2,n_3} |c^{(\mathbf{k},\alpha)}_{n_1,n_2,n_3}|^2 = 1, \tag{2.14}$$

which is equivalent to working in units of the real space unit cell volume $V_{\text{unit cell}} = 1$. The Bloch and the u functions are thus not normalized to unity when integrated over the entire real-space lattice, but instead over the unit cell

$$\int_{\text{unit cell}} d^3r\ |\psi_{\mathbf{k},\alpha}(\mathbf{r})|^2 = \int_{\text{unit cell}} d^3r\ |u_{\mathbf{k},\alpha}(\mathbf{r})|^2 = 1. \tag{2.15}$$

The Bloch states on a lattice with L sites can then be expressed explicitly as

$$|\mathbf{k},\,\alpha\rangle = \frac{1}{\sqrt{L}} \int d^3r \sum_{n_1,n_2,n_3} c^{(\mathbf{k},\alpha)}_{n_1,n_2,n_3}\, e^{i(\mathbf{k}+n_1\mathbf{b}_1+n_2\mathbf{b}_2+n_3\mathbf{b}_3)\cdot\mathbf{r}}\ |\mathbf{r}\rangle. \tag{2.16}$$

The set of all Bloch states, being eigenstates of the Hermitian operator $H_{\text{s.p.}}$, constitute an orthonormal basis of the single-particle space

$$\langle \mathbf{k},\alpha|\mathbf{k}',\alpha'\rangle = \delta_{\mathbf{k},\mathbf{k}'}\,\delta_{\alpha,\alpha'} \tag{2.17}$$

$$\sum_{\mathbf{k},\alpha} |\mathbf{k},\alpha\rangle\langle\mathbf{k},\alpha| = \mathbb{1}. \tag{2.18}$$

and the single particle Hamiltonian is by construction diagonal in this basis

$$H_{\text{s.p.}} = \sum_{\mathbf{k},\alpha} E_{\mathbf{k},\alpha}|\mathbf{k},\alpha\rangle\langle\mathbf{k},\alpha|. \tag{2.19}$$

2.2 Bloch States in a $1D$ Optical Lattice

As a specific example, we now consider the Bloch states in a simple 1D optical lattice

$$V(x) = sE_r\left(\sin^2(k_L x) - \frac{1}{2}\right) = -\frac{sE_r}{4}\left(e^{2ik_L x} + e^{-2ik_L x}\right). \tag{2.20}$$

Here s is the lattice depth in units of the recoil energy $E_r = \frac{\hbar^2 k_L^2}{2m}$, which is the kinetic energy an atom gains by absorbing a photon from the lattice laser beam and defines the natural energy scale of the system.

In this case the potential leads to a tridiagonal matrix with matrix elements

$$H^{(k)}_{n,n'} = E_r\left(\frac{k}{k_L} + 2n\right)^2 \delta_{n,n'} - \frac{sE_r}{4}(\delta_{n,n'+1} + \delta_{n,n'-1}). \tag{2.21}$$

Typical Bloch functions for the sinusoidal potential are shown in Fig. (2.1).

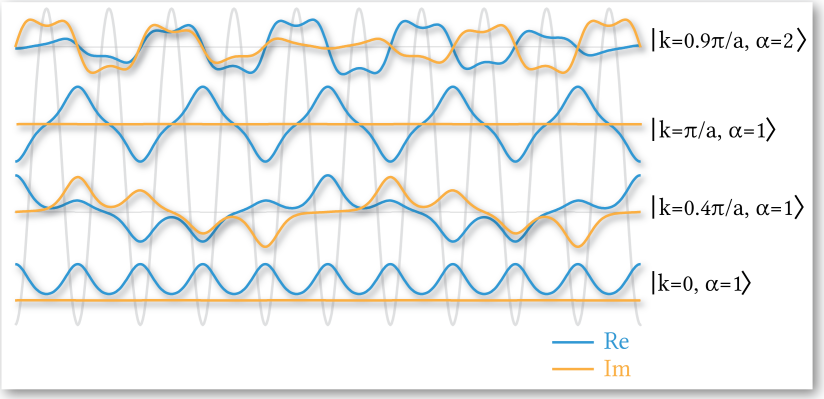

Figure 2.1: Typical Bloch functions for a one-dimensional optical lattice of depth $s = 8E_r$. At the high symmetry points in the Brillouin zone ($k = 0$ and $k = k_L$ here) these can be chosen purely real, as shown here for the lowest band $\alpha = 1$. However, in general this is not possible.

Plotting the set of eigenenergies $E_{\mathbf{k},\alpha}$ as a function of the quasi-momentum $\mathbf{k}$, Fig. (2.2) shows the emergence of a band structure in the single particle dispersion relation, as the lattice depth s is increased.

As discussed previously, every state can be represented as a point in the first Brillouin zone in conjunction with an additional quantum number, the band index α. In the limit of vanishing lattice intensity, the free quadratic dispersion relation is simply folded back into the first Brillouin zone at the zone edge, as shown on the left of Fig. (2.2). The periodic potential couples pure momentum states corresponding to the same quasi-momentum, i.e. lying on the same vertical line. As the lattice depth is increased, states lying with an energy difference of the order of the coupling by the lattice potential hybridize and band gaps open up. These lead to avoided crossings at the points where the free particle energy lines initially intersected and bands form. For a lattice with L sites, each band contains exactly L different Bloch states and in the limit of an infinitely large lattice, the points within each band move mutually closer, forming a continuous band.

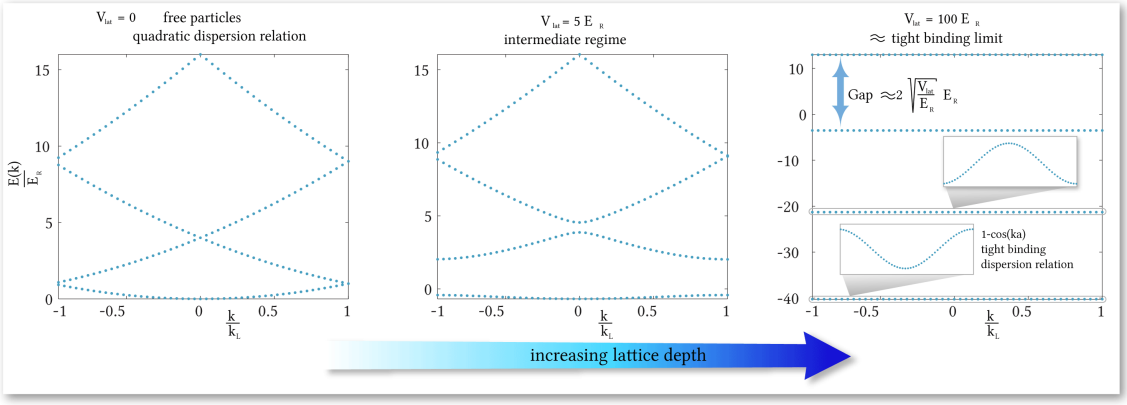

Figure 2.2: Single Particle Dispersion relations in a 1D optical lattice for three different lattice intensities. Every point corresponds to the eigenenergy $E_{\mathbf{k},\alpha}$ of a specific Bloch state, which can be uniquely classified according to a quasi-momentum $\mathbf{k}$ and a band index α. For a free system (left subfigure), the quadratic dispersion relation is simply folded back into the first Brillouin zone. As the lattice intensity is increased, energy gaps open up (center subfigure), bands form and these converge to the tight binding dispersion relation. For very deep lattices, the band width is suppressed and the band gaps become equidistant (right subfigure), corresponding to the associated harmonic oscillator energy spacing.

A ubiquitous feature of the dispersion relations for general lattices in the limit of a strong lattice depth, is cosine shape of the individual bands, shown in the insets on the right of Fig. (2.2). Typically, the lowest band becomes proportional to $1-\cos(ka)$, corresponding to a positive effective mass $m^* = \left(\frac{\partial^2 E}{\partial k^2}\right)^{-1}$, which alternates in sign with increasing band number in one dimension. This is the tight binding limit of a particle in a strong lattice and can also be understood as the limit where only spatially localized Wannier states on nearest neighboring sites are coupled by a tunneling element J and all longer range tunneling can be neglected, as discussed in the next section.

The Bloch states discussed above are fully delocalized and extend over the entire lattice. The Bloch functions depicted in Fig. (2.1) can be understood to be either appropriately scaled cutouts of a state on a much larger lattice or to calculated using periodic boundary conditions. In a finite system with open boundaries, the structure of the Bloch states in the bulk of the system is not significantly changed.

2.3 Eigenstates in an Optical Lattice with a Trap

Clearly describing the single particle eigenstates as extended Bloch states, albeit the eigenstates calculated with hard wall boundary conditions, is a crude approximation for cold atom experiments, where a Gaussian trap is usually present. It should be pointed out that if the external trapping potential originates from the beam profile of the lattice laser, the intensity profile is multiplied (and not added) with the lattice potential, which also implies that the Hubbard parameters become site dependent. Only within a first order approximation, can it be considered as an additional harmonic potential and the system is described by the Hamiltonian

$$\mathcal{H} = \mathcal{H}_{\text{lat}} + V_0 \int dx \left(\frac{x}{a}\right)^2 |x\rangle\langle x|. \tag{2.22}$$

Here, V_0 is the harmonic trapping strength, which has the dimension of an energy. Working in the multiband basis of Bloch states of the lattice without a harmonic trap, the trap potential couples Bloch states from different bands. Thus, the eigenstates of the harmonic lattice and the trap contain higher band contributions and are furthermore no longer spread out over the entire system. The amplitudes of states in the low energy eigenstates from high bands of the homogeneous system is strongly suppressed, justifying a truncation of the entire space to the relevant low energy bands of the original, homogeneous system. In the presence of an inhomogeneous potential, which does not possess the lattice symmetry, the eigenstates cannot be classified according to their quasi-momentum (i.e. this is no longer a good quantum number) and the energy eigenvalues cannot be plotted as a dispersion relation. In Fig. (2.3) we therefore plot the eigenenergy values according to their index (which is given in monotonically increasing order) for a strong lattice. In the absence of a trap, the lowest band has the expected tight binding shape and the spectrum features a large gap to the next highest band.

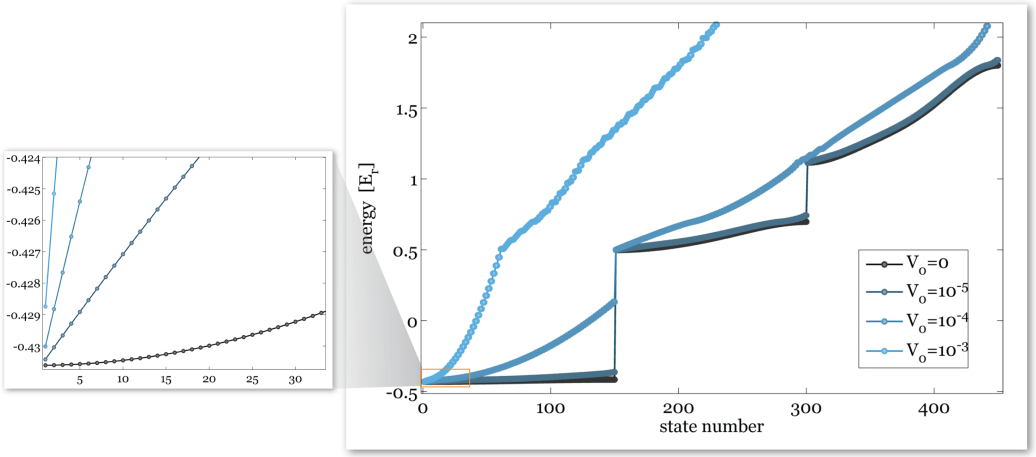

Figure 2.3: Single particle eigenstates in an optical lattice with a trap. The inset shows shows a close-up version of the behavior at low energies. Whereas the dispersion relation for atoms in a lattice without any confining trap is quadratic at low energies ϵ (low momenta in the tight-binding relation $1-\cos(ka)$), corresponding to a density of states diverging as $\propto \epsilon^{-\frac{1}{2}}$, the density of states is constant at low energies as soon as any quadratic trapping potential is added (corresponding to a linear increase of the energy values with their numbering). This agrees with the results found by Hooley and Quintanilla [76] within a single band treatment. In the main figure on the right, it can be seen that the band structure is preserved if the additional trapping potential is not too strong. The band gap survives, although each individual eigenstate is no longer a fully extended Bloch state. If the trap potential does not change too fast, the eigenstates retain the local structure of a homogeneous Bloch state at an energy corresponding to the inhomogeneous eigenstate energy minus the potential energy offset (known as the local density approximation).

As the external quadratic trap is turned on, both the eigenstate and the energy eigenvalues evolve continuously from the Bloch states (calculated for the finite size system with periodic boundary

conditions for $V_0 = 0$) into localized eigenstates of the trapped lattice. If the trapping potential V_0 is not too strong, the band structure is thus preserved, transforming into *dressed bands*. Only when the external spatial potential becomes very strong[3], do the gaps close and the dressed band structure breaks down.

Typical representative eigenstates of the lowest dressed band of a sinusoidal potential with a harmonic trap are shown in Fig. (2.4). Note that V_0, together with the lattice depth set an effective harmonic oscillator length scale, where the effective mass m^* of the particle in the lattice takes the role of the mass in the usual harmonic oscillator length scale. For weak V_0, this is simply the coarse grained version of the harmonic oscillator and we expect the low energy eigenstates to be the harmonic oscillator eigenstates, convolved with the local Wannier function (which will be introduced in the next section). This can clearly be seen for the two lowest states $|1\rangle$ and $|6\rangle$ shown in Fig. (2.4). For higher energy excited states, a qualitative difference to the usual harmonic oscillator arises. In the homogeneous lattice, the Bloch eigenstates can only take on energies which lie inside one of the energy bands, the lowest of which has the width $4J$. If the energy of a trapped lattice eigenstate is larger than the band width $4J$, the central region of the trap (where the additional potential energy is close to zero) becomes classically forbidden and the wave functions of the excited states decay exponentially at the classical turning points. This is in accordance with the results found by Hooley and Quintanilla within a single band, tight binding basis system of the homogeneous system [76]. Depending on the energy eigenvalue of the trapped lattice eigenstate, its wave function is localized to an outer radial region, as shown for the excited state $|66\rangle$ in Fig. (2.4).

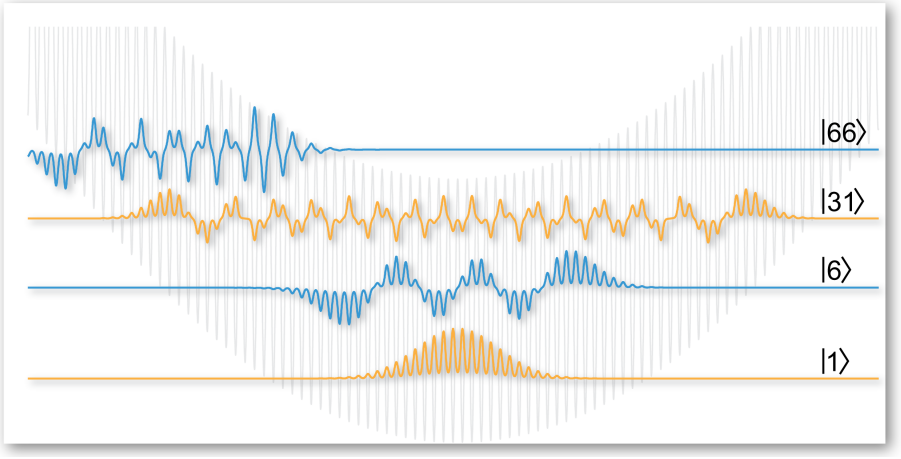

Figure 2.4: A few representative single particle eigenstates in a $s = 10$ optical lattice consisting of $L = 150$ sites with a trap of strength $V_0 = 10^{-5}E_r$ in the lowest dressed band. These were determined within a full multi-band calculation of the original lattice Hamiltonian. Since the system is invariant under time reversal, the real-space representation of the eigenstates can be and are chosen real. If the energy of the eigenstate lies within the band, the state corresponds to a coarse grained version of the usual harmonic oscillator eigenstate. If the energy of the eigenstate is higher than the bandwidth (note: not the lattice depth, as may be misinterpreted from the lattice potential shown in light gray), the states are localized either on the left or right, if the system is not fully spatially symmetric under reflection.

If the lattice well minimum coincides with the trap minimum, the system is symmetric under reflection and all eigenstates are also either fully symmetric or antisymmetric under reflection. For the 1D case, the excited states with exponentially suppressed amplitude at the trap center have weight on both the left and right sides of the trap. However, such states are very susceptible to decoherence and a very small shift of the trap center position relative to the lattice minima localizes the amplitude of the eigenstates to either the left or the right side, as shown in the excited eigenstate $|66\rangle$ in Fig. (2.4).

[3] A close analysis shows that the spatial potential is considered to be strong if the variation in local on-site energies of neighboring sites becomes comparable to the relevant band gap.

2.4 Maximally Localized Wannier States

We will now discuss the construction of Wannier states [168, 91], which are a set of spatially localized states within a given band of a lattice and play a central role in the formulation of lattice models when including local effects, such as interactions or spatial potentials. Independently, they have also been found in context of chemical covalent bonding by Boys [22]. Wannier states constitute an orthonormal basis of eigenstates within each band, but in contrast to the Bloch eigenstates, they are exponentially localized to a given lattice site. The existence of a unique set of exponentially localized Wannier states in 1D was shown in a seminal work by Kohn [90], but the extension to higher dimensions remained one of the last unresolved problems in single particle quantum mechanics. Only in 2007 was this shown for systems with time reversal symmetry in two and three dimensions by Brouder et al. [23]. We will first give and discuss the standard definition and the commonly used *construction recipe*, which is however only applicable for simple lattice geometries and seldom explained. For more complicated lattice geometries, such as inseparable 2D hexagonal lattice structures, this heuristic, symmetry-based approach to choosing the phases of the Bloch states, becomes very cumbersome and potentially misleading, since it is often not clear that the resulting Wannier states are the maximally localized states within each given band. An alternative approach, which has commonly been used to determine Wannier states in complicated solid state lattice structures is based on the numerical minimization of the spatial variance as a function of the Bloch states' complex phases, is technically and numerically challenging [112, 111], but of fundamental importance to the construction of microscopic models from first principles.

We suggest a novel, different approach to numerically determine maximally localized Wannier for arbitrary lattices, based on an idea by Kivelson [89]. Here, the Wannier states are defined as the eigenstates of the position operator projected onto a given band[4]. We show that this definition of Wannier states is not only theoretically appealing, but also well suited and efficient for explicit numerical calculation, requiring no numerical minimization and circumventing the associated pitfalls of convergence local minima. We furthermore show that the matrix elements of the band projected position operator, initially expressed as spatial integrals over weighted Bloch functions, can be evaluated analytically, reducing the numerical effort to a summation containing the Bloch state eigenvector elements expressed in the momentum basis. It can be extended to inhomogeneous lattice systems, allowing a unique definition of orthogonal Wannier functions in inhomogeneous lattice systems. In chapter (5) we extend the procedure to inseparable potentials in two dimensions, showing that this method is also well suited for more complicated lattice geometries.

2.4.1 Usual Definition

In most of the literature, the Wannier state in band α and at site $\boldsymbol{\ell}$ and position $\mathbf{R}_{\boldsymbol{\ell}}$ is defined as the discrete Fourier transform of the Bloch states within the same band

$$|\boldsymbol{\ell}, \alpha\rangle = \frac{1}{\sqrt{L}} \sum_{\mathbf{k}} e^{-i\mathbf{k}\cdot\mathbf{R}_{\boldsymbol{\ell}}} |\mathbf{k}, \alpha\rangle. \tag{2.23}$$

However, this definition[5] is not the whole truth and it may even be misleading, as it insinuates a uniqueness, which it does not possess. Assume that the above definition does indeed lead to the correct, maximally localized Wannier states, which implies a certain a priori choice for the complex phases for the Bloch states. We may, however, transform to another set of Bloch states $|\mathbf{k}, \alpha\rangle'$, which differ only by a complex phase factor from $|\mathbf{k}, \alpha\rangle$, such that Eq. (2.23) applied to $|\mathbf{k}, \alpha\rangle'$ will not give localized Wannier states. This shows that the definition (2.23) by itself is incomplete: starting from an arbitrary set of Bloch states, the complex phases $\phi_{\mathbf{k},\alpha}$ such that

$$|\mathbf{k}, \alpha\rangle = e^{i\phi_{\mathbf{k},\alpha}} |\mathbf{k}, \alpha\rangle' \tag{2.24}$$

[4] Or onto multiple bands for lattice geometries with multiple potential minima per unit cell.

[5] Note that this definition must be extended to a summation over different bands if more than a single potential minimum exists in each unit cell, for each of which one seeks a separate Wannier state.

have to be determined additionally. This may seem trivial at first sight, but it comprises the main effort of determining maximally localized Wannier states, especially for the case of inseparable lattice geometries and when the potential within the unit cell is not symmetric under spatial reflection.

One might be tempted to think that requiring the Wannier functions to be purely real, uniquely fixes the phases. However it can be shown that phases of time-reversed states can always be chosen, such that the superposition $|\mathbf{k}, \alpha\rangle + |-\mathbf{k}, \alpha\rangle$ always has a purely real real-space representation. This essentially halves[6] the number of degrees of freedom.

Choosing the Bloch States' Complex Phases for a simple 1D Optical Lattice

We now give a simple *heuristic recipe* for choosing the phases $\phi_{\mathbf{k},\alpha}$ in the band α for the 1D case. Let $\psi_{k,\alpha}(x) = \langle x|k, \alpha\rangle$ be the real-space representation of the Bloch states and x_0 the spatial position of the $l = 0$ site's center. Here we have to distinguish between odd and even bands. Starting with a set of Bloch states $|\mathbf{k}, \alpha\rangle'$ from the band structure calculation with arbitrary phases, the phases for odd bands α[7] are chosen such that $\psi_{k,\alpha}(x = x_0)$ is real and positive for each k. For even bands, on the other hand, $\phi_{\mathbf{k},\alpha}$ is chosen such that the spatial derivative $\frac{d\psi_{k,\alpha}}{dx}(x = x_0)$ is real and positive. This procedure guarantees that the resulting real-space representation of the Wannier states is purely real everywhere and seems like a plausible choice in the limit of very strong lattices, where the Wannier states at any given site converge to the eigenstates of the harmonic oscillator. These are known to be even functions under reflection for odd α and odd functions for even α. From this construction procedure for odd (even) α it is clear that the resulting Wannier function will have the maximum possible value (maximum possible slope) out of all possible choices of phases at $x = x_0$, since at this point all local function values (slopes) are added with the same phase and *interfere constructively*. It thus seems plausible that such a wave function with the largest possible value (slope) at the position it is localized to, also has the smallest possible spatial variance. This is not a rigorous proof, however, it can be verified numerically and in the limit of deep lattices by comparison with the harmonic oscillator eigenstates.

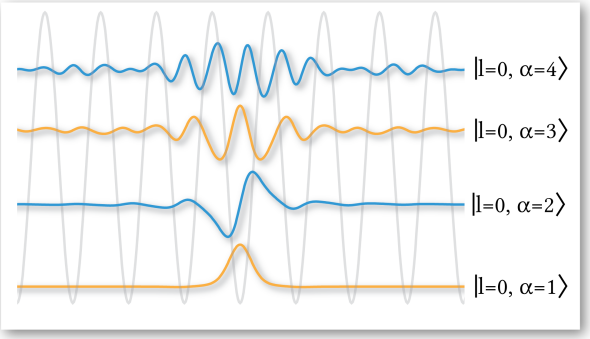

Figure 2.5: The maximally localized Wannier functions from the lowest four bands at a given site in a simple optical lattice of depth $s = 8$. These are purely real and their parity alternates with the band index. With increasing band index, the Wannier functions become less localized. The energetic band gaps and the lattice potential are drawn to scale.

2.4.2 Wannier Functions as Maximally Localized States

As mentioned above, one has to introduce a constraint in addition to Eq. (2.23), such as minimizing the spatial variance[8] $\langle \boldsymbol{\ell}, \alpha|\hat{x}_i^2|\boldsymbol{\ell}, \alpha\rangle - (\langle \boldsymbol{\ell}, \alpha|\hat{x}_i|\boldsymbol{\ell}, \alpha\rangle)^2$ to uniquely define the Wannier states. Such a

[6] neglecting high symmetry points, where the phases are individually fixed by this requirement.
[7] The lowest band is denoted by $\alpha = 1$.
[8] In general, any measure of spatial localization can be used. In the solid state community, a maximization of the on-site Coulomb repulsion energy has for instance also been used as a measure [44].

minimization has also commonly been used to determine the Wannier states on a numerical level [112, 111]. This is conceptually similar to minimizing the energy with respect to a variational state and numerical procedures analogous to imaginary time evolution have been devised. However one does not run along paths of steepest decent in energy, but in spatial variance within the parameter space of complex phases. For complicated lattice geometries, where the complex phases of the Bloch states can not easily be determined by reasons of symmetry, there has thus far been no other way to generally determine the Wannier states. Depending on the lattice structure, this spatial variance landscape may contain false local minima [113] in which a minimization algorithm may get stuck. It thus has to be guaranteed additionally that the true global minimum of the spatial variance has been determined, which complicates this approach.

2.5 Alternative Definition: Wannier States as Eigenstates of the Band Projected Position Operator

We now introduce a different technique to numerically determine Wannier states. This builds on an alternative definition of Wannier states by Kivelson [89] as eigenstate of the position operator, projected onto a given band or set of bands. Up to now, this technique has not been used as a basis to numerically calculate Wannier functions. As shown in [113], the Wannier states defined in this way correspond exactly to the Wannier states minimizing the spatial variance. Due to this fundamental correspondence, the spatial variance takes on a special role compared to other spatial localization measures.

Here we discuss the 1D case as not to obscure the presentation. We start with a set of Bloch states $|\mathbf{k}, \alpha\rangle$ from a band structure calculation and define the projection operator onto band α to be

$$\mathcal{P}_\alpha = \sum_k |k, \alpha\rangle\langle k, \alpha|. \tag{2.25}$$

The projection of the real space position operator onto the band α

$$\hat{x}_\alpha = \mathcal{P}_\alpha \, \hat{x} \, \mathcal{P}_\alpha \tag{2.26}$$

is again a Hermitian operator on the L-dimensional subspace of band α. The Wannier states in this band can now be defined [89] as the eigenstates of $\hat{x}_\alpha$

$$\hat{x}_\alpha |l, \alpha\rangle = la|l, \alpha\rangle. \tag{2.27}$$

This definition is independent of the Bloch states' complex phases and, as eigenstates of a Hermitian operator, the resulting Wannier states are automatically guaranteed to be mutually orthogonal in addition to the orthogonality between different bands. The eigenvalues indicate the spatial position the respective Wannier state is localized to and degeneracies only appear in higher dimensional lattices, when there is more than one Wannier state localized along a certain real space lattice direction within any given band. Up to now we have made no reference to the size of the system or the role finite size effects play. They do indeed affect the Wannier states obtained as eigenstate close to the edge of a finite system. However, with increasing distance from the edge the effect on the eigenstates is reduced exponentially. The entire information about the choice of phases $\phi_{\mathbf{k},\alpha}$, such that Eq. (2.23) applies, is contained within any one of the properly determined Wannier states. From this information all the states, including the ones located at the edge, can be constructed without finite size effects.

Evaluation of the Matrix Elements

In this section it is shown that the matrix elements $X^{(\alpha)}_{k,k'} = \langle k, \alpha|\hat{x}_\alpha|k', \alpha\rangle$, which are initially written as spatial integrals containing two Bloch functions and the position coordinate, can be

reduced to a sum containing the Fourier components of the Bloch states. This form allows for an efficient numerical evaluation of the matrix elements.

We consider a lattice consisting of L sites. This restricts the possible values the quasi-momentum can take on the L distinct values

$$k = \frac{2\pi}{a}\frac{m}{L}, \tag{2.28}$$

where the integer m is chosen such that all corresponding values of k lie within the first Brillouin zone. To construct Wannier states with the local reflectional symmetries of the lattice, it is required that $k = 0$ is included in the set of quasi-momenta. For even L, the range of k is $[(-1 + \frac{2}{L})\frac{\pi}{a}, \frac{\pi}{a}]$, whereas for odd L the range is $[-(1 - \frac{1}{L})\frac{\pi}{a}, (1 - \frac{1}{L})\frac{\pi}{a},]$. In both cases, k is evenly space with a step size of $\frac{2\pi}{aL}$. Note that for the simple 1D case, $\frac{2\pi}{a}$ is the (only) reciprocal lattice vector.

In the most straight-forward implementation to calculate the matrix elements of the position operator, the real space integration is restricted to the domain of the actual real space lattice as shown in Fig. 2.6, i.e.

$$X_{k,k'} = \int_{-\frac{a}{2}}^{(L-\frac{1}{2})a} \tilde{\psi}_k^*(x)\, \tilde{\psi}_{k'}(x)\, x\, dx, \tag{2.29}$$

which applies to every band α individually and we omitted the band index.

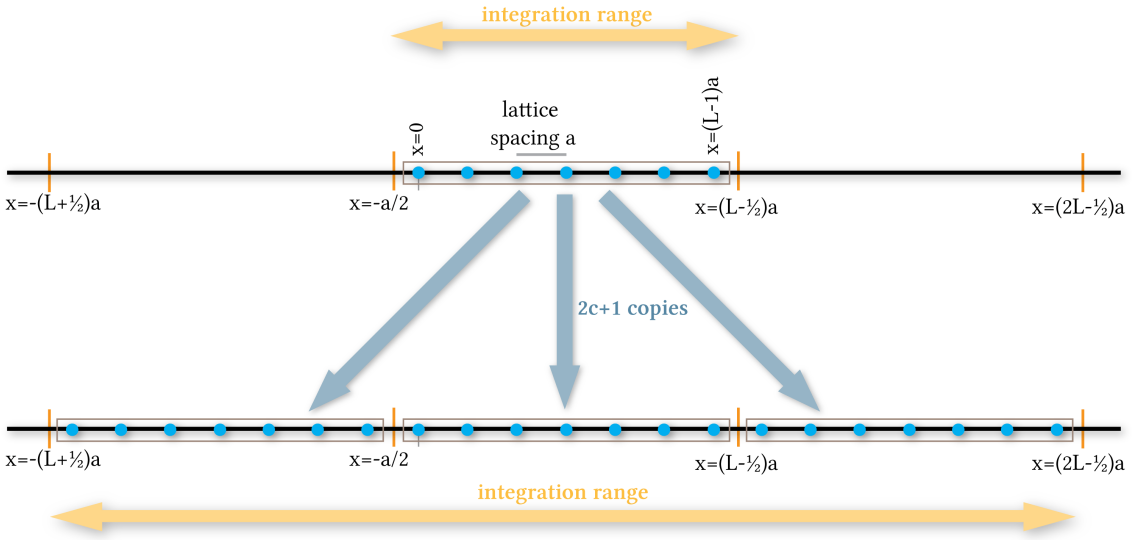

Figure 2.6: The original integration range to calculate the matrix elements $X_{k,k'}$ extends over the actual lattice from $x = -\frac{a}{2}$ to $x = (L - \frac{1}{2})a$, as shown in the upper part. However, the position operator does not have the same periodic structure (obeying periodic boundary conditions) as all allowed Bloch functions for this lattice. To minimize the finite size effect on the resulting eigenstates at the edge of the lattice, one may consider placing c (shown here for $c = 1$ in the lower part) copies of the original lattice both to the left and the right of the original lattice (all allowed Bloch states are fully periodic with period La) and integrating over the entire range.

However, although all Bloch functions are fully periodic over the extent of the full real-space lattice, this is not the case for the position operator $\hat{x}$. As a consequence, the Wannier states obtained as eigenstates close to the boundary may be affected and don't correspond to the true, maximally localized Wannier states. As shown in Fig. (2.6), one could try to minimize the finite size effects by exploiting the periodic nature of the Bloch states and formally extending the integration region by adding c copies of the original single lattice to both the left and the right hand side

$$X_{k,k'} = \int_{-(cL+\frac{1}{2})a}^{[(c+1)L-\frac{1}{2}]a} \tilde{\psi}_k^*(x)\, \tilde{\psi}_{k'}(x)\, x\, dx \tag{2.30}$$

while accounting for the correct normalization of the Bloch state

$$\tilde{\psi}_{k'}(x) = A\, e^{ikx} \sum_n c_n^{(k)}\, e^{in\frac{2\pi}{a}x} \tag{2.31}$$

over the entire integration range. This is achieved by choosing the normalization factor

$$A = \sqrt{\frac{1}{aL(2c+1)}} \tag{2.32}$$

for a given artificial lattice, consisting of $(2c+1)$ replicas of the initial, real lattice. This ensures the correct normalization

$$\int_{-(cL+\frac{1}{2})a}^{[(c+1)L-\frac{1}{2}]a} \tilde{\psi}_k^*(x)\, \tilde{\psi}_{k'}(x)\, dx = \delta_{k,k'}. \tag{2.33}$$

To explicitly calculate the matrix elements in Eq. (2.30), we introduce the integration parameter λ, such that the position coordinate is parametrized by

$$x = -(cL + \frac{1}{2})a + \lambda a, \tag{2.34}$$

such that, for the limit specified in Eq. (2.30), i.e. $x \in [-(cL+1/2)a,\, \{(c+1)L - 1/2\}a]$, the corresponding domain is $\lambda \in [0,\, (2c+1)L]$.

Using the parameterization in Eq. (2.28) for the quasi-momentum k with the integer m and the Fourier expansion of the Bloch state (2.31), we can simplify the expression for the matrix elements in Eq. (2.30)

$$\begin{aligned}
X_{m,m'} &= \langle k|\hat{x}|k'\rangle \\
&= \frac{1}{L(2c+1)} \int_0^{(2c+1)L} d\lambda\, e^{-i\frac{2\pi}{aL}(m-m')[-(cL+\frac{1}{2})a+\lambda a]} \sum_{n,n'=-\infty}^{\infty} c_n^{(k)*} c_{n'}^{(k')} \\
&\times\ (-1)^{n-n'}\ e^{-2\pi i(n-n')[-(cL+\frac{1}{2})+\lambda]}\, [-(cL+\frac{1}{2})a + \lambda a] \\
&= \frac{a}{L(2c+1)} e^{i\frac{\pi}{L}(m-m')} \sum_{n,n'=-\infty}^{\infty} c_n^{(k)*} c_{n'}^{(k')}\, (-1)^{n-n'} \left\{ -(cL+\frac{1}{2})(2c+1)L\, \delta_{m,m'}\, \delta_{n,n'} \right. \\
&\left. +\delta_{m,m'}\, \delta_{n,n'} \frac{(2c+1)^2 L^2}{2} + (1-\delta_{m,m'}\, \delta_{n,n'}) \left[\frac{i(2c+1)L}{2\pi(n-n'+\frac{m-m'}{L})} \right] \right\}
\end{aligned} \tag{2.35}$$

The last only to contribute if the denominator is non-zero, which is indicated by a multiplication with the factor $(1-\delta_{m,m'}\, \delta_{n,n'})$. Considering that both $n-n'$ and $m-m'$ both lie within the range $[-(L-1),\, (L-1)]$, the denominator only vanishes iff $m = m'$ and $n = n'$. The same reasoning was used to derive the factors containing the product $\delta_{m,m'}\, \delta_{n,n'}$. Furthermore, we used the identities

$$\int_0^L d\lambda\, e^{it\lambda} = \begin{cases} -\frac{i}{t}(e^{itL} - 1) & \text{if } t \neq 0 \\ L & \text{if } t = 0 \end{cases} \tag{2.36}$$

$$\int_0^L d\lambda\, e^{it\lambda}\, \lambda = \begin{cases} -\frac{1}{t^2} + \left[\frac{1}{t^2} - i\frac{L}{t}\right] e^{itL} & \text{if } t \neq 0 \\ \frac{L^2}{2} & \text{if } t = 0 \end{cases} \tag{2.37}$$

to obtain the expressions in the last line. Rearranging and simplifying terms in Eq. (2.35), we obtain the final form for the matrix elements

$$\begin{aligned}
X_{m,m'} = a\, e^{i\frac{\pi}{L}(m-m')} \sum_{n,n'=-\infty}^{\infty} c_n^{(k)*} c_{n'}^{(k')} (-1)^{n-n'} \left\{ \delta_{m,m'}\, \delta_{n,n'} \frac{1}{2}(L-1) \right. \\
\left. +(1-\delta_{m,m'}\, \delta_{n,n'}) \frac{i}{2\pi(n-n'+\frac{m-m'}{L})} \right\}
\end{aligned} \tag{2.38}$$

Note that all of these matrix elements are independent of multiplicative extension c of the lattice, to which the integration range was extended. Therefore this approach leads to the same result as when using the usual integration domain restricted to the actual real space lattice only, i.e. setting $c = 0$. Although not required for the calculation of the correct Wannier states, since the entire set may always be determined from any Wannier state at the center, it would be desirable to resolve this issue. It is however not clear, whether such a solution even exists.

To demonstrate the procedure, the eigenvalues of $X_{m,m'}$ and a corresponding Wannier function for the lowest band of a 1D $L = 10$ optical lattice are shown in Fig. (2.7).

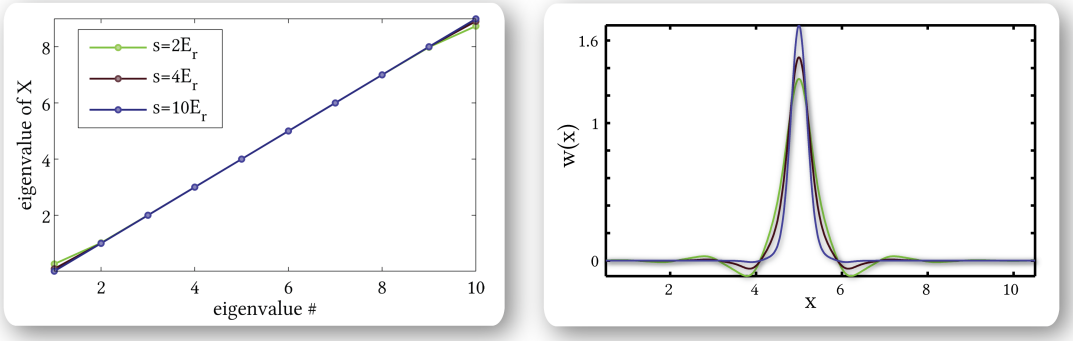

Figure 2.7: Spectrum of the matrix $X_{k,k'}$ (left subfigure) for three different lattice depth in an optical lattice consisting of $L = 10$ sites and corresponding Wannier functions (right subfigure). Finite size effects are only visible in the outermost eigenvalues for weak lattices. Fortunately, the complex phases for the Bloch states can be uniquely set using any of the corresponding eigenvalues, determining all Wannier states.

As expected for a large system, the eigenvalues corresponding to the lattice positions of the Wannier states away from the border are equidistantly spaced, i.e. a linear spectrum. The eigenvalues close to the border are however distorted, since the position operator $\hat{x}_\alpha$ is not periodic at the boundaries, but the Wannier functions are periodic, i.e. the weight leaking out on one side reenters on the opposite side of the lattice. Since the Wannier functions decay exponentially in space, the deviation of the eigenvalues from a precisely linear spectrum also falls off exponentially with the distance from the edge. The decay constant increases with the lattice depth s, as the Wannier functions become more localized and also decay faster. Thus the error in the determined Wannier states at the center of the lattice is exponentially small both in the lattice depth s and the size of the system L and practically negligible. For a system size of $L = 10$ and a lattice depth of $s = 5$, it is of the order 10^{-10}.

Setting the complex Bloch phases

We now shortly discuss how the phases of the Bloch states can be extracted if a single Wannier state at a central lattice site l_c (i.e. the eigenstate of X corresponding to the eigenvalue al_c) has been determined from the procedure above. Let $|k, \alpha\rangle$ be the basis of Bloch states with some random phase, which we directly obtain from the exact diagonalization procedure and in the basis of which, the operator $X_{k,k'}$ is represented. An alternative Bloch basis

$$|k, \alpha\rangle' = e^{i\phi_k} |k, \alpha\rangle \tag{2.39}$$

exists, where the complex phases are chosen such that the maximally localized Wannier states emerge from the natural definition

$$|l, \alpha\rangle = \frac{1}{\sqrt{L}} \sum_k e^{-iakl} |k, \alpha\rangle'. \tag{2.40}$$

Using this transformation relation specifically for the central site l_c, where the Wannier state corresponds to the eigenvector v_k^c of $X_{k,k'}$, we have

$$|l_c, \alpha\rangle = \frac{1}{\sqrt{L}} \sum_k e^{-iakl_c} |k, \alpha\rangle' = e^{i\gamma} \sum_k v_k^c |k, \alpha\rangle, \tag{2.41}$$

where γ is the global phase of this Wannier state chosen, such that the real-space representation $w_{l_c,\alpha}(x) = \langle x|l_c, \alpha\rangle$ is purely real and positive at the reflectional symmetry point for even bands. From Eq. (2.41) we conclude that the modulus of all eigenvector entries must be $|v_k^c| = \frac{1}{\sqrt{L}}$ and obtain the explicit expression to determine the phases

$$\phi_k = \gamma + akl_c + \arg(v_k^c). \tag{2.42}$$

This simultaneously determines all Wannier states in the lattice (not only at the site l_c) in Eq. (2.40), which are all purely real and mutually related by real-space translations. This allows us to avoid finite size effects present in the eigenvectors corresponding to Wannier state close to the edge of the lattice, by reconstructing these from the well-represented Wannier states at the center of the lattice.

2.6 Wannier Functions in Higher Dimensions

For higher dimensional lattices the task of determining the Wannier states can be reduced to that of fewer dimensions if the lattice is separable, i.e. the potential can be written as a direct sum of lower-dimensional potentials. For the well known 3D hypercubic lattice, this is the case with $V(x, y, z) = V_x(x) + V_y(y) + V_z(z)$, which implies that both the 3D Bloch eigenstates, as well as the Wannier states are direct product states, each of which is associated with one dimension only.

In the real-space representation the three-dimensional Bloch (Wannier) function can thus be written as a product of three one-dimensional Bloch (Wannier) functions $\psi_n(x, y, z) = \psi_{n_x}^{(x)} \psi_{n_y}^{(y)} \psi_{n_z}^{(z)}$. The collective state index n then represents one of all possible combination of 1D indices $n \leftrightarrow (n_x, n_y, n_z)$ and the single-particle energy is simply the sum of energies of the $1D$ states. As shown in Fig. (2.8) for the $2D$ case, the lowest two Wannier states are both fully symmetric in one dimension, but the first excited state is antisymmetric in the other dimension.

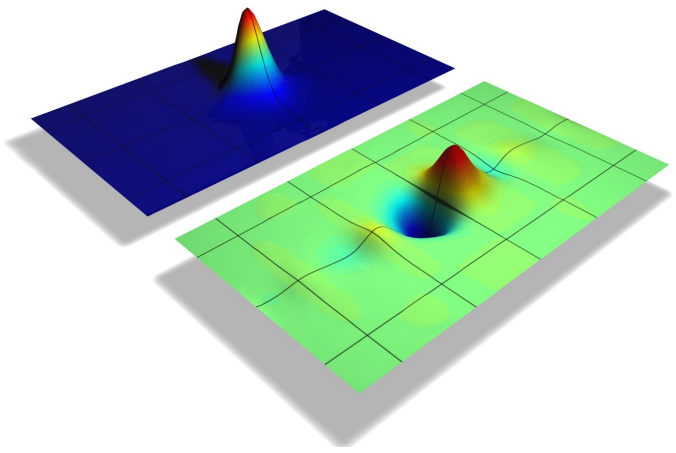

Figure 2.8: The lowest two Wannier functions in a 2D cubic optical lattice. For separable lattices, these are simply the direct product states of the individual dimensions, i.e. the real-space representation of this state is a scalar product of two one-dimensional functions $w_{2D}(x, y) = w(x) \cdot w(y)$.

If the potential is not separable, the calculation has to be performed on the full direct product space of the individual dimensions. The position operators along the directions of the reciprocal basis vectors can then be diagonalized successively, as shown and discussed in detail for the case of a 2D honeycomb lattice in chapter (5).

2.7 Wannier States in Inhomogeneous Lattices

To determine Wannier states in idealized fully periodic lattices, it does not matter whether these are determined from the Bloch states using symmetry arguments, minimizing the spatial variance or from the diagonalization of the projected position operator. Each of these approaches, when used correctly, leads to the same result and it can be shown that the definitions are equivalent. This is no longer true once one tries to determine or even define maximally localized Wannier for inhomogeneous lattices. Here the power of the generalized definition of Wannier states as eigenstates of the band projected position operator becomes clear, allowing for an unambiguous and rigorous definition of these states. In a work by Zhou and Ceperley [181], the task of determining Wannier states for a speckle disordered lattice and the resulting distribution of microscopic Hubbard parameters was addressed within the context of imaginary time evolution, starting from the original Wannier states in the pure lattice system. In this section we will give and discuss the general procedure to determine spatially localized Wannier states in inhomogeneous systems, as well as the limitations, when these can sensibly be defined.

Formulation of the Problem

The applicability of Wannier states as a suitable basis relies on the existence of an underlying lattice structure and any inhomogeneity to be weak in some sense, compared to this lattice. We thus formally split the potential into a perfectly periodic lattice potential part $V_{lat}(x)$ and an additional inhomogeneous part $V_{ih}(x)$. The exact single particle Hamiltonian is thus

$$\mathcal{H} = \int dp \frac{1}{2m} |p\rangle\langle p| + \int dx \, [V_{lat}(x) + \lambda \, V_{ih}(x)] |x\rangle\langle x|, \tag{2.43}$$

where we couple the inhomogeneity via a scalar parameter λ, such that this can artificially be *turned* on continuously by increasing λ from 0 to 1. If Wannier states exist for $\lambda = 1$, we expect these to evolve continuously from the well known Wannier states of the homogeneous system $\lambda = 0$, as λ is increased. One might be tempted to expect Wannier states to exist if J/W, where W is the typical variation in energy offset of the inhomogeneous potential $V_{ih}(x)$ over one lattice spacing[9]. This is however not the correct small parameter, since it also vanishes in the limit of large lattice depth at constant $V_{ih}(x)$, where we expect the Wannier states of the inhomogeneous system to be well defined. Rather, the correct small parameter is Δ/W, where Δ is the band gap between the band(s) within which the Wannier states are constructed[10]. Generally, the existence of a band structure can clearly be seen from the single particle energy spectrum: for an inhomogeneous system the eigenstates cannot be classified according to a quasi-momentum, i.e. this is no longer a good quantum number, and it does not make sense to depict the energy spectrum as a dispersion relation. However, one can of course sort and plot the single particle states according to their energies, as shown for the eigenstates of a lattice with a trap in Fig. (2.3). The existence of a gap Ãős clearly visible as the discontinuity in the energy spectrum in this picture, also for an inhomogeneous system where the gap may close with increasing λ. As long as such a band gap exists in the single-particle spectrum, we can generalize our Wannier state construction procedure uniquely to the inhomogeneous case: the n-th single particle eigenstate $|n(\lambda)\rangle$ evolves continuously from a Bloch state with λ and the projection operator $P_\alpha = \sum_n |n(\lambda)\rangle\langle n(\lambda)|$ on the lowest band(s) α is well defined and unique [11]. The projected position operator on this subspace

$$X_\alpha = \sum_{m,n \in \alpha} |m\rangle\langle n| \tag{2.44}$$

is Hermitian (as projection generally preserves hermiticity). The Wannier states to different sites, the position of which is indicated by the respective eigenvalue λ_l, can then be expressed as

$$|\lambda_l\rangle = \sum_n d_n^{(l)} |n\rangle \tag{2.45}$$

[9] This could for instance be determined as the difference in expectation values of $V_{ih}(x)$, determined within neighboring Wannier states of the pure system.

[10] For lattices with N_u potential minima per unit cell, Wannier states localized at each of these minima are constructed by the superposition of states from the lowest N_u bands.

[11] i.e., degeneracies that may be present do not influence P_α.

where $d_n^{(l)}$ is the l-th eigenvector of the matrix $X_{m,n} = \langle m|\hat{x}|n\rangle$. All properties of its eigenstates $|\lambda_l\rangle$ do not depend on the initial choice of complex phases of the energy eigenstates $|n\rangle$, although representation of $\hat{x}$ and the eigenstates in the basis $|n\rangle$ do. Hence, the projection method of constructing the Wannier states is also applicable to the inhomogeneous case and intrinsically circumvents the problem of appropriately choosing the phases of the initial eigenstates. It also follows directly from this construction procedure, that the resulting Wannier states are mutually orthogonal, since they are different eigenstates of the Hermitian operator X_α. In contrast to the case of simple homogeneous lattices, the amplitudes $|d_n^{(l)}|$ may generally depend on n, i.e. different energy eigenstates are contained with different amplitudes in a given Wannier state. This property directly renders the usual symmetry-based approach to constructing Wannier states invalid for inhomogeneous systems. Considering the inverse transformation, this is no surprise: the single particle energy eigenstates in an inhomogeneous system may generally be localized to certain regions in space, while being mutually orthogonal. Thus when constructing a Wannier state at a given lattice site as a superposition of energy eigenstates, the amplitude of energy eigenstates located to some distant spatial region is necessarily small. A further difference to the homogeneous lattice case is that the different Wannier functions within each band are generally not interrelated by spatial translations, but may differ in their local *shape*, adapting to any features in the inhomogeneous potential.

To explicitly obtain the single-particle energy eigenstates $|n\rangle$ of the inhomogeneous system, it is often convenient to work in the multi-band basis of Wannier or Bloch states of the homogeneous system. If all bands are taken along, these constitute valid bases to represent any state and it is a straight-forward task to set up the Hamiltonian, including the inhomogeneity $V_{ih}(x)$ in this basis. Using the Bloch basis has the advantage that the pure lattice part (i.e. not containing the inhomogeneity) of the Hamiltonian is diagonal, but many matrix elements of the inhomogeneity may be significant. Within the Wannier basis, on the other hand, the pure lattice part of the Hamiltonian is only Block diagonal, but the matrix elements of a real space potential decay exponentially with the distance of the respective Wannier states, allowing many to safely be neglected.

Once the Wannier states have been determined, it is again a straight-forward task to determine the different Hubbard parameters. In a trapped lattice, for instance, both the hopping J and the interaction U become site-dependent

$$J_{\boldsymbol{\ell},\boldsymbol{\ell}'}^{(\alpha)} = \langle \boldsymbol{\ell}, \alpha|\mathcal{H}|\boldsymbol{\ell}', \alpha\rangle \tag{2.46}$$

$$U_{\boldsymbol{\ell}}^{(\alpha)} = \frac{g}{2}\int d^3r\, |\langle \mathbf{r}|\boldsymbol{\ell}, \alpha\rangle|^4. \tag{2.47}$$

Further examples of systems where the procedure described here would be of interest to apply to are:

1. Disordered lattices for a specific type of spatial disorder, such as the potential created by a speckle laser. Here one would expect to recover the results obtained by Zhou and Ceperley [181] using imaginary time evolution for an appropriately chosen imaginary time. However, within this approach the Wannier states are uniquely defined and no *artificial* imaginary time period has to be chosen to construct them in an approximate fashion. Moreover, they do not have to be reorthogonalized, as they are orthogonal by construction.

2. Wannier states in a trap. The spatial dependence of the Hubbard parameters has often been pointed out and mentioned in literature, but to the best of the author's knowledge never been substantiated and rigorously calculated.

3. Tilted optical lattices with Wannier-Stark states as eigenstates within a description of the original homogeneous lowest band. For a strong tilt of the lattice, as can easily be realized in experiment by accelerating the lattice, higher band effects are expected to play a role, which would be captured within this treatment.

4. Systems with an additional, artificial magnetic flux. For specific values of the flux strength, the original discrete translational invariance of the lattice is reduced to a periodicity of the

magnetic unit cell. The Wannier states localized to a single lattice site are then be constructed from a superposition of eigenstates from a band structure calculation from multiple bands. They may generally differ from the Wannier states without an artificial magnetic field, as may the microscopic Hubbard parameters.

2.8 The Lattice Hamiltonian in the Wannier Basis

Now that the multiband Wannier basis $|\boldsymbol{\ell}, \alpha\rangle$ has been defined, we can express any operator in it. The lattice Hamiltonian (2.1) is of specific interest and using the transformation (2.23) can be exactly rewritten as

$$\begin{aligned} H_{\text{s.p.}} &= \sum_{\mathbf{k},\alpha} E_{\mathbf{k},\alpha} |\mathbf{k}, \alpha\rangle\langle \mathbf{k}, \alpha| \\ &= \sum_{\boldsymbol{\ell},\boldsymbol{\ell}',\alpha} J^{(\alpha)}_{\boldsymbol{\ell},\boldsymbol{\ell}'} |\boldsymbol{\ell}, \alpha\rangle\langle \boldsymbol{\ell}', \alpha| \end{aligned} \tag{2.48}$$

where the hopping matrix element between sites $\boldsymbol{\ell}$, $\boldsymbol{\ell}'$ within the band α is naturally defined as

$$J^{(\alpha)}_{\boldsymbol{\ell},\boldsymbol{\ell}'} = \frac{1}{L} \sum_{\mathbf{k}} E_{\mathbf{k},\alpha}\, e^{i\mathbf{k}\cdot(\mathbf{R}_{\boldsymbol{\ell}} - \mathbf{R}_{\boldsymbol{\ell}'})}. \tag{2.49}$$

Within the Wannier basis, the lattice Hamiltonian is block diagonal within each band and $J^{(\alpha)}_{\boldsymbol{\ell},\boldsymbol{\ell}'}$ only depends on and decays exponentially with the distance $\boldsymbol{\ell} - \boldsymbol{\ell}'$ between sites, as shown in Fig. (2.9).

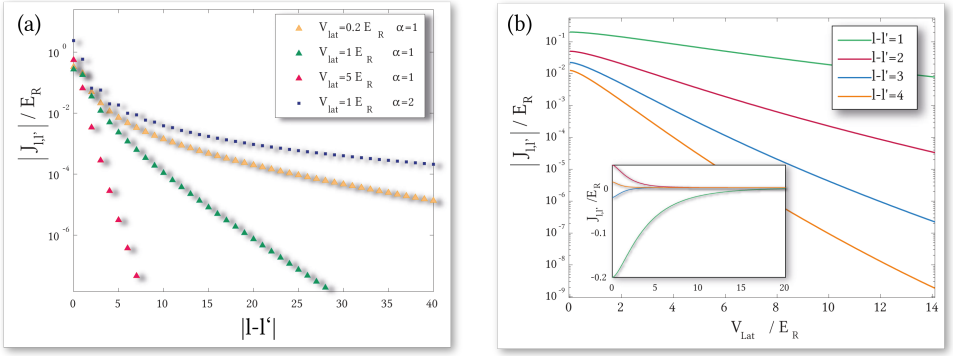

Figure 2.9: The modulus of the tunneling matrix elements $J_{l,l'}$ for a cubic optical lattice on a logarithmic scale. In subfigure (a) $|J|$ is plotted as a function of the distance $|l - l'|$ between lattice sites, featuring an exponential decay, with the decay constant increasing as the lattice depth increases. Subfigure (b) shows the dependence on the optical lattice depth, which is also exponential. The inset in (b) shows the corresponding plot on a linear scale, revealing that the sign of the matrix elements alternates with increasing band index.

The tunneling matrix elements for a 1D optical lattice are shown in Fig (2.9), both at a fixed lattice distance as a function of the lattice depth and at at fixed lattice depth as a function of the discrete lattice distance. In both cases, they decay exponentially with the decay constant depending on the lattice depth or the distance respectively. For higher bands, the tunneling elements alternate in sign and strongly grow in magnitude. This effect has a strong impact on the renormalization of the tunneling energies within an effective dressed band description for interacting atoms in an optical lattice, which will be derived and discussed in detail in chapter (4).

Tunneling Elements in Higher Dimensional Separable Lattices

We now consider how the tunneling matrix elements on a 3D cubic lattice are related to the corresponding elements in 1D. Considering only a single band, we know, that for a separable potential, the energy of the single particle 3D state is exactly the sum of energies of the 1D states and we can explicitly calculate the tunneling energy as

$$\begin{aligned} J^{(\alpha)}_{\boldsymbol{\ell},\boldsymbol{\ell}'} &= \frac{1}{L_x L_y L_z} \sum_{k_x,k_y,k_z} \left(E_{k_x} + E_{k_y} + E_{k_z}\right) e^{i(k_x(x_{l_x} - x_{l'_x}) + k_y(y_{l_y} - y_{l'_y}) + k_z(z_{l_z} - z_{l'_z}))} \\ &= J^{(x)}_{l_x,l'_x}\, \delta_{l_y,l'_y}\, \delta_{l_z,l'_z} + J^{(y)}_{l_y,l'_y}\, \delta_{l_x,l'_x}\, \delta_{l_z,l'_z} + J^{(z)}_{l_z,l'_z}\, \delta_{l_x,l'_x}\, \delta_{l_y,l'_y}. \end{aligned} \tag{2.50}$$

Hence, the tunneling energy is only non-zero along lines of either of the three dimensions, where it is simply the corresponding 1D element. The tunneling element vanishes exactly for any process along any diagonal direction, as shown in Fig. (2.10) for the analogous 2D case. This may seem counterintuitive at first, but is an exact statement valid beyond the tight-binding approximation, where it would apply by definition.

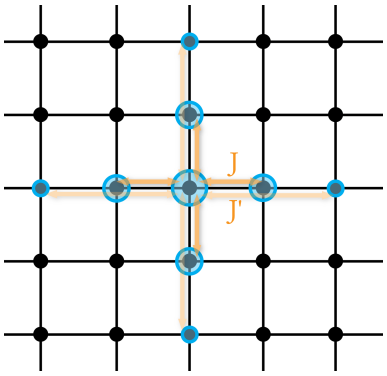

Figure 2.10: The magnitude of tunneling elements on a 2D lattice from the central site are indicated by the magnitude of the blue circles. If the potential is separable, only tunneling elements along one dimension can be non-zero and all other elements vanish exactly.

Any non-zero matrix element between diagonally connected lattice sites indicates the non-separability of the underlying lattice potential.

The Tight Binding Limit

For moderately strong lattices $s \gtrapprox 10$, the tunneling elements decay rapidly with the lattice distance in the lowest band $\alpha = 1$. The zeroth order term $J^{(\alpha=1)}_{\boldsymbol{\ell},\boldsymbol{\ell}}$ is simply the local on-site energy, which is equal for every Wannier state and can be absorbed into an effective chemical potential. The lowest order term that is of physical significance is thus the tunneling $J = -J^{(\alpha=1)}_{\boldsymbol{\ell},\boldsymbol{\ell}'}$ on nearest neighboring sites $\boldsymbol{\ell}$ and $\boldsymbol{\ell}'$. The tight binding approximation consists of neglecting all tunneling terms beyond this order, which is energetically well justified for moderately deep lattices. The lowest band single particle tight binding Hamiltonian is thus of the form

$$\mathcal{H}_{\text{t.b.}} = -J \sum_{\langle \boldsymbol{\ell},\boldsymbol{\ell}' \rangle} |\boldsymbol{\ell}\rangle\langle\boldsymbol{\ell}'| + \text{h.c.}, \tag{2.51}$$

where $|\boldsymbol{\ell}\rangle$ is the lowest band Wannier state at site $\boldsymbol{\ell}$. Within this approximation, the dispersion relation is always of the form

$$\epsilon(\mathbf{k}) = -2J \sum_{i=1}^{3} \cos(\mathbf{k} \cdot \mathbf{a}_i). \tag{2.52}$$

The validity of the tight binding approximation can also be verified from the importance of the higher Fourier components in the true single particle dispersion relation, i.e. the deviation from the form (2.52).

2.9 Interactions in the Wannier Basis

Up to now we have described a single particle in a periodic potential. To describe interactions between different atoms, we enter the realm of many-particle quantum mechanics, which is very conveniently expressed within the formalism of second quantization. Here, the Hilbert space at hand is extended to the many-particle Fock space $\mathscr{H} = \mathscr{H}_0 \oplus \mathscr{H}_1 \oplus \mathscr{H}_2 \oplus \ldots$, which is the direct sum of all n-particle Hilbert spaces $\mathscr{H}_n$. Operators originally given on $\mathscr{H}_1$ within a given single particle basis[12], for instance the real space basis via their matrix elements $a(\mathbf{r}, \mathbf{r}')$, are promoted to single particle operators on the Fock space by using field operators

$$A = \int d\mathbf{r}\, d\mathbf{r}'\, a(\mathbf{r}, \mathbf{r}')|\mathbf{r}\rangle\langle\mathbf{r}'| \rightarrow A = \int d\mathbf{r}\, d\mathbf{r}'\, a(\mathbf{r}, \mathbf{r}')\psi^\dagger(\mathbf{r})\psi(\mathbf{r}'), \tag{2.53}$$

where the operators $\psi^\dagger(\mathbf{r})$ and $\psi(\mathbf{r})$ respectively create and annihilate a particle at position $\mathbf{r}$.

Two-particle interactions, on the other hand, are described by a two-particle operator. For a sufficiently dilute, weakly interacting atomic gas, the short ranged interactions are well approximated by an effective zero-range contact interaction Hamiltonian

$$\mathcal{H}_{\text{int}} = \frac{g}{2} \int d^3r\, \psi^\dagger(\mathbf{r})\, \psi^\dagger(\mathbf{r})\, \psi(\mathbf{r})\, \psi(\mathbf{r}), \tag{2.54}$$

where the interaction strength g is related to the s-wave scattering length and the mass of the atoms by

$$g = \frac{4\pi\hbar^2 a_s}{m}. \tag{2.55}$$

To express the effective interaction Hamiltonian in the lowest Band Wannier basis, we define the creation operator for the lowest band Wannier orbital $w_{\boldsymbol{\ell}}(\mathbf{r}) = \langle \mathbf{r}|\boldsymbol{\ell}, \alpha = 1\rangle$ at site $\boldsymbol{\ell}$

$$b^\dagger_{\boldsymbol{\ell}} = \int d^3r\, w_{\boldsymbol{\ell}}(\mathbf{r})\, \psi^\dagger(\mathbf{r}). \tag{2.56}$$

Projected onto the lowest band and considering only the lowest order, on-site contribution (i.e. justified by tightly bound Wannier states), this two-body operator becomes

$$\mathcal{H}_{\text{int}} = \frac{U}{2} \sum_{\boldsymbol{\ell}} b^\dagger_{\boldsymbol{\ell}} b^\dagger_{\boldsymbol{\ell}} b_{\boldsymbol{\ell}} b_{\boldsymbol{\ell}}, \tag{2.57}$$

where

$$U = \frac{g}{2} \int d^3r\, |w_{\boldsymbol{\ell}}(\mathbf{r})|^4 \tag{2.58}$$

is the on-site interaction energy. In the limit of strong lattices, the on-site local shape of the Wannier functions is approximately captured by the harmonic oscillator ground state and the integral in Eq. (2.58) can be performed analytically, leading to the well known approximate result for the interaction energy

$$U \approx \sqrt{\frac{8}{\pi}} \frac{2\pi a_s}{\lambda}\, s^{3/4}\, E_r. \tag{2.59}$$

[12] Single particle states are henceforth referred to as *orbitals*, to distinguish them from the states in the Fock space.

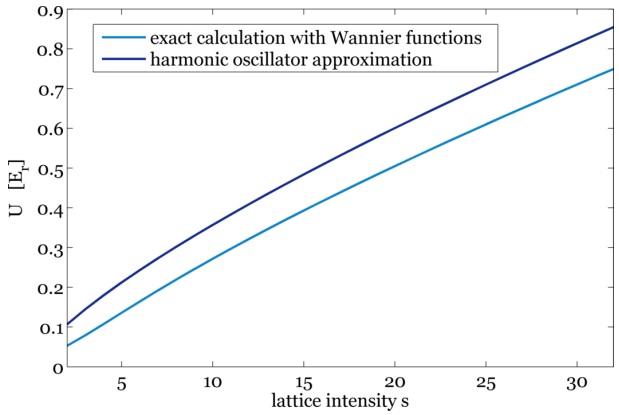

Figure 2.11: The interaction constant U for ^{87}Rb as a function of the lattice depth s obtained from an exact band structure calculation and within the harmonic oscillator approximation in a 812nm 3D cubic optical lattice.

This approximate value is compared to interaction energy calculated from the exact Wannier functions in Fig. (2.11). As the lattice depth increases and the lowest band Wannier state approaches the harmonic oscillator ground state (a Gaussian), the relative error, i.e. the deviation divided by the absolute value, decreases. However, the absolute deviation increases and the applicability and quality of the harmonic oscillator approximation for the interaction element U is commonly overestimated.

2.10 Scaling of the Hubbard Parameters U and J

The Tunneling Energy J

The tunneling matrix element J has a simple scaling behavior with the laser wavelength. For a given dimensionless lattice depth s (the lattice depth in units of the recoil energy E_r), the resulting (dimensionless) tunneling energy in units of the recoil energy J/E_r is a function of s alone, which does not depend on λ_{lat} beyond the scaling of E_r. This follows from the fact that the recoil energy E_r is the only energy that can be constructed from the microscopic variables in the single-particle system. Hence, the dependence on the lattice depth s (which has the units of energy) of any dimensionless quantities has to be a universal and scalar function of s/E_r.

The Interaction Energy U

The situation is more complicated for the interaction energy

$$U = \frac{4\pi\hbar^2 a_s}{m} \int d^3r \, |w(\mathbf{r})|^4, \tag{2.60}$$

which is not independent of s, in the sense that U/E_R does depend on λ_{lat}.

In contrast, the effective interaction constant U does not follow this simple scaling behavior (U/E_R does not only depend on s, but additionally on λ_{lat}) and a more detailed analysis is required to understand its scaling behavior. We restrict our analysis to the case of a 3D cubic lattice with the same wavelength λ_{lat} and the same lattice depth s in each dimension. It is useful to introduce dimensionless coordinate $\mathbf{y} = \mathbf{x}/a$, where $a = \lambda_{lat}/2$ is the lattice spacing. Note that the usual Wannier functions have the dimension of an inverse square root of a volume, since $\int d^3r \, |w(\mathbf{x})|^2 = 1$ and it is furthermore useful to define the dimensionless Wannier functions of the dimensionless variable $\mathbf{y}$, such that

$$w(\mathbf{x}) = C \, \tilde{w}(\mathbf{x}/a). \tag{2.61}$$

Here, $C = \frac{1}{a^{3/2}}$ is determined by the normalization

$$\int_{\tilde{V}} d^3y \, |\tilde{w}(\mathbf{y})|^2 = 1. \tag{2.62}$$

Specifying the dimensionless lattice height s uniquely fixes the shape of the Wannier function $\tilde{w}(\mathbf{y})$ on a single dimensionless lattice site where unit cell $\tilde{V}$ has a volume of 1. In a lattice, however, the scaled Wannier function $w(\mathbf{x})$ is related by $\mathbf{x} = a\,\mathbf{y}$

$$w(\mathbf{x}) = C\,\tilde{w}(\mathbf{x}/a) \tag{2.63}$$

where $C = \frac{1}{a^{3/2}}$ is determined by the normalization. This means that the interaction constant can also be expressed as

$$U = \frac{4\pi\hbar^2 a_s}{ma^3} \int d^3y \, |\tilde{w}(\mathbf{y})|^4 \tag{2.64}$$

where the integral is dimensionless and only depends on s. Therefore, in a 3D optical lattice the scaling behavior for fixed $s = V_{\text{lat}}/E_R$ in λ_{lat} is

$$U/E_r \propto \lambda_{lat}^{-1}. \tag{2.65}$$

2.11 The Bose-Hubbard Model

Combining the kinetic tunneling, a spatial potential described by a local energy offset $\epsilon_{\boldsymbol{\ell}}$ within the lowest band description and the interaction term leads to the Bose Hubbard Hamiltonian

$$H_{\text{BH}} = -J \sum_{\langle \boldsymbol{\ell}, \boldsymbol{\ell}' \rangle} (b_{\boldsymbol{\ell}}^\dagger b_{\boldsymbol{\ell}'} + b_{\boldsymbol{\ell}'}^\dagger b_{\boldsymbol{\ell}}) + \sum_{\boldsymbol{\ell}} (\epsilon_{\boldsymbol{\ell}} - \mu) b_{\boldsymbol{\ell}}^\dagger b_{\boldsymbol{\ell}} + \frac{U}{2} \sum_{\boldsymbol{\ell}} b_{\boldsymbol{\ell}}^\dagger b_{\boldsymbol{\ell}}^\dagger b_{\boldsymbol{\ell}} b_{\boldsymbol{\ell}}. \tag{2.66}$$

Typical tunneling and interaction energies, as well as their ratios are shown in Fig. (2.12).

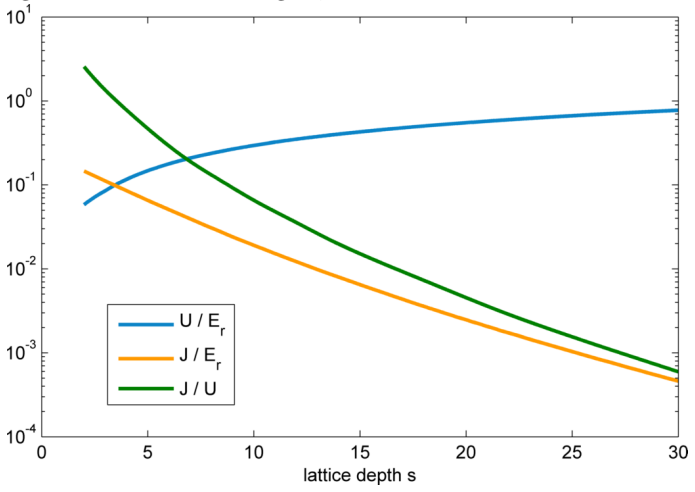

Figure 2.12: The microscopic Bose-Hubbard parameters J and U, as well as their ratio shown as a function of the lattice depth s (in units of the recoil energy E_r) for ^{87}Rb in a 812nm optical lattice. It can be seen on the logarithmic scale that a very deep lattice suppresses the tunneling energy J, and thus also the ratio J/U approximately exponentially.

This is the simplest interacting bosonic lattice model, and was first proposed to describe liquid helium in porous media by Fisher et al. in [56]. An almost perfect realization of this model is given by ultracold bosonic atoms in optical lattices in recent experiments, which is illustrated in the cartoon in Fig. (2.13).

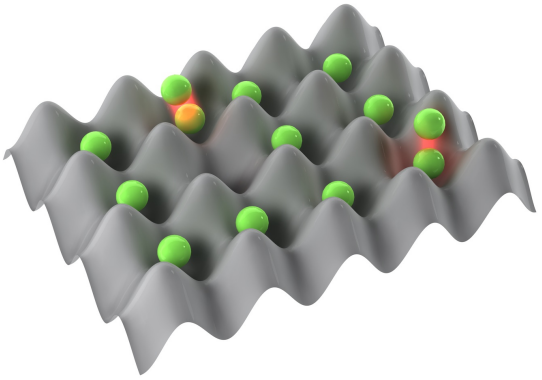

Figure 2.13: The Bose-Hubbard model describes a many-body system of atoms in an optical lattice, which can tunnel between nearest neighboring sites with an amplitude J. Multiple particles on the same site interact repulsively, characterized by an interaction energy U.

The derivation also applies to the fermionic case, with the difference that within the lowest band description, only fermions in different internal atomic states can occupy the same lattice site due to the Pauli exclusion principle. For an interacting single band model thus requires more than a single spin species. The single-particle operator terms from the bosonic Hamiltonian (2.66) are simply extended to all spin species accordingly, whereas the inter-species interaction prefactor is U and not $U/2$ as in the bosonic case.

3. Phases in the Bose-Hubbard Model & Theoretical Methods

In the previous chapter we have derived the many-body Bose- and Fermi-Hubbard Hamiltonians from first principles on a microscopic level for interacting atoms in an optical lattice. In this chapter we will focus on the bosonic case and discuss the many-body aspects and phases of the Bose-Hubbard model at zero temperature. In contrast to most single particle quantum mechanical problems, a direct exact diagonalization of the many-particle Hamiltonian is not feasible (and also not within foreseeable reach) for realistic system sizes and particle numbers due to the exponential growth of the Hilbert space with the system size. For one dimensional systems, significant progress has been made over the past decade on the development of numerical techniques to treat interacting many-body systems. The density matrix renormalization group is essentially capable of numerically solving most problems, both static or dynamic, for the time scales of interest. In higher dimensions on the other hand, there is no comparable method to treat arbitrary bosonic or fermionic problems with or without time dependence. In most case, approximations, such as mean-field theory are required. For clarity, we begin by shortly reviewing the static Gutzwiller mean-field approach to interacting bosons in a lattice, while discussing the phases of the Bose-Hubbard model in parallel. We then move on to dynamics in the model and introduce the time-dependent bosonic Gutzwiller approach. Thereafter we proceed with technically more advanced methods and derive and discuss the projection operator approach, which captures a wider range of physical phenomena than the Gutzwiller mean-field approach, such as dynamics in the Mott insulator (MI). It is one of the most promising, if not the best method, to describe real time dynamics of strongly interacting lattice bosons in three dimensions, which is a notoriously difficult problem to date. For the static case, the homogeneous 3D phase diagram is in excellent agreement with quantum Monte Carlo simulations.

3.1 Static Bosonic Gutzwiller

On a conceptual level, there are two different approaches to bosonic Gutzwiller mean-field theory, which are however fundamentally equivalent.

- The mean-field decoupling approach typically refers to an approximation on the level of the Hamiltonian, where the bosonic annihilation operator b_ℓ is approximated by a static mean-field, leading to an effective, decoupled mean-field Hamiltonian in conjunction with a self-consistency condition.
- The second approach, commonly referred to as the bosonic Gutzwiller variational approach, simply consists of a variational many-particle state, where the state on the entire lattice

consisting of L sites is restricted to a product state over different lattice sites. The Gutzwiller ground state is then determined by minimizing the variational energy of the full Bose-Hubbard Hamiltonian with respect to the variational state.

We first discuss the variational approach before relating it to the self-consistent mean-field theory.

Variational Approach

The many-particle Gutzwiller variational state on the entire lattice can be expressed as the direct product state

$$|\mathrm{GW}\rangle = |\phi_1\rangle_1 \otimes \ldots \otimes |\phi_L\rangle_L. \tag{3.1}$$

The local state $|\phi_{\boldsymbol{\ell}}\rangle_{\boldsymbol{\ell}}$ at a lattice site $\boldsymbol{\ell}$ can be expressed in any local basis, such as the local occupation number Fock basis of the lowest band Wannier orbitals

$$|\phi_{\boldsymbol{\ell}}\rangle_{\boldsymbol{\ell}} = \sum_{n=0}^{\infty} c_n^{(\boldsymbol{\ell})} |n\rangle_{\boldsymbol{\ell}} \tag{3.2}$$

within the lowest band description. Here, $|n\rangle_{\boldsymbol{\ell}} = \frac{1}{\sqrt{n!}}(b_{\boldsymbol{\ell}}^\dagger)^n|\mathrm{vac}\rangle$ denotes the Fock state with n particles in the lowest band Wannier state at site $\boldsymbol{\ell}$. The bosonic Gutzwiller approach can readily be applied to the extended dressed band description derived in chapter (4), which gives the best possible effective single band description for finite interactions at the cost of density-dependent Hubbard parameters. Within this approach the local n-particle ground states contain correlations and admixtures of higher bands (seen in the original single-particle basis). The local ground states in the lowest dressed band can nevertheless be labeled by the local particle number n (i.e. this is still a good quantum number), and can be used synonymously within the Gutzwiller approach, i.e. $|n\rangle_{\boldsymbol{\ell}}$ then denotes the local n-particle correlated ground state. Furthermore, the lowest dressed band Hamiltonian with density-dependent parameters has to be used, which can be conveniently expressed in terms of newly defined dressed band bosonic creation and annihilation operators.

We now return to the simple Bose-Hubbard Hamiltonian and consider a homogeneous system. If the ground state does not spontaneously break the discrete translational symmetry, the variational Gutzwiller Fock amplitudes $c_n^{(\boldsymbol{\ell})}$ become site independent and the variational energy per site is

$$\frac{E(c_n)}{L} = \frac{1}{\sum_{n=0}^{\infty}|c_n|^2}\left[\sum_{n=0}^{\infty}|c_n|^2\left(\frac{U}{2}n(n-1)-\mu\, n\right) - JZ\left|\sum_{n=0}^{\infty} c_n^*\, c_{n+1}\sqrt{n+1}\right|^2\right] \tag{3.3}$$

If the variational parameters are restricted to the manifold of normalized states $\langle \mathrm{GW}|\mathrm{GW}\rangle = 1$, the first normalization in Eq. (3.3) can be omitted. Z is the coordination number of the lattice, i.e. the number of nearest neighbors for any given site. The variational energy for the general inhomogeneous state is of an analogous form, but the counterpart of the last term in Eq. (3.3) contains products of variational parameters on nearest neighboring sites.

Site-Decoupling Approach

A conceptually different approach consists of starting on the level of the Bose-Hubbard Hamiltonian and derive an effective mean-field Hamiltonian, which is a direct sum of Hamiltonians on the individual lattice sites. The symmetry-breaking mean-field approach consists of decompose the Wannier field operator into a scalar mean-field part $\psi_l = \langle b_{\boldsymbol{\ell}}\rangle$, which can acquire a non-zero expectation value, and a fluctuation part $\delta b_{\boldsymbol{\ell}}$

$$b_{\boldsymbol{\ell}} = \psi_{\boldsymbol{\ell}} + \delta b_{\boldsymbol{\ell}}. \tag{3.4}$$

The expectation value of $b_{\boldsymbol{\ell}}$ is to be taken in the final resulting mean-field ground state, i.e. determined self-consistently. This is equivalent to requiring $\langle \delta b_{\boldsymbol{\ell}}\rangle = 0$ within the self-consistent state, i.e. expectation values of the fluctuations has to vanish. This decomposition spontaneously

breaks the continuous $U(1)$ symmetry of the original Bose-Hubbard Hamiltonian, which is related to the total particle number conservation. Whereas this is invariant under a transformation of all $b_{\boldsymbol{\ell}} \mapsto e^{i\varphi} b_{\boldsymbol{\ell}}$, the order parameters $\psi_{\boldsymbol{\ell}}$ are not invariant under such a transformation and in this sense a self-consistently determined mean-field ground state with $\psi_{\boldsymbol{\ell}} \neq 0$ spontaneously breaks the original $U(1)$ symmetry. Self-consistent states $|\psi(\varphi)\rangle$ to order parameters $\psi_{\boldsymbol{\ell}} = |\psi_{\boldsymbol{\ell}}| e^{i\varphi}$ with a different phase have the same energy expectation value $\langle\psi(\varphi)|H_{\mathrm{BH}}|\psi(\varphi)\rangle$, but are different beyond a complex phase factor of the entire state, i.e. $|\langle\psi(\varphi)|\psi(\varphi)\rangle|^2 < 1$. While all local terms (i.e. interaction, chemical and on-site potentials) of the Bose-Hubbard Hamiltonian are taken along exactly in the mean-field Hamiltonian, this decomposition is used on the nearest neighbor tunneling term on the operators

$$b^\dagger_{\boldsymbol{\ell}} b_{\boldsymbol{\ell}'} = \psi^*_{\boldsymbol{\ell}}\, b_{\boldsymbol{\ell}'} + \psi_{\boldsymbol{\ell}'}\, b^\dagger_{\boldsymbol{\ell}} - \psi^*_{\boldsymbol{\ell}}\, \psi_{\boldsymbol{\ell}'} + \delta b^\dagger_{\boldsymbol{\ell}}\, b_{\boldsymbol{\ell}'} \,. \tag{3.5}$$

The mean-field approximation consists of neglecting all terms of second order in the fluctuations $\delta b^\dagger_{\boldsymbol{\ell}}\, \delta b_{\boldsymbol{\ell}'} \to 0$. In a sense not discussed in further detail here, the fluctuations are small in high dimensions. In the limit of high dimensions, as well as in the non-interacting limit $U/J \to 0$, they vanish (within the correct scaling) and the resulting mean-field theory becomes exact. The resulting mean-field Hamiltonian is a sum of on-site Hamiltonians

$$H_{\mathrm{mf}} = \sum_{\boldsymbol{\ell}} H^{(\boldsymbol{\ell})}_{\mathrm{mf}} \,, \tag{3.6}$$

each of which is of the form

$$H^{(\boldsymbol{\ell})}_{\mathrm{mf}} = \frac{U}{2} b^\dagger_{\boldsymbol{\ell}} b^\dagger_{\boldsymbol{\ell}} b_{\boldsymbol{\ell}} b_{\boldsymbol{\ell}} + (\epsilon_{\boldsymbol{\ell}} - \mu)\, b^\dagger_{\boldsymbol{\ell}} b_{\boldsymbol{\ell}} - J \sum_{\boldsymbol{\ell}' \in \mathrm{n.n.}(\boldsymbol{\ell})} \left[\psi^*_{\boldsymbol{\ell}'}\, b_{\boldsymbol{\ell}} + \psi_{\boldsymbol{\ell}'}\, b^\dagger_{\boldsymbol{\ell}} - \frac{\psi^*_{\boldsymbol{\ell}'}\, \psi_{\boldsymbol{\ell}} + \psi_{\boldsymbol{\ell}'}\, \psi^*_{\boldsymbol{\ell}}}{2} \right] . \tag{3.7}$$

Here, n.n.($\boldsymbol{\ell}$) denotes the set of all nearest neighboring sites of a given site $\boldsymbol{\ell}$.

Equivalence of the Variational and Site-Decoupling Approach

The equivalence of the two approaches above is proven shown in [16] and we will only shortly outline the relation. Since the mean-field Hamiltonian (3.6) is a direct sum of on-site Hamiltonians, its eigenstates can always be chosen to be direct product states over different sites. Thus the exact ground state of any mean-field Hamiltonian can be chosen to be of the Gutzwiller variational form. It can furthermore be shown that the energy expectation value of the mean-field Hamiltonian evaluated within the self-consistently determined mean-field ground state is identical to the energy expectation value of the full Bose-Hubbard Hamiltonian evaluated within the same state. Requiring the derivative of the mean-field variational energy with respect to the order parameter, for which the mean-field eigenstate is determined, to vanish exactly leads to the self-consistency equation from the site decoupling mean-field theory. Thus the self-consistency condition and the minimization of the Gutzwiller variational energy are equivalent.

3.2 The Bose-Hubbard Phase Diagram within the Gutzwiller Approach

Both the energy minimization approach, as well as the self-consistent mean-field approach[1], can be used to determine the approximate Gutzwiller ground state of the system for a given set of microscopic parameters (U, J, μ). The latter is typically more efficient for an efficient numerical implementation. For the homogeneous case, where all order parameters can be chosen to be purely real and positive, this amounts to determining the root of a non-linear equation. It is also useful to shortly discuss the units and scaling in the problem. We have three distinct energies for the static homogeneous case. If all energies in the system are rescaled by an arbitrary positive factor λ, the Hamiltonian will also only be rescaled by the same factor (the energy is simply an extensive quantity), but this cannot affect the eigenvectors or any dimensionless quantity in this system. All dimensionless quantities can thus only depend on the ratios of energies and we choose to express all energies in scaled by the interaction energy U.

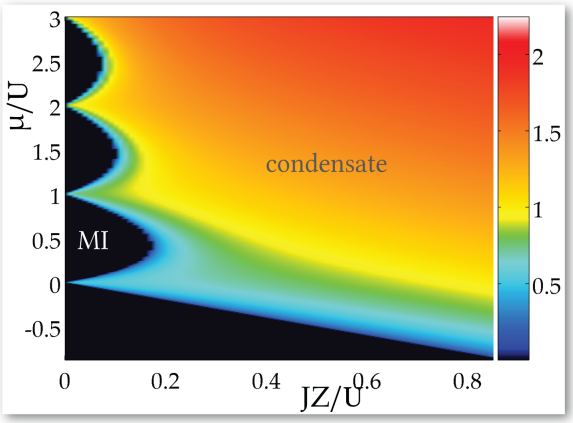

Figure 3.1: The Gutzwiller ground state order parameter $\langle b \rangle$ for the homogeneous Bose-Hubbard model as a function of the chemical potential μ/U and the scaled tunneling energy JZ/U in units of the interaction energy U. For strong interactions, i.e. small JZ/U the system is in a Mott insulating state, described by a direct product of local Fock number states on the mean-field level. The different lobes correspond to different integer values of filling. With increasing tunneling energy JZ/U, the system undergoes a transition into a condensed state, where a macroscopic number of particles occupy the $\mathbf{k} = 0$ single particle Bloch state. Within the mean-field description, the condensate is characterized by a non-zero order parameter, which increases continuously with JZ/U. The tunneling energy J is multiplied with the coordination number Z (related to the dimensionality of the system), since the mean-field results only depend on the product of these two quantities.

Determining the mean-field ground state and the resulting order parameter $\langle b \rangle$ for all values of μ/U and JZ/U, leads to the phase diagram shown in Fig. (3.1). At zero temperature, two distinct phases can exist in the homogeneous system: the black lobes indicating a vanishing order parameter correspond to the Mott insulator (MI) in the symmetry-breaking description, whereas the other regions with a non-zero order parameter indicate a state corresponding to a Bose-Einstein condensate. We will shortly discuss these two phases separately.

[1] Furthermore one can also use imaginary time evolution using the equations from the dynamical Gutzwiller approach. This is particularly useful if the ground state at a given total particle number of an inhomogeneous system is sought after, since the total particle number is also conserved under imaginary time evolution. One can thus simply start with some approximate condensate state at the given particle number and the imaginary time evolution will drive the system into the ground state along a trajectory corresponding to this particle number. This circumvents the additional problem of adjusting the chemical potential appropriately, which one has within the other approaches.

The quantum phase transition (i.e. at $T = 0$) between the Mott insulator and the condensed state can also be considered within a Landau-Ginzburg approach, where the grand canonical potential[2] is considered as a function of the order parameter ψ. As motivated above, the state corresponding to the energy minimum is the self-consistent mean-field ground state. The energy is plotted as a function of the (real) order parameter in Fig. (3.2).

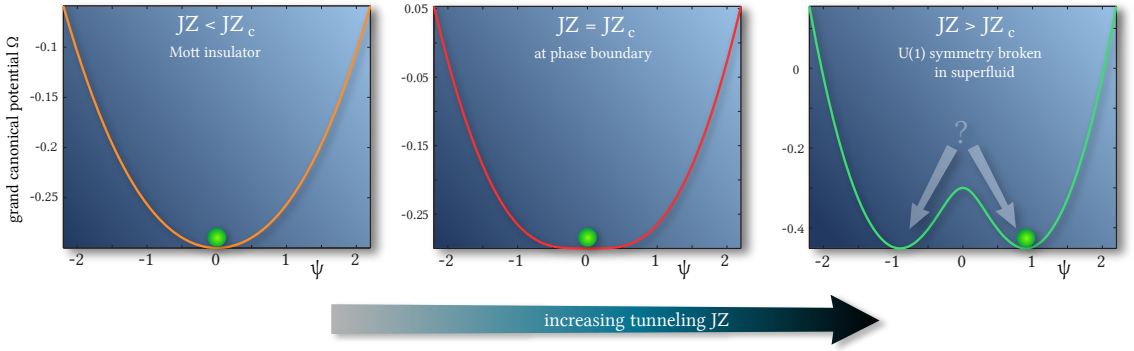

Figure 3.2: The Ginzburg-Landau energy as a function of the order parameter for three different regimes in the phase diagram. The physical ground state corresponds to the state at the energy minimum. In the Mott insulator, the global minimum lies at $\psi = 0$. Upon approaching the phase border to the condensate, the curvature (i.e. the second derivative) at $\psi = 0$ decreases and vanishes at the phase transition. Beyond the phase transition in the condensate, the minimum appears at a non-zero ψ. Keeping in mind that the order parameter ψ is a complex number and that the energy only depends on $|\psi|$, the energy function shown in the right figure corresponds to a mexican hat potential when plotted in the complex plane. Here, the energy is minimal at an arbitrary point along the continuous manifold, reflecting the $U(1)$ symmetry of the original Bose-Hubbard Hamiltonian. If a single fixed value of the order parameter ψ is chosen, this specific choice spontaneously breaks the symmetry.

Condensate

The condensate is a quantum phase of matter, in which a macroscopic number of bosonic particles occupy one single particle state. It thereby reflects the quantum mechanical character of the single particle state on a macroscopic scale. Within the above mean-field approximation, the condensed state is indicated by a non-zero order parameter $\langle b \rangle \neq 0$, which is associated with a breaking of the $U(1)$ symmetry. Although such a breaking of the $U(1)$ symmetry may physically well be the case in some systems, such as lasers, it is only an effective description for systems with a well-defined total particle number, such as cold atom experiments. In such a system, the exact ground state (which may very well not be exactly known) has one fixed particle number N and hence the expectation value of a particle annihilation operator for any single particle mode vanishes identically. This means that $\langle b \rangle$ is not always a good order parameter for Bose-Einstein condensation, which may very well occur in systems with a very large, but fixed particle number, as has been observed in various experiments and such states can also be explicitly constructed in theory. A better and more general definition of BEC was given by Penrose and Onsager [123] within the context of the single particle density matrix (SPDM). This is the matrix defined via its matrix elements $\rho_{\boldsymbol{\ell},\boldsymbol{\ell}'} = \langle b^\dagger_{\boldsymbol{\ell}} b_{\boldsymbol{\ell}'} \rangle$ with each index running over an entire set of single particle eigenstates. The expectation value is to be taken within a specific many-particle state or density operator in case of a statistical ensemble. The spectrum of ρ, which is invariant under unitary transformations, is thus independent of the single particle operators in which the matrix elements are evaluated. Being a Hermitian matrix, it is diagonalizable and the eigenvalues correspond to the occupation numbers of the natural orbitals, the eigenvectors to the corresponding state in the respective single particle basis. The definition

[2]The grand canonical potential is misleadingly, but conventionally referred to as the energy in this context. We will adopt this convention henceforth, nevertheless keeping the true meaning in mind.

of BEC according to the Penrose-Onsager criterion is now given via the eigenvalue structure of ρ when taking the appropriate thermodynamic limit for the system: if a single eigenvalue scales proportional to the system size (i.e. is macroscopic) and all other eigenvalues do not, then the state is in a Bose-condensed state. Commonly, the scaling behavior is not verified and it is only examined if one eigenvalue is large for practical reasons. The macroscopic eigenvalue N_0 is the condensate particle number and the condensate fraction is simply defined as the ratio $f_c = N_0/N$, where $N = \mathrm{Tr}\,(\rho)$ is the total particle number.

To relate this criterion to our Gutzwiller mean-field state above, we explicitly calculate the single particle density matrix in this case. This can be calculated without any approximation on a lattice consisting of L sites. We distinguish between diagonal elements, which are simply the density n for the homogeneous system and off-diagonal elements, which are products of two on-site order parameters

$$\rho_{\boldsymbol{\ell},\boldsymbol{\ell}'} = \langle b^\dagger_{\boldsymbol{\ell}}\, b_{\boldsymbol{\ell}'}\rangle = \begin{cases} |\psi|^2 & \text{if } \boldsymbol{\ell} \neq \boldsymbol{\ell}' \\ \langle b^\dagger b\rangle = n & \text{if } \boldsymbol{\ell} = \boldsymbol{\ell}' \end{cases} = |\psi|^2 + (n - |\psi|^2)\,\delta_{\boldsymbol{\ell},\boldsymbol{\ell}'}. \tag{3.8}$$

The largest eigenvalue is

$$N_0 = |\psi|^2\,(L-1) + n \tag{3.9}$$

leading to the condensate fraction in the thermodynamic limit at constant filling n

$$f_c = \lim_{L\to\infty} \frac{N_0}{L} = \frac{|\psi|^2}{n}. \tag{3.10}$$

Thus, if the order parameter of the Gutzwiller state is non-zero, this also applies to the condensate fraction in the thermodynamic limit. Note that the spatial extent of the condensate orbital has to scale with the system size at any finite interaction strength U/J, since otherwise the energy would eventually scale quadratically with the particle number, which is at variance with the energy being an extensive quantity.

It can furthermore be seen that the condensate fraction of a coherent state in the thermodynamic limit is one and the system is fully condensed. Such a coherent state can either be seen as a direct product of on-site coherent states or, alternatively, as a coherent state in an arbitrary single particle state on the entire lattice. Projecting this state onto a subspace with fixed total particle number N simply yields the N-particle Fock state in the respective single particle mode, in agreement with the system being fully condensed.

Since the matrix elements of the single particle density matrix in the Wannier representation for the homogeneous system do not decay to zero with increasing spatial distance of the lattice sites, the condensed state is said to have off-diagonal long range order. As will be shown in chapter (7) in detail, there are collective quasi-particle states at arbitrarily low energy present in the superfluid, related to a Goldstone mode. Hence the condensate is not gapped, but there is always spectral weight in the single particle spectral function at low frequencies and the state is also compressible.

At any non-zero interaction strength $U/J > 0$ the condensed state is also superfluid and exhibits frictionless flow. Since no roton minimum appears in the dispersion relation, the critical velocity, which sets the lower bound on the speed at which any object moving through the superfluid can excite quasi-particles, is thus set by the slope of the sound mode in the limit of small $\mathbf{k}$.

Mott Insulator

The Mott insulator is an interaction dominated phase at $T = 0$, which can only appear at integer filling in the homogeneous system. The single particle density matrix does not possess a single macroscopic eigenvalue, but an extensive number of single particle orbitals have eigenvalues on the order of the particle density. The eigenvectors of the single particle density matrix, i.e. the natural orbitals are all spatially localized and approach the individual Wannier orbitals in the strongly interacting limit $J/U \to 0$. Within the Gutzwiller approximation for the homogeneous system, the single particle density matrix is diagonal (and a multiple of the unit matrix) in any single particle basis at any J/U in the Mott insulating phase. Furthermore, the Mott insulator is characterized

by an exponential decay of all n-particle correlation functions with spatial distance. The single particle spectrum features a finite energy gap[3], which closes upon approaching the phase border to the condensed state. The collective quasi-particle excitations are particle and hole excitations, which are dispersive and fully delocalized at any finite J/U.

Analytical Expression for the Phase Boundary

The phase border, i.e. the line determining the mean-field transition between the Mott insulator and the condensed phase, can in fact be determined analytically [167, 16]. Since the transition is always of second order, the order parameter approaches zero continuously when approaching the transition from the condensate side. The critical value $JZ_c(\mu)/U$ can be determined from second order perturbation theory, starting with the Mott insulating mean-field state. The hopping part of the Hamiltonian is considered as the perturbation. In contrast to the Mott insulator, the energy of the second order perturbed state is reduced with respect to the Mott insulating Fock state if the system is in the condensate region of the phase diagram. This condition leads to the critical phase border

$$\frac{JZ_c(\mu)}{U} = \frac{(\overline{n}_\mu - \mu/U) - (\overline{n}_\mu - \mu/U)^2}{1 + \mu/U}\,, \tag{3.11}$$

where $\overline{n}_\mu = \max\left(\lceil \frac{\mu}{U} \rceil,\, 0\right)$ is the integer filling value in the $J \to 0$ limit at a given chemical potential μ. This function exactly corresponds to the lobe structure of the Mott insulator in Fig. (3.1).

Phases at Finite Temperature

The Penrose-Onsager definition of the condensate state carries over to finite temperature T: the single particle density matrix is now not evaluated within the ground state, but within the thermal density operator

$$\rho_{\boldsymbol{\ell},\boldsymbol{\ell}'} = \langle b^\dagger_{\boldsymbol{\ell}} b_{\boldsymbol{\ell}'} \rangle = \frac{1}{Z} \mathrm{Tr}\left(e^{-H/k_B T}\, b^\dagger_{\boldsymbol{\ell}} b_{\boldsymbol{\ell}'} \right) \tag{3.12}$$

where $Z = \mathrm{Tr}\left(e^{-H/k_B T}\right)$ is the partition function. Also in this case, the single particle density matrix is Hermitian and can readily be diagonalized, which allows for the same definition of BEC via the largest eigenvalue of the SPDM the thermodynamic limit as in the zero temperature case. Typically, temperature (i.e. thermal fluctuations) decrease the condensate fraction and even in the non-interacting case, the system may be driven out of the condensed phase by increasing the temperature. We thus have at least two phases: the condensate (as in the $T = 0$ case) and a non-condensed phase in the high temperature limit, which is referred to as the **normal** phase. It is characterized by a vanishing condensate fraction $f_c = 0$ and a finite single particle density of states (DOS) at low frequencies, as higher single particle orbitals are also thermally populated in equilibrium. The latter also implies a finite compressibility.

One may now also expect a phase transition from the Mott insulating state (which exists for the zero temperature case) into the normal phase. However, this is only a crossover. Strictly speaking, a Mott insulator (characterized by a gap in the single particle DOS) can never exist at finite temperature, since at any non-zero temperature, the DOS is non-zero (although possibly exponentially small in the inverse temperature) at low frequencies, which may for all practical purposes behave like a Mott insulator. With increasing temperature, there is however never any thermodynamic phase transition when starting in the Mott insulating state and there are only two possible phases at any $T > 0$: the normal phase and the condensate.

The Gutzwiller Variational Ansatz at Fixed Particle Number

One may argue that the variational Gutzwiller state is unphysical for ultracold atoms in an optical lattice, as these systems have a well defined particle number, which is violated by the Gutzwiller

[3] i.e. any many-particle excitation from the ground state to an excited state costs an energy greater than a finite value set by the energy gap Δ in the thermodynamic limit.

state in the condensate. Here we shortly introduce a remedy for this problem. Instead of taking the original Gutzwiller state of the form (3.1) as a variational state, let us consider the state

$$|\mathrm{GW}(N_0)\rangle = C \int_0^{2\pi} \frac{d\varphi}{2\pi} e^{i\varphi(\sum_{\boldsymbol{\ell}} b_{\boldsymbol{\ell}}^\dagger b_{\boldsymbol{\ell}} - N_0)} |\mathrm{GW}\rangle. \tag{3.13}$$

This has exactly the same variational parameters $c_n^{(\boldsymbol{\ell})}$ as the original Gutzwiller state, as well as a parameter N_0. It can thus also be considered as a variational state, such as in the usual Gutzwiller theory and the parameters are chosen, such that the energy is minimized. C is a normalization constant, chosen such that $\langle \mathrm{GW}(N_0)|\mathrm{GW}(N_0)\rangle = 1$. It can be verified that the state $|\mathrm{GW}(N_0)\rangle$ precisely has the total particle number N_0, i.e. zero fluctuations

$$\langle \mathrm{GW}(N_0)|(\sum_{\boldsymbol{\ell}} b_{\boldsymbol{\ell}}^\dagger b_{\boldsymbol{\ell}})^2|\mathrm{GW}(N_0)\rangle - (\langle \mathrm{GW}(N_0)|\sum_{\boldsymbol{\ell}} b_{\boldsymbol{\ell}}^\dagger b_{\boldsymbol{\ell}}|\mathrm{GW}(N_0)\rangle)^2 = 0. \tag{3.14}$$

The state (3.13) leads to the same expectation values of any particle number conserving operator as the Gutzwiller variational state in the thermodynamic limit, but contains (relevant and physically existent) corrections for finite particle number. As one expects from any physically relevant state for an ensemble of an arbitrarily large, but fixed number of bosons, the expectation value of any anomalous operator (such as the $\langle b\rangle$, $\langle bb\rangle$, etc.) vanishes and this state does not artificially break the $U(1)$ symmetry. Of course it can nevertheless describe the phase transition to a condensate, where the order parameter is the condensate fraction defined via the largest eigenvalue of the single particle density matrix. Note that in contrast to the Gutzwiller state (3.1), the state $|\mathrm{GW}(N_0)\rangle$ is generally not a direct product state over different lattice sites, i.e. contains entanglement between different lattice sites in the condensate.

3.3 Expressing any single particle Operator within the Gutzwiller approximation

Any operator can be expressed in the basis of localized Wannier functions in multiple bands. For a single band Gutzwiller calculation, two approximations have to be made.

- The lowest band approximation entails neglecting all terms that do not couple states within the lowest band, i.e. terms that describe transitions into or out of any higher band. Within this approximation, any single particle operator can be written as

$$\hat{A} = \sum_{l,l'} A_{l,l'} b_l^\dagger b_{l'}. \tag{3.15}$$

- To enable the application of an operator of this form to a bosonic Gutzwiller product state, the mean-field approximation has to be applied to the non-local terms on an operator level. After this further approximation, which reduces the quantum mechanical coupling between different sites to a scalar one, the operator takes on the form

$$\begin{aligned} \hat{A}(t) = &\sum_l A_{l,l} b_l^\dagger b_l \\ &+ \sum_m \sum_{l\neq m} A_{l,m}(t)\, \psi_l^*\, b_m \\ &+ \sum_m \sum_{l\neq m} A_{m,l}(t)\, \psi_l\, b_m^\dagger \\ &- \sum_m \sum_{l\neq m} Re(A_{m,l}(t)\, \psi_l\, \psi_m^*). \end{aligned} \tag{3.16}$$

  This can also be understood in the sense that the expectation value of any non-local operator evaluated within the Gutzwiller state is identical to the product of the local expectation values.

3.4 Time-Dependent Bosonic Gutzwiller

Hitherto we have considered static properties of the Bose-Hubbard model within the Gutzwiller approach. The Gutzwiller variational approach can however also be extended to treat time-dependent problems. Here it constitutes a relatively simple, but remarkably powerful method which is capable of treating dynamics of interacting bosons beyond the time-dependent Gross-Pitaevskii approach. In this section we shortly describe the method and derive the time-dependent equations of motion by extremizing the Gutzwiller variational action. The time-dependent equations of motion are sometimes also derived by postulating a Schrödinger equation, where the time evolution is generated by the mean-field Hamiltonian, which itself depends non-linearly on the mean-field state at every point in time. Here we follow a different approach which is more systematic: we simply use the Gutzwiller variational ansatz, but now in time-dependent form. In full analogy to determining the ground state by minimizing the energy in the time-independent case, we extremize the variational action, which leads to the equations of motion for the variational coefficients.

As before, the variational ansatz within the bosonic Gutzwiller approach for the state on the total lattice is the direct product state

$$|\mathrm{GW}(t)\rangle = \prod_{\otimes \boldsymbol{\ell}} |\phi_{\boldsymbol{\ell}}(t)\rangle_{\boldsymbol{\ell}} \tag{3.17}$$

with the most general form of a local lattice state. Again, this can be expanded in any local basis[4], such as the local Wannier Fock basis $|\phi_{\boldsymbol{\ell}}(t)\rangle_{\boldsymbol{\ell}} = \sum_n c_n^{(\boldsymbol{\ell})}(t)|n\rangle_{\boldsymbol{\ell}}$, where $c_n^{(\boldsymbol{\ell})}(t)$ are now time-dependent fields within the dynamic approach. As the action

$$\mathcal{S} = \int dt\, \left[-i\langle \mathrm{GW}(t)|(\partial_t|\mathrm{GW}(t)\rangle) + \langle \mathrm{GW}(t)|\mathcal{H}_{\mathrm{BH}} + \mathcal{B}(t)|\mathrm{GW}(t)\rangle\right] \tag{3.18}$$

becomes extremal for the physical path and the energy function is a continuous function of the amplitudes $c_n^{(\boldsymbol{\ell})}(t)$, the variation with respect to any of the fields $c_n^{(\boldsymbol{\ell})*}(t)$ leads to the equations of motion. Here, the time-dependent operator $\mathcal{B}(t)$ can be any additional perturbing operator, not necessarily weak. Within the context of Bragg spectroscopy discussed in chapter (9), this is for instance the operator describing the effect of the probing beams. The dynamics defined by these equations for $c_n^{(\boldsymbol{\ell})}(t)$ is fully equivalent to a physically more intuitive formulation, where the time evolution of the local state $|\phi_{\boldsymbol{\ell}}(t)\rangle_{\boldsymbol{\ell}}$ (at site $\boldsymbol{\ell}$) is generated by the effective local Hamiltonian

$$\mathcal{H}_{\boldsymbol{\ell}} = \frac{U}{2} b_{\boldsymbol{\ell}}^\dagger b_{\boldsymbol{\ell}}^\dagger b_{\boldsymbol{\ell}}\, b_{\boldsymbol{\ell}} - [\mu - B_{\boldsymbol{\ell},\boldsymbol{\ell}}(t)]\, b_{\boldsymbol{\ell}}^\dagger b_{\boldsymbol{\ell}} - \eta^*(t) b_{\boldsymbol{\ell}} - \eta(t) b_{\boldsymbol{\ell}}^\dagger. \tag{3.19}$$

Within this picture, all local on-site operators (or sums thereof) are accounted for exactly, whereas the non-local terms of any single particle operator are decoupled as

$$\sum_{\substack{\boldsymbol{\ell},\boldsymbol{\ell}' \\ \boldsymbol{\ell}\neq\boldsymbol{\ell}'}} A_{\boldsymbol{\ell},\boldsymbol{\ell}'} b_{\boldsymbol{\ell}}^\dagger b_{\boldsymbol{\ell}'} \mapsto \sum_{\substack{\boldsymbol{\ell},\boldsymbol{\ell}' \\ \boldsymbol{\ell}\neq\boldsymbol{\ell}'}} A_{\boldsymbol{\ell},\boldsymbol{\ell}'} (\langle b_{\boldsymbol{\ell}}^\dagger\rangle b_{\boldsymbol{\ell}'} + b_{\boldsymbol{\ell}}^\dagger \langle b_{\boldsymbol{\ell}'}\rangle - \langle b_{\boldsymbol{\ell}}^\dagger\rangle\langle b_{\boldsymbol{\ell}'}\rangle). \tag{3.20}$$

In our specific case this leads to the time-dependent complex parameters

$$\eta_{\boldsymbol{\ell}}(t) = J \sum_{\boldsymbol{\ell}'\in n(\boldsymbol{\ell})} \psi_{\boldsymbol{\ell}'} - \sum_{\boldsymbol{\ell}'\neq\boldsymbol{\ell}} B_{\boldsymbol{\ell},\boldsymbol{\ell}'}\, \psi_{\boldsymbol{\ell}'} \tag{3.21}$$

in Eq. (3.19), where $\psi_{\boldsymbol{\ell}}(t) = \langle b_{\boldsymbol{\ell}}\rangle$ is the local order parameter, directly related to the Wannier space representation of the condensate state and $n(\boldsymbol{\ell})$ denoting the set of all sites, which are nearest neighbors of sites of $\boldsymbol{\ell}$. The parameter $\eta_{\boldsymbol{\ell}}(t)$ thus accounts for both the non-linear nearest neighbor coupling through the hopping term in $\mathcal{H}_{\mathrm{BH}}$, as well as the long range coupling to all other sites in the plane, mediated by $\mathcal{B}(t)$.

[4]The basis is always chosen to be time-independent. Only the coefficients are promoted to time-dependent fields.

By choosing sufficiently small time steps during the evolution, the numerical error is well controlled. Furthermore, various constants of motion (e.g. the total particle number, the energy for time independent Hamiltonians, the quasi-momentum for translationally invariant lattice potentials, etc.) are also conserved during the dynamic Gutzwiller time evolution. The average particle number conservation is shown in appendix (E.1). Numerically, realistically large (i.e. of the order 10^6 sites), strongly interacting non-equilibrium 3D lattice systems can be treated for all experimentally relevant time scales within this approach.

At every point in time physical quantities, such as the total energy (evaluated in the pure BHM Hamiltonian) $E(t) = \langle \mathrm{GW}(t)|\mathcal{H}_{\mathrm{BH}}|\mathrm{GW}(t)\rangle$, the condensate fraction or the quasi-momentum distribution $n(\mathbf{k}, t) = \langle \mathrm{GW}(t)|b_k^\dagger b_k|\mathrm{GW}(t)\rangle$ are directly accessible from the many-particle state. When all particles are in the lowest band, the physical momentum distribution $\langle a_p^\dagger a_p\rangle$ simply consists of scaled replicas in the higher Brillouin zones and can be quantitatively determined using the coefficients obtained from the single particle band structure calculation.

Within a straight-forward implementation, the numerical complexity of calculating the quasi-momentum distribution for a bosonic Gutzwiller state scales quadratically with the number of lattice sites, which would restrict the systems to sizes of $\lessapprox 50^3$ lattice sites for reasonable computation times. In appendix (E.2) a more efficient implementation to calculate the quasi-momentum distribution is derived. Using a suitable variable transformation, the problem is mapped onto a discrete Fourier transform, which can be computed using the FFT algorithm and hence the complexity scales differently.

3.5 The Projection Operator Approach

We now introduce the projection operator approach for strongly interacting bosons in a lattice. Analogous to bosonic Gutzwiller theory, it can be used to determine both static and dynamic properties and relies on performing a Schrieffer-Wolff transformation to the Hamiltonian before evaluating the transformed Hamiltonian within a Gutzwiller state. This seemingly simple approach was devised and implemented for the homogeneous system (analogous to the single site case) by Trefzger and Sengupta in [163]. Here, we give a detailed derivation and discuss the extension to inhomogeneous systems.

One starts by decomposing the original Bose-Hubbard Hamiltonian into two parts: the local part containing the interactions, on-site energies and the chemical potential.

$$\begin{aligned} \mathcal{H}_0 &= \sum_i \mathcal{H}_0^{(i)} \\ \mathcal{H}_0^{(i)} &= \frac{U}{2} n_i(n_i - 1) - \mu n_i \end{aligned} \tag{3.22}$$

Since this operator is diagonal in the Wannier Fock basis, its many-body eigenstates and energies are exactly known. The second part is the hopping term in the Hamiltonian, which can be written as the sum over all hopping operators over different bonds σ on the entire lattice.

$$\mathcal{T}_\sigma = -J(b_{\sigma_1}^\dagger b_{\sigma_2} + b_{\sigma_2}^\dagger b_{\sigma_1}) \tag{3.23}$$

The entire Bose-Hubbard Hamiltonian thus reads

$$\mathcal{H}_{\mathrm{BH}} = \mathcal{H}_0 + \sum_\sigma \mathcal{T}_\sigma, \tag{3.24}$$

where the sum extends over all bonds σ on the lattice, as shown in Fig. (3.3). A bond refers to one specific pair of nearest neighboring sites and is not counted twice under a permutation of the two site indices.

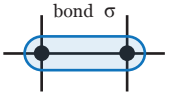

Figure 3.3: The sum $\sum_\sigma$ contains each bond, connecting two sites σ_1 and σ_2 on that bond, exactly once.

The goal now consists of finding an Hermitian operator $\mathcal{S}$ generating to a unitary transformation $e^{-i\mathcal{S}}$, which fulfills the following requirement: if it is applied to the Bose-Hubbard Hamiltonian, the all terms of order J/U resulting transformed Hamiltonian, which take the system out of the low energy manifold of eigenstates of $\mathcal{H}_0$, have to cancel. Expanding the transformation up to second order in J/U, the transformed Hamiltonian is given by

$$\begin{aligned}\mathcal{H}^* &= e^{i\mathcal{S}}\ \mathcal{H}_{\text{BH}}\ e^{-i\mathcal{S}} \\ &= \mathcal{H}_{\text{BH}} + [i\mathcal{S}, \mathcal{H}_0 + \sum_\sigma \mathcal{T}_\sigma] + \frac{1}{2}[i\mathcal{S}, [i\mathcal{S}, \mathcal{H}_0]] + \mathcal{O}(J^3/U^2).\end{aligned} \tag{3.25}$$

Since the transformation is unitary (i.e. before truncating the exponential), $\mathcal{H}^*$ has the same energy spectrum as $\mathcal{H}_{\text{BH}}$. Furthermore, this expansion by the Baker-Hausdorff equation is equivalent to an expansion of the Hamiltonian in J/U.

To construct a suitable transformation operator $e^{-i\mathcal{S}}$, it is useful to introduce the projection operator on a bond σ

$$\mathcal{P}_\sigma = |\overline{n}\rangle_{\sigma_1\sigma_1}\langle\overline{n}| \otimes |\overline{n}\rangle_{\sigma_2\sigma_2}\langle\overline{n}| \otimes \prod_{i\neq\sigma_1,\sigma_2} \mathbb{1}_i. \tag{3.26}$$

Together with the orthogonal projection operator

$$\mathcal{P}_\sigma^\perp = \mathbb{1} - \mathcal{P}_\sigma \tag{3.27}$$

and the property

$$\mathcal{P}_\sigma \mathcal{T}_\sigma \mathcal{P}_\sigma = 0, \tag{3.28}$$

the kinetic term can be rewritten as

$$\begin{aligned}\mathcal{T}_\sigma &= (\mathcal{P}_\sigma + \mathcal{P}_\sigma^\perp)\mathcal{T}_\sigma(\mathcal{P}_\sigma + \mathcal{P}_\sigma^\perp) \\ &= \mathcal{P}_\sigma\mathcal{T}_\sigma + \mathcal{T}_\sigma\mathcal{P}_\sigma + \mathcal{P}_\sigma^\perp\mathcal{T}_\sigma\mathcal{P}_\sigma^\perp.\end{aligned} \tag{3.29}$$

We now define the Hermitian generator for the unitary transformation as

$$\begin{aligned}\mathcal{S} =& \sum_\sigma \frac{i}{U}[\mathcal{P}_\sigma, \mathcal{T}_\sigma] \\ =& i\frac{J}{U}\sqrt{\overline{n}(\overline{n}+1)}\sum_\sigma (|\overline{n}+1, \overline{n}-1\rangle_{\sigma\sigma}\langle\overline{n}, \overline{n}| + |\overline{n}-1, \overline{n}+1\rangle_{\sigma\sigma}\langle\overline{n}, \overline{n}| \\ & -|\overline{n}, \overline{n}\rangle_{\sigma\sigma}\langle\overline{n}-1, \overline{n}+1| - |\overline{n}, \overline{n}\rangle_{\sigma\sigma}\langle\overline{n}+1, \overline{n}-1|)\end{aligned} \tag{3.30}$$

$|n_1, n_2\rangle_\sigma$ denotes the state on the two sites σ_1 and σ_2, belonging to the bond σ in the Fock number representation. The subsequent operator acts on the Hilbert space of **all** sites, with the unit operator on all sites other than σ_1 and σ_2, being implicit.

Note, that since $\mathcal{P}_\sigma$ and $\mathcal{T}_\sigma$ are all Hermitian, the commutators in Eq. (3.30) are anti-Hermitian, yielding a Hermitian $\mathcal{S}$, as required for the generator of an unitary transformation.

The different terms in Eq. (3.25) can now be evaluated, which leads

$$\begin{aligned}
[i\mathcal{S},\mathcal{H}_0] =& -\sum_\sigma(\mathcal{P}_\sigma\mathcal{T}_\sigma+\mathcal{T}_\sigma\mathcal{P}_\sigma)\\
[i\mathcal{S},\sum_\sigma\mathcal{T}_\sigma] =& \frac{1}{U}\sum_\sigma(2\mathcal{T}_\sigma\mathcal{P}_\sigma\mathcal{T}_\sigma-\mathcal{P}_\sigma\mathcal{T}_\sigma^2-\mathcal{T}_\sigma^2\mathcal{P}_\sigma)\\
&+\frac{1}{U}\sum_{\langle\sigma,\sigma'\rangle}(\mathcal{T}_\sigma\mathcal{P}_\sigma\mathcal{T}_{\sigma'}+\mathcal{T}_{\sigma'}\mathcal{P}_\sigma\mathcal{T}_\sigma+\mathcal{T}_{\sigma'}\mathcal{P}_{\sigma'}\mathcal{T}_\sigma+\mathcal{T}_\sigma\mathcal{P}_{\sigma'}\mathcal{T}_{\sigma'}\\
&-\mathcal{P}_\sigma\mathcal{T}_\sigma\mathcal{T}_{\sigma'}-\mathcal{T}_{\sigma'}\mathcal{T}_\sigma\mathcal{P}_\sigma-\mathcal{P}_{\sigma'}\mathcal{T}_{\sigma'}\mathcal{T}_\sigma-\mathcal{T}_\sigma\mathcal{T}_{\sigma'}\mathcal{P}_{\sigma'})\\
\frac{1}{2}[i\mathcal{S},[i\mathcal{S},\mathcal{H}_0]] =& \frac{1}{U}\sum_\sigma(\mathcal{P}_\sigma\mathcal{T}_\sigma^2\mathcal{P}_\sigma-\mathcal{T}_\sigma\mathcal{P}_\sigma\mathcal{T}_\sigma)\\
&+\frac{1}{U}\sum_{\langle\sigma,\sigma'\rangle}(\mathcal{P}_\sigma\mathcal{T}_\sigma\mathcal{T}_{\sigma'}\mathcal{P}_{\sigma'}+\mathcal{P}_{\sigma'}\mathcal{T}_{\sigma'}\mathcal{T}_\sigma\mathcal{P}_\sigma-\mathcal{T}_\sigma\mathcal{P}_\sigma\mathcal{P}_{\sigma'}\mathcal{T}_{\sigma'}-\mathcal{T}_{\sigma'}\mathcal{P}_{\sigma'}\mathcal{P}_\sigma\mathcal{T}_\sigma)
\end{aligned} \tag{3.31}$$

Here, the sum $\sum_{\langle\sigma,\sigma'\rangle}$ contains all pairs of bonds, sharing exactly one site (i.e. consisting of three different sites), as shown in Fig. (3.4). In a lattice consisting of L sites and with a coordination number Z and periodic boundary conditions (or fixed boundary conditions in the thermodynamic limit), there are exactly $Z(Z-1)L/2$ distinct pairs of bonds.

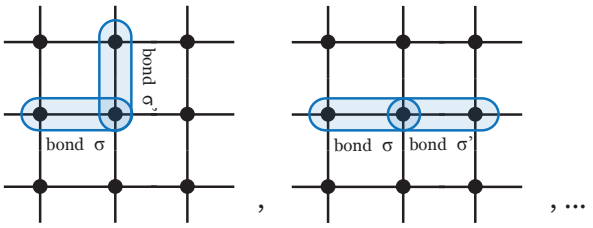

Figure 3.4: The sum $\sum_{\langle\sigma,\sigma'\rangle}$ contains the set of all pairs of connected bonds σ and σ', avoiding double-counting.

The transformed Hamiltonian from Eq. (3.25) can now be expressed as

$$\begin{aligned}
\mathcal{H}^* =& \frac{U}{2}\sum_i n_i(n_i-1)-\mu\sum_i n_i+\sum_\sigma\mathcal{P}_\sigma^\perp\mathcal{T}_\sigma\mathcal{P}_\sigma^\perp\\
&+\frac{1}{U}\sum_\sigma(\mathcal{P}_\sigma\mathcal{T}_\sigma^2\mathcal{P}_\sigma+\mathcal{T}_\sigma\mathcal{P}_\sigma\mathcal{T}_\sigma-\mathcal{P}_\sigma\mathcal{T}_\sigma^2-\mathcal{T}_\sigma^2\mathcal{P}_\sigma)\\
&+\frac{1}{U}\sum_{\langle\sigma,\sigma'\rangle}[(\mathcal{T}_\sigma\mathcal{P}_\sigma\mathcal{T}_{\sigma'}+\mathcal{T}_{\sigma'}\mathcal{P}_{\sigma'}\mathcal{T}_\sigma-\mathcal{P}_\sigma\mathcal{T}_\sigma\mathcal{T}_{\sigma'}-\mathcal{P}_{\sigma'}\mathcal{T}_{\sigma'}\mathcal{T}_\sigma+\mathcal{P}_\sigma\mathcal{T}_\sigma\mathcal{T}_{\sigma'}\mathcal{P}_{\sigma'}-\mathcal{T}_\sigma\mathcal{P}_\sigma\mathcal{P}_{\sigma'}\mathcal{T}_{\sigma'})+\text{ h.c.}]\,.
\end{aligned} \tag{3.32}$$

Note that in this expression, the operator terms taking the system out of the low energy manifold $\sum_\sigma(\mathcal{P}_\sigma\mathcal{T}_\sigma+\mathcal{T}_\sigma\mathcal{P}_\sigma)$ exactly cancel, proving the suitability of the $\mathcal{S}$ chosen above in Eq. (3.30).

For a variational calculation, we use the bosonic Gutzwiller ansatz to evaluate the energy of the transformed Hamiltonian $\mathcal{H}^*$

$$|\mathrm{GW}\rangle=\prod_i\left(\sum_{n=0}^\infty c_n^{(i)}|n\rangle_i\right) \tag{3.33}$$

to obtain an approximate ground state and determine the phase diagram of the system. The coefficients $c_n^{(i)}$ for the ground state can be determined by minimizing the total energy

$$E_0=\langle\mathrm{GW}|\mathcal{H}^*|\mathrm{GW}\rangle=\langle\mathrm{GW}|e^{i\mathcal{S}}\,\mathcal{H}_{\mathrm{BH}}\,e^{-i\mathcal{S}}|\mathrm{GW}\rangle. \tag{3.34}$$

Conversely, this method can also be seen, not as a transformation to a effective operator $\mathcal{H}^*$, but using an extended trial state

$$|\psi\rangle = e^{-i\mathcal{S}}|\mathrm{GW}\rangle \tag{3.35}$$

and minimizing the energy of the original Bose-Hubbard Hamiltonian, as shown by the last expression in Eq. (3.34).

Determining the Ground State

Evaluating this energy for all terms in Eq. (3.32), it is useful to introduce the following definitions:

$$\varphi_{i,n} \equiv \sqrt{n+1}\, c_n^{(i)*}\, c_{n+1}^{(i)} \tag{3.36}$$

$$\varphi_i \equiv \langle \mathrm{GW}|b_i|\mathrm{GW}\rangle = \sum_{n=0}^{\infty} \varphi_{i,n} \tag{3.37}$$

$$\phi_{i,n} \equiv \sqrt{(n+1)(n+2)}\, c_n^{(i)*}\, c_{n+2}^{(i)} \tag{3.38}$$

$$\phi_i \equiv \langle \mathrm{GW}|b_i^2|\mathrm{GW}\rangle = \sum_{n=0}^{\infty} \phi_{i,n} \tag{3.39}$$

Adding up all contributions for the homogeneous system, leads to the expression

$$\begin{aligned}
E =& \sum_i \sum_{n=0}^{\infty} |c_n^{(i)}|^2 (Un(n-1)/2 - \mu n) + J \sum_{\sigma} 2\mathrm{Re}(\varphi_{j,\overline{n}}\, \varphi_{i,\overline{n}-1}^* + \varphi_{i,\overline{n}}\, \varphi_{j,\overline{n}-1}^* - \varphi_i^* \varphi_j) \\
&+ \frac{J^2}{U} \sum_{\sigma} \Big[-2\overline{n}(\overline{n}+1)|c_{\overline{n}}^{(i)}|^2 |c_{\overline{n}}^{(j)}|^2 + \overline{n}(\overline{n}+1)|c_{\overline{n}+1}^{(i)}|^2 |c_{\overline{n}-1}^{(j)}|^2 + \overline{n}(\overline{n}+1)|c_{\overline{n}-1}^{(i)}|^2 |c_{\overline{n}+1}^{(j)}|^2 \\
&+ \phi_{i,\overline{n}-1}^*\, \phi_{j,\overline{n}-1} + \phi_{i,\overline{n}-1}\, \phi_{j,\overline{n}-1}^* - \phi_{i,\overline{n}-2}^*\, \phi_{j,\overline{n}} - \phi_{i,\overline{n}-2}\, \phi_{j,\overline{n}}^* - \phi_{j,\overline{n}-2}^*\, \phi_{i,\overline{n}} - \phi_{j,\overline{n}-2}\, \phi_{i,\overline{n}}^* \Big] \\
&+ 2\frac{J^2}{U} \sum_{\langle \sigma,\sigma' \rangle} \mathrm{Re} \Big[\overline{n}\, (\varphi_{i,\overline{n}}^*\, \varphi_l + \varphi_{l,\overline{n}}^*\, \varphi_i) |c_{\overline{n}-1}^{(j)}|^2 + (\overline{n}+1)\, (\varphi_{i,\overline{n}-1}\, \varphi_l^* + \varphi_{l,\overline{n}-1}\, \varphi_i^*) |c_{\overline{n}+1}^{(j)}|^2 \\
&+ (\varphi_{i,\overline{n}-1}\, \varphi_l + \varphi_{l,\overline{n}-1}\, \varphi_i)\, \phi_{j,\overline{n}-1}^* + (\varphi_{i,\overline{n}}^*\, \varphi_l^* + \varphi_{l,\overline{n}}^*\, \varphi_i^*)\, \phi_{j,\overline{n}-1} \\
&- (\overline{n}+1)\, (\varphi_{i,\overline{n}-1}^*\, \varphi_l + \varphi_{l,\overline{n}-1}^*\, \varphi_i) |c_{\overline{n}}^{(j)}|^2 - \overline{n}\, (\varphi_{i,\overline{n}}\, \varphi_l^* + \varphi_{l,\overline{n}}\, \varphi_i^*) |c_{\overline{n}}^{(j)}|^2 \\
&- (\varphi_{i,\overline{n}-1}^*\, \varphi_l^* + \varphi_{l,\overline{n}-1}^*\, \varphi_i^*)\, \phi_{j,\overline{n}} - (\varphi_{i,\overline{n}}\, \varphi_l + \varphi_{l,\overline{n}}\, \varphi_i)\, \phi_{j,\overline{n}-2}^* \\
&+ (\overline{n}+1)\, \varphi_{i,\overline{n}-1}^*\, \varphi_{l,\overline{n}-1} |c_{\overline{n}}^{(j)}|^2 + \overline{n}\, \varphi_{i,\overline{n}}\, \varphi_{l,\overline{n}}^* |c_{\overline{n}}^{(j)}|^2 - \varphi_{i,\overline{n}}^*\, \phi_{j,\overline{n}-1}\, \varphi_{l,\overline{n}-1}^* \\
&- \varphi_{i,\overline{n}-1}\, \phi_{j,\overline{n}-1}^*\, \varphi_{l,\overline{n}} - \overline{n}\, \varphi_{i,\overline{n}}^*\, \varphi_{l,\overline{n}} |c_{\overline{n}-1}^{(j)}|^2 - (\overline{n}+1)\, \varphi_{i,\overline{n}-1}\, \varphi_{l,\overline{n}-1}^* |c_{\overline{n}+1}^{(j)}|^2 \Big]
\end{aligned} \tag{3.40}$$

for the energy. In the last sum i, j and l denote the three sites within the connected pair of bonds σ, σ'. The sum extends over all sets of three connected sites exactly once (if a term with l and i appears in the sum, the term with l and i interchanged does not appear), with j always denoting the site connecting i and l, as shown in Fig. 3.5.

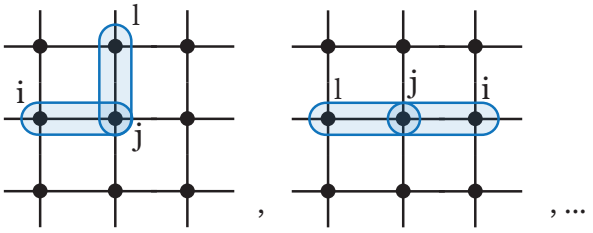

Figure 3.5: j always denotes the central site connecting i and l.

Even in the homogeneous case, the energy landscape described by Eq. (3.40) possesses many local minima and common minimization methods, such as the downhill simplex, conjugate gradient and Powell's method fail to find the true minimum, not leading the correct approximate ground state

and and incorrect phase diagram. To circumvent this problem, a simulated annealing algorithm was adapted to find a point in the vicinity of the global minimum in the space of c_n-coefficients, before the downhill simplex method is applied for the small final steps, to obtain a very high precision. In contrast to the usual energy functional minimization of $E = \langle\psi|\mathcal{H}|\psi\rangle/\langle\psi|\psi\rangle$ when the normalization of the state is not guaranteed, special attention has to be paid here, since the energy contains more than only binomial terms in c_n, invalidating this approach.

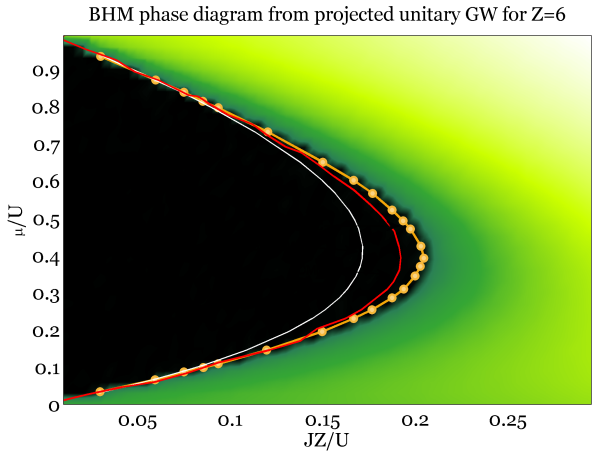

Figure 3.6: Order parameter phase diagram for the BHM in 3D, obtained by minimizing the ground state energy. White line: bosonic Gutzwiller mean-field theory. Red line: Bosonic DMFT for the Bethe lattice with $Z = 6$ from [77]. Orange line: quantum Monte Carlo phase diagram from [26].

In Fig. (3.6) the order parameter, obtained by minimizing the energy per site Eq. (3.40), is shown. The phase border is determined by the largest value of JZ/U, for which the ground state order parameters vanishes. This is not particularly clear from the colormap, but it was shown in [163] that for a three-dimensional cubic lattice, the phase border agrees remarkably well with the Quantum Monte Carlo (QMC) result from [26] on the level of below 1%. Furthermore, the phase diagram is compared with that obtained by bosonic Dynamical Mean-Field Theory (DMFT) on the Bethe lattice, as well as the Gutzwiller mean-field result.

Equations of Motion

A very important advantage of the projection operator approach over other methods, such as QMC and bosonic DMFT, is that it can be extended to treat out of equilibium, real time dynamics. To describe the temporal evolution of the system in a non-equilibrium situation or to apply imaginary time evolution as an alternative method of determining the ground state, the equations of motion for the coefficients $c_n^{(i)}$ have to be determined. We do this by using the principle of least action. The action for the system is given by

$$\mathcal{S} = \int_{t_i}^{t_f} dt \, \left[-i\hbar\langle \mathrm{GW}(t)|e^{i\mathcal{S}} \, \partial_t \, e^{-i\mathcal{S}}|\mathrm{GW}(t)\rangle + E(t)\right], \tag{3.41}$$

where $E(t)$ denotes the total, but now time-dependent (i.e. $c_n^{(i)}(t)$, $\varphi_{i,n}(t)$, $\varphi_i(t)$, $\phi_{i,n}(t)$ and $\phi_i(t)$ are now time dependent functions) energy expression given in Eq. (3.40). Evaluating the first term in Eq. (3.41) (here for the case of Hamiltonian, that is not explicitly time dependent) and formally treating $c_n^{(i)}(t)$ and ${c_n^{(i)}}^*(t)$ as independent variables, it can be given explicitly as

$$\langle \mathrm{GW}(t)|e^{i\mathcal{S}} \, \partial_t \, e^{-i\mathcal{S}}|\mathrm{GW}(t)\rangle = \sum_j \sum_{m=0}^{\infty} {c_m^{(j)}}^*(t) \, \dot{c}_m^{(j)}(t). \tag{3.42}$$

The principle of least action, stating that the S takes is extremal along the physical path, i.e. $\delta S = 0$, implies in particular that the action does not change for any infinitesimal variation $\delta {c_n^{(i)}}^*(t)$

$$\frac{\delta \mathcal{S}}{\delta {c_n^{(l)}}^*(t)} = 0. \tag{3.43}$$

Since the explicit equations of motion for the coefficients are lengthy and technical, they are given in appendix (F). Note that the above derivation is already for the inhomogeneous case, where either the variational state or the variational state and the potential are not translationally invariant. If the density distribution undergoes large changes during the evolution, the projection operator has to be adjusted accordingly. Alternatively, a generalized construction procedure for the projection operator may be used. The projection operator approach is capable of describing non-trivial dynamics in the Mott insulating state, which is beyond the scope of bosonic Gutzwiller theory. Its applicability to time-dependent problems far away from equilibrium, as well as the excellent agreement of the static phase diagram with the QMC result, make it a very promising candidate for future use in treating a variety of time-dependent problems of lattice bosons in the Mott insulator and strongly interacting condensate.

4. The Extended Bose-Hubbard Model in the Lowest Dressed Band

With the ever increasing precision in recent experiments [172, 171, 164], as well as development of new probing techniques and remarkable technical advances [119, 13, 110, 12], it has become possible to observe effects beyond the standard Hubbard model. Specifically, a density dependence of the interaction parameter U has been observed by using quantum phase revival spectroscopy [172, 171], which has been predicted and described using effective many-body interactions. A recent experiment using multi-band spectroscopy to investigate the effect of bosons in a Bose-Fermi mixture found a significant reduction of the fermionic tunneling energy J [73].

While the Fock space spanned by the Fock states generated by the full multi-band single-particle Wannier orbitals is a perfectly valid basis for the interacting many-body system, where by construction the parameters are density-independent, it is customary to work in an effective single band basis. However, such a description requires a density dependence of the parameters, or alternatively the introduction of effective higher order terms as will be shown.

It has been proposed [106, 108, 116] that the density dependence of the bosonic tunneling parameter induced by the Bose-Fermi interaction can explain the shift in the bosonic superfluid-Mott insulator transition observed in Bose-Fermi mixtures [119, 13]. This topic is still under debate with an alternative cause suggested to be the heating of the system as the lattice is ramped up [34, 33, 150]. Furthermore, several new phases have recently been predicted for the effective single-band density-dependent Bose-Hubbard model [72, 43]. An effective density-dependent change of the Hubbard parameters has been calculated using a mean-field decoupling of the densities in Bose-Fermi mixtures [106, 108] and also beyond this approximation [116], where two-particle hopping amplitudes and further relevant Bose-Fermi Hubbard parameters were calculated within the full multi-orbital picture. In a single species bosonic lattice gas, the density-dependence of J, the on-site interactions U, as well as nearest neighbor interactions have been calculated within a Gaussian approximation for the Wannier functions [72]. The density-dependence of the single particle tunneling amplitude J and the interaction parameter U, as well as the effect on the phase diagram were considered in [43, 107]. In [107] a fully correlated, multi-orbital calculation was performed in the Wannier basis to quantitatively determine the density-dependence of J.

In this work we rigorously derive and define the effective lowest-band representation used in these previous works, where the localized many-body low-energy states are **dressed** with contributions from higher bands, analogous to the dressed state basis in quantum optics. We define new ladder operators connecting only states within this dressed low-energy manifold, which exactly fulfill bosonic commutation relations. For finite interaction strength $|g| > 0$, these do not coincide with the usual single-particle Wannier creation and annihilation operators and we give the exact

prescription for transforming operators between the multi-orbital Wannier and the dressed single-band basis in the low-energy description. This transformation is also vital to translate any operator into the new basis, which is usually given in the real space, Bloch or Wannier representation, e.g. observables, additional terms in the Hamiltonian or perturbations. On a local level, our transformation recovers the effective multi-body interactions found in [84] in the limit of strong lattice depths s, where a gaussian approximation for the Wannier functions applies. Furthermore our basis transformation procedure allows for a systematic treatment of all non-local terms. These have been addressed in the context of Bose-Fermi mixtures in [116] and identify the counterparts of local multi-body interactions: multi-particle induced tunneling and correlated-pair tunneling terms arising from the usual bosonic interacting lattice Hamiltonian.

This article is organized as follows: in section (4.1) we juxtapose the multi-orbital Wannier and the effective single band descriptions and introduce the basis states of the latter. In section (4.2) and section (4.4) we define the low-energy subspace and the new effective bosonic ladder operators, from which the transformation properties are derived. Subsequently, they are applied in the systematic derivation of additional terms to the standard Bose-Hubbard model and are shown to give rise to n-particle induced single- and correlated two-particle tunneling in in section (4.5.1) and in section (4.5.2) respectively, as well as multi-body nearest neighbor interactions in section (4.5.3). Finally, we investigate the main energy reduction mechanism in section (4.7), showing that mutual particle avoidance visible in the second order correlation function is more important than the commonly used explanation of broadened single-particle orbitals.

4.1 Multi-Orbital vs. Dressed-Band Description

We start with the single-particle Hamiltonian describing atoms of mass m in a 3D cubic optical lattice

$$\mathcal{H}_{\text{lat}} = \frac{\hat{\mathbf{p}}^2}{2m} + \int d^3r \sum_{d=x,y,z} s\left(\sin^2(\pi r_i/a) - \frac{1}{2}\right) |\mathbf{r}\rangle\langle\mathbf{r}| \tag{4.1}$$

with the same lattice depth s and spacing a in each dimension. We work in units of the recoil energy $E_r = \frac{1}{2m}\left(\frac{\pi\hbar}{a}\right)^2$. Performing a band structure calculation and Fourier transforming the single-particle Bloch eigenstates leads to a multi-orbital basis of Wannier orbitals [1], for which we introduce the bosonic annihilation (creation) operators $a_{i,\alpha}$ ($a^\dagger_{i,\alpha}$) at site i and in the band $\alpha = (\alpha_x, \alpha_y, \alpha_z)$. A short-ranged interaction for two atoms scattering in the s-wave channel only at the relevant energy scale can be well approximated by a δ-type contact interaction and characterized completely by the s-wave scattering length a_s. The interaction strength parameter for the effective contact interaction is given by $g = 4\pi\hbar a_s/m$ and the interaction Hamiltonian can thus be expressed in the multiband Wannier basis as

$$\begin{aligned}\mathcal{H}_{\text{int}} &= \frac{g}{2}\int d^3r\, \psi^\dagger(\mathbf{r})\psi^\dagger(\mathbf{r})\psi(\mathbf{r})\psi(\mathbf{r}) \\ &= \sum_{\substack{\alpha_1,\alpha_2,\alpha_3,\alpha_4 \\ i_1,i_2,i_3,i_4}} U^{(i_1,i_2,i_3,i_4)}_{\alpha_1,\alpha_2,\alpha_3,\alpha_4}\, a^\dagger_{i_1,\alpha_1} a^\dagger_{i_2,\alpha_2} a_{i_3,\alpha_3} a_{i_4,\alpha_4}\end{aligned} \tag{4.2}$$

where the matrix elements are defined in terms of the single-particle Wannier functions

$$U^{(i_1,i_2,i_3,i_4)}_{\alpha_1,\alpha_2,\alpha_3,\alpha_4} = \frac{g}{2}\int d^3r\, w^*_{i_1,\alpha_1}(\mathbf{r})\, w^*_{i_2,\alpha_2}(\mathbf{r})\, w_{i_3,\alpha_3}(\mathbf{r})\, w_{i_4,\alpha_4}(\mathbf{r}) \tag{4.3}$$

Together with the contact interaction term, the full many-body interacting lattice Hamiltonian can be be written in terms of five contributions:

$$\begin{aligned}\mathcal{H}_{\text{tot}} &= \mathcal{H}_{\text{lat}} + \mathcal{H}_{\text{int}} - \mu\sum_{i,\alpha} a^\dagger_{i,\alpha} a_{i,\alpha} \\ &= \mathcal{H}_\epsilon + \mathcal{H}_{U,\text{loc}} + \mathcal{H}_t + \mathcal{H}_{U,\text{nn}} + \mathcal{H}_{\text{lr}}\end{aligned} \tag{4.4}$$

[1] Choosing the complex phases of the individual Bloch states appropriately is vital for the real-space localization of the resulting Wannier states.

Here, $\mathcal{H}_\epsilon = \sum_\alpha (\epsilon^{(\alpha)} - \mu) \sum_i a^\dagger_{i,\alpha} a_{i,\alpha}$ is the on-site contribution of the single-particle lattice Hamiltonian Eq. (4.1) with $\epsilon^{(\alpha)}$ being the mean energy of the band α and μ the chemical potential when switching to the grand canonical ensemble. The term $\mathcal{H}_t = \sum_\alpha t^{(\alpha)} \sum_{\langle i,j \rangle} (a^\dagger_{i,\alpha} a_{j,\alpha} + \text{h.c.})$ is the tunneling between all pairs of nearest neighboring sites $\langle i, j \rangle$ within the different bands α. $t^{(\alpha)} = \frac{1}{L} \sum_{\mathbf{k}} e^{ia\mathbf{k}\cdot\mathbf{e}_i} E^{(\alpha,\mathbf{k})}$ is the nearest neighbor tunneling energy along direction $\mathbf{e}_i$, i.e. the first component of the energy band $E^{(\alpha,\mathbf{k})}$'s Fourier transform, with the sum of quasi-momenta $\mathbf{k}$ extending over the first Brillouin zone of a lattice containing L sites.

Note that the terms $\mathcal{H}_\epsilon, \mathcal{H}_t$ and a part of $\mathcal{H}_{\text{lr}}$ do not couple different bands, whereas the on-site interaction term $\mathcal{H}_{U,\text{loc}}$ conserves the local many-body parity

$$Q_i^{(x)} = \prod_{\alpha_x = 1,3,5,\ldots} \prod_{\alpha_y, \alpha_z = 0}^{\infty} (-1)^{\hat{n}_{i,\alpha}} \tag{4.5}$$

(for the x-dimension, others are analogous) along each dimension.The local interacting Hamiltonian at every site can thus be diagonalized in the subspace corresponding to all multiorbital local states with the same parity as the ground state. The resulting eigenstates subsequently constitute an alternative set of basis states for the n-particle local Hilbert space.

We now shortly recap the approximations made in the derivation of the standard Bose-Hubbard model: Firstly, one relies on a strong spatial localization of the single particle Wannier functions. For a sufficiently strong lattice depth s, this justifies to take only nearest-neighbor tunneling as well as only on-site interactions into account and neglect all others. Secondly, one assumes that all interband couplings (for any relevant operator) are negligible, thus justifying a truncation to the lowest single-particle band before constructing the many-particle Fock space. The presence of additional terms of the first kind is intrinsic to the problem and cannot be remedied. In a lattice of finite depth and with discrete translational symmetry, the basis states in which all of these couplings would disappear necessarily has spatially completely delocalized basis states (i.e. are the Bloch Fock states in the absence of interactions), which contradicts the initial goal of finding a spatially localized basis. On the other hand, the problem of interband couplings can be remedied by switching to the basis of local eigenstates. Here, the local interband couplings are contained to infinite order in each local eigenstate and the subsequent coupling between the different lattice sites gives rise to a new band structure, which we refer to as dressed bands. This evolution of the local many-particle energy spectrum, where the non-interacting bands continuously evolve into dressed bands is shown in Fig. (4.1).

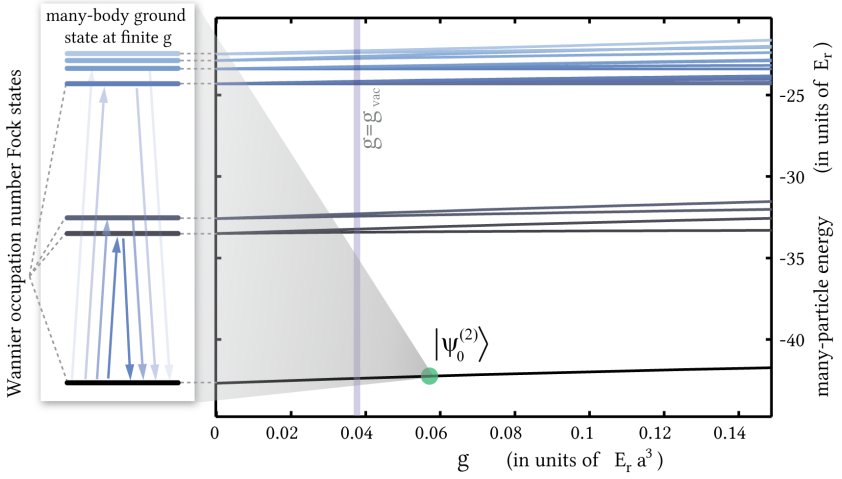

Figure 4.1: Two-particle energy spectrum of the local Hamiltonian $\mathcal{H}_{\text{loc}}^{(i)}$ in a 3D cubic 768nm lattice of depth $s = 10$ as a function of the interaction strength g. For any finite g the local ground state $|\psi_o^n\rangle$ is no longer the pure Fock state, with all particles occupying the lowest local Wannier orbital, but an admixture of higher Wannier orbitals is coupled by the local interaction terms. This lowers the total energy (including all orders in perturbation theory) and can be thought of as a dressed state in an effective lowest-band, as it evolves continuously from the $g = 0$ limit and remains gapped from all higher dressed bands for typical interaction strengths. g_{vac} is the two-body inter-atomic interaction strength of ^{87}Rb without the presence of an external magnetic field addressing the Feshbach resonance. In contrast to working in the truncated single orbital Wannier basis, this state gives a much better low-energy description containing local correlations, as was confirmed experimentally [172, 171]. Spatial localization is furthermore guaranteed, since only higher Wannier orbitals at the same site are occupied.

For a non-interacting system, the Fock state with $|n\rangle_i$ particles occupying the lowest Wannier orbital $\alpha = 1$ at site i is the local lowest energy state and therefore well suited as a basis vector for a low-energy description of the system. In the presence of interactions $|n\rangle_i$ is no longer the local lowest energy state, although the Fock states still provide a complete basis when taking all bands into account. However, for the simulation of interacting many-particle systems, one is often interested in a single-band description, and it is of great importance to find the best possible effective single-band basis. From these many-particle basis states one requires that they

1. Have the highest possible spatial localization, i.e. minimize a localization measure such as the spatial variance of the density profile.
2. Contain the local interaction-induced correlations, also lowering the many-particle energy expectation values of these states (evaluated with the full interacting Hamiltonian).
3. Possess a well defined local particle number, such that the occupation number representation can be associated with these states.
4. Are mutually orthogonal and span the complete low-energy subspace, i.e. formally constitute a basis.
5. Recover the standard Bose-Hubbard model in the non-interacting limit.

Having defined these requirements which we impose on an optimized effective single-band basis, the next task is to find a set of such states fulfilling the above requirements. We propose to use the many-particle eigenstates of the local interacting Hamiltonian $\mathcal{H}_{\text{loc}} = \mathcal{H}_\epsilon + \mathcal{H}_{U,\text{loc}}$ (which is a direct sum of local Hamiltonians $\mathcal{H}_{\text{loc}}^{(i)}$), projected onto the Fock space spanned by the set of all non-interacting Wannier orbitals at a single site i. The above criteria are then fulfilled for the following reasons:

1. Maximal spatial localization [2] carries over from the maximum localization of the single-particle Wannier orbitals at a given site.
2. The multi-orbital, many-particle local ground state by definition minimizes the local energy and contains correlations in the interacting case, where the eigenstates are entangled with respect to the single-particle basis.
3. Since the local truncated interacting Hamiltonian conserves the local particle number

$$[H_{\text{loc}}^{(i)}, \sum_\alpha a_{i,\alpha}^\dagger a_{i,\alpha}] = 0, \tag{4.6}$$

[2] Clearly this property competes with the energy minimization, we do however not require spatial localization beyond the lattice spacing a for the validity of a discretized lattice model. Therefore the energy reduction criterion dominates, once spatial localization on the order of the lattice spacing is guaranteed.

the eigenstates of $H_{\mathrm{loc}}^{(i)}$ can all be chosen to have a fixed local particle number. For all typical experimental interaction strengths, the ground state is non-degenerate (thus necessarily possessing a fixed particle number). This allows a clear translation from the initial truncated single-band Wannier occupation into the new dressed band formalism: the initial local Fock state $|n_i\rangle_i$ is formally replaced by the local correlated ground state with n particles $|\psi_0(n)\rangle$ at the cost of renormalizing the Bose-Hubbard parameters.

4. Local ground states with different particle number are orthogonal (or can be chosen as such in the case of degeneracy) since they are simultaneously eigenstates of the Hermitian local many-particle Hamiltonian. States at different sites on the other hand are orthogonal, since by construction they only occupy Wannier orbitals at different sites, which are orthogonal on the single-particle level.

5. In the non-interacting limit, the local n-particle ground state continuously converges to the local Wannier Fock state, thus recovering this limit.

All longer-range matrix elements (beyond nearest neighbor) from both the lattice, as well as the interaction Hamiltonian are contained in the long-range term $\mathcal{H}_{\mathrm{lr}}$. These will not be discussed in further detail, since their translation into the effective single band basis is identical to that of the nearest neighbor terms, they are however generally smaller in magnitude. The remaining terms (on-site and terms connecting nearest neighbors) from the interaction Hamiltonian can be classified into four groups: on-site interaction terms forming the local interaction Hamiltonian $\mathcal{H}_{U,\mathrm{loc}}^{(i)} = \sum_{\alpha_1,\alpha_2,\alpha_3,\alpha_4,i} U_{\alpha_1,\alpha_2,\alpha_3,\alpha_4}^{(i,i,i,i)} a_{i,\alpha_1}^\dagger a_{i,\alpha_2}^\dagger a_{i,\alpha_3} a_{i,\alpha_4}$, the density-induced single-particle tunneling Hamiltonian $\mathcal{H}_{U,\mathrm{nn}}^J$ containing terms of the form $a_{i,\alpha_1}^\dagger a_{i,\alpha_2}^\dagger a_{i,\alpha_3} a_{j,\alpha_4} + h.c.$ (as well as their counterparts under exchange $i \leftrightarrow j$), pair tunneling terms of the form $a_{i,\alpha_1}^\dagger a_{i,\alpha_2}^\dagger a_{j,\alpha_3} a_{j,\alpha_4} + h.c.$ in $\mathcal{H}_{U,\mathrm{nn}}^I$, as well as the nearest-neighbor interaction Hamiltonian $\mathcal{H}_{U,\mathrm{nn}}^{\mathrm{int}}$ with terms $a_{i,\alpha_1}^\dagger a_{i,\alpha_2} a_{j,\alpha_3}^\dagger a_{j,\alpha_4} + \mathrm{h.c.}$ All terms of the latter three types are contained in the nearest neighbor interaction Hamiltonian $\mathcal{P}_{\mathrm{lowE}} \mathcal{H}_{U,\mathrm{nn}} \mathcal{P}_{\mathrm{lowE}} = \mathcal{H}_{U,\mathrm{nn}}^J + \mathcal{H}_{U,\mathrm{nn}}^I + \mathcal{H}_{U,\mathrm{nn}}^{\mathrm{int}}$.

4.2 Definition of the low-energy subspace

In this section we systematically construct the effective low-energy subspace. The full Hamiltonian projected onto this subspace gives the best possible description of interacting bosons in a lattice at a sufficiently low temperature, where all higher dressed bands can be neglected. Our procedure is summarized in Fig. (4.2).

We diagonalize the local part of the Hamiltonian in Eq. (4.4), which is a direct sum of local Hamiltonians

$$\mathcal{H}_{\mathrm{loc}} = \mathcal{H}_\epsilon + \mathcal{H}_{U,\mathrm{loc}} = \sum_i \mathcal{H}_{\mathrm{loc}}^{(i)} \otimes \prod_{\otimes j \neq i} \mathbb{1}_j. \tag{4.7}$$

This can be achieved by diagonalizing the local Hamiltonian at each site separately, although for a homogeneous lattice the diagonalizations are of course identical and it suffices to perform one only. Our formalism is however directly extensible to inhomogeneous systems, e.g. in the presence of additional spatial potentials or spatially dependent interactions. Note that in our notation $\mathcal{H}_{\mathrm{loc}}^{(i)}$ operates only on the **local** Hilbert space of a single site (i.e. not on the complete lattice Fock space), the complete many-particle lattice Hilbert space is the direct product of all local Fock spaces over all sites.

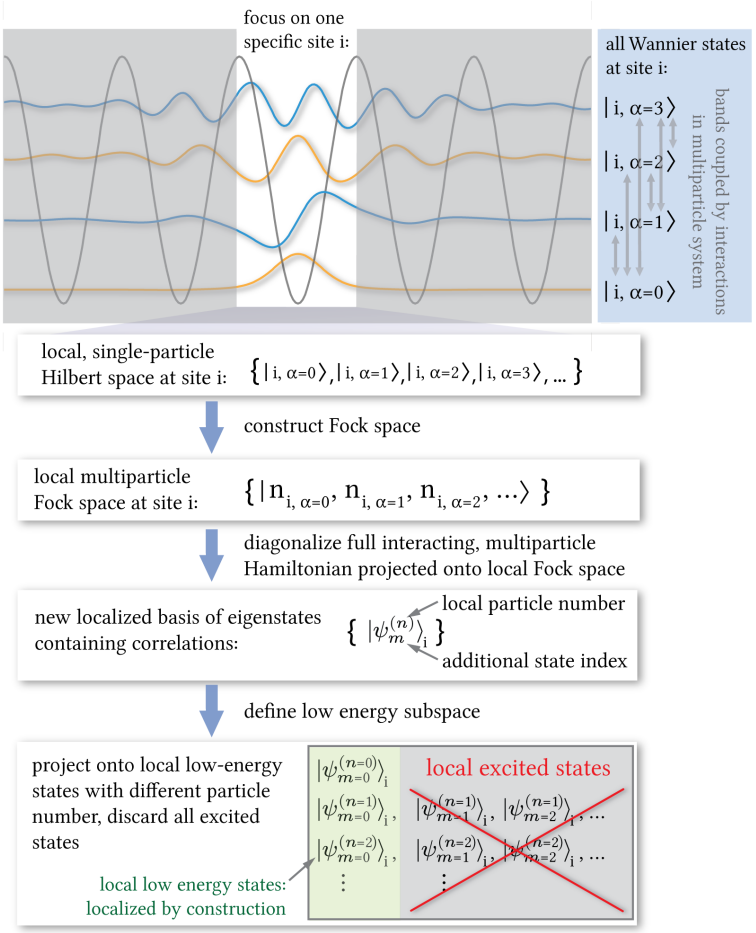

Figure 4.2: Cartoon depicting our procedure to construct the localized low-energy, dressed band basis. The Wannier functions (shown for a lattice of depth $s = 8E_r$) are obtained from an exact single-particle band structure calculation on a large lattice, before one focuses on the diagonalization of the interacting many-particle Hamiltonian on the Fock subspace of multiorbital maximally localized Wannier states on a single site. This is not to be confused with a truncation of the spatial potential to a single lattice site.

Truncating the local single particle space to the $\alpha_{\max}$ lowest bands, we diagonalize the local Hamiltonian in the Wannier Fock representation at fixed particle number and parity, leading to

$$\mathcal{H}^{(i)}_{\text{loc}} = \sum_{m,n} E^{(n)}_m |\psi^{(n)}_m\rangle_{ii}\langle\psi^{(n)}_m|. \tag{4.8}$$

Due to number conservation of $\mathcal{H}^{(i)}_{\text{loc}}$, the eigenstates $|\psi^{(n)}_m\rangle_i$ can always be chosen to be of fixed particle number n and contain an additional excitation index m. On a local level, a projection onto the many-particle low-energy space means only considering the local correlated local ground states

$$|\psi^{(n)}_0\rangle_i = \sum_{n_{i,0},\ldots,n_{i,\alpha_{\max}}} c_{n_{i,0},\ldots,n_{i,\alpha_{\max}}} |n_{i,0},\ldots,n_{i,\alpha_{\max}}\rangle \tag{4.9}$$

with all different particle numbers $n = n_{i,0} + \ldots + n_{i,\alpha_{\max}}$. This low-energy projection can be extended to the whole system by defining the subspace spanned by the basis states

$$|\psi^{(n_1,\ldots,n_L)}_0\rangle \equiv \prod_{\otimes i=1}^{L} |\psi^{(n_i)}_0\rangle_i \tag{4.10}$$

for all possible sets of integer local occupation numbers $(n_1, \ldots, n_L)$. By construction, these states are all mutually orthogonal

$$\langle \psi_0^{(n_1,\ldots,n_L)} | \psi_0^{(n_1',\ldots,n_L')} \rangle = \delta_{n_1,n_1'} \ldots \delta_{n_L,n_L'}, \tag{4.11}$$

which follows from the properties of the direct product in combination with the local states being different eigenstates of the same Hermitian Hamiltonian. It is also useful to define a low-energy projection operator

$$\mathcal{P}_{\text{lowE}} = \sum_{n_1,\ldots,n_L} |\psi_0^{(n_1,\ldots,n_L)}\rangle\langle\psi_0^{(n_1,\ldots,n_L)}| \tag{4.12}$$

which projects any state from the full multi-orbital Fock space to the low-energy subspace of the full lattice.

4.3 Numerical Implementation

To numerically compute the local, many-particle energy eigenstates, energies and all parameters for the effective dressed band model, we use use exact diagonalization. To reduce the numerical effort to a minimum, we exploit both the $U(1)$-symmetry of the local Hamiltonian, implying that all eigenstates can be chosen to be of fixed particle number, as well as the reflectional symmetry of the Hamiltonian in all three spatial dimensions. Using these symmetries is effectively equivalent to bringing the total Hamiltonian into block diagonal form and numerically diagonalizing the individual subblocks separately. If an eigenstate is non-degenerate and has non-zero elements throughout the whole subspace of a given subblock, it is assured that no additional symmetries, which would further reduce the computational effort, have been overlooked. Apart from the algorithm for the diagonalizing large, sparse matrices and are readily available, the implementation consists of efficiently constructing a basis of the many-particle system within each irreducible subspace and efficiently determining and setting the matrix elements of the Hamiltonian, as described in Appendix (D). Whereas all subspaces to different particle number are relevant for our system, only the fully symmetric subspace (on the many-particle level) with respect to reflections in all three dimensions is of significance for the local N-particle ground state. This can easily be seen in the non-interacting limit: Here the many-particle ground state is the direct product state of single-particle states, where each atom is in the lowest 3D orbital, i.e. the lowest band 3D Wannier state, which is symmetric under reflections in all three spatial directions for the hypercubic lattice. Turning on the interaction, all other many-particle eigenstates remain energetically gapped and hence, for all interaction strengths where the many-particle energy levels don't cross[3], the many-particle ground state at finite interactions remains in the same symmetry class.

4.4 Transformation into the new dressed band basis

Having defined the effective single band space of interest, we now focus on expressing arbitrary operators in this subspace. Here it proves very useful to define a set of new ladder operators

$$b_i = \left(\sum_{n=1}^{\infty} \sqrt{n} |\psi_0^{(n-1)}\rangle_{ii} \langle \psi_0^{(n)}| \right) \otimes \prod_{\otimes j \neq i} \mathbb{1}_j \tag{4.13}$$

where i again refers to a physical site. It can be seen from the structure of these operators that any operator containing only transition elements between low-energy states of the type in Eq. (4.10) can be expressed in terms of these ladder operators and their Hermitian conjugates. Furthermore it can be directly verified that these operators fulfill bosonic commutation relations

$$[b_i, b_j^\dagger] = \delta_{i,j}. \tag{4.14}$$

[3]This is fulfilled for typically relevant regimes.

Consequently, these ladder operators take over the role of the Wannier orbital creation and annihilation operators within a more appropriate single band description of an interacting bosonic lattice system. The next step is to express the original Hamiltonian and any other N-particle operator in terms of the operators b_i and $b_i^\dagger$, after projection onto the lowest dressed band. This does not mean that all Wannier creation and annihilation operators $a_{i,\alpha}$ and $a_{i,\alpha}^\dagger$ are directly substituted by b_i and $b_i^\dagger$, but a systematic transformation is required. An arbitrary operator (acting on the full lattice) $\mathcal{D} = \sum_l \mathcal{D}^{(l)}$ expressed in terms of multiorbital lattice Wannier operators can be decomposed into normally ordered terms, where each term $\mathcal{D}^{(l)}$ can contain operators corresponding to many different lattice sites. Projecting this operator onto the lowest dressed band, i.e. multiplying with operator $\mathcal{P}_{\text{lowE}}$ from both the left and right, decouples this operator in the sense that the contribution to each lattice site can be considered individually. Omitting the site index, one such local term is thus generally of the normally ordered form

$$A = a_{i,\alpha_1}^\dagger ... a_{i,\alpha_p}^\dagger a_{i,\beta_1} ... a_{i,\beta_q}, \tag{4.15}$$

containing p creation and q annihilation operators and acting as the unit operator on all other sites. Thus, they transfer any basis state from the local $(m+q-1)$-particle subspace to the $(m+p-1)$-particle subspace for integer $m \geq 1$. We now use the fact that the set of all operators which change the local particle number of any state by some fixed integer number $p-q$ and which annihilate all states containing less than q particles form a subspace of the complete operator vector space. We are however only interested in the low-energy subspace of this subspace, spanned by the operators $\{|\psi_0^{(p)}\rangle_{ii}\langle\psi_0^{(q)}|, |\psi_0^{(p+1)}\rangle_{ii}\langle\psi_0^{(q+1)}|, |\psi_0^{(p+2)}\rangle_{ii}\langle\psi_0^{(q+2)}|, \ldots\}$ or equivalently by the set of operators $\{{b_i^\dagger}^{p+m-1} {b_i}^{q+m-1}\}$, defined in Eq. (4.13). Since the operator A from Eq. (4.15) changes the local particle number by exactly $p-q$, and the set $\{{b_i^\dagger}^{p+m-1} {b_i}^{q+m-1}\}$ for different integer $m \geq 1$ constitutes a basis for all operators with this property in the low-energy subspace, we know that any transformation between the operator A and the new dressed band creation and annihilation operators has to be of the form

$$\begin{aligned} &\mathcal{P}_{\text{lowE}} a_{i,\alpha_1}^\dagger \ldots a_{i,\alpha_p}^\dagger a_{i,\beta_1} \ldots a_{i,\beta_q} \mathcal{P}_{\text{lowE}} \\ &= \sum_m h^{(m)}_{(\alpha_1,\ldots,\alpha_p),(\beta_1,\ldots,\beta_q)} {b_i^\dagger}^{p+m-1} {b_i}^{q+m-1}, \end{aligned} \tag{4.16}$$

with coefficients $h^{(m)}_{(\alpha_1,\ldots,\alpha_p),(\beta_1,\ldots,\beta_q)}$, which are still to be determined. To explicitly determine the transformation coefficients h, we evaluate both sides of Eq. (4.16) in the local low energy basis $|\psi_0^{(n)}\rangle$.

We first rewrite the first part of Eq. (4.16) by inserting the completeness relation in the low-energy subspace in the form $\mathcal{P}_{\text{lowE}} = \sum_{n=0}^\infty |\psi_0^{(n)}\rangle_{ii}\langle\psi_0^{(n)}| \otimes \prod_{j\neq i} \mathbb{1}_j$ on both the left and right side to obtain

$$\begin{aligned} &\mathcal{P}_{\text{lowE}} a_{i,\alpha_1}^\dagger \ldots a_{i,\alpha_p}^\dagger a_{i,\beta_1} \ldots a_{i,\beta_q} \mathcal{P}_{\text{lowE}} \\ &= \sum_{n=0}^\infty \frac{\sqrt{n!(n+p-q)!}}{(n-q)!} f^{(n-q+1)}_{(\alpha_1,\ldots,\alpha_p),(\beta_1,\ldots,\beta_q)} |\psi_0^{(n+p-q)}\rangle_{ii}\langle\psi_0^{(n)}| \end{aligned} \tag{4.17}$$

where we defined the correlation factors

$$\begin{aligned} f^{(n-q+1)}_{(\alpha_1,\ldots,\alpha_p),(\beta_1,\ldots,\beta_q)} &= \frac{(n-q)!}{\sqrt{n!(n+p-q)!}} \\ &\times \langle\psi_0^{(n+p-q)}| a_{\alpha_1}^\dagger \ldots a_{\alpha_p}^\dagger a_{\beta_1} \ldots a_{\beta_q} |\psi_0^{(n)}\rangle. \end{aligned} \tag{4.18}$$

For notational convenience, we have dropped the site index i of which the f's are independent for a homogeneous lattice. The factor in the definition of the f's is chosen such that these obey a number of simple symmetry properties and will also be convenient of later quantities. The upper indices are labeled in a fashion, such that $f^{(r)}_{(\alpha_1,\ldots,\alpha_p),(\beta_1,\ldots,\beta_q)}$ is defined and can be non-zero for any integer $r \geq 1$. These coefficients can be directly calculated once the local eigenstates $|\psi_0^{(n)}\rangle$ are

obtained from the exact diagonalization of the local Hamiltonian. It is furthermore sufficient to restrict the indices to $q \geq p$, since all other cases are related by conjugation. For the special case of only annihilation operators being locally present (i.e. $p = 0$), we define $f^{(r)}_{\beta_1,\ldots,\beta_q} = f^{(r)}_{(),(\beta_1,\ldots,\beta_q)}$ for notational convenience. In Fig. (4.3) the coefficients $f^{(n)}_{\alpha}$ for a single annihilation operator $p = 0$, $q = 1$ are shown. These coefficients have the symmetry property

$$f^{(r)}_{(\beta_1,\ldots,\beta_q),(\alpha_1,\ldots,\alpha_p)} = f^{(r)^*}_{(\alpha_1,\ldots,\alpha_p),(\beta_1,\ldots,\beta_q)} \tag{4.19}$$

and are furthermore invariant under permutations of indices within each bracket

$$f^{(r)}_{(\sigma(\alpha_1),\ldots,\sigma(\alpha_p)),(\tilde{\sigma}(\beta_1),\ldots,\tilde{\sigma}(\beta_q))} = f^{(r)}_{(\alpha_1,\ldots,\alpha_p),(\beta_1,\ldots,\beta_q)}. \tag{4.20}$$

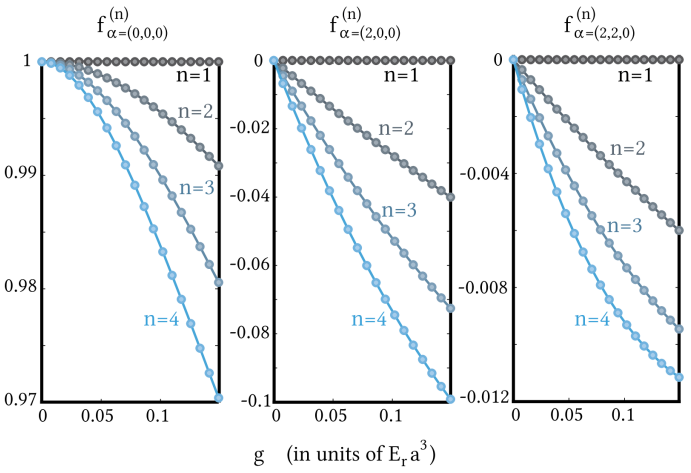

Figure 4.3: The coefficients $f^{(n)}_{\alpha}$ as a function of interaction strength g for a 738nm 3D cubic lattice of depth $s = 10E_r$. Note the symmetry relation $f^{(n)}_{\alpha=(2,0,0)} = f^{(n)}_{\alpha=(0,2,0)} = f^{(n)}_{\alpha=(0,0,2)}$ and $f^{(n)}_{\alpha=(2,2,0)} = f^{(n)}_{\alpha=(2,0,2)} = f^{(n)}_{\alpha=(0,2,2)}$ if the lattice is isotropic. In the non-interacting limit where all particles occupy the lowest local Wannier orbital, the coefficients $f^{(n)}_{\alpha=(0,0,0)}$ approach 1, whereas all coefficients corresponding to other orbitals vanish.

We now evaluate both sides of Eq. (4.16) (using Eq. (4.17)) in the basis of local low-energy basis states $\langle\psi_0^{(n')}|$ and $|\psi_0^{(n)}\rangle$, noting that only elements with $n' = n + p - q$ can be non-zero. Equating identical elements from both sides leads to the linear transformation between the f and h coefficients, which can be written in matrix form as

$$f^{(r)}_{(\alpha_1,\ldots,\alpha_p)(\beta_1,\ldots,\beta_q)} = \sum_{m=1}^{\infty} \mathcal{B}_{r,m} h^{(m)}_{(\alpha_1,\ldots,\alpha_p)(\beta_1,\ldots,\beta_q)} \tag{4.21}$$

with the matrix

$$\mathcal{B}_{n,m} = \frac{(n-1)!}{(n-m)!}\Theta(n-m) \tag{4.22}$$

and $\Theta(x)$ being the step function with $\Theta(0) = 1$. Explicitly, the first truncated part of the matrix is of the form

$$\mathcal{B} = \begin{pmatrix} 1 & 0 & 0 & 0 & 0 & 0 & 0 & \\ 1 & 1 & 0 & 0 & 0 & 0 & 0 & \\ 1 & 2 & 2 & 0 & 0 & 0 & 0 & \\ 1 & 3 & 6 & 6 & 0 & 0 & 0 & \ldots \\ 1 & 4 & 12 & 24 & 24 & 0 & 0 & \\ 1 & 5 & 20 & 60 & 120 & 120 & 0 & \\ 1 & 6 & 30 & 120 & 360 & 720 & 720 & \\ & & & \vdots & & & & \end{pmatrix} \tag{4.23}$$

The lower triangular form of the matrix is a consequence of the fact that the operator $(b^\dagger)^{p+m}(b)^{q+m}$ annihilates any state with less than $(q+m)$ particles. In the non-interacting case, when the n-particle ground state is simply the state with all particles occupying the lowest Wannier orbital $\alpha = 0$, we have $f^{(r)}_{(\alpha_1,\ldots,\alpha_p)(\beta_1,\ldots,\beta_q)} = \delta_{\alpha_1,0}\ldots\delta_{\alpha_p,0}\delta_{\beta_1,0}\ldots\delta_{\beta_q,0}$ and $h^{(r)}_{(\alpha_1,\ldots,\alpha_p)(\beta_1,\ldots,\beta_q)} = \delta_{r,1}\delta_{\alpha_1,0}\ldots\delta_{\alpha_p,0}\delta_{\beta_1,0}\ldots\delta_{\beta_q,0}$, in which case the density-induced transitions between the local ground states of different particle number vanish and the effective low energy creation and annihilation operators are identical to the Wannier creation and annihilation operators.

To explicitly calculate the density-induced transition parameters $h^{(m)}_{(\alpha_1,\ldots,\alpha_p)(\beta_1,\ldots,\beta_q)}$, we require the inverse matrix, which is found to be

$$(\mathcal{B}^{-1})_{m,n} = \frac{(-1)^{m+n}}{(n-1)!\,(m-n)!}\Theta(m-n) \tag{4.24}$$

with the first elements explicitly being

$$\mathcal{B}^{-1} = \begin{pmatrix} 1 & 0 & 0 & 0 & 0 & 0 & 0 & \\ -1 & 1 & 0 & 0 & 0 & 0 & 0 & \\ \frac{1}{2} & -1 & \frac{1}{2} & 0 & 0 & 0 & 0 & \\ -\frac{1}{6} & \frac{1}{2} & -\frac{1}{2} & \frac{1}{6} & 0 & 0 & 0 & \ldots \\ \frac{1}{24} & -\frac{1}{6} & \frac{1}{4} & -\frac{1}{6} & \frac{1}{24} & 0 & 0 & \\ -\frac{1}{120} & \frac{1}{24} & -\frac{1}{12} & \frac{1}{12} & -\frac{1}{24} & \frac{1}{120} & 0 & \\ \frac{1}{720} & -\frac{1}{120} & \frac{1}{48} & -\frac{1}{36} & \frac{1}{48} & -\frac{1}{120} & \frac{1}{720} & \\ & & & \vdots & & & & \end{pmatrix}. \tag{4.25}$$

It should be pointed out that due to this structure, the truncated inverse matrix is identical to the inverse truncated matrix. This finally allows us to express $\mathcal{P}_{\text{lowE}}A\mathcal{P}_{\text{lowE}}$ in terms of effective low energy creation and annihilation operators, which explicitly reads

$$\begin{aligned} \mathcal{P}_{\text{lowE}}a^\dagger_{\alpha_1}\ldots a^\dagger_{\alpha_p}a_{\beta_1}\ldots a_{\beta_q}\mathcal{P}_{\text{lowE}} &= f^{(1)}_{\boldsymbol{\alpha}_p\boldsymbol{\beta}_q}(b^\dagger)^p(b)^q \\ &+ \left(-f^{(1)}_{\boldsymbol{\alpha}_p\boldsymbol{\beta}_q} + f^{(2)}_{\boldsymbol{\alpha}_p\boldsymbol{\beta}_q}\right)(b^\dagger)^{p+1}(b)^{q+1} \\ &+ \left(\frac{1}{2}f^{(1)}_{\boldsymbol{\alpha}_p\boldsymbol{\beta}_q} - f^{(2)}_{\boldsymbol{\alpha}_p\boldsymbol{\beta}_q} + \frac{1}{2}f^{(3)}_{\boldsymbol{\alpha}_p\boldsymbol{\beta}_q}\right)(b^\dagger)^{p+2}(b)^{q+2} + \ldots \end{aligned} \tag{4.26}$$

with $\boldsymbol{\alpha}_p = (\alpha_1,\ldots,\alpha_p)$ and $\boldsymbol{\beta}_q = (\beta_1,\ldots,\beta_q)$. Note that in the non-interacting limit we have $f^{(r)}_{\boldsymbol{\alpha}_p\boldsymbol{\beta}_q} = \delta_{\boldsymbol{\alpha}_p,\mathbf{0}}\,\delta_{\boldsymbol{\beta}_q,\mathbf{0}}$, all coefficients in brackets in Eq. (4.26) of higher order terms cancel and all operators $a_{i,\alpha}$ ($a^\dagger_{i,\alpha}$) for the lowest band can directly be replaced with b_i ($b^\dagger_i$).

For the specific case of a single annihilation operator $\mathcal{P}_{\text{lowE}}a_\alpha\mathcal{P}_{\text{lowE}}$ the transformation is given by

$$\begin{aligned} \mathcal{P}_{\text{lowE}}a_\alpha\mathcal{P}_{\text{lowE}} &= f^{(1)}_\alpha\, b + \left(-f^{(1)}_\alpha + f^{(2)}_\alpha\right)b^\dagger bb \\ &+ \left(\frac{1}{2}f^{(1)}_\alpha - f^{(2)}_\alpha + \frac{1}{2}f^{(3)}_\alpha\right)b^\dagger b^\dagger bbb + \ldots \end{aligned} \tag{4.27}$$

for which we show the first coefficients $f^{(r)}_\alpha$ in Fig. (4.3) as a function of the interaction strength. We point out that the local particle number operator transforms as

$$\sum_\alpha a^\dagger_\alpha a_\alpha = \sum_{r=1}^{\infty}\left[\sum_\alpha h^{(r)}_{(\alpha)(\alpha)}\right](b^\dagger)^r(b)^r = b^\dagger b, \tag{4.28}$$

since $\sum_\alpha f^{(r)}_{(\alpha)(\alpha)} = 1$ for all r and the property of the transformation matrix in Eq. (4.24) $\sum_n(\mathcal{B}^{-1})_{m,n} = \delta_{m,1}$. Hence the local particle operator in our single dressed band counts all particle in all local orbitals.

The transformation relations are the central result of this section: given any physical operator in the single-particle Wannier basis (as is usually the case) which acts on the system or is measured, one cannot simply substitute the Wannier creation and annihilation operators $a_{i,\alpha}$ with the b_i operators from the effective single-band model with density dependent parameters! Rather, the transformation relations from Eqns. (4.16,4.26) have to be used to systematically express this operator in the effective low-energy subspace.

In the following sections we will apply this transformation to the various terms of the original Hamiltonian. The purely local terms exactly recover the effective multibody interactions found in [84] and are diagonal in the dressed band basis with density-dependent interaction parameters. Non-local nearest neighbor terms originate from $\mathcal{H}_t + \mathcal{H}_{U,\mathrm{nn}}$ and are non-diagonal in the new basis, leading to the low-energy representation

$$\begin{aligned}\mathcal{P}_{\mathrm{lowE}}\mathcal{H}_{\mathrm{tot}}\mathcal{P}_{\mathrm{lowE}} = \mathcal{P}_{\mathrm{lowE}}\mathcal{H}_{\mathrm{loc}}\mathcal{P}_{\mathrm{lowE}} + \mathcal{H}_J + \mathcal{H}^I_{U,\mathrm{nn}} + \mathcal{H}^{int}_{U,\mathrm{nn}} \\ + \mathcal{P}_{\mathrm{lowE}}\mathcal{H}_{\mathrm{lr}}\mathcal{P}_{\mathrm{lowE}}\end{aligned} \tag{4.29}$$

of the full initial Hamiltonian. We neglect all long-range (beyond nearest neighbor) terms contained in $\mathcal{H}_{\mathrm{lr}}$ in this work, their transformation is however identical to that of the nearest neighbor terms. Thereafter we will discuss an equivalent formulation of the extension of the Bose-Hubbard model using density-dependent parameters for the various terms at the cost of additionally summing over the set of all local low-energy states.

4.5 Application to the Bose-Hubbard model: Multi-body induced tunneling and interactions

In this section we discuss the four relevant terms in the dressed single-band Bose-Hubbard model. These contain all relevant local and nearest neighbor processes. The amplitudes for processes on neighboring sites in the multi-body induced picture are shown in Fig. (4.4).

4.5.1 Single-particle tunneling term

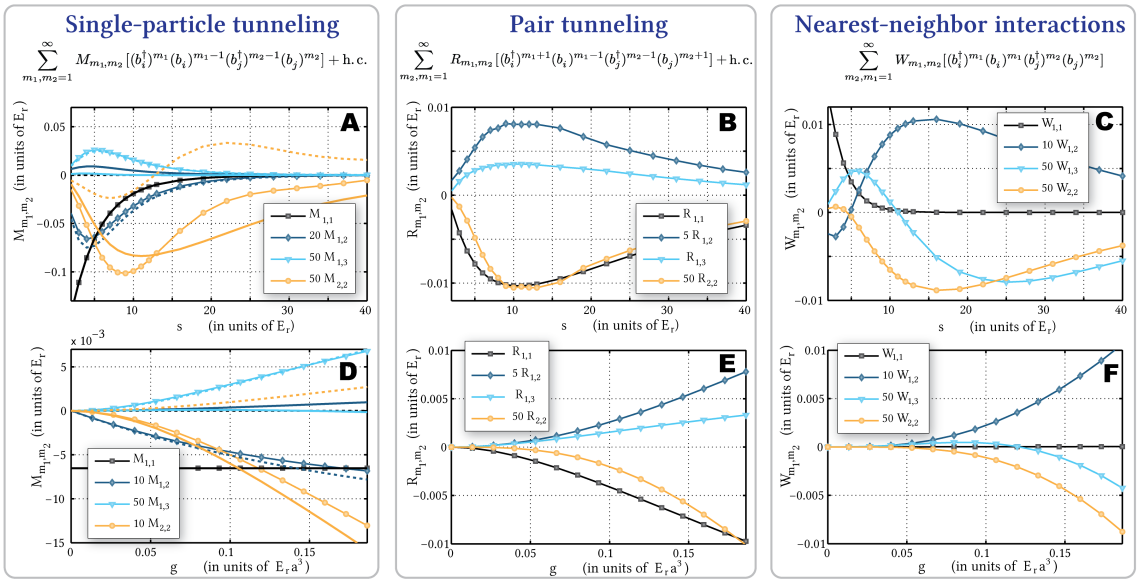

Figure 4.4: Amplitudes for all multibody-induced transitions on nearest neighboring sites. The lowest order, most relevant processes are shown as functions of the lattice depth s at a fixed interaction strength $g = 5g_{\text{vac}} = 0.186E_r a^3$ for ^{87}Rb in the upper row, as well as their dependence on the interaction strength g at a fixed lattice depth $s = 10E_r$ in the lower row. Note the different scaling of individual graphs for visual clarity, which is given in the legends. The subplots (A,D) in the left column show the effective single-particle tunneling, the dotted and solid lines show the contributions from the interaction term $\mathcal{H}_{U,\text{nn}}$ and the single particle particle tunneling term $\mathcal{H}_t$ respectively. With increasing order (m_1, m_2) the contribution from the interaction becomes more important and eventually dominates. Whereas the dependence of all three amplitudes on the interaction strength g is monotonic, the dependence on the lattice depth is more complicated, being non-monotonic and even leading to sign changes. We point out that as a function of the lattice depth s, the magnitude of the higher order terms is most significant in the region of $s \approx 10E_r$ or slightly below, which is also the relevant region for the superfluid-Mott insulator transition (depending on the interaction strength g, i.e. the Feshbach resonance). In the noninteracting limit $g \to 0$ all terms, except the lowest order single particle tunneling $M_{1,1}$ vanish, recovering the usual lowest band Bose-Hubbard model. However, at any finite interaction strength with other terms becoming non-zero, the Bose-Hubbard model truncated to the lowest single particle Bloch band does not give the correct low-energy description. The numerical calculations were performed using 6 bands per dimension, amounting to 216 single-particle orbitals.

We now have to gather all operator contributions in the total Hamiltonian $\mathcal{H}_{\text{tot}}$ that give rise to single-particle tunneling transitions between nearest neighboring sites i and j. Clearly, the tunneling term from the original single-particle lattice Hamiltonian $\mathcal{H}_t$ is such a term, but also the interaction Hamiltonian $\mathcal{H}_{U,\text{nn}}$ contains single-particle transition terms of this type, which we denote by $\mathcal{H}^J_{U,\text{nn}}$. For each fixed set of nearest neighbor sites i and j there are four relevant terms for this process and thus the total single-particle hopping Hamiltonian originating from the interaction term is

$$\begin{aligned}\mathcal{H}^J_{U,\text{nn}} = \sum_{\langle i,j\rangle} \sum_{\alpha_1,\alpha_2,\alpha_3,\alpha_4} [&U^{(i,i,i,j)}_{\alpha_1,\alpha_2,\alpha_3,\alpha_4}\, a^\dagger_{i,\alpha_1} a^\dagger_{i,\alpha_2} a_{i,\alpha_3} a_{j,\alpha_4} \\ &+U^{(i,j,j,j)}_{\alpha_1,\alpha_2,\alpha_3,\alpha_4}\, a^\dagger_{i,\alpha_1} a^\dagger_{j,\alpha_2} a_{j,\alpha_3} a_{j,\alpha_4}] + \text{h.c.}\end{aligned} \tag{4.30}$$

Note that in contrast to $\mathcal{H}_t$, which is diagonal in the band index, $\mathcal{H}^J_{U,\text{nn}}$ couples Wannier states in different bands on neighboring sites.

The single-particle tunneling $\mathcal{H}_J$ can also directly be written in terms of b-operators, giving rise to multiparticle induced single-particle tunneling

$$\begin{aligned}\mathcal{H}_J &= \mathcal{P}_{\text{lowE}} \mathcal{H}_t \mathcal{P}_{\text{lowE}} + \mathcal{H}^J_{U,\text{nn}} \\ &= \sum_{m_1,m_2=1}^{\infty} M_{m_1,m_2} \sum_{\langle i,j\rangle} [(b^\dagger_i)^{m_1} (b_i)^{m_1-1} (b^\dagger_j)^{m_2-1} (b_j)^{m_2}] + \text{h.c.}\end{aligned} \tag{4.31}$$

with the (m_1, m_2)-particle-induced tunneling amplitude

$$\begin{aligned}M_{m_1,m_2} = \sum_\alpha t^{(\alpha)} h^{(m_1)^*}_\alpha h^{(m_2)}_\alpha + \sum_{\alpha_1,\alpha_2,\alpha_3,\alpha_4} \Big[&U^{(i,i,i,j)}_{\alpha_1,\alpha_2,\alpha_3,\alpha_4} \\ &\times h^{(m_1-1)^*}_{(\alpha_3)(\alpha_2\alpha_1)} h^{(m_2)}_{\alpha_4} + U^{(i,j,j,j)}_{\alpha_1,\alpha_2,\alpha_3,\alpha_4} h^{(m_2-1)}_{(\alpha_2)(\alpha_3\alpha_4)} h^{(m_1)^*}_{\alpha_1} \Big],\end{aligned} \tag{4.32}$$

shown in Fig. (4.4) A and D. For $m_1 = m_2 = 1$ Eq. (4.31) is simply a usual single-particle tunneling term, containing all multi-orbital contributions in $\mathcal{H}_t$, but no contribution from $\mathcal{H}^J_{U,\text{nn}}$, since $h^{(m_2)}_{(\alpha_1)(\alpha_2\alpha_3)}$ vanishes for any $m_2 < 1$. However, there are also additional **multibody-induced** single-particle tunneling terms present: for $m_2 > 1$ or $m_1 > 1$ a single particle can tunnel between neighboring lattice sites with an amplitude M_{m_1,m_2} if $m_2 - 1$ and $m_1 - 1$ **additional** particles (additional to the one tunneling) are present on the lattice sites. We therefore refer to these processes as being multibody-induced.

4.5.2 Two-particle correlated hopping

In contrast to the non-interacting lattice Hamiltonian, the interaction term $\mathcal{H}_{U,\mathrm{nn}}$ also contains two-particle correlated tunneling transition elements in the term $\mathcal{H}^I_{U,\mathrm{nn}}$. A single application of such a term to the state $|\psi_0^{(n_i)}\rangle_i|\psi_0^{(n_j)}\rangle_j$ leads to a correlated tunneling of two particles on neighboring sites i and j, leading to states of the form $|\psi_0^{(n_i+2)}\rangle_i|\psi_0^{(n_j-2)}\rangle_j$. Clearly such operator terms are beyond the standard Bose-Hubbard model and cannot be contained in a renormalized tunneling parameter. They may however lead to interesting effects and we additionally include them in an extended description of the interacting lattice model.

$$\begin{aligned}\mathcal{H}^I_{U,\mathrm{nn}} = \sum_{m_1,m_2=1}^{\infty} R_{m_1,m_2} \sum_{\langle i,j\rangle} [(b_i^\dagger)^{m_1+1}(b_i)^{m_1-1} \\ \times (b_j^\dagger)^{m_2-1}(b_j)^{m_2+1}] + \mathrm{h.c.}\end{aligned} \tag{4.33}$$

with the (m_1, m_2)-particle-induced two-particle tunneling amplitude

$$R_{m_1,m_2} = \sum_{\alpha_1,\alpha_2,\alpha_3,\alpha_4} U^{(i,i,j,j)}_{\alpha_1,\alpha_2,\alpha_3,\alpha_4} h^{(m_1)^*}_{\alpha_1,\alpha_2} h^{(m_2)}_{\alpha_3,\alpha_4}. \tag{4.34}$$

The lowest order processes are shown as a function of the lattice depth s and interaction strength g in Fig. (4.4) B and E. The magnitude of these amplitudes decrease with increasing order (m_1, m_2) of the processes. At large s however, the two-particle tunneling amplitudes decay much slower than the bare single-particle tunneling J, such that these processes become relevant on this nearest neighbor energy scale.

4.5.3 Nearest neighbor interactions

Counting terms corresponding to nearest neighbor interactions in the total nearest neighboring part of the Hamiltonian $\sum_{\alpha_1,\alpha_2,\alpha_3,\alpha_4} U^{(i_1,i_2,i_3,i_4)}_{\alpha_1,\alpha_2,\alpha_3,\alpha_4} a^\dagger_{i_1,\alpha_1} a^\dagger_{i_2,\alpha_2} a_{i_3,\alpha_3} a_{i_4,\alpha_4}$ with all i_m being one of two nearest neighbor sites i and j, there are four terms corresponding to nearest neighbor interactions. These are all equivalent and after permuting indices the full nearest neighbor interaction Hamiltonian can be written in the form

$$\begin{aligned}\mathcal{H}^{int}_{U,\mathrm{nn}} &= 4 \sum_{\langle i,j\rangle} \sum_{\alpha_1,\alpha_2,\alpha_3,\alpha_4} U^{(i,i,j,j)}_{\alpha_1,\alpha_2,\alpha_3,\alpha_4} \\ &\times \mathcal{P}_{\mathrm{lowE}}\, a^\dagger_{i,\alpha_1} a_{i,\alpha_2} a^\dagger_{j,\alpha_3} a_{j,\alpha_4} \mathcal{P}_{\mathrm{lowE}} \\ &= \sum_{m_1,m_2=1}^{\infty} \sum_{\langle i,j\rangle} W_{m_1,m_2}\, (b_i^\dagger)^{m_1}(b_i)^{m_1}(b_j^\dagger)^{m_2}(b_j)^{m_2},\end{aligned} \tag{4.35}$$

where the last line is in the effective multibody nearest neighbor interaction picture with the parameters

$$W_{m_1,m_2} = 4 \sum_{\alpha_1,\alpha_2,\alpha_3,\alpha_4} U^{(i,i,j,j)}_{\alpha_1,\alpha_2,\alpha_3,\alpha_4} h^{(m_1)}_{(\alpha_1)(\alpha_2)}\, h^{(m_2)}_{(\alpha_3)(\alpha_4)}. \tag{4.36}$$

These are shown in Fig. (4.4 C and F). Note that in contrast to the tunneling Hamiltonians, Eq. (4.35) does not contain the addition of the Hermitian conjugate, since this is equivalent to the respective process itself and leads to a factor of 2.

4.5.4 On-site terms

After diagonalization, we explicitly have the Hamiltonian containing all local terms in diagonal form

$$\mathcal{P}_{\mathrm{lowE}} \mathcal{H}_{\mathrm{loc}} \mathcal{P}_{\mathrm{lowE}} = \sum_i \sum_n E_0^{(n)} |\psi_0^{(n)}\rangle_{ii} \langle\psi_0^{(n)}|. \tag{4.37}$$

In the density-induced picture containing effective higher order interaction terms, we seek a representation in terms of the b operators. Since by construction this is diagonal in the lowest dressed band basis, it can be written as a series of local terms, each containing the same number of creation and annihilation operators

$$\mathcal{P}_{\mathrm{lowE}}\mathcal{H}_{U,\mathrm{loc}}\mathcal{P}_{\mathrm{lowE}} = \sum_i (\epsilon^{(0)} - \mu) b_i^\dagger b_i + \sum_i \sum_{m=2}^{\infty} \frac{V_m}{m!} (b_i^\dagger)^m (b_i)^m. \tag{4.38}$$

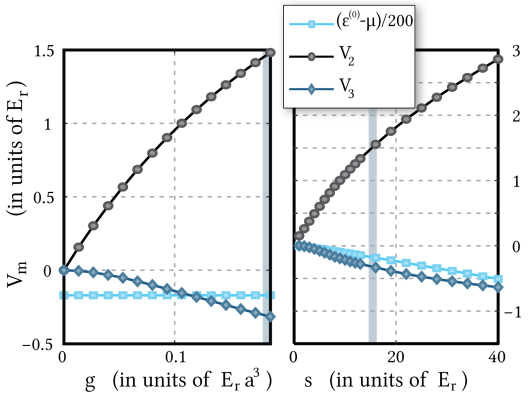

Figure 4.5: The density-induced local parameters as a function of the interaction strength g at constant $s = 15E_r$ (left) and as a function of the lattice depth s at constant $g = 5g_{vac}$ (right). The single particle term $(\epsilon^{(0)} - \mu)$ coupling to the local density operator is not invariant under a single particle energy shift. All higher order terms V_m with $m \geq 2$ are invariant under such a transformation. The two gray shaded areas correspond to the respective region of the other plot.

The first term is the single particle contribution and contains the energy offset of every particle due to the on-site Wannier energy and the chemical potential. It only contains the single particle lowest band energy, since for the case of a single local particle, interactions do not play a role and the local state $|\psi_0^{(n=1)}\rangle_i$ is simply the lowest band Wannier state. Letting the two equations (4.38) and (4.37) act on the local low energy basis states $|\psi_0^{(n)}\rangle_i$ for all integer n leads to the expression of the higher order interaction amplitudes in terms of on-site many-particle eigenenergies

$$V_m = m! \sum_{n=1}^{\infty} (\mathcal{B}^{-1})_{m,n} \frac{E_0^{(n)}}{n}. \tag{4.39}$$

These terms are exactly the effective many-body interactions introduced in [84] and experimentally observed in [172]. They gain significance with both increasing lattice depth s and interaction strength g, as shown in Fig. (4.5).

4.6 Density-dependent parameter formulation of the Bose-Hubbard model

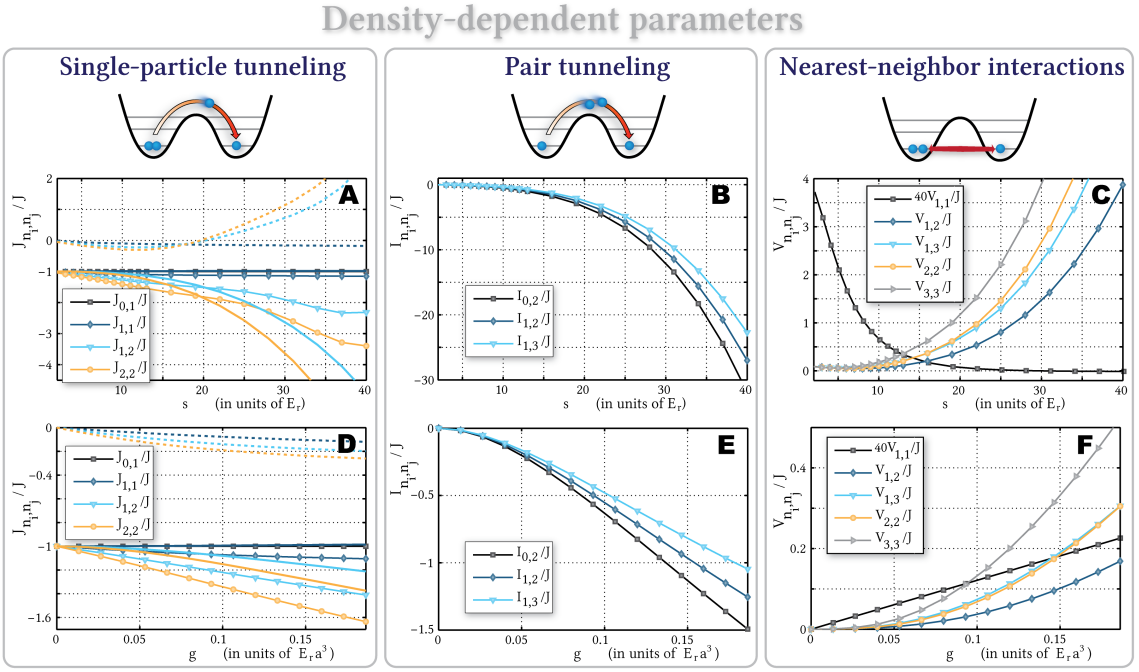

Figure 4.6: Density-dependent parameters in the lowest dressed band as a function of the lattice depth s at fixed $g = 5g_{vac}$ (upper subfigures A,B,C) and as a function of the interaction strength g at fixed $s = 15E_r$ (lower subfigures D,E,F). For the single-particle tunneling terms (subplots A and D) the solid lines indicate the contribution from the multi-orbital single particle lattice Hamiltonian, whereas the dashed lines are the contributions from the interacting Hamiltonian $\mathcal{H}_{\text{int}}$ respectively. The relevant energy scale for nearest neighbor processes is set by the bare single particle tunneling $J = -J_{0,1}$ by which we scale all other quantities in this figure. Note that for strong lattice depths the two-particle tunneling amplitudes and nearest neighbor interaction energies, which are usually neglected, become relevant and can even dominate on the relevant energy scale J. In the non-interacting limit and approximately in the limit of shallow lattice depths, the single-particle tunneling amplitudes become density-independent and approach the single bare particle tunneling amplitude, whereas the pair tunneling amplitudes (subplots B and E) and nearest neighbor interaction energies (subplots C and F) vanish.

An alternative and equivalent description to the multibody induced picture is a formulation in terms of density-dependent parameters. In this picture, one performs a summation over all local occupation numbers and allows the matrix elements, which are coefficients of operators of the form $|\psi_0^{n_i}\rangle_{ii}\langle\psi_0^{n_i'}|$ to acquire a density dependence beyond the bosonic statistical factor. This picture is convenient to directly infer certain multiorbital effects, such as the observed energy peak positions in quantum phase revival spectroscopy experiments [172, 171]. However, the density-dependent representation is not always the most convenient approach for treating multiorbital effects with usual many-body methods. For instance, bosonization or even the site decoupling mean-field theory cannot be performed within this framework. The effective representation discussed in the previous section section (4.5), which does not require an external summation over all local occupation numbers is more favorable in this sense and has been successfully applied for the pure on-site terms in describing effective multibody interactions [84]. We show that, especially in the regime of deep lattices, the density-dependent parameters are strongly modified. Two-particle tunneling and nearest neighbor interaction processes, beyond the usual Bose-Hubbard model, become significant, even becoming an order of magnitude stronger than the bare single-particle hopping J in certain experimentally accessible regimes.

4.6.1 Single-particle tunneling term

We first seek the single-particle tunneling term in the Hamiltonian with a density-dependent tunneling parameter, i.e. of the form

$$\begin{aligned}\mathcal{H}_J = &\sum_{\langle i,j\rangle}\sum_{n_i,n_j} J_{n_i,n_j}\sqrt{n_i+1}\,|\psi_0^{(n_i+1)}\rangle_{ii}\langle\psi_0^{(n_i)}| \\ &\otimes\sqrt{n_j}\,|\psi_0^{(n_j-1)}\rangle_{jj}\langle\psi_0^{(n_j)}| + \text{h.c.}\end{aligned} \tag{4.40}$$

In a recent independent calculation by Lühmann et al. [107], similar results to the ones presented here were obtained for the density-dependent single-particle tunneling parameters within the fully correlated many-body framework. In this section we omit writing the unit operator on other sites for any local operator: i.e. any operator $A^{(i)}$ acting only on the local Fock space of site i is to be implicitly understood as being extended to the full lattice Fock space as $A^{(i)}\otimes\prod_{\otimes j\neq i}\mathbb{1}_j$. Each operator term in Eq. (4.40) can also be written with the use of local projectors $\mathcal{P}_n^{(i)} = |\psi_0^{(n)}\rangle_{ii}\langle\psi_0^{(n)}|$ on the n-particle ground state at site i as

$$\begin{aligned}&\sqrt{n_i+1}\,|\psi_0^{(n_i+1)}\rangle_{ii}\langle\psi_0^{(n_i)}|\otimes\sqrt{n_j}\,|\psi_0^{(n_j-1)}\rangle_{jj}\langle\psi_0^{(n_j)}| \\ &\qquad = b_i^\dagger\, b_j\,\mathcal{P}_{n_i}^{(i)}\mathcal{P}_{n_j}^{(j)}.\end{aligned} \tag{4.41}$$

The final summation over all occupation numbers n_i, n_j is however always necessary in this density-dependent parameter representation of any operator, alternatively an operator $\hat{J}_{n_i,n_j}$, diagonal in the local particle number operators $\hat{n}_i$ and containing the density-dependent coefficients, can be constructed.

To transform the total single-particle tunneling Hamiltonian $\mathcal{H}_J = \mathcal{H}_t + \mathcal{H}_{U,\text{nn}}^J$ to the density-dependent parameter form of Eq. (4.40), we insert the unit operator of the low-energy subspace on both the left and the right. For one given operator term, such as $\mathcal{A}_{i,j} = a_{i,\alpha_1}^\dagger a_{i,\alpha_2}^\dagger a_{i,\alpha_3} a_{j,\alpha_4}$, the expectation reduces to a product of expectation values at different sites

$$\begin{aligned}{}_i\langle\psi_0^{(n_i')}|_j\langle\psi_0^{(n_j')}|A_{i,j}|\psi_0^{(n_i)}\rangle_i|\psi_0^{(n_j)}\rangle_j &= \delta_{n_i',n_i+1}\delta_{n_j',n_j-1} \\ &\times\sqrt{n_j(n_i+1)}n_i\, f_{(\alpha_3)(\alpha_2,\alpha_1)}^{(n_i)^*} f_{\alpha_4}^{(n_j)},\end{aligned} \tag{4.42}$$

where the coefficients $f_{(\alpha_3)(\alpha_2,\alpha_1)}^{(n_i)^*}$ are defined in Eq. (4.18). On all other lattice sites different from i or j, $\mathcal{A}_{i,j}$ acts as the unit operator. The same procedure can be used for $\mathcal{H}_t$. We furthermore use the fact that for a time reversal symmetric system, all Wannier functions can be chosen purely real and the matrix element $U_{\alpha_1,\alpha_2,\alpha_3,\alpha_4}^{(i_1,i_2,i_3,i_4)}$ is invariant under the 24 possible permutations of index pairs (i_n,α_n). Together with the discrete translational symmetry we thus have $U_{\alpha_1,\alpha_2,\alpha_3,\alpha_4}^{(i,j,j,j)} = U_{\alpha_4,\alpha_2,\alpha_3,\alpha_1}^{(i,i,i,j)}$ and upon relabeling the summation indices $\alpha_1\leftrightarrow\alpha_4$ obtain the total density dependent single-particle tunneling parameter after collecting all terms of $\mathcal{H}_J$

$$\begin{aligned}J_{n_i,n_j} &= J_{n_i,n_j}^t + J_{n_i,n_j}^U \\ &= \sum_\alpha t^{(\alpha)} f_\alpha^{(n_j)} f_\alpha^{(n_i+1)^*} + \sum_{\alpha_1,\alpha_2,\alpha_3,\alpha_4} U_{\alpha_1,\alpha_2,\alpha_3,\alpha_4}^{(i,i,i,j)} \\ &\times\left[n_i\, f_{(\alpha_3)(\alpha_2,\alpha_1)}^{(n_i)^*} f_{\alpha_4}^{(n_j)} + (n_j-1) f_{(\alpha_2)(\alpha_3,\alpha_1)}^{(n_j-1)} f_{\alpha_4}^{(n_i+1)^*}\right].\end{aligned} \tag{4.43}$$

The first term contains all multi-orbital contributions from the single-particle lattice Hamiltonian, whereas the second term contains the nearest-neighbor couplings originating directly from the two-body interaction Hamiltonian $\mathcal{H}_{\text{int}}$, which are referred to as *non-linear tunneling* in [116] and *bond-charge tunneling* in [107]. The former are plotted as solid lines, whereas the latter are the dotted lines in Fig. (4.6) A and D. For moderate lattice depths $s\lesssim 17E_r$ both contributions J_{n_i,n_j}^t and J_{n_i,n_j}^U are negative in sign and favor a condensation in the $k=0$ mode. In contrast, at

larger lattice depths, the sign of the contribution from the interaction $J^U_{n_i,n_j}$ changes, favoring a condensation in the $k = \frac{\pi}{a}$ mode, competing with the $J^t_{n_i,n_j}$ processes. In the regime we considered, the single-particle multi-orbital terms outweigh the interaction terms for reasonably deep lattices. Compared to the bare single-particle tunneling amplitudes, the resulting effective single-particle tunneling is changed on the order of 60% for strong lattices. This effect is enhanced by using Feshbach resonances to adjust the scattering length a_s.

4.6.2 Two-particle correlated hopping

For a density-dependent representation of the two-particle tunneling parameter, they are represented by an additional term in the total Hamiltonian

$$\begin{aligned}\mathcal{H}^I_{U,\mathrm{nn}} = &\sum_{\langle i,j\rangle}\sum_{n_i,n_j} I_{n_i,n_j}\sqrt{(n_i+1)(n_i+2)}\,|\psi_0^{(n_i+2)}\rangle_{ii}\langle\psi_0^{(n_i)}| \\ &\otimes\sqrt{n_j(n_j-1)}\,|\psi_0^{(n_j-2)}\rangle_{jj}\langle\psi_0^{(n_j)}| + \mathrm{h.c.}\end{aligned} \tag{4.44}$$

The same procedure as described in section (4.5.1) can be used to obtain the density-dependent two-particle tunneling coefficients

$$I_{n_i,n_j} = \sum_{\alpha_1,\alpha_2,\alpha_3,\alpha_4} U^{(i,i,j,j)}_{\alpha_1,\alpha_2,\alpha_3,\alpha_4} f^{(n_i+1)^*}_{\alpha_1,\alpha_2} f^{(n_j-1)}_{\alpha_3,\alpha_4} \tag{4.45}$$

As shown in Fig. (4.6) B and E, the two-particle tunneling amplitudes are exponentially sensitive on the lattice depth s and can become very strong on the nearest neighbor energy scale, set by the single particle tunneling J, even exceeding this by an order of magnitude for the strongly interacting case $g = 5g_{vac}$ we considered. The density-dependent amplitude I_{n_i,n_j} furthermore increases with increasing occupation numbers and for reasonably strong interactions ($g \gtrsim 1.5g_{vac}$ for ^{87}Rb in a 738nm lattice) the dependence on the interaction strength g is approximately linear.

We point out that a transformation between the density-induced and density-dependent two-particle hopping amplitudes exists, which is of the form of a second order tensor with the $\mathcal{B}$ matrix defined in Eq. (4.22)

$$I_{n_i,n_j} = \sum_{m_1,m_2=1}^{\infty} \mathcal{B}_{n_1+1,m_1}\mathcal{B}_{n_2-1,m_2}R_{m_1,m_2} \tag{4.46}$$

$$R_{m_1,m_2} = \sum_{n_i=0,n_j=2}^{\infty} (\mathcal{B}^{-1})_{m_1,n_i+1}(\mathcal{B}^{-1})_{m_2,n_j-1}I_{n_i,n_j}. \tag{4.47}$$

4.6.3 Nearest neighbor interactions

The nearest neighbor interaction Hamiltonian in its density-dependent parameter representation reads

$$\mathcal{H}^{\mathrm{int}}_{U,\mathrm{nn}} = \sum_{\langle i,j\rangle}\sum_{n_i,n_j} V_{n_i,n_j}\, n_i\,|\psi_0^{(n_i)}\rangle_{ii}\langle\psi_0^{(n_i)}| \otimes n_j\,|\psi_0^{(n_j)}\rangle_{jj}\langle\psi_0^{(n_j)}| \tag{4.48}$$

with the coefficients

$$V_{n_i,n_j} = 4\sum_{\alpha_1,\alpha_2,\alpha_3,\alpha_4} U^{(i,i,j,j)}_{\alpha_1,\alpha_2,\alpha_3,\alpha_4} f^{(n_i)}_{(\alpha_1)(\alpha_2)} f^{(n_j)}_{(\alpha_3)(\alpha_4)} \tag{4.49}$$

Note that the coefficient $f^{(n)}_{(\alpha_1,\alpha_2)}$ in this case is exactly the local single-particle density matrix in the multi-orbital Wannier representation for the local many-particle ground state $|\psi_0^{(n)}\rangle$. The amplitudes V_{n_i,n_j} scaled by the bare single particle tunneling J depend exponentially on the lattice

depth s, as shown in Fig. (4.6 C). Note that while $V_{1,1}/J$ decreases with increasing s, higher order terms $V_{n_i,n_j}/J$ with $n_i, n_j > 1$ grow exponentially. These also become very strong and can become more relevant than the single particle hopping elements at large s, which is of relevance for processes in the Mott insulating regime. An analogous second order tensor transformation property as Eq. (4.46) applies to the nearest neighbor interaction amplitudes

$$V_{n_i,n_j} = \sum_{m_1,m_2=1}^{\infty} \mathcal{B}_{n_1,m_1}\mathcal{B}_{n_2,m_2}W_{m_1,m_2} \tag{4.50}$$

$$W_{m_1,m_2} = \sum_{n_i,n_j=1}^{\infty} (\mathcal{B}^{-1})_{m_1,n_i}(\mathcal{B}^{-1})_{m_2,n_j}V_{n_i,n_j}. \tag{4.51}$$

4.6.4 On-site energies

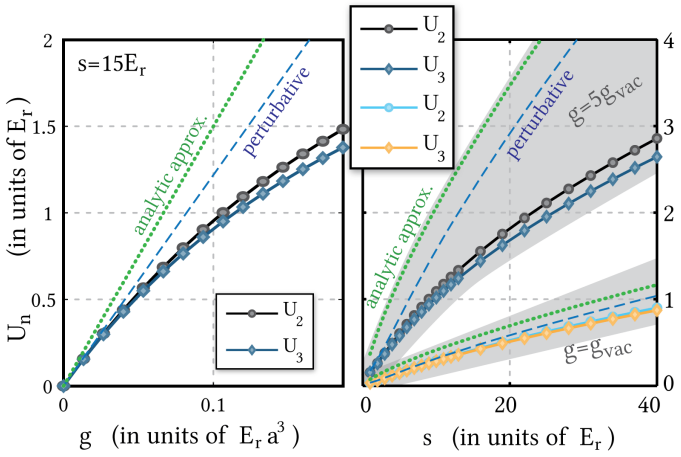

Figure 4.7: The density-dependent local parameters as a function of the interaction strength g at constant $s = 15E_r$ (left) and as a function of the lattice depth s at two fixed values of the interaction strength $g = g_{\text{vac}}$ and $g = 5g_{\text{vac}}$. Shown as green dotted lines is the analytic approximation $U = \sqrt{8\pi}\frac{a_s}{a}(s/E_r)^{3/4}E_r$. The perturbative result from a single particle band structure calculation is shown as blue dashed lines.

The exact diagonalization procedure yields the Hamiltonian containing all on-site terms in the form

$$\mathcal{P}_{\text{lowE}}\mathcal{H}_{\text{loc}}\mathcal{P}_{\text{lowE}} = \sum_i \sum_n E_0^{(n)}|\psi_0^{(n)}\rangle_{ii}\langle\psi_0^{(n)}| \tag{4.52}$$

with the n-particle ground state energies $E_0^{(n)}$ being the numerically found lowest eigenvalues. Within a Bose-Hubbard formulation of the same Hamiltonian with density-dependent interaction parameters U_n, each on-site term of this Hamiltonian is to be expressed in the form

$$\mathcal{P}_{\text{lowE}}\mathcal{H}_{\text{loc}}^{(i)}\mathcal{P}_{\text{lowE}} = \sum_n(\epsilon^{(0)} - \mu)n|\psi_0^{(n)}\rangle_{ii}\langle\psi_0^{(n)}| + \sum_n \frac{U_n}{2}n(n-1)|\psi_0^{(n)}\rangle_{ii}\langle\psi_0^{(n)}| \tag{4.53}$$

and is of course identical to the single particle energy formally obtained from the many-particle diagonalization

$$E_0^{(1)} = \epsilon^{(0)} - \mu. \tag{4.54}$$

Since for $n = 1$ interactions do not play a role and the particle is in the lowest Wannier orbital only, thus only the lowest band single particle energy $\epsilon^{(0)}$ contributes. Subtracting the single particle energy shift for higher occupations $n > 1$, the density-dependent interaction parameter is found to be

$$U_n = 2\frac{E_0^{(n)} - (\epsilon^{(0)} - \mu)n}{n(n-1)}. \tag{4.55}$$

In the limit of very weak interactions (compared to the single particle hopping energy), where the interaction can be treated perturbatively, the parameters U_n become independent of the local density n and all coincide with the usual interaction energy U, as shown in Fig. (4.7).

4.7 Correlations vs. Orbital Deformation

We demonstrate now that the deformation of single-particle orbitals by the interactions is not the main effect to lower the local on-site energy. The higher order correlations, which cannot be understood as such a deformation, are the dominant effect to lower the energy. Therefore, a single-particle picture and wave functions are not sufficient for understanding the effect of interactions on the local level, since entanglement becomes important. This can best be seen in the two-particle correlation function in Fig. (4.9).

Given the state $|\psi_0^{(n)}\rangle_i$, the local single-particle density matrix is Hermitian and can thus be expressed in terms of its orthogonal eigenvectors (corresponding to single-particle states in the respective basis) $\phi_\alpha^{(l)}$ and the corresponding real, positive eigenvalues λ_l

$$\begin{aligned}\rho_{\alpha,\alpha'} &= \langle\psi_0^{(n)}|a_{i,\alpha}^\dagger a_{i,\alpha'}|\psi_0^{(n)}\rangle \\ &= \sum_l \lambda_l\, \phi_\alpha^{(l)}\, \phi_{\alpha'}^{(l)*}.\end{aligned} \tag{4.56}$$

The eigenvalues λ_l and the associated single-particle states do of course not depend on the basis in which the single-particle density matrix is evaluated in.

We can now construct an artificial state

$$|\psi_{uc}\rangle = \sum_l \sqrt{\frac{\lambda_l}{n}}\,\frac{1}{\sqrt{n!}}(d_l^\dagger)^n\,|0\rangle \tag{4.57}$$

for comparison, which leads to the identical single-particle density matrix, but does not contain the higher order correlations.

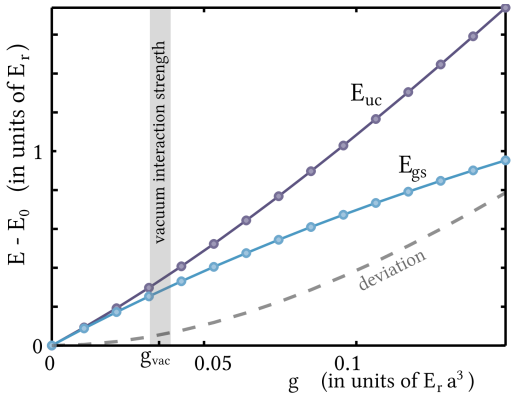

Figure 4.8: Comparison of the true many-body local ground state energy E_{gs} and the energy E_{uc} of the artificially created state $|\psi_{uc}\rangle$ of Eq. (4.57) with the same single-particle density matrix (i.e. the same broadened orbitals and their occupation), but no higher order correlations. The deviation between the two becomes very significant with increasing interaction strength and is well in the experimentally observable regime (here for $s = 10$, but the effect becomes stronger with increasing lattice depth), showing that the usual simple picture of broadened single-particle orbitals is insufficient to explain the effects of interactions on the local many-body state.

Here we defined the creation operators for the eigenstates of the single-particle density matrix $d_l^\dagger = \sum_\alpha \phi_\alpha^{(l)} a_{i,\alpha}^\dagger$. The state in Eq. (4.57) can be thought of as having the identical single-particle

properties as the true local ground state, and would be the most natural many-particle state for thinking in terms of spatially broadened single-particle orbitals due to the interactions, as commonly referred to in literature [172]. It does however not contain the same higher order correlations as the original state, for instance the two-particle correlation function $G^{(2)}_{l,l'} = \langle\psi_{uc}|d_l^\dagger\, d_{l'}^\dagger d_{l'} d_l\,|\psi_{uc}\rangle = \lambda_l\,\delta_{l,l'}$ for $n = 2$ particles or more. In Fig. (4.8) the energy expectation value of the uncorrelated state $E_{uc} = \langle\psi_{uc}|\mathcal{H}|\psi_{uc}\rangle$ is compared to the true ground state energy as a function of the interaction strength g. Since the above constructed state $|\psi_{uc}\rangle$ becomes the true ground state in the non-interacting limit, the energies agree in this limit. However, significant deviations arise at finite interaction strengths g, indicating that the simple picture of spatially broadened single-particle orbitals cannot explain the main energy reduction mechanism.

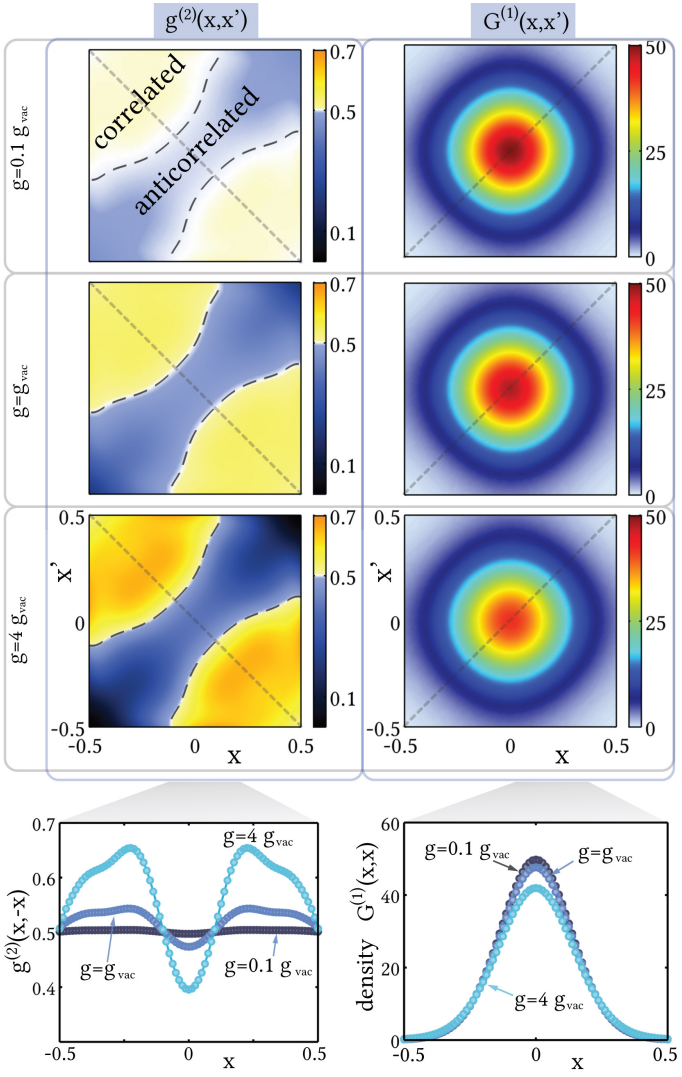

Figure 4.9: Correlation functions $g^{(2)}(x, x')$ (left column) and single-particle density matrix $G^{(1)}(x, x') = \langle\Psi^\dagger(x)\Psi(x')\rangle$ (right column) in real space at $y = y' = z = z' = 0$ for a single site in units of the lattice constant a. Results are shown for $n = 2$ ^{87}Rb atoms in a 768nm $s = 10E_r$ lattice for three different interaction strengths, up to four times the vacuum interaction strength g_{vac}. The lower graphs are cuts along the dotted lines in the plots above. With increasing interaction strength, the atoms mutually avoid each other, as can be seen in the decrease of $g^{(2)}(x, x)$ along the diagonal ($x = x'$) and an increase for $|x - x'| \gtrapprox 0.2$, as compared to the non-interacting case where $g^{(2)}(x, x') = 0.5$ for $n = 2$. The effect on the density distribution along one direction is significantly weaker, with the main effect being a reduction of density at the center of the lattice site.

The significant change of the on-site many-body state lies in the higher order correlation functions, with particles mutually reducing their spatial overlap. It is not contained in and cannot be understood on single-particle level (since all single-particle properties of the local state are contained in $\rho^{(i)}_{\alpha,\alpha}$). To substantiate this point, we calculated the normalized second-order correlation function

$$g^{(2)}(\mathbf{r},\mathbf{r}') = \frac{\langle\psi|\Psi^\dagger(\mathbf{r})\,\Psi^\dagger(\mathbf{r}')\,\Psi(\mathbf{r}')\,\Psi(\mathbf{r})|\psi\rangle}{(\langle\psi|\Psi^\dagger(\mathbf{r})\,\Psi(\mathbf{r})|\psi\rangle)(\langle\psi|\Psi^\dagger(\mathbf{r}')\,\Psi(\mathbf{r}')|\psi\rangle)} \tag{4.58}$$

for a local interacting two-particle ground state $|\psi_0^{(2)}\rangle$, shown in Fig. (4.9). The normalized second order correlation function can be understood as a conditional probability: for the non-interacting state $|n=2\rangle$ we have $g^{(2)}(\mathbf{r},\mathbf{r}') = 1 - \frac{1}{n} = \frac{1}{2}$, which is our reference and which we refer to as uncorrelated by interactions. A value of $g^{(2)}(\mathbf{r},\mathbf{r}') < \frac{1}{2}$ indicates a reduced probability for a particle to be found at location $\mathbf{r}'$ if another particle is located at $\mathbf{r}$ or vice versa and is therefore anticorrelated in this sense. This anticorrelation can be seen along the diagonal line $x = x'$ in Fig. (4.9), where two repulsively interacting atoms have a reduced probability to be found at the same spatial position $x = x'$. Since all particles are restricted to occupy Wannier orbitals at the same site, the conditional probability $g^{(2)}(\mathbf{r},\mathbf{r}')$ has to be increased elsewhere, i.e. correlated. With increasing interactions, the specific shape of $g^{(2)}(\mathbf{r},\mathbf{r}')$ is independent of the interaction strength g in this regime in the sense that the deviation from the uncorrelated case scales linearly with g. This can clearly be seen by comparing the different functions in the left column of Fig. (4.9). In contrast, the density profile shown in the right column is only slightly changed by the interactions. The main effect is a reduction of the maximal density at the center of the lattice site, whereas only a minimal broadening of the density profile is visible.

4.8 Conclusions

We have formulated a systematic derivation of an effective low-energy, single-band basis for ultracold bosonic atoms in optical lattices in the presence of interactions. Some properties intrinsic to our formalism, such as density-dependent interaction parameters or the appearance of effective multibody interactions have been previously discussed and experimentally confirmed. We introduce ladder operators fulfilling bosonic commutation relations within the new dressed band basis, which are shown to be the bosonic operators used within an effective Bose-Hubbard model for the system. It is however shown that these are not the original lowest band Wannier creation and annihilation operators beyond lowest order and we derive a simple prescription for the transformation of arbitrary operators into the new low-energy dressed band basis. These transformations are used to systematically treat all terms in the interacting lattice Hamiltonian and give rise to multibody-induced single and pair particle tunneling, as well as multibody local and nearest neighbor interactions. The amplitudes for these processes are calculated and compared to renormalized parameters in the density-dependent representation of the Bose-Hubbard model. The latter formulation, although fully equivalent, is however less favorable for the treatment with a number of common theoretical methods, since it contains an external summation over the set of all n-particle states at each lattice site. We furthermore show that the commonly used single-particle picture of spatially broadened Wannier orbitals cannot describe the observed energy reduction of the local many-body state. The relevant mechanism is mutual avoidance of the various atoms at a given lattice site, which is a many-particle effect contained only in the higher order correlation functions.

5. Honeycomb Optical Lattices

We now come to the problem of determining the Wannier states in a non-separable lattice potential in dimensions higher than one. For the general case, where a lattice unit cell may contain more than a single potential minimum, it is no longer possible to find a simple, general prescription for choosing the complex phases of the Bloch states, such that the maximally localized Wannier states result from a direct discrete Fourier transform of these. In solid state systems, intricate approaches to numerically minimize the spatial variance have been devised [113, 112, 111].

We propose a completely different approach: In this chapter we show that the method of diagonalizing the position operator projected onto a specific set of bands (introduced for the one-dimensional case in section (2.5)), can be extended to treat higher-dimensional, non-separable lattices. We explicitly demonstrate it for the specific case of a optical honeycomb potential, which was recently experimentally realized in the Esslinger group [162].

This approach is numerically highly efficient, requiring only a few seconds of computation time on a current commercially available notebook. Furthermore, it does not suffer under numerical complications, such as getting stuck in local minima, which has been reported to occur when numerically minimizing the spatial variance in certain parameter regimes. Furthermore it may directly be used to determine the maximally localized Wannier states in any given (set of) bands.

5.1 The ETH Honeycomb Lattice Potential

In general, the 2D part is not separable with respect to the individual dimensions. The third part, if this is present, is separable. In real space, the 2D part takes on the form

$$V(x,y) = -V_{\bar{x}}\cos^2(k_l x + \frac{\theta}{2}) - V_x\cos^2(k_l x) - V_y\cos^2(k_l y) - 2\alpha_{\text{lat}}\sqrt{V_x V_y}\cos(\varphi_{\text{lat}})\cos(k_l x)\cos(k_l y) \tag{5.1}$$

with the lattice momentum $k_L = \lambda_L/(2\pi)$. The real-space lattice vectors are orthogonal

$$\begin{aligned}\mathbf{a}_1 &= \frac{\lambda_L}{2}(\mathbf{e}_x + \mathbf{e}_y)\\ \mathbf{a}_2 &= \frac{\lambda_L}{2}(\mathbf{e}_x - \mathbf{e}_y),\end{aligned} \tag{5.2}$$

and are thus parallel to the reciprocal lattice vectors

$$\begin{aligned}\mathbf{b}_1 &= k_L(\mathbf{e}_x + \mathbf{e}_y)\\ \mathbf{b}_2 &= k_L(\mathbf{e}_x - \mathbf{e}_y).\end{aligned} \tag{5.3}$$

the spatial potential for a typical choice of parameters is shown in Fig. (5.1).

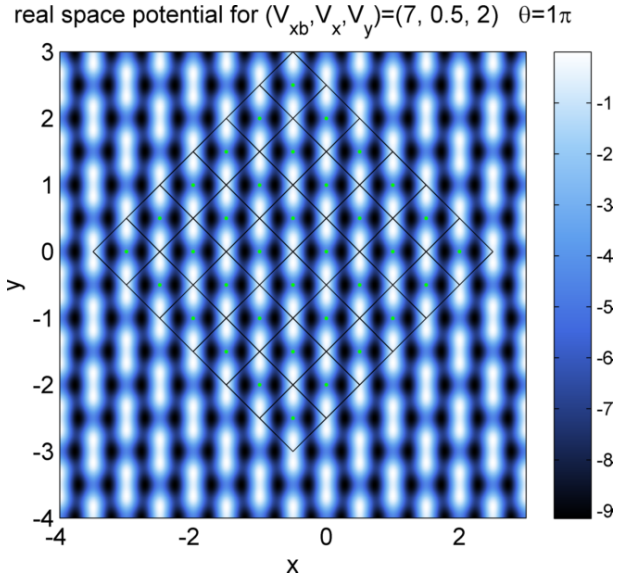

Figure 5.1: Real-space potential in the honeycomb regime.

With the potential being fully periodic in real-space, it can be written as a discrete Fourier sum

$$V(x,y) = \sum_{\mathbf{K}} V_{\mathbf{K}}\, e^{i\mathbf{K}\cdot\mathbf{r}} = \sum_{n_1,n_2} V_{n_1,n_2}\, e^{i(n_1\,\mathbf{b}_1 + n_2\,\mathbf{b}_2)\cdot\mathbf{r}} \tag{5.4}$$

with $\mathbf{K} = n_1\,\mathbf{b}_1 + n_2\,\mathbf{b}_2$ running over the infinite set of reciprocal lattice vectors. This is equivalent to (n_1, n_2) taking on all possible integer values. For smooth spatial potentials the Fourier coefficients decay exponentially in $|n_1|$ and $|n_2|$ leading to the low energy eigenstates also having an exponentially decaying amplitude in $|n_1|$ and $|n_2|$. Within a numerical implementation, this allows for a simple truncation to a restricted set of (n_1, n_2) with a well-controlled error.

Writing the specific lattice 5.1 above in terms of complex exponentials, one sees that only a finite number of Fourier coefficients are non-zero

$$\begin{aligned}
V_{0,0} &= -\frac{1}{2}(V_{\overline{x}} + V_x + V_y) \\
V_{1,1} &= -\frac{1}{4}(V_x + e^{i\theta} V_{\overline{x}}) \\
V_{-1,-1} &= -\frac{1}{4}(V_x + e^{-i\theta} V_{\overline{x}}) \\
V_{1,-1} &= -\frac{V_y}{4} \\
V_{-1,1} &= -\frac{V_y}{4} \\
V_{1,0} = V_{-1,0} = V_{0,1} = V_{0,-1} &= -\frac{\alpha_{\text{lat}}}{2}\sqrt{V_x V_y}\cos(\varphi_{\text{lat}}).
\end{aligned} \tag{5.5}$$

All other coefficients vanish identically for the homogeneous lattice.

5.2 Band Structure & Bloch States

In consequence of the discrete translational invariance and Bloch's theorem, the real-space representation of the Bloch states can be written as

$$\psi_{\mathbf{k},\alpha}(\mathbf{r}) = e^{i\mathbf{k}\cdot\mathbf{r}}\, u_{\mathbf{k},\alpha}(\mathbf{r}) \tag{5.6}$$

where $u_{\mathbf{k},\alpha}(\mathbf{r})$ are functions with the full lattice periodicity and hence of the spectrally decomposed form

$$u_{\mathbf{k},\alpha}(\mathbf{r}) = \sum_{n_1,n_2} c^{(\mathbf{k},\alpha)}_{n_1,n_2}\; e^{i(n_1\,\mathbf{b}_1+n_2\,\mathbf{b}_2)\cdot\mathbf{r}}. \tag{5.7}$$

By definition, the Bloch functions are the exact single particle eigenstates of the single-particle lattice Hamiltonian. Inserting Eq. (5.6) into the Schrödinger equation

$$\left[-\frac{\hbar^2}{2m}\Delta \;+\; V(x,y)\right]\psi_{(\mathbf{k},\alpha)} = E_{\mathbf{k},\alpha}\;\psi_{(\mathbf{k},\alpha)} \tag{5.8}$$

leads to an effective Schrödinger equation for the u-states. Expressed in the basis of physical momentum states, this renders the eigenvalue equation

$$E_r\left[\mathbf{k}/k_L + n_1\mathbf{b}_1/k_L + n_2\mathbf{b}_2/k_L\right]^2 c^{(\mathbf{k},\alpha)}_{n_1,n_2} \;+\; \sum_{n_1',n_2'} V_{n_1-n_1',n_2-n_2'}\; c^{(\mathbf{k},\alpha)}_{n_1',n_2'} = E_{\mathbf{k},\alpha}\; c^{(\mathbf{k},\alpha)}_{n_1,n_2} \tag{5.9}$$

and we see that the vectors $c^{(\mathbf{k},\alpha)}_{n_1,n_2}$ are exactly the eigenvectors of the effective Hamiltonian matrix expressed in this basis. The set $(\mathbf{k},\alpha)$ labels the eigenvector corresponding to the eigenvalue $E_{\mathbf{k},\alpha}$, whereas the set of indices (n_1,n_2) specifies the position of the element within the respective eigenvector, i.e. the row index.

Note that we will use the normalization convention, where each eigenvector is normalized with respect to the canonical norm

$$\sum_{n_1,n_2} |c^{(\mathbf{k},\alpha)}_{n_1,n_2}|^2 = 1, \tag{5.10}$$

which however implies that the Bloch (and u) functions are not normalized to unity when integrated over the entire real-space lattice, but over the unity cell.

$$\int_{\text{unit cell}} d^2r\; |\psi_{\mathbf{k},\alpha}(\mathbf{r})|^2 = \int_{\text{unit cell}} d^2r\; |u_{\mathbf{k},\alpha}(\mathbf{r})|^2 = 1 \tag{5.11}$$

Since the reciprocal lattice vectors are orthogonal and of equal length, the first Brillouin zone is of square form - a property which holds throughout the regime of arbitrary system parameters $(V_{\overline{x}}, V_x, V_y, \alpha_{\text{lat}}, \theta, \varphi_{\text{lat}})$.

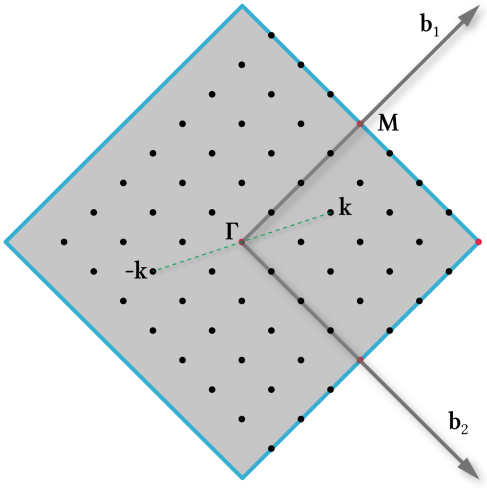

Figure 5.2: The first Brillouin zone for a 8×8 lattice. The dots indicate the possible quasi-momentum values.

5.3 Wannier States

We define the real-space coordinate operators along the direction of $\mathbf{b}_1$ and $\mathbf{b}_2$

$$\hat{r}_1 = \mathbf{b}_1 \cdot \begin{pmatrix} \hat{x} \\ \hat{y} \end{pmatrix} = k_L(\hat{x} + \hat{y}) \tag{5.12}$$

$$\hat{r}_2 = \mathbf{b}_2 \cdot \begin{pmatrix} \hat{x} \\ \hat{y} \end{pmatrix} = k_L(\hat{x} - \hat{y}), \tag{5.13}$$

which are dimensionless by construction. Clearly, they commute in this form

$$[\hat{r}_1, \hat{r}_2] = 0, \tag{5.14}$$

which is however no longer necessarily true once we project them onto the subspace of the lowest two bands. We define the projected operators in the basis of normalized Bloch states

$$R_j = \sum_{\mathbf{k},\mathbf{k}',\alpha,\alpha'} \overline{\langle \mathbf{k},\alpha|} \hat{r}_j \overline{|\mathbf{k}',\alpha'\rangle} \quad \overline{|\mathbf{k},\alpha\rangle}\,\overline{\langle \mathbf{k}',\alpha'|} \tag{5.15}$$

5.3.1 Evaluation of the real-space coordinate operator matrix elements

Once the Bloch states and their real-space representation have been determined numerically, all matrix elements can be calculated by numerical integration over the entire real-space lattice. However, the integration can also be performed analytically and the matrix elements can be transformed into a compact form, containing only a summation over elements of the various eigenvectors $c^{(\mathbf{k},\alpha)}_{n_1,n_2}$, as shown in the following.

Using the real-space representation of a Bloch state

$$\psi_{\mathbf{k},\alpha}(\mathbf{r}) = \langle \mathbf{r}|\mathbf{k},\alpha\rangle = e^{i\phi_{\mathbf{k},\alpha}}\, e^{i\mathbf{k}\cdot\mathbf{r}} \sum_{n_1,n_2} c^{(\mathbf{k},\alpha)}_{n_1,n_2}\, e^{i(n_1\,\mathbf{b}_1 + n_2\,\mathbf{b}_2)\cdot\mathbf{r}} \tag{5.16}$$

we can evaluate the matrix element (the '$\pm$' refers to operators R_1 and R_2 respectively and 'r.s.l.' to the region of the entire *real-space lattice*). Furthermore, we parametrize the allowed vectorial quasi-momenta by

$$\mathbf{k} = \frac{m_1}{L}\mathbf{b}_1 + \frac{m_2}{L}\mathbf{b}_2, \tag{5.17}$$

where (m_1, m_2) are integer values chosen such that the corresponding $\mathbf{k}$ always lies within the first Brillouin zone. Consequently, a single Bloch state is uniquely defined by the three indices (m_1, m_2, α), which are mapped onto a single collective index $I(m_1, m_2, \alpha)$ by the indexing function I.

$$\begin{aligned} R^{(1,2)}_{I(m_1,m_2,\alpha),I(m_1',m_2',\alpha')} &= \overline{\langle \mathbf{k},\alpha|} k_L(\hat{x}+\hat{y}) \overline{|\mathbf{k}',\alpha'\rangle} \\ &= A^2 k_L \int_{\text{r.s.l.}} d^2r\; e^{-i(\phi_{\mathbf{k},\alpha} - \phi_{\mathbf{k}',\alpha'})} \sum_{\substack{n_1,n_2 \\ n_1',n_2'}} {c^{(\mathbf{k},\alpha)}_{n_1,n_2}}^*\; c^{(\mathbf{k}',\alpha')}_{n_1',n_2'} \\ &\quad \times e^{-i(n_1\,\mathbf{b}_1 + n_2\,\mathbf{b}_2 + \mathbf{k})\cdot\mathbf{r}}\, e^{i(n_1'\,\mathbf{b}_1 + n_2'\,\mathbf{b}_2 + \mathbf{k}')\cdot\mathbf{r}}\; (x \pm y) \end{aligned} \tag{5.18}$$

To perform the two-dimensional integration, we parametrize the position vector

$$\mathbf{r}(\lambda_1, \lambda_2) = \mathbf{r}_0 + \lambda_1\mathbf{a}_1 + \lambda_2\mathbf{a}_2. \tag{5.19}$$

The vector $\mathbf{r}_0 = -m_0(\mathbf{a}_1 + \mathbf{a}_2)$ with $m_0 = \lceil \frac{L-1}{2} \rceil + \frac{1}{2}$ is the outermost left corner of the integration area and the whole area is covered when both the dimensionless parameters run in the interval $\lambda_{1,2} \in [0, L]$.

To perform the integration, the Jacobian for the correct measure has to furthermore be considered

$$d^2r = dx\,dy = \frac{\lambda_L^2}{2}\,d\lambda_1\,d\lambda_2 \tag{5.20}$$

and the coordinates are expressed as functions of the integration parameters

$$x(\lambda_1,\lambda_2) = -x_0 + \frac{\lambda_L}{2}(\lambda_1+\lambda_2) \tag{5.21}$$

$$y(\lambda_1,\lambda_2) = \frac{\lambda_L}{2}(\lambda_1-\lambda_2) \tag{5.22}$$

with $x_0 = -\mathbf{r}_0\cdot\mathbf{e}_x = \lambda_L m_0$. We therefore have

$$x+y = -x_0+\lambda_L\lambda_1 \tag{5.23}$$

$$x-y = -x_0+\lambda_L\lambda_2 \tag{5.24}$$

and can now evaluate the matrix elements

$$\begin{aligned} R^{(1,2)}_{I(m_1,m_2,\alpha),I(m_1',m_2',\alpha')} &= A^2 k_L\; e^{-i(\phi_{\mathbf{k},\alpha}-\phi_{\mathbf{k}',\alpha'})} \sum_{\substack{n_1,n_2\\ n_1',n_2'}} c^{(\mathbf{k},\alpha)\,*}_{n_1,n_2}\, c^{(\mathbf{k}',\alpha')}_{n_1',n_2'} \\ &\quad\times \int_{\text{r.s.l.}} d^2r\, e^{i[(n_1'-n_1)\mathbf{b}_1+(n_2'-n_2)\mathbf{b}_2+\mathbf{k}'-\mathbf{k}]\cdot\mathbf{r}}\;(x\pm y) \\ &= A^2 k_L\; e^{-i(\phi_{\mathbf{k},\alpha}-\phi_{\mathbf{k}',\alpha'})} \sum_{\substack{n_1,n_2\\ n_1',n_2'}} c^{(\mathbf{k},\alpha)\,*}_{n_1,n_2}\, c^{(\mathbf{k}',\alpha')}_{n_1',n_2'} \\ &\quad\times \int_{\text{r.s.l.}} d^2r\, e^{i[(n_1'-n_1)\mathbf{b}_1+(n_2'-n_2)\mathbf{b}_2+\mathbf{k}'-\mathbf{k}]\cdot\mathbf{r}}\;(x\pm y) \end{aligned} \tag{5.25}$$

5.3.2 Determining the Wannier States

Firstly, one has to distinguish between two qualitatively different regimes of the lattice geometry, depending on the parameters: For the case of a single real-space unit cell containing two local potential minima, the Wannier states are constructed in the subspace of the **two** lowest bands. In contrast, if only one potential minimum exists within the unit cell, a maximally localized Wannier state can be constructed within the lowest band only. In the prior case, each Wannier state contains an additional sublattice index $\mathcal{A}$ or $\mathcal{B}$, specifying, in addition to the unit cell indices, on which sublattice the state is localized.

It can of course be verified explicitly, that both operators R_1 and R_2 are Hermitian (numerically we work in the basis of Bloch states, where the matrices representation in Eq. (5.25) carries the same name), since a projection retains Hermiticity. For a finite system the two projected position operators do not commute $[R_1,R_2]\neq 0$. We first diagonalize one of the operators, for instance R_1. As shown in Figure 5.3, the eigenvalues split into groups of 5, which are almost, but not completely degenerate [1]. Note that there are twice as many such almost degenerate groups as the number of unit cells. This is a consequence of the two potential minima within a real-space Wigner-Seitz cell have different locations with respect to the direction $\mathbf{b}_1$.

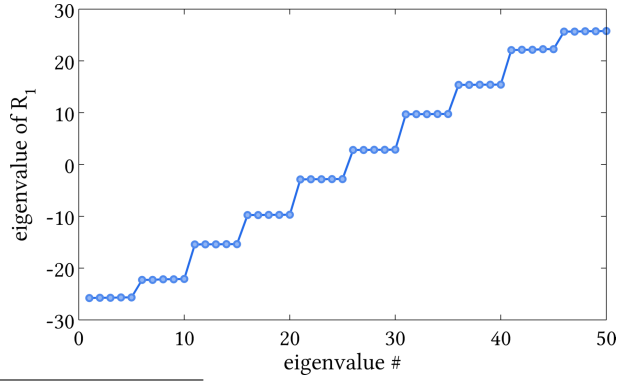

[1] We refer to such states as semi-degenerate.

Figure 5.3: Spectrum of the real-space position operator along the direction $\mathbf{b}_1$ projected onto the lowest two bands of a lattice in the honeycomb regime. Here the eigenvalues for a lattice consisting of 5×5 unit cells, i.e. 50 potential minima, are shown.

The corresponding eigenstates of R_1 are all maximally localized along the $\mathbf{b}_1$ direction, but not necessarily along the direction $\mathbf{b}_2$. However, any state consisting only of a superposition of eigenstates corresponding to an almost degenerate subspace, will necessarily be strongly spatially localized to the region of the respective eigenvalue of R_1. We therefore focus on one such degenerate subspace, within which we subsequently diagonalize the complementary position operator R_2, leading to a states which are maximally localized along all directions. For a real-space lattice consisting of L unit cells along the direction $\mathbf{b}_1$, there are $2L$ almost degenerate sets of eigenvalues, corresponding to states on sublattices $\mathcal{A}$ and $\mathcal{B}$ in alternating order.Even when, due to finite size effects, the eigenvalues are not exactly degenerate, the different eigenstates are exactly mutually orthogonal.

For periodic boundary conditions or an infinitely large system, the Wannier states localized at different unit cells are all related by translation in real-space, or analogously, a linear change of the complex phase in k-space of the respective Bloch states. Hence, it suffices to determine all Wannier states on a single real-space unit cell only. To minimize finite size effects from the edge, we construct the Wannier states at the center of the real-space lattice. Subsequently, the complex phase of each Bloch state is set, such that every Wannier state on either of the two sublattices is directly obtained as

$$|\boldsymbol{\ell}, \mathcal{A}\rangle = \frac{1}{\sqrt{2L_x L_y}} \sum_{\mathbf{k}} e^{-i\mathbf{k}\cdot\mathbf{R}_{\boldsymbol{\ell}}} \left[|\mathbf{k}, \alpha = 0\rangle + |\mathbf{k}, \alpha = 1\rangle\right] \tag{5.26}$$

$$|\boldsymbol{\ell}, \mathcal{B}\rangle = \frac{1}{\sqrt{2L_x L_y}} \sum_{\mathbf{k}} e^{-i\mathbf{k}\cdot\mathbf{R}_{\boldsymbol{\ell}}} \left[|\mathbf{k}, \alpha = 0\rangle + e^{i\beta_{\mathbf{k}}}|\mathbf{k}, \alpha = 1\rangle\right]. \tag{5.27}$$

Using this procedure, also the states at the edge do not contain finite size effects, but behave like states in a system with periodic boundary conditions.

Choosing the set of almost degenerate eigenvalues of R_1 defines the sublattice to which the resulting Wannier state will be localized. When crossing from the double-well into the triangular lattice regime, where there is only a single potential minimum per unit cell, pairs of such degenerate sets of eigenvalues will furthermore become degenerate.

Let us denote the spectral decomposition of the operator

$$R_1 = \sum_i \lambda_i |\lambda_i\rangle\langle\lambda_i| \tag{5.28}$$

and construct the projection operator onto the subspace of eigenstates with corresponding eigenvalues lying in the vicinity of the fixed value λ up to a tolerance parameter ϵ_{tol}

$$P_\lambda = \sum_{i \text{ with } |\lambda_i - \lambda| < \epsilon_{\text{tol}}} |\lambda_i\rangle\langle\lambda_i|. \tag{5.29}$$

For suitably chosen ϵ_{tol} and discrete values corresponding to the approximate eigenvalue of a semi-degenerate group, the rank of each projector is L and we have

$$P_\lambda P_\mu = \delta_{\lambda,\mu} P_\lambda. \tag{5.30}$$

Let $\lambda_{\mathcal{A}}$ denote the eigenvalue of R_1 corresponding to a potential minimum on sublattice $\mathcal{A}$ in a central unit cell and, analogously, $\lambda_{\mathcal{B}}$ to the alternate potential minimum on sublattice $\mathcal{B}$ in the same unit cell.

The two different Wannier states in the given unit call are found by diagonalizing $P_{\lambda_{\mathcal{A}}} R_2 P_{\lambda_{\mathcal{A}}}$ and $P_{\lambda_{\mathcal{B}}} R_2 P_{\lambda_{\mathcal{B}}}$, of which they are the respective eigenstate to the eigenvalue corresponding to the coordinate along the $\mathbf{b}_2$ coordinate.

With the Wannier states being constructed as eigenstates of an Hermitian operators within mutually orthogonal subspaces, their orthogonality is inherent by construction.

To finally obtain the Wannier states, which are maximally localized along both directions $\mathbf{b}_1$ and $\mathbf{b}_2$, we subsequently diagonalize the complementary position operator R_2 in the semi-degenerate subspaces of R_1.

5.3.3 Sublattice conjugate Wannier states for unit cells with reflectional symmetry

If the lattice unit cell is symmetric under spatial reflection, i.e. the potential fulfills $V(\mathbf{r}_0+\mathbf{r}) = V(\mathbf{r}_0-\mathbf{r})$ and $\mathbf{r}_0$ lies at the center of the unit cell, then the Wannier functions on the two sublattices are also related by a spatial reflection. Without loss of generality, let us assume that the phases of the Bloch states have been chosen, such that the Wannier state at site $\boldsymbol{\ell} = (0,0)$ and sublattice $\mathcal{A}$ is given by

$$|\boldsymbol{\ell} = (0,0), \mathcal{A}\rangle = \frac{1}{\sqrt{2L_xL_y}} \sum_{\mathbf{k}} \sum_{\alpha=0,1} |\mathbf{k}, \alpha\rangle \tag{5.31}$$

with the purely real real-space representation $w_{\boldsymbol{\ell}=(0,0),\mathcal{A}}(\mathbf{r}) = \langle \mathbf{r}|\boldsymbol{\ell} = (0,0), \mathcal{A}\rangle$. The Wannier function for the same unit cell, but sublattice $\mathcal{B}$ is then simply given by

$$\begin{aligned} \langle \mathbf{r}|\boldsymbol{\ell} = (0,0), \mathcal{B}\rangle &= w_{\boldsymbol{\ell}=(0,0),\mathcal{B}}(\mathbf{r}) \\ &= w_{\boldsymbol{\ell}=(0,0),\mathcal{A}}(-\mathbf{r}). \end{aligned} \tag{5.32}$$

The state on sublattice $\mathcal{B}$ must necessarily also be representable as a superposition of Bloch states of the lowest two bands (retaining the complex phase convention defined by Eq. (5.31))

$$|\boldsymbol{\ell} = (0,0), \mathcal{B}\rangle = \frac{1}{\sqrt{2L_xL_y}} \sum_{\mathbf{k}} \sum_{\alpha=0,1} v_{\mathbf{k},\alpha} |\mathbf{k}, \alpha\rangle. \tag{5.33}$$

The intermediate goal is to determine the coefficients $v_{\mathbf{k},\alpha}$, all of which are expected to be of modulus 1, since the Wannier state on sublattice $\mathcal{A}$ also contains an equal admixture of all Bloch states in the two lowest bands. Let $\mathcal{T}$ denote the parity operator, which is implicitly defined by reflecting all real-space eigenstates (constituting a basis) with respect to the origin $\mathcal{T}|\mathbf{r}\rangle = |-\mathbf{r}\rangle$. A short analysis reveals that the action on the basis of physical momentum states $\mathcal{T}|\mathbf{p}\rangle = |-\mathbf{p}\rangle$ is of similar form. Using this property, Eq. (5.32) and expanding the Bloch states in the basis of momentum states,

$$|\mathbf{k}, \alpha\rangle = \frac{1}{\sqrt{2L_xL_y}} \sum_{n_1,n_2} c^{(\mathbf{k},\alpha)}_{n_1,n_2} |\mathbf{p} = n_1\mathbf{b}_1 + n_2\mathbf{b}_2 + \mathbf{k}\rangle, \tag{5.34}$$

one obtains

$$\begin{aligned} |\boldsymbol{\ell} = (0,0), \mathcal{B}\rangle &= \mathcal{T}|\boldsymbol{\ell} = (0,0), \mathcal{A}\rangle \\ &= \frac{1}{\sqrt{2L_xL_y}} \sum_{\mathbf{k}} \sum_{\alpha=0,1} \sum_{n_1,n_2} c^{(\mathbf{k},\alpha)}_{n_1,n_2} \mathcal{T}|\mathbf{p} = n_1\mathbf{b}_1 + n_2\mathbf{b}_2 + \mathbf{k}\rangle \\ &= \frac{1}{\sqrt{2L_xL_y}} \sum_{\mathbf{k}} \sum_{\alpha=0,1} \sum_{n_1,n_2} c^{(-\mathbf{k},\alpha)}_{-n_1,-n_2} |\mathbf{p} = n_1\mathbf{b}_1 + n_2\mathbf{b}_2 + \mathbf{k}\rangle. \end{aligned} \tag{5.35}$$

In the last step a transformation of summation variables was performed. This is not of the desired form, being expressed in the Bloch basis, yet. For this purpose, we insert the unity operator within the two lowest bands in form of the Bloch state completeness relation

$$\mathbb{1}_{\alpha=0,1} = \sum_{\mathbf{k}} \sum_{\alpha=0,1} |\mathbf{k}, \alpha\rangle\langle \mathbf{k}, \alpha| \tag{5.36}$$

into Eq. (5.35), which leads to

$$|\boldsymbol{\ell}=(0,0),\mathcal{B}\rangle = \frac{1}{\sqrt{2L_xL_y}}\sum_{\mathbf{k},\mathbf{k}'}\sum_{\alpha,\alpha'=0,1}\sum_{n_1',n_2'} c^{(-\mathbf{k}',\alpha')}_{-n_1',-n_2'}\langle \mathbf{k},\alpha|\mathbf{p}=n_1'\mathbf{b}_1+n_2'\mathbf{b}_2+\mathbf{k}'\rangle\ |\mathbf{k},\alpha\rangle. \tag{5.37}$$

This is of the sought-after form of Eq. (5.33) and a comparison directly reveals the coefficients for expressing the conjugate Wannier state in the Bloch basis. Here we use the conjugate of Eq. (5.34) and exploit the orthogonality of momentum states, as well as the injectivity of the mapping $\mathbf{p}\mapsto(\mathbf{k},n_1,n_2)$, where $\mathbf{k}\in 1BZ$, yielding the relation

$$\langle \mathbf{p}=n_1\mathbf{b}_1+n_2\mathbf{b}_2+\mathbf{k}|\mathbf{p}=n_1'\mathbf{b}_1+n_2'\mathbf{b}_2+\mathbf{k}'\rangle = \delta_{n_1,n_1'}\,\delta_{n_2,n_2'}\,\delta_{\mathbf{k},\mathbf{k}'}. \tag{5.38}$$

Finally, we can evaluate the coefficients to be

$$\begin{aligned} v_{\mathbf{k},\alpha} &= \sum_{\mathbf{k}'}\sum_{\alpha'=0,1}\sum_{n_1',n_2'} c^{(-\mathbf{k}',\alpha')}_{-n_1',-n_2'}\langle \mathbf{k},\alpha|\mathbf{p}=n_1'\mathbf{b}_1+n_2'\mathbf{b}_2+\mathbf{k}'\rangle \\ &= \sum_{\mathbf{k}'}\sum_{\alpha'=0,1}\sum_{n_1,n_2,n_1',n_2'} {c^{(\mathbf{k},\alpha)}_{n_1,n_2}}^{*} c^{(-\mathbf{k}',\alpha')}_{-n_1',-n_2'}\langle \mathbf{p}=n_1\mathbf{b}_1+n_2\mathbf{b}_2+\mathbf{k}|\mathbf{p}=n_1'\mathbf{b}_1+n_2'\mathbf{b}_2+\mathbf{k}'\rangle \\ &= \sum_{\alpha'=0,1}\sum_{n_1,n_2} {c^{(\mathbf{k},\alpha)}_{n_1,n_2}}^{*} c^{(-\mathbf{k},\alpha')}_{-n_1,-n_2}. \end{aligned} \tag{5.39}$$

It was verified numerically, that these coefficients $v_{\mathbf{k},\alpha}$ are indeed all of modulus one, which is not directly clear from the form of Eq. (5.39).

5.3.3.1 Symmetry properties of the c-coefficients

In setting up the single-particle lattice Hamiltonian, the diagonal kinetic energy terms are of the form $(n_1\mathbf{b}_1+n_2\mathbf{b}_2+\mathbf{k})^2$ and thus invariant under a simultaneous change

$$(n_1,n_2,\mathbf{k})\mapsto(-n_1,-n_2,-\mathbf{k}). \tag{5.40}$$

In the case of a symmetric unit cell under reflection, i.e. $\theta=m\pi$ with $m\in\mathbb{Z}$, the Fourier coefficients V_{n_1,n_2} of the potential are purely real and also invariant under the transformation in Eq. (5.40), the eigenvalue spectrum of the of the lattice Hamiltonian's momentum-space representation $\mathcal{H}^{(\mathbf{k})}_{\text{lat}}$ is identical for pairs[2] of $\mathbf{k}$ and $-\mathbf{k}$. The eigenvectors to a common eigenvalue are interrelated by a permutation $(n_1,n_2)\leftrightarrow(-n_1,-n_2)$ if the two overall phases are chosen accordingly

$$c^{(\mathbf{k},\alpha)}_{n_1,n_2} = c^{(-\mathbf{k},\alpha)}_{-n_1,-n_2}. \tag{5.41}$$

However, this only holds before the Bloch states' phases have been chosen and absorbed into the c-coefficients, such that the Wannier state in Eq. (5.31) is maximally localized and purely real in the real-space representation. After fulfilling the latter requirement, the coefficients no longer necessarily obey Eq. (5.42), but much rather

$${c^{(\mathbf{k},\alpha)}_{n_1,n_2}}^{*} = c^{(-\mathbf{k},\alpha)}_{-n_1,-n_2}, \tag{5.42}$$

which guarantees that the superposition of each pair of conjugate Bloch functions is purely real: $[\langle\mathbf{r}|\mathbf{k},\alpha\rangle+\langle\mathbf{r}|-\mathbf{k},\alpha\rangle]\in\mathbb{R}$.

[2]The total lattice Hamiltonian is separable into sub-blocks, each corresponding to a different quasi-momentum $\mathbf{k}$. For each such sub-block, $\mathbf{k}$ is to be seen as a fixed parameter.

5.3.4 Alternate representation of the conjugate Wannier states

All Wannier states in the Bloch basis have now been determined to be of the form

$$|\boldsymbol{\ell}, \mathcal{A}\rangle = \frac{1}{\sqrt{2L_xL_y}} \sum_{\mathbf{k}} \sum_{\alpha=0,1} e^{-i\mathbf{k}\cdot\mathbf{R}_{\boldsymbol{\ell}}} |\mathbf{k}, \alpha\rangle \tag{5.43}$$

$$|\boldsymbol{\ell}, \mathcal{B}\rangle = \frac{1}{\sqrt{2L_xL_y}} \sum_{\mathbf{k}} \sum_{\alpha=0,1} e^{-i\mathbf{k}\cdot\mathbf{R}_{\boldsymbol{\ell}}}\, v_{\mathbf{k},\alpha}\, |\mathbf{k}, \alpha\rangle. \tag{5.44}$$

It turns out, that the coefficients $v_{\mathbf{k},\alpha}$ are always of modulus one and, for a given quasi-momentum $\mathbf{k}$, the complex phases exactly differ by π

$$\arg(v_{\mathbf{k},1}) - \arg(v_{\mathbf{k},0}) = \pi. \tag{5.45}$$

Thus, the Wannier states on sublattice $\mathcal{B}$ can also be written in the form

$$|\boldsymbol{\ell}, \mathcal{B}\rangle = \frac{1}{\sqrt{2L_xL_y}} \sum_{\mathbf{k}} e^{-i\mathbf{k}\cdot\mathbf{R}_{\boldsymbol{\ell}}}\, e^{i\beta_{\mathbf{k}}} (|\mathbf{k}, \alpha = 0\rangle - |\mathbf{k}, \alpha = 1\rangle). \tag{5.46}$$

From this representation it is directly evident that all Wannier states on sublattice $\mathcal{B}$ are exactly orthogonal to all Wannier states on sublattice $\mathcal{A}$.

Instead of calculating $v_{\mathbf{k},\alpha}$ via Eq. (5.39) and subsequently extracting the complex phases, we seek a more direct method to determine $\beta_{\mathbf{k}}$. For the case of a symmetric unit cell under spatial reflection, the two Wannier states on sublattices $\mathcal{A}$ and $\mathcal{B}$ are also interrelated by reflection, as expressed in Eq.(5.32). From the spectral decomposition of the Wannier states and the orthogonality of the plane wave basis, one finds the relation between pairs of Bloch functions in the lowest two bands

$$e^{i\beta_{\mathbf{k}}} [\psi_{\mathbf{k},0}(\mathbf{r}) - \psi_{\mathbf{k},1}(\mathbf{r})] = \psi_{-\mathbf{k},0}(-\mathbf{r}) + \psi_{-\mathbf{k},1}(-\mathbf{r}). \tag{5.47}$$

Using the expression of Bloch functions in terms of plane waves

$$\psi_{\mathbf{k},\alpha}(\mathbf{r}) = e^{i\mathbf{k}\cdot\mathbf{r}} \sum_{n_1,n_2} c^{(\mathbf{k},\alpha)}_{n_1,n_2}\, e^{i(n_1\mathbf{b}_1 + n_2\mathbf{b}_2)\cdot\mathbf{r}} \tag{5.48}$$

the above relation Eq. (5.47) implies

$$e^{i\beta_{\mathbf{k}}} \sum_{n_1,n_2} \left[c^{(\mathbf{k},0)}_{n_1,n_2} - c^{(\mathbf{k},1)}_{n_1,n_2}\right] e^{i(n_1\mathbf{b}_1 + n_2\mathbf{b}_2 + \mathbf{k})\cdot\mathbf{r}} = \sum_{n_1,n_2} \left[c^{(-\mathbf{k},0)}_{n_1,n_2} + c^{(-\mathbf{k},1)}_{n_1,n_2}\right] e^{i(-n_1\mathbf{b}_1 - n_2\mathbf{b}_2 + \mathbf{k})\cdot\mathbf{r}}. \tag{5.49}$$

Performing a summation variable transformation and using the orthogonality of the plane waves again, this implies the equality of the individual coefficients

$$e^{i\beta_{\mathbf{k}}} \left[c^{(\mathbf{k},0)}_{n_1,n_2} - c^{(\mathbf{k},1)}_{n_1,n_2}\right] = c^{(-\mathbf{k},0)}_{-n_1,-n_2} + c^{(-\mathbf{k},1)}_{-n_1,-n_2} \tag{5.50}$$

for all n_1 and n_2. Using the symmetry relation in Eq. (5.42), the phase factor can be written as

$$e^{i\beta_{\mathbf{k}}} = \frac{c^{(\mathbf{k},0)\,*}_{n_1,n_2} + c^{(\mathbf{k},1)\,*}_{n_1,n_2}}{c^{(\mathbf{k},0)}_{n_1,n_2} - c^{(\mathbf{k},1)}_{n_1,n_2}} = \frac{c^{(\mathbf{k},0)^*\,2}_{n_1,n_2} - c^{(\mathbf{k},1)^*\,2}_{n_1,n_2}}{\left|c^{(\mathbf{k},0)}_{n_1,n_2} - c^{(\mathbf{k},1)}_{n_1,n_2}\right|^2} \tag{5.51}$$

and hence

$$\beta_{\mathbf{k}} = \arg\left[c^{(\mathbf{k},0)^*\,2}_{n_1,n_2} - c^{(\mathbf{k},1)^*\,2}_{n_1,n_2}\right]. \tag{5.52}$$

Note that the structure of the eigenvectors $c^{(\mathbf{k},\alpha)}_{n_1,n_2}$, such that the expressions in Eq. (5.51) are guaranteed to be of modulus one, arises naturally from the diagonalization of the lattice Hamiltonian.

Once the phases $\beta_{\mathbf{k}}$ have been determined, all tunneling matrix elements for the reflectionally symmetric lattice can easily be determined. The matrix elements between Wannier states on different sublattices

$$\begin{aligned} J_{(\boldsymbol{\ell},\mathcal{A}),(\boldsymbol{\ell}',\mathcal{B})} &= -\langle \boldsymbol{\ell},\mathcal{A}|\mathcal{H}_{\mathrm{lat}}|\boldsymbol{\ell}',\mathcal{B}\rangle \\ &= \frac{1}{2L_xL_y}\sum_{\mathbf{k}} e^{i[\mathbf{k}\cdot(\mathbf{R}_{\boldsymbol{\ell}}-\mathbf{R}_{\boldsymbol{\ell}'})+\beta_{\mathbf{k}}]}\left(E_{\mathbf{k},\alpha=1}-E_{\mathbf{k},\alpha=0}\right) \end{aligned} \tag{5.53}$$

contain an the phase factor $\beta_{\mathbf{k}}$. These elements can thus not be determined solely from the dispersion relation, i.e. the relative phase factors $\beta_{\mathbf{k}}$ also have to be determined.

This is different to the hopping matrix elements between Wannier states on the same sublattice

$$\begin{aligned} J_{(\boldsymbol{\ell},\mathcal{A}),(\boldsymbol{\ell}',\mathcal{A})} = J_{(\boldsymbol{\ell},\mathcal{B}),(\boldsymbol{\ell}',\mathcal{B})} &= -\langle \boldsymbol{\ell},\mathcal{B}|\mathcal{H}_{\mathrm{lat}}|\boldsymbol{\ell}',\mathcal{B}\rangle \\ &= -\frac{1}{2L_xL_y}\sum_{\mathbf{k}} e^{i\mathbf{k}\cdot(\mathbf{R}_{\boldsymbol{\ell}}-\mathbf{R}_{\boldsymbol{\ell}'})}\left(E_{\mathbf{k},\alpha=0}+E_{\mathbf{k},\alpha=1}\right), \end{aligned} \tag{5.54}$$

which is directly the Fourier transform of the dispersion relation and the Wannier states do not have to be calculated.

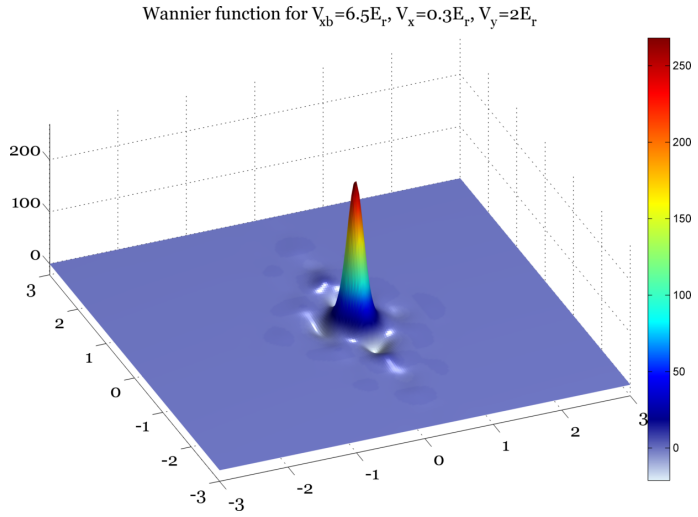

Figure 5.4: A typical (pureley real) Wannier function in the honeycomb regime for $V_{\overline{x}} = 6.5E_r$, $V_x = 0.3E_r$ and $V_y = 2E_r$.

A typical Wannier function in the honeycomb regime, localized to one of the two sublattice minima, is shown in Fig. (5.4). As expected, this is exponentially localized in all spatial directions and reflects all required symmetry properties of the lattice. The imaginary part of the Wannier function resulting from our calculation procedure is of the order of the machine precision. This indicates that the Wannier functions are obtained with high numerical precision within this approach.

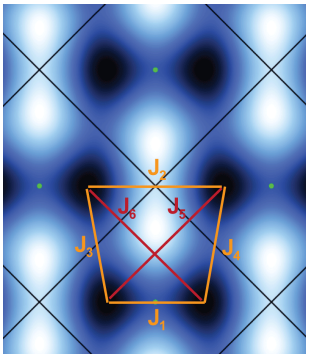

Figure 5.5

The hopping matrix elements for the various couplings defined in Fig. (5.5), as well as the on-site interaction constant U are plotted as functions of V_x and $V_{\overline{x}}$ in Fig. (5.6).

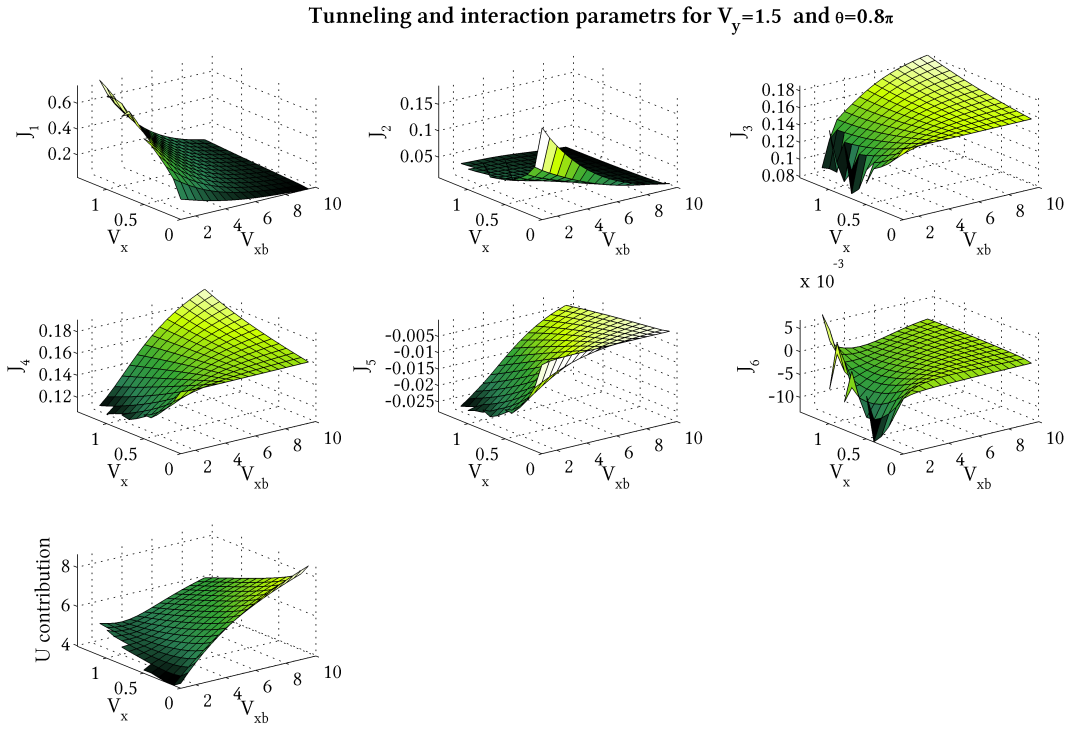

Figure 5.6: The most relevant different hopping parameters, as well as the on-site interaction energy U as functions of the lattice depths V_x and $V_{\overline{x}}$ at fixed $V_y = 1.5$ and a relative phase angle $\theta = 0.8\pi$ between the two laser beams in x-direction.

6. A Generalized Approach to Bogoliubov Theory

The usual method to derive Bogoliubov theory consists of identifying the macroscopically occupied condensate orbital and subsequently approximating both the corresponding annihilation operator a_0 and creation operator $a_0^\dagger$ by a complex number. This number is the square root of the modulus of the condensate number. Subsequently, the interacting Hamiltonian is expanded in the remaining operators up to quadratic order and this part can be diagonalized by a Bogoliubov transformation of the operators. However, this approach neglects some relevant physics, since the condensate orbital is no longer treated on an operator level and, is colloquially said to neglect *quantum fluctuations* in this sense.

We will not review this standard approach to Bogoliubov theory, but discuss two alternative derivations:

1. Replacing the annihilation operators $b_{\boldsymbol{\ell}} = \phi_{\boldsymbol{\ell}} + \delta b_{\boldsymbol{\ell}}$, expanding the Hamiltonian in different orders in the fluctuation operators and diagonalizing it up to second order in the fluctuations. Within this approach, one retains the operator structure of the fluctuations throughout the entire derivation.

2. Linearizing the time-dependent Gross-Pitaevskii equation of motion for the condensate field around the energy-minimizing static field configuration. The eigenmodes of the linearized equations of motion correspond to coherent states of the respective quasi-particles modes. By systematically quantizing these modes from the classical theory, Bogoliubov theory with its rich structure beyond the realm of Gross-Pitaevskii physics, is fully derived.

Although these two derivations may seem very different at a first glance, they are fundamentally connected: up to linear order the equations of motion determined by time-dependent Gross-Pitaevskii theory for the classical fluctuation amplitudes are related to the Heisenberg equations of motion of the fluctuation field operators $\delta b_{\boldsymbol{\ell}}(t)$ by the Ehrenfest theorem. It is on this level that time-dependent Gross-Pitaevskii theory is the classical limit of Bogoliubov theory, where all quasi-particle Bogoliubov modes are coherently excited[1]. In contrast to the continuum version, which is presented in most textbooks, we will always consider the lattice version in the following. Apart from being directly applicable to interacting lattice models, it has the advantage of containing a natural ultraviolet cutoff and does hence not lead to unphysical divergences of quantities such as the ground state energy shift, which appear in the continuum version.

[1] In the sense of coherent states.

6.1 Derivation of Bogoliubov Theory on an Operator Level

In this section we review the derivation of Bogoliubov theory on an operator level. The advantage of this route is its transparency, where it becomes very clear how the quasi-particle creation and annihilation operators are related to the original fluctuation operators, which in turn are directly related to the bosonic annihilation operators by a scalar mean-field shift. Furthermore, this derivation is not restricted to homogeneous systems and constitutes one of the simplest forms to practically implement Bogoliubov theory for inhomogeneous systems, e.g. in the presence of a trap or disorder. Throughout this derivation, there is no need to consider time-dependence and we remain in the Schrödinger picture.

We begin with the Bose-Hubbard Hamiltonian from Eq. (2.66) and write every annihilation operator (the creation operator analogously by the adjoint) as a sum of a mean-field shift and a fluctuation operator, which is implicitly defined hereby

$$b_{\boldsymbol{\ell}} = \phi_{\boldsymbol{\ell}} + \delta b_{\boldsymbol{\ell}}. \tag{6.1}$$

Note that this replacement is completely general and does not imply any specific choice for $\phi_{\boldsymbol{\ell}}$, nor does it imply a symmetry-breaking effective theory. The different choices for $\phi_{\boldsymbol{\ell}}$ differs for various theories: the most common and simplest choice of $\phi_{\boldsymbol{\ell}} = \langle b_{\boldsymbol{\ell}} \rangle$ (or to the appropriately scaled value of the largest eigenvector of the single particle density matrix within a number-conserving formulation) leads to Bogoliubov theory, whereas the depletion of the condensate can also be included within extensions, such as the Hartree-Fock Bogoliubov approximation.

Inserting Eq. (6.1) into the Bose-Hubbard Hamiltonian

$$\begin{aligned} H_{\text{BH}} &= -J \sum_{\langle \boldsymbol{\ell},\boldsymbol{\ell}' \rangle} (b_{\boldsymbol{\ell}}^\dagger b_{\boldsymbol{\ell}'} + b_{\boldsymbol{\ell}'}^\dagger b_{\boldsymbol{\ell}}) + \sum_{\boldsymbol{\ell}} (\epsilon_{\boldsymbol{\ell}} - \mu) b_{\boldsymbol{\ell}}^\dagger b_{\boldsymbol{\ell}} + \frac{U}{2} \sum_{\boldsymbol{\ell}} b_{\boldsymbol{\ell}}^\dagger b_{\boldsymbol{\ell}}^\dagger b_{\boldsymbol{\ell}} b_{\boldsymbol{\ell}} \\ &= E^{(0)} + \mathcal{H}^{(1)} + \mathcal{H}^{(2)} + \mathcal{H}^{(3)} + \mathcal{H}^{(4)}, \end{aligned} \tag{6.2}$$

we separate the resulting terms by their different orders, where $\mathcal{H}^{(n)}$ denotes the term containing n fluctuation operators $\delta b_{\boldsymbol{\ell}}$ and $\delta b_{\boldsymbol{\ell}}^\dagger$. Explicitly, these are of the form

$$E^{(0)} = -J \sum_{\langle \boldsymbol{\ell},\boldsymbol{\ell}' \rangle} (\phi_{\boldsymbol{\ell}}^* \phi_{\boldsymbol{\ell}'} + \phi_{\boldsymbol{\ell}'}^* \phi_{\boldsymbol{\ell}}) + \sum_{\boldsymbol{\ell}} (\epsilon_{\boldsymbol{\ell}} - \mu) |\phi_{\boldsymbol{\ell}}|^2 + \frac{U}{2} \sum_{\boldsymbol{\ell}} |\phi_{\boldsymbol{\ell}}|^4 \tag{6.3}$$

$$\begin{aligned} \mathcal{H}^{(1)} = &-J \sum_{\langle \boldsymbol{\ell},\boldsymbol{\ell}' \rangle} (\phi_{\boldsymbol{\ell}}^* \delta b_{\boldsymbol{\ell}'} + \phi_{\boldsymbol{\ell}} \delta b_{\boldsymbol{\ell}'}^\dagger + \phi_{\boldsymbol{\ell}'} \delta b_{\boldsymbol{\ell}}^\dagger + \phi_{\boldsymbol{\ell}'}^* \delta b_{\boldsymbol{\ell}}) + \sum_{\boldsymbol{\ell}} (\epsilon_{\boldsymbol{\ell}} - \mu)(\phi_{\boldsymbol{\ell}}^* \delta b_{\boldsymbol{\ell}} + \phi_{\boldsymbol{\ell}} \delta b_{\boldsymbol{\ell}}^\dagger) \\ &+ U \sum_{\boldsymbol{\ell}} |\phi_{\boldsymbol{\ell}}|^2 (\phi_{\boldsymbol{\ell}}^* \delta b_{\boldsymbol{\ell}} + \phi_{\boldsymbol{\ell}} \delta b_{\boldsymbol{\ell}}^\dagger) \end{aligned} \tag{6.4}$$

$$\begin{aligned} \mathcal{H}^{(2)} = &-J \sum_{\langle \boldsymbol{\ell},\boldsymbol{\ell}' \rangle} (\delta b_{\boldsymbol{\ell}}^\dagger \delta b_{\boldsymbol{\ell}'} + \delta b_{\boldsymbol{\ell}'}^\dagger \delta b_{\boldsymbol{\ell}}) + \sum_{\boldsymbol{\ell}} (\epsilon_{\boldsymbol{\ell}} - \mu) \delta b_{\boldsymbol{\ell}}^\dagger \delta b_{\boldsymbol{\ell}} \\ &+ \frac{U}{2} \sum_{\boldsymbol{\ell}} (\phi_{\boldsymbol{\ell}}^* \phi_{\boldsymbol{\ell}}^* \delta b_{\boldsymbol{\ell}} \delta b_{\boldsymbol{\ell}} + 4 |\phi_{\boldsymbol{\ell}}|^2 \delta b_{\boldsymbol{\ell}}^\dagger \delta b_{\boldsymbol{\ell}} + \phi_{\boldsymbol{\ell}} \phi_{\boldsymbol{\ell}} \delta b_{\boldsymbol{\ell}}^\dagger \delta b_{\boldsymbol{\ell}}^\dagger) \end{aligned} \tag{6.5}$$

$$\mathcal{H}^{(3)} = U \sum_{\boldsymbol{\ell}} (\phi_{\boldsymbol{\ell}}^* \delta b_{\boldsymbol{\ell}}^\dagger \delta b_{\boldsymbol{\ell}} \delta b_{\boldsymbol{\ell}} + \phi_{\boldsymbol{\ell}} \delta b_{\boldsymbol{\ell}}^\dagger \delta b_{\boldsymbol{\ell}}^\dagger \delta b_{\boldsymbol{\ell}}) \tag{6.6}$$

$$\mathcal{H}^{(4)} = \frac{U}{2} \sum_{\boldsymbol{\ell}} \delta b_{\boldsymbol{\ell}}^\dagger \delta b_{\boldsymbol{\ell}}^\dagger \delta b_{\boldsymbol{\ell}} \delta b_{\boldsymbol{\ell}} \tag{6.7}$$

We will now shortly discuss each of these terms separately in the context of a $U(1)$-symmetry breaking formulation of Bogoliubov theory.

Zeroth Order Term

The term $E^{(0)}$ in Eq. (6.3) contains no fluctuation operators and is exactly the scalar Gross-Pitaevskii energy function, with all field operators $b_{\boldsymbol{\ell}}(t)$ having been replaced by $\phi_{\boldsymbol{\ell}}(t)$. As shown

in section (6.2), the same energy function can be obtained within a number conserving approach when evaluating the expectation value of the Bose-Hubbard Hamiltonian H_{BH} within the variational state $|\psi_{GP}\rangle = \frac{1}{\sqrt{N!}} \left(\sum_{\boldsymbol{\ell}} \phi_{\boldsymbol{\ell}}(t)\, b_{\boldsymbol{\ell}}^\dagger\right)^N |\text{vac}\rangle$, i.e.

$$E^{(0)} = \langle \psi_{GP} | H_{\text{BH}} | \psi_{GP} \rangle. \tag{6.8}$$

Within the Bogoliubov approach, the ground state field configuration $\phi_{\boldsymbol{\ell}}$ is determined such that it minimizes $E^{(0)}$ and, since this is a continuously differentiable function of all $\phi_{\boldsymbol{\ell}}$, necessarily implies

$$0 \stackrel{!}{=} \frac{\partial E^{(0)}}{\partial \phi_{\boldsymbol{\ell}}} = -J \sum_{\boldsymbol{\ell}' \in \text{n.n.}(\boldsymbol{\ell})} \phi_{\boldsymbol{\ell}'}^* + \left(\epsilon_{\boldsymbol{\ell}} - \mu + U|\phi_{\boldsymbol{\ell}}|^2\right)\phi_{\boldsymbol{\ell}}^* \tag{6.9}$$

for all $\boldsymbol{\ell}$.

First Order Term

If the total energy takes on a minimum for the chosen configuration of the scalar field $\phi_{\boldsymbol{\ell}}$, the expectation value of the first oder term in Eq. (6.4) has to vanish identically. If this expectation value were not zero in the state around which the fluctuation expansion is performed, the system could lower its energy further if $\langle \mathcal{H}^{(1)} \rangle$ were non-zero. This can be seen explicitly from the coefficient of $\delta b_{\boldsymbol{\ell}}$ being exactly the expression $\frac{\partial E^{(0)}}{\partial \phi_{\boldsymbol{\ell}}}$, i.e. the derivative of the scalar energy expectation value and we can rewrite the first order Hamiltonian as

$$\mathcal{H}^{(1)} = \sum_{\boldsymbol{\ell}} \left[\frac{\partial E^{(0)}}{\partial \phi_{\boldsymbol{\ell}}}\, \delta b_{\boldsymbol{\ell}} + \frac{\partial E^{(0)}}{\partial \phi_{\boldsymbol{\ell}}^*}\, \delta b_{\boldsymbol{\ell}}^\dagger \right]. \tag{6.10}$$

A vanishing first order Hamiltonian is thus a sufficient and necessary condition for the scalar energy taking on a minimum value for the choice of the static background field $\phi_{\boldsymbol{\ell}}$. Taken together, the set of all conditions in Eq. (6.9) for different $\boldsymbol{\ell}$ is nothing but the static Gross-Pitaevskii equation.

Second Order Term

The second order terms from Eq. (6.5) are thus the leading order beyond the Gross-Pitaevskii energy and by construction a quadratic form in the fluctuation operators. Let us define the column vectors of operators and the conjugate[2]

$$\boldsymbol{\delta \mathbf{b}} = \begin{pmatrix} \delta b_1 \\ \vdots \\ \delta b_n \end{pmatrix}, \qquad \boldsymbol{\delta \mathbf{b}}^\dagger = \begin{pmatrix} \delta b_1^\dagger \\ \vdots \\ \delta b_n^\dagger \end{pmatrix}. \tag{6.11}$$

As discussed in Sec. (K.1), and paying attention to the scalar shift originating from the commutation relations $[\delta b_l, \delta b_{l'}^\dagger] = \delta_{l,l'}$ of the fluctuation operators, the second order Hamiltonian can be written as a bilinear form in matrix notation

$$\mathcal{H}^{(2)} = \frac{1}{2} \begin{pmatrix} \boldsymbol{\delta \mathbf{b}} \\ \boldsymbol{\delta \mathbf{b}}^\dagger \end{pmatrix}^\dagger H_{\text{QP}} \begin{pmatrix} \boldsymbol{\delta \mathbf{b}} \\ \boldsymbol{\delta \mathbf{b}}^\dagger \end{pmatrix} - \frac{1}{2} \text{Tr}\,(h)\,. \tag{6.12}$$

In this case the $2L \times 2L$-dimensional Bogoliubov quasi-particle Hamiltonian is defined as

$$H_{\text{QP}} = \begin{pmatrix} h & \Delta \\ \Delta^* & h^* \end{pmatrix} \tag{6.13}$$

with the $L \times L$-dimensional Hermitian matrix h and symmetric matrix Δ, defined via their matrix elements

$$h_{\boldsymbol{\ell},\boldsymbol{\ell}'} = -J_{\boldsymbol{\ell},\boldsymbol{\ell}'} + (\epsilon_{\boldsymbol{\ell}} - \mu + 2U|\phi_{\boldsymbol{\ell}}|^2)\delta_{\boldsymbol{\ell},\boldsymbol{\ell}'} \tag{6.14}$$

$$\Delta_{\boldsymbol{\ell},\boldsymbol{\ell}'} = U\phi_{\boldsymbol{\ell}}^2\, \delta_{\boldsymbol{\ell},\boldsymbol{\ell}'}, \tag{6.15}$$

where $J_{\boldsymbol{\ell},\boldsymbol{\ell}'}$ is defined as J if $\boldsymbol{\ell}$ and $\boldsymbol{\ell}'$ are nearest neighboring sites and zero otherwise.

[2]Note that they are not truly related by Hermitian conjugation, since both are column vectors. It is nevertheless convenient to define this notation. and one has $(\boldsymbol{\delta \mathbf{b}}^\dagger)^\dagger = \boldsymbol{\delta \mathbf{b}}^t$.

Diagonalizing is not enough

One might be tempted to directly diagonalize the matrix H_{QP}, which is Hermitian, since h is Hermitian and Δ is symmetric. One could then define new operators corresponding to the eigenvectors, however these would generally not obey bosonic commutation relations (or analogously Poisson bracket relations for a classical bosonic theory). In addition to diagonalizing the quadratic form, we thus need the additional physical requirement, that the new quasi-particle operators β_r also obey bosonic commutation relations $[\beta_r, \beta_s^\dagger] = \delta_{r,s}$. This gives the bosonic vector space a symplectic structure[3], where a scalar product[4] is defined by the matrix $\Sigma = \begin{pmatrix} \mathbb{1}_L & 0 \\ 0 & -\mathbb{1}_L \end{pmatrix}$. All overlaps, norms of vectors and orthogonality relations are to be understood in terms of this scalar product.

Explicitly, a generalized unitary transformation is of the form

$$\begin{pmatrix} \boldsymbol{\delta}\mathbf{b} \\ \boldsymbol{\delta}\mathbf{b}^\dagger \end{pmatrix} = W \begin{pmatrix} \boldsymbol{\beta} \\ \boldsymbol{\beta}^\dagger \end{pmatrix}, \tag{6.16}$$

where we for now neglect an additional complication as not to obscure the presentation of the structure here. As will be shown in Sec. (6.1.1), a complete basis of bosonic eigenstates of the quasi-particle Hamiltonian does not exist. The eigenvectors, which constitute the column vector entries of the matrix W, have to be complemented by additional vectors. For now, we focus on the space spanned by the collective bosonic modes of the system. As shown in Sec. (K.1), requiring the operators β_r to obey canonical commutation relations (i.e. to be of a bosonic nature), imposes the inversion relation

$$W^{-1} = \Sigma W^\dagger \Sigma \tag{6.17}$$

on the generalized unitary transformation matrix. Hence W is not unitary and its column vectors are not mutually orthogonal with respect to the canonical scalar product, but with respect to the scalar product Σ. We therefore have to take care with the diagonalization procedure: a general diagonalization procedure of a matrix A consists of finding a non-singular basis transformation matrix U, such that $U^{-1}AU = D$ is a diagonal matrix. Note that U is generally not unitary, and hence the matrix U^{-1} on the left cannot simply be substituted by $U^\dagger$. We begin with the bilinear form in Eq. (6.12) and insert the transformation Eq. (6.16), as well as its adjoint

$$\begin{aligned} \mathcal{H}^{(2)} &= \frac{1}{2}\begin{pmatrix} \boldsymbol{\delta}\mathbf{b} \\ \boldsymbol{\delta}\mathbf{b}^\dagger \end{pmatrix}^\dagger H_{\mathrm{QP}} \begin{pmatrix} \boldsymbol{\delta}\mathbf{b} \\ \boldsymbol{\delta}\mathbf{b}^\dagger \end{pmatrix} - \frac{1}{2}\mathrm{Tr}\,(h) \\ &= \frac{1}{2}\begin{pmatrix} \boldsymbol{\beta} \\ \boldsymbol{\beta}^\dagger \end{pmatrix}^\dagger \Sigma W^{-1} \Sigma H_{\mathrm{QP}} W \begin{pmatrix} \boldsymbol{\beta} \\ \boldsymbol{\beta}^\dagger \end{pmatrix} - \frac{1}{2}\mathrm{Tr}\,(h)\,. \end{aligned} \tag{6.18}$$

This representation shows that the basis transformation matrix W contains the eigenvectors when diagonalizing the matrix ΣH_{QP} and $W^{-1}(\Sigma H_{\mathrm{QP}})W$ is of diagonal form, which the subsequent multiplication with Σ does not change, but acts in the context of the scalar product, taken with the row vector to the left. Up to now we have not restricted the derivation to any specific form of the spatial potential and determining the eigenvectors of ΣH_{QP} amounts to the Bogoliubov de Gennes equations, which is the most common approach to weakly interacting bosons in inhomogeneous systems and can be performed numerically.

6.1.1 Homogeneous Case

We now consider the case of a homogeneous system $\epsilon_{\boldsymbol{\ell}} = 0$, where the diagonalization can be performed analytically and leads to the well known usual Bogoliubov result. Here the condensate

[3] In contrast, life is easier here for fermionic systems, where the analogous space has a euclidean structure.
[4] In the strict mathematical sense, this is only a bilinear form, since it is not positive definite.

state is the $\mathbf{k} = 0$ Bloch state and correspondingly the mean-field parameters are site independent $\phi_{\boldsymbol{\ell}} = \phi$ when the zeroth order energy is minimized. Here we introduce intermediate Bloch fluctuation operators

$$\delta a_{\mathbf{k}} = \frac{1}{\sqrt{L}} \sum_{\boldsymbol{\ell}} e^{-i\mathbf{k}\cdot\mathbf{r}_{\boldsymbol{\ell}}}\, \delta b_{\boldsymbol{\ell}} \tag{6.19}$$

$$\delta a^{\dagger}_{\mathbf{k}} = \frac{1}{\sqrt{L}} \sum_{\boldsymbol{\ell}} e^{i\mathbf{k}\cdot\mathbf{r}_{\boldsymbol{\ell}}}\, \delta b^{\dagger}_{\boldsymbol{\ell}} \tag{6.20}$$

as well as the corresponding column vectors, analogous to Eq. (6.11). In matrix form, this transformation can be expressed as

$$\begin{pmatrix} \boldsymbol{\delta}\mathbf{b} \\ \boldsymbol{\delta}\mathbf{b}^{\dagger} \end{pmatrix} = \begin{pmatrix} K & 0 \\ 0 & K^{*} \end{pmatrix} \begin{pmatrix} \boldsymbol{\delta}\mathbf{a} \\ \boldsymbol{\delta}\mathbf{a}^{\dagger} \end{pmatrix} \qquad \text{with} \qquad K_{l,\mathbf{k}} = \frac{1}{\sqrt{L}} e^{i\mathbf{k}\cdot\mathbf{r}_{\boldsymbol{\ell}}} \tag{6.21}$$

and $K = K^{\dagger}$ is a $L \times L$ unitary matrix. Inserting this into Eq. (6.12), the second order Hamiltonian becomes

$$\mathcal{H}^{(2)} = \frac{1}{2} \begin{pmatrix} \boldsymbol{\delta}\mathbf{a} \\ \boldsymbol{\delta}\mathbf{a}^{\dagger} \end{pmatrix}^{\dagger} \tilde{H}_{\mathrm{QP}} \begin{pmatrix} \boldsymbol{\delta}\mathbf{a} \\ \boldsymbol{\delta}\mathbf{a}^{\dagger} \end{pmatrix} - \frac{1}{2} \mathrm{Tr}\,(h)\,. \tag{6.22}$$

where the quasi-particle Hamiltonian in Bloch space

$$\tilde{H}_{\mathrm{QP}} = \begin{pmatrix} \tilde{h} & \tilde{\Delta} \\ \tilde{\Delta}^{*} & \tilde{h}^{*} \end{pmatrix} = \begin{pmatrix} K & 0 \\ 0 & K^{*} \end{pmatrix}^{\dagger} \begin{pmatrix} h & \Delta \\ \Delta^{*} & h^{*} \end{pmatrix} \begin{pmatrix} K & 0 \\ 0 & K^{*} \end{pmatrix} = \begin{pmatrix} K^{\dagger} h K & K^{\dagger} \Delta K^{*} \\ K^{t} \Delta^{*} K & K^{t} h^{*} K^{*} \end{pmatrix}. \tag{6.23}$$

Note that under the unitary single particle transformation, h and $\tilde{h}$ are related by the unitary transformation K. In contrast, the anomalous coupling Δ does not transform unitarily. Although Δ is a multiple of the unit matrix (which is invariant under any unitary transformation) in Wannier space, its counterpart $\tilde{\Delta}$ in Bloch space is non-diagonal. The matrix multiplication in Eq. (6.23) can be performed explicitly and the matrix elements are found to be

$$\tilde{h}_{\mathbf{k},\mathbf{k}'} = \delta_{\mathbf{k},\mathbf{k}'} \left[2U|\phi|^2 - \mu - JZ + \epsilon(\mathbf{k}) \right] \tag{6.24}$$

$$\tilde{\Delta}_{\mathbf{k},\mathbf{k}'} = \delta_{\mathbf{k},-\mathbf{k}'} U \phi^2. \tag{6.25}$$

Let us shortly discuss the coupling structure of $\tilde{H}_{\mathrm{QP}}$. For each single particle Bloch state $|\mathbf{k}\rangle$, which is an eigenstate of the single particle Hamiltonian, there exists a time reversed state eigenstate $|-\mathbf{k}\rangle$. Only at high symmetry points in the Brillouin zone $\mathbf{k} = 0$ and on the edge, does the Bloch state coincide with its time-reversed state and, in principle, these cases have to be considered separately. The matrix $\tilde{h}$ is already diagonal, however the matrix $\tilde{\Delta}$ couples a particle in the $|\mathbf{k}\rangle$ mode with a hole in the $|-\mathbf{k}\rangle$ mode. Through a unitary permutation transformation, the matrix $\tilde{H}_{\mathrm{QP}}$ can be brought into Block diagonal form, consisting of two-dimensional irreducible subblocks, see Fig. (6.1).

$$P_{\sigma}^{\dagger}\, \Sigma\, \tilde{H}_{\mathrm{QP}} P_{\sigma} = \begin{pmatrix} \begin{pmatrix} \Sigma\tilde{H}^{(\mathbf{k}_1)} \end{pmatrix} & 0 & & \\ 0 & \begin{pmatrix} \Sigma\tilde{H}^{(\mathbf{k}_2)} \end{pmatrix} & & \\ & & \begin{pmatrix} \Sigma\tilde{H}^{(\mathbf{k}_3)} \end{pmatrix} & \\ & & & \ddots \end{pmatrix}$$

Figure 6.1: The two coupled modes correspond to the creation of a particle in a given mode $|\mathbf{k}\rangle$ and the annihilation of a particle (i.e. a hole) in the time reversed mode $|-\mathbf{k}\rangle$.

The time dependence of the Gross-Pitaevskii field can be determined from the $U(1)$-symmetry breaking formulation as the time-dependent expectation value of the condensate mode a_0 annihilation operator

$$\phi_{\boldsymbol{\ell}}(t) = \langle \psi_{N-1} | a_c^{(\boldsymbol{\ell})} | \psi_N \rangle. \tag{6.26}$$

Here $|\psi_N(t)\rangle$ and $|\psi_{N-1}(t)\rangle$ are the condensate states with N and $N-1$ particles, which evolve in time with phase factors of $e^{-iE_N t}$ and $e^{-iE_{N-1}t}$ respectively and a_c is the annihilation operator for the condensate mode. Hence, a the evolution of a stationary solution of the time-dependent GP is determined by difference in the N and $N-1$ condensate energies, i.e. the chemical potential $\mu = E_N - E_{N-1}$

$$\phi_{\boldsymbol{\ell}}(t) = e^{-i\mu t}\phi_{\boldsymbol{\ell}}(0). \tag{6.27}$$

It is convenient to choose the global energy offset such that the solutions for the fluctuations of the order parameter from the mean field ground state are stationary, which imposes

$$\mu = -JZ + U|\phi|^2. \tag{6.28}$$

In contrast to the free space analogue, the term $-JZ$ arises in the lattice, which is the trapping energy per particle in a red detuned (attractive) lattice. Inserting Eq. (6.28) into the 2×2 subblock of $P_\sigma^\dagger \Sigma \tilde{H}_{\mathrm{QP}} P_\sigma$ for fixed $\mathbf{k}$ and writing the constant condensate state in terms of modulus and phase $\phi = |\phi| e^{i\varphi}$, this becomes

$$\Sigma\mathcal{H}^{(\mathbf{k})} = \begin{pmatrix} U|\phi|^2 + \epsilon(\mathbf{k}) & U|\phi|^2 e^{2i\varphi} \\ -U|\phi|^2 e^{-2i\varphi} & -[U|\phi|^2 + \epsilon(-\mathbf{k})] \end{pmatrix}, \tag{6.29}$$

and the diagonalization of the entire matrix can be performed analytically for each subblock, leading to the well known usual Bogoliubov result. For each $\mathbf{k}$ the 2×2 matrix (6.29) is of the structure (K.14), we know that for the case that two eigenvalues exist (which is guaranteed if one eigenvalue is non-zero), these are real, equal in magnitude and differ in sign. We denote these by $\omega_\pm^{(\mathbf{k})}$. In the following discussion we will consider the case of non-zero eigenvectors and treat the case of a vanishing eigenvalue later.

Eigenvalues

Determining the eigenvalues as the roots of the characteristic polynomial $\chi(\lambda) = |\mathcal{H}^{(\mathbf{k})} - \lambda \mathbb{1}|$, directly leads to

$$\omega_\pm^{(\mathbf{k})} = \pm\sqrt{\epsilon^2(\mathbf{k}) + 2U|\phi|^2\epsilon(\mathbf{k})}, \tag{6.30}$$

which is the well known Bogoliubov dispersion relation in a lattice. Note that the eigenvalues, which are measurable physical quantities, are independent of the complex phase of the condensate state ϕ. For homogeneous condensates, such as the ground state of a homogeneous system, it turns out that eigenvectors $\mathbf{x}$ to a positive eigenvalue also have a positive norm $x^\dagger \Sigma_2 x > 0$, which is not always true as in the case of vortex states for example [51]. Since the structure of the 2×2 matrix is of the form in Eq. (K.14), it is no surprise that the two eigenvalues only differ in sign and they refer to the same physical excitation. Whereas the positive eigenvalue $\omega_+^{(\mathbf{k})}$ corresponds to the creation of a quasi-particle, the negative eigenvalue $\omega_-^{(\mathbf{k})}$ and the corresponding operator refers to the operator creating a hole in the same quasi-particle mode, thus reducing the energy by the amount of the positive eigenvalue. We henceforth only consider the positive eigenvalue, keeping this in mind.

Eigenvectors

The elements of the eigenvector $\mathbf{x}^{(\mathbf{k})} = \begin{pmatrix} u_{\mathbf{k}} \\ -v_{\mathbf{k}} \end{pmatrix}$ on this two-dimensional subspace to the positive eigenvalue $\omega_+^{(\mathbf{k})}$ can conveniently be expressed as

$$u_{\mathbf{k}} = \left[\frac{\epsilon(\mathbf{k}) + U|\phi|^2}{2\omega_+^{(\mathbf{k})}} + \frac{1}{2} \right]^{\frac{1}{2}} \tag{6.31}$$

$$v_{\mathbf{k}} = e^{-2i\varphi} \left[\frac{\epsilon(\mathbf{k}) + U|\phi|^2}{2\omega_+^{(\mathbf{k})}} - \frac{1}{2} \right]^{\frac{1}{2}} \tag{6.32}$$

which automatically guarantees that $\mathbf{x}^{(\mathbf{k})}$ is normalized to unity

$$1 = \mathbf{x}^{(\mathbf{k})\dagger} \Sigma \, \mathbf{x}^{(\mathbf{k})} = |u_{\mathbf{k}}|^2 - |v_{\mathbf{k}}|^2, \tag{6.33}$$

as can be verified explicitly. Using the relation

$$U^2|\phi|^4 = (\epsilon(\mathbf{k}) + U|\phi|^2 - \omega_+)(\epsilon(\mathbf{k}) + U|\phi|^2 + \omega_+), \tag{6.34}$$

it can also be directly verified that $\mathbf{x}^{(\mathbf{k})}$ is an eigenvector of $\mathcal{H}^{(\mathbf{k})}$ to the eigenvalue $\omega_+^{(\mathbf{k})}$. As discussed in Sec. (K.1) the corresponding eigenvector to the negative eigenvalue $\omega_-^{(\mathbf{k})}$ is $\mathbf{y}^{(\mathbf{k})} = \begin{pmatrix} -\mathbf{v}^{(\mathbf{k})*} \\ \mathbf{u}^{(\mathbf{k})*} \end{pmatrix}$. Using the linear independence of the two eigenvectors in conjunction with their orthogonality with respect to Σ, the completeness relation within one such diagonalizable sub-block can be expressed as

$$\mathbb{1}_{\mathbf{k}} = (\mathbf{x}^{(\mathbf{k})}\mathbf{x}^{(\mathbf{k})\dagger} - \mathbf{y}^{(\mathbf{k})}\mathbf{y}^{(\mathbf{k})\dagger})\Sigma. \tag{6.35}$$

The Non-Diagonalizable Sub-Block

For any non-zero single-particle energy $\epsilon(\mathbf{k}) > 0$ the 2×2 subblock in Eq. (6.29) possesses a basis of eigenvectors. This is however not true for the mode corresponding to the single particle condensate state with $\epsilon(\mathbf{k}) = 0$ for finite interactions $U|\phi|^2 > 0$. Here, the matrix

$$\Sigma H^{(\mathbf{k}=0)} = U|\phi|^2 \begin{pmatrix} 1 & e^{2i\varphi} \\ -e^{-2i\varphi} & -1 \end{pmatrix} \tag{6.36}$$

always has one eigenvector $\mathbf{p} = \frac{1}{\sqrt{2}} \begin{pmatrix} e^{i\varphi} \\ -e^{-i\varphi} \end{pmatrix}$ to an eigenvalue 0. Clearly, its norm vanishes $\mathbf{p}^\dagger \Sigma \mathbf{p} = 0$ and thus any vector that is orthogonal to $\mathbf{p}$ in this 2D subspace, will be a multiple of $\mathbf{p}$. A second eigenvector of $\Sigma H^{(\mathbf{k}=0)}$ does not exist, rather $\Sigma H^{(\mathbf{k}=0)}$ maps any vector onto a multiple of $\mathbf{p}$ (i.e. $\Sigma H^{(\mathbf{k}=0)}$ is of rank 1). Hence, there exists no basis of eigenvectors of $\Sigma H^{(\mathbf{k}=0)}$ and we have to complete the basis with some other vector. Using $\mathbf{p}$ as the first basis vector, it is convenient to choose the second basis vector

$$\mathbf{q} = \frac{-i}{\sqrt{2}} \begin{pmatrix} e^{i\varphi} \\ e^{-i\varphi} \end{pmatrix} \tag{6.37}$$

to be orthogonal to $\mathbf{p}$ with respect to the euclidean scalar product[5]. This is mapped onto

$$\Sigma H^{(\mathbf{k}=0)} \mathbf{q} = -\frac{i}{\tilde{m}} \mathbf{p}, \tag{6.38}$$

[5]Since it can't be chosen orthogonal to $\mathbf{p}$ with respect to Σ.

where $\tilde{m} = \frac{1}{2U|\phi|^2}$ takes on the role of a mass, as will become apparent. We thus have the relations

$$\mathbf{q}^\dagger \Sigma \mathbf{q} = 0 \tag{6.39}$$

$$\mathbf{q}^\dagger H^{(\mathbf{k}=0)} \mathbf{p} = \frac{1}{\tilde{m}} \tag{6.40}$$

$$\mathbf{q}^\dagger \Sigma \mathbf{p} = i \tag{6.41}$$

and the completeness relation on this subspace in terms of $\mathbf{p}$ and $\mathbf{q}$ can be expressed as

$$i(\mathbf{q}\,\mathbf{p}^\dagger - \mathbf{p}\,\mathbf{q}^\dagger)\Sigma = \mathbb{1}_2. \tag{6.42}$$

Multiplying $\Sigma H^{(\mathbf{k}=0)}$ with (6.42) from the right and using (6.38) as well as the eigenvector relation, the block-diagonal part of ΣH on the 2D subspace can be expressed as

$$\Sigma H^{(\mathbf{k}=0)} = \frac{1}{\tilde{m}} \mathbf{p}\,\mathbf{p}^\dagger \Sigma. \tag{6.43}$$

The corresponding part of the quasi-particle Hamiltonian on this subspace becomes

$$\begin{aligned} \mathcal{H}^{(2,\mathbf{k}=0)} &= \frac{1}{2} \begin{pmatrix} \delta a_0 \\ \delta a_0^\dagger \end{pmatrix}^\dagger \tilde{H}^{(0)} \begin{pmatrix} \delta a_0 \\ \delta a_0^\dagger \end{pmatrix} - \frac{1}{2} U|\phi|^2 \\ &= \frac{1}{2\tilde{m}} \mathscr{P}^2 - \frac{1}{2} U|\phi|^2. \end{aligned} \tag{6.44}$$

The last term comes from the permutation of operators into normal order. Here we defined the Hermitian operator

$$\mathscr{P} = \mathbf{p}^\dagger \Sigma \begin{pmatrix} \delta a_0 \\ \delta a_0^\dagger \end{pmatrix} = \frac{e^{-i\varphi}\,\delta a_0 + e^{i\varphi}\,\delta a_0^\dagger}{\sqrt{2}}, \tag{6.45}$$

which takes on the role of a momentum operator for a particle of mass $\tilde{m}$ without a restoring force, which is ubiquitous to quasi-particle Hamiltonians in systems with a spontaneously broken symmetry [19].

Transformation of the entire Hamiltonian

We now revert to the original, full space (i.e. not the subspaces of the individual subblocks) and synonymously use the notation $\mathbf{x}, \mathbf{y}, \mathbf{q} = -i \begin{pmatrix} \mathbf{v}^{(0)} \\ \mathbf{v}^{(0)*} \end{pmatrix}$, $\mathbf{p} = \begin{pmatrix} \mathbf{u}^{(0)} \\ -\mathbf{u}^{(0)*} \end{pmatrix}$ for the respective vectors.

For the general inhomogeneous case, the upper index in the vectors $\mathbf{u}^{(s)}$, $\mathbf{v}^{(s)}$ is the collective mode index. Only in the homogeneous case is this labeled with a quasi-momentum. In the scalar coefficients $u_\mathbf{k}$ and $v_\mathbf{k}$ (the eigenvector elements in Eqns. (6.31, 6.32)) are the only non-zero elements in the vectors $\mathbf{u}^{(\mathbf{k})}$ and $\mathbf{v}^{(\mathbf{k})}$ at the positions corresponding to the $|\mathbf{k}\rangle$ and $|-\mathbf{k}\rangle$ modes respectively. Within the index notation, we thus have

$$\mathbf{u}_\mathbf{k}^{(s)} = \delta_{s,\mathbf{k}}\, u_\mathbf{k} \tag{6.46}$$

$$\mathbf{v}_\mathbf{k}^{(s)} = \delta_{s,-\mathbf{k}}\, v_{-\mathbf{k}}. \tag{6.47}$$

Except for these two elements, all other entries of the vectors $\mathbf{u}^{(s)}$, $\mathbf{v}^{(s)}$ are zero for the homogeneous case.

Combining the completeness relations on the diagonalizable and non-diagonalizable subspaces, the unit operator on the entire space becomes

$$\mathbb{1} = \left[\sum_{\mathbf{k}\neq 0} (\mathbf{x}^{(\mathbf{k})} \mathbf{x}^{(\mathbf{k})\dagger} - \mathbf{y}^{(\mathbf{k})} \mathbf{y}^{(\mathbf{k})\dagger}) \Sigma \right] + i(\mathbf{q}\,\mathbf{p}^\dagger - \mathbf{p}\,\mathbf{q}^\dagger)\Sigma. \tag{6.48}$$

Multiplying $\tilde{H}_{\mathrm{QP}}$ with $\mathbb{1} = \Sigma^2$ from the left and Eq. (6.48) from the right, the second order fluctuation Hamiltonian (6.22) becomes

$$\begin{aligned}\mathcal{H}^{(2)} &= \frac{1}{2}\begin{pmatrix}\boldsymbol{\delta a}\\ \boldsymbol{\delta a}^\dagger\end{pmatrix}^\dagger \tilde{H}_{\mathrm{QP}} \begin{pmatrix}\boldsymbol{\delta a}\\ \boldsymbol{\delta a}^\dagger\end{pmatrix} - \frac{1}{2}\mathrm{Tr}\left(\tilde{h}\right) \\ &= \frac{1}{2}\begin{pmatrix}\boldsymbol{\delta a}\\ \boldsymbol{\delta a}^\dagger\end{pmatrix}^\dagger \left[\sum_{\mathbf{k}\neq 0}(\omega_+^{(\mathbf{k})}\Sigma\,\mathbf{x}^{(\mathbf{k})}\mathbf{x}^{(\mathbf{k})\,\dagger}\Sigma - \omega_-^{(\mathbf{k})}\Sigma\,\mathbf{y}^{(\mathbf{k})}\mathbf{y}^{(\mathbf{k})\,\dagger}\Sigma) + \frac{1}{\tilde{m}}\Sigma\mathbf{p}\mathbf{p}^\dagger\Sigma\right]\begin{pmatrix}\boldsymbol{\delta a}\\ \boldsymbol{\delta a}^\dagger\end{pmatrix} - \frac{1}{2}\mathrm{Tr}\left(\tilde{h}\right).\end{aligned} \tag{6.49}$$

Defining the quasi-particle annihilation operators

$$\beta_{\mathbf{k}} = \mathbf{x}^{(\mathbf{k})\,\dagger}\Sigma\begin{pmatrix}\boldsymbol{\delta a}\\ \boldsymbol{\delta a}^\dagger\end{pmatrix} \tag{6.50}$$

and the momentum-like operator

$$\mathscr{P} = \mathbf{p}^\dagger\Sigma\begin{pmatrix}\boldsymbol{\delta a}\\ \boldsymbol{\delta a}^\dagger\end{pmatrix} = \frac{1}{\sqrt{2}}(e^{-i\varphi}\,\delta a_{\mathbf{k}=0} + e^{i\varphi}\,\delta a_{\mathbf{k}=0}^\dagger) \tag{6.51}$$

the second order Hamiltonian can be expressed in terms of these as

$$\mathcal{H}^{(2)} = \sum_{\mathbf{k}\neq 0}\omega_+^{(\mathbf{k})}\beta_{\mathbf{k}}^\dagger\beta_{\mathbf{k}} + \frac{1}{2\tilde{m}}\mathscr{P}^2 + \Delta E^{(2)} \tag{6.52}$$

with the (negative) scalar energy shift

$$\Delta E^{(2)} = \frac{1}{2}\sum_{\mathbf{k}\neq 0}\omega_+^{(\mathbf{k})} - \frac{1}{2}\mathrm{Tr}\left(\tilde{h}\right). \tag{6.53}$$

Here first term arises from bringing the second term in Eq. (6.49) into normal order. For the homogeneous system, the quasi-particle annihilation and creation operators can be expressed both in terms of $\mathbf{x}$ and $\mathbf{y}$ vectors:

$$\begin{aligned}\beta_{\mathbf{k}}^\dagger &= u_{\mathbf{k}}\,\delta a_{\mathbf{k}}^\dagger + v_{\mathbf{k}}\,\delta a_{-\mathbf{k}} \\ &= -\mathbf{y}^{(\mathbf{k})\,\dagger}\Sigma\begin{pmatrix}\boldsymbol{\delta a}\\ \boldsymbol{\delta a}^\dagger\end{pmatrix} \\ &= \begin{pmatrix}\boldsymbol{\delta a}\\ \boldsymbol{\delta a}^\dagger\end{pmatrix}^\dagger \Sigma\,\mathbf{x}^{(\mathbf{k})}.\end{aligned} \tag{6.54}$$

Here we implicitly used the relations in Eqns. (6.46,6.47), which directly leads to

$$\mathbf{u}^{(\mathbf{k})\,\dagger}\cdot\boldsymbol{\delta a} = u_{\mathbf{k}}^*\,\delta a_{\mathbf{k}} \tag{6.55}$$

$$\mathbf{v}^{(\mathbf{k})\,\dagger}\cdot\boldsymbol{\delta a}^\dagger = v_{\mathbf{k}}^*\,\delta a_{-\mathbf{k}}^\dagger. \tag{6.56}$$

Explicit Form of the p and q Vectors

We now prove by construction, that one eigenvector $\mathbf{p}$ to a zero eigenvalue of ΣH_{QP} exists. In the initial fluctuation expansion of the Hamiltonian in Eq. (6.3 - 6.7), we saw that the minimization of the scalar energy term was fully equivalent to the first order term in the Hamiltonian vanishing identically. We will now see, that this condition is also reflected in the second order term, where it relates the eigenvector $\mathbf{p}$ to the condensate state. We know that the vector $\mathbf{p}$ is of the form $\mathbf{p} = \begin{pmatrix}\mathbf{u}^{(0)}\\ -\mathbf{u}^{(0)*}\end{pmatrix}$, where the L-dimensional vector $\mathbf{u}^{(0)}$ is normalized as $\mathbf{u}^{(0)\,\dagger}\mathbf{u}^{(0)} = 1/2$. If we define the vector

$$\mathbf{u}^{(0)} = \frac{1}{\sqrt{2N}}\begin{pmatrix}\phi_1\\ \vdots\\ \phi_L\end{pmatrix}, \tag{6.57}$$

we see that for the upper half of the elements (i.e. $1 \leq l \leq L$)

$$\begin{aligned}(\Sigma H_{\mathrm{QP}}\mathbf{p})_{\boldsymbol{\ell}} &= \sum_{\boldsymbol{\ell}'} \left[h_{\boldsymbol{\ell},\boldsymbol{\ell}'}\,\phi_{\boldsymbol{\ell}'} - \Delta_{\boldsymbol{\ell},\boldsymbol{\ell}'}\,\phi^*_{\boldsymbol{\ell}'}\right] \\ &= -J \sum_{\boldsymbol{\ell}'\in \mathrm{n.n.}(\boldsymbol{\ell})} \phi_{\boldsymbol{\ell}'} + \left(\epsilon_{\boldsymbol{\ell}} - \mu + U|\phi_{\boldsymbol{\ell}}|^2\right)\phi_{\boldsymbol{\ell}} \\ &= 0\end{aligned} \tag{6.58}$$

vanishes, since it is equivalent to the conjugate of the condition in Eq. (6.9). The lower half of the elements vanish by virtue of the conjugate calculation. This explicitly proves that $\mathbf{p}$, as defined via (6.57) is an eigenvector to the eigenvalue zero.

Furthermore, within Bogoliubov theory for the homogeneous case with $\phi_{\boldsymbol{\ell}} = \phi$, we can also explicitly construct the vector $\mathbf{q}$ and extract the effective mass $\tilde{m}$. It was shown that $\mathbf{q} = -i\begin{pmatrix}\mathbf{v}^{(0)}\\ \mathbf{v}^{(0)*}\end{pmatrix}$ and we here define $\mathbf{v}^{(0)} = \mathbf{u}^{(0)}$, as in Eq. (6.57). By explicit multiplication, one finds

$$\begin{aligned}(\Sigma H_{\mathrm{QP}}\mathbf{q})_{\boldsymbol{\ell}} &= -\frac{i}{\sqrt{2N}} \sum_{\boldsymbol{\ell}'} \left[h_{\boldsymbol{\ell},\boldsymbol{\ell}'}\,\phi_{\boldsymbol{\ell}'} + \Delta_{\boldsymbol{\ell},\boldsymbol{\ell}'}\,\phi^*_{\boldsymbol{\ell}'}\right] \\ &= -2iU|\phi|^2(\mathbf{p})_{\boldsymbol{\ell}},\end{aligned} \tag{6.59}$$

from which we can extract

$$\tilde{m} = \frac{1}{2U|\phi|^2} \tag{6.60}$$

via Eq. (6.38).

Structure of the Modes

Each mode, other than the condensate mode, corresponds to an harmonic oscillator mode with an equidistant energy spectrum and the excitations being of a bosonic nature $[\beta_{\mathbf{k}}, \beta^\dagger_{\mathbf{k}'}] = \delta_{\mathbf{k},\mathbf{k}'}$. Within this extended treatment, an additional effective kinetic energy term without a restoring force appears from the condensate subspace, with the inverse mean-field interaction energy per site $\tilde{m} = \frac{1}{2U|\phi|^2}$ acting as an inertial prefactor. The spectrum of $\mathscr{P}^2$ is bounded from below, since $\mathscr{P}$ is Hermitian and for any state $|\psi\rangle$ the expectation value $(\langle\psi|\mathscr{P}^\dagger)(\mathscr{P}|\psi\rangle)$ is non-negative.

A comparison with Eq. (6.32) shows that the scalar energy shift can also be expressed in terms of the Bogoliubov coefficients $v^{(\mathbf{k})}$ as

$$\Delta E^{(2)} = -\sum_{\mathbf{k}\neq 0} \omega_+^{(\mathbf{k})}\,|v_{\mathbf{k}}|^2 - \frac{1}{2}U|\phi|^2. \tag{6.61}$$

Note that in the non-interacting limit, where the true ground state approaches the Gross-Pitaevskii state, the coefficients $|v^{(\mathbf{k})}|^2$ and hence also the ground state energy shift $\Delta E^{(2)}$ vanish.

The Bogoliubov ground state

Since the ground state energy of the Bogoliubov Hamiltonian $E^{(0)} + \Delta E^{(2)}$ is lower than the GP energy $E^{(0)}$, the Bogoliubov ground state $|\psi_{\mathrm{Bog}}\rangle$ cannot be the GP state. Rather, the Bogoliubov ground state is a superposition of states with pairs of particle hole excitations, which can be clearly seen in the number-conserving, variational state approach in Eq. (6.164). Colloquially, these are referred to as *quantum fluctuations* and they lower the energy expectation value of $|\psi_{\mathrm{Bog}}\rangle$.

The ground state of the Bogoliubov Hamiltonian (6.52) can be implicitly defined by considering the various terms individually. For each of the harmonic oscillator modes, the ground state is the harmonic oscillator ground state

$$\beta_{\mathbf{k}}|\psi_{\mathrm{Bog}}\rangle = 0. \tag{6.62}$$

and furthermore also the self-consistent ground state, which minimizes the energy of the operator $\mathscr{P}^2$. Within the momentum operator, the eigenstates correspond correspond to plane waves and the ground state would be the $p = 0$ state (this abstract momentum is not to be confused with the physical momentum or quasi-momentum of the atoms).

Although the implicit definition (6.62) of the ground state is very compact and the expectation value of any operator can be implicitly calculated by expressing it in terms of quasi-particle creation and annihilation operators, the explicit form of the ground state is of interest. This can be constructed by determining the unitary operator S on the full many-particle Hilbert space, which relates the quasi-particle to the original annihilation operators

$$\beta_{\mathbf{k}} = S a_{\mathbf{k}} S^\dagger. \tag{6.63}$$

The explicit form of S can be found by solving an effective differential equation for the expectation values within coherent states [19], or alternatively by using an extended version of the transformation relation presented in appendix (J). Subsequently, the Bogoliubov ground state can be expressed explicitly in terms of the a unitary transformation acting on the Gross-Pitaevskii ground state

$$\begin{aligned} |\psi_{\mathrm{Bog}}\rangle &= S|\psi_{\mathrm{GP}}\rangle \\ &= \det(U^\dagger U)^{-1/4} \exp\left[\frac{1}{2}\boldsymbol{\delta}\mathbf{a}_{\mathbf{k}}^{\dagger\, t} U^{*-1} V^* \boldsymbol{\delta}\mathbf{a}_{\mathbf{k}}^\dagger\right] |\psi_{\mathrm{GP}}\rangle, \end{aligned} \tag{6.64}$$

where U and V are the matrices containing the column vectors $\mathbf{u}^{(\mathbf{k})}$ and $\mathbf{v}^{(\mathbf{k})}$ respectively for all $\mathbf{k}$. In both matrices U and V, as well as in the operator vector $\boldsymbol{\delta}\mathbf{a}_{\mathbf{k}}^\dagger$, the $|\mathbf{k} = 0\rangle$ is omitted, since no annihilation operator can be associated with it. To simplify the expression $|\psi_{\mathrm{Bog}}\rangle$ further, we use the relation

$$\frac{v_{\mathbf{k}}}{u_{\mathbf{k}}} = 2e^{-2i\varphi} \frac{\omega_+^{(\mathbf{k})} |v_{\mathbf{k}}|^2}{U|\phi|^2} \tag{6.65}$$

and obtain

$$|\psi_{\mathrm{Bog}}\rangle = \det(U^\dagger U)^{-1/4} \exp\left[e^{-2i\varphi} \frac{\omega_+^{(\mathbf{k})} |v_{\mathbf{k}}|^2}{U|\phi|^2} \delta a_{\mathbf{k}}^\dagger \delta a_{-\mathbf{k}}^\dagger\right] |\psi_{\mathrm{GP}}\rangle. \tag{6.66}$$

This expression clearly reveals, that with increasing interaction strength, more and more correlated excitations in opposite momenta (as well as states with a higher number of such excitations, due to the exponential structure) are admixed to the original GP ground state.

For the non-interacting case, S is simply the unit operator and the Bogoliubov ground state is the GP ground state. Increasing the interaction, the unitary operator S smoothly rotates the Bogoliubov state away from the GP state, increasing the amplitude of correlated pair excitations at finite momenta.

6.1.2 Transformation of Operators

Up to now we have determined the eigenvectors of $\Sigma\tilde{H}_{\mathrm{QP}}$ and expressed the second order Hamiltonian in terms of operators corresponding to these. Operators corresponding to eigenvectors other than the condensate mode (i.e. where the eigenvector is orthogonal to the condensate orbital with respect to the scalar product Σ) are bosonic ladder operators. Conjugate pairs of eigenvectors $\mathbf{x}^{(s)}$ and $\mathbf{y}^{(s)} = \gamma \mathbf{x}^{(s)^*}$ correspond to the same physical mode. Within Bogoliubov theory for a system consisting of L bosonic degrees of freedom, $\Sigma\tilde{H}_{\mathrm{QP}}$ possesses $2L - 1$ eigenvectors, corresponding to $L - 1$ bosonic modes. In the condensate (which is always the case for Bogoliubov theory), there exists one eigenvector $\mathbf{p}$ to an eigenvalue of zero, corresponding to the condensate mode in the respective single particle basis. There is no additional, linearly independent conjugate eigenvector to $\mathbf{p}$ and the associated operator $\mathscr{P}$ is not a bosonic ladder operator, i.e. $[\mathscr{P}, \mathscr{P}^\dagger] \neq 1$. In fact, this commutator vanishes, as $\mathscr{P}$ is Hermitian. In the sense that we do not have a complete basis

of eigenvectors, i.e. only $2L-1$ eigenvectors in the $2L$-dimensional space for within Bogoliubov theory, we are also missing one operator in addition to $\{\beta_s, \beta_s^\dagger, \mathscr{P}\}$, which we require to express an arbitrary operator given in terms of δa and $\delta a^\dagger$. Clearly, this is the operator associated with the additional basis vector $\mathbf{q}$ and we define

$$\mathcal{Q} = -\mathbf{q}^\dagger \Sigma \begin{pmatrix} \boldsymbol{\delta a} \\ \boldsymbol{\delta a}^\dagger \end{pmatrix} = \frac{e^{-i\varphi}\,\delta a_0 - e^{i\varphi}\,\delta a_0^\dagger}{\sqrt{2}\,i}, \tag{6.67}$$

which is also Hermitian.

Generalized Transformation in the Non-Diagonalizable Case

The transformation in the diagonalizable case is simpler than in the non-diagonalizable case. We therefore only describe the latter here - the diagonalizable case is equivalent to neglecting the non-diagonalizable subspace.

In the non-diagonalizable case, a basis of eigenvectors does not exist. Here we complete the set of eigenvectors to a basis by including the additional vector $\mathbf{q}$. We begin by defining the matrix by its column vectors

$$W = \Big[\mathbf{x}^{(1)}, \ldots, \mathbf{x}^{(L-1)},\, i\mathbf{p},\, \mathbf{y}^{(1)}, \ldots, \mathbf{y}^{(L-1)}, i\mathbf{q}\Big]. \tag{6.68}$$

The factors of i and the ordering are chosen such that the resulting transformations take on a particularly simple form. Since all column vectors are linearly independent, the matrix W is non-singular and the inverse W^{-1} exists. Next, we explicitly determine the matrix product

$$W^\dagger \Sigma W = \begin{pmatrix} \mathbb{1}_{L-1} & & & \\ & 0 & \ldots & -i \\ & \vdots & -\mathbb{1}_{L-1} & \vdots \\ & i & \ldots & 0 \end{pmatrix} =: \tilde{\Sigma}, \tag{6.69}$$

where we used the relations

$$\mathbf{x}^{(r)\dagger}\Sigma\mathbf{x}^{(s)} = \delta_{r,s} \tag{6.70}$$
$$\mathbf{y}^{(r)\dagger}\Sigma\mathbf{y}^{(s)} = -\delta_{r,s} \tag{6.71}$$
$$\mathbf{x}^{(r)\dagger}\Sigma\mathbf{y}^{(s)} = 0 \tag{6.72}$$
$$\mathbf{p}^\dagger\Sigma\mathbf{p} = 0 \tag{6.73}$$
$$\mathbf{p}^\dagger\Sigma\mathbf{x}^{(s)} = 0 \tag{6.74}$$
$$\mathbf{p}^\dagger\Sigma\mathbf{y}^{(s)} = 0 \tag{6.75}$$
$$\mathbf{q}^\dagger\Sigma\mathbf{q} = 0 \tag{6.76}$$
$$\mathbf{q}^\dagger\Sigma\mathbf{x}^{(s)} = 0 \tag{6.77}$$
$$\mathbf{q}^\dagger\Sigma\mathbf{y}^{(s)} = 0 \tag{6.78}$$
$$\mathbf{q}^\dagger\Sigma\mathbf{p} = i \tag{6.79}$$

to determine the individual matrix elements. In Eq. (6.69) we defined the Hermitian and unitary matrix $\tilde{\Sigma} = \tilde{\Sigma}^\dagger$ with $\tilde{\Sigma}^2 = \mathbb{1}$. To determine the transformation between the original bosonic creation and annihilation operators and the operators $\{\boldsymbol{\beta}, \boldsymbol{\beta}^\dagger, \mathscr{P}, \mathcal{Q}\}$, we explicitly multiply out

$$\begin{pmatrix} \boldsymbol{\beta} \\ -i\mathscr{P} \\ -\boldsymbol{\beta}^\dagger \\ i\mathcal{Q} \end{pmatrix} = W^\dagger \Sigma \begin{pmatrix} \boldsymbol{\delta a} \\ \boldsymbol{\delta a}^\dagger \end{pmatrix}. \tag{6.80}$$

By multiplying both sides of Eq. (6.69) by $\tilde{\Sigma}$ from the left, one finds $\tilde{\Sigma}W^\dagger\Sigma W = \mathbb{1}$. This directly gives us the inverse matrix[6]

$$W^{-1} = \tilde{\Sigma}W^\dagger\Sigma = \begin{pmatrix} U^\dagger, & V^\dagger \\ -i\mathbf{v}^{(0)\dagger}, & i\mathbf{v}^{(0)t} \\ V^t, & U^t \\ \mathbf{u}^{(0)\dagger}, & \mathbf{u}^{(0)t} \end{pmatrix}. \tag{6.81}$$

[6]This is both the left and right inverse, since these are identical for any finite dimensional space.

Using this and multiplying EQ. (6.80) by $\tilde{\Sigma}$, we find the explicit form of both the forward and backward transformation of operators

$$\begin{pmatrix} \boldsymbol{\beta} \\ \mathcal{Q} \\ \boldsymbol{\beta}^\dagger \\ \mathscr{P} \end{pmatrix} = \tilde{\Sigma} W^\dagger \Sigma \begin{pmatrix} \boldsymbol{\delta a} \\ \boldsymbol{\delta a}^\dagger \end{pmatrix} \tag{6.82}$$

$$\begin{pmatrix} \boldsymbol{\delta a} \\ \boldsymbol{\delta a}^\dagger \end{pmatrix} = W \begin{pmatrix} \boldsymbol{\beta} \\ \mathcal{Q} \\ \boldsymbol{\beta}^\dagger \\ \mathscr{P} \end{pmatrix}. \tag{6.83}$$

These are the exact operator transformations and can be understood as a basis change on the space of bosonic creation and annihilation operators. Since any many-body operator can be expressed in terms of creation and annihilation operators (possibly containing multiple products of these), it can also be expressed exactly in terms of operators $\{\boldsymbol{\beta}, \boldsymbol{\beta}^\dagger, \mathscr{P}, \mathcal{Q}\}$.

Using the explicit expression (6.81), the transformation in Eq. (6.82) corresponds to the initial definition of the $\{\boldsymbol{\beta}, \boldsymbol{\beta}^\dagger, \mathscr{P}, \mathcal{Q}\}$ operators. The explicit form of the reverse transformation in Eq. (6.83) reads

$$\delta a_{\mathbf{k}} = \sum_s \mathbf{u}_{\mathbf{k}}^{(s)} \beta_s - \sum_s \mathbf{v}_{\mathbf{k}}^{(s)^*} \beta_s^\dagger + i \mathbf{u}_{\mathbf{k}}^{(0)} \mathcal{Q} + \mathbf{v}_{\mathbf{k}}^{(0)} \mathscr{P} \tag{6.84}$$

$$\delta a_{\mathbf{k}}^\dagger = \sum_s \mathbf{u}_{\mathbf{k}}^{(s)^*} \beta_s^\dagger - \sum_s \mathbf{v}_{\mathbf{k}}^{(s)} \beta_s - i \mathbf{u}_{\mathbf{k}}^{(0)^*} \mathcal{Q} + \mathbf{v}_{\mathbf{k}}^{(0)^*} \mathscr{P}. \tag{6.85}$$

The transformation relations discussed in this paragraph are generic and applicable to arbitrary spatial potentials. Furthermore, they are independent of the single particle basis in which the initial Hamiltonian is expressed and instead of the quasi-momentum orbitals $\mathbf{k}$, an arbitrary other mode basis may be used. The collective eigenmodes β_s and the spectrum ω_s obtained are independent of this basis.

Comparison with Bogoliubov Theory in Its Usual Form

In most textbooks, Bogoliubov theory is derived within a symmetry-breaking approach by identifying the single particle condensate mode and approximating the associated creation and annihilation operators by a scalar field $a_0, a_0^\dagger \mapsto \sqrt{N_0}$. In this *classical* approach to the bosonic field, the operator character is lost and higher order processes of particles being transferred between the condensate mode and other modes can no longer be captured. This is justified by the fluctuations, i.e. the fluctuations of the associated coherent state field within a path integral approach, being small relative to the averaged expectation value of the field $\sqrt{N_0}$. Within this approach, two operator degrees of freedom are discarded, namely δa_0 and $\delta a_0^\dagger$. On the remaining operator subspace, the complications of the eigenvectors of $\Sigma \tilde{H}_{\mathrm{QP}}$ not forming a complete basis set do not arise.

Since in our approach above, the eigenvector to the eigenvalue zero (corresponding to the condensate orbital) is not coupled to any of the excited collective modes, the Bogoliubov modes in the usual approach exactly coincide with the collective modes in our extended approach.

The two approaches are however also conceptually different: In the usual approach, it is assumed within the derivation that for any state at hand $a_0 \approx \sqrt{N_0}$, i.e. the depletion is small. Here a restriction is made on the level of the state to which the theory applies. In the approach above, we in principle exactly reexpress the full original Hamiltonian in terms of new operators $\{\boldsymbol{\beta}, \boldsymbol{\beta}^\dagger, \mathscr{P}, \mathcal{Q}\}$ when all higher order terms are taken along. No approximation is made to the state. The new operators are however usually chosen appropriately for a given parameter regime (such as J, U, μ and the spatial potential), such that no first order terms in the new operators appear when writing the specific Hamiltonian in terms of these. The operators thus have parametric dependence on the system parameters and in this sense they depend on the corresponding Gross-Pitaevskii state for

the system. The approximation to obtain effective, approximate descriptions of the system is made a posteriori here and different theories can be obtained.

Time-dependent Gross-Pitaevskii theory is recovered when using a variational state where all particles are condensed and all higher order terms are taken along in the action, from which the equations of motion are deduced. In this case, conservation laws which are violated within the lowest order Bogoliubov approximation, such as the total particle number, are again fulfilled. This is different in the usual form of Bogoliubov theory: if the condensate mode is approximated by a scalar field, the total particle number is not conserved (especially not when going away from equilibrium and for long times), since the operator coupling back to the condensate mode is missing.

Expressed in the basis of new new operators, the equations of motion for the bosonic modes are decoupled to lowest order. In other words, if one such quasi-particle mode is slightly populated, it is only coupled to other modes by higher order terms. If these couplings are weak, this occurs slowly on the inverse time scale of this mode's energy and it makes sense to consider this as a quasi-particle with a well-defined energy.

6.2 Gross-Pitaevskii Theory

In this section we shortly review the derivation of Gross-Pitaevskii theory. This is the simplest approach to describe weakly or non-interacting bosons, where it is assumed that every particle occupies the same single particle orbital

$$a_c^\dagger = \sum_{\boldsymbol{\ell}} \frac{\psi_{\boldsymbol{\ell}}}{\sqrt{N}} b_{\boldsymbol{\ell}}^\dagger \tag{6.86}$$

and thus implies a condensate fraction of one[7]. Gross-Pitaevskii theory can, in its most general form, be stated in terms of a variational many-particle state, where the variational parameters characterize the single particle condensate orbital.

We will determine the Gross-Pitaevskii energy and action both for a variational coherent state, as well as a condensate Fock state with fixed particle number. These are equivalent in the limit of large particle number N, but differ in $1/N$ corrections for finite. Thereafter we will derive Bogoliubov theory from the linearized form of time-dependent Gross-Pitaevskii theory, which demonstrates that Bogoliubov theory can also be derived within a particle number conserving approach without artificially breaking the $U(1)$-symmetry. Furthermore the physically relevant $1/N$ corrections for finite particle number are explicitly contained, which are contained neither in the operator-based approach in the previous section, nor in the coherent state Gross-Pitaevskii approach.

The Action and Equations of Motion for a Variational State

Specifying a variational state $|\psi(t)\rangle$ does not only allow to determine the ground state within that approximation, but also gives access to dynamics. In this case the variables determining the variational state become time-dependent fields (for Gross-Pitaevskii theory $\psi_{\boldsymbol{\ell}} \to \psi_{\boldsymbol{\ell}}(t)$) and, analogous to minimizing the energy for the static case, the physical field trajectories are those, which minimize the variational action

$$\mathcal{S} = \int_{t_i}^{t_f} dt \left[-i\langle\psi(t)|\partial_t|\psi(t)\rangle + \langle\psi(t)|H|\psi(t)\rangle \right]. \tag{6.87}$$

The temporal derivative is understood to act on the ket to its right only. If the action (6.87) is a sufficiently smooth functional of the variational fields, an extremum for a given field configuration implies that the action does not change (to infinitesimal order) for any infinitesimal change of the field configuration. In other words, any functional derivative with respect to a variational field vanishes along such an extremal field configuration. For a given action, expressed in terms of the variational fields and their temporal derivatives, the explicit equations of motion are obtained by taking the functional derivatives with respect to the conjugate fields

$$0 \stackrel{!}{=} \frac{\delta S_{GP}}{\delta \psi_{\boldsymbol{\ell}}^*(t)} \tag{6.88}$$

and subsequently rearranging and solving the resulting equations into appropriate form.

Note that the action (6.87) is the generic for any variational state. For a variational state of the most general form, i.e. an arbitrary state in the full Hilbert space expressed as a superposition of basis states with the variational parameters being the coefficients, it reproduces the time-dependent Schrödinger equation in the basis at hand. Here we use this procedure to determine the time-dependent Gross-Pitaevskii equation, where the condensate state on the lattice $\psi_{\boldsymbol{\ell}}(t)$ is the variational field. A rigorous derivation of the equations of motion for time-dependent Gutzwiller method, as discussed in section (3.4), also relies on this principle.

[7] This does however not imply that methods derived from Gross-Pitaevskii theory also always imply a fully condensed system. For instance, Bogoliubov theory can be derived from time-dependent Gross-Pitaevskii theory and allows for a small, but finite depletion.

Formulation in terms of Coherent States

The many-particle variational state can be of non-definite particle number, such as a coherent state

$$|\psi_{\mathrm{GP}}^{\mathrm{coh}}\rangle = e^{-N/2} e^{\sqrt{N} a_c^\dagger} |\mathrm{vac}\rangle, \tag{6.89}$$

which is particularly suited for calculations, since it is also a direct product of local coherent states on different sites and an eigenstate to any annihilation operator. Indeed, this state has a particle number expectation value $\langle\psi_{\mathrm{GP}}^{\mathrm{coh}}| \sum_{\boldsymbol{\ell}} b_{\boldsymbol{\ell}}^\dagger b_{\boldsymbol{\ell}} |\psi_{\mathrm{GP}}^{\mathrm{coh}}\rangle = N$ and the expectation value of any single particle operator can be expressed in terms of the elements of the single particle density matrix

$$\rho_{\boldsymbol{\ell},\boldsymbol{\ell}'} = \langle\psi_{\mathrm{GP}}^{\mathrm{coh}}| b_{\boldsymbol{\ell}}^\dagger b_{\boldsymbol{\ell}'} |\psi_{\mathrm{GP}}^{\mathrm{coh}}\rangle = \psi_{\boldsymbol{\ell}}^* \psi_{\boldsymbol{\ell}'}. \tag{6.90}$$

Within this formulation, the $U(1)$ symmetry is broken and the usual order parameter

$$\psi_{\boldsymbol{\ell}} = \langle\psi_{\mathrm{GP}}^{\mathrm{coh}}| b_{\boldsymbol{\ell}} |\psi_{\mathrm{GP}}^{\mathrm{coh}}\rangle \tag{6.91}$$

is directly proportional to the condensate state in the respective single particle basis. It may however be argued, that such a symmetry breaking formulation does not reflect the true experimentally realized state in an experimental system, which is of definite particle number and thus directly implies that any anomalous expectation value[8] such as $\langle b_{\boldsymbol{\ell}}\rangle = 0$, vanishes exactly. Therefore $U(1)$-symmetry breaking formulations have to be used with care and not to be understood as the true physical state of the system, but are often very convenient for calculation purposes.

We can easily evaluate the energy of the Bose-Hubbard Hamiltonian (6.2) within this variational state (6.89) and obtain the energy function

$$\begin{aligned} E_{GP}(\psi_1, \ldots, \psi_L) &= \langle\psi_{\mathrm{GP}}^{\mathrm{coh}}| H_{\mathrm{BH}} |\psi_{\mathrm{GP}}^{\mathrm{coh}}\rangle \\ &= -J \sum_{\langle \boldsymbol{\ell},\boldsymbol{\ell}'\rangle} (\psi_{\boldsymbol{\ell}}^* \psi_{\boldsymbol{\ell}'} + \psi_{\boldsymbol{\ell}'}^* \psi_{\boldsymbol{\ell}}) + \sum_{\boldsymbol{\ell}} (\epsilon_{\boldsymbol{\ell}} - \mu) |\psi_{\boldsymbol{\ell}}|^2 + \frac{U}{2} \sum_{\boldsymbol{\ell}} |\psi_{\boldsymbol{\ell}}|^4, \end{aligned} \tag{6.92}$$

which exactly coincides with the lowest order scalar energy term in Eq. (6.3). The coherent state representation is particularly appealing for evaluating the expectation values of normally ordered operators. Using the eigenvalue properties, annihilation and creation operators are simply replaced with the coherent state parameter or its conjugate respectively.

To obtain the action, one furthermore requires the term containing the temporal derivative in the action (6.87). This calculation is explicated in appendix (H) and one obtains

$$\langle\psi_{\mathrm{GP}}^{\mathrm{coh}}| \partial_t |\psi_{\mathrm{GP}}^{\mathrm{coh}}\rangle = \sum_{\boldsymbol{\ell}} \psi_{\boldsymbol{\ell}}^*(t)\, \dot{\psi}_{\boldsymbol{\ell}}(t) + \mathcal{C}, \tag{6.93}$$

where the constant $\mathcal{C}$ depends on the boundary conditions. This constant only leads to an additional irrelevant phase evolution of the time-dependent state, and we neglect it henceforth. The full coherent state Gross-Pitaevskii action is thus

$$\mathcal{S}_{\mathrm{GP}}^{\mathrm{coh}} = \int_{t_i}^{t_f} dt \left[-i \sum_{\boldsymbol{\ell}} \psi_{\boldsymbol{\ell}}^*(t)\, \dot{\psi}_{\boldsymbol{\ell}}(t) - J \sum_{\langle \boldsymbol{\ell},\boldsymbol{\ell}'\rangle} (\psi_{\boldsymbol{\ell}}^*(t) \psi_{\boldsymbol{\ell}'}(t) + \psi_{\boldsymbol{\ell}'}^*(t) \psi_{\boldsymbol{\ell}}(t)) + \sum_{\boldsymbol{\ell}} \left(\epsilon_{\boldsymbol{\ell}} - \mu + \frac{U}{2} |\psi_{\boldsymbol{\ell}}(t)|^2 \right) |\psi_{\boldsymbol{\ell}}(t)|^2 \right]. \tag{6.94}$$

To obtain the equations of motion, we extremize the action and explicitly take the functional derivative (6.88) of the action with respect to the conjugate field and find

$$i\, \dot{\psi}_{\boldsymbol{\ell}}(t) = -J \sum_{\boldsymbol{\ell}' \in \mathrm{n.n.}(\boldsymbol{\ell})} \psi_{\boldsymbol{\ell}'}(t) + (\epsilon_{\boldsymbol{\ell}} - \mu) \psi_{\boldsymbol{\ell}}(t) + U |\psi_{\boldsymbol{\ell}}(t)|^2 \psi_{\boldsymbol{\ell}}(t), \tag{6.95}$$

where n.n.($\boldsymbol{\ell}$) denotes the set of all sites, which are nearest neighbors of the site $\boldsymbol{\ell}$. Eq. (6.95) is the well-known time-dependent Gross-Pitaevskii equation, which has been remarkably successful at describing a vast variety of properties and phenomena in weakly or non-interacting condensates. It is not restricted to regimes close to the ground state, but can also applicable out of equilibrium, as long as the condensate fraction is large.

[8] i.e. the expectation value of an operator that does not conserve the total particle number.

Formulation in Terms of States with Fixed Particle Number

In cold atom experiments to date, the number of particles in a trapped ensemble of atoms is fixed and the $U(1)$-symmetry is not broken. To show that the physics described by the Gross-Pitaevskii equation are not an artifact of the artificial symmetry breaking, we here derive a similar form of the action using a canonical variational state

$$|\psi_{\mathrm{GP}}^{\mathrm{can}}\rangle = \frac{1}{\sqrt{N!}}(a_c^\dagger)^N|\mathrm{vac}\rangle, \tag{6.96}$$

containing exactly N particles in the variational single particle mode $a_c^\dagger$. This is the exact ground state of a system of N non-interacting bosons in a lattice.

Using this state, the expectation value any operator which does not conserve the total particle number vanishes and specifically $\langle\psi_{\mathrm{GP}}^{\mathrm{can}}|b_{\boldsymbol{\ell}}|\psi_{\mathrm{GP}}^{\mathrm{can}}\rangle = 0$, although the system described by this state is fully condensed.

To evaluate the expectation values of operators and specifically the energy, we use the commutation relation

$$\left[b_{\boldsymbol{\ell}},\ \left(\sum_{\boldsymbol{\ell}'}\frac{\psi_{\boldsymbol{\ell}'}}{\sqrt{N}}b_{\boldsymbol{\ell}'}^\dagger\right)^N\right] = \sqrt{N}\psi_{\boldsymbol{\ell}}\left(\sum_{\boldsymbol{\ell}'}\frac{\psi_{\boldsymbol{\ell}'}}{\sqrt{N}}b_{\boldsymbol{\ell}'}^\dagger\right)^{N-1}. \tag{6.97}$$

The matrix elements of the single particle density matrix

$$\langle\psi_{\mathrm{GP}}^{\mathrm{can}}|b_{\boldsymbol{\ell}}^\dagger b_{\boldsymbol{\ell}'}|\psi_{\mathrm{GP}}^{\mathrm{can}}\rangle = \psi_{\boldsymbol{\ell}}^*\psi_{\boldsymbol{\ell}'}, \tag{6.98}$$

which contains the entire information for the expectation value of any single-particle operator, are identical to the matrix elements using the corresponding coherent state. To evaluate the interaction energy, we furthermore require the two-particle correlator

$$\langle\psi_{\mathrm{GP}}^{\mathrm{can}}|b_{\boldsymbol{\ell}_1}^\dagger b_{\boldsymbol{\ell}_2}^\dagger b_{\boldsymbol{\ell}_3}b_{\boldsymbol{\ell}_4}|\psi_{\mathrm{GP}}^{\mathrm{can}}\rangle = \frac{N(N-1)}{N^2}\psi_{\boldsymbol{\ell}_1}^*\psi_{\boldsymbol{\ell}_2}^*\psi_{\boldsymbol{\ell}_3}\psi_{\boldsymbol{\ell}_4}, \tag{6.99}$$

which differs from its coherent state counterpart by a factor of $(1-N^{-1})$. To explicitly express the action as a function of the complex fields $\psi_{\boldsymbol{\ell}}(t)$, we again require the term containing the temporal derivative in the action (6.87). Here, we use the relations

$$\partial_t\left(\sum_{\boldsymbol{\ell}}\psi_{\boldsymbol{\ell}}(t)\,b_{\boldsymbol{\ell}}^\dagger\right)^N = N\left(\sum_{\boldsymbol{\ell}}\psi_{\boldsymbol{\ell}}(t)\,b_{\boldsymbol{\ell}}^\dagger\right)^{N-1}\left(\sum_{\boldsymbol{\ell}}\dot{\psi}_{\boldsymbol{\ell}}(t)\,b_{\boldsymbol{\ell}}^\dagger\right) \tag{6.100}$$

$$[a_c^N, a_c^\dagger] = N\,a_c^{N-1} \tag{6.101}$$

to explicitly obtain

$$\begin{aligned}\langle\psi_{\mathrm{GP}}^{\mathrm{can}}|\partial_t|\psi_{\mathrm{GP}}^{\mathrm{can}}\rangle &= \frac{1}{N!}\langle\mathrm{vac}|a_c^N(a_c^\dagger)^{N-1}\left(\sum_{\boldsymbol{\ell}}\dot{\psi}_{\boldsymbol{\ell}}(t)\,b_{\boldsymbol{\ell}}^\dagger\right)|\mathrm{vac}\rangle \\ &= \sum_{\boldsymbol{\ell}}\psi_{\boldsymbol{\ell}}^*(t)\,\dot{\psi}_{\boldsymbol{\ell}}(t).\end{aligned} \tag{6.102}$$

This is identical to the corresponding term in the coherent state formulation up to the constant term $\mathcal{C}$. Explicitly evaluating the energy for the Bose-Hubbard Hamiltonian (6.2), we arrive at the canonical action

$$\begin{aligned}\mathcal{S}_{\mathrm{GP}}^{\mathrm{can}} = \int_{t_i}^{t_f}dt\Big[&-i\sum_{\boldsymbol{\ell}}\psi_{\boldsymbol{\ell}}^*(t)\,\dot{\psi}_{\boldsymbol{\ell}}(t) - J\sum_{\langle\boldsymbol{\ell},\boldsymbol{\ell}'\rangle}[\psi_{\boldsymbol{\ell}}^*(t)\psi_{\boldsymbol{\ell}'}(t)+\psi_{\boldsymbol{\ell}'}^*(t)\psi_{\boldsymbol{\ell}}(t)] \\ &+\sum_{\boldsymbol{\ell}}\Big(\epsilon_{\boldsymbol{\ell}}-\mu+\frac{U}{2}\frac{N(N-1)}{N^2}|\psi_{\boldsymbol{\ell}}(t)|^2\Big)|\psi_{\boldsymbol{\ell}}(t)|^2\Big].\end{aligned} \tag{6.103}$$

Analogously, the minimization of the action leads to the time-dependent Gross-Pitaevskii equation with the finite particle number correction

$$i\,\dot{\psi}_{\boldsymbol{\ell}}(t) = -J \sum_{\boldsymbol{\ell}' \in \text{n.n.}(\boldsymbol{\ell})} \psi_{\boldsymbol{\ell}'}(t) + (\epsilon_{\boldsymbol{\ell}} - \mu)\psi_{\boldsymbol{\ell}}(t) + U|\psi_{\boldsymbol{\ell}}(t)|^2\psi_{\boldsymbol{\ell}}(t) - \frac{U}{N}|\psi_{\boldsymbol{\ell}}(t)|^2\psi_{\boldsymbol{\ell}}(t). \tag{6.104}$$

Comparison Between Coherent and Canonical Formulation

Clearly, the coherent and canonical actions in Eq. (6.94) and Eq. (6.103) are interrelated by

$$\mathcal{S}_{\text{GP}}^{\text{coh}} = \mathcal{S}_{\text{GP}}^{\text{can}} + \frac{U}{2N}\sum_{\boldsymbol{\ell}} |\psi_{\boldsymbol{\ell}}(t)|^4. \tag{6.105}$$

Physically, the difference between the two formulations originates from the (absence of the) self-interaction of the particles in the condensate. In the thermodynamic limit of large N, this becomes negligible in comparison to the inter-particle interactions and the two formulations, including the equations of motion, become equivalent. For small N in cold atom experiments, the canonical is superior to the coherent state formulation. It is interesting to note, that neither Gross-Pitaevskii theory, nor Bogoliubov theory, which will be derived on the basis of this, rely on a $U(1)$-symmetry breaking description of BEC.

Symmetries and Conserved Quantities

It is worthwhile looking at the symmetries of the effective action (6.94), each of which leads to a conserved quantity under the corresponding equations of motion, as related by Noether's theorem. For our specific case, the action is invariant $\mathcal{S}_{GP} \mapsto \mathcal{S}_{GP}$, under a global complex phase shift of all order parameters $\psi_{\boldsymbol{\ell}} \mapsto e^{i\theta}\psi_{\boldsymbol{\ell}}$, an arbitrary translation in time $t \mapsto t + \Delta t$ and in case of translational invariance $\epsilon_{\boldsymbol{\ell}} = \epsilon$, an arbitrary discrete spatial translation $\psi_{\boldsymbol{\ell}} \mapsto \psi_{\boldsymbol{\ell}+\Delta\boldsymbol{\ell}}$. This implies that under time evolution of an arbitrary state, the Gross-Pitaevskii equation conserves particle number, energy and quasi-momentum respectively. Furthermore, the Gross-Pitaevskii ground state can be chosen to obey all of these symmetries[9].

Grandcanonical Potential or Energy

We shortly comment on the practical implementation of the procedure described above. Throughout the derivation we assumed a given particle number N imposing the constraint $\sum_{\boldsymbol{\ell}} |\psi_{\boldsymbol{\ell}}|^2 = N$. Numerically determining the Gross-Pitaevskii ground state using a minimization procedure as a function of the complex[10] parameters $\psi_{\boldsymbol{\ell}}$ is cumbersome if the additional constraint is to be fulfilled. One possibility to inherently guarantee a fixed particle particle number would be via a parameterization of the condensate field $\psi_{\boldsymbol{\ell}}$ by high-dimensional polar coordinates. Usually, one however chooses another route via a Legendre transformation by adding the term $-\mu\sum_{\boldsymbol{\ell}} b_{\boldsymbol{\ell}}^\dagger b_{\boldsymbol{\ell}}$, which was already performed for the Bose-Hubbard Hamiltonian (6.2). It is important to keep in mind, that the expectation value of the Hamiltonian in this form is not the physical energy, but the grand canonical potential (although it is commonly referred to as the *energy* and we shall adopt this convention). For fixed chemical potential μ, one determines the variational state which minimizes the expectation value $\langle H_{\text{BH}}\rangle$ without any additional constraint. The resulting particle number $\langle\hat{N}\rangle$ expectation value for this state is then monotonically related to the chemical potential μ. A given particle number can thus be set by the appropriate choice of μ and is often efficiently implemented via a root finding algorithm.

[9] Note that the time translation symmetry differs from all other symmetries here, since it is always a parameter in such a non-relativistic theory. The fact that a stationary state (under the effective time evolution) exists, is attributed to this symmetry and no further *internal* conserved quantity is associated within such a static state.

[10] If the system is invariant under time reversal symmetry, these can all be chosen purely real for a ground state.

6.3 Derivation of Bogoliubov Theory from Classical Gross-Pitaevskii Theory

In this section we will show that Bogoliubov theory, which can describe phenomena beyond Gross-Pitaevskii theory (such as depletion of the condensate) and encompasses a much larger set of effective states, can be derived from a linearization of the time-dependent Gross-Pitaevskii equation and a subsequent quantization of the collective modes. Bogoliubov theory, both in its static and dynamical form, recovers Gross-Pitaevskii theory if one restricts the excitation of the quasi-particle modes to coherent states.

We split the time-dependent scalar field at each site

$$\psi_{\boldsymbol{\ell}}(t) = \phi_{\boldsymbol{\ell}} + \delta\psi_{\boldsymbol{\ell}}(t) \tag{6.106}$$

into a static background term $\phi_{\boldsymbol{\ell}}$ and a time-dependent scalar fluctuation $\delta\psi_{\boldsymbol{\ell}}(t)$. For simplicity, we again restrict ourselves to the homogeneous system $\epsilon_{\boldsymbol{\ell}} = 0$. Rewriting the Gross-Pitaevskii equation (6.95) in terms of these variables, we arrive at

$$\begin{aligned} i\,\dot{\delta\psi}_{\boldsymbol{\ell}}(t) = &- J \sum_{\boldsymbol{\ell}'\in \mathrm{n.n.}(\boldsymbol{\ell})} \phi_{\boldsymbol{\ell}'} \; + (\epsilon_{\boldsymbol{\ell}} - \mu)\,\phi_{\boldsymbol{\ell}} + U|\phi_{\boldsymbol{\ell}}|^2\phi_{\boldsymbol{\ell}} \\ &- J \sum_{\boldsymbol{\ell}'\in \mathrm{n.n.}(\boldsymbol{\ell})} \delta\psi_{\boldsymbol{\ell}'}(t) + (\epsilon_{\boldsymbol{\ell}} - \mu)\,\delta\psi_{\boldsymbol{\ell}}(t) + 2U|\phi_{\boldsymbol{\ell}}|^2\,\delta\psi_{\boldsymbol{\ell}}(t) + U\phi_{\boldsymbol{\ell}}^2\,\delta\psi^*_{\boldsymbol{\ell}}(t) \\ &+ 2U\phi_{\boldsymbol{\ell}}\,\delta\psi^*_{\boldsymbol{\ell}}(t)\,\delta\psi_{\boldsymbol{\ell}}(t) + U\phi^*_{\boldsymbol{\ell}}\,\delta\psi_{\boldsymbol{\ell}}(t)\,\delta\psi_{\boldsymbol{\ell}}(t) \\ &+ U\delta\psi^*_{\boldsymbol{\ell}}(t)\,\delta\psi_{\boldsymbol{\ell}}(t)\,\delta\psi_{\boldsymbol{\ell}}(t), \end{aligned} \tag{6.107}$$

where the terms in the different lines are grouped according to their order in the fluctuations. Note that no approximation has been made here, as this is only a transformation of classical variables and is equivalent to the original Gross-Pitaevskii equation in (6.95) for any choice of $\phi_{\boldsymbol{\ell}}$. Note that the constant term in the first line of Eq. (6.107) is nothing but a part of the static Gross-Pitaevskii equation on the lattice. As elucidated in Eq. (6.9), this vanishes identically if the fluctuation expansion is performed around the energy minimum, which we now impose. For a given particle number N, this fixes the chemical potential as a function of the physical parameters. Specifically for a homogeneous system ($\epsilon_{\boldsymbol{\ell}} = 0$), this implies the particularly simple relation $\mu = -JZ + U|\phi|^2$.

We now consider the time evolution of the system in the limit of small fluctuations, i.e. the system being close to the Gross-Pitaevskii ground state. In this case, the higher order terms are irrelevant and the time evolution is generated by the terms of first order in $\delta\psi_{\boldsymbol{\ell}}$ and $\delta\psi^*_{\boldsymbol{\ell}}$, which correspond exactly to the terms of second order in the fluctuations in the action in Eq. (6.94). Defining the column vectors of the fluctuations

$$\boldsymbol{\delta\psi}(t) = \begin{pmatrix} \delta\psi_1(t) \\ \vdots \\ \delta\psi_L(t) \end{pmatrix}, \tag{6.108}$$

we can express the equations of motion up to linear order in matrix form together with the conjugate equations as

$$i\frac{d}{dt}\begin{pmatrix} \boldsymbol{\delta\psi}(t) \\ \boldsymbol{\delta\psi}^*(t) \end{pmatrix} = \Sigma H_{\mathrm{QP}} \begin{pmatrix} \boldsymbol{\delta\psi}(t) \\ \boldsymbol{\delta\psi}^*(t) \end{pmatrix}, \tag{6.109}$$

with the same non-Hermitian matrix given in Eq. (6.175)

$$\Sigma H_{\mathrm{QP}} = \begin{pmatrix} h & \Delta \\ -\Delta^* & -h^* \end{pmatrix}. \tag{6.110}$$

and the same Hermitian matrix h and symmetric matrix Δ as appearing in the operator case in Eqns. (6.14, 6.15)

$$h_{\boldsymbol{\ell},\boldsymbol{\ell}'} = -J_{l,l'} + (\epsilon_{\boldsymbol{\ell}} - \mu + 2U|\phi_{\boldsymbol{\ell}}|^2)\delta_{l,l'} \tag{6.111}$$

$$\Delta_{\boldsymbol{\ell},\boldsymbol{\ell}'} = U\phi^2_{\boldsymbol{\ell}}\,\delta_{l,l'}. \tag{6.112}$$

Time Evolution in the Quasi-Particle Basis

To determine the time evolution of an arbitrary state $\begin{pmatrix}\boldsymbol{\delta\psi}(t)\\ \boldsymbol{\delta\psi}^*(t)\end{pmatrix}$, determined by the equation of motion (6.109), it is convenient to change into a more suitable basis. As discussed in section (6.1.1), a basis of eigenvectors of ΣH_{QP} does not exist in the condensate. We do not repeat the derivation of the eigenvector structure, but use the same notation and build on the results of section (6.1.1).

The generalized form of the completeness relation for inhomogeneous systems reads

$$\mathbb{1} = \sum_s{}' (\mathbf{x}^{(s)}\mathbf{x}^{(s)\,\dagger} - \mathbf{y}^{(s)}\mathbf{y}^{(s)\,\dagger})\Sigma + i(\mathbf{q}\,\mathbf{p}^\dagger - \mathbf{p}\,\mathbf{q}^\dagger)\Sigma. \tag{6.113}$$

Here, s refers to the collective mode index with associated eigenvectors $\mathbf{x}^{(s)} = \begin{pmatrix}\mathbf{u}^{(s)}\\ -\mathbf{v}^{(s)}\end{pmatrix}$ and $\mathbf{y}^{(s)} = \begin{pmatrix}-\mathbf{v}^{(s)\,*}\\ \mathbf{u}^{(s)\,*}\end{pmatrix}$ to eigenvalues ω_s and $-\omega_s$ respectively. $\mathbf{p}$ is the only eigenvector to a zero eigenvalue and $\mathbf{q}$, required to complete the basis, is not an eigenvector of ΣH_{QP}, but fulfills $\Sigma H_{\mathrm{QP}}\mathbf{q} = -\frac{i}{\tilde{m}}\mathbf{p}$. The $\sum_s'$ denotes the summation over all bosonic modes and does include the eigenvector $\mathbf{p}$.

Clearly, it is convenient to work in the basis of as many eigenvectors as possible, since in this basis the coefficients of the eigenvectors simply evolve with a constant complex phase in time. We therefore expand the vector in the basis $\{\mathbf{x}^{(s)}, \mathbf{y}^{(s)}, \mathbf{p}, \mathbf{q}\}$ using Eq. (6.113)

$$\begin{pmatrix}\boldsymbol{\delta\psi}(t)\\ \boldsymbol{\delta\psi}^*(t)\end{pmatrix} = \sum_s \alpha_s(t)\,\mathbf{x}^{(s)} + \sum_s \alpha_s^*(t)\,\mathbf{y}^{(s)} + i\rho(t)\,\mathbf{q} + i\chi(t)\,\mathbf{p}, \tag{6.114}$$

where we defined the overlap coefficients

$$\alpha_s(t) = \mathbf{x}^{(s)\,\dagger}\Sigma\begin{pmatrix}\boldsymbol{\delta\psi}(t)\\ \boldsymbol{\delta\psi}^*(t)\end{pmatrix} = \sum_{\boldsymbol{\ell}}\left[u_{\boldsymbol{\ell}}^{(s)\,*}\delta\psi_{\boldsymbol{\ell}}(t) + v_{\boldsymbol{\ell}}^{(s)\,*}\delta\psi_{\boldsymbol{\ell}}^*(t)\right] \tag{6.115}$$

$$\alpha_s^*(t) = -\mathbf{y}^{(s)\,\dagger}\Sigma\begin{pmatrix}\boldsymbol{\delta\psi}(t)\\ \boldsymbol{\delta\psi}^*(t)\end{pmatrix} = \sum_{\boldsymbol{\ell}}\left[v_{\boldsymbol{\ell}}^{(s)}\delta\psi_{\boldsymbol{\ell}}(t) + u_{\boldsymbol{\ell}}^{(s)}\delta\psi_{\boldsymbol{\ell}}^*(t)\right] \tag{6.116}$$

$$\rho(t) = \mathbf{p}^\dagger\Sigma\begin{pmatrix}\boldsymbol{\delta\psi}(t)\\ \boldsymbol{\delta\psi}^*(t)\end{pmatrix} \tag{6.117}$$

$$\chi(t) = -\mathbf{q}^\dagger\Sigma\begin{pmatrix}\boldsymbol{\delta\psi}(t)\\ \boldsymbol{\delta\psi}^*(t)\end{pmatrix}. \tag{6.118}$$

Note that the basis vectors are always understood to be stationary and only the coefficients, representing the physical state at hand, are possibly time-dependent.

Analogous to the operator case in Eqns. (6.82, 6.83), the forward and reverse transformations can also be expressed in matrix form

$$\begin{pmatrix}\boldsymbol{\alpha}(t)\\ \chi(t)\\ \boldsymbol{\alpha}^*(t)\\ \rho(t)\end{pmatrix} = \tilde{\Sigma}W^\dagger\Sigma\begin{pmatrix}\boldsymbol{\delta\psi}(t)\\ \boldsymbol{\delta\psi}^*(t)\end{pmatrix} \tag{6.119}$$

$$\begin{pmatrix}\boldsymbol{\delta\psi}(t)\\ \boldsymbol{\delta\psi}^*(t)\end{pmatrix} = W\begin{pmatrix}\boldsymbol{\alpha}(t)\\ \chi(t)\\ \boldsymbol{\alpha}^*(t)\\ \rho(t)\end{pmatrix}, \tag{6.120}$$

where the transformation matrix was defined in Eq. (8.55) and we defined the vector $\boldsymbol{\alpha}(t) = [\alpha_1(t), \ldots, \alpha_L(t)]^t$. The inverse transformation (6.120) is explicitly given by

$$\delta\psi_{\boldsymbol{\ell}} = \sum_s u_{\boldsymbol{\ell}}^{(s)}\alpha_s(t) - \sum_s v_{\boldsymbol{\ell}}^{(s)\,*}\alpha_s^*(t) + iu_{\boldsymbol{\ell}}^{(0)}\,\chi(t) + v_{\boldsymbol{\ell}}^{(0)}\,\rho(t) \tag{6.121}$$

$$\delta\psi_{\boldsymbol{\ell}}^* = \sum_s u_{\boldsymbol{\ell}}^{(s)}\alpha_s^*(t) - \sum_s v_{\boldsymbol{\ell}}^{(s)}\alpha_s(t) - iu_{\boldsymbol{\ell}}^{(0)\,*}\,\chi(t) + v_{\boldsymbol{\ell}}^{(0)\,*}\,\rho(t) \tag{6.122}$$

Although the vectors $[\boldsymbol{\delta\psi}(t), \boldsymbol{\delta\psi}^*(t)]^t$ contain the $2L$ complex variables, there are only L degrees of freedom since two entries are always interrelated by conjugation. The same number of degrees of freedom are contained in the vector $[\boldsymbol{\alpha}(t), \chi(t), \boldsymbol{\alpha}^*(t), \rho(t)]^t$. However, here the variables $\chi(t)$ and $\rho(t)$ are independent, but restricted to purely real values by the structure of the transformation. This property is equivalent to the operators $\mathscr{P}$ and $\mathcal{Q}$ being Hermitian. In fact, the coefficients are related by being the time-dependent expectation values of these operators $\rho(t) = \langle \mathscr{P}(t) \rangle$ and $\chi(t) = \langle \mathcal{Q}(t) \rangle$.

Time Evolution under $\mathcal{H}^{(2)}$

If we consider the time evolution generated by the second order Hamiltonian $\mathcal{H}^{(2)}$, the equations of motion (6.109) are easily solved explicitly in the basis of $\{\mathbf{x}^{(s)}, \mathbf{y}^{(s)}, \mathbf{p}, \mathbf{q}\}$. Using the representation (6.121s) in (6.109) and multiplying by one of the new basis vectors and Σ from the left, one directly finds the decoupled equations of motion

$$\dot{\alpha}_s(t) = -i\omega_s\, \alpha_s(t) \tag{6.123}$$
$$\dot{\alpha}^*_s(t) = i\omega_s\, \alpha^*_s(t) \tag{6.124}$$
$$\dot{\rho}(t) = 0 \tag{6.125}$$
$$\dot{\chi}(t) = -\frac{\rho(t)}{\tilde{m}}. \tag{6.126}$$

These are uniquely solved by

$$\alpha_s(t) = \alpha_s(0)\, e^{-i\omega_s t} \tag{6.127}$$
$$\rho(t) = \rho(0) \tag{6.128}$$
$$\chi(t) = \chi(0) - \frac{\rho(0)}{\tilde{m}} t. \tag{6.129}$$

We see that if the time evolution is generated by the second order term only, the quasi-particle amplitude fields are fully decoupled and evolve in time by changing their complex phase at a constant rate ω_s only. The mode occupation $|\alpha_s(t)|$ is constant in time, corresponding to an infinite lifetime. In the associated quantum theory, the time-dependent field amplitude $\alpha_s(t)$ corresponds to the corresponding quasi-particle annihilation operator $\beta_s(t)$ in the Heisenberg representation, where the time-dependence is contained in the operators.

The temporal evolution of the amplitudes $\rho(t)$ and $\chi(t)$ is quite different, when considering terms up to second order only. Whereas $\rho(t)$, corresponding to the expectation value of $\mathscr{P}$ remains constant in time and is fixed by the initial, $\chi(t)$ corresponding to the expectation value of $\mathcal{Q}$ grows linearly in time at a rate $\frac{\rho(0)}{\tilde{m}}$, analogous to a particle with momentum $\langle \mathscr{P} \rangle$ and mass $\tilde{m}$.

Classical Correspondence and Quantization of Collective Modes

Having determined the collective modes of linearized Gross-Pitaevskii theory, we can now express the original classical energy (6.92) in this new basis. We first express it in different orders in the fluctuations, analogous to the ordering in Eqns. (6.3 - 6.7)

$$E_{GP}(\boldsymbol{\delta\psi}, \boldsymbol{\delta\psi}^*) = E^{(0)} + \sum_{m=2}^{4} E^{(m)}(\boldsymbol{\delta\psi}, \boldsymbol{\delta\psi}^*), \tag{6.130}$$

where $E^{(0)}$ is the same Gross-Pitaevskii energy and the first order term vanishes identically. The energy term of second order in the fluctuations can be expressed as the bilinear form in the complex fluctuation amplitudes $\boldsymbol{\delta\psi}$, analogous to the operator case expressed in *fluctuation operators*

$$E^{(2)}(\boldsymbol{\delta\psi}, \boldsymbol{\delta\psi}^*) = \frac{1}{2} \begin{pmatrix} \boldsymbol{\delta\psi}(t) \\ \boldsymbol{\delta\psi}^*(t) \end{pmatrix}^\dagger H_{\mathrm{QP}} \begin{pmatrix} \boldsymbol{\delta\psi}(t) \\ \boldsymbol{\delta\psi}^*(t) \end{pmatrix}. \tag{6.131}$$

As discussed, we have a bijective transformation to amplitudes $\boldsymbol{\alpha}, \rho, \chi$, in terms of which we can equally well express any variational state. Using the transformation (6.120), the second order energy in these variables becomes

$$\begin{aligned} E^{(2)}(\boldsymbol{\alpha}, \boldsymbol{\alpha}^*, \rho, \chi) &= \frac{1}{2} \begin{pmatrix} \boldsymbol{\alpha}(t) \\ \chi(t) \\ \boldsymbol{\alpha}^*(t) \\ \rho(t) \end{pmatrix}^\dagger W^\dagger \Sigma (\Sigma H_{\mathrm{QP}}) W \begin{pmatrix} \boldsymbol{\alpha}(t) \\ \chi(t) \\ \boldsymbol{\alpha}^*(t) \\ \rho(t) \end{pmatrix} \\ &= \sum_s \omega_s \left|\alpha_s(t)\right|^2 + \frac{1}{2\tilde{m}} \rho^2(t) \end{aligned} \tag{6.132}$$

and is diagonal in the collective mode amplitudes. To obtain the last line, we used the eigenvector relations and the orthogonality relations in Eqns. (7.26 - 7.35).

The first term in $E^{(2)}$ corresponds to a set of $L-1$ decoupled harmonic oscillators in the classical limit. Here the classical complex coordinate α_s is related to the position x_s and momentum p_s by

$$\alpha_s(t) = \frac{1}{2x_s^{(0)}} x_s(t) + i x_s^{(0)}\, p_s(t), \tag{6.133}$$

where $x_s^{(0)} = (2\tilde{m}\omega_s)^{-1}$ is the corresponding quantum harmonic oscillator length scale for a particle of mass $\tilde{m}$ in a quadratic potential $V(x) = \frac{1}{2}\tilde{m}\omega_s^2 x^2$. In these effective coordinates and momenta, the second order energy becomes

$$E^{(2)}(\{x_s\}, \{p_s\}, \rho, \chi) = \sum_s \left(\frac{1}{2}\tilde{m}\omega_s x_s^2(t) + \frac{1}{2m} p_s^2 \right) + \frac{1}{2\tilde{m}} \rho^2(t). \tag{6.134}$$

The equations of motion for the complex classical variable $\alpha(t)$ in Eq. (6.123) are fully equivalent to Hamilton's equations of motion for the classical position and momenta

$$\frac{d}{dt} x_s = \frac{\partial E^{(2)}}{\partial p_s} = \{x_s, E^{(2)}\} \tag{6.135}$$

$$\frac{d}{dt} p_s = -\frac{\partial E^{(2)}}{\partial x_s} = \{p_s, E^{(2)}\}, \tag{6.136}$$

where

$$\{A, B\} = \sum_s \left(\frac{\partial A}{\partial x_s}\frac{\partial B}{\partial p_s} - \frac{\partial A}{\partial p_s}\frac{\partial B}{\partial x_s} \right) \tag{6.137}$$

denotes the Poisson bracket. Since these new variables mutually fulfill Poisson bracket relations

$$\{x_r, p_s\} = \delta_{r,s}, \tag{6.138}$$

these are conjugate variables in the sense of Hamiltonian mechanics and the procedure to construct a corresponding quantum theory, which contains this theory as a classical limit is clear: we promote these classical variables to operators $x_s \mapsto \hat{x}_s$ and $p_s \mapsto \hat{p}_s$, which fulfill the corresponding commutation relations

$$[\hat{x}_r, \hat{p}_s] = i\delta_{r,s}. \tag{6.139}$$

From these, we now define the operators

$$\beta_s(t) = \frac{1}{2x_s^{(0)}} \hat{x}_s(t) + i x_s^{(0)}\, \hat{p}_s(t) \tag{6.140}$$

which can easily be verified to fulfill the commutation relations

$$[\beta_r, \beta_s^\dagger] = \delta_{r,s}. \tag{6.141}$$

These operators correspond to ladder operators between harmonic oscillator eigenstates and it follows solely from the commutation relation (6.141), that the operator $\beta_s^\dagger \beta_s$ has an equidistant spectrum, which is bounded from below [53]. Each harmonic oscillator eigenstate can be associated with a state containing a fixed number of quasi-particles in the respective mode and we refer to β_s and $\beta_s^\dagger$ quasi-particle creation and annihilation operators.

Expressing Operators in Quasi-Particle Operators

We now know that the collective excitations around the ground state correspond to bosonic quasi-particles and a natural next step is to relate the bosonic quasi-particle operators β_s and $\beta_s^\dagger$ to microscopic creation and annihilation operators in our initial Hamiltonian, before going to the classical limit. We stress that this correspondence is not unique. For instance, our derivation above may be understood to have been performed in a system with constant particle number N. We also obtain bosonic modes in this system, i.e. also the excited Bogoliubov states have the same fixed particle number N. In such a system the operators β_s and $\beta_s^\dagger$ cannot coincide with the usual Bogoliubov operators: if we created a state containing a single Bogoliubov quasi-particle, this would be a many-body state consisting of a superposition $N+1$ and $N-1$ particle states, which has zero overlap with a N-particle state. This number-conserving approach devised by Leggett is shortly discussed in subsection (6.3.3).

Here, we derive the relation of the quantized operators β_s and $\beta_s^\dagger$ to the standard Bogoliubov operators. Following the prescription of replacing all classical field amplitudes α_s and $\alpha_s^\dagger$ by bosonic operators β_s and $\beta_s^\dagger$, we find the quantum counterpart of the transformation (6.121) to local (or any other single particle basis for that sake) fluctuation amplitudes

$$\theta_{\boldsymbol{\ell}} = \sum_s \mathbf{u}_{\boldsymbol{\ell}}^{(s)} \beta_s(t) - \sum_s \mathbf{v}_{\boldsymbol{\ell}}^{(s)^*} \beta_s^\dagger + \mathcal{A}_{\boldsymbol{\ell}}. \tag{6.142}$$

Here $\mathcal{A}_{\boldsymbol{\ell}}$ is an operator, the time-dependent expectation value of which is fixed to $\langle \mathcal{A}_{\boldsymbol{\ell}}(t) \rangle = i u_{\boldsymbol{\ell}}^{(0)} \chi(t) + v_{\boldsymbol{\ell}}^{(0)} \rho(t)$ by the classical correspondence principle. From the classical equations of motion, where the evolution of the quasi-particles is decoupled from $\rho(t)$ and $\chi(t)$, we know that $[\beta_s, \mathcal{A}] = 0$ for all modes s. If we require that the operator space spanned by the set of all original creation and annihilation operators $b_{\boldsymbol{\ell}}$ and $b_{\boldsymbol{\ell}}^\dagger$ is also spanned by the $2(L-1)$ operators β_s and $\beta_s^\dagger$, we additionally have to take the condensate mode operators a_0 and $a_0^\dagger$ into account with the latter. Alternatively, one can also express $\mathcal{A}_{\boldsymbol{\ell}}$ in terms of the Hermitian operators $\mathscr{P}$ and $\mathcal{Q}$ (defined in (6.51) and (6.67))

$$\mathcal{A}_{\boldsymbol{\ell}} = i \mathbf{u}_{\boldsymbol{\ell}}^{(0)} Q + \mathbf{v}_{\boldsymbol{\ell}}^{(0)} \mathscr{P}. \tag{6.143}$$

These are the operator counterparts of the classical variables $\rho(t)$ and $\chi(t)$ respectively.

From matching the expectation values of $\langle \theta_{\boldsymbol{\ell}} \rangle$ with the classical variables $\delta\psi_{\boldsymbol{\ell}}$, we find the relation of these fluctuation operators to the original bosonic annihilation operators $b_{\boldsymbol{\ell}}$

$$\theta_{\boldsymbol{\ell}} = b_{\boldsymbol{\ell}} - \phi_{\boldsymbol{\ell}} \tag{6.144}$$

$$\theta_{\boldsymbol{\ell}}^\dagger = b_{\boldsymbol{\ell}}^\dagger - \phi_{\boldsymbol{\ell}}^*. \tag{6.145}$$

Combining all these properties, we end up with the transformations on operator level in matrix form

$$\begin{pmatrix} \boldsymbol{\beta} \\ \mathcal{Q} \\ \boldsymbol{\beta}^\dagger \\ \mathscr{P} \end{pmatrix} = \tilde{\Sigma} W^\dagger \Sigma \begin{pmatrix} \boldsymbol{\theta} \\ \boldsymbol{\theta}^\dagger \end{pmatrix} \tag{6.146}$$

$$\begin{pmatrix} \boldsymbol{\theta} \\ \boldsymbol{\theta}^\dagger \end{pmatrix} = W \begin{pmatrix} \boldsymbol{\beta} \\ \mathcal{Q} \\ \boldsymbol{\beta}^\dagger \\ \mathscr{P} \end{pmatrix}, \tag{6.147}$$

where we defined the column vector of fluctuation operators $\boldsymbol{\theta} = (\theta_1, \ldots, \theta_L)^t$. Using this form of the Bogoliubov operators, these are fully equivalent to transformations (6.82, 6.83) obtained in the previous chapter without going to the classical limit. We stress however, that the choice (6.144) of associating quantum mechanical operators to the bosonic degrees of freedom is not unique and this is only one possible form.

The Bogoliubov Quasi-Particle Hamiltonian

For the above choice of Bogoliubov operators (6.142), we have precisely the same transformations on an operator level as before. Thus the Bogoliubov Hamiltonian up to second order in the fluctuations is of precisely the same form as in section (6.1). For an inhomogeneous system, it is of the general form

$$\mathcal{H}^{(2)} = \sum_s \omega_s \beta_s^\dagger \beta_s + \frac{1}{2\tilde{m}} \mathscr{P}^2 + \Delta E^{(2)}. \tag{6.148}$$

Compared to the Gross-Pitaevskii state, the energy is lowered by

$$\Delta E^{(2)} = \frac{1}{2} \sum_s \omega_s - \frac{1}{2} \mathrm{Tr}\,(h)\,, \tag{6.149}$$

indicating that the Bogoliubov ground state is different from the Gross-Pitaevskii ground state for any finite interaction strength.

Coherent States and the Classical Limit

This limit is not achieved by considering high energy eigenstates, but rather restricting the allowed states to coherent states, which minimize the uncertainty $(\Delta x)(\Delta p)$. Assuming that $\rho(t=0) = 0$, a quasi-particle coherent state is explicitly of the form

$$|\alpha_1, \ldots, \alpha_{L-1}\rangle = e^{-\sum_s |\lambda_s|^2/2}\, e^{\sum_s \lambda_s \beta_s^\dagger} |0\rangle, \tag{6.150}$$

where $|0\rangle$ is the Bogoliubov vacuum. Being a coherent state, the quasi-particles in different modes are not entangled. Equivalently, the state can also be understood to be a single coherent state in the single mode $\beta^\dagger \propto \sum_s \lambda_s \beta_s^\dagger$.

In the limit of small fluctuations $\sum_s |\lambda_s|^2 \ll L$, where the higher order terms can be neglected, the time evolution of the coherent state becomes particularly simple, remaining a coherent state at all times with the time-dependent parameters

$$\begin{aligned} |\lambda_1(t), \ldots, \lambda_{L-1}(t)\rangle &= e^{-i(E^{(0)} + \mathcal{H}^{(2)})t} |\lambda_1(0), \ldots, \lambda_{L-1}(0)\rangle \\ &= e^{-iE^{(0)}t} |e^{-i\omega_1 t}\lambda_1(0), \ldots, e^{-i\omega_{L-1}t}\lambda_{L-1}(0)\rangle. \end{aligned} \tag{6.151}$$

Thus, the coherent state parameters λ_s follow exactly the same trajectories as the classical variables $\alpha_s(t)$ and we use them synonymously. The classical evolution of the system can therefore be associated with a coherent variational state in the quantum system.

Order Parameter and Density Response

To understand the physical significance of a state coherently excited in a single quasi-particle mode $\mathbf{q}$, we determine its spatial order parameter response $\langle b_{\boldsymbol{\ell}} \rangle$ and density response $\langle b_{\boldsymbol{\ell}}^\dagger b_{\boldsymbol{\ell}} \rangle$. For clarity, this is done for a homogeneous system. We begin by expressing the local annihilation operator $b_{\boldsymbol{\ell}}$ in terms of quasi-particle operators $\beta_{\boldsymbol{\ell}}$ and $\beta_{\boldsymbol{\ell}}^\dagger$, using the transformation relations

$$a_{\mathbf{k}} = \phi_{\mathbf{k}} + u_{\mathbf{k}} \beta_{\mathbf{k}} - v_{-\mathbf{k}}^* \beta_{-\mathbf{k}}^\dagger + \mathcal{A}_{\mathbf{k}} \qquad \text{for } \mathbf{k} \neq 0 \tag{6.152}$$

$$a_{\mathbf{k}=0} = \sqrt{N_0} + \frac{\mathscr{P} + i\mathcal{Q}}{\sqrt{2}} \qquad \text{for } \mathbf{k} = 0. \tag{6.153}$$

to arrive at

$$b_{\boldsymbol{\ell}} = \sqrt{\frac{N_0}{L}} + \frac{\mathscr{P} + i\mathcal{Q}}{\sqrt{2L}} + \frac{1}{\sqrt{L}} \sum_{\mathbf{k} \neq 0} e^{i\mathbf{k}\cdot\mathbf{R}_{\boldsymbol{\ell}}} (u_{\mathbf{k}} \beta_{\mathbf{k}} - v_{-\mathbf{k}}^* \beta_{-\mathbf{k}}^\dagger). \tag{6.154}$$

We evaluate these two quantities in the state

$$|\lambda_{\mathbf{q}}, \mathbf{q}\rangle = e^{-|\lambda_{\mathbf{q}}|^2/2}\, e^{\lambda_{\mathbf{q}} \beta^\dagger_{\mathbf{q}}} |0\rangle, \tag{6.155}$$

where $|0\rangle$ denotes the Bogoliubov ground state and a single Bogoliubov quasi particle mode $\mathbf{q}$ is weakly excited, i.e. in the limit of small $\lambda_{\mathbf{q}}$. The state at a time t, according to Eq. (6.151), is given by

$$e^{-i\mathcal{H}t}|\lambda_{\mathbf{q}}, \mathbf{q}\rangle = |\lambda_{\mathbf{q}} \cdot e^{-i\omega_{\mathbf{q}}t}, \mathbf{q}\rangle \tag{6.156}$$

and the expectation values of $b_{\boldsymbol{\ell}}$ and $b^\dagger_{\boldsymbol{\ell}} b_{\boldsymbol{\ell}}$ can be evaluated up to linear order in $\lambda_{\mathbf{q}}$

$$\begin{aligned}
\langle b_{\boldsymbol{\ell}}(t)\rangle &= \langle \lambda_{\mathbf{q}} \cdot e^{-i\omega_{\mathbf{q}}t}, \mathbf{q}| b_{\boldsymbol{\ell}} |\lambda_{\mathbf{q}} \cdot e^{-i\omega_{\mathbf{q}}t}, \mathbf{q}\rangle \\
&= \sqrt{\frac{N_0}{L}} + \lambda_{\mathbf{q}} u_{\mathbf{q}} e^{i(a\mathbf{q}\cdot\boldsymbol{\ell} - \omega_{\mathbf{q}}t)} + \lambda^*_{\mathbf{q}} v_{-\mathbf{q}} e^{-(ia\mathbf{q}\cdot\boldsymbol{\ell} - \omega_{\mathbf{q}}t)} \\
&= \sqrt{\frac{N_0}{L}} + |\lambda_{\mathbf{q}}| \left(u_{\mathbf{q}} e^{i(a\mathbf{q}\cdot\boldsymbol{\ell} - \omega_{\mathbf{q}}t + \psi)} + v_{-\mathbf{q}} e^{-(ia\mathbf{q}\cdot\boldsymbol{\ell} - \omega_{\mathbf{q}}t - \psi)} \right),
\end{aligned} \tag{6.157}$$

where the phase shift is implicitly defined by $\lambda_{\mathbf{q}} = |\lambda_{\mathbf{q}}| e^{i\varphi}$ at time $t = 0$. This form of the order parameter modulation verifies the assumption of a coherent excitation of Bogoliubov particles, which is in a sense the 'most classical' form of a quantum mechanically excited state, as also in the case for the harmonics oscillator. Furthermore, this coherent Bogoliubov state also corresponds to a density modulation of the condensate, with the density expectation value up to first order in $\sqrt{N_0}$ being

$$\langle \hat{n}_{\boldsymbol{\ell}}(t)\rangle = 2\frac{\sqrt{N_0}}{L} |\lambda_{\mathbf{q}}| (u_{\mathbf{q}} + v_{-\mathbf{q}}) \cos(a\mathbf{q}\cdot\boldsymbol{\ell} - \omega_{\mathbf{q}}t + \varphi). \tag{6.158}$$

Relation to the operators equations of motion

Formally, the equations of motion for the fluctuation operators $\boldsymbol{\delta}\mathbf{b}_{\boldsymbol{\ell}}(t)$ in the Heisenberg picture[11] (6.172) and for the scalar fluctuation amplitudes[12] $\boldsymbol{\delta\psi}_{\boldsymbol{\ell}}(t)$ in Eq. (6.107) are fully equivalent (hence they also coincide in linear order). Conceptually, they are however quite different: The operator equations of motion are exact and performing imaginary time evolution, for instance, would lead to the precise many-body ground state. Practically, these equations of motion are nothing but the full Schrödinger equation in a different form and not of much use without subsequent approximations. According to Ehrenfest's theorem, the time-dependent expectation values of the fluctuation operators in the Heisenberg picture exactly correspond to the scalar fluctuation variables in time-dependent Gross-Pitaevskii theory. Thus, up to second order in both theories, the equations of motion are of the identical structure. In this picture the correspondence between the quantum time evolution of the operators and the classical fluctuation variables governed by time-dependent Gross-Pitaevskii theory, becomes particularly clear. Furthermore it shows in which sense the time-dependent classical mean-field theory is related to the full quantum version of the time-independent theory.

[11] Note that fluctuation operators are to appear in normal order for this equivalence.
[12] Determined by the Gross-Pitaevskii equation transformed to these variables.

6.3.1 Final step: quantizing the Gross-Pitaevskii energy functional

In the final step, we now construct a quantized theory by the correspondence principle, based on the energy expression for the harmonic oscillators. Here we promote the conjugate fields $\alpha_j^*(t)$ and the corresponding generalized momentum $\pi_j(t) = \frac{\delta S}{\delta \alpha_j^*(t)}$ to creation and annihilation operators $\beta_j(t)$ and $\beta_j^\dagger(t)$ of the harmonic oscillator respectively. Replacing the scalar fluctuating field $\delta\psi_{\boldsymbol{\ell}}(t)$ with a the new quasiparticle operator, reveals how these are related to the initial fluctuation operator field

$$\hat{\theta}_{\boldsymbol{\ell}}(t) = b_{\boldsymbol{\ell}}(t) - \phi_{\boldsymbol{\ell}}(t) = \sum_j \left[u_{\boldsymbol{\ell}}^{(j)} e^{-i\omega_j t} \beta_j + v_{\boldsymbol{\ell}}^{(j)^*} e^{i\omega_j t} \beta_j^\dagger \right] \tag{6.159}$$

. Note that here the fluctuation operator is given in the Heisenberg representation, while the quasiparticle operators β_j and $\beta_j^\dagger$ are in the Schrödinger picture. Due to the structure of the quasiparticle Hamiltonian, they take on the form

$$\begin{aligned} \beta_j(t) =& e^{-i\omega_j t}\, \beta_j \\ \beta_j^\dagger(t) =& e^{i\omega_j t}\, \beta_j^\dagger \end{aligned} \tag{6.160}$$

in the Heisenberg picture.

6.3.2 Higher Order Decay and Interaction Processes

One can now consider the higher order terms in the original Hamiltonian, which were argued to be small in comparison to the quasi-particle Hamiltonian of second order in the fluctuations. The original Bose-Hubbard Hamiltonian contained at most four fluctuation operators and all fluctuation operators up to second order were absorbed exactly into the quasi-particle Hamiltonian. Since the quasi-particle operators transform linearly into the fluctuation operators θ and their conjugates, all remaining terms (which were neglected before) are of third and fourth order in both the fluctuation operators and the quasi-particle operators. Expressed in fluctuation operators, they are of the explicit form

$$\mathcal{T}_1 = U \sum_{\boldsymbol{\ell}} \phi_{\boldsymbol{\ell}}^* \theta_l^\dagger \theta_l \theta_l \tag{6.161}$$

$$\mathcal{T}_2 = U \sum_l \phi_l \theta_l^\dagger \theta_l^\dagger \theta_l \tag{6.162}$$

$$\mathcal{T}_3 = \frac{U}{2} \sum_l \theta_l^\dagger \theta_l^\dagger \theta_l \theta_l \tag{6.163}$$

and can readily be expressed in terms of quasi-particle operators using the derived transformation relations. Expressed in these operators, it becomes evident that these terms correspond to decay and interaction processes of quasi-particles. These also lead to Landau and Beliaev damping processes, as discussed in [126, 49, 101, 165] and also measured experimentally [85]. To first order the decay rate can be calculated within Fermi's golden rule and the dominant process is the decay of a Bogoliubov quasi-particle into two energetically lower quasi-particles.

6.3.3 Leggett's Number-Conserving Formulation of Bogoliubov Theory

In contrast to the number non-conserving formulation of Bogoliubov theory given above, this can also be formulated within a variational approach with a fixed particle number [102]. Apart from giving Extending on Gross-Pitaevskii theory where the number-conserving variational formulation

amounts to using a variational many-particle state with all particles occupying the same single-particle orbital, Bogoliubov theory can be constructed using the N-particle variational state, where all pairs of particles occupy the same two-particle state

$$\begin{aligned} |\psi_{\text{Bog}}, N\rangle &= \frac{1}{\sqrt{N!}} \left[\sum_{\boldsymbol{\ell},\boldsymbol{\ell}'} \varphi(\boldsymbol{\ell}-\boldsymbol{\ell}')\, b^\dagger_{\boldsymbol{\ell}} b^\dagger_{\boldsymbol{\ell}'} \right]^{N/2} |\text{vac}\rangle \\ &\propto \frac{1}{\sqrt{N!}} \left[a_0^\dagger a_0^\dagger - \sum_{\mathbf{k}\neq 0} \lambda_{\mathbf{k}} a^\dagger_{\mathbf{k}} a^\dagger_{-\mathbf{k}} \right]^{N/2} |\text{vac}\rangle. \end{aligned} \tag{6.164}$$

The above state is for discrete translationally invariant systems and can also be formulated in first quantization as a product of two-particle wave functions, which is subsequently symmetrized with respect to all particle permutations. The two-particle wave function $\varphi(\boldsymbol{\ell}-\boldsymbol{\ell}')$ or, alternatively, the coefficients $\lambda_{\mathbf{k}}$ are determined by minimizing the energy $\langle \psi_{\text{Bog}}, N|H_{\text{BH}}|\psi_{\text{Bog}}, N\rangle \to \text{min}$. Performing this minimization and neglecting the interactions between mutually excited single particle states leads to the same expressions $u_{\mathbf{k}} = \cosh\theta_{\mathbf{k}}$, $v_{\mathbf{k}} = \sinh\theta_{\mathbf{k}}$ and energies as above, which are related to the coefficients $\lambda_{\mathbf{k}} = \tanh\theta_{\mathbf{k}}$.

The particle number conserving, bosonic quasi-particle operators take on the form

$$\alpha^\dagger_{\mathbf{k}} = \frac{1}{\sqrt{N_0}} (u_{\mathbf{k}}\, a^\dagger_{\mathbf{k}} a_0 + v_{\mathbf{k}}\, a_0^\dagger a_{-\mathbf{k}}) \tag{6.165}$$

and it can be directly verified that these obey the commutation relations

$$[\alpha_{\mathbf{k}},\, \alpha^\dagger_{\mathbf{k}'}] = \delta_{\mathbf{k},\mathbf{k}'} \frac{1}{N_0} a_0^\dagger a_0 - \frac{u^*_{\mathbf{k}} u_{\mathbf{k}'}}{N_0} a^\dagger_{\mathbf{k}'} a_{\mathbf{k}} + \frac{v^*_{\mathbf{k}} v_{\mathbf{k}'}}{N_0} a^\dagger_{-\mathbf{k}} a_{-\mathbf{k}'}. \tag{6.166}$$

Only the first term is macroscopic and when evaluated within a state where N_0 particles are condensed, the coefficient equals unity. The two latter terms are of order N_0^{-1} and not scale macroscopically with increasing system size. In this sense the operators $\alpha_{\mathbf{k}}$ are approximately bosonic for a sufficiently large system, but there are $1/N$ corrections for a finite system.

6.4 Deriving Bogoliubov Theory from the Heisenberg Equations of Motion for the Fluctuation Operators

In this section we derive Bogoliubov theory from the equations of motion for the fluctuation operators and only taking the lowest order terms into account. This is fully equivalent to bringing the second order Hamiltonian $\mathcal{H}^{(2)}$ into its most diagonal form. The importance of this derivation is its close connection to the linearized Gross-Pitaevskii equations of motion for the classical fluctuations.

As will become apparent, these are exactly the expectation values of the fluctuation operators, when evaluated in coherent quasi-particle states. Since throughout this derivation all commutation relations on an operator level are fully accounted for. Thus it serves as a guideline for the correct quantization procedure when deriving Bogoliubov theory from the classical GP equation, where the commutation relations are initially not contained (here one works with complex scalar fields) and only reintroduced in the quantization procedure.

Throughout this section, we work in the Heisenberg picture, where the time-dependence of the system is contained in the operators. To keep a simple notation, we denote all operators by the same symbols used in the Schrödinger picture, and only the explicit notation of time-dependence $A(t)$ indicates a Heisenberg operator. In this picture the temporal evolution of any operator is governed by the Heisenberg equation of motion

$$\frac{d}{dt} A(t) = i[H(t), A(t)]. \tag{6.167}$$

As before, we start by decomposing the Wannier annihilation operator into a constant mean expectation and a fluctuation operator

$$b_{\boldsymbol{\ell}}(t) = \phi_{\boldsymbol{\ell}} + \delta b_{\boldsymbol{\ell}}(t). \tag{6.168}$$

Note that $\delta b_{\boldsymbol{\ell}}(t)$ also exactly fulfills bosonic commutation relations and $\phi_{\boldsymbol{\ell}}$ is chosen to be time-independent. We again restrict ourselves to the translationally invariant system and use commutation relations of the type

$$[\delta b^\dagger_{\boldsymbol{\ell}_1}(t)\, \delta b_{\boldsymbol{\ell}_2}(t),\ \delta b_{\boldsymbol{\ell}}(t)] = -\delta_{\boldsymbol{\ell}_1,\boldsymbol{\ell}}\, \delta b_{\boldsymbol{\ell}_2}(t) \tag{6.169}$$

$$[\delta b_{\boldsymbol{\ell}_1}(t)\, \delta b_{\boldsymbol{\ell}_2}(t),\ \delta b_{\boldsymbol{\ell}}(t)] = 0 \tag{6.170}$$

$$[\delta b^\dagger_{\boldsymbol{\ell}_1}(t)\, \delta b^\dagger_{\boldsymbol{\ell}_2}(t),\ \delta b_{\boldsymbol{\ell}}(t)] = -\delta_{\boldsymbol{\ell}_1,\boldsymbol{\ell}}\, \delta b^\dagger_{\boldsymbol{\ell}_2}(t) - \delta_{\boldsymbol{\ell}_2,\boldsymbol{\ell}}\, \delta b^\dagger_{\boldsymbol{\ell}_1}(t) \tag{6.171}$$

in conjunction with the decomposition of the Bose-Hubbard Hamiltonian (6.2) into terms of different order in the fluctuation operators, to obtain the exact equations of motion for the field operators

$$\begin{aligned} i\frac{d}{dt}\delta b_{\boldsymbol{\ell}}(t) = {} & (-JZ + U|\phi|^2 - \mu)\phi \\ & - J \sum_{\boldsymbol{\ell}' \in \text{n.n.}(\boldsymbol{\ell})} \delta b_{\boldsymbol{\ell}'}(t) - \mu\, \delta b_{\boldsymbol{\ell}}(t) + 2U|\phi|^2 \delta b_{\boldsymbol{\ell}}(t) + U\phi^2 \delta b^\dagger_{\boldsymbol{\ell}}(t) \\ & + 2U\phi\, \delta b^\dagger_{\boldsymbol{\ell}}(t)\, \delta b_{\boldsymbol{\ell}}(t) + U\phi^*\, \delta b_{\boldsymbol{\ell}}(t)\, \delta b_{\boldsymbol{\ell}}(t) \\ & + U\phi\, \delta b^\dagger_{\boldsymbol{\ell}}(t)\, \delta b_{\boldsymbol{\ell}}(t)\, \delta b_{\boldsymbol{\ell}}(t). \end{aligned} \tag{6.172}$$

Since it is scalar, the zeroth order energy term (6.3) does not generate any time evolution and neither does the first order energy term (6.4) when using relation (6.28) to set the chemical potential, i.e. the first term in Eq. (6.172) vanishes if the background field ϕ satisfies the static Gross-Pitaevskii equations. If the system is close to the ground state in the sense that expectation values of $\delta b_{\boldsymbol{\ell}}$ are small, the terms of different order constitute a hierarchy and the terms of order higher than 1 in $\delta b_{\boldsymbol{\ell}}$ on the right of Eq. (6.172) can be neglected in a first approximation. Within this approximation, corresponding to the time evolution generated by the second order Hamiltonian in $\delta b_{\boldsymbol{\ell}}$, the equations of motion for the fulctuation operators can be written as

$$i\frac{d}{dt}\delta b_{\boldsymbol{\ell}}(t) = \sum_{\boldsymbol{\ell}'} h_{\boldsymbol{\ell},\boldsymbol{\ell}'}\, \delta b_{\boldsymbol{\ell}'}(t) + \sum_{\boldsymbol{\ell}'} \Delta_{\boldsymbol{\ell},\boldsymbol{\ell}'}\, \delta b^\dagger_{\boldsymbol{\ell}'}(t), \tag{6.173}$$

where the matrix elements $h_{\boldsymbol{\ell},\boldsymbol{\ell}'}$ and $\Delta_{\boldsymbol{\ell},\boldsymbol{\ell}'}$ are the same as before, defined in Eq. (6.14) and Eq. (6.15) respectively. Together with the conjugate set of equations of motion, these can be written in matrix form

$$i\frac{d}{dt}\begin{pmatrix} \boldsymbol{\delta b}(t) \\ \boldsymbol{\delta b}^\dagger(t) \end{pmatrix} = \Sigma H_{\text{QP}} \begin{pmatrix} \boldsymbol{\delta b}(t) \\ \boldsymbol{\delta b}^\dagger(t) \end{pmatrix}, \tag{6.174}$$

with the non-Hermitian matrix

$$\Sigma H_{\text{QP}} = \begin{pmatrix} h & \Delta \\ -\Delta^* & -h^* \end{pmatrix} \tag{6.175}$$

determining the evolution.

6.5 Comparison of the Derivations

Let us recap what we have achieved in this chapter. We have derived Bogoliubov theory in three different way, each of which leads to the task of bringing the same matrix ΣH_{QP} into its Jordan normal form, and are thus – in this sense – equivalent. The diagonalization and transformation procedure was therefore not repeated in the previous section (6.4).

- The first path, discussed in section (6), was the derivation on an operator level of the Hamiltonian. The full Bose-Hubbard Hamiltonian is expressed in terms of fluctuation operator δb and Bogoliubov theory consists of diagonalizing the quadratic form containing all terms up to second order in these operators. The advantage of this approach is that the full quantum operator character is retained throughout the entire derivation. There is no ambiguity in expressing any given operator in terms of the quasi-particle operators.

- The second path, taken in section (6.2) and (6.3), consisted of first deriving the much simpler Gross-Pitaevskii theory and showing that Bogoliubov theory can be obtained by linearizing the non-linear equations of motion around the classical Gross-Pitaevksii minimum, determining the collective eigenmodes of these coupled differential equations and subsequently quantizing the theory. Within this path the quantum character of the theory is lost in between. After the requantization, the ordering of the non-commuting bosonic operators, when expressing operators of higher order in the Bogoliubov operators β, is not directly clear. This form of the derivation is however valuable and pedagogical as an analogy to the derivation of the extended quasi-particle theory in the following chapter: here the non-linear Gutzwiller equations of motion (instead of the non-linear time-dependent Gross-Pitaevskii equation) are linearized around the minimum and subsequently quantized.

- The last derivation of Bogoliubov theory given in section (6.4) reveals the conceptual connection between these two, seemingly different, approaches: being formulated in terms of time-dependent Heisenberg operators, the full quantum character is retained throughout. The equations of motion for the fluctuation operators can also be classified in different order of the fluctuation operators. Here, the n-th order Hamiltonian $\mathcal{H}^{(n)}$ term (as given in section (6), containing n fluctuation operators) gives a term in the Heisenberg equations of motion containing $(n-1)$ fluctuation operators. The connection to time-dependent Gross-Pitaevskii theory is that the scalar fluctuation amplitudes $\delta\psi_{\boldsymbol{\ell}}(t) = \langle \delta b_{\boldsymbol{\ell}}(t) \rangle$ are the (time-dependent) expectation values of the Heisenberg fluctuation operators when evaluated in the appropriate variational state: the Gross-Pitaevskii in form of a coherent state. The fact that these – conceptually very different – degrees of freedom are governed by exactly the same equations of motion is a consequence of the Ehrenfest theorem. On should however keep in mind, that the formulation in terms of Heisenberg fluctuation operators discussed in this section is more powerful, since it is not restricted to the coherent Gross-Pitaevskii state.

7. Quasi-Particle Theory for Strongly Interacting Lattice Bosons

A remarkable number of dynamical and static properties of weakly interacting bosons have been described within the context of Bogoliubov theory over he past decades. The concept of quasi-particles has lead to a much deeper understanding of the collective phenomena in many correlated systems, and Bogoliubov quasi-particles are one of prime textbook examples and drosophila of this concept in condensed matter physics. However, Bogoliubov theory by construction relies on a large condensate fraction, a condition which is mostly not fulfilled for strong interparticle interactions. The latter regime is however of large interest, especially with the developments of cold atom systems over the last years, where the interaction is tunable over a large range. Whereas the phenomena in weakly interacting systems are typically single-particle like and smoothly connected to the non-interacting case where all properties are usually known, strongly interacting systems are much harder to describe theoretically.

Here we focus on the case of interacting bosons in a three-dimensional lattice, which are typically described by Hubbard-type models. Significant progress in the development of theoretical methods has been made in the last decade. In one dimension, the density matrix renormalization group (or equivalently the time evolved block decimation algorithm) can be used to calculate essentially all static and time-dependent properties. For bosonic problems, the quantum Monte-Carlo worm algorithm can be used to determine arbitrary static expectation values at equilibrium.

One of the challenging problems is thus to describe out of equilibrium dynamics of strongly interacting bosons in dimensions higher than one. Here, we develop a quasi-particle theory for such systems, which goes beyond the realm of Bogoliubov theory and is also valid for strong interactions. As shown in the previous chapter, Bogoliubov theory can be understood as the quantized theory counterpart of the linearized equations of motion around the classical, fully condensed Gross-Pitaevskii variational state. Here we start with a different variational state for bosons in a lattice: the bosonic Gutzwiller variational state takes the place of the Gross-Pitaevskii state. This provides a much better starting point for finite interactions, taking finite depletion into account and describing the Mott insulator phase transition in 3D on a qualitatively correct level, while recovering Bogoliubov theory in the weakly interacting limit. It therefore provides a much better starting point for a fluctuation expansion treatment than the Gross-Pitaevskii state at the cost of a larger number of variational parameters.

From the mathematical structure, the generalized unitary operator transformations are analogous to the Bogoliubov case. Both the classical fluctuation variables, as well as the corresponding operators in the quantized theory presented in chapter (8) live on a symplectic space and the transformations preserving the Poisson bracket relations or bosonic commutation relations respectively, are of the generalized unitary type discussed in appendix (K). Since the derivation in the previous

chapter was presented in such a detailed form, since it is the same mathematical formalism, but the physical context is better known for Bogoliubov theory.

At first, we present the derivation for the single species Bose-Hubbard model, but results for the two-species case will also be presented in section (8.10). The variational Gutzwiller state is of the form

$$|\mathrm{GW}\rangle = \prod_{\otimes \boldsymbol{\ell}} \left[\sum_n c_n^{(\boldsymbol{\ell})} |n\rangle_{\boldsymbol{\ell}} \right], \tag{7.1}$$

where $|n\rangle_{\boldsymbol{\ell}}$ is the local Fock state at site $\boldsymbol{\ell}$ containing n particles. The complex variables $c_n^{(\boldsymbol{\ell})}$ are to be seen as variational parameters, with the additional constraints $\sum_n |c_n^{(\boldsymbol{\ell})}|^2 = 1$ for each $\boldsymbol{\ell}$, which guarantees that each local state is normalized. This is not to be confused with the particle number constraint in Gross-Pitaevskii theory. Here the total particle number is given by $N = \sum_{n,\boldsymbol{\ell}} n\, |c_n^{(\boldsymbol{\ell})}|^2$.

Within this approximation, the ground state can be uniquely obtained (up to a trivial complex phase factor in all coefficients $c_n^{(\boldsymbol{\ell})}$) by minimizing the energy expectation value of the Bose-Hubbard Hamiltonian

$$\langle \mathrm{GW}|H_{\mathrm{BH}}|\mathrm{GW}\rangle \to \min. \tag{7.2}$$

This defines the set of ground state variational parameters $g_n^{(\boldsymbol{\ell})}$, and we can equally well perform a variable transformation and work in terms of the fluctuation amplitudes $\delta c_n^{(\boldsymbol{\ell})}$, where $c_n^{(\boldsymbol{\ell})} = g_n^{(\boldsymbol{\ell})} + \delta c_n^{(\boldsymbol{\ell})}$.

Normalization of the Local State

However, working in the Fock basis has a disadvantage associated with it. Enforcing the normalization condition of the local state $\langle \mathrm{GW}(\{\delta c_n^{(\boldsymbol{\ell})}\})|\mathrm{GW}(\{\delta c_n^{(\boldsymbol{\ell})}\})\rangle = 1$ essentially means, that we have more variables $\{\delta c_n^{(\boldsymbol{\ell})}\}$ than actual degrees of freedom. If we change the state by some infinitesimal amount in $\{\delta c_n^{(\boldsymbol{\ell})}\}$, the norm of the state will generally also change in first order. If the quasi-particle matrix is set up with including these redundant degrees of freedom, this will result in additional zero eigenvalues with the eigenvectors along the direction of the local ground states or superpositions thereof. For a lattice of size L, there are L such eigenvalues. These are not to be confused with the single zero eigenvalue in the condensate.

Working in the Gutzwiller Eigenbasis

To circumvent this problem from the very beginning and to allow for a more elegant formulation, we choose to work in a different local basis from the very beginning. Having determined the ground state $|\mathrm{GW}_0\rangle$ within the variational approach defines a the set of local order parameters $\phi_{\boldsymbol{\ell}} = \langle \mathrm{GW}_0|b_{\boldsymbol{\ell}}|\mathrm{GW}_0\rangle$, and a mean-field Hamiltonian

$$H_{\mathrm{mf}} = \sum_{\boldsymbol{\ell}} \left[-J \sum_{\boldsymbol{\ell}' \in nn(\boldsymbol{\ell})} (\phi_{\boldsymbol{\ell}'}\, b_{\boldsymbol{\ell}}^\dagger + \phi_{\boldsymbol{\ell}'} b_{\boldsymbol{\ell}}) + (\epsilon_{\boldsymbol{\ell}} - \mu) b_{\boldsymbol{\ell}}^\dagger b_{\boldsymbol{\ell}} + \frac{U}{2} b_{\boldsymbol{\ell}}^\dagger b_{\boldsymbol{\ell}}^\dagger b_{\boldsymbol{\ell}} b_{\boldsymbol{\ell}} \right] \tag{7.3}$$

to which $|\mathrm{GW}_0\rangle$ is also the self-consistent ground state. Since H_{mf} is Hermitian and a direct sum of on-site Hamiltonians $\mathcal{H}_{\boldsymbol{\ell}}$, its eigenstates constitute a complete basis of the entire space. Each of these multi-site eigenstates is a direct product of local eigenstates $|i\rangle_{\boldsymbol{\ell}}$, where i is the mean-field eigenstate index and $i = 0$ denotes the ground state. By construction, each local mean-field Hamiltonian (as well as the entire H_{mf}) is diagonal in this basis

$$\mathcal{H}_{\boldsymbol{\ell}} = \sum_{i=0}^{\infty} E_i^{(\boldsymbol{\ell})} |i\rangle_{\boldsymbol{\ell}\boldsymbol{\ell}} \langle i| \tag{7.4}$$

and we choose the energy offset such that the ground state energy vanishes. We emphasize that working in the basis mean-field eigenstates does not imply a restriction to the variational approach,

i.e. an arbitrary many-body state can be exactly represented in terms of mean-field eigenstates. Furthermore the Gutzwiller eigenbasis is static: also when considering non-equilibrium states with time-dependent order parameters, the basis $|i\rangle_{\boldsymbol{\ell}}$ is always the eigenbasis of the H_{mf} for the ground state order parameter.

The variational Gutzwiller state (7.1) can now also be expressed in this eigenbasis

$$|\mathrm{GW}\rangle = \prod_{\otimes \boldsymbol{\ell}} \left[\sum_{i \geq 0} \lambda_i^{(\boldsymbol{\ell})} |i\rangle_{\boldsymbol{\ell}} \right]. \tag{7.5}$$

To describe a time-dependent evolution of the variational state, the amplitudes $\lambda_i^{(\boldsymbol{\ell})}$ are promoted to time-dependent fields and the fluctuation expansion around in this basis the mean-field ground state takes on the particularly simple form

$$\lambda_i^{(\boldsymbol{\ell})}(t) = \delta_{i,0} + \delta\lambda_i^{(\boldsymbol{\ell})}(t). \tag{7.6}$$

The norm $\langle \mathrm{GW}(\delta\lambda_i^{(\boldsymbol{\ell})}) | \mathrm{GW}(\delta\lambda_i^{(\boldsymbol{\ell})}) \rangle$ is preserved to first order in the fluctuations $\delta\lambda_i^{(\boldsymbol{\ell})}$ if the fluctuation amplitude of each mean-field ground state $|i=0\rangle$ is kept fixed $\delta\lambda_0^{(\boldsymbol{\ell})}(t) = 0$. To uniquely characterize the variational state, one may thus simply exclude the ground state amplitudes $\delta\lambda_0^{(\boldsymbol{\ell})}$ from the set of variational parameters. Also for states further away from the mean-field ground state, the remaining amplitudes uniquely parametrize the entire variational state up to an irrelevant overall complex phase:

$$|1 + \delta\lambda_0^{(\boldsymbol{\ell})}| = \sqrt{1 - \sum_{i>0} |\delta\lambda_i^{(\boldsymbol{\ell})}|^2} \tag{7.7}$$

implicitly determines the amplitudes of the local mean-field ground states up to a phase. Clearly, the parameters describing physically relevant variational states are restricted to the manifold $\sum_{i>0} |\delta\lambda_i^{(\boldsymbol{\ell})}|^2 \leq 1$.

Equations of Motion

The non-linear Gutzwiller equations of motion can be formulated within any basis by extremizing the action with respect to the variational amplitude fields $\lambda_i^{(\boldsymbol{\ell})}(t)$. For a non-equilibrium state, the equations of motion are equivalent to the time evolution of each local state $|\psi_{\boldsymbol{\ell}}(t)\rangle$ at site $\boldsymbol{\ell}$ being generated by

$$i\partial_t |\psi_{\boldsymbol{\ell}}(t)\rangle = \left[\mathcal{H}_{\boldsymbol{\ell}} - \delta\eta_{\boldsymbol{\ell}}(t)\, b_{\boldsymbol{\ell}}^\dagger - \delta\eta_{\boldsymbol{\ell}}^*(t)\, b_{\boldsymbol{\ell}} \right] |\psi_{\boldsymbol{\ell}}(t)\rangle. \tag{7.8}$$

Here the coupling to the nearest neighboring site is contained in the contained in the time-dependent function

$$\delta\eta_{\boldsymbol{\ell}}(t) = J \sum_{\boldsymbol{\ell}' \in nn(\boldsymbol{\ell})} (\psi_{\boldsymbol{\ell}'}(t) - \phi_{\boldsymbol{\ell}'}) \tag{7.9}$$

and $\psi_{\boldsymbol{\ell}}(t) = {}_{\boldsymbol{\ell}}\langle \psi_{\boldsymbol{\ell}}(t) | b_{\boldsymbol{\ell}} | \psi_{\boldsymbol{\ell}}(t) \rangle_{\boldsymbol{\ell}}$ is the local order parameter.

In the mean-field basis, this amounts to a set of coupled differential equations

$$i\partial_t \lambda_j^{(\boldsymbol{\ell})}(t) = E_j^{(\boldsymbol{\ell})}\, \lambda_j^{(\boldsymbol{\ell})}(t) - \delta\eta_{\boldsymbol{\ell}}(t) \sum_i \lambda_i^{(\boldsymbol{\ell})}(t) B_{i,j}^{(\boldsymbol{\ell})^*} - \delta\eta_{\boldsymbol{\ell}}^*(t) \sum_i \lambda_i^{(\boldsymbol{\ell})}(t) B_{j,i}^{(\boldsymbol{\ell})}, \tag{7.10}$$

where we defined the matrix elements of the annihilation operators in the mean-field basis

$$B_{i,j}^{(\boldsymbol{\ell})} = {}_{\boldsymbol{\ell}}\langle i | b_{\boldsymbol{\ell}} | j \rangle_{\boldsymbol{\ell}}. \tag{7.11}$$

Note that the coupling $\delta\eta_{\boldsymbol{\ell}}$ is a non-linear function in the fluctuation amplitudes $\delta\lambda$. Using the relation $\psi_{\boldsymbol{\ell}} = \sum_{i,j \geq 0} B_{i,j}^{(\boldsymbol{\ell})}\, \lambda_i^{(\boldsymbol{\ell})^*}\, \lambda_j^{(\boldsymbol{\ell})}$, we can express $\delta\eta_{\boldsymbol{\ell}}$ up to linear in the fluctuations $\delta\lambda$ as

$$\delta\eta_{\boldsymbol{\ell}}(t) = J \sum_{\boldsymbol{\ell}' \in \mathrm{n.n.}(\boldsymbol{\ell})} \sum_i \left[B_{0,i}^{(\boldsymbol{\ell}')}\, \delta\lambda_i^{(\boldsymbol{\ell}')}(t) + B_{i,0}^{(\boldsymbol{\ell}')}\, \delta\lambda_i^{(\boldsymbol{\ell}')^*}(t) \right] + \mathcal{O}(\delta\lambda^2). \tag{7.12}$$

Choosing the energy offset $E_0^{(\boldsymbol{\ell})} = 0$ and using (7.12) in the equations of motion (7.10) leads to the linearized equations of motion for the fluctuation amplitudes

$$\begin{aligned} i\partial_t \delta\lambda_j^{(\boldsymbol{\ell})}(t) = E_j^{(\boldsymbol{\ell})}\, \delta\lambda_j^{(\boldsymbol{\ell})}(t) - J \sum_{\boldsymbol{\ell}' \in \mathrm{nn}(\boldsymbol{\ell})} \sum_{i=0}^{\infty} \Big[\big(B_{0,i}^{(\boldsymbol{\ell}')}\, \delta\lambda_i^{(\boldsymbol{\ell}')}(t) + B_{i,0}^{(\boldsymbol{\ell}')}\, \delta\lambda_i^{(\boldsymbol{\ell}')^*}(t)\big) B_{0,j}^{(\boldsymbol{\ell})^*} \\ + \big(B_{0,i}^{(\boldsymbol{\ell}')^*}\, \delta\lambda_i^{(l')^*}(t) + B_{i,0}^{(\boldsymbol{\ell}')^*}\, \delta\lambda_i^{(\boldsymbol{\ell}')}(t)\big) B_{j,0}^{(\boldsymbol{\ell})} \Big] \end{aligned} \tag{7.13}$$

which exactly recover the dynamics of the full non-linear time evolution in the limit of weak fluctuations $\delta\lambda$.

Matrix Representation

To analyze the structure of these equations of motion and their solutions in a more rigorous and thorough mathematical framework, we express these equations in matrix form. We begin by truncating the local Hilbert space on every site to the energetically lowest $N_{\max}$ mean-field eigenstates and define the vector

$$\boldsymbol{\delta\lambda}^{(\boldsymbol{\ell})} \equiv \begin{pmatrix} \delta\lambda_1^{(\boldsymbol{\ell})} \\ \vdots \\ \delta\lambda_{N_{\max}}^{(\boldsymbol{\ell})} \end{pmatrix}. \tag{7.14}$$

Here we did not include the ground state fluctuation amplitude $\lambda_0^{(\boldsymbol{\ell})}$, as motivated above. We furthermore define the $\mathcal{D} = LN_{\max}$ dimensional vector parametrizing the entire variational state on all L sites

$$\boldsymbol{\delta\lambda} \equiv \begin{pmatrix} \boldsymbol{\delta\lambda}^{(1)} \\ \vdots \\ \boldsymbol{\delta\lambda}^{(L)} \end{pmatrix}. \tag{7.15}$$

The construction of the theory is done for finite $N_{\max}$, which amounts to an energy truncation in the initial mean-field basis. Only at the very end is the limit $N_{\max} \to \infty$ taken and all relevant observables, seen as a function of $N_{\max}$, converge to the physically correct result.

The elements of $\boldsymbol{\delta\lambda}$ are complex variables and the differential equations (7.13) can be understood as twice the number of differential equations for the imaginary and real parts of $\delta\lambda$. The appearance of conjugate terms $\delta\lambda^*$ in the temporal derivative $\frac{d}{dt}\delta\lambda$ lead to a coupling of real and imaginary parts. As shown in appendix (I), one can formally treat $\delta\lambda$ and $\delta\lambda^*$ as independent variables, which is equivalent to considering real and imaginary parts individually. In this spirit, we can write the entire set of differential equations (7.13) together with their conjugates in $2\mathcal{D}$-dimensional matrix form as

$$i\frac{d}{dt}\begin{pmatrix} \boldsymbol{\delta\lambda} \\ -\boldsymbol{\delta\lambda}^* \end{pmatrix} = H_{\mathrm{QP}} \begin{pmatrix} \boldsymbol{\delta\lambda} \\ \boldsymbol{\delta\lambda}^* \end{pmatrix}. \tag{7.16}$$

The quasi-particle Hamiltonian in this mean-field fluctuation basis takes on the form

$$H_{\mathrm{QP}} = \begin{pmatrix} h & \Delta \\ \Delta^* & h^* \end{pmatrix}, \tag{7.17}$$

where h is a $\mathcal{D} \times \mathcal{D}$ Hermitian matrix with the elements

$$h_{(i,\boldsymbol{\ell}),(j,\boldsymbol{\ell}')} = \delta_{\boldsymbol{\ell},\boldsymbol{\ell}'}\, \delta_{i,j}\, E_i^{(\boldsymbol{\ell})} - J_{\boldsymbol{\ell},\boldsymbol{\ell}'}\, F_{i,0,0,j}^{(\boldsymbol{\ell},\boldsymbol{\ell}')} \tag{7.18}$$

and Δ is also $\mathcal{D} \times \mathcal{D}$-dimensional, but symmetric with matrix elements

$$\Delta_{(i,\boldsymbol{\ell}),(j,\boldsymbol{\ell}')} = -J_{\boldsymbol{\ell},\boldsymbol{\ell}'} F_{i,j,0,0}^{(\boldsymbol{\ell},\boldsymbol{\ell}')}. \tag{7.19}$$

Here, we defined the quantity

$$F_{i_1,i_2,j_1,j_2}^{(\boldsymbol{\ell}_1,\boldsymbol{\ell}_2)} = \tilde{B}_{j_1,i_1}^{(\boldsymbol{\ell}_1)^*} \tilde{B}_{i_2,j_2}^{(\boldsymbol{\ell}_2)} + \tilde{B}_{i_1,j_1}^{(\boldsymbol{\ell}_1)} \tilde{B}_{j_2,i_2}^{(\boldsymbol{\ell}_2)^*} \tag{7.20}$$

to express the matrix elements in a convenient form. Furthermore, $J_{\boldsymbol{\ell},\boldsymbol{\ell}'}$ is defined to be J if the indices $\boldsymbol{\ell}$ and $\boldsymbol{\ell}'$ refer to nearest neighboring sites, and zero otherwise.

To bring the equations of motion (7.16) into a form where we can decompose the initial state vector in terms of eigenmodes, we multiply both sides of Eq. (7.16) by $\Sigma = \begin{pmatrix} \mathbb{1}_{\mathcal{D}} & 0 \\ 0 & -\mathbb{1}_{\mathcal{D}} \end{pmatrix}$ to obtain

$$i\frac{d}{dt}\begin{pmatrix} \boldsymbol{\delta\lambda} \\ \boldsymbol{\delta\lambda}^* \end{pmatrix} = \Sigma H_{\mathrm{QP}} \begin{pmatrix} \boldsymbol{\delta\lambda} \\ \boldsymbol{\delta\lambda}^* \end{pmatrix}. \tag{7.21}$$

Since the matrix h is Hermitian and Δ is symmetric, H_{QP} is Hermitian. However, as in the Bogoliubov case, the equations of motion (7.21) reveal that the collective modes are not the eigenvectors of H_{QP}, but of the matrix ΣH_{QP}, which is not Hermitian, nor normal. As discussed on general ground in appendix (K), we can infer many properties of the eigenvectors and eigenvalues. For the quasi-particle theory discussed here, there is one crucial difference to Bogoliubov theory in the qualitative eigenvector structure: In Bogoliubov theory, which necessarily relies on the existence of a condensate, a complete basis of eigenvectors of ΣH_{QP} never exists in any parameter regime. The same applies within the quasi-particle theory derived here, if a condensate is present. If, however, we are in an insulating phase, this is no longer necessarily true and it turns out that a basis of eigenvectors of ΣH_{QP} does very well exist. This is not at variance with the matrix ΣH_{QP} being non-normal, since the eigenvectors are not orthogonal with respect to the euclidean norm, but *orthogonal* with respect to the bilinear form defined by Σ. Since the completeness relations and the qualitative structure of the resulting quasi-particle Hamiltonians are different in the case of a condensate or an insulator, we discuss them individually.

7.0.1 Eigenvector Structure in the Condensate

For the general inhomogeneous case, it turns out that ΣH_{QP} possesses $2\mathcal{D}-1$ eigenvectors. One eigenvector $\mathbf{p}$ to an eigenvalue zero is associated with the condensate and generally of the structure

$$\mathbf{p} = \begin{pmatrix} \mathbf{u}^{(0)} \\ -\mathbf{u}^{(0)*} \end{pmatrix}. \tag{7.22}$$

We choose the normalization $\mathbf{p}^\dagger\mathbf{p} = 1$.

All other eigenvectors appear have non-zero eigenvalues and appear in pairs: if $\mathbf{x}^{(s)} = \begin{pmatrix} \mathbf{u}^{(s)} \\ -\mathbf{v}^{(s)} \end{pmatrix}$ is an eigenvector to an eigenvalue ω_s, then an associated eigenvector $\mathbf{y}^{(s)} = \gamma\mathbf{x}^{(s)*} = \begin{pmatrix} -\mathbf{v}^{(s)*} \\ \mathbf{u}^{(s)*} \end{pmatrix}$ to an eigenvalue $-\omega_s^*$ exists. Here $\gamma = \begin{pmatrix} 0 & \mathbb{1}_{\mathcal{D}} \\ \mathbb{1}_{\mathcal{D}} & 0 \end{pmatrix}$ is a permutation matrix. Both eigenvectors $\mathbf{x}^{(s)}$ and $\mathbf{y}^{(s)}$ correspond to the same quasi-particle mode: the prior to the creation of a quasi-particle, the latter to the removal, i.e. a quasi-particle hole.

For a state expanded around the mean-field minimum, the eigenvalues ω_s turn out to be real and we omit the complex conjugation. With ω_s we furthermore always denote the positive eigenvalue. If the initial mean-field state corresponds to the global energy minimum, the eigenvector $\mathbf{x}^{(s)}$ to a positive eigenvalue ω_s has a positive norm $\mathbf{x}^{(s)\dagger}\Sigma\mathbf{x}^{(s)} > 0$ with respect to the metric Σ, whereas eigenvectors $\mathbf{y}^{(s)}$ to negative eigenvalues $-\omega_s$ have a negative norm $\mathbf{y}^{(s)\dagger}\Sigma\mathbf{y}^{(s)} < 0$. This property is no longer true when considering self-consistent mean-field states corresponding to local minima, such as vortex states. The sign of the norm of a vector in the symplectic space is invariant under arbitrary renormalization. We choose to normalize the eigenvectors to non-zero eigenvalues such that $\mathbf{x}^{(s)\dagger}\Sigma\mathbf{x}^{(s)} = 1$ and $\mathbf{y}^{(s)\dagger}\Sigma\mathbf{y}^{(s)} = -1$. Eigenvectors to different eigenvalues are generally orthogonal with respect to the scalar product associated with Σ.

In the condensate there are $\mathcal{D}-1$ eigenvectors $\mathbf{x}^{(s)}$ and the same number of associated eigenvectors $\mathbf{y}^{(s)}$, as well as the eigenvector $\mathbf{p}$ to a zero eigenvalue. To span the entire space, we thus require

one additional vector, which lies in the extended eigenspace to the eigenvalue zero and we denote by $\mathbf{q}$, analogous to the Bogoliubov case. This vector is implicitly defined by

$$\Sigma H_{\mathrm{QP}}\,\mathbf{q} = -\frac{i}{\tilde{m}}\mathbf{p}, \tag{7.23}$$

where the mass-like number $\tilde{m}$ is purely real and is not to be confused with the effective mass of the various quasi-particles. Since $\mathbf{p}$ and $\mathbf{q}$ both lie in the generalized eigenspace to the eigenvalue zero, Eq. (8.45) does not uniquely define the vector $\mathbf{q}$: an arbitrary vector within this generalized eigenspace fulfills this condition. The form (7.22) of the vector $\mathbf{p}$ guarantees that the expectation value of the corresponding variable is always purely real[1]. This property can also be fulfilled for the variable associated with the vector $\mathbf{q}$ if we choose it to be of the form

$$\mathbf{q} = -i\begin{pmatrix}\mathbf{v}^{(0)}\\ \mathbf{v}^{(0)*}\end{pmatrix}, \tag{7.24}$$

which is linearly independent of $\mathbf{p}$. The Σ-norm of $\mathbf{q}$ vanishes and we choose to normalize it via the overlap with the $\mathbf{p}$

$$\mathbf{q}^\dagger\Sigma\mathbf{p} = i. \tag{7.25}$$

The structure of (7.24) and (7.22) is in accordance with this overlap (7.25) being purely imaginary. Together with the normalization $\mathbf{p}^\dagger\mathbf{p} = 1$, the two equations (8.45) and (7.25) uniquely determine $\mathbf{q}$, up to a global complex phase of both $\mathbf{p}$ and $\mathbf{q}$.

Note that in contrast to Bogoliubov theory[2], the subvector $\mathbf{u}^{(0)}$ from the eigenvector $\mathbf{p}$ in Eq. (8.39) is generally linearly independent of the subvector $\mathbf{v}^{(0)}$ of the vector $\mathbf{q}$.

One general way to explicitly determine $\mathbf{q}$ is to start with an arbitrary vector lying outside the space spanned by ($\{\mathbf{x}^{(s)}\}$, $\{\mathbf{y}^{(s)}\}$, $\mathbf{p}$) and subsequently orthogonalize it to the other basis vectors with respect to Σ.

What have we achieved? We have determined a uniquely defined basis set of vectors ($\{\mathbf{x}^{(s)}\}$, $\{\mathbf{y}^{(s)}\}$, $\mathbf{p}, \mathbf{q}$) which span the space of variational states parametrized in the Gutzwiller form. In summary, these obey the orthogonality relations

$$\mathbf{x}^{(r)\dagger}\Sigma\mathbf{x}^{(s)} = \delta_{r,s} \tag{7.26}$$
$$\mathbf{y}^{(r)\dagger}\Sigma\mathbf{y}^{(s)} = -\delta_{r,s} \tag{7.27}$$
$$\mathbf{x}^{(r)\dagger}\Sigma\mathbf{y}^{(s)} = 0 \tag{7.28}$$
$$\mathbf{p}^\dagger\Sigma\mathbf{p} = 0 \tag{7.29}$$
$$\mathbf{p}^\dagger\Sigma\mathbf{x}^{(s)} = 0 \tag{7.30}$$
$$\mathbf{p}^\dagger\Sigma\mathbf{y}^{(s)} = 0 \tag{7.31}$$
$$\mathbf{q}^\dagger\Sigma\mathbf{q} = 0 \tag{7.32}$$
$$\mathbf{q}^\dagger\Sigma\mathbf{x}^{(s)} = 0 \tag{7.33}$$
$$\mathbf{q}^\dagger\Sigma\mathbf{y}^{(s)} = 0 \tag{7.34}$$
$$\mathbf{q}^\dagger\Sigma\mathbf{p} = i. \tag{7.35}$$

Only by using these orthogonality relations, together with the normalization $\mathbf{p}^\dagger\mathbf{p} = 1$, we find the completeness relation by explicit construction of the unit operator

$$\mathbb{1}_{2\mathcal{D}} = \sum_s (\mathbf{x}^{(s)}\mathbf{x}^{(s)\dagger} - \mathbf{y}^{(s)}\mathbf{y}^{(s)\dagger})\Sigma + i(\mathbf{q}\,\mathbf{p}^\dagger - \mathbf{p}\,\mathbf{q}^\dagger)\Sigma. \tag{7.36}$$

This can be seen by letting the right hand side of (8.49) act on the basis set ($\{\mathbf{x}^{(s)}\}$, $\{\mathbf{y}^{(s)}\}$, $\mathbf{p}, \mathbf{q}$), which maps each vector onto itself. The only matrix fulfilling this property is the unit matrix.

7.0.2 Eigenvector Structure in the Insulator

The construction of a basis is much simpler than in the condensate case. Here, a complete basis of eigenvectors ($\{\mathbf{x}^{(s)}\}$, $\{\mathbf{y}^{(s)}\}$) exists (i.e. s runs from 1 to $\mathcal{D}$) and all eigenvalues ω_s (and the conjugate counterparts) are non-zero. The same orthogonality relations as in the previous case exist and the completeness relation is found to be

$$\mathbb{1}_{2\mathcal{D}} = \sum_s (\mathbf{x}^{(s)}\mathbf{x}^{(s)\dagger} - \mathbf{y}^{(s)}\mathbf{y}^{(s)\dagger})\Sigma. \tag{7.37}$$

[1] In the quantized corresponding theory, the associated operator is Hermitian.

[2] Here the generalized eigenspace to the condensate mode is to-dimensional and the subvector $\mathbf{u}^{(0)}$ thus a complex number.

7.1 Structure of the Quasi-Particle Transformation

We now have two different bases in which the variational state (which is basis-independent) can be expressed: the canonical mean-field basis in which the state is parametrized by $(\boldsymbol{\delta\lambda}, \boldsymbol{\delta\lambda}^*)^t$, as well as the basis $(\{\mathbf{x}^{(s)}\}, \{\mathbf{y}^{(s)}\}, \mathbf{p}, \mathbf{q})$ in the condensate or $(\{\mathbf{x}^{(s)}\}, \{\mathbf{y}^{(s)}\})$ in the insulator. These two cases have to be considered separately throughout this section. We will discuss the more complicated condensate case first. The corresponding results for the insulating case are easily deduced and are considered at the end.

Condensate Case

Given an arbitrary variational state parametrized by the vector of Gutzwiller fluctuation amplitudes $(\boldsymbol{\delta\lambda}, \boldsymbol{\delta\lambda}^*)^t$, we can use the completeness relation in the condensate (8.49) to directly express this in the extended quasi-particle eigenbasis as

$$\begin{pmatrix} \boldsymbol{\delta\lambda}(t) \\ \boldsymbol{\delta\lambda}^*(t) \end{pmatrix} = \sum_s \alpha_s(t)\, \mathbf{x}^{(s)} + \sum_s \alpha_s^*(t)\, \mathbf{y}^{(s)} + i\rho(t)\, \mathbf{q} + i\chi(t)\, \mathbf{p}, \tag{7.38}$$

where, analogous to the transformation structure in Bogoliubov case (6.115), we defined the overlap coefficients

$$\alpha_s(t) = \mathbf{x}^{(s)\dagger} \Sigma \begin{pmatrix} \boldsymbol{\delta\lambda}(t) \\ \boldsymbol{\delta\lambda}^*(t) \end{pmatrix} = \sum_{i>0} \sum_{\boldsymbol{\ell}} \left[u_{i,\boldsymbol{\ell}}^{(s)*} \delta\lambda_i^{(\boldsymbol{\ell})}(t) + v_{i,\boldsymbol{\ell}}^{(s)*} \delta\lambda_i^{(\boldsymbol{\ell})*}(t) \right] \tag{7.39}$$

$$\alpha_s^*(t) = -\mathbf{y}^{(s)\dagger} \Sigma \begin{pmatrix} \boldsymbol{\delta\lambda}(t) \\ \boldsymbol{\delta\lambda}^*(t) \end{pmatrix} = \sum_{i>0} \sum_{\boldsymbol{\ell}} \left[v_{i,\boldsymbol{\ell}}^{(s)} \delta\lambda_i^{(\boldsymbol{\ell})}(t) + u_{i,\boldsymbol{\ell}}^{(s)} \delta\lambda_i^{(\boldsymbol{\ell})*}(t) \right] \tag{7.40}$$

$$\rho(t) = \mathbf{p}^\dagger \Sigma \begin{pmatrix} \boldsymbol{\delta\lambda}(t) \\ \boldsymbol{\delta\lambda}^*(t) \end{pmatrix} \tag{7.41}$$

$$\chi(t) = -\mathbf{q}^\dagger \Sigma \begin{pmatrix} \boldsymbol{\delta\lambda}(t) \\ \boldsymbol{\delta\lambda}^*(t) \end{pmatrix}. \tag{7.42}$$

The coefficients $\alpha(t)$ in Eq. (7.39) and $\alpha^*(t)$ in Eq. (7.40) are related by conjugation, since the eigenvectors $\mathbf{x}^{(s)}$ and $\mathbf{y}^{(s)}$ are related by $\mathbf{x}^{(s)} = \gamma \mathbf{y}^{(s)*}$.

Let us define the matrix W via its column vectors

$$W = \left[\mathbf{x}^{(1)}, \ldots, \mathbf{x}^{(\mathcal{D}-1)}, i\mathbf{p}, \mathbf{y}^{(1)}, \ldots, \mathbf{y}^{(\mathcal{D}-1)}, i\mathbf{q} \right]. \tag{7.43}$$

Extending on the Bogoliubov case (6.69), one finds the relation

$$W^\dagger \Sigma W = \begin{pmatrix} \mathbb{1}_{\mathcal{D}-1} & & & \\ & 0 & \cdots & -i \\ & \vdots & -\mathbb{1}_{\mathcal{D}-1} & \vdots \\ & i & \cdots & 0 \end{pmatrix} =: \tilde{\Sigma} \tag{7.44}$$

by using the orthogonality relations in Eqns. (7.39 - 7.42). The matrix $\tilde{\Sigma}$ is Hermitian and unitary

$$\tilde{\Sigma}^{-1} = \tilde{\Sigma} = \tilde{\Sigma}^\dagger. \tag{7.45}$$

Multiplying both sides of (7.44) by $\tilde{\Sigma}$, one finds $\tilde{\Sigma} W^\dagger \Sigma W = \mathbb{1}_{2\mathcal{D}}$, which allows the inverse matrix W^{-1} to be obtained to be obtained by a simple matrix multiplication

$$W^{-1} = \tilde{\Sigma} W^\dagger \Sigma = \begin{pmatrix} U^\dagger, & V^\dagger \\ -i\mathbf{v}^{(0)\dagger}, & i\mathbf{v}^{(0)t} \\ V^t, & U^t \\ \mathbf{u}^{(0)\dagger}, & \mathbf{u}^{(0)t} \end{pmatrix}. \tag{7.46}$$

The $\mathcal{D} \times (\mathcal{D}-1)$-dimensional matrices U and V are defined by their column vectors $\mathbf{u}^{(s)}$ and $\mathbf{v}^{(s)}$, ordered in the same fashion as the eigenvectors in W, respectively.

Defining the column vector of amplitudes in the extended quasi-particle basis

$$\boldsymbol{\alpha} = \begin{pmatrix} \alpha_1 \\ \vdots \\ \alpha_{\mathcal{D}-1} \end{pmatrix}, \tag{7.47}$$

we note that the transformation relations in Eqns. (7.39 - 7.42) can be written in matrix form as

$$\begin{pmatrix} \boldsymbol{\alpha}(t) \\ -i\rho(t) \\ -\boldsymbol{\alpha}^*(t) \\ i\chi(t) \end{pmatrix} = W^\dagger \Sigma \begin{pmatrix} \boldsymbol{\delta\lambda}(t) \\ \boldsymbol{\delta\lambda}^*(t) \end{pmatrix}. \tag{7.48}$$

Multiplying (7.48) by $\tilde{\Sigma}$ and using (7.54), we find the central transformation relations in both directions in matrix form

$$\begin{pmatrix} \boldsymbol{\alpha}(t) \\ \chi(t) \\ \boldsymbol{\alpha}^*(t) \\ \rho(t) \end{pmatrix} = \tilde{\Sigma} W^\dagger \Sigma \begin{pmatrix} \boldsymbol{\delta\lambda}(t) \\ \boldsymbol{\delta\lambda}^*(t) \end{pmatrix} \tag{7.49}$$

$$\begin{pmatrix} \boldsymbol{\delta\lambda}(t) \\ \boldsymbol{\delta\lambda}^*(t) \end{pmatrix} = W \begin{pmatrix} \boldsymbol{\alpha}(t) \\ \chi(t) \\ \boldsymbol{\alpha}^*(t) \\ \rho(t) \end{pmatrix}. \tag{7.50}$$

These are the central transformation relations: If we have any (also time-dependent) Gutzwiller state, which one can easily express in terms of the coefficients $\boldsymbol{\delta\lambda}(t)$, the transformation (7.55) is the prescription to explicitly calculate the occupation numbers of the various quasi-particle modes and the position and momentum expectation values of the effective free particle associated with the condensate mode. On the other hand, the inverse transformation (7.56) allows us to calculate the Gutzwiller coefficients of a state, which we can prepare at will, occupying specific quasi-particle modes are as coherent states with a given number of quasi-particles. For instance, one may ask what the form of the Gutzwiller state is, where only the amplitude mode at a given $\mathbf{k}$ is excited. In the limit that this coherent excitation is weak, this state evolves as a mode eigenstate when evolved with the Gutzwiller equations of motion.

For later calculations, it is furthermore useful to write the transformation (7.56) in component form for the individual fluctuation coefficients, which then reads

$$\delta\lambda_i^{(\boldsymbol{\ell})^*}(t) = \sum_s u_{i,\boldsymbol{\ell}}^{(s)} \alpha_s(t) - \sum_s v_{i,\boldsymbol{\ell}}^{(s)^*} \alpha_s^*(t) + i u_{i,\boldsymbol{\ell}}^{(0)} \chi(t) + v_{i,\boldsymbol{\ell}}^{(0)} \rho(t). \tag{7.51}$$

Insulator Case

Here the eigenvectors $\{\mathbf{x}^{(s)}\}$ and $\{\mathbf{y}^{(s)}\}$ constitute a complete basis and the vectors $\mathbf{p}$ and $\mathbf{q}$ do not appear in the expansion. The transformations from Eqns. (7.39) and (7.40) hold in the same form. The matrix W is of the form

$$W = \left[\mathbf{x}^{(1)}, \ldots, \mathbf{x}^{(\mathcal{D})}, \mathbf{y}^{(1)}, \ldots, \mathbf{y}^{(\mathcal{D})}\right] \tag{7.52}$$

and fulfills

$$W^\dagger \Sigma W = \Sigma. \tag{7.53}$$

Thus

$$W^{-1} = \tilde{\Sigma} W^\dagger \Sigma = \begin{pmatrix} U^\dagger, & V^\dagger \\ V^t, & U^t \end{pmatrix} \tag{7.54}$$

and the main transformations in both direction become

$$\begin{pmatrix} \boldsymbol{\alpha}(t) \\ \boldsymbol{\alpha}^*(t) \end{pmatrix} = \Sigma W^\dagger \Sigma \begin{pmatrix} \boldsymbol{\delta\lambda}(t) \\ \boldsymbol{\delta\lambda}^*(t) \end{pmatrix} \tag{7.55}$$

$$\begin{pmatrix} \boldsymbol{\delta\lambda}(t) \\ \boldsymbol{\delta\lambda}^*(t) \end{pmatrix} = W \begin{pmatrix} \boldsymbol{\alpha}(t) \\ \boldsymbol{\alpha}^*(t) \end{pmatrix} \tag{7.56}$$

with the explicit form of the latter

$$\delta\lambda_i^{(\boldsymbol{\ell})^*}(t) = \sum_s u_{i,\boldsymbol{\ell}}^{(s)} \alpha_s(t) - \sum_s v_{i,\boldsymbol{\ell}}^{(s)^*} \alpha_s^*(t). \tag{7.57}$$

7.2 Time Evolution Close to Equilibrium

To solve the equations of motion within the linearized, i.e. generated by the second order Hamiltonian, we use the expression (7.38) in the equations of motion (7.21), noting that the basis vectors are time independent. Furthermore, we use the eigenvector properties, which lead to the relations

$$i\sum_s \dot{\alpha}_s(t)\,\mathbf{x}^{(s)} + i\sum_s \dot{\alpha}_s^*(t)\,\mathbf{y}^{(s)} - \dot{\rho}(t)\,\mathbf{q} - \dot{\chi}(t)\,\mathbf{p} = \sum_s \omega_s\,\alpha_s(t)\,\mathbf{x}^{(s)} - \sum_s \omega_s\,\alpha_s^*(t)\,\mathbf{y}^{(s)} + \frac{1}{\tilde{m}}\rho(t)\,\mathbf{p} \tag{7.58}$$

Multiplying by $\mathbf{v}^\dagger\Sigma$ from the left, where $\mathbf{v}$ is one of the new basis vectors, and using the orthogonality relations, one obtains the most uncoupled form for the equations of motion of the coefficients in the new basis

$$\dot{\alpha}_s(t) = -i\omega_s\,\alpha_s(t) \tag{7.59}$$

$$\dot{\alpha}_s^*(t) = i\omega_s\,\alpha_s^*(t) \tag{7.60}$$

$$\dot{\rho}(t) = 0 \tag{7.61}$$

$$\dot{\chi}(t) = -\frac{\rho(t)}{\tilde{m}}. \tag{7.62}$$

For a given set of initial values $\boldsymbol{\alpha}(0)$, $\rho(0)$, $\chi(0)$, these equations possess the unique solution

$$\alpha_s(t) = \alpha_s(0)\,e^{-i\omega_s t} \tag{7.63}$$

$$\rho(t) = \rho(0) \tag{7.64}$$

$$\chi(t) = \chi(0) - \frac{\rho(0)}{\tilde{m}}\,t. \tag{7.65}$$

Classical Correspondence

The evolution of each complex variable α_s corresponds to the evolution of a classical harmonic oscillator, where the relation to the corresponding classical position and momentum is given by Eq. (6.133). Qualitatively, the physics of all harmonic oscillator modes is equivalent. The situation for the ρ and χ variables is however quite different: here the equations correspond to those of a free classical particle with mass $\tilde{m}$, momentum $-\rho$ and position χ. In the absence of any force, the momentum is conserved, i.e. $\rho(t) = \rho(0)$ and the position $\chi(t)$ changes linearly in time at a rate proportional to the momentum $-\rho$.

Note that also when considering the dynamics of a particle in a harmonic potential $V(x) = \frac{\tilde{m}\omega^2}{2}x^2$ within classical mechanics, the solutions to the equations of motion for the two cases $\omega > 0$ and $\omega = 0$, are qualitatively different. Taking the limit $\omega \to 0$ does not smoothly lead to the $\omega = 0$ solution. This is fundamentally related with the components of the eigenvectors $\mathbf{x}^{(s)}$ and $\mathbf{y}^{(s)}$ in the quasi-particle operator space diverging in this limit $\omega \to 0$. For any finite ω, $\mathbf{x}^{(s)}$ and $\mathbf{y}^{(s)}$ linearly independent, but for $\omega = 0$ case, the situation is also qualitatively different and only a single, non-normalizable (with respect to the Σ-norm) eigenvector exists.

The time evolution of the system in this classical limit can be pictured as a trajectory of a classical particle of mass $\tilde{m}$ in a $\mathcal{D}$-dimensional (spatial) space[3]. In the condensate this particle has a mass $\tilde{m}$ and the potential $V(x_1,\ldots,x_{\mathcal{D}}) = \sum_{s=1}^{\mathcal{D}-1} \frac{\tilde{m}\omega_s^2}{2} x_s^2$ is harmonic along $\mathcal{D}-1$ dimensions. Along one dimension however, the particle is free.

This potential shape arises when taking only the second order terms in the fluctuations along. The trajectories would be $\mathcal{D}-1$ dimensional Lissajous curves, but the particle would drift at a constant momentum $-\rho(0)$ along the coordinate $\chi(t)$. Only when taking higher order terms (beyond $E^{(2)}$ in the energy fluctuation expansion) along, is the potential for the classical particle deformed at larger radii. These terms result in the potential being non-separable and, correspondingly in the time-dependent picture, couple the equations of motion (7.59) - (7.62) for the quasi-particle amplitudes. A coupling of the free dimension (corresponding to the position χ) to the harmonic potentials would arise. This coupling is also responsible for the exact particle number conservation within the full description (also within time-dependent Gutzwiller theory), which is not fulfilled within the linearized equations of motion.

7.3 Fluctuation Expansion of the Classical Energy

The energy for the Gutzwiller is a well-defined, real function of the complex variational parameters $\delta\lambda$ and takes on a minimum if all of these are zero. We now express this energy exactly in terms of $\delta\lambda$ and group the different terms by the number of contained fluctuation amplitudes. The energy can be evaluated in any basis and the mean-field basis is allows for the most efficient evaluation. The exact Bose-Hubbard Hamiltonian is decomposed into the mean-field Hamiltonian and a fluctuation part

$$H_{\text{BH}} = H_{\text{mf}} + H_\delta. \tag{7.66}$$

The former is a sum of on-site Operators and the expectation value of any such operator is of second order in the fluctuations

$$\langle \text{GW}|H_{\text{mf}}|\text{GW}\rangle = \sum_{\boldsymbol{\ell}} \sum_{i>0}^{\infty} E_i^{(\boldsymbol{\ell})} |\delta\lambda_i^{(l)}|^2. \tag{7.67}$$

The fluctuation operator

$$H_\delta = -J \sum_{\langle \boldsymbol{\ell},\boldsymbol{\ell}'\rangle} (\delta b_{\boldsymbol{\ell}}^\dagger \delta b_{\boldsymbol{\ell}'} + \delta b_{\boldsymbol{\ell}'}^\dagger \delta b_{\boldsymbol{\ell}}). \tag{7.68}$$

induces coupling between sites, and we defined the mean-field shifted bosonic annihilation operators

$$\begin{aligned} \delta b_{\boldsymbol{\ell}} &= b_{\boldsymbol{\ell}} - \phi_{\boldsymbol{\ell}} \\ &= \sum_{i,j=0}^{\infty} \tilde{B}_{i,j}^{(\boldsymbol{\ell})} \; |i\rangle_{\boldsymbol{\ell}\,\boldsymbol{\ell}} \langle j|. \end{aligned} \tag{7.69}$$

Their matrix elements are related to (7.11) by $\tilde{B}_{i,j}^{(\boldsymbol{\ell})} = B_{i,j}^{(\boldsymbol{\ell})} - \phi_{\boldsymbol{\ell}}\,\delta_{i,j}$. It is useful to define the complex coefficients

$$F_{i_1,i_2,j_1,j_2}^{(\boldsymbol{\ell}_1,\boldsymbol{\ell}_2)} = \tilde{B}_{j_1,i_1}^{(\boldsymbol{\ell}_1)^*} \tilde{B}_{i_2,j_2}^{(\boldsymbol{\ell}_2)} + \tilde{B}_{i_1,j_1}^{(\boldsymbol{\ell}_1)} \tilde{B}_{j_2,i_2}^{(\boldsymbol{\ell}_2)^*}, \tag{7.70}$$

which, by virtue of $\tilde{B}_{0,0}^{(\boldsymbol{\ell})} = 0$, possess the properties

$$F_{0,i_2,0,j_2}^{(\boldsymbol{\ell}_1,\boldsymbol{\ell}_2)} = F_{i_1,0,j_1,0}^{(\boldsymbol{\ell}_1,\boldsymbol{\ell}_2)} = 0 \tag{7.71}$$

$$F_{i_2,i_1,j_2,j_1}^{(\boldsymbol{\ell}_2,\boldsymbol{\ell}_1)} = F_{j_1,j_2,i_1,i_2}^{(\boldsymbol{\ell}_1,\boldsymbol{\ell}_2)^*} = F_{i_1,i_2,j_1,j_2}^{(\boldsymbol{\ell}_1,\boldsymbol{\ell}_2)}. \tag{7.72}$$

[3]The phase space, including the momenta of all particles is of course $2\mathcal{D}$ dimensional.

In terms of these coefficients, the expectation value of H_δ can be expressed as

$$\langle \mathrm{GW}|H_\delta|\mathrm{GW}\rangle = -J \sum_{\langle \boldsymbol{\ell}_1,\boldsymbol{\ell}_2\rangle} \sum_{\substack{i_1,i_2\\ j_1,j_2}} F^{(\boldsymbol{\ell}_1,\boldsymbol{\ell}_2)}_{i_1,i_2,j_1,j_2} (\delta_{i_1,0}+\delta\lambda^{(\boldsymbol{\ell}_1)^*}_{i_1})(\delta_{i_2,0}+\delta\lambda^{(\boldsymbol{\ell}_2)^*}_{i_2})(\delta_{j_1,0}+\delta\lambda^{(\boldsymbol{\ell}_1)}_{j_1})(\delta_{j_2,0}+\delta\lambda^{(\boldsymbol{\ell}_2)}_{j_2}). \tag{7.73}$$

The total variational energy can now be written in various orders in the fluctuations

$$E_{\mathrm{tot}}(\boldsymbol{\delta\lambda},\boldsymbol{\delta\lambda}^*) = \langle \mathrm{GW}|H_{\mathrm{BH}}|\mathrm{GW}\rangle = \sum_{m=0}^{4} E^{(m)}. \tag{7.74}$$

Zeroth and first order terms do not arise from H_δ, since the F coefficients identically vanish if three or more lower indices are zero. Higher order terms do not exist, since the Hamiltonian only contains terms where at most two sites are coupled. The lowest order term $E^{(0)}$ is nothing but the Gutzwiller ground state energy. Analogous to the Bogoliubov fluctuation expansion, the first order term $E^{(1)}$ vanishes if the variational state is chosen to minimize $E^{(0)}$. The remaining higher order terms are given by

$$\begin{aligned} E^{(2)} = &\sum_{\boldsymbol{\ell}} \sum_{i>0}^{\infty} E^{(\boldsymbol{\ell})}_i |\delta\lambda^{(l)}_i|^2 - J \sum_{\langle \boldsymbol{\ell}_1,\boldsymbol{\ell}_2\rangle} \sum_{i,j>0} \Big[2F^{(\boldsymbol{\ell}_1,\boldsymbol{\ell}_2)}_{i,0,0,j} \delta\lambda^{(\boldsymbol{\ell}_1)^*}_i \delta\lambda^{(\boldsymbol{\ell}_2)}_j + F^{(\boldsymbol{\ell}_1,\boldsymbol{\ell}_2)}_{0,0,i,j} \delta\lambda^{(\boldsymbol{\ell}_1)}_i \delta\lambda^{(\boldsymbol{\ell}_2)}_j \\ &+ F^{(\boldsymbol{\ell}_1,\boldsymbol{\ell}_2)}_{i,j,0,0} \delta\lambda^{(\boldsymbol{\ell}_1)^*}_i \delta\lambda^{(\boldsymbol{\ell}_2)^*}_j \Big] \end{aligned} \tag{7.75}$$

$$\begin{aligned} E^{(3)} = -J &\sum_{\langle \boldsymbol{\ell}_1,\boldsymbol{\ell}_2\rangle} \sum_{i_1,i_2,i_3} \Big[F^{(\boldsymbol{\ell}_1,\boldsymbol{\ell}_2)}_{0,i_1,i_2,i_3} \delta\lambda^{(\boldsymbol{\ell}_2)^*}_{i_1} \delta\lambda^{(\boldsymbol{\ell}_1)}_{i_2} \delta\lambda^{(\boldsymbol{\ell}_2)}_{i_3} + F^{(\boldsymbol{\ell}_1,\boldsymbol{\ell}_2)}_{i_1,0,i_2,i_3} \delta\lambda^{(\boldsymbol{\ell}_1)^*}_{i_1} \delta\lambda^{(\boldsymbol{\ell}_1)}_{i_2} \delta\lambda^{(\boldsymbol{\ell}_2)}_{i_3} \\ &+ F^{(\boldsymbol{\ell}_1,\boldsymbol{\ell}_2)}_{i_1,i_2,0,i_3} \delta\lambda^{(\boldsymbol{\ell}_1)^*}_{i_1} \delta\lambda^{(\boldsymbol{\ell}_2)^*}_{i_2} \delta\lambda^{(\boldsymbol{\ell}_2)}_{i_3} + F^{(\boldsymbol{\ell}_1,\boldsymbol{\ell}_2)}_{i_1,i_2,i_3,0} \delta\lambda^{(\boldsymbol{\ell}_1)^*}_{i_1} \delta\lambda^{(\boldsymbol{\ell}_2)^*}_{i_2} \delta\lambda^{(\boldsymbol{\ell}_1)}_{i_3} \Big] \end{aligned} \tag{7.76}$$

$$E^{(4)} = -J \sum_{\langle \boldsymbol{\ell}_1,\boldsymbol{\ell}_2\rangle} \sum_{i_1,i_2,i_3,i_4} F^{(\boldsymbol{\ell}_1,\boldsymbol{\ell}_2)}_{i_1,i_2,i_3,i_4} \delta\lambda^{(\boldsymbol{\ell}_1)^*}_{i_1} \delta\lambda^{(\boldsymbol{\ell}_2)^*}_{i_2} \delta\lambda^{(\boldsymbol{\ell}_1)}_{i_3} \delta\lambda^{(\boldsymbol{\ell}_2)}_{i_4} \tag{7.77}$$

This explicitly shows that, in contrast to Bogoliubov theory where the non-linearity arises from the physical interaction term, the higher order terms here are purely proportional to the hopping J. In fact, any local operator in the Hamiltonian is taken into account exactly by construction of the Gutzwiller ansatz. In this sense, the quasi-particle theory here is not only a higher order extension of Bogoliubov theory, but constructed upon the strongly correlated, spatially localized limit. It is therefore a non-trivial, although appealing feature, that this extended quasi-particle theory furthermore correctly describes the opposite, non-interacting limit correctly. Here it systematically recovers Bogoliubov theory in second order in the fluctuations, as Gutzwiller theory recovers Gross-Pitaevskii theory in zeroth fluctuation order. At any finite interaction strength, it however contains quantitative corrections to Bogoliubov theory, as a finite depletion is accounted for.

7.3.1 Diagonalization of the Quasi-Particle Hamiltonian

Comparing the definitions of h and Δ in Eqns. (7.19, 7.18) with the second order energy (7.75), one notices that the second order energy can be written in matrix form as

$$E^{(2)}(\boldsymbol{\delta\lambda},\boldsymbol{\delta\lambda}^*) = \frac{1}{2} \begin{pmatrix} \boldsymbol{\delta\lambda} \\ \boldsymbol{\delta\lambda}^* \end{pmatrix}^\dagger H_{\mathrm{QP}} \begin{pmatrix} \boldsymbol{\delta\lambda} \\ \boldsymbol{\delta\lambda}^* \end{pmatrix}. \tag{7.78}$$

Care has to be taken with the factor of two: in the matrix notation the sum runs over all pairs of sites $\boldsymbol{\ell}$ and $\boldsymbol{\ell}'$ and each nearest neighbor bond is implicitly contained twice. The sum $\sum_{\langle \boldsymbol{\ell},\boldsymbol{\ell}'\rangle}$ in Eq. (7.75) only contains each nearest neighbor bond once.

We now use $H_{\mathrm{QP}} = \Sigma(\Sigma H_{\mathrm{QP}})\mathbb{1}_{2\mathcal{D}}$ in conjunction with the completeness relations (8.49) or (7.37) in the condensate or insulator case respectively, as well as the eigenvector properties to bring the second order energy into diagonal form.

Condensate

Here, the second order energy expressed as a function of the new variables ($\{\alpha_s\}$, ρ, χ) becomes

$$\begin{aligned} E^{(2)} &= \frac{1}{2}\begin{pmatrix}\boldsymbol{\delta\lambda}\\ \boldsymbol{\delta\lambda}^*\end{pmatrix}^\dagger \sum_s \left[\sum_s \omega_s \Sigma \mathbf{x}^{(s)}\mathbf{x}^{(s)\,\dagger} + \sum_s \omega_s \Sigma \mathbf{y}^{(s)}\mathbf{y}^{(s)\,\dagger} + \frac{1}{\tilde{m}}\Sigma \mathbf{p}\mathbf{p}^\dagger\right] \Sigma \begin{pmatrix}\boldsymbol{\delta\lambda}\\ \boldsymbol{\delta\lambda}^*\end{pmatrix} \\ &= \sum_s \omega_s |\alpha_s|^2 + \frac{\rho^2}{2\tilde{m}}. \end{aligned} \tag{7.79}$$

The sum $\sum_s$ runs over $\mathcal{D}-1$ collective modes and to obtain the last line, we used the definitions in Eqns. (7.39 - 7.42).

Insulator

In the insulator the last term, corresponding to a classical free particle, is absent and we have

$$E^{(2)} = \sum_s \omega_s |\alpha_s|^2, \tag{7.80}$$

where the sum extends over $\mathcal{D}$ different collective modes.

7.4 Quantization of the Theory

As expected, the classical energy when taking all second order terms along is the sum of uncoupled harmonic oscillators. In the condensate, an additional contribution $\frac{\rho^2}{2\tilde{m}}$, reminiscent of the kinetic energy of a free particle also contributes. The classical energy is thus analogous to the Gross-Pitaevskii energy in Eq. (6.132), with the important difference, that there are more independent collective modes in this theory. Within Bogoliubov theory, there are $L-1$ bosonic sound modes, which also exist within this extended quasi-particle theory and are renormalized at any finite interaction strength. In contrast, within this theory, there are $N_{\max}L-1$ and $\mathcal{D}=N_{\max}L$ independent collective modes in the limit of weak fluctuations for the superfluid and insulating case respectively.

The quantization procedure is completely analogous to the one given in the corresponding section (6.3) to Bogoliubov theory. We again discuss the condensate case including the effective free particle degree of freedom. Omitting the latter corresponds to the insulating case.

Again, we assign real position and momentum variables to each complex, classical coherent state parameter $\alpha_s(t)$. Translating the equations of motion for the $\alpha_s(t)$ into equations of motion for $x_s(t)$ and $p_s(t)$ shows that these are exactly the generalized coordinates and momenta for a particle of mass $\tilde{m}$ in a $\mathcal{D}$ dimensional space, confined with a harmonic trapping frequency ω_s along $\mathcal{D}-1$ dimensions and free along one. Along the free dimension, the canonical variables are $x_0(t)=\chi(t)$ and $p_0(t)=-\rho(t)$. Since the set $(\{x_s\},\{p_s\})$ with $0\leq s\leq\mathcal{D}$ are a complete set of canonically conjugate classical variables, they obey the Poisson bracket relations $\{x_r,p_s\}=\delta_{r,s}$. For the corresponding quantized version of the theory, these are promoted to operators $\hat{x}_s$ and $\hat{p}_s$, fulfilling the commutation relations $[\hat{x}_r,\hat{p}_s]=i\delta_{r,s}$. Only for the case $s>0$ can we define the ladder operators $\beta_s(t)=\frac{1}{2x_s^{(0)}}\hat{x}_s(t)+ix_s^{(0)}\hat{p}_s(t)$, where $x_s^{(0)}=(2\tilde{m}\omega_s)^{-1}$ is the quantum harmonic oscillator length scale along the corresponding dimension.

It is not possible to define ladder operators along the free dimension, since the harmonic oscillator length scale diverges here. Here, we simply work in terms of the associated position and momentum operators $\chi\mapsto\mathcal{Q}$ and $\rho\mapsto\mathscr{P}$. Note that within our notation, the operator $\mathscr{P}$ corresponds to the negative physical momentum $p_0(t)=-\rho(t)\mapsto-\mathscr{P}$ and an additional minus sign appears in the commutator

$$[\mathcal{Q},\mathscr{P}]=-i. \tag{7.81}$$

Additionally, we have the commutation relations

$$[\beta_r, \beta_s^\dagger] = \delta_{r,s} \tag{7.82}$$
$$[\beta_r, \mathscr{P}] = 0 \tag{7.83}$$
$$[\beta_r, \mathcal{Q}] = 0. \tag{7.84}$$

Note that the operators $\mathscr{P}$ and $\mathcal{Q}$ are Hermitian, since the directly correspond to physical coordinates and momenta. The latter two commutators vanish, since the associated Poisson brackets in the classical vanish

$$\{x_s(t), \chi(t)\} = 0 \tag{7.85}$$
$$\{x_s(t), \rho(t)\} = 0 \tag{7.86}$$
$$\{p_s(t), \chi(t)\} = 0 \tag{7.87}$$
$$\{p_s(t), \rho(t)\} = 0 \tag{7.88}$$

for all $s \geq 1$.

7.4.1 The Quasi-Particle Hamiltonian

To obtain the Hamiltonian in quantized form, we promote the classical fields in the Hamilton function to the newly defined operators. Since the classical scalar fields commute, but the corresponding operators do not, the ordering of the fields plays a role. When only considering the second order Hamiltonian, this ordering determines the energy shift of the quantum mechanical ground state in comparison to the classical energy minimum. This shift is however not physically measurable, its existence however clearly signals that the ground state of the new quantized Hamiltonian differs from the initial variational ansatz, i.e. the Gutzwiller state in our case.

As became clear in the comparison of the derivation of Bogoliubov theory on an operator level and from the classical, linearized Gross-Pitaevskii equations of motion, the correct energy shift is obtained if the Hamiltonian with the fields α_s and their conjugates are arranged into a symmetrized form before quantization. An additional energy shift, arising from the initial permutation of the bosonic operators into symmetric order and written as a bilinear form with the matrix H_{QP} also has to be considered. By analogy to the Bogoliubov case, it may be argued that the same energy shifts have to be taken into account in the quantization of this quasi-particle theory.

Condensate

In the condensate case, the Hamilton function of second order in the fluctuations (7.79) thus leads to the quasi-particle Hamiltonian of second order

$$\mathcal{H}^{(2)} = \sum_s \omega_s \beta_s^\dagger \beta_s + \frac{\mathscr{P}^2}{2\tilde{m}} + \frac{1}{2}\left[\sum_s \omega_s - \mathrm{Tr}\,(h)\right], \tag{7.89}$$

where h is the upper left submatrix of H_{QP}.

Insulator

In the insulator, the identical reasoning applies and the second order Hamiltonian becomes

$$\mathcal{H}^{(2)} = \sum_s \omega_s \beta_s^\dagger \beta_s + \frac{1}{2}\left[\sum_s \omega_s - \mathrm{Tr}\,(h)\right]. \tag{7.90}$$

Clearly, also the higher order terms (7.76) and (7.77) from the fluctuation expansion of the classical energy can be expressed as operator contributions to the Hamiltonian. Since there are more than two terms, the order in which the classical field amplitudes are arranged before quantization is not entirely clear. The analogous terms appearing in the two derivations of Bogoliubov theory may be

used for comparison, however a much clearer procedure is given in the next chapter (8), where the quantized theory is derived without going into the intermediate classical regime and the ordering of operators is fully taken into account throughout the entire derivation.

With each operator β_s fulfilling the commutation relation (7.82), it is an annihilation operator and the existence of a ground state, implicitly defined by $\beta_s|0\rangle = 0$ is guaranteed [53]. If the energy shift $\Delta E = [\sum_s \omega_s - \mathrm{Tr}\,(h)]/2$ relative to the classical Gutzwiller energy is non-zero, the ground state within this quasi-particle theory differs from the initial variational Gutzwiller state. With respect to the $\mathcal{Q}$ and $\mathscr{P}$ degrees of freedom, the ground state is defined as the zero momentum state $\mathscr{P}|0\rangle = 0$, which exactly corresponds to $\langle \mathscr{P}(t)\rangle = \rho(t) = 0$ in the classical system.

7.5 Quasi-Particles in the Translationally Invariant System

We now focus on the specific case of a translationally invariant system. Here the local on-site eigenenergies $E_i^{(l)}$, as well as the quantities $F^{(l_1,l_2)}_{i_1,i_2,j_1,j_2}$ become independent of the site indices l, l_1 and l_2, which we thus omit.

For the diagonalization of ΣH_{QP} in the case of a translationally invariant system, it is useful to perform an intermediate basis change into the quasi-momentum, mean-field eigenstate basis, in which the equations of motion largely decouple and the quasi-particle Hamiltonian becomes block diagonal. We denote the amplitudes in this new basis by $\nu_i^{(k)}$ and define the (unitary, discrete Fourier) transformation as

$$\delta\lambda_i^{(l)}(t) = \frac{1}{\sqrt{L}} \sum_{\mathbf{k}} e^{i\mathbf{k}\cdot\mathbf{r}_{\boldsymbol{\ell}}}\, \nu_i^{(\mathbf{k})}(t) \tag{7.91}$$

$$\nu_i^{(\mathbf{k})}(t) = \frac{1}{\sqrt{L}} \sum_{\mathbf{k}} e^{-i\mathbf{k}\cdot\mathbf{r}_{\boldsymbol{\ell}}}\, \delta\lambda_i^{(l)}(t). \tag{7.92}$$

This is nothing more but a generalized unitary transformation discussed in appendix (K), which defines a new set of canonical variables (or the bosonic character of the quasi-particles on an operator level). In matrix form, this can be expressed as

$$\begin{pmatrix} \boldsymbol{\delta\lambda}(t) \\ \boldsymbol{\delta\lambda}^*(t) \end{pmatrix} = \begin{pmatrix} K & 0 \\ 0 & K^* \end{pmatrix} \begin{pmatrix} \boldsymbol{\nu}(t) \\ \boldsymbol{\nu}^*(t) \end{pmatrix}, \tag{7.93}$$

where K is the $\mathcal{D}\times\mathcal{D}$-dimensional matrix with elements

$$K_{(i,l),(j,\mathbf{k})} = \frac{1}{\sqrt{L}} \delta_{i,j}\, e^{i\mathbf{k}\cdot\mathbf{r}_{\boldsymbol{\ell}}}. \tag{7.94}$$

Using the relation

$$\sum_{\boldsymbol{\ell}} \sum_{\boldsymbol{\ell}'\in \mathrm{n.n.}(\boldsymbol{\ell})} e^{-i\mathbf{k}\cdot\mathbf{r}_{\boldsymbol{\ell}}}\, e^{i\mathbf{k}'\cdot\mathbf{r}_{\boldsymbol{\ell}'}} = 2L\, \delta_{\mathbf{k},\mathbf{k}'} \sum_{d=1}^{Z/2} \cos(\mathbf{k}\cdot\mathbf{a}_d) \tag{7.95}$$

for a $Z/2$-dimensional hypercubic lattice, the linearized equations of motion in this basis become

$$\begin{aligned} i\frac{d}{dt}\nu_i^{(\mathbf{k})}(t) =& E_i\, \nu_i^{(\mathbf{k})}(t) + \sum_j F_{i,0,0,j} \left[-2J \sum_{d=1}^{Z/2} \cos(\mathbf{k}\cdot\mathbf{a}_d) \right] \nu_j^{(\mathbf{k})}(t) \\ &+ \sum_j F_{i,j,0,0} \left[-2J \sum_{d=1}^{Z/2} \cos(\mathbf{k}\cdot\mathbf{a}_d) \right] \nu_j^{(-\mathbf{k})^*}(t). \end{aligned} \tag{7.96}$$

With the definition of the free dispersion energy

$$\epsilon_{\mathbf{k}} = 2J \sum_{d=1}^{Z/2} \left[1 - \cos(\mathbf{k} \cdot \mathbf{a}_d)\right], \tag{7.97}$$

these equations of motion and their complex conjugates can also be written in matrix form

$$i \frac{d}{dt} \begin{pmatrix} \boldsymbol{\nu}(t) \\ \boldsymbol{\nu}^*(t) \end{pmatrix} = \Sigma \tilde{H}_{\mathrm{QP}} \begin{pmatrix} \boldsymbol{\nu}(t) \\ \boldsymbol{\nu}^*(t) \end{pmatrix} \tag{7.98}$$

where the matrices $\tilde{H}_{\mathrm{QP}}$, $\tilde{h}$ and $\tilde{\Delta}$ are defined as

$$\tilde{H}_{\mathrm{QP}} = \begin{pmatrix} \tilde{h} & \tilde{\Delta} \\ \tilde{\Delta}^* & \tilde{h}^* \end{pmatrix} \tag{7.99}$$

$$\tilde{h}_{(i,\mathbf{k}),(j,\mathbf{k}')} = \left[E_i \, \delta_{i,j} + (\epsilon_{\mathbf{k}} - JZ) \, F_{i,0,0,j}\right] \delta_{\mathbf{k},\mathbf{k}'} \tag{7.100}$$

$$\tilde{\Delta}_{(i,\mathbf{k}),(j,\mathbf{k}')} = (\epsilon_{\mathbf{k}} - JZ) \, F_{i,j,0,0} \, \delta_{\mathbf{k},-\mathbf{k}'}. \tag{7.101}$$

For a suitable choice of a collective indexing notation, the matrices $\tilde{h}$ and $\tilde{\Delta}$ are a sum of a diagonal matrix and a Kronecker product of matrices operating on the space of sites (or equivalently quasi-momentum) and the internal mean-field degrees of freedom. Consequently, the quasi-particle Hamiltonian $\tilde{H}_{\mathrm{QP}}$ is block diagonal, with blocks coupling states with opposite quasi-momenta $(\mathbf{k}, -\mathbf{k})$. The diagonalization of the complete quasi-particle Hamiltonian $\Sigma\tilde{H}_{\mathrm{QP}}$ can thus be reduced to the individual diagonalization of the subblocks. Each of these subblocks, labeled by a fixed $\mathbf{k}$, contains the coefficients of fluctuation coefficients $\nu_i^{(\mathbf{k})}$ and conjugate coefficients to $\nu_i^{(\mathbf{k})^*}$ to the opposite quasi-momentum $-\mathbf{k}$. In this sense particle-like fluctuations $\mathbf{k}$ are coupled to hole-like fluctuations $-\mathbf{k}$. If $\mathbf{k}$ and $-\mathbf{k}$ refer to different single-particle modes, there are two such distinct subblocks to $\mathbf{k}$ and $-\mathbf{k}$, which both (seen as a subblock only) have exactly the same subblocks, since $\epsilon(-\mathbf{k}) = \epsilon(\mathbf{k})$. For every collective mode in the $+\mathbf{k}$ sector, there is thus a related, although independent and orthogonal mode in the $-\mathbf{k}$ sector with the same energy. Note that for the high symmetry points in the Brillouin zone where $\mathbf{k}$ and $-\mathbf{k}$ refer to the identical mode (e.g. $\mathbf{k} = 0$ or certain points at the edge of the Brillouin zone), the corresponding non-diagonal subblocks are only half as large as in the other cases.

The set of all eigenvalues of $\Sigma\tilde{H}_{\mathrm{QP}}$ is the combined set of eigenvalues of all individual subblocks. The corresponding eigenvectors have non-zero elements only at positions in the respective subblocks. Hence, modes from different subblocks are mutually orthogonal, both with respect to the standard and Σ scalar product. For the translationally invariant case, the label of any collective mode s can be split into a label of the respective subblock $\mathbf{k}$ (referring to the particle-like fluctuation) and and an additional mode index γ, i.e. $s \to (\mathbf{k}, \gamma)$.

Dispersion Relations

One of the central quantities characterizing the collective excitation spectrum of a transversally invariant system is the dispersion relation. As a consequence of the overall discrete translational invariance (also in the interacting system), all (many-body) excitations can be chosen to have a well defined quasi-momentum. Within Bogoliubov theory, the quasi-momentum fully characterizes the excitation, since only the sound mode exists in this case. Generally, as is the case within this extended quasi-particle theory, there can be different excited states (i.e. in different modes) for a given quasi-momentum and we uniquely characterize the excited state by the pair of quantum numbers $(\mathbf{k}, \gamma)$, where γ is an additional mode label. We assign increasing integer values to γ in energetically increasing order, beginning with $\gamma = 1$ for the energetically lowest mode. The dispersion relation of the system is the set of mode eigenenergies shown in dependence of the quasi-momentum $\mathbf{k}$.

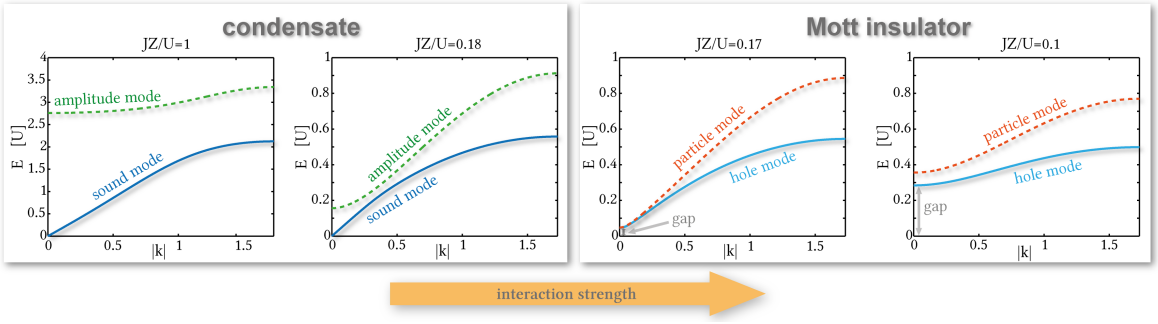

Figure 7.1: Dispersion relations in the single component homogeneous Bose-Hubbard model at constant integer filling $n = 1$ for different interaction strengths. The dispersion relations are shown within the first Brillouin zone along the diagonal line from $\mathbf{k} = (0, 0, 0)$ to $\mathbf{k} = (1, 1, 1)\pi/a$. In the condensate (left figures), the two lowest modes are the gapless sound mode and the massive amplitude mode. In the Mott insulator, the lowest two single particle excitations are the particle and hole modes.

The dispersion relation at integer filling $n = 1$ is shown along the diagonal of the first Brillouin zone for the Mott insulator, as well as the strongly and weakly interacting condensate in Fig. (7.1). For strong interactions in the Mott insulator, the system is gapped, i.e. there are no quasi-particle states at arbitrarily low energy. The two lowest modes are the particle and hole modes. Although the sum of particle and hole energy at any given $\mathbf{k}$ only depends on the (integer) density, their individual energy depends on the chemical potential μ, which is not uniquely determined by the density in the Mott insulator. Approaching the transition to the condensate from the Mott insulator side, the particle and hole modes lower their energy at small $\mathbf{k}$. Which of these two modes in the Mott insulator closes the energy gap first depends on the chemical potential and whether the transition takes place through the upper (above the tip) or lower part of the Mott lobe in the JZ/U-μ/U Bose-Hubbard phase diagram. If it occurs above (below) the tip, the particle (hole) branch has a lower energy. In the vicinity of the phase boundary, but remaining on the Mott insulator side, it becomes energetically favorable for the system to populate these quasi-particle modes[4], as their energy becomes arbitrarily low. The transition is determined by the point, where the quasi-particle energy vanishes and can be understood as a condensation of particle (hole) quasi-particles on the upper (lower) side of the Mott lobe [115]. If the transitions takes place at a chemical potential running through the tip of the lobe, both particle and hole modes close their gaps simultaneously and the transition corresponds to a condensation of particles and holes. This scenario corresponds to the one shown in Fig. (7.1), where the transition at integer filling occurs between the $JZ/U = 0.17$ and $JZ/U = 0.18$.

One of the major differences between this extended quasi-particle theory and Bogoliubov theory is its ability to describe more than a single collective mode at a given quasi-momentum $\mathbf{k}$, which becomes relevant at strong interactions. In the Mott insulator, we have discussed the two lowest modes, but there are more, energetically higher modes, corresponding to two-particle excitations (and holes, depending on the density) etc. These are dispersionless (i.e. the mode energies are independent of the quasi-momentum) within this quasi-particle theory, sice they are not coupled to the mean-field ground state within first order in the fluctuation Hamiltonian. On a structural level, these modes are contained since this quasi-particle theory is built on an action containing more degrees of freedom (i.e. all the local mean-field eigenstate coefficients) than simply the order parameter field (as is the case for Gross-Pitaevskii and the resulting Bogoliubov theory). As a result, a much larger number of collective modes, which are the eigenstates of such a theory under

[4]The mechanism through which the system can lower its energy by the population of these modes is derived and shown in chapter 8. Within perturbation theory, it can easily be seen that the coupling term originating from the difference of the full Bose-Hubbard and the mean-field Hamiltonian lowers the energy. As the energetic difference between the original many-particle Gutzwiller eigenstates is reduced, the admixture of the higher energy eigenstates increases,reducing the energy. Commonly, this admixture of other eigenstates in the original basis is referred to as quantum fluctuations.

an effective time evolution of these degrees of freedom in the vicinity of an energy minimum, can appear.

In the condensate there are indeed also a number of higher modes at each $\mathbf{k}$. The most important is the amplitude mode, which energetically lies above the sound mode. It name originates from the response of the order parameter when a single collective mode is excited as a coherent state: whereas in the limit of low $\mathbf{k}$ the fluctuation of the order parameter is purely in the phase (i.e. imaginary if the ground state order parameters are chosen to be real), the response for an analogous amplitude mode excitation also contains a large amplitude component. It is important to note that within this quasi-particle theory, the various quasi-particle modes are mutually orthogonal, i.e. it is impossible to express amplitude mode excitations terms of sound mode excitations. At higher energies, many other collective modes exist, which have not been blessed with a name thus far. These become ever less important in the sense that their weight in the spectral functions vanishes with increasing mode index. In this thesis, the focus will be cast on the sound and amplitude modes.

Although the **energies** of the particle and hole modes in the insulator continuously cross over into the energies of the collective sound and amplitude modes when crossing the transition to the condensate side, the internal structure of the modes (determined by the eigenstates, not the energy eigenvalues) changes abruptly at the transition. This will be elucidated later. In the condensate, the lowest collective mode $\gamma = 1$ is the gapless sound mode, which features a linear dependence of the energy on $|\mathbf{k}|$ for any finite interaction strength. The momentum up to which the dispersion of the sound mode is linear is set by the inverse healing length, which depends on the interaction strength. As will be shown, density fluctuations in the condensate correspond mainly to quasi-particle excitations of the sound mode. If a wave packet is constructed from a superposition of such sound quasi-particles from the linear regime of the dispersion relation, this wave packet will propagate with the speed of sound set by the slope of the sound mode $c = \frac{\partial \omega_{\mathbf{k},\gamma=1}}{\partial k_i}$ without dispersing, i.e. keeping its shape during the propagation. If, however, higher frequency components from the quasi-momentum regime beyond the linear region are contained (which is necessarily the case once the wave packet becomes strongly localized in space), it will disperse and change its shape during propagation. The propagation in time and the dispersion is explicitly shown for a wave packet much larger than the lattice spacing (i.e. the continuum limit) in appendix (N) for different interaction strengths in the Bogoliubov limit. In the weakly interacting Bogoliubov limit, the Bogoliubov sound excitations can be understood as coherent superposition of particle hole excitations $\beta^\dagger_{\mathbf{k}} = u_{\mathbf{k}} a^\dagger_{\mathbf{k}} + v_{\mathbf{k}} a_{-\mathbf{k}}$. In the linear dispersion regime both $u_{\mathbf{k}}$ and v_bk are large and a single quasi-particle excitation can be understood as strong coherent particle-hole excitation, involving many particles collectively. In the limit of large $\mathbf{k}$ (which is limited by the edge of the Brillouin zone in the lattice case) on the other hand, $v_{\mathbf{k}}$ weakens and $u_{\mathbf{k}}$ approaches unit. Such a quasi-particle excitation can be understood to be particle-like in the sense of it corresponding to an additional *free* particle propagating on top of the condensate, with its energy being shifted by a mean-field proportional to the interactions strength and the background density.

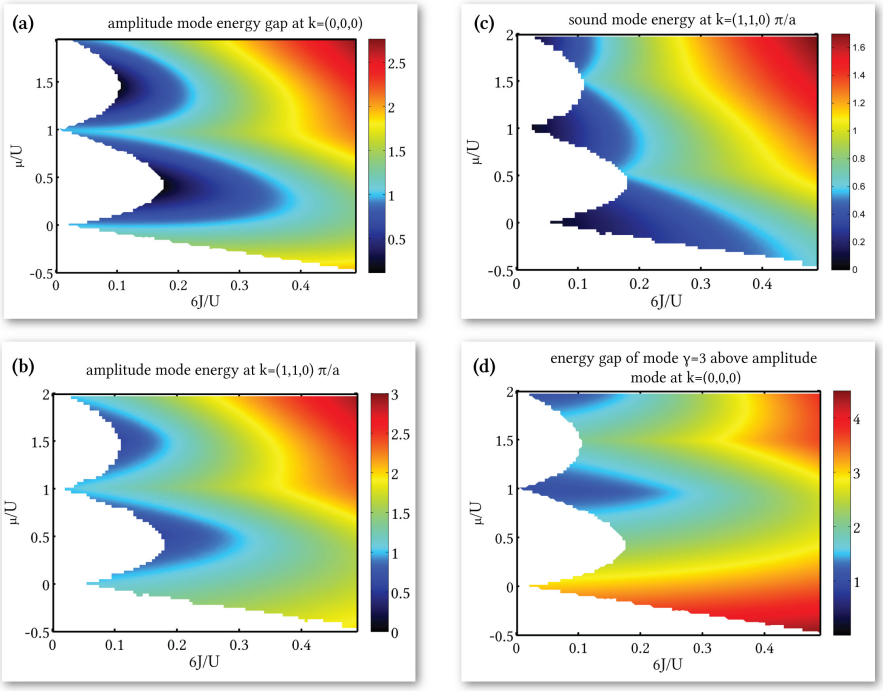

Figure 7.2: Various energies of different modes in the condensate shown in units of the interaction energy U. Subfigures (a) and (d) show the energy gap of the amplitude mode and the next highest mode $\gamma = 2$ in the condensate at $\mathbf{k} = 0$. The latter features qualitatively similar behavior as the amplitude mode energy gap for weak interactions. For strong interactions however, its energy gap never closes at the transition and, in contrast to the amplitude mode energy gap, takes on its minimum in the vicinity of integer values of μ/U, between the various Mott lobes. It can be seen that the amplitude mode energy gap is not simply the interaction energy U, but depends on the parameter regime. It vanishes only when crossing the transition to the Mott insulator at the tip of the lobes at integer filling. The energy gap for the sound mode would vanish everywhere in the condensate. For comparison, the energy at a finite quasi-momentum $\mathbf{k} = (1, 1, 0)\pi/a$ is shown for both the amplitude and the sound mode in subfigures (b) and (c) respectively.

We now turn to the behavior of the amplitude mode's energy gap in the phase diagram, which is shown in units of U in Fig. (7.2 a). No typical order of magnitude can be assigned to it over the global parameter range. The minimum energy over all momenta is always the energy at $\mathbf{k} = 0$, which thus determines the gap. This gap closes at transition to the Mott insulator, but only at integer values of the density. This is in accordance with the particle and hole mode approaching zero energy on the Mott insulator side of the transition, if the energy eigenvalues cross over continuously into the energy eigenvalues of the sound and amplitude modes. With increasing tunneling energy J, as well as with increasing density in the weakly interacting regime, the energy gap (scaled in units of U) increases.

Interaction-Dependent Energy Range of the Modes

Up to now we have considered the energies of the various modes at a specific quasi-momentum. To better understand the range of energies over which a given mode extends, i.e. the set of energy values at which single-particle excitations lie (at some $\mathbf{k}$), we plot this range as a function of the inverse interaction strength J/U at constant filling $n = 1$ in Fig. (7.3). The lowest mode energy is generally at $\mathbf{k} = 0$, whereas the highest mode energy is always at the outer corner $\mathbf{k} = [1, 1, 1]\pi/a$ of the first Brillouin zone.

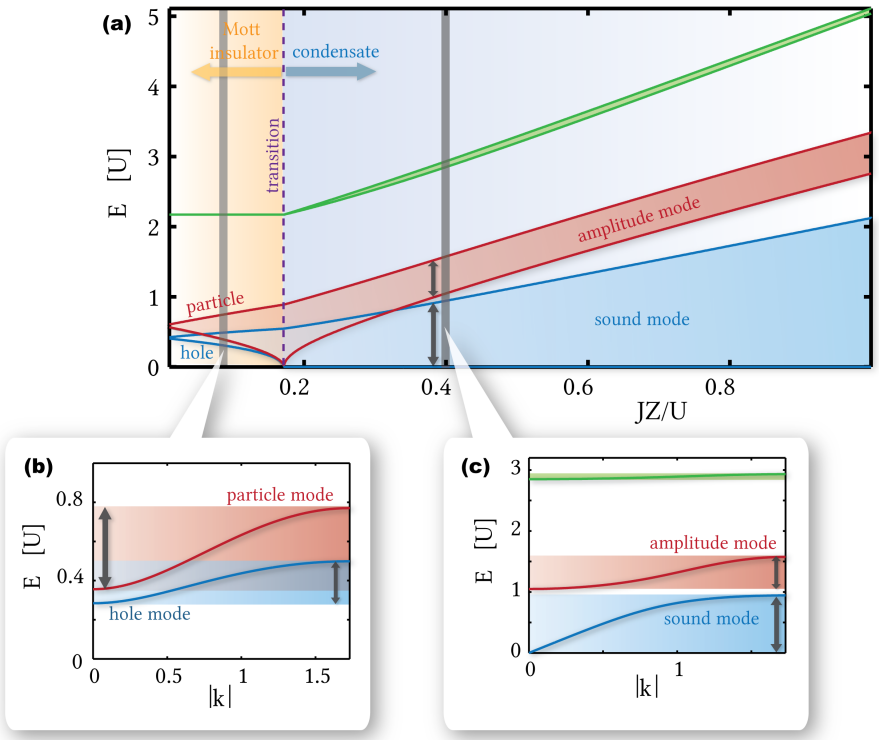

Figure 7.3: Width of the modes in units of U as a function of JZ/U for fixed density $n = 1$. In the Mott insulator, the density does not uniquely define the dispersion relation and the chemical potential is set to the value at the tip of the Mott lobe. In subfigures (b) and (c) the dispersion relations along the diagonal $(1, 1, 1)$ direction are shown for a point in the Mott insulator and the condensate respectively. The energy range of the modes (marked in blue and red for the hole and particle, or sound and amplitude modes respectively in all subfigure) depicted in (a) corresponds to the energy range of the dispersion relations at every given (U, J, n) and may generally overlap for different modes.

Due to the fluctuation operator and coupling structure in the Mott insulator, all collective modes other than the particle and hole modes are dispersionless in this regime. The behavior of the amplitude mode in the non-interacting limit $U/J \to \infty$ at constant filling can be seen in Fig. (7.3a): both the upper and lower energy boundaries grow linearly with U/J and remain above and energetically separated from the sound mode. In the appropriate energy units of J in this limit, the amplitude mode energy approaches a constant (density-dependent) value above the sound mode's maximum energy and its energetic range decreases. Furthermore, its single particle spectral weight, which cannot be seen from Fig. (7.3) , vanishes in the non-interacting limit.

Speed of Sound

Sound is characterized by a collective mode with a linear dispersion relation in the large wavelength limit. If a wave packet is only composed of frequencies within a range where the dispersion relation is exactly linear, it travels through the system at a constant speed and does not disperse. The speed of sound c is given by the slope of the sound mode (with respect to $\mathbf{k}$ in the dispersion relation) and is shown in Fig. (7.4) as a function of the interaction strength.

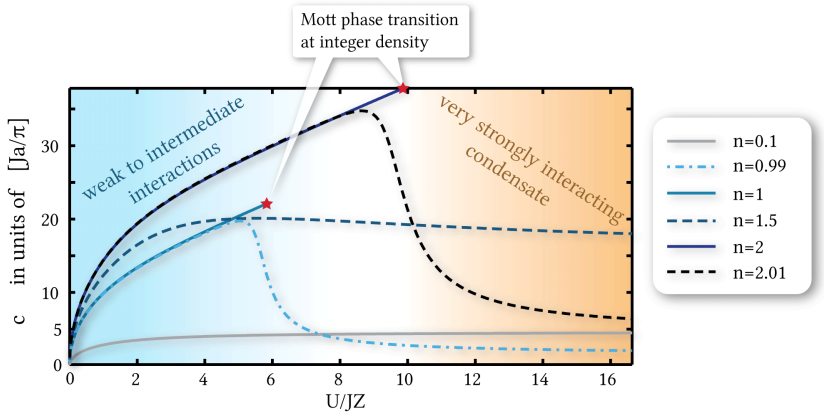

Figure 7.4: The speed of sound as a function of the interaction strength U/J at various densities. Expressed in units of the tunneling energy J, the speed of sound vanishes in the non-interacting limit. For non-integer density the system is condensed at any interaction strength and the sound mode exists. The speed of sound is however strongly reduced in this very strongly interacting regime. At integer values of the density, the system undergoes a transition into the Mott phase at sufficiently large U/J, beyond which the sound mode ceases to exist.

For weak interactions, the Bogoliubov result is recovered: the speed of sound grows with the interaction strength and vanishes in the non-interacting limit. For strong interactions at integer values, the system undergoes a phase transition into the Mott insulating state and a sound mode no longer exists. At non-integer filling, where the system remains condensed at even stronger interactions, the speed of sound is significantly reduced, as the energy cost for multiple occupancy becomes very large.

Effective Mass

A further quantity, which characterizes the dynamical behavior of quasi-particles, is the effective mass. For a given quasi-particle mode, this is defined as $m_{\text{eff}} = \left(\frac{\partial^2 \epsilon(\mathbf{k})}{\partial k_i^2}\right)^{-1}$. When composing a spatially localized wave packet of excited states by a superposition of quasi-particle states with a quasi-momentum lying within a small range around $\mathbf{k}$, this wave packet may behave similar to a free particle in its propagation in the continuum limit of the lattice theory to some approximation, while dispersing. The effective mass is the associated mass of this effective free particle description, which may in general depend on the quasi-momentum $\mathbf{k}$. For the sound mode in the condensate, the effective mass is not defined in the $\mathbf{k} \to 0$ limit, as the dispersion relation becomes linear at small $\mathbf{k}$ for any finite interaction strength. Note, that although phonons are often referred to as *massless*, the effective mass at $\mathbf{k} = 0$ actually diverges when coming from finite $\mathbf{k}$. The amplitude mode, on the other hand, have a well defined effective mass at $\mathbf{k} = 0$, as do the higher modes in the condensate and the particle and hole mode in the Mott insulator. We plot the effective mass of these modes as a function of the interaction strength U/JZ at constant filling in Fig. (7.5) for various values of the filling.

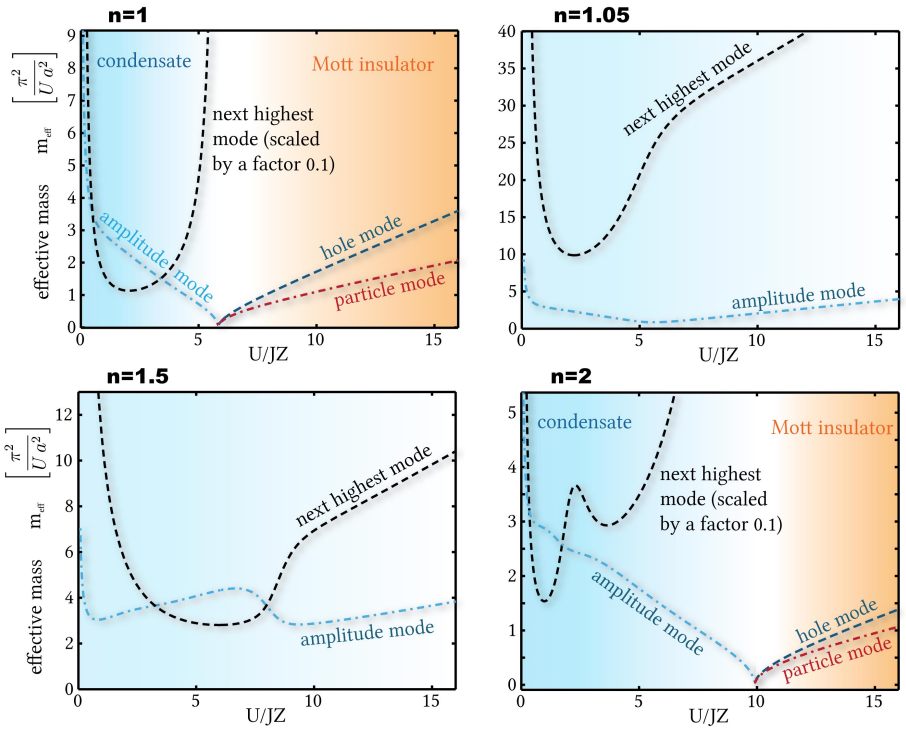

Figure 7.5: Effective masses of the various modes at $\mathbf{k} = 0$ in units of $\pi^2(Ua^2)^{-1}$ as a function of the interaction strength at different densities. At integer values of the filling, where the system undergoes a Mott transition, the effective masses of the amplitude, particle and hole modes approach zero and vanish at the transition. In contrast, the effective masses of the higher modes above the amplitude mode in the condensate diverge when approaching the transition. At non-integer filling, the system is always in a condensed state and the effective masses of the amplitude and higher modes in the condensate have a non-monotonic behavior in U/JZ, taking on a minimum value in the vicinity of the regime where the transition would occur at the closest related integer filling value. In both the non-interacting and strongly interacting limits, the effective mass of these modes diverges.

8. Diagonalization of the Fluctuation Hamiltonian above the Gutzwiller Ground State

In this section we will derive the quasi-particle theory for strongly interacting lattice bosons without leaving the full quantum operator domain, i.e. not by a quantization of the classical eigenmodes from the time-dependent Gutzwiller equations of motion. The strategy consists of the following steps:

1. We define fluctuation operators via the static mean-field eigenstates.
2. These operators are shown to obey bosonic commutation relations in the limit weak excitations, i.e. when the state at hand is close to the static Gutzwiller ground state.
3. It is shown that for the Gutzwiller ground state, none of these fluctuations are excited. The mean-field Hamiltonian is diagonal in terms of these operators. This justifies the identification of these operators with fluctuation operators.
4. The entire Bose-Hubbard Hamiltonian is expressed in terms of these fluctuation operators. First order terms do not appear. The quasi-particle Hamiltonian corresponds to all terms of second order in the fluctuation operators and is expressed in diagonal form in newly defined quasi-particle operators via a generalized unitary transformation.
5. Higher order terms associated with quasi-particle decay, creation and interactions are taken along exactly on an operator level and can subsequently be expressed in terms of quasi-particle operators. In contrast to the previous approach of quantizing the classical eigenmodes, no ambiguity concerning the ordering of operators arises here.
6. The new quasi-particle vacuum is related to the Gutzwiller ground state by the same unitary transformation, which transforms the quasi-particle operators into the fluctuation operators.

After diagonalizing the static mean-field Hamiltonian, the exact Bose-Hubbard Hamiltonian can be expressed in terms of these mean-field eigenstates, which are all combinations of direct product states of the local eigenstate $|i\rangle$. To draw the connection to the derivation of Bogoliubov theory by diagonalizing the GP fluctuation operators up to quadratic order, we define fluctuation operators, which will be shown to be bosonic for low quasi-particle occupation numbers. The full Bose-Hubbard Hamiltonian will then be expressed in terms of these operators. The quasi-particle Hamiltonian contains all terms up to second order in these fluctuations and can be diagonalized

by a generalized unitary transformation, which retains the approximate bosonic character of the original fluctuation operators.

We start with Bose-Hubbard Hamiltonian

$$H_{\text{BH}} = -J \sum_{\langle \boldsymbol{\ell}, \boldsymbol{\ell}' \rangle} (b^\dagger_{\boldsymbol{\ell}} b_{\boldsymbol{\ell}'} + b^\dagger_{\boldsymbol{\ell}'} b_{\boldsymbol{\ell}}) - \mu \sum_{\boldsymbol{\ell}} b^\dagger_{\boldsymbol{\ell}} b_{\boldsymbol{\ell}} + \frac{U}{2} \sum_{\boldsymbol{\ell}} b^\dagger_{\boldsymbol{\ell}} b^\dagger_{\boldsymbol{\ell}} b_{\boldsymbol{\ell}} b_{\boldsymbol{\ell}} \tag{8.1}$$

and determine the Gutzwiller ground state with self-consistent ground state order parameters $\phi_{\boldsymbol{\ell}} = \langle b_{\boldsymbol{\ell}} \rangle$. This is equivalent to minimizing the variational energy $\langle \psi_{GW} | H_{\text{BH}} | \psi_{GW} \rangle \to \min$ within the variational Gutzwiller product state $|\psi_{GW}\rangle = \prod_{\boldsymbol{\ell}} |\psi_{\boldsymbol{\ell}}\rangle_{\boldsymbol{\ell}}$ with an arbitrary local state $|\psi_l\rangle_{\boldsymbol{\ell}} = \sum_{n=0}^{\infty} c_n^{(\boldsymbol{\ell})} |n\rangle_{\boldsymbol{\ell}}$. The state minimizing the energy $|i=0\rangle_{\boldsymbol{\ell}}$ is the local ground state of the mean-field Hamiltonian $H^{(\boldsymbol{\ell})}_{\text{mf}}(\eta_{\boldsymbol{\ell}}) |i=0\rangle_{\boldsymbol{\ell}} = E_0^{(\boldsymbol{\ell})} |i=0\rangle_{\boldsymbol{\ell}}$, where the MF Hamiltonian depends on the neighboring sites $\eta_{\boldsymbol{\ell}} = J \sum_{\boldsymbol{\ell}' \in nn(\boldsymbol{\ell})} \phi_{\boldsymbol{\ell}}$.

This mean-field state acts as the background state upon which the extended, quasi-particle ground state is constructed. In this sense it is analogous to the GP state, upon which the Bogoliubov state is constructed.

As in the classical case, we decompose the full Hamiltonian

$$H_{\text{BH}} = H_{\text{mf}} + H_\delta \tag{8.2}$$

into a mean-field Hamiltonian, which is exactly diagonal in the mean-field basis and depends on the ground state order parameters $\phi_{\boldsymbol{\ell}}$ (which after being determined self-consistently, are kept constant throughout the entire further procedure)

$$H_{\text{mf}} = \sum_{\boldsymbol{\ell}} H^{(\boldsymbol{\ell})}_{\text{mf}} = \sum_{\boldsymbol{\ell}} \sum_{i=0}^{\infty} E_i^{(\boldsymbol{\ell})} |i\rangle_{\boldsymbol{\ell}\boldsymbol{\ell}} \langle i|, \tag{8.3}$$

as well as a fluctuating part

$$H_\delta = -J \sum_{\langle \boldsymbol{\ell}, \boldsymbol{\ell}' \rangle} (\delta b^\dagger_{\boldsymbol{\ell}} \delta b_{\boldsymbol{\ell}'} + \delta b^\dagger_{\boldsymbol{\ell}'} \delta b_{\boldsymbol{\ell}}). \tag{8.4}$$

Note that the mean-field eigenenergies $E_i^{(\boldsymbol{\ell})}$ also contain the shift proportional to $\phi^*_{\boldsymbol{\ell}} \phi_{\boldsymbol{\ell}'}$. The energy gauge is chosen such that total ground state mean-field energy vanishes and for each site $E_i^{(\boldsymbol{\ell})} = 0$. One might be tempted to directly apply a single-particle basis or Bogoliubov transformation to the operators $\delta b_{\boldsymbol{\ell}}$, to bring H_δ into diagonal form. This is possible, but is not the desired result corresponding to the collective eigenmodes in the Gutzwiller time evolution, simply yielding the term $-2J \sum_{\mathbf{k}} \sum_d \cos(\mathbf{k} \cdot \mathbf{a}_d) \delta b^\dagger_{\mathbf{k}} \delta b_{\mathbf{k}}$.

8.1 Fluctuation Operators in the Gutzwiller Approach

We now define the fluctuation *annihilation* operators

$$\sigma^{(i)}_{\boldsymbol{\ell}} = |0\rangle_{\boldsymbol{\ell}\boldsymbol{\ell}} \langle i| \otimes \prod_{\otimes \boldsymbol{\ell}' \neq \boldsymbol{\ell}} \mathbb{1}_{\boldsymbol{\ell}'}, \tag{8.5}$$

which only acts at site $\boldsymbol{\ell}$, transferring an excited mean-field state $|i\rangle_{\boldsymbol{\ell}}$ to the local mean-field ground state $|0\rangle_{\boldsymbol{\ell}}$. Henceforth we will not explicate the unit operators on other sites and any operator defined on a subset of sites will be implicitly understood to be of this form on other sites. Furthermore defining the operator

$$s^{(i)}_{\boldsymbol{\ell}} = |0\rangle_{\boldsymbol{\ell}\boldsymbol{\ell}} \langle 0| - |i\rangle_{\boldsymbol{\ell}\boldsymbol{\ell}} \langle i|, \tag{8.6}$$

which is analogous to the s_z operator in two-level spin systems and measures the population imbalance between the mean-field ground state and the i^{th} mean-field state, it is easy to show that the fluctuation operators satisfy the commutation relations

$$[\sigma_{\boldsymbol{\ell}}^{(i)},\, {\sigma_{\boldsymbol{\ell}'}^{(j)}}^{\dagger}] = \delta_{\boldsymbol{\ell},\boldsymbol{\ell}'}\,(\delta_{i,j}\, s_{\boldsymbol{\ell}}^{(i)} - (1-\delta_{i,j}){\sigma_{\boldsymbol{\ell}}^{(j)}}^{\dagger}\sigma_{\boldsymbol{\ell}}^{(i)}) \tag{8.7}$$

$$[{\sigma_{\boldsymbol{\ell}}^{(i)}}^{\dagger}, {\sigma_{\boldsymbol{\ell}'}^{(j)}}^{\dagger}] = [\sigma_{\boldsymbol{\ell}}^{(i)}, \sigma_{\boldsymbol{\ell}'}^{(j)}] = 0 \tag{8.8}$$

Note that the fluctuation operators are defined only for the excited states $i > 0$. It is useful to transform the fluctuation operators from Wannier into quasi-momentum space, where their approximate bosonic nature becomes more apparent.

$$\tilde{\sigma}_{\mathbf{k}}^{(i)} = \frac{1}{\sqrt{L}} \sum_{\boldsymbol{\ell}} e^{-i\mathbf{k}\cdot\mathbf{R}_{\boldsymbol{\ell}}}\, \sigma_{\boldsymbol{\ell}}^{(i)} \tag{8.9}$$

Within the Gutzwiller approach, the occupation of quasi-particle modes is reflected by a non-vanishing amplitude of excited mean-field states. Considering a single site, the modulus of an excited state amplitude can take on a maximum value of 1, which is fundamentally incompatible with a true bosonic nature of the quasi-particles. In other words: the maximum number of quasi-particles is restricted by the structure of the original state. At a first glance, this may seem to be an unfortunate artifact and shortcoming of this approach. However, an analysis of the degrees of freedom reveals that any theory capable of describing more than a single mode, can never have truly bosonic quasi-particles. Starting with a lattice with L sites in the single-band approximation, one has L bosonic creation operators in any single particle basis. Successively applying these to the vacuum state, a complete basis of Fock states can be generated. An arbitrary generalized unitary transformation of these creation operators cannot change the number of resulting bosonic operators, from which an equivalent basis, spanning the identical Hilbert space, can be constructed. If more than L resulting bosonic operators would exist, a larger and thus different Hilbert space would be spanned. Hence, in any theory describing the amplitude mode in addition to the sound mode, the quasi-particles are at best approximately bosonic.

The fluctuation operators in quasi-momentum space fulfill the commutation relations

$$[\tilde{\sigma}_{\mathbf{k}'}^{(j)}, {\tilde{\sigma}_{\mathbf{k}}^{(i)}}^{\dagger}] = \delta_{\mathbf{k},\mathbf{k}'}\,\delta_{i,j} - \frac{1}{L} R_{\mathbf{k},\mathbf{k}'}^{(i,j)} \tag{8.10}$$

with

$$\begin{aligned} R_{\mathbf{k},\mathbf{k}'}^{(i,j)} &= \sum_{\boldsymbol{\ell}} e^{i(\mathbf{k}-\mathbf{k}')\cdot\mathbf{R}_{\boldsymbol{\ell}}} \left({\sigma_{\boldsymbol{\ell}}^{(i)}}^{\dagger}\, \sigma_{\boldsymbol{\ell}}^{(j)} + \delta_{i,j} \sum_{j'>0} {\sigma_{\boldsymbol{\ell}}^{(j')}}^{\dagger}\, \sigma_{\boldsymbol{\ell}}^{(j')} \right) \\ &= \sum_{\mathbf{k}_1} \left({\tilde{\sigma}_{\mathbf{k}_1+\mathbf{k}-\mathbf{k}'+\mathbf{G}}^{(i)}}^{\dagger}\, \tilde{\sigma}_{\mathbf{k}_1}^{(j)} + \delta_{i,j} \sum_{j'>0} {\tilde{\sigma}_{\mathbf{k}_1+\mathbf{k}-\mathbf{k}'+\mathbf{G}}^{(j')}}^{\dagger}\, \tilde{\sigma}_{\mathbf{k}_1}^{(j')} \right). \end{aligned} \tag{8.11}$$

The first term in the commutation relation (8.10) is the usual bosonic part and of order one. The additional term $R_{\mathbf{k},\mathbf{k}'}^{(i,j)}$ is proportional to and of the order of the number of quasi-particles in the system, but scales with L^{-1} in the commutator. It is in this sense that in the limit of weak quasi-particle occupation, the fluctuation operators $\tilde{\sigma}_{\mathbf{k}}^{(i)}$ are bosonic. In Eq. (8.11), the lattice vector $\mathbf{G}$ is chosen for given $\mathbf{k}_1$, such that $\mathbf{k}_1 + \mathbf{k} - \mathbf{k}' + \mathbf{G}$ lies within the first Brillouin zone.

Completeness of the Fluctuations Operators

The set of all fluctuation operators $\sigma_{\boldsymbol{\ell}}^{(i)}$ and their conjugates is complete in the sense that an arbitrary many-body operator can be expressed in terms of them. It suffices to show that an arbitrary on-site operator can be expressed in terms of fluctuation operators, since any operator can be written as a superposition of products of on-site operators. The local mean-field eigenstates constitute a local basis and thus any local operator can be expanded in terms of these

$$\mathcal{A}^{(l)} = \sum_{i,j\geq 0} A_{i,j}^{(l)} |i\rangle_{\boldsymbol{\ell}\boldsymbol{\ell}}\langle j|. \tag{8.12}$$

Now we consider the four qualitatively different cases of the operator $|i\rangle_{\boldsymbol{\ell}\boldsymbol{\ell}}\langle j|$ and write these in terms of fluctuation operators

$$|j\rangle_{\boldsymbol{\ell}\boldsymbol{\ell}}\langle i| = {\sigma_{\boldsymbol{\ell}}^{(j)}}^{\dagger}\sigma_{\boldsymbol{\ell}}^{(i)} \qquad \text{if } i,j>0 \tag{8.13}$$

$$|0\rangle_{\boldsymbol{\ell}\boldsymbol{\ell}}\langle i| = \sigma_{\boldsymbol{\ell}}^{(i)} \qquad \text{if } \quad i>0 \tag{8.14}$$

$$|i\rangle_{\boldsymbol{\ell}\boldsymbol{\ell}}\langle 0| = {\sigma_{\boldsymbol{\ell}}^{(i)}}^{\dagger} \qquad \text{if } \quad i>0 \tag{8.15}$$

$$|0\rangle_{\boldsymbol{\ell}\boldsymbol{\ell}}\langle 0| = \mathbb{1} - \sum_{i>0} {\sigma_{\boldsymbol{\ell}}^{(i)}}^{\dagger}\sigma_{\boldsymbol{\ell}}^{(i)}. \tag{8.16}$$

The operator $|0\rangle_{\boldsymbol{\ell}\boldsymbol{\ell}}\langle 0|$ in the last relation (8.16) can, in principle, be expressed as $\sigma_{\boldsymbol{\ell}}^{(i)}{\sigma_{\boldsymbol{\ell}}^{(i)}}^{\dagger}$ for any i. However, if we require all fluctuation operators to appear in normal order, the representation (8.16) is unique. We furthermore note, that this form is closely related to the conservation of the local norm of a Gutzwiller state (7.7) in the classical case.

8.2 Expressing the Full Bose-Hubbard Hamiltonian in Terms of Fluctuation Operators σ

We now consider a homogeneous system, where the on-site energies $E_i^{(\boldsymbol{\ell})}$ become site independent and choosing $E_{i=0}=0$, the mean-field Hamiltonian (8.3) can be written as

$$\begin{aligned} H_{\mathrm{mf}} &= \sum_{i>0}\sum_{\boldsymbol{\ell}} E_i\, {\sigma_{\boldsymbol{\ell}}^{(i)}}^{\dagger}\,\sigma_{\boldsymbol{\ell}}^{(i)} \\ &= \sum_{i>0}\sum_{\mathbf{k}} E_i\, {\tilde{\sigma}_{\mathbf{k}}^{(i)}}^{\dagger}\,\tilde{\sigma}_{\mathbf{k}}^{(i)} \end{aligned} \tag{8.17}$$

and is diagonal in both the Wannier and quasi-momentum space representation. To express H_δ in terms of σ, it is useful to define the annihilation operator matrix elements and shifted counterparts as

$$B_{i,j}^{(\boldsymbol{\ell})} = {}_{\boldsymbol{\ell}}\langle i|b_{\boldsymbol{\ell}}|j\rangle_{\boldsymbol{\ell}} \tag{8.18}$$

$$\tilde{B}_{i,j}^{(\boldsymbol{\ell})} = B_{i,j}^{(\boldsymbol{\ell})} - \phi_{\boldsymbol{\ell}}\,\delta_{i,j}. \tag{8.19}$$

The mean-field shifted bosonic annihilation operator can then be written terms of local mean-field eigenstates as

$$\delta b_{\boldsymbol{\ell}} = \sum_{i,j=0}^{\infty} \tilde{B}_{i,j}^{(\boldsymbol{\ell})}\; |i\rangle_{\boldsymbol{\ell}}\,{}_{\boldsymbol{\ell}}\langle j|. \tag{8.20}$$

Note that the element $B_{0,0}^{(\boldsymbol{\ell})} = \phi_{\boldsymbol{\ell}}$ is the local order parameter for the mean-field ground state and $\tilde{B}_{0,0}^{(\boldsymbol{\ell})} = 0$. The non-diagonal part H_δ can now be written as

$$\begin{aligned} H_\delta &= -J \sum_{\langle \boldsymbol{\ell}_1,\boldsymbol{\ell}_2\rangle} \sum_{\substack{i_1,i_2\\ j_1,j_2}} \tilde{B}_{j_1,i_1}^{(\boldsymbol{\ell}_1)^*}\tilde{B}_{i_2,j_2}^{(\boldsymbol{\ell}_2)} |i_1\rangle_{\boldsymbol{\ell}_1\boldsymbol{\ell}_1}\langle j_1| \otimes |i_2\rangle_{\boldsymbol{\ell}_2\boldsymbol{\ell}_2}\langle j_2| \;+\text{h.c.} \\ &= -J \sum_{\langle \boldsymbol{\ell}_1,\boldsymbol{\ell}_2\rangle} \sum_{\substack{i_1,i_2\\ j_1,j_2}} F_{i_1,i_2,j_1,j_2}^{(\boldsymbol{\ell}_1,\boldsymbol{\ell}_2)} |i_1\rangle_{\boldsymbol{\ell}_1\boldsymbol{\ell}_1}\langle j_1| \otimes |i_2\rangle_{\boldsymbol{\ell}_2\boldsymbol{\ell}_2}\langle j_2| \end{aligned} \tag{8.21}$$

We again use the complex coefficients

$$F_{i_1,i_2,j_1,j_2}^{(\boldsymbol{\ell}_1,\boldsymbol{\ell}_2)} = \tilde{B}_{j_1,i_1}^{(\boldsymbol{\ell}_1)^*}\tilde{B}_{i_2,j_2}^{(\boldsymbol{\ell}_2)} + \tilde{B}_{i_1,j_1}^{(\boldsymbol{\ell}_1)}\tilde{B}_{j_2,i_2}^{(\boldsymbol{\ell}_2)^*}. \tag{8.22}$$

Due to the property (7.71), no terms of zeroth or first order in σ appear in H_δ. The lowest order terms contain fluctuation operators on nearest neighboring sites in the Wannier representation. At most, four fluctuation operators appear in any terms of H_δ. We therefore group the full Bose-Hubbard Hamiltonian into terms of different orders in σ

$$H_{\mathrm{BH}} = E^{(0)} + \mathcal{H}^{(2)} + \mathcal{H}^{(3)} + \mathcal{H}^{(4)}. \tag{8.23}$$

We emphasize that no approximation is made and this is an exact rewriting of H_{BH} in terms of σ. The second order Hamiltonian $\mathcal{H}^{(2)}$ determines the quasi-particle structure and gives rise to quasi-particles with an infinite lifetime. The two higher order terms $\mathcal{H}^{(3)}$ and $\mathcal{H}^{(4)}$ couple quasi-particles in different modes and lead to decay and interaction processes of these, resulting in a finite lifetime.

To explicitly obtain the contributions of $\mathcal{H}_\delta$ to $\mathcal{H}_2$, $\mathcal{H}_3$ and $\mathcal{H}_4$, one has to consider all combinations of terms in Eq. (8.21) where 2, 1 or 0 indices are zero respectively and all others are non-zero. The third order term thus becomes

$$\begin{aligned}\mathcal{H}^{(3)} = -J \sum_{\langle \boldsymbol{\ell}_1,\boldsymbol{\ell}_2\rangle} \sum_{i_1,i_2,i_3>0} \Big[& F^{(\boldsymbol{\ell}_1,\boldsymbol{\ell}_2)}_{0,i_1,i_2,i_3} |0\rangle_{\boldsymbol{\ell}_1\boldsymbol{\ell}_1}\langle i_2| \otimes |i_1\rangle_{\boldsymbol{\ell}_2\boldsymbol{\ell}_2}\langle i_3| + F^{(\boldsymbol{\ell}_1,\boldsymbol{\ell}_2)}_{i_1,0,i_2,i_3} |i_1\rangle_{\boldsymbol{\ell}_1\boldsymbol{\ell}_1}\langle i_2| \otimes |0\rangle_{\boldsymbol{\ell}_2\boldsymbol{\ell}_2}\langle i_3| \\ & + F^{(\boldsymbol{\ell}_1,\boldsymbol{\ell}_2)}_{i_1,i_2,0,i_3} |i_1\rangle_{\boldsymbol{\ell}_1\boldsymbol{\ell}_1}\langle 0| \otimes |i_2\rangle_{\boldsymbol{\ell}_2\boldsymbol{\ell}_2}\langle i_3| + F^{(\boldsymbol{\ell}_1,\boldsymbol{\ell}_2)}_{i_1,i_2,i_3,0} |i_1\rangle_{\boldsymbol{\ell}_1\boldsymbol{\ell}_1}\langle i_3| \otimes |i_2\rangle_{\boldsymbol{\ell}_2\boldsymbol{\ell}_2}\langle 0| \Big].\end{aligned} \tag{8.24}$$

For the fourth order term, no index is zero and there is only one combination

$$\mathcal{H}^{(4)} = -J \sum_{\langle \boldsymbol{\ell}_1,\boldsymbol{\ell}_2\rangle} \sum_{i_1,i_2,j_1,j_2>0} F^{(\boldsymbol{\ell}_1,\boldsymbol{\ell}_2)}_{i_1,i_2,j_1,j_2} |i_1\rangle_{\boldsymbol{\ell}_1\boldsymbol{\ell}_1}\langle j_1| \otimes |i_2\rangle_{\boldsymbol{\ell}_2\boldsymbol{\ell}_2}\langle j_2|. \tag{8.25}$$

Second order quasi-particle Hamiltonian

All terms from H_{mf}, as well as four different types of terms from H_δ (the four different combinations of creation and annihilation operators on two neighboring sites) contribute to the second order Hamiltonian $\mathcal{H}^{(2)}$. The latter terms make it off-diagonal unless $J = 0$. Using the property that one can rewrite $|i\rangle_{\boldsymbol{\ell}_1\boldsymbol{\ell}_1}\langle 0| \otimes |0\rangle_{\boldsymbol{\ell}_2\boldsymbol{\ell}_2}\langle j| = \sigma^{(i)^\dagger}_{\boldsymbol{\ell}_1}\sigma^{(j)}_{\boldsymbol{\ell}_2}$ and analogues thereof, we find

$$\mathcal{H}^{(2)} = \sum_{i>0}\sum_{\boldsymbol{\ell}} E^{(\boldsymbol{\ell})}_i \, \sigma^{(i)^\dagger}_{\boldsymbol{\ell}} \, \sigma^{(i)}_{\boldsymbol{\ell}} - J \sum_{i,j>0} \sum_{\langle \boldsymbol{\ell}_1,\boldsymbol{\ell}_2\rangle} \left[2F^{(\boldsymbol{\ell}_1,\boldsymbol{\ell}_2)}_{i,0,0,j} \, \sigma^{(i)^\dagger}_{\boldsymbol{\ell}_1}\sigma^{(j)}_{\boldsymbol{\ell}_2} + F^{(\boldsymbol{\ell}_1,\boldsymbol{\ell}_2)}_{0,0,i,j} \, \sigma^{(i)}_{\boldsymbol{\ell}_1}\sigma^{(j)}_{\boldsymbol{\ell}_2} + F^{(\boldsymbol{\ell}_1,\boldsymbol{\ell}_2)}_{i,j,0,0} \, \sigma^{(i)^\dagger}_{\boldsymbol{\ell}_1}\sigma^{(j)^\dagger}_{\boldsymbol{\ell}_2} \right] \tag{8.26}$$

In grouping the terms we used $F^{(\boldsymbol{\ell}_1,\boldsymbol{\ell}_2)}_{i,0,0,j} = F^{(\boldsymbol{\ell}_2,\boldsymbol{\ell}_1)}_{0,i,j,0}$ from Eq. (7.72). We define $J_{\boldsymbol{\ell},\boldsymbol{\ell}'}$ to be J if sites $\boldsymbol{\ell}$ and $\boldsymbol{\ell}'$ are nearest neighbors and zero otherwise. Thus for the same site, $J_{\boldsymbol{\ell},\boldsymbol{\ell}}$ always vanishes and using the property that $\sigma^{(i)^\dagger}_{\boldsymbol{\ell}_1}$ and $\sigma^{(j)}_{\boldsymbol{\ell}_2}$ always commute for neighboring lattice sites, we rewrite Eq. (8.26) as

$$\begin{aligned}\mathcal{H}^{(2)} = & \sum_{i>0}\sum_{\boldsymbol{\ell}} E^{(\boldsymbol{\ell})}_i \, \sigma^{(i)^\dagger}_{\boldsymbol{\ell}} \, \sigma^{(i)}_{\boldsymbol{\ell}} - \frac{1}{2} \sum_{i,j>0} \sum_{\boldsymbol{\ell}_1,\boldsymbol{\ell}_2} J_{\boldsymbol{\ell}_1,\boldsymbol{\ell}_2} \Big[F^{(\boldsymbol{\ell}_1,\boldsymbol{\ell}_2)}_{i,0,0,j} \, \sigma^{(i)^\dagger}_{\boldsymbol{\ell}_1}\sigma^{(j)}_{\boldsymbol{\ell}_2} + F^{(\boldsymbol{\ell}_1,\boldsymbol{\ell}_2)}_{i,0,0,j} \, \sigma^{(j)}_{\boldsymbol{\ell}_2}\sigma^{(i)^\dagger}_{\boldsymbol{\ell}_1} \\ & + F^{(\boldsymbol{\ell}_1,\boldsymbol{\ell}_2)}_{0,0,i,j} \, \sigma^{(i)}_{\boldsymbol{\ell}_1}\sigma^{(j)}_{\boldsymbol{\ell}_2} + F^{(\boldsymbol{\ell}_1,\boldsymbol{\ell}_2)}_{i,j,0,0} \, \sigma^{(i)^\dagger}_{\boldsymbol{\ell}_1}\sigma^{(j)^\dagger}_{\boldsymbol{\ell}_2} \Big],\end{aligned} \tag{8.27}$$

which is a more suitable to express $\mathcal{H}^{(2)}$ in matrix form. Note that a factor $\frac{1}{2}$ enters in the second term, since the sum $\sum_{\boldsymbol{\ell}_1,\boldsymbol{\ell}_2}$ contains twice as many non-vanishing terms as before.

It is now possible to express the second order Hamiltonian in matrix form, using the same coefficient matrices h and Δ as in the classical case in Eqn. (7.18) and Eqn. (7.19)

$$\mathcal{H}^{(2)} = \frac{1}{2} \begin{pmatrix} \tilde{\boldsymbol{\sigma}} \\ \tilde{\boldsymbol{\sigma}}^\dagger \end{pmatrix}^\dagger H_{\mathrm{QP}} \begin{pmatrix} \tilde{\boldsymbol{\sigma}} \\ \tilde{\boldsymbol{\sigma}}^\dagger \end{pmatrix} \tag{8.28}$$

8.3 Homogeneous Case

We now restrict ourselves to homogeneous systems, where the coefficients $F_{i_1,i_2,j_1,j_2} = F^{(\boldsymbol{\ell}_1,\boldsymbol{\ell}_2)}_{i_1,i_2,j_1,j_2}$ and the local mean-field energies $E_i = E_i^{(\boldsymbol{\ell})}$ become site independent and express $\mathcal{H}^{(2)}$ in terms of quasi-momentum fluctuation operators $\sigma^{(i)}_{\mathbf{k}}$, which transforms the quasi-particle matrix H_{QP} into block-diagonal form. Using the relation

$$\begin{aligned} -2J \sum_{\langle \boldsymbol{\ell}_1,\boldsymbol{\ell}_2\rangle} e^{-i(\mathbf{k}_1\cdot\mathbf{R}_{\boldsymbol{\ell}_1}-\mathbf{k}_2\cdot\mathbf{R}_{\boldsymbol{\ell}_2})} &= -2JL\,\delta_{\mathbf{k}_1,\mathbf{k}_2}\sum_d \cos(\mathbf{k}_1\cdot\mathbf{a}_d) \\ &= L\,\delta_{\mathbf{k}_1,\mathbf{k}_2}(\epsilon(\mathbf{k}_1)-JZ), \end{aligned} \tag{8.29}$$

where

$$\epsilon(\mathbf{k}) \equiv 2J\big[Z/2 - \sum_{d=1}^{Z/2}\cos(\mathbf{a}_d\cdot\mathbf{k})\big]. \tag{8.30}$$

is the non-interacting dispersion relation, we express the second order Hamiltonian (8.26) as

$$\begin{aligned} \mathcal{H}^{(2)} &= \sum_{i>0}\sum_{\mathbf{k}} E_i\,\tilde{\sigma}^{(i)^\dagger}_{\mathbf{k}}\,\tilde{\sigma}^{(i)}_{\mathbf{k}} \\ &\quad + \sum_{i,j>0}\sum_{\mathbf{k}}\frac{1}{2}[\epsilon(\mathbf{k})-JZ]\left[F_{i,0,0,j}\,(\tilde{\sigma}^{(i)^\dagger}_{\mathbf{k}}\tilde{\sigma}^{(j)}_{\mathbf{k}} + \tilde{\sigma}^{(j)}_{\mathbf{k}}\tilde{\sigma}^{(i)^\dagger}_{\mathbf{k}}) + F_{0,0,i,j}\,\tilde{\sigma}^{(i)}_{-\mathbf{k}}\tilde{\sigma}^{(j)}_{\mathbf{k}} + F_{i,j,0,0}\,\tilde{\sigma}^{(i)^\dagger}_{-\mathbf{k}}\tilde{\sigma}^{(j)^\dagger}_{\mathbf{k}}\right]. \end{aligned} \tag{8.31}$$

Using the commutation relation (8.10), the first line in (8.31) can be rewritten as

$$\begin{aligned} \sum_{i>0}\sum_{\mathbf{k}} E_i\,\tilde{\sigma}^{(i)^\dagger}_{\mathbf{k}}\,\tilde{\sigma}^{(i)}_{\mathbf{k}} &= \frac{1}{2}\sum_{i>0}\sum_{\mathbf{k}} E_i\,(\tilde{\sigma}^{(i)^\dagger}_{\mathbf{k}}\,\tilde{\sigma}^{(i)}_{\mathbf{k}} + \tilde{\sigma}^{(i)}_{\mathbf{k}}\,\tilde{\sigma}^{(i)^\dagger}_{\mathbf{k}}) \\ &\quad - \frac{1}{2}\sum_{i>0}\sum_{\mathbf{k}} E_i + \frac{1}{2L}\sum_{i>0}\sum_{\mathbf{k}_1} E_i\left(\tilde{\sigma}^{(i)^\dagger}_{\mathbf{k}_1}\,\tilde{\sigma}^{(i)}_{\mathbf{k}_1} + \sum_{j'>0}\tilde{\sigma}^{(j')^\dagger}_{\mathbf{k}_1}\,\tilde{\sigma}^{(j')}_{\mathbf{k}_1}\right) \end{aligned} \tag{8.32}$$

and the second order quasi-particle Hamiltonian can finally be expressed in matrix form in the quasi-momentum representation as

$$\mathcal{H}^{(2)} = \frac{1}{2}\begin{pmatrix}\tilde{\boldsymbol{\sigma}}\\ \tilde{\boldsymbol{\sigma}}^\dagger\end{pmatrix}^\dagger \tilde{H}_{\mathrm{QP}}\begin{pmatrix}\tilde{\boldsymbol{\sigma}}\\ \tilde{\boldsymbol{\sigma}}^\dagger\end{pmatrix} - \frac{1}{2}\mathrm{Tr}\,(h) + \frac{D}{L} \tag{8.33}$$

with

$$\tilde{H}_{\mathrm{QP}} = \begin{pmatrix}\tilde{h} & \tilde{\Delta}\\ \tilde{\Delta}^* & \tilde{h}^*\end{pmatrix}, \tag{8.34}$$

and the $n\times n$ matrices h and Δ have the matrix elements

$$\tilde{h}_{(i,\mathbf{k}),(j,\mathbf{k}')} = \delta_{\mathbf{k},\mathbf{k}'}\,[\delta_{i,j}\,E_i + (\epsilon(\mathbf{k})-JZ)F_{i,0,0,j}] \tag{8.35}$$

$$\tilde{\Delta}_{(i,\mathbf{k}),(j,\mathbf{k}')} = \delta_{-\mathbf{k},\mathbf{k}'}\,(\epsilon(\mathbf{k})-JZ)\,F_{i,j,0,0} \tag{8.36}$$

and

$$D = \frac{1}{2}\sum_{i>0}\sum_{\mathbf{k}_1} E_i\left(\tilde{\sigma}^{(i)^\dagger}_{\mathbf{k}_1}\,\tilde{\sigma}^{(i)}_{\mathbf{k}_1} + \sum_{j'>0}\tilde{\sigma}^{(j')^\dagger}_{\mathbf{k}_1}\,\tilde{\sigma}^{(j')}_{\mathbf{k}_1}\right). \tag{8.37}$$

Note that the pair of an internal mean-field eigenstate index and a site index $(i,\mathbf{k})$ are to be understood as a single collective index for the matrix. The vectors $\tilde{\boldsymbol{\sigma}}$ and $\tilde{\boldsymbol{\sigma}}^\dagger$ are defined as the column vectors of all fluctuation operators $\tilde{\sigma}^{(i)}_{\mathbf{k}}$ and $\tilde{\sigma}^{(i)^\dagger}_{\mathbf{k}}$ respectively, with some given ordering structure for the modes $(i,\mathbf{k})$. The fluctuation operators are only defined for positive internal

state indices $i > 0$. If the index $i = 0$ were taken along (as can be done in the classical Gutzwiller equations of motion for the scalar fluctuations), for each $\mathbf{k}$ particle[1] and $-\mathbf{k}$ hole mode, the subspace corresponding to $i = 0$ would totally decouple from all other modes. With the convention $E_i = 0$, this would lead to two additional eigenvalues of zero in every $\mathbf{k}$ particle and $-\mathbf{k}$ hole subspace, which would not correspond to physical collective modes of freedom. It is therefore also justified in the classical case to neglect these decoupled subspaces from the beginning. This does however not imply, that no additional eigenvalue of zero, corresponding to a physical zero-energy collective mode, may appear in $\tilde{H}_{\mathrm{QP}}$ (which is the case for the homogeneous system in the $\mathbf{k} = 0$ subspace).

Note that in this expansion in fluctuation operators, there is a fundamental difference to Bogoliubov theory: whereas the off-diagonal terms and non-linearities in Bogoliubov theory are proportional to U and the higher order terms are at first diagonal in the Wannier representation, the off-diagonal fluctuations and higher order terms in this quasi-particle theory are proportional to the hopping J and are at first diagonal in the quasi-momentum representation.

Symmetry of the Matrices

Using the symmetry property $F_{j,0,0,i} = F^*_{i,0,0,j}$ from Eq. (7.72) and the property that all energies E_i are always real (since the self-consistent on-site mean-field Hamiltonian is always Hermitian), it directly follows from the definition (8.35) that the matrix $\tilde{h}$ is Hermitian $\tilde{h}_{(i,\mathbf{k}),(j,\mathbf{k}')} = \tilde{h}^*_{(j,\mathbf{k}'),(i,\mathbf{k})}$.

Similarly, using $F_{j,i,0,0} = F^*_{i,j,0,0}$ from Eq. (7.72) implies that the matrix $\tilde{\Delta}$ is symmetric $\tilde{\Delta}_{(i,\mathbf{k}),(j,\mathbf{k}')} = \tilde{\Delta}_{(j,\mathbf{k}'),(i,\mathbf{k})}$. Hence the quasi-particle Hamiltonian (8.34) is Hermitian $\tilde{H}_{\mathrm{QP}} = \tilde{H}^\dagger_{\mathrm{QP}}$.

8.3.1 Determining the Quasi-Particle Mode Structure

Concerning its mathematical structure, the matrix $\tilde{H}_{\mathrm{QP}}$ is of the same form as the Bogoliubov quasi-particle matrix (6.13) and we can use all of the previously derived properties. As before, directly diagonalizing the Hermitian matrix $\tilde{H}_{\mathrm{QP}}$ does not lead to the correct collective mode spectrum and structure, since the bosonic structure of the operators (and the Poisson bracket relations for the classical degrees of freedom) are not preserved under the transformation defined by the eigenvectors.

Rather, the diagonalization has to be performed on the symplectic space, leading to transformation of the generalized unitary type, preserving the commutation relations. This amounts to determining the eigenvectors of the matrix $\Sigma\tilde{H}_{\mathrm{QP}}$, which is however again not necessarily fully diagonalizable. In the quasi-momentum representation, $\Sigma\tilde{H}_{\mathrm{QP}}$ is not block diagonal as shown in Fig. (8.1 a), but consists of non-diagonal subblocks of fixed $\mathbf{k}$ on the diagonal. The $+\mathbf{k}$ particle modes are however also coupled to the $-\mathbf{k}$ hole modes by $\tilde{\Delta}$. A permutation P_σ can directly bring $\Sigma\tilde{H}_{\mathrm{QP}}$ into block diagonal form $P^\dagger_\sigma \Sigma\tilde{H}_{\mathrm{QP}} P_\sigma$ as shown in Fig. (8.1 b), where the non-diagonal subblocks $\Sigma\mathcal{H}^{(\mathbf{k})}$ can then be diagonalized individually.

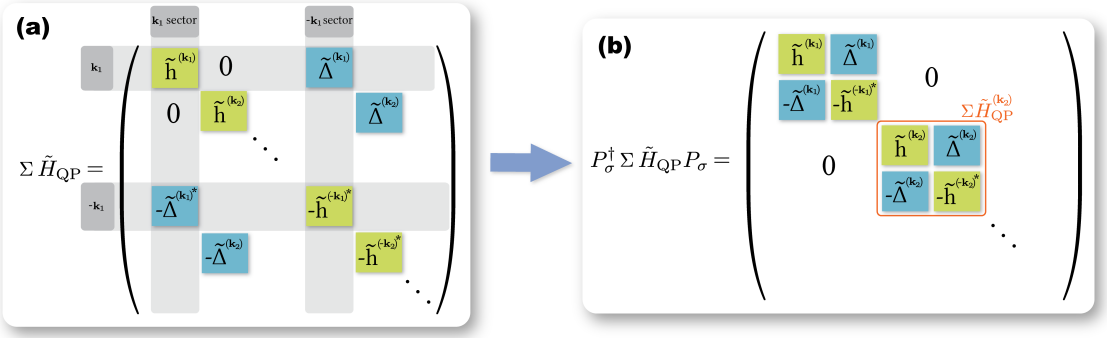

[1] Note that "particle" does and "hole" do not necessarily refer to an addition or removal of a physical particle or atom, but rather to the addition of removal of a fluctuation through the operator $\tilde{\sigma}^{(i)\dagger}_{\mathbf{k}}$ or $\tilde{\sigma}^{(i)}_{\mathbf{k}}$ respectively. It is therefore the addition or removal of a quantum in the Gutzwiller eigenbasis fields, which possess a particle-like structure close to equilibrium.

Figure 8.1: Structure of the quasi-particle Hamiltonian: if the collective index corresponding to $(i, \mathbf{k})$ is grouped such that for fixed $\mathbf{k}$ the elements for different i follow successively, the matrix initially consists of non-zero subblocks in these subspaces of fixed $\mathbf{k}$. The $|\mathbf{k}\rangle$ particle modes are coupled to the $|-\mathbf{k}\rangle$ hole modes by the anomalous terms Δ. A simple permutation can bring this matrix into block diagonal form.

Symmetries

We shortly discuss the multiplicity of eigenvalues and the interrelation of corresponding eigenvectors of $\Sigma\tilde{H}_{\mathrm{QP}}$. For homogeneous systems, one has to distinguish two different classes of single particle states:

1. High symmetry points in the Brillouin zone where $|\mathbf{k}\rangle$ is physically the same state as $|-\mathbf{k}\rangle$. This applies to the $|\mathbf{k}=0\rangle$ state and certain states on the edge of the Brillouin zone.

2. All other states $|\mathbf{k}\rangle$ in the Brillouin zone, which do not fulfill the criterion above.

For both of these classes of points, the structure of the individual non-diagonal sub-block $\Sigma\tilde{H}^{(\mathbf{k})}_{\mathrm{QP}}$ is identical. For each such block eigenvalues, if they are non-zero, always appear in pairs $(\omega_{\mathbf{k},\gamma}, -\omega_{\mathbf{k},\gamma})$ and the related eigenvectors respectively correspond to a particle-like addition and a hole-like removal of a quasi-particle into the physically same mode.

This is not to be confused with the implications of the reflective symmetry in a homogeneous system. For all points $\mathbf{k}$ not belonging to the high symmetry class, a totally independent sub-block corresponding to $-\mathbf{k}$ exists. This is fully decoupled from the $+\mathbf{k}$ subspace and the eigenmodes in the $-\mathbf{k}$ will thus be physically different and orthogonal to all eigenmodes in the $\mathbf{k}$ subspace. However, since the single particle energy is symmetric under reflection $\epsilon(\mathbf{k}) = \epsilon(-\mathbf{k})$, the two subblocks will have the identical matrix elements and thus also same eigenvector and eigenvalue structure. Hence, for each quasi-particle $\beta^{\dagger}_{\mathbf{k},\gamma}$ with energy $\omega_{\mathbf{k},\gamma}$ where $\mathbf{k}$ is not a high symmetry point in the Brillouin zone, there will exist a physically distinct time reversed quasi-particle state $\beta^{\dagger}_{-\mathbf{k},\gamma}$ with the same energy $\omega_{-\mathbf{k},\gamma} = \omega_{\mathbf{k},\gamma}$ with a very similar structure (i.e. the entries of the eigenvectors are identical, but located in different subspaces).

For a system without reflectional symmetry, there is in general no analogue of the $|-\mathbf{k}\rangle$ single particle state related to any given $|\mathbf{k}\rangle$ state [50] and the simple Block structure of $\Sigma\tilde{H}_{\mathrm{QP}}$ breaks down. For a given $|\mathbf{k}\rangle$ quasi-particle orbital, a physically distinct quasiparticle orbital $|-\mathbf{k}\rangle$ does not necessarily exist. However, the corresponding quasi-particle hole mode for the quasi-particle orbital $|\mathbf{k}\rangle$ with an eigenvalue $\omega_{\mathbf{k}}$ will always appear as an eigenvector of $\Sigma\tilde{H}_{\mathrm{QP}}$ with an associated eigenvalue $-\omega_{\mathbf{k}}$.

Eigenvalue and Eigenvector Structure of $\Sigma\tilde{H}_{\mathbf{QP}}$

The goal is to bring $\Sigma\tilde{H}_{\mathrm{QP}}$ into its Jordan normal form. For each $\mathbf{k} \neq 0$ with a positive single-particle energy $\epsilon(\mathbf{k}) > 0$, the corresponding sub-block $\Sigma\tilde{H}^{(\mathbf{k})}_{\mathrm{QP}}$ is diagonalizable in the sense that a basis of eigenvectors exists. This is however no longer true for the $\mathbf{k} = 0$ sub-block in the condensate phase: here one eigenvalue is zero[2] with only one eigenvector, i.e. a second linearly independent eigenvector does not exist here. Hence, the eigenvectors do not constitute a complete basis here, rendering the matrix $\Sigma\tilde{H}_{\mathrm{QP}}$ non-diagonalizable.

[2]Here we restrict ourselves to points in the phase diagram, which are not at the tip of the Mott lobe. In this case the eigenvalues of two physically distinct modes approach zero simultaneously and this case has to be considered separately.

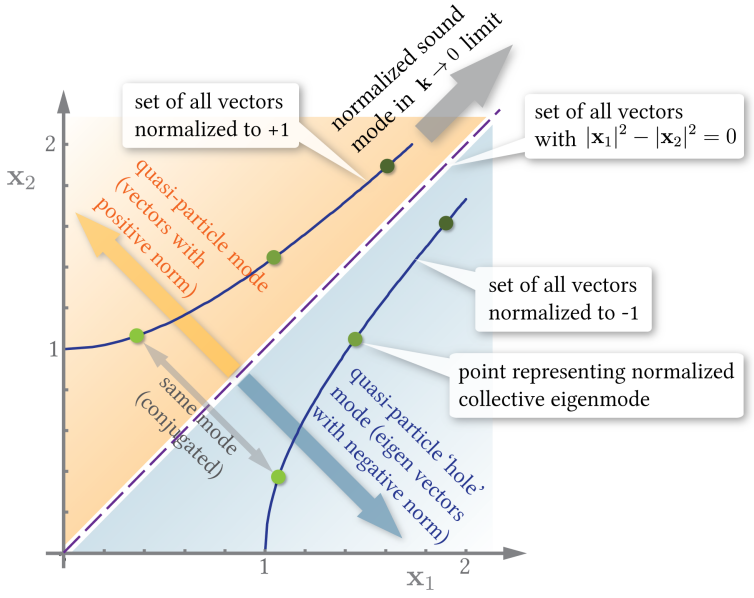

Figure 8.2: Structure of the symplectic quasi-particle space: every eigenvector $\mathbf{x}^{(\mathbf{k},\gamma)} = \begin{pmatrix} \mathbf{u}^{(\mathbf{k},\gamma)} \\ -\mathbf{v}^{(\mathbf{k},\gamma)} \end{pmatrix}$ can be mapped onto a two-dimensional real vector $\mathbf{x} = \begin{pmatrix} x_1 \\ x_2 \end{pmatrix}$ with the components being defined as the euclidean norms of the fluctuation particle $x_1 = |\mathbf{u}^{(\mathbf{k},\gamma)}|$ and hole $x_2 = |\mathbf{v}^{(\mathbf{k},\gamma)}|$ parts. Thus the norm of $\mathbf{x}$ with respect to the 2D Σ is exactly the norm of the original vector $\mathbf{x}^{(\mathbf{k},\gamma)}$. A general vector can either have a positive (upper left region in the figure), negative (lower right region in the figure) or zero norm (dashed diagonal line), which is invariant under rescaling. The set of all vectors normalized to -1, 0 and 1 are indicated by the lower blue, dashed purple and upper blue line respectively. For each given vector, an orthogonal counterpart can be obtained by reflection on the diagonal. Hence, any vector with a non-zero norm is linearly independent of its orthogonal counterpart. Physically, a positive normalized vector (on the upper blue line) and its normalized orthogonal counterpart correspond to particle and hole excitations of the same fluctuation mode. Note that within the extended quasi-particle theory, the dimension of the irreducible subspaces is of higher dimension than two and this structure applies to each set of conjugated eigenstates with different mode indices separately.

To understand how the one basis vector disappears, we look at the eigenvalues and eigenvectors of the sub-block $\Sigma\tilde{H}_{\mathrm{QP}}^{(\mathbf{k})}$ as a function of the parameter $\mathbf{k}$, as it approaches zero. For any non-zero $\mathbf{k}$, all eigenvalues are non-zero, real and appear in mutual pairs $(\omega_{\mathbf{k},\gamma}, -\omega_{\mathbf{k},\gamma})$, as shown in App. (K.1.1). The eigenvectors $\mathbf{x}^{(\mathbf{k},\gamma)} = \begin{pmatrix} \mathbf{u}^{(\mathbf{k},\gamma)} \\ -\mathbf{v}^{(\mathbf{k},\gamma)} \end{pmatrix}$ and $\mathbf{y}^{(\mathbf{k},\gamma)} = \begin{pmatrix} -\mathbf{v}^{(\mathbf{k},\gamma)^*} \\ \mathbf{u}^{(\mathbf{k},\gamma)^*} \end{pmatrix}$ are orthogonal with respect to Σ and linearly independent, as well as of opposite sign in the norm. In normalized form, they lie on the upper and lower blue line in Fig. (8.2), interrelated by a reflection on the diagonal. As $\epsilon(\mathbf{k})$ approaches zero, both $|\mathbf{u}^{(\mathbf{k},\gamma)}|$ and $|\mathbf{v}^{(\mathbf{k},\gamma)}|$ to ensure the normalization, corresponding to the point representing the eigenvectors in Fig. (8.2) moving out along the diagonal. At $\mathbf{k} = 0$ the point has moved out infinitely far on the diagonal and the eigenvectors $\mathbf{x}^{(\mathbf{k},\gamma)}$ and $\mathbf{y}^{(\mathbf{k},\gamma)}$ have become linearly dependent in this limit, i.e. there is only a single eigenvector with norm zero to the eigenvalue zero.

8.4 Completeness Relation

Insulator

If no eigenvalue vanishes, we have a complete basis of eigenvectors $\mathbf{x}^{(\mathbf{k},\gamma)}$ and $\mathbf{y}^{(\mathbf{k},\gamma)}$. This structure also applies to each subblock $\mathbf{k} \neq 0$ of $\Sigma\tilde{H}_{\mathrm{QP}}$ in the condensate. As can be checked using the

orthogonality relations and the application to the basis set of eigenvectors, the unit operator can be written as

$$\mathbb{1}^{(\mathbf{k})} = \sum_{\gamma} (\mathbf{x}^{(\mathbf{k},\gamma)} \mathbf{x}^{(\mathbf{k},\gamma)\dagger} - \mathbf{y}^{(\mathbf{k},\gamma)} \mathbf{y}^{(\mathbf{k},\gamma)\dagger}) \Sigma. \tag{8.38}$$

Non-Diagonalizable Sub-Blocks in the Condensate

In the condensate regime, the sub-block corresponding to $\mathbf{k} = 0$ does not possess a basis of eigenvectors and this case, which leads to a qualitatively different Hamiltonian, has to be treated separately. This is not the case in the Mott insulator regime, where all eigenvalues of $\tilde{H}_{\mathrm{QP}}^{(\mathbf{k}=0)}$ are non-zero, can be treated as described in the previous paragraph.

Let us denote the dimension of $\tilde{H}_{\mathrm{QP}}^{(\mathbf{k}=0)}$ by $2\mathcal{D}$, where the limit $\mathcal{D} \to \infty$ can be taken at the very end, when calculating any expectation values within this theory. If one zero eigenvalue of $\tilde{H}_{\mathrm{QP}}^{(\mathbf{k}=0)}$ appears, one corresponding eigenvector of the structure

$$\mathbf{p} = \begin{pmatrix} \mathbf{u}^{(0)} \\ -\mathbf{u}^{(0)^*} \end{pmatrix} \tag{8.39}$$

appears, the Σ-norm of which vanishes exactly $\mathbf{p}^\dagger \Sigma \mathbf{p} = 0$. We choose to normalize it to unity with respect to the euclidean norm $\mathbf{p}^\dagger \mathbf{p} = 1$, which uniquely determines the $\mathbf{p}$ up to a overall complex phase.

Assuming that only one pair of conjugated eigenvalues has become zero, the eigenvectors $\mathbf{x}^{(\mathbf{k}=0,\gamma)}$ and $\mathbf{y}^{(\mathbf{k}=0,\gamma)}$ to all non-zero eigenvalues (i.e. $\gamma > 1$ by convention) span the $(2\mathcal{D}-2)$-dimensional subspace and are mutually orthogonal and normalized as

$$\mathbf{x}^{(\mathbf{k}=0,\gamma)^\dagger} \Sigma \, \mathbf{x}^{(\mathbf{k}=0,\gamma')} = \delta_{\gamma,\gamma'} \tag{8.40}$$

$$\mathbf{y}^{(\mathbf{k}=0,\gamma)^\dagger} \Sigma \, \mathbf{y}^{(\mathbf{k}=0,\gamma')} = -\delta_{\gamma,\gamma'} \tag{8.41}$$

$$\mathbf{x}^{(\mathbf{k}=0,\gamma)^\dagger} \Sigma \, \mathbf{y}^{(\mathbf{k}=0,\gamma')} = 0. \tag{8.42}$$

Since they are eigenvectors to different eigenvalues, $\mathbf{p}$ is also orthogonal to and linearly independent of all other eigenvectors

$$\mathbf{p}^\dagger \Sigma \mathbf{x}^{(\mathbf{k}=0,\gamma)} = 0 \tag{8.43}$$

$$\mathbf{p}^\dagger \Sigma \, \mathbf{y}^{(\mathbf{k}=0,\gamma)} = 0. \tag{8.44}$$

Hence, together with $\mathbf{p}$, all eigenvectors span the entire subspace of the sub-block, up to a single basis vector. Considering the eigenvector structure parametrically as a function of $\mathbf{k}$ approaching zero, the missing basis vector $\mathbf{q}$ must lie in the two-dimensional subspace of the lowest eigenvalue pair for any non-zero $\mathbf{k}$. One might therefore hope to construct it Σ-orthogonal to $\mathbf{p}$ in this subspace. However, this is impossible since for $\mathbf{k} = 0$, it implies that the basis vector is a multiple of $\mathbf{p}$. We could choose $\mathbf{q}$ to lie anywhere within this limiting subspace as long as it is linearly independent of $\mathbf{p}$. However, this would not allow for a direct representation of the identity in terms of eigenvectors and the vector $\mathbf{q}$. The vector $\mathbf{q}$ lies within the generalized subspace to the eigenvalue zero and can be chosen, such that its euclidean norm vanishes $\mathbf{q}^\dagger \Sigma \, \mathbf{q} = 0$. The application of $\Sigma \tilde{H}_{\mathrm{QP}}$ maps $\mathbf{q}$ onto a multiple of $\mathbf{p}$

$$\Sigma \tilde{H}_{\mathrm{QP}} \, \mathbf{q} = -\frac{i}{\tilde{m}} \mathbf{p}, \tag{8.45}$$

and we fix its normalization by requiring

$$\tag{8.46}$$

$$\mathbf{q}^\dagger \Sigma \mathbf{p} = i. \tag{8.47}$$

The mass-like constant $\tilde{m}$ is real, which can easily be determined once $\mathbf{p}$ and $\mathbf{q}$ are known. The vector $\mathbf{q}$ is of the form

$$\mathbf{q} = -i \begin{pmatrix} \mathbf{v}^{(0)} \\ \mathbf{v}^{(0)*} \end{pmatrix}, \tag{8.48}$$

from which it is also directly clear, that it has vanishing norm.

Hence we see that in the basis spanned by all ($\mathbf{x}^{(\mathbf{k}=0,\gamma)}$, $\mathbf{y}^{(\mathbf{k}=0,\gamma)}$, $\mathbf{p}$, $\mathbf{q}$), the matrix $\Sigma\tilde{H}_{\mathrm{QP}}$ is in its Jordan normal form. We can now write the completeness relation for the $\mathbf{k}=0$ subspace in the condensate can be expressed as

$$\mathbb{1}^{(\mathbf{k}=0)} = \sum_{\gamma>1} (\mathbf{x}^{(\mathbf{k}=0,\gamma)} \mathbf{x}^{(\mathbf{k}=0,\gamma)\dagger} - \mathbf{y}^{(\mathbf{k}=0,\gamma)} \mathbf{y}^{(\mathbf{k}=0,\gamma)\dagger}) \Sigma + \; i(\mathbf{q}\,\mathbf{p}^\dagger - \mathbf{p}\,\mathbf{q}^\dagger)\Sigma. \tag{8.49}$$

8.5 Transformation Relations

8.5.1 Condensate

Now that we have established the properties of the eigenvectors of $\Sigma\tilde{H}_{\mathrm{QP}}$, we can define the quasi-particle operators analogous to the classical variables (corresponding to their expectation values)

$$\beta_s = \mathbf{x}^{(s)\dagger} \Sigma \begin{pmatrix} \tilde{\boldsymbol{\sigma}} \\ \tilde{\boldsymbol{\sigma}}^\dagger \end{pmatrix} = \mathbf{u}^{(s)\dagger} \tilde{\boldsymbol{\sigma}} + \mathbf{v}^{(s)\dagger} \tilde{\boldsymbol{\sigma}}^\dagger \tag{8.50}$$

$$\beta_s^\dagger = -\mathbf{y}^{(s)\dagger} \Sigma \begin{pmatrix} \tilde{\boldsymbol{\sigma}} \\ \tilde{\boldsymbol{\sigma}}^\dagger \end{pmatrix} = \mathbf{v}^{(s)t} \tilde{\boldsymbol{\sigma}} + \mathbf{u}^{(s)t} \tilde{\boldsymbol{\sigma}}^\dagger \tag{8.51}$$

$$\mathscr{P} = \mathbf{p}^\dagger \Sigma \begin{pmatrix} \tilde{\boldsymbol{\sigma}} \\ \tilde{\boldsymbol{\sigma}}^\dagger \end{pmatrix} = \sum_{i>0} \left(u_i^{(0)*} \, \tilde{\sigma}^{(i)}_{\mathbf{k}=0} + u_i^{(0)} \, \tilde{\sigma}^{(i)\dagger}_{\mathbf{k}=0} \right) \tag{8.52}$$

$$\mathcal{Q} = -\mathbf{q}^\dagger \Sigma \begin{pmatrix} \tilde{\boldsymbol{\sigma}} \\ \tilde{\boldsymbol{\sigma}}^\dagger \end{pmatrix}. \tag{8.53}$$

In the Heisenberg picture this transformation would also apply in the form, where all operators would be time-dependent.

Care has to be taken with the indices if the diagonalization is performed within a specific subblock $\Sigma\tilde{H}^{(\mathbf{k})}_{\mathrm{QP}}$: the lower half of the eigenvectors $\mathbf{x}^{(\mathbf{k},\gamma)} = \begin{pmatrix} \mathbf{u}^{(\mathbf{k},\gamma)} \\ -\mathbf{v}^{(\mathbf{k},\gamma)} \end{pmatrix}$ implicitly refers to the $-\mathbf{k}$ sector and hence

$$\mathbf{v}^{(\mathbf{k},\gamma)\dagger} \cdot \tilde{\boldsymbol{\sigma}}^\dagger = \sum_{i>0} v_i^{(\mathbf{k},\gamma)*} \tilde{\sigma}^{(i)\dagger}_{-\mathbf{k}}\,. \tag{8.54}$$

The upper index $\mathbf{k}$ in $\mathbf{v}^{(\mathbf{k},\gamma)}$ (which is a vector in the subspace of the respective subblock) thus has to be distinguished from the notation with the lower index $\mathbf{k}$, as in $\mathbf{v}^{(s)}_{\mathbf{k},i}$ (which is a vector in the entire $2\mathcal{D}$-dimensional space), where $(\mathbf{k}, i)$ refers to the mode index.

In analogy to the matrix Eq. (7.43), we define the matrix

$$W = \Big[\mathbf{x}^{(1)}, \ldots, \mathbf{x}^{(\mathcal{D}-1)}, \, i\mathbf{p}, \, \mathbf{y}^{(1)}, \ldots, \mathbf{y}^{(\mathcal{D}-1)}, i\mathbf{q} \Big]. \tag{8.55}$$

through its column vectors. Note that for the derivation considered in this section, the explicit form of W is different from Eq. (7.43), since the vectors are expressed in the single particle Bloch basis and not the Wannier basis. As before, the inverse matrix can be obtained by multiplication

$$W^{-1} = \tilde{\Sigma} W^\dagger \Sigma. \tag{8.56}$$

In matrix form, the transformations can be written as

$$\begin{pmatrix} \boldsymbol{\beta} \\ \mathcal{Q} \\ \boldsymbol{\beta}^\dagger \\ \mathscr{P} \end{pmatrix} = \tilde{\Sigma} W^\dagger \Sigma \begin{pmatrix} \tilde{\boldsymbol{\sigma}} \\ \tilde{\boldsymbol{\sigma}}^\dagger \end{pmatrix}, \tag{8.57}$$

as well as the inverse

$$\begin{pmatrix} \tilde{\boldsymbol{\sigma}} \\ \tilde{\boldsymbol{\sigma}}^\dagger \end{pmatrix} = W \begin{pmatrix} \boldsymbol{\beta} \\ \mathcal{Q} \\ \boldsymbol{\beta}^\dagger \\ \mathscr{P} \end{pmatrix}. \tag{8.58}$$

The explicit form for the individual components of (8.58) read

$$\tilde{\sigma}_{\mathbf{k}}^{(i)} = \sum_s u_{i,\mathbf{k}}^{(s)} \beta_s - \sum_s v_{i,\mathbf{k}}^{(s)^*} \beta_s^\dagger + i u_{i,\mathbf{k}}^{(0)} \mathcal{Q} + v_{i,\mathbf{k}}^{(0)} \mathscr{P} \tag{8.59}$$

$$\tilde{\sigma}_{\mathbf{k}}^{(i)^\dagger} = \sum_s u_{i,\mathbf{k}}^{(s)^*} \beta_s^\dagger - \sum_s v_{i,\mathbf{k}}^{(s)} \beta_s - i u_{i,\mathbf{k}}^{(0)^*} \mathcal{Q} + v_{i,\mathbf{k}}^{(0)^*} \mathscr{P}. \tag{8.60}$$

8.5.2 Insulator

For the insulator, where a basis of eigenvectors exists, the transformation structure is simpler than in the condensate case. We use the identical definition for the quasi-particle creation and annihilation operators $\beta_s^\dagger$ and β_s as in (8.50) and (8.51), but now the quasi-particle mode index s can take on $\mathcal{D}$ distinct values. In this case we again define the matrix

$$W = \left[\mathbf{x}^{(1)}, \ldots, \mathbf{x}^{(\mathcal{D})}, \mathbf{y}^{(1)}, \ldots, \mathbf{y}^{(\mathcal{D})}\right] \tag{8.61}$$

through its column vectors. The transformations in matrix form then become

$$\begin{pmatrix} \boldsymbol{\beta} \\ \boldsymbol{\beta}^\dagger \end{pmatrix} = \Sigma W^\dagger \Sigma \begin{pmatrix} \tilde{\boldsymbol{\sigma}} \\ \tilde{\boldsymbol{\sigma}}^\dagger \end{pmatrix} \tag{8.62}$$

$$\begin{pmatrix} \tilde{\boldsymbol{\sigma}} \\ \tilde{\boldsymbol{\sigma}}^\dagger \end{pmatrix} = W \begin{pmatrix} \boldsymbol{\beta} \\ \boldsymbol{\beta}^\dagger \end{pmatrix}. \tag{8.63}$$

The transformation matrix and its inverse are of the form

$$W = \begin{pmatrix} U & -V^* \\ -V & U^* \end{pmatrix} \qquad \text{and} \qquad W^{-1} = \Sigma W^\dagger \Sigma = \begin{pmatrix} U^\dagger & V^\dagger \\ V^t & U^t \end{pmatrix}, \tag{8.64}$$

where U and V are the $\mathcal{D} \times \mathcal{D}$-dimensional matrices respectively containing the eigenvectors $\mathbf{u}^{(s)}$ and $\mathbf{v}^{(s)}$ as their column vectors. The transformation from quasi-particle operators β to fluctuation operators σ in the Bloch basis can thus be given explicitly as

$$\tilde{\sigma}_{\mathbf{k}}^{(i)} = \sum_s u_{i,\mathbf{k}}^{(s)} \beta_s - \sum_s v_{i,\mathbf{k}}^{(s)^*} \beta_s^\dagger \tag{8.65}$$

$$\tilde{\sigma}_{\mathbf{k}}^{(i)^\dagger} = \sum_s u_{i,\mathbf{k}}^{(s)^*} \beta_s^\dagger - \sum_s v_{i,\mathbf{k}}^{(s)} \beta_s. \tag{8.66}$$

Orthogonality and Completeness Relations

Using the explicit form of the matrices W and W^{-1} in Eq. (8.64) and $\mathbb{1}_{2\mathcal{D}} = WW^{-1} = W^{-1}W$, we find the matrix relations

$$UU^\dagger - V^* V^t = \mathbb{1}_{\mathcal{D}} \tag{8.67}$$

$$UV^\dagger - V^* U^t = 0 \tag{8.68}$$

$$U^\dagger U - V^\dagger V = \mathbb{1}_{\mathcal{D}} \tag{8.69}$$

$$V^t U - U^t V = 0. \tag{8.70}$$

Explicating these in terms of the column vectors of U and V can be understood as orthogonality and completeness relations for the subvectors $\mathbf{u}^{(s)}$ and $\mathbf{v}^{(s)}$. For the condensate case, similar, but extended versions of these relations can be found analogously.

Determining the Eigenmodes

In contrast to Bogoliubov theory, where only two fluctuation modes are coupled for each quasi-particle eigenmode and the diagonalization is easily performed analytically, the two coupled subblocks of mean-field states within this quasi-particle theory are somewhat larger and can be determined numerically. For a homogeneous system, the numerical diagonalization can be performed in every subblock to fixed $\mathbf{k}$ and it is typically sufficient to truncate the system to the lowest ≈ 10 mean-field states, which amounts to the diagonalization of (18×18) matrices. The convergence of the low energy modes as a function of the cutoff is easily controlled. In inhomogeneous systems with symmetries, such as a harmonically trapped system with discrete rotational invariance, the respective symmetry can be exploited in the diagonalization. For particular cases, such as a homogeneous Mott insulator, it may even be possible to determine the eigenmode structure analytically.

Notation for the Translationally Invariant Case

Care has to be taken in the translationally invariant case. Here, the collective mode s can be split into a pair of independent quantum numbers $s \to (\mathbf{k}, \gamma)$, where γ is the internal mode index. However, $\mathbf{k}$ can also be used as an index set $(i, \mathbf{k})$, referring to an element of a given vector, as for instance $v^{(s)}_{(i,\mathbf{k})}$. These two different meanings may not be confused and a minus may appear from the nature of the generalized unitary transformation, where particle and hole fluctuations are coupled.

Let us consider an eigenvector $\mathbf{x}^{(s)} = \begin{pmatrix} \mathbf{u}^{(s)} \\ -\mathbf{v}^{(s)} \end{pmatrix}$ to a given collective mode $s = (\mathbf{k}, \gamma)$. This can be obtained from the diagonalization of the subblock $\Sigma H^{(\mathbf{k})}_{\mathrm{QP}}$, which, by **convention**, contains the $\mathbf{k}$-particle sector in the upper half, but the $-\mathbf{k}$ sector in the lower half. Let us denote the eigenvectors in this lower dimensional subspace by $\mathbf{x}^{(\mathbf{k},\gamma)} = \begin{pmatrix} \mathbf{u}^{(\mathbf{k},\gamma)} \\ -\mathbf{v}^{(\mathbf{k},\gamma)} \end{pmatrix}$ and $\mathbf{y}^{(\mathbf{k},\gamma)} = \begin{pmatrix} -\mathbf{v}^{(\mathbf{k},\gamma)^*} \\ \mathbf{u}^{(\mathbf{k},\gamma)^*} \end{pmatrix}$. In index notation these vectors only have a single index i. If these are promoted to the corresponding vectors $\mathbf{x}^{(s)}$ and $\mathbf{y}^{(s)}$ on the entire space, the upper halves contain the vectors $\mathbf{u}^{(\mathbf{k},\gamma)}$ and $-\mathbf{v}^{(\mathbf{k},\gamma)^*}$ in the $\mathbf{k}$ sector and the vectors $-\mathbf{v}^{(\mathbf{k},\gamma)}$ and $\mathbf{u}^{(\mathbf{k},\gamma)^*}$ in the $-\mathbf{k}$ sector in the lower halves respectively. Thus, we have the relation for the matrix elements in the total and the reduced subspaces

$$u^{(\mathbf{k},\gamma)}_{i,\mathbf{k}'} = \delta_{\mathbf{k},\mathbf{k}'}\, u^{(\mathbf{k},\gamma)}_i \tag{8.71}$$

$$v^{(\mathbf{k},\gamma)}_{i,\mathbf{k}'} = \delta_{\mathbf{k},-\mathbf{k}'}\, v^{(\mathbf{k},\gamma)}_i. \tag{8.72}$$

Also note that conjugated vectors $\mathbf{x}^{(s)}$ and $\mathbf{y}^{(s)}$ on the full space do not correspond to conjugated vectors obtained from the diagonalization of a single subblock $\Sigma H^{(\mathbf{k})}_{\mathrm{QP}}$, but from eigenvectors of two different subblocks: if $\mathbf{x}^{(s)}$ is the vector on the entire space promoted from a positive eigenvector of $\Sigma H^{(\mathbf{k})}_{\mathrm{QP}}$, then $\mathbf{y}^{(s)}$ on the entire space is the vector promoted from a negative eigenvector of $\Sigma H^{(-\mathbf{k})}_{\mathrm{QP}}$. This implies that the subvectors $\mathbf{u}^{(\mathbf{k},\gamma)}$ and $\mathbf{v}^{(\mathbf{k},\gamma)}$ determined from the diagonalization of different subblocks have to be chosen such that

$$\mathbf{u}^{(\mathbf{k},\gamma)} = \mathbf{u}^{(-\mathbf{k},\gamma)} \tag{8.73}$$

$$\mathbf{v}^{(\mathbf{k},\gamma)} = \mathbf{v}^{(-\mathbf{k},\gamma)}. \tag{8.74}$$

In the homogeneous case, the general transformation relations (8.59) and (8.60) for the condensate then become

$$\tilde{\sigma}^{(i)}_{\mathbf{k}} = \sum_{\gamma} \left[u^{(\mathbf{k},\gamma)}_i\, \beta_{\mathbf{k},\gamma} - v^{(\mathbf{k},\gamma)^*}_i\, \beta^\dagger_{-\mathbf{k},\gamma} \right] + \delta_{\mathbf{k},0} \left[v^{(0)}_{i,\mathbf{k}}\, \mathscr{P} + i u^{(0)}_{i,\mathbf{k}}\, \mathcal{Q} \right] \tag{8.75}$$

$$\tilde{\sigma}^{(i)^\dagger}_{\mathbf{k}} = \sum_{\gamma} \left[u^{(\mathbf{k},\gamma)^*}_i\, \beta^\dagger_{\mathbf{k},\gamma} - v^{(\mathbf{k},\gamma)}_i\, \beta_{-\mathbf{k},\gamma} \right] + \delta_{\mathbf{k},0} \left[v^{(0)^*}_{i,\mathbf{k}}\, \mathscr{P} - i u^{(0)^*}_{i,\mathbf{k}}\, \mathcal{Q} \right] \tag{8.76}$$

Here, $u^{(\mathbf{k},\gamma)}_i$ is the i-th element of the subvector $\mathbf{u}$ of the γ-th eigenvector obtained by diagonalizing the $2N_{\max} \times 2N_{\max}$-dimensional subblock labeled by $\mathbf{k}$. In the homogeneous insulator case, the transformations are identical up to the last two terms, which are to be neglected.

8.6 Jordan Normal Form of the Quasi-Particle Hamiltonian

The qualitative form of $\mathcal{H}^{(2)}$ depends on whether ΣH_{QP} possesses a basis of eigenvectors. If this is not the case, an additional term analogous to a kinetic energy of a free particle without a restoring force appears in the resulting Hamiltonian. Such a term generally appears in the condensate phase (also at strong interactions), but not in the Mott insulator and we consider these two cases separately. To express $\mathcal{H}^{(2)}$ in terms of quasi-particle operators and $\mathscr{P}$, we multiply the coefficient matrix $\tilde{H}_{\mathrm{QP}}$ by the completeness relation from the right and $\Sigma\Sigma = \mathbb{1}$ from the left and then use the eigenvector and orthogonality relations.

8.6.1 Condensate

In the condensate, we use the completeness relation (8.49) and find

$$\begin{aligned}\tilde{H}_{\mathrm{QP}} &= \Sigma(\Sigma\tilde{H}_{\mathrm{QP}})\mathbb{1} \\ &= \sum_{\mathbf{k},\gamma}{}' (\Sigma\,\mathbf{x}^{(\mathbf{k},\gamma)}\,\omega_{\mathbf{k},\gamma}\,\mathbf{x}^{(\mathbf{k},\gamma)\,\dagger}\Sigma + \Sigma\,\mathbf{y}^{(\mathbf{k},\gamma)}\,\omega_{\mathbf{k},\gamma}\,\mathbf{y}^{(\mathbf{k},\gamma)\,\dagger}\Sigma) + \frac{1}{\tilde{m}}\Sigma\,\mathbf{p}\,\mathbf{p}^{\dagger}\Sigma.\end{aligned} \tag{8.77}$$

Here the $\sum'_{\mathbf{k},\gamma}$ denotes the sum over all bosonic modes, i.e. all quasi-momenta $\mathbf{k}$ and internal mode indices γ, except for the combination $(\mathbf{k}=0,\gamma=1)$, since there is no bosonic sound mode at $\mathbf{k}=0$. Using the quasi-particle operator definitions (8.50) and (8.51), as well as the momentum-like operator (8.52), the second order quasi-particle Hamiltonian (8.33) can be rewritten as

$$\begin{aligned}\mathcal{H}^{(2)} &= \frac{1}{2}\sum_{\mathbf{k},\gamma}{}' \omega_{\mathbf{k},\gamma}\left(\beta^{\dagger}_{\mathbf{k},\gamma}\beta_{\mathbf{k},\gamma} + \beta_{\mathbf{k},\gamma}\,\beta^{\dagger}_{\mathbf{k},\gamma}\right) + \frac{\mathscr{P}^2}{2\tilde{m}} - \frac{1}{2}\mathrm{Tr}\,(h) + \frac{D}{L} \\ &\approx \sum_{\mathbf{k},\gamma}{}' \omega_{\mathbf{k},\gamma}\beta^{\dagger}_{\mathbf{k},\gamma}\,\beta_{\mathbf{k},\gamma} + \frac{\mathscr{P}^2}{2\tilde{m}} + \frac{1}{2}\left(\sum_{\mathbf{k},\gamma}{}' \omega_{\mathbf{k},\gamma} - \mathrm{Tr}\,(h)\right).\end{aligned} \tag{8.78}$$

To obtain the last line, we neglected the term D/L, where $\langle D\rangle$ is of the order of the number of quasi-particle excitations and L is the number of sites. If the concentration of quasi-particles is low (both excitations and fluctuations in the ground state), this term is small and can be neglected.Furthermore, we used the bosonic commutation relations to bring β and $\beta^{\dagger}$ into normal order, which gives rise to an additional scalar term $\frac{1}{2}\sum'_{\mathbf{k},\gamma}\omega_{\mathbf{k},\gamma}$. Note that each of the scalar terms, taken by itself, diverges in the limit of a large local bosonic cutoff $N_{\max}\to\infty$. Only when taking the limit of the sum of the two, does this remain finite and lowers the energy of the new quasi-particle ground state.

8.6.2 Insulator

When not in the condensate, the same derivation applies, except for the difference that the quasi-particle matrix can be fully expressed in terms of eigenvectors and no spurious mode arises. The Hamiltonian in this case then becomes

$$\mathcal{H}^{(2)} \approx \sum_{\mathbf{k},\gamma}\omega_{\mathbf{k},\gamma}\beta^{\dagger}_{\mathbf{k},\gamma}\,\beta_{\mathbf{k},\gamma} + \frac{1}{2}\left(\sum_{\mathbf{k},\gamma}\omega_{\mathbf{k},\gamma} - \mathrm{Tr}\,(h)\right). \tag{8.79}$$

Note that here the sum extends over all modes, including the bosonic $(\mathbf{k}=0,\gamma=1)$ mode, which exists in contrast to the condensate case. In the Mott insulator, the lowest two modes correspond to collective particle and hole excitations, which are fully delocalized and each quasi-particle possesses a well-defined quasi-momentum. Only for $J=0$ do these become degenerate and the quasi-particles can also be chosen to be localized.

8.6.2.1 The Spurious Mode's Effective Mass

In the non-interacting limit $U \to 0$ the Bogoliubov result in Eq.(6.60) is recovered, where $\tilde{m}$ is given by $\tilde{m} = \frac{1}{2U|\phi|^2}$. In the non-interacting limit, where the condensate fraction approaches 1 at zero temperature, approaches the density of particles in the lattice $\lim_{U/J\to 0} |\phi|^2 = n$. In the non-interacting limit, the effective mass $\tilde{m}$ thus scales inversely with the density, which is however no longer true at stronger interactions U/J, as shown in Fig. (8.3).

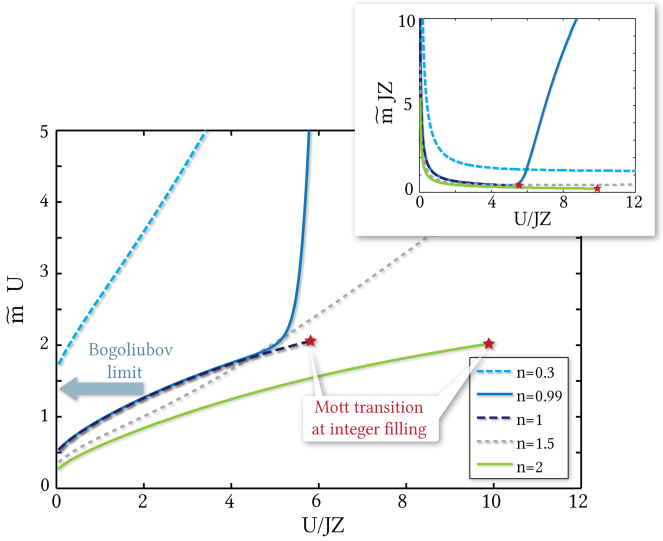

Figure 8.3: The effective mass $\tilde{m}$ of the momentum-like term $\frac{\mathscr{P}^2}{2\tilde{m}}$ in the condensate quasi-particle Hamiltonian shown as a function of the interaction strength U/JZ for various fixed densities. $\tilde{m}$ has the units of an inverse energy and is plotted here in units U^{-1}. At integer filling (solid green and dashed dark blue line) the system undergoes a Mott transition at a critical value of U/J, beyond which an effective mass $\tilde{m}$ is not defined in the Mott insulator. We point out that $\tilde{m}U$ does not diverge at the transition, but approaches a value of 2.06 and 2.02 for filling $n = 1$ and $n = 2$ respectively. For non-integer fillings the system remains condensed for arbitrarily large U/J and $\tilde{m}U$ increases linearly (thus diverging) with U/J in this strongly interacting limit. Note that (scaled in units of inverse JZ), $\tilde{m}JZ$ does not diverge in the strongly interacting limit, but converges to a density-dependent value, as shown in the inset for the same data.

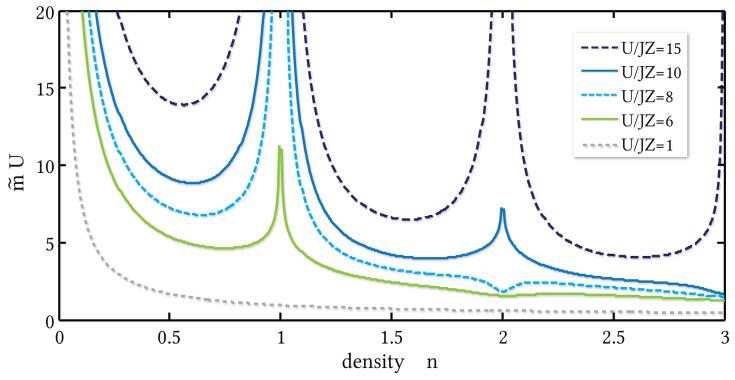

Figure 8.4: Density dependence of the mass-like term $\tilde{m}$ for various interaction strengths. For weak interactions (dashed gray line), the Bogoliubov result, where $\tilde{m} \propto 1/n$ is recovered. At stronger interactions, there is however a very strong density dependence. For sufficiently strong values of U/J, the quantity $\tilde{m}U$ diverges when approaching integer values of the density, where the system enters a Mott insulating state. In the insulator, $\tilde{m}$ is not defined and does not appear in the quasi-particle Hamiltonian. Note however, that the dependence on the density is non-trivial: for certain interaction strengths (such as $U/J = 8$ here), approaching integer filling ($n = 2$ here) may suppress $\tilde{m}$, in contrast to the usual case.

8.6.2.2 The Quasi-Particle Ground State

Together with the quasi-particle transformation prescription, these quasi-particle Hamiltonians (8.78,8.79) are the main result of this section. It describes a set of independent, non-interacting bosonic quasi-particles, each characterized by a quasi-momentum index $\mathbf{k}$ and an internal mode index γ. As in the (uncommon), but more complete derivation of Bogoliubov theory given in the previous chapter and in [19, 103], there is no quasi-particle sound mode at $\mathbf{k} = 0$, but an additional momentum-like degree of freedom $\mathscr{P}$ with a mass-like prefactor $1/(2\tilde{m})$ appears. The last term is the energy reduction relative to the mean-field energy. Note that while each of the two terms diverges individually when taking the limit of an infinite number of mean-field states, the sum of both does not diverge, but gives a finite energy correction proportional to the number of lattice sites. The ground state $|\psi_0\rangle$ of this Hamiltonian can be implicitly defined as the state where no quasi-particle modes are occupied and it is thus annihilated by the application of any annihilation operator

$$\beta_{\mathbf{k},\gamma}|\psi_0\rangle = 0. \tag{8.80}$$

Since $\mathscr{P}$ is a Hermitian, momentum-like operator with a continuous spectrum and the term $\mathscr{P}^2/2\tilde{m}$ appears in the quasi-particle Hamiltonian, the ground state is furthermore characterized by

$$\mathscr{P}|\psi_0\rangle = 0. \tag{8.81}$$

The operator $\mathcal{Q}$ does not appear in the Hamiltonian and the time-dependent expectation value $\langle\mathcal{Q}\rangle$ changes linearly in time in any state, at a rate proportional to $\langle P\rangle$. Since the latter vanishes in the ground state, the expectation value of $\mathcal{Q}$ is constant and the quasi-particle ground state can be chosen such that $\langle\mathcal{Q}\rangle = 0$.

Any finite lowering in energy $\left(\sum'_{\mathbf{k},\gamma} \omega_{\mathbf{k},\gamma} - \mathrm{Tr}\,(h)\right)$ (or the counterpart containing the ($\mathbf{k} = 0, \gamma = 1$) mode in the Mott insulator) indicates that ground state of this Hamiltonian differs from the original Gutzwiller ground state. This ground state contains correlated pairs of quasi-particle excitations, which lower its energy for any non-zero or non-infinite J/U, which are colloquially sometimes referred to as *quantum fluctuations*.

8.7 Expressing Operators in Quasi-Particle Operators

To incorporate the effect of any external perturbation on the system or calculate expectation values, it is of central importance to express a given operator in terms of the new quasi-particle operators $\beta^\dagger_{\mathbf{k},\gamma}$ and $\beta_{\mathbf{k},\gamma}$. Typically, an operator for our many-particle system is given in second quantization, in terms of momentum, quasi-momentum or Wannier creation and annihilation operators. It is a straightforward task to express such an operator in terms of local mean-field states in the form $|i\rangle_{\ell\ell}\langle j|$ and direct products thereof[3]. Expressing a given operator in quasi-particle operators, the maximum number of $\beta^\dagger_{\mathbf{k},\gamma}$ and $\beta_{\mathbf{k},\gamma}$ appearing in any term is twice as large as the maximum number of on-site operators appearing as a product in a given term. For instance, any on-site operator

[3]Since the set of all direct product mean-field states constitute a basis of the entire Fock space.

contains a maximum of two quasi-particle operator, any two site operator (such as the hopping term) a maximum of four, etc.

We now consider the transformation to a special, but common class of operators: a sum of on-site operators $\tilde{A}_{\boldsymbol{\ell}}$, each weighted by a complex exponential and parametrized by a quasi-momentum index

$$\mathcal{A}_{\mathbf{k}} = \frac{1}{\sqrt{L}} \sum_{\boldsymbol{\ell}} e^{i\mathbf{k}\cdot\mathbf{R}_{\boldsymbol{\ell}}} \tilde{\mathcal{A}}_{\boldsymbol{\ell}}. \tag{8.82}$$

We define the matrix elements in the local Gutzwiller eigenbasis $A_{i,j}^{(\boldsymbol{\ell})} = {}_{\boldsymbol{\ell}}\langle i|\tilde{\mathcal{A}}_{\boldsymbol{\ell}}|j\rangle_{\boldsymbol{\ell}}$, which become site independent for a homogeneous system and for the case that $\tilde{\mathcal{A}}_{\boldsymbol{\ell}}$ are the same local operator. Grouping by different orders in the fluctuations and using the fact that any local operator can be expressed in terms of at most two local fluctuation operators given by Eqns. (8.13 - 8.16), we find

$$\begin{aligned}\mathcal{A}_{\mathbf{k}} =& \frac{1}{\sqrt{L}} \sum_{\boldsymbol{\ell}} e^{i\mathbf{k}\cdot\mathbf{R}_{\boldsymbol{\ell}}} \left[A_{0,0}|0\rangle_{\boldsymbol{\ell}\boldsymbol{\ell}}\langle 0| + \sum_{i>0} \left(A_{i,0}|i\rangle_{\boldsymbol{\ell}\boldsymbol{\ell}}\langle 0| + A_{0,i}|0\rangle_{\boldsymbol{\ell}\boldsymbol{\ell}}\langle i|\right) + \sum_{i,j>0} A_{i,j}|i\rangle_{\boldsymbol{\ell}\boldsymbol{\ell}}\langle j| \right] \\ =& \sqrt{L}\, A_{0,0}\, \delta_{\mathbf{k},0} + \sum_{i>0} \left(A_{i,0}\, \tilde{\sigma}_{\mathbf{k}}^{(i)^\dagger} + A_{0,i}\, \tilde{\sigma}_{-\mathbf{k}}^{(i)} \right) + \frac{1}{\sqrt{L}} \sum_{i,j>0} \sum_{\mathbf{k}'} (A_{i,j} - A_{0,0}\delta_{i,j})\, \tilde{\sigma}_{\lfloor \mathbf{k}+\mathbf{k}' \rfloor}^{(i)^\dagger} \tilde{\sigma}_{\mathbf{k}'}^{(j)}\end{aligned} \tag{8.83}$$

where the function $\lfloor\ \rfloor : \mathbf{k} \mapsto \lfloor \mathbf{k} \rfloor = \mathbf{k} + \mathbf{G}$ maps a momentum vector into the first Brillouin zone (referred to as *umklapp processes*) by addition of an appropriate reciprocal lattice vector $\mathbf{G}$ if $\mathbf{k}$ lies outside the first Brillouin zone. To obtain the last line, we used

$$|0\rangle_{\boldsymbol{\ell}\boldsymbol{\ell}}\langle 0| = \mathbb{1} - \sum_{i>0} \sigma_{\boldsymbol{\ell}}^{(i)^\dagger} \sigma_{\boldsymbol{\ell}}^{(i)}, \tag{8.84}$$

and decomposed the first term in (8.83) into a constant and a sum of normally ordered fluctuation operators

$$\frac{1}{\sqrt{L}} \sum_{\boldsymbol{\ell}} e^{i\mathbf{k}\cdot\mathbf{R}_{\boldsymbol{\ell}}} A_{0,0}|0\rangle_{\boldsymbol{\ell}\boldsymbol{\ell}}\langle 0| = \sqrt{L}\, A_{0,0}\, \delta_{\mathbf{k},0} - \frac{A_{0,0}}{\sqrt{L}} \sum_{i>0} \sum_{\mathbf{k}'} \tilde{\sigma}_{\lfloor \mathbf{k}+\mathbf{k}' \rfloor}^{(i)^\dagger} \tilde{\sigma}_{\mathbf{k}'}^{(i)}. \tag{8.85}$$

The first term is simply the scalar contribution to the operator from the Gutzwiller ground state. The second term accounts for the *depletion* from the Gutzwiller state: if quasi-particle modes are excited, the amplitudes of the Gutzwiller ground state $|i = 0\rangle$ are reduced, which is directly related to the amplitudes with which the local excited mean-field states are occupied. This second order *depletion* term is grouped together with the other second order terms in Eq. (8.83). Note that no approximation was made so far and the last line of Eq. (8.83) is exact. To express all fluctuation operators in terms of quasi-particle operators, we use the transformations (8.75) and (8.76) for the homogeneous case. Inserting these into (8.85), one obtains

$$\mathcal{A}_{\mathbf{k}} = \sqrt{L}\, A_{0,0}\, \delta_{\mathbf{k},0} + \sum_{\gamma} \left[D_{\mathbf{k},\gamma}\, \beta_{\mathbf{k},\gamma}^\dagger + \tilde{D}_{-\mathbf{k},\gamma}\, \beta_{-\mathbf{k},\gamma} \right] + D_P \mathscr{P} + D_Q \mathcal{Q} + \mathcal{O}(\beta^2). \tag{8.86}$$

Here we defined the coefficients

$$D_{\mathbf{k},\gamma} = \sum_{i>0} \left[A_{i,0}\, u_i^{(\mathbf{k},\gamma)^*} - A_{0,i}\, v_i^{(-\mathbf{k},\gamma)^*} \right] \tag{8.87}$$

$$\tilde{D}_{\mathbf{k},\gamma} = \sum_{i>0} \left[A_{0,i}\, u_i^{(\mathbf{k},\gamma)} - A_{i,0}\, v_i^{(-\mathbf{k},\gamma)} \right] \tag{8.88}$$

$$D_P = \delta_{\mathbf{k},0} \sum_{i>0} \left[A_{0,i}\, v_{i,-\mathbf{k}}^{(0)} + A_{i,0}\, v_{i,\mathbf{k}}^{(0)^*} \right] \tag{8.89}$$

$$D_Q = i\delta_{\mathbf{k},0} \sum_{i>0} \left[A_{0,i}\, u_{i,-\mathbf{k}}^{(0)} - A_{i,0}\, u_{i,\mathbf{k}}^{(0)^*} \right] \tag{8.90}$$

of the quasi-particle operators in the first order term. Typically, the last term of second order in β in Eq. (8.86) can be neglected for low concentrations of quasi-particles, as is the case for linear response calculations. Also note that for Hermitian operators $\mathcal{A}_{\mathbf{k}}$, the coefficients D_P and D_Q of the condensate mode position and momentum operators are purely real. The notation $\mathcal{O}(\beta^2)$ denotes terms of second order in any of the products of $\beta, \beta^\dagger, \mathscr{P}, \mathcal{Q}$.

Higher Order Decay & Interaction Processes

Up to now, we have reexpressed the second order Hamiltonian, which is quadratic in both the original fluctuation and the quasi-particle operators. It is also $\mathcal{H}^{(2)}$, which determines the form of the quasi-particle operators $\beta_{\mathbf{k},\gamma}$. It is now possible to express the higher order terms $\mathcal{H}^{(3)} + \mathcal{H}^{(4)}$ from the original Bose-Hubbard Hamiltonian, which were previously neglected, in terms of the quasi-particle operators. Although straightforward, the result is somewhat lengthy and not shown here. These terms, containing three or four quasi-particle operators, physically correspond to quasi-particle decay, creation and interaction processes. These give excited quasi-particle states a finite lifetime with the associated broadening of the peaks in the spectral functions. In both the non-interacting and zero-tunneling limits, these terms disappear and the quasi-particles become infinitely long-lived.

8.8 Results

8.8.1 Structure of the Excitations

Up to now, we have focused on the structure of the spectrum, i.e. the eigenvalues of the quasi-particle Hamiltonian. It is furthermore of interest to analyze the structure of the associated quasi-particle eigenstates, both the ground state, as well as excited states.

Mott Insulator

In the Mott insulator, it is useful to start from the Gutzwiller product state (shown at the top of Fig. (8.5)). The lowest energy excited states in of the mean-field Hamiltonian in the insulator are particle states $|\gamma = p, \boldsymbol{\ell}\rangle$ containing one additional particle, or hole states $|\gamma = h, \boldsymbol{\ell}\rangle$ containing one less particle at one site $\boldsymbol{\ell}$. These states are distinct and orthogonal, as well as degenerate with respect to the mean-field Hamiltonian and graphically shown in the two boxed of Fig. (8.5). This degeneracy is however lifted by the fluctuating part H_δ of the Bose-Hubbard Hamiltonian beyond the mean-field term.

To understand the structure of the excitations and the states involved, it is useful to view the diagonalization of the second order Hamiltonian $\mathcal{H}^{(2)}$ from a different angle: in the insulator, this is equivalent to the diagonalization of the full Bose-Hubbard Hamiltonian, projected to the subspace of particle and hole states. Each of these subspaces is L-dimensional and the fluctuation term H_δ (beyond the static mean-field term) couples these many-particle states containing either one additional particle, or one additional hole at one site. For the translationally invariant case, the resulting particle and hole eigenstates are superpositions $|\gamma = p/h, \mathbf{k}\rangle = \frac{1}{\sqrt{L}} \sum_{\boldsymbol{\ell}} e^{i\mathbf{k}\cdot\mathbf{r}_{\boldsymbol{\ell}}} |\gamma = p/h, \boldsymbol{\ell}\rangle$, where the particle or hole excitation is completely delocalized on the lattice and the many-particle eigenstate can be characterized by a quantum number corresponding to the quasi-momentum of the excitation (in addition to the mode index γ).

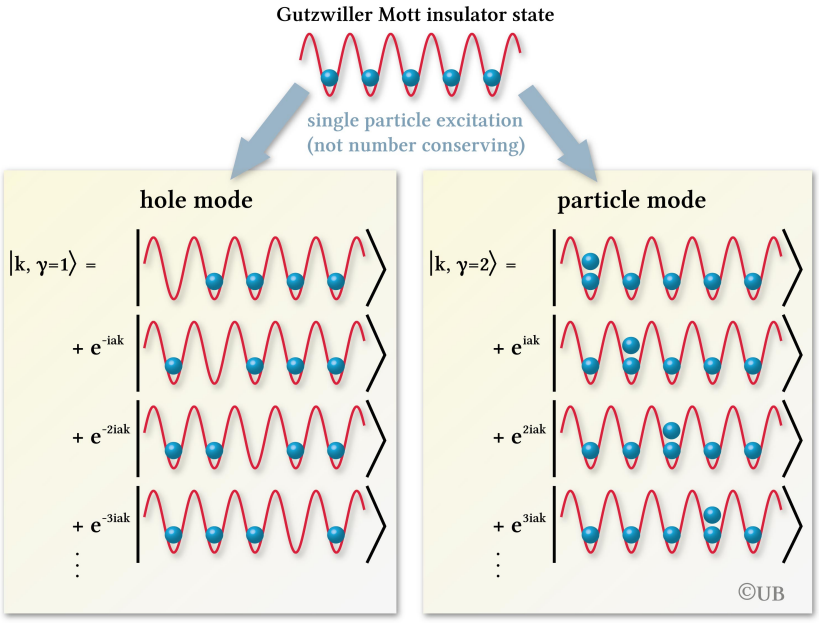

Figure 8.5: The approximate many-particle eigenstates with the lowest energy in the Mott insulator are spatially delocalized hole and particle states containing exactly $(N-1)$ and $N+1$ respectively. Starting from the Gutzwiller Mott insulating state and creating excited states by removing or adding a particle at one given lattice site, the eigenstates in the homogeneous system can be constructed by taking the superposition of all such spatially localized hole and particle states with a complex phase factor determined by the quasi-momentum.

This quasi-momentum determines the complex phase factor with which the localized particle or hole states are superimposed, and a graphical representation of such excited eigenstates is shown in Fig. (8.5). The many-particle energy of such an excited state is given by the tight-binding energy rescaled by a bosonic factor and furthermore shifted by the chemical potential, which accounts for the removal or the addition of one particle. For both the particle and the hole case, the state characterized by $\mathbf{k} = 0$ has the lowest energy within the entire mode.

Note that in the Mott insulator, the single particle spectrum and these eigenstates are **not** the energies and states measured by atom number conserving probing techniques, such as Bragg spectroscopy or lattice modulation spectroscopy. These techniques measure the excitation spectrum within the subspace of fixed particle number N. The N-particle excited states can be constructed within this quasi-particle theory approach by adding both a particle and a hole excitation. To lowest order (i.e. on the level of the quasi-particle Hamiltonian), the particle and the hole quasi-particle do not interact and the energy of such an excited state is given by the sum of individual excitation energies. The set of such particle-hole N-particle excited states which the probing operator couples to is further restricted by quasi-momentum conservation laws.

Condensate

The excited many-particle states are harder to picture in the condensate. Let us first consider the non-interacting, where it is favorable to think in terms of the occupation number basis of the Bloch states. The N-particle ground state is given by the state where all particles occupy the lowest single particle mode, i.e. the $\mathbf{k} = 0$ mode for a homogeneous system $|\psi_{\text{g.s.}}\rangle \propto (a^\dagger_{\mathbf{k}=0})^N |\text{vac}\rangle$. The N-particle excited states can be explicitly constructed by removing one particle from the $\mathbf{k} = 0$ mode and placing it in an excited quasi-momentum mode $\mathbf{q}$, i.e. $|\psi_{\mathbf{q}}\rangle \propto a^\dagger_{\mathbf{q}} a_{\mathbf{k}=0} |\psi_{\text{g.s.}}\rangle$. Clearly, these states are mutually orthogonal, contain N particles and are exact eigenstates of the non-interacting Hamiltonian. The number of particles removed from the $\mathbf{k} = 0$ mode and inserted into a given mode $\mathbf{q}$ can be associated with the quasi-particle number in the quasi-particle mode we label with the same quantum number $\mathbf{q}$. This can be related to Leggett's number-conserving formulation of

Bogoliubov theory discussed in section (6.3.3): since, for the non-interacting system, the energies of such excitations are exactly additive, the quasi-particles are non-interacting and bosonic up to a deviation in the construction of the associated particle number conserving bosonic operator, the deviation of which vanishes in the thermodynamic limit.

The concept discussed above for the non-interacting states can formally be extended (although physically not useful, this makes calculations much easier) to the symmetry-breaking approach in terms of coherent states. Since all operations can be formulated in terms in terms of number-conserving operators, it is guaranteed that all relevant expectation values coincide with those of the number conserving approach up to prefactors, which approach unity in the thermodynamic limit (see [16] for a proof of this statement). Within this formulation, the effect of interactions can be incorporated on the level of Gutzwiller and the quasi-particle theory, where the coherent states from the non-interacting case are now replaced by a more general class of number non-conserving states.

When considering states excited with a single or a fixed number of quasi-particles in the condensate, there is a qualitative difference to the Mott insulator: If the initial ground state contains an average of N particles (and the many-particle state's projection onto the N-particle subspace being non-zero) and adding a single quasi-particle in any mode, the resulting state may contain a slightly different particle number on average, but the projection of this state onto the N-particle subspace is still **non-zero**. In this sense, the single-particle spectrum for a N-particle state, predicted by the quasi-particle theory in the condensate contains a contribution from N-particle excited states. This would not be the case in a hypothetical exact calculation of the single particle spectrum in the condensate, but can be remedied (if required) by a number-conserving formulation of the quasi-particle theory, as discussed for Gutzwiller theory in section (3.2).

This property does however tell us, that the excitational structure calculated within the symmetry-breaking approach also contains information relevant for number-conserving probing techniques (which is not the case in the insulator). For this reason, the quasi-particle sound and amplitude mode energies measured in the condensate are directly contained in the resulting energy spectrum. In the Mott insulator, on the other hand, the sum of particle and hole quasi-particle energies has to be taken for comparison with experimental data. The particle and hole mode energies in their bare form would be relevant for the spectrocopic measurement with an experimental technique, which adds or ejects an atom during each probing process, respectively (such as photo-emission spectroscopy in solid state systems, where an electron is ejected).

Order Parameter Response of the Various Modes

One possibility to gain insight into the structure of collective modes is to analyze the properties of a state, excited in a given quasi-particle mode. Here we will analyze the resulting spatial order parameter and density distribution. Let us first consider a state excited with a single quasi-particle $|\psi\rangle = \beta_{\mathbf{k},\gamma}|\psi\rangle_0$, where $|\psi_0\rangle$ is the quasi-particle ground state. Since no lattice site can be singled out and as can be verified explicitly, this does not break the discrete translational symmetry in any way: it does not describe a density wave (which would be composed mainly of sound mode quasi-particles), nor a order parameter wave. To describe the latter, we require a state corresponding to the classical limit, features which are extremized by coherent states. This is analogous to the harmonic oscillator: the best description of a classical particle, with which both a position and a momentum can be associated with minimal uncertainty is never a harmonic oscillator eigenstate, no matter how high the excitational index is. Here, as state featuring a well defined density wave would never correspond to a quasi-particle eigenstate with $\tilde{n}\ |\psi\rangle = \frac{1}{\sqrt{\tilde{n}}}\beta^{\tilde{n}}_{\mathbf{k},\gamma}|\psi_0\rangle$, but a coherent state

$$|z, \mathbf{k}, \gamma\rangle = e^{-|z|^2/2} e^{z\beta^\dagger_{\mathbf{k},\gamma}}|\psi_0\rangle. \tag{8.91}$$

This state contains $|z|^2 = \langle z, \mathbf{k}, \gamma|\beta^\dagger_{\mathbf{k},\gamma}\,\beta_{\mathbf{k},\gamma}|z, \mathbf{k}, \gamma\rangle$ quasi-particles on average. The complex phase of the coherent state parameter $z = |z|e^{i\varphi}$ however also determines the structure of the state and, together with the overall complex phase contained in the definition of $\beta^\dagger_{\mathbf{k},\gamma}$, determines the spatial symmetry breaking (i.e. at which lattice sites the density, a measurable quantity, takes on its maximum). If this state is time evolved with the quasi-particle Hamiltonian, which is simply a harmonic oscillator Hamiltonian for each individual quasi-particle mode, the state remains a coherent state with the time-dependent coherent state parameter z rotating in the complex plane at a rate set by the quasi-particle mode energy $\omega_{\mathbf{k},s}$. The corresponding time-dependent state would feature an order parameter and density wave propagating with a phase velocity $\omega_{\mathbf{k},s}/|\mathbf{k}|$. For a linear mode, such as the sound mode at small $\mathbf{k}$, this leads to a quasi-momentum-independent phase velocity at small $\mathbf{k}$ (and hence a dispersionless propagation). In contrast, this however implies a highly $|\mathbf{k}|$-dependent phase velocity, which diverges for $|\mathbf{k}| \to 0$ for any gapped mode, such as the amplitude or particle and holes modes.

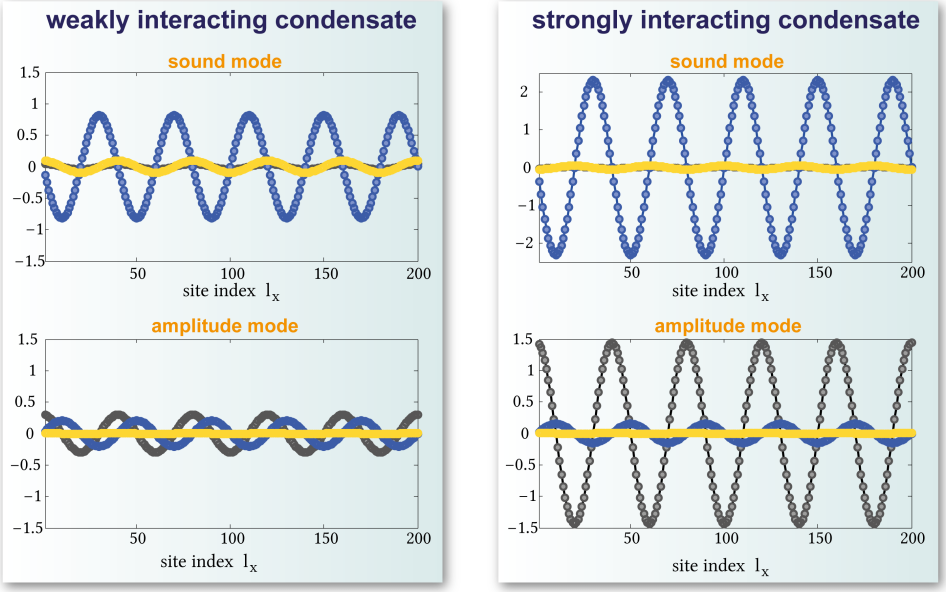

Figure 8.6: The spatial density distribution and order parameter response for a weakly interacting condensate at $6J/U = 1.45$ (left subfigures) and for the strongly interacting case $6J/U = 0.2$ (right subfigures) at integer density $n = 1$.

We are now interested in the signatures of a coherent quasi-particle state of type (8.91), for which we can calculate arbitrary expectation values. For strong excitations amplitudes, there is generally no simple scaling relation with the amplitude z. Here we restrict ourselves to the regime of weak quasi-particle excitations $|z| \ll 1$, for which we derived the quasi-particle theory. For a general operator A, with an expectation value of $A_0 = \langle\psi_0|A|\psi_0\rangle$ in the ground state, the lowest order term in the deviation of the ground state expectation value may generally scale linearly in z, i.e.

$$\langle z, \mathbf{k}, \gamma|A|z, \mathbf{k}, \gamma\rangle = A_0 + A_1 z + \mathcal{O}(z^2). \tag{8.92}$$

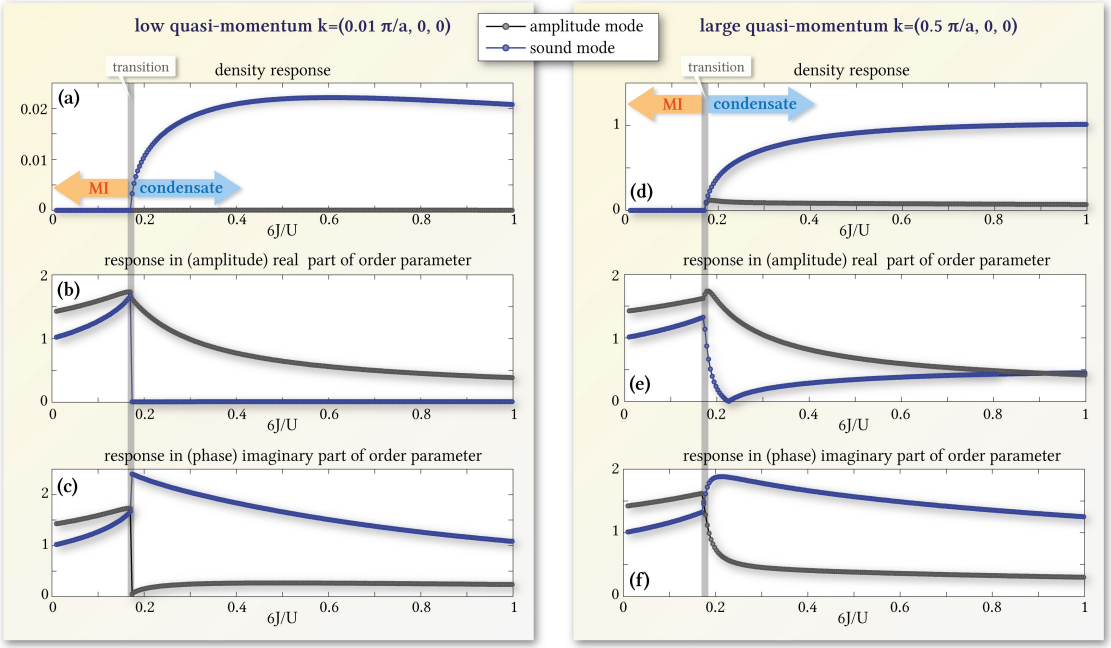

Figure 8.7: Response in density and the real and imaginary parts of the order parameter for a coherent excitation of the lowest two quasi-particle modes at integer density $n = 1$ as a function of the tunneling energy J.

To illustrate the properties of the two lowest modes in the regime of weak excitations, the response A_1 for the spatial density, as well as for the real and imaginary parts of the order parameters $\langle b_\ell \rangle$ are shown in Fig. (8.7). Both the density, as well as the order parameter oscillate spatially at the wave vector of the quasi-particle excitation $\mathbf{k}$. Thus, the amplitude of this oscillation is shown. The response of the order parameter depends on the ground state configuration of the order parameters. Here, the (dimensionless) response is shown for purely real and positive ground state order parameters, in which the case the real and imaginary parts of the response coincide with the amplitude and phase response in linear order.

The three different response quantities are shown as functions of the tunneling energy J/U for very low quasi-momentum $\mathbf{k} = (0.05, 0, 0)\pi/a$, close to zero, and for large quasi-momentum $\mathbf{k} = (0.5, 0, 0)\pi/a$, halfway between zero and the edge of the Brillouin zone. In the $|\mathbf{k}| \to 0$ limit the order parameter response features a discontinuous jump at the transition, both in the amplitude, as well as in the phase component. This discontinuity shows that the internal structure of the collective modes, which cannot be seen from the energy eigenvalue itself, undergoes a qualitative change at the phase transition and that the amplitude mode cannot be undestood as a continuation of the particle or hole mode into the condensate regime. As can be seen from Fig. (8.7b), the sound mode has a pure phase response in the $\mathbf{k} \to 0$ limit at any interaction strength. At higher momenta, it however also has a amplitude response in the order parameter, which can even outweigh the amplitude response of the amplitude mode for sufficiently weak interactions.

In contrast, the amplitude mode does **not** generally have a pure amplitude response in the order parameter for the $\mathbf{k} \to 0$ limit, but may also contain a phase component, as shown in Fig. (8.7c). It does however become a pure amplitude response in the limit of approaching the Mott transition and the $\mathbf{k} \to 0$.

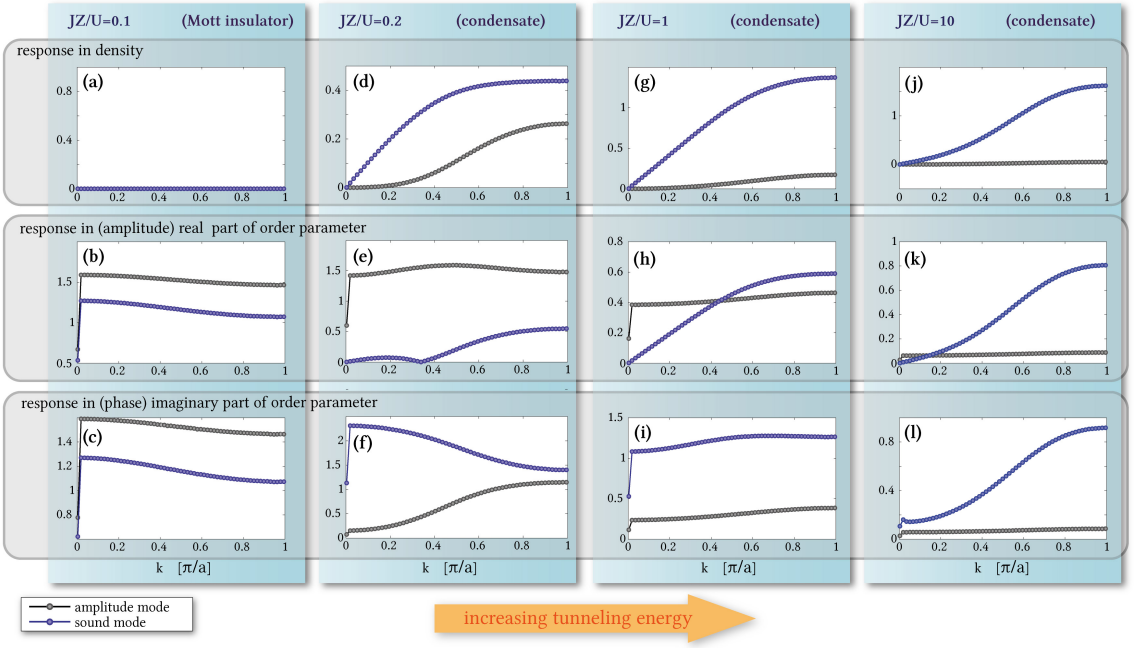

Figure 8.8: density $n = 1$ along k_x direction.

At finite quasi-momentum, the discontinuities become continuous functions at the transition, as shown in Fig. (8.7 d-f). It is interesting to note that the phase response of the amplitude mode increases when the transition is approached, which is the opposite of what happens at low momenta. The quasi-momentum dependence of these response quantities at various interaction strengths is shown in Fig. (8.8). In the Mott insulator, the density response vanishes identically for both particle and hole excitations, since the density operator is diagonal in the Gutzwiller eigenbasis and the and quasi-particle operators $\beta^\dagger_{\mathbf{k},\gamma}$ either increase or decrease the particle number by one (as becomes apparent from the quasi-particle Hamiltonian and resulting eigenvector structure). For both the sound and the amplitude mode, the density response vanishes in the $\mathbf{k} \to 0$ limit at any interaction strength. For the sound mode, the density response increases linearly at small $|\mathbf{k}|$, whereas for the amplitude mode also the derivative at $\mathbf{k} = 0$ vanishes. This implies a state featuring a density wave with a certain amplitude with a large wavelength is excited with many more quasi-particles than a comparable state with the same density wave amplitude, but at a shorter wavelength. At large quasi-momenta (outer half of the Brillouin zone) in the strongly interacting condensate, also the amplitude mode can carry a significant density response, comparable to the sound mode, as can be seen in Fig. (8.8 d). This implies that in the strongly interacting regime also the amplitude can contribute to mass transport if the associated wave packet contains high momentum components.

8.8.2 Spectral Functions

We now explicitly calculate the spectral functions for the Bose-Hubbard model within the extended quasi-particle theory approach. This is derived and discussed in appendix (L). We explicitly calculate the greater spectral function

$$\mathcal{A}^{>}_{\mathbf{k}',\mathbf{k}}(\omega) = \langle\psi_0|a_{\mathbf{k}'}\ \delta(H - E_0 - \omega)\ a^\dagger_{\mathbf{k}}|\psi_0\rangle \tag{8.93}$$

in the single-particle Bloch basis.

We begin by expressing the Bloch state creation and annihilation operators in terms of fluctuation operators

$$a^\dagger_{\mathbf{k}} = \sqrt{L}\delta_{\mathbf{k},0}B^*_{0,0}\mathbb{1} + \sum_{i>0}(B^*_{i,0}\tilde{\sigma}^{(i)}_{-\mathbf{k}} + B^*_{0,i}\tilde{\sigma}^{(i)^\dagger}_{\mathbf{k}}) + \frac{1}{\sqrt{L}}\sum_{i,j>0}(B^*_{i,j} - \delta_{i,j}B^*_{0,0})\sum_{\mathbf{k}_1}\tilde{\sigma}^{(j)^\dagger}_{\lfloor\mathbf{k}+\mathbf{k}_1\rfloor}\tilde{\sigma}^{(i)}_{\mathbf{k}_1} \tag{8.94}$$

Using the transformation relations from Eq. (8.75, 8.76) for the homogeneous condensate (in the insulator case the respective terms can again be omitted), we first consider the state

$$\begin{aligned}
a^\dagger_{\mathbf{k}}|\psi_0\rangle =& \sqrt{L}\delta_{\mathbf{k},0}B^*_{0,0}|\psi_0\rangle - \sum_{i>0,\gamma}B^*_{i,0}v_i^{(\mathbf{k},\gamma)^*}\beta^\dagger_{\mathbf{k},\gamma}|\psi_0\rangle + \sum_{i>0,\gamma}B^*_{0,i}u_i^{(\mathbf{k},\gamma)^*}\beta^\dagger_{\mathbf{k},\gamma}|\psi_0\rangle \\
&+ i\delta_{\mathbf{k},0}\sum_{i>0}B^*_{i,0}u^{(0)}_{i,\mathbf{k}}\,\mathcal{Q}|\psi_0\rangle - i\delta_{\mathbf{k},0}\sum_{i>0}B^*_{0,i}u^{(0)}_{i,\mathbf{k}}\,\mathcal{Q}|\psi_0\rangle \\
&+ \frac{1}{\sqrt{L}}\sum_{i,j>0}(B^*_{i,j} - \delta_{i,j}B^*_{0,0})\sum_{\mathbf{k}_1}\tilde{\sigma}^{(j)^\dagger}_{\lfloor\mathbf{k}+\mathbf{k}_1\rfloor}\tilde{\sigma}^{(i)}_{\mathbf{k}_1}|\psi_0\rangle
\end{aligned} \tag{8.95}$$

The last term involving two fluctuation operators is evaluated separately

$$\begin{aligned}
\tilde{\sigma}^{(j)^\dagger}_{\lfloor\mathbf{k}+\mathbf{k}_1\rfloor}\tilde{\sigma}^{(i)}_{\mathbf{k}_1}|\psi_0\rangle =& -\sum_{\gamma_1,\gamma_2}v_i^{(\mathbf{k}_1,\gamma_1)^*}u_j^{(\lfloor\mathbf{k}+\mathbf{k}_1\rfloor,\gamma_2)^*}\beta^\dagger_{\lfloor\mathbf{k}+\mathbf{k}_1\rfloor,\gamma_2}\beta^\dagger_{-\mathbf{k}_1,\gamma_1}|\psi_0\rangle \\
&+ \delta_{-\lfloor\mathbf{k}+\mathbf{k}_1\rfloor,-\mathbf{k}_1}\sum_{\gamma}v_i^{(\mathbf{k}_1,\gamma)^*}v_j^{(\lfloor\mathbf{k}+\mathbf{k}_1\rfloor,\gamma)}|\psi_0\rangle \\
&+ i\delta_{\lfloor\mathbf{k}+\mathbf{k}_1\rfloor,0}\ u^{(0)^*}_{j,0}\sum_{\gamma}v_i^{(\mathbf{k}_1,\gamma)^*}\beta^\dagger_{-\mathbf{k}_1,\gamma}\mathcal{Q}|\psi_0\rangle \\
&+ i\delta_{\mathbf{k}_1,0}\ u^{(0)}_{i,0}\sum_{\gamma}u_i^{(\lfloor\mathbf{k}+\mathbf{k}_1\rfloor,\gamma)^*}\beta^\dagger_{\lfloor\mathbf{k}+\mathbf{k}_1\rfloor,\gamma}\mathcal{Q}|\psi_0\rangle \\
&+ i\delta_{\mathbf{k}_1,0}\ \delta_{\lfloor\mathbf{k}+\mathbf{k}_1\rfloor,0}\ u^{(0)}_{i,0}\ v^{(0)^*}_{j,0}\,\mathscr{P}\mathcal{Q}|\psi_0\rangle \\
&+ \delta_{\mathbf{k}_1,0}\ \delta_{\lfloor\mathbf{k}+\mathbf{k}_1\rfloor,0}\ u^{(0)}_{i,0}\ u^{(0)^*}_{j,0}\,\mathcal{Q}\mathcal{Q}|\psi_0\rangle
\end{aligned} \tag{8.96}$$

and thus the summation over all $\mathbf{k}_1$ within the first Brillouin zone yields

$$\begin{aligned}
\sum_{\mathbf{k}_1}\tilde{\sigma}^{(j)^\dagger}_{\lfloor\mathbf{k}+\mathbf{k}_1\rfloor}\tilde{\sigma}^{(i)}_{\mathbf{k}_1}|\psi_0\rangle =& -\sum_{\gamma_1,\gamma_2,\mathbf{k}_1}v_i^{(\mathbf{k}_1,\gamma_1)^*}u_j^{(\lfloor\mathbf{k}+\mathbf{k}_1\rfloor,\gamma_2)^*}\beta^\dagger_{\lfloor\mathbf{k}+\mathbf{k}_1\rfloor,\gamma_2}\beta^\dagger_{-\mathbf{k}_1,\gamma_1}|\psi_0\rangle \\
&+ \delta_{\mathbf{k},0}\Big(-u^{(0)}_{i,0}\ v^{(0)^*}_{j,0} + \sum_{\gamma,\mathbf{k}_1}v_i^{(\mathbf{k}_1,\gamma)^*}v_j^{(\lfloor\mathbf{k}+\mathbf{k}_1\rfloor,\gamma)}\Big)|\psi_0\rangle \\
&+ i\sum_{\gamma}\Big(u^{(0)^*}_{j,0}v_i^{(-\mathbf{k},\gamma)^*} + u^{(0)}_{i,0}u_i^{(\mathbf{k},\gamma)^*}\Big)\beta^\dagger_{\mathbf{k},\gamma}\mathcal{Q}|\psi_0\rangle \\
&+ \ \delta_{\mathbf{k},0}\ u^{(0)}_{i,0}\ u^{(0)^*}_{j,0}\,\mathcal{Q}\mathcal{Q}|\psi_0\rangle
\end{aligned} \tag{8.97}$$

We now focus on the spectral function for the Mott insulating case, where a complete basis of eigenmodes exists and the operators $\mathcal{Q}$ and $\mathscr{P}$ do not appear. Here, the state in Eq. (8.95) is

$$\begin{aligned} a_{\mathbf{k}}^\dagger|\psi_0\rangle =& \delta_{\mathbf{k},0}\sqrt{L}C_0|\psi_0\rangle \\ &+ \sum_{i>0,\gamma}\left[B_{0,i}^* {u_i^{(\mathbf{k},\gamma)}}^* - B_{i,0}^* {v_i^{(\mathbf{k},\gamma)}}^*\right]\beta_{\mathbf{k},\gamma}^\dagger|\psi_0\rangle \\ &- \frac{1}{\sqrt{L}}\sum_{i,j>0}(B_{i,j}^* - \delta_{i,j}B_{0,0}^*)\sum_{\gamma_1,\gamma_2,\mathbf{k}_1} {v_i^{(-\mathbf{k}_1,\gamma_1)}}^* {u_j^{(\lfloor\mathbf{k}-\mathbf{k}_1\rfloor,\gamma_2)}}^* \beta_{\lfloor\mathbf{k}-\mathbf{k}_1\rfloor,\gamma_2}^\dagger \beta_{\mathbf{k}_1,\gamma_1}^\dagger|\psi_0\rangle \end{aligned} \tag{8.98}$$

with

$$C_0 := B_{0,0}^* + \frac{1}{L}\sum_{i,j>0}(B_{i,j}^* - \delta_{i,j}B_{0,0}^*)\Big(\sum_{\gamma,\mathbf{k}_1} {v_i^{(\mathbf{k}_1,\gamma)}}^* v_j^{(\lfloor\mathbf{k}+\mathbf{k}_1\rfloor,\gamma)}\Big) \tag{8.99}$$

$$S_{\mathbf{k},\gamma} := \sum_{i>0}\left[B_{0,i}^* {u_i^{(\mathbf{k},\gamma)}}^* - B_{i,0}^* {v_i^{(\mathbf{k},\gamma)}}^*\right] \tag{8.100}$$

$$S_{\mathbf{k}_1,\mathbf{k}_2,\gamma_1,\gamma_2} := -\frac{1}{\sqrt{L}}\sum_{i,j>0}(B_{i,j}^* - \delta_{i,j}B_{0,0}^*) {v_i^{(-\mathbf{k}_1,\gamma_1)}}^* {u_j^{(\mathbf{k}_2,\gamma_2)}}^* \tag{8.101}$$

Hence, the state becomes

$$a_{\mathbf{k}}^\dagger|\psi_0\rangle = \delta_{\mathbf{k},0}\sqrt{L}C_0|\psi_0\rangle + \sum_\gamma S_{\mathbf{k},\gamma}\beta_{\mathbf{k},\gamma}^\dagger|\psi_0\rangle + \sum_{\gamma_1,\gamma_2,\mathbf{k}_1} S_{\mathbf{k}_1,\lfloor\mathbf{k}-\mathbf{k}_1\rfloor,\gamma_1,\gamma_2}\beta_{\lfloor\mathbf{k}-\mathbf{k}_1\rfloor,\gamma_2}^\dagger\beta_{\mathbf{k}_1,\gamma_1}^\dagger|\psi_0\rangle \tag{8.102}$$

in which form the greater spectral function can be directly evaluated

$$\begin{aligned} \mathcal{A}_{\mathbf{k}',\mathbf{k}}^>(\omega) =& \delta_{\mathbf{k},0}\,\delta_{\mathbf{k}',0}\,\delta(\omega)\,L|C_0|^2 + \delta_{\mathbf{k},\mathbf{k}'}\sum_\gamma |S_{\mathbf{k},\gamma}|^2\,\delta(\omega_{\mathbf{k},\gamma} - E_0 - \omega) \\ &+ \delta_{\mathbf{k},\mathbf{k}'}\sum_{\mathbf{k}_1,\gamma_1,\gamma_2}\left[|S_{\mathbf{k}_1,\lfloor\mathbf{k}-\mathbf{k}_1\rfloor,\gamma_1,\gamma_2}^*|^2 + S_{\lfloor\mathbf{k}-\mathbf{k}_1\rfloor,\mathbf{k}_1,\gamma_2,\gamma_1}^*\,S_{\mathbf{k}_1,\lfloor\mathbf{k}-\mathbf{k}_1\rfloor,\gamma_1,\gamma_2}\right] \\ &\times \delta(\omega_{\mathbf{k}_1,\gamma_1} + \omega_{\lfloor\mathbf{k}-\mathbf{k}_1\rfloor,\gamma_2} - E_0 - \omega) \end{aligned} \tag{8.103}$$

The calculation of the greater spectral function in the condensate regime entails more terms (corresponding to the $\mathscr{P}$ and $\mathcal{Q}$ operators), which becomes rather technical and is not explicated here. The lesser spectral function is essentially analogous up to an interchange of $b_{\boldsymbol{\ell}}$ and $b_{\boldsymbol{\ell}}^\dagger$ and a minus sign in the frequency. Subsequently, the full spectral function is the difference of the greater and the lesser spectral functions

$$\mathcal{A}_{\boldsymbol{\ell},\boldsymbol{\ell}'}(\omega) = \theta(\omega)\,\mathcal{A}_{\boldsymbol{\ell},\boldsymbol{\ell}'}^>(\omega) - \theta(-\omega)\,\mathcal{A}_{\boldsymbol{\ell},\boldsymbol{\ell}'}^<(\omega). \tag{8.104}$$

The terms of the first line of Eq. (8.103) simply correspond to a weighted delta-peak positioned along the dispersion relation. On the other hand, the lower two lines of this equation contribute to a broad background of two-particle processes. This term is fundamentally different from and does not appear in the weakly interacting case within Bogoliubov theory. Whereas in Bogoliubov theory removing or adding a particle to the ground state results in a state containing a single quasi-particle, this is not the case within this extended quasi-particle theory, as Eq. (8.102) also contains a contribution of a state containing two quasi-particles.

Green's Functions

As derived in appendix (L), the time-ordered, retarded and advanced Green's functions can explicitly be given in terms of the spectral function as

$$G_{\boldsymbol{\ell},\boldsymbol{\ell}'}(\omega) = \int_{-\infty}^{\infty} d\omega'\,\frac{\mathcal{A}_{\boldsymbol{\ell},\boldsymbol{\ell}'}(\omega')}{\omega - \omega' + i0^+\,\mathrm{sgn}(\omega' - \mu)} \tag{8.105}$$

$$G_{\boldsymbol{\ell},\boldsymbol{\ell}'}^{r\atop a}(\omega) = \int_{-\infty}^{\infty} d\omega'\,\frac{\mathcal{A}_{\boldsymbol{\ell},\boldsymbol{\ell}'}(\omega')}{\omega - \omega' \pm i0^+}. \tag{8.106}$$

8.8.3 Single-Particle Density of States

The positive frequency part of the single particle density of states for a given many-particle state $|\psi_0^{(N)}\rangle$ containing N particles, is a measure for the number of many particle eigenstates per energy interval in the $(N+1)$-particle subspace, which are all weighted by a certain overlap factor as discussed in appendix (L.5). For a non-interacting system, this simply reproduces the intuitive result, which is the density of single-particle states per unit energy. The non-interacting density of states for the 1D, 2D and 3D hypercubic lattices is shown in Fig. (8.9).

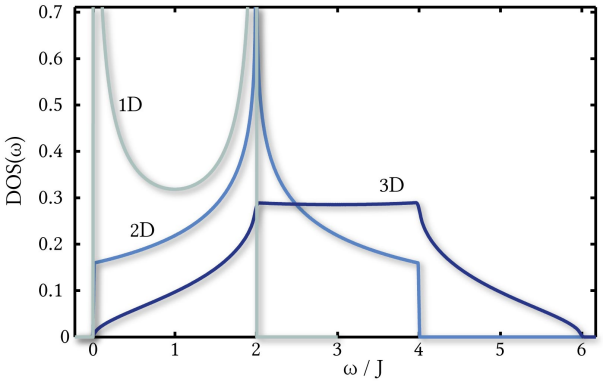

Figure 8.9: The non-interacting single-particle density of states on hypercubic lattices in one, two and three dimensions. Clearly, their shape is qualitatively different.

We are now however interested in how the spectral function changes in the presence of interactions. In Fig. (8.10) we plot the positive part of the single particle DOS for various interaction strengths at fixed filling, associated with the larger the spectral function in Eq. (8.103).

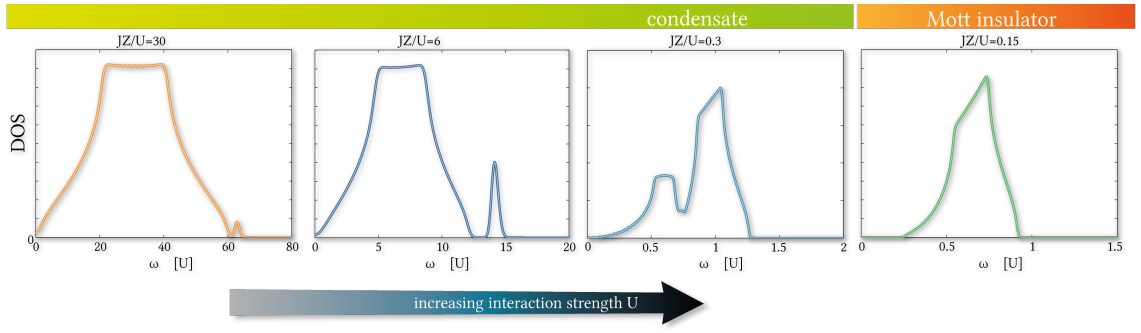

Figure 8.10: The positive frequency part of the single particle DOS for the homogeneous system at integer filling $n = 1$ for different interaction strengths JZ/U. Note the evolution of the amplitude mode with decreasing interaction strength: In the very strongly interacting condensate at $JZ/U = 0.3$, it corresponds to the peak at higher energy and carries more spectral weight than the sound mode in this regime. With decreasing interaction strength, it continuously looses spectral weight and transforms into a small peak just above the wide peak, corresponding to the sound mode. Scaled in units of U, its width also decreases with decreasing U/JZ. The DOS in the Mott insulator, shown on the right, corresponds to the particle mode quasi-particles and the spectrum possesses a finite gap, in contrast to the condensate regime.

8.8.4 Dynamic Structure Factor

The dynamic structure factor is the discrete spatial Fourier transform of the on-site density operator $\hat{n}_{\boldsymbol{\ell}} = b^\dagger_{\boldsymbol{\ell}} b_{\boldsymbol{\ell}}$

$$S(\mathbf{k},\omega) = \frac{1}{2\pi}\sum_{\boldsymbol{\ell},\boldsymbol{\ell}'}\int_{-\infty}^{\infty} dt\, e^{i\omega t}\, e^{i\mathbf{k}\cdot(\mathbf{R}_{\boldsymbol{\ell}'}-\mathbf{R}_{\boldsymbol{\ell}})}\, \langle\psi_0|\hat{n}_{\boldsymbol{\ell}}(t)\,\hat{n}^\dagger_{\boldsymbol{\ell}'}(0)|\psi_0\rangle, \tag{8.107}$$

where the density operators are in the Heisenberg representation. This is of the same structure as the single particle Green's function, except that the local density operators take on the role of the bosonic creation and annihilation operators. Subsequently, the calculation of the dynamic structure factor within the extended quasi-particle theory proceeds in the same fashion, except for these matrix elements, and is not repeated here.

8.8.5 Single Particle Density Matrix

In principle, all expectation values of single particle operators are contained in the single particle density matrix, which is the equal time Green's function. Here, we however calculate the single particle density matrix in a different way, to minimize the deviation induced in the result by the non-bosonic nature of the quasi-particle operators. The single-particle density matrix depends on two single-particle basis indices and transforms like a second order tensor under unitary single particle basis transformations. We explicitly calculate it in the lowest band Wannier basis, where it is defined by

$$\rho_{\boldsymbol{\ell},\boldsymbol{\ell}'} = \langle b^\dagger_{\boldsymbol{\ell}} b_{\boldsymbol{\ell}'}\rangle. \tag{8.108}$$

The expectation value is to be taken in the quasi-particle ground state $|0\rangle$. For the explicit calculation of the matrix elements, we distinguish two qualitatively different cases.

Diagonal Elements

The elements on the diagonal ($\boldsymbol{\ell} = \boldsymbol{\ell}'$) of the single-particle density matrix simply correspond to the on-site density of particles on the respective lattice site. For a translationally invariant system and excluding the possibility of a spontaneous formation of a density wave (which does not occur for the single component Bose-Hubbard model), the density is homogeneous and

$$\rho_{\boldsymbol{\ell},\boldsymbol{\ell}} = \langle b^\dagger_{\boldsymbol{\ell}} b_{\boldsymbol{\ell}}\rangle = \frac{N}{L}, \tag{8.109}$$

where N is the total number of particles and L the number of sites. This result is exact and we can circumvent the explicit calculation of the matrix elements within the quasi-particle theory.

Off-Diagonal Elements

On the other hand, the off-diagonal elements of $\rho_{\boldsymbol{\ell},\boldsymbol{\ell}'}$ with $\boldsymbol{\ell} \neq \boldsymbol{\ell}'$, have to be evaluated explicitly. We express the local Wannier creation and annihilation operators in terms of fluctuation operators using the relations in Eqns. (8.13-8.16)

$$b^\dagger_{\boldsymbol{\ell}} = B^*_{0,0}\mathbb{1} + \sum_{i>0}\left(B^*_{i,0}\sigma^{(i)}_{\boldsymbol{\ell}} + B^*_{0,i}{\sigma^{(i)}_{\boldsymbol{\ell}}}^\dagger\right) + \sum_{i,j>0}\left(B^*_{i,j} - \delta_{i,j}B^*_{0,0}\right){\sigma^{(j)}_{\boldsymbol{\ell}}}^\dagger\sigma^{(i)}_{\boldsymbol{\ell}}. \tag{8.110}$$

We now evaluate the off-diagonal elements

$$\begin{aligned}\langle b^\dagger_{\boldsymbol{\ell}} b_{\boldsymbol{\ell}'}\rangle = \Big\langle &\Big[B^*_{0,0}\mathbb{1} + \sum_{i>0}\left(B^*_{i,0}\sigma^{(i)}_{\boldsymbol{\ell}} + B^*_{0,i}{\sigma^{(i)}_{\boldsymbol{\ell}}}^\dagger\right) + \sum_{i,j>0}\left(B^*_{i,j} - \delta_{i,j}B^*_{0,0}\right){\sigma^{(j)}_{\boldsymbol{\ell}}}^\dagger\sigma^{(i)}_{\boldsymbol{\ell}}\Big]\\ \times &\Big[B_{0,0}\mathbb{1} + \sum_{i'>0}\left(B_{i',0}{\sigma^{(i')}_{\boldsymbol{\ell}'}}^\dagger + B_{0,i'}\sigma^{(i')}_{\boldsymbol{\ell}'}\right) + \sum_{i',j'>0}\left(B_{i',j'} - \delta_{i',j'}B_{0,0}\right){\sigma^{(i')}_{\boldsymbol{\ell}'}}^\dagger\sigma^{(j')}_{\boldsymbol{\ell}'}\Big]\Big\rangle\end{aligned} \tag{8.111}$$

taking all terms up to second order in the fluctuation operators σ and their conjugates into account. Since in the transformation between these fluctuations operators and the quasi-particle operators β and $\beta^\dagger$ is linear, this guarantees that all terms up to second order in the quasi-particle operators are taken along. Another advantage of evaluating the matrix elements in the single particle Wannier basis is the property that, by construction, all fluctuation operators on different sites commute exactly. We thus bring them into normal order before transforming into the Bloch basis. Furthermore, when evaluating the operators in the ground state $|0\rangle$, all terms of first order in σ and $\sigma^\dagger$ vanish identically. Up to second order, one thus obtains

$$\begin{aligned}\langle b_{\boldsymbol{\ell}}^\dagger b_{\boldsymbol{\ell}'}\rangle &= |B_{0,0}|^2 + B_{0,0}^* \sum_{i',j'>0} \left(B_{i',j'} - \delta_{i',j'} B_{0,0}\right) \langle {\sigma_{\boldsymbol{\ell}'}^{(i')}}^\dagger \sigma_{\boldsymbol{\ell}'}^{(j')}\rangle \\ &+ B_{0,0} \sum_{i,j>0} \left(B_{i,j}^* - \delta_{i,j} B_{0,0}^*\right) \langle {\sigma_{\boldsymbol{\ell}}^{(j)}}^\dagger \sigma_{\boldsymbol{\ell}}^{(i)}\rangle \\ &+ \sum_{i,j>0} \Big[B_{i,0}^* B_{j,0} \langle {\sigma_{\boldsymbol{\ell}'}^{(j)}}^\dagger \sigma_{\boldsymbol{\ell}}^{(i)}\rangle + B_{i,0}^* B_{0,j} \langle \sigma_{\boldsymbol{\ell}}^{(i)} \sigma_{\boldsymbol{\ell}'}^{(j)}\rangle + B_{0,i}^* B_{j,0} \langle {\sigma_{\boldsymbol{\ell}}^{(i)}}^\dagger {\sigma_{\boldsymbol{\ell}'}^{(j)}}^\dagger\rangle + B_{0,i}^* B_{0,j} \langle {\sigma_{\boldsymbol{\ell}}^{(i)}}^\dagger \sigma_{\boldsymbol{\ell}'}^{(j)}\rangle\Big] \\ &+ \mathcal{O}(\sigma^3).\end{aligned} \tag{8.112}$$

We now evaluate the individual expectation values individually by expressing the fluctuation operators in terms of quasi-particle, $\mathscr{P}$ and $\mathcal{Q}$ operators. It turns out that when taking the additional property $\mathrm{Tr}\,(\rho) = N$ into account, the $\mathscr{P}$ and $\mathcal{Q}$ operators, which only operate in the $\mathbf{k} = 0$ sector, do not have to be taken into account explicitly. We thus omit them in the following and determine the only matrix element, to which they would contribute in the Bloch representation of the single-particle density matrix from

$$\langle a_{\mathbf{k}=0}^\dagger a_{\mathbf{k}=0}\rangle = N - \sum_{\mathbf{k}\neq 0} \langle a_{\mathbf{k}}^\dagger a_{\mathbf{k}}\rangle. \tag{8.113}$$

Using the transformation to quasi-momentum fluctuation operators in Eq. (8.9) and Eqns. (8.76,8.75), we find

$$\langle {\sigma_{\boldsymbol{\ell}}^{(i)}}^\dagger \sigma_{\boldsymbol{\ell}'}^{(j)}\rangle = \frac{1}{L} \sum_{\mathbf{k}} e^{-i\mathbf{k}\cdot(\mathbf{R}_{\boldsymbol{\ell}} - \mathbf{R}_{\boldsymbol{\ell}'})} \sum_\gamma v_i^{(\mathbf{k},\gamma)}\, v_j^{(\mathbf{k},\gamma)^*} \tag{8.114}$$

$$\langle \sigma_{\boldsymbol{\ell}}^{(i)} \sigma_{\boldsymbol{\ell}'}^{(j)}\rangle = -\frac{1}{L} \sum_{\mathbf{k}} e^{i\mathbf{k}\cdot(\mathbf{R}_{\boldsymbol{\ell}} - \mathbf{R}_{\boldsymbol{\ell}'})} \sum_\gamma u_i^{(\mathbf{k},\gamma)}\, v_j^{(\mathbf{k},\gamma)^*} \tag{8.115}$$

$$\langle {\sigma_{\boldsymbol{\ell}}^{(i)}}^\dagger {\sigma_{\boldsymbol{\ell}'}^{(j)}}^\dagger\rangle = -\frac{1}{L} \sum_{\mathbf{k}} e^{i\mathbf{k}\cdot(\mathbf{R}_{\boldsymbol{\ell}} - \mathbf{R}_{\boldsymbol{\ell}'})} \sum_\gamma u_j^{(\mathbf{k},\gamma)^*}\, v_i^{(\mathbf{k},\gamma)}. \tag{8.116}$$

The Full Single-Particle Density Matrix

Combining the diagonal and off-diagonal case, the single particle density matrix in combined form can thus be written

$$\begin{aligned}\rho_{\boldsymbol{\ell},\boldsymbol{\ell}'} = \delta_{\boldsymbol{\ell},\boldsymbol{\ell}'} \frac{N}{L} + (1 - \delta_{\boldsymbol{\ell},\boldsymbol{\ell}'}) \Big[&|B_{0,0}|^2 + \frac{1}{L} B_{0,0}^* \sum_{i,j>0} \left(B_{i,j} - \delta_{i,j} B_{0,0}\right) \sum_{\mathbf{k}_1,\gamma} v_i^{(\mathbf{k}_1,\gamma)}\, v_j^{(\mathbf{k}_1,\gamma)^*} \\ &+ \frac{1}{L} B_{0,0} \sum_{i,j>0} \left(B_{i,j}^* - \delta_{i,j} B_{0,0}^*\right) \sum_{\mathbf{k}_1,\gamma} v_j^{(\mathbf{k}_1,\gamma)}\, v_i^{(\mathbf{k}_1,\gamma)^*} + \frac{1}{L} \sum_{\mathbf{k}_1} e^{-i\mathbf{k}_1\cdot(\mathbf{R}_{\boldsymbol{\ell}} - \mathbf{R}_{\boldsymbol{\ell}'})} N_{\mathbf{k}_1}\Big]\end{aligned} \tag{8.117}$$

where we defined

$$\begin{aligned}N_{\mathbf{k}} = \sum_{i,j>0} \Big[&B_{i,0}^* B_{j,0} \sum_\gamma v_j^{(\mathbf{k},\gamma)}\, v_i^{(\mathbf{k},\gamma)^*} + B_{0,i}^* B_{0,j} \sum_\gamma v_i^{(-\mathbf{k},\gamma)}\, v_j^{(-\mathbf{k},\gamma)^*} \\ &- B_{i,0}^* B_{0,j} \sum_\gamma u_i^{(\mathbf{k},\gamma)}\, v_j^{(-\mathbf{k},\gamma)^*} - B_{0,i}^* B_{j,0} \sum_\gamma v_i^{(-\mathbf{k},\gamma)}\, u_j^{(\mathbf{k},\gamma)^*}\Big].\end{aligned} \tag{8.118}$$

The first three terms in the square brackets in Eq. (8.117) only contribute in the condensed phase and give rise to the constant background term, often referred to as of-diagonal long-range order in the condensate. The last term in the square brackets, which is the spatial Fourier transform of $N_{\mathbf{k}}$ arises from the non-trivial quasi-particle correlations in the different modes and is present in both the condensate and the Mott-insulator at any non-zero J/U. Also note that the sum rule $\sum_{\boldsymbol{\ell}} \rho_{\boldsymbol{\ell},\boldsymbol{\ell}} = N$ is exactly fulfilled.

The Single-Particle Density Matrix in Quasi-Momentum Space

In momentum space, the single particle density matrix is related to its Wannier space counterpart in Eq. (8.117) by

$$\begin{aligned}
\tilde{\rho}_{\mathbf{k},\mathbf{k}'} =& \langle a_{\mathbf{k}}^\dagger \, a_{\mathbf{k}'} \rangle \\
=& \frac{1}{L} \sum_{\boldsymbol{\ell},\boldsymbol{\ell}'} e^{i(\mathbf{k}\cdot\mathbf{R}_{\boldsymbol{\ell}} - \mathbf{k}'\cdot\mathbf{R}_{\boldsymbol{\ell}'})} \rho_{\boldsymbol{\ell},\boldsymbol{\ell}'} \\
=& \delta_{\mathbf{k},\mathbf{k}'} (L\,\delta_{\mathbf{k},0} - 1) \Big[|B_{0,0}|^2 + \frac{1}{L} B_{0,0}^* \sum_{i,j>0} (B_{i,j} - \delta_{i,j} B_{0,0}) \sum_{\mathbf{k}_1,\gamma} v_i^{(\mathbf{k}_1,\gamma)} \, v_j^{(\mathbf{k}_1,\gamma)^*} \\
&+ \frac{1}{L} B_{0,0} \sum_{i,j>0} \left(B_{i,j}^* - \delta_{i,j} B_{0,0}^* \right) \sum_{\mathbf{k}_1,\gamma} v_j^{(\mathbf{k}_1,\gamma)} \, v_i^{(\mathbf{k}_1,\gamma)^*} \Big] + \delta_{\mathbf{k},\mathbf{k}'} \, N_{\mathbf{k}} + \delta_{\mathbf{k},\mathbf{k}'} \left[\frac{N}{L} - \frac{1}{L} \sum_{\mathbf{k}_1} N_{\mathbf{k}_1} \right].
\end{aligned} \tag{8.119}$$

8.8.6 The Quasi-Momentum Distribution

The explicit form of the single particle density matrix in quasi-momentum space shows that the only non-vanishing elements appear on the diagonal. This is nothing but the quasi-momentum distribution

$$\begin{aligned}
n(\mathbf{k}) &= \langle a_{\mathbf{k}}^\dagger \, a_{\mathbf{k}} \rangle \\
&= N_{\mathbf{k}} + \left[\frac{N}{L} - \frac{1}{L} \sum_{\mathbf{k}_1} N_{\mathbf{k}_1} \right] + (L\,\delta_{\mathbf{k},0} - 1) \Big[|B_{0,0}|^2 + \frac{1}{L} B_{0,0}^* \sum_{i,j>0} (B_{i,j} - \delta_{i,j} B_{0,0}) \\
&\times \sum_{\mathbf{k}_1,\gamma} v_i^{(\mathbf{k}_1,\gamma)} \, v_j^{(\mathbf{k}_1,\gamma)^*} + \frac{1}{L} B_{0,0} \sum_{i,j>0} \left(B_{i,j}^* - \delta_{i,j} B_{0,0}^* \right) \sum_{\mathbf{k}_1,\gamma} v_j^{(\mathbf{k}_1,\gamma)} \, v_i^{(\mathbf{k}_1,\gamma)^*} \Big].
\end{aligned} \tag{8.120}$$

It is interesting to note that for the homogeneous system, the entire information of any single-particle measurement is thus contained in the quasi-momentum distribution. Typical momentum distributions at constant integer filling for the homogeneous Bose-Hubbard model are shown in Fig. (8.11).

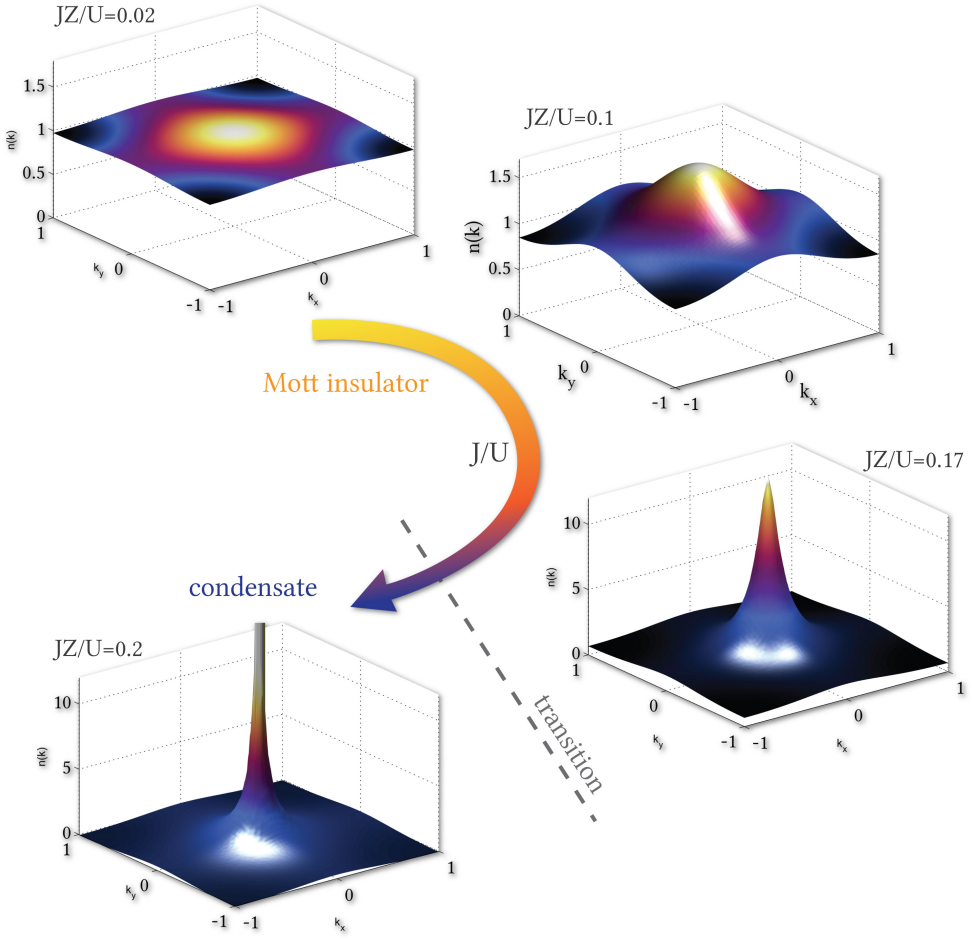

Figure 8.11: The quasi-momentum distributions $n(\mathbf{k})$ for the 3D Bose-Hubbard model at an integer filling of $n = 1$, shown for the $k_z = 0$ plane for various ratios of JZ/U. In contrast to the quasi-momentum distributions obtained from Gutzwiller theory, the quasi-particle theory results leads to non-trivial (i.e. non-constant) distributions in the MI at any finite JZ/U. As the system approaches the phase boundary in the MI, shown shown in the upper three figures, the particle-hole modes become occupied by an increasing number of quasi-particles in the ground state, an effect which becomes stronger for small $\mathbf{k}$. Although the quasi-momentum profile for $JZ/U = 0.17$ features a pronounced peak at $\mathbf{k} = 0$, none of the quasi-particle modes is macroscopically occupied yet. As the transition into the condensate is crossed, a macroscopic number of particles occupies the (**single**) $\mathbf{k} = 0$ mode. This is reflected by an additional delta-peak in $n(\mathbf{k})$ at $\mathbf{k} = 0$, which is however not directly visible in the lowest figure, due to its singular structure. The population of the quasi-particle modes diverges with decreasing $|\mathbf{k}|$, although any mode at non-zero $\mathbf{k}$ is not macroscopically populated.

8.9 Deviation of the Quasi-Particle Ground State from the Gutzwiller Ground State

As in Bogoliubov theory, the consistency of the theory can be verified retrospectively. The assumption for the validity of the expansion of the Bose-Hubbard Hamiltonian in different order of the fluctuation operators, relies on the fact that these fluctuations are small, i.e. that the fluctuation modes are sparsely populated. Within Bogoliubov theory, this can be quantified by the number

of particles in modes other than the condensate $\sum_{\mathbf{k}\neq 0}\langle a_{\mathbf{k}}^\dagger a_{\mathbf{k}}\rangle$. The analogous quantity within this theory is

$$\left\langle -\sum_{i>0}\sigma_{\boldsymbol{\ell}}^{(i)\dagger}\sigma_{\boldsymbol{\ell}}^{(i)}\right\rangle = \frac{1}{L}\sum_{\mathbf{k},\gamma}\sum_{i>0}|v_i^{(\mathbf{k},\gamma)}|^2, \tag{8.121}$$

where Eq. (8.114) was used to obtain this expression. It does not have the simple interpretation as the number of non-condensed particles, which is a desirable property, since we also want to be able to perform the fluctuation expansion around a depleted state. That is, even if no fluctuations were present, corresponding to the Gutzwiller state, this state may already have a finite depletion. In an extreme form, it may even be an insulating state with a condensate fraction of zero. Much rather, the quantity in Eq. (8.121) should be understood on the level of many-body states: The set of all Gutzwiller states constitutes a perfectly valid basis of the many-body Hilbert space, in which the true many-body ground state could be expressed. Eq. (8.121) is exactly the modulus squared amplitude of the quasi-particle ground state lying outside of the one-dimensional subspace of the Gutzwiller ground state. In other words, it is one minus the overlap of the quasi-particle ground state with the Gutzwiller ground state.

Except in the non-interacting and the zero-tunneling limit, the quasi-particle ground state is not the true ground state. It does however give a good approximation beyond the Gutzwiller state, which we know to be good if the control parameter in Eq. (8.121) is small in comparison to one. Since this can be explicitly calculated after performing the fluctuation expansion, the consistency can be verified.

8.10 Results for the Two-Species Case

We now shortly discuss results for the two-component bosonic case, described by the Hamiltonian

$$\begin{aligned}\mathcal{H} = &\sum_{\boldsymbol{\ell}}\left[\frac{U_a}{2}b_{\boldsymbol{\ell}}^{(a)\dagger}b_{\boldsymbol{\ell}}^{(a)\dagger}b_{\boldsymbol{\ell}}^{(a)}b_{\boldsymbol{\ell}}^{(a)} - \mu_a\, b_{\boldsymbol{\ell}}^{(a)\dagger}b_{\boldsymbol{\ell}}^{(a)}\right] - J_a\sum_{\langle\boldsymbol{\ell},\boldsymbol{\ell}'\rangle}(b_{\boldsymbol{\ell}}^{(a)\dagger}b_{\boldsymbol{\ell}'}^{(a)} + b_{\boldsymbol{\ell}'}^{(a)\dagger}b_{\boldsymbol{\ell}}^{(a)})\\ &+\sum_{\boldsymbol{\ell}}\left[\frac{U_b}{2}b_{\boldsymbol{\ell}}^{(b)\dagger}b_{\boldsymbol{\ell}}^{(b)\dagger}b_{\boldsymbol{\ell}}^{(b)}b_{\boldsymbol{\ell}}^{(b)} - \mu_b\, b_{\boldsymbol{\ell}}^{(b)\dagger}b_{\boldsymbol{\ell}}^{(b)}\right] - J_b\sum_{\langle\boldsymbol{\ell},\boldsymbol{\ell}'\rangle}(b_{\boldsymbol{\ell}}^{(b)\dagger}b_{\boldsymbol{\ell}'}^{(b)} + b_{\boldsymbol{\ell}'}^{(b)\dagger}b_{\boldsymbol{\ell}}^{(b)})\\ &+U_{ab}\sum_{\boldsymbol{\ell}}b_{\boldsymbol{\ell}}^{(a)\dagger}b_{\boldsymbol{\ell}}^{(a)}b_{\boldsymbol{\ell}}^{(b)\dagger}b_{\boldsymbol{\ell}}^{(b)}.\end{aligned} \tag{8.122}$$

The two species a and b are both described by a Bose-Hubbard Hamiltonian with intra-species interaction energies U_{ab} and U_b, as well as tunneling energies J_a and J_b. Additionally, there is an intra-species on-site interaction with an energy U_{ab}. We perform the analogous quasi-particle theory derivation for the two-particle case, where the local Hilbert space for each site is given by the direct product space of the local Hilbert spaces of each component. The procedure is largely analogous and we will not discuss it in detail here.

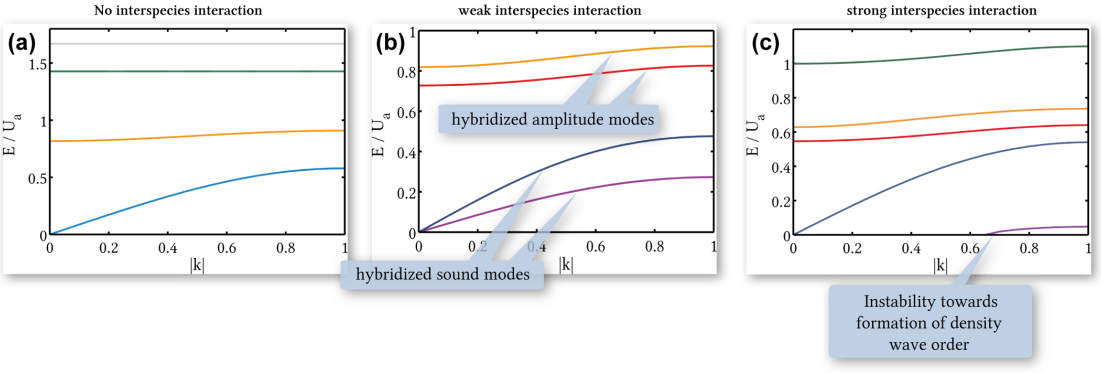

Figure 8.12: Dispersion relations of the collective modes of a two-component Bose mixture with repulsive interactions along the $\mathbf{k} = |\mathbf{k}|\mathbf{e}_x$ direction. For all plots we chose $J_a = J_b = 0.05U_a$, $\mu_a = \mu_b = 0.5U_a$ and $U_b = U_a$. The three subfigures correspond to different interaction strengths. Without inter-species interactions (subfigure (a)) $U_{ab} = 0$, the system corresponds to two separate although identical single-species systems and the collective mode energies lie above one another. For weak inter-species interactions $U_{ab} = 0.5U_a$ (subfigure (b)), the collective modes involve both species and all modes are hybridized and split up energetically. For strong interactions $U_{ab} = 1.5$ (subfigure (c)) the lowest hybridized sound mode only emerges at finite $\mathbf{k}$, indicating an instability with a diverging susceptibility towards a different state at lower momenta.

In Fig. (8.12), we restrict ourselves to identical parameters in the condensate regime for both species and vary the inter-species interaction. A homogeneous mean-field ground state is assumed, above which the fluctuation expansion is performed. For a weak, but non-zero interaction, the collective modes, which lie above one another for the non-interacting case split up energetically. Neither of them can be associated with the dynamics of a one of the two species alone, but they both are collective excitations of the two species combined, i.e. hybridized sound and amplitude modes of the two species' individual sound and amplitude modes. The energetically lower modes involve an order parameter and density fluctuation of the two species which is out of phase (i.e. in the regions where the density of species a is increased, that of species b is decreased), whereas the energetically higher modes correspond to an in phase oscillation of the two species' density and order parameters fluctuations. With increasing U_{ab} the speed of sound in the condensate (i.e. the slope of the lower sound mode at $\mathbf{k} = 0$ in this case) is reduced up to a critical U_{ab} where an interesting feature appears: beyond this inter-species interaction strength the lower sound mode only emerges at positive energies at a non-zero quasi-momentum. This indicates an energetic instability at low $\mathbf{k}$ and may signal the formation of a density wave. Further investigation to whether the extended quasi-particle theory is also able to capture magnetic ordering in the Mott insulator and other phases beyond the reach of bosonic Gutzwiller theory is of high interest.

8.11 Conclusion

In the last two chapters, we have developed an alternative quasi-particle theory (in contrast to Bogoliubov theory), which is also applicable to the Bose-Hubbard model for strong interactions. In fact, the procedure by which we derived it building upon a variational state (here: the bosonic Gutzwiller state) is generic.

The classical route consists of finding some variational state which captures the relevant degrees of freedom, and explicitly parametrize it by real or complex variables. One then allows these variational parameters to acquire a time dependence and evaluates the energy, yielding a classical energy function. Furthermore, evaluating the relevant term containing the temporal derivative of the variational state, one explicitly obtains the classical action in terms of the scalar variables, from which the equations of motion can be derived. Determining the energy minimum of the static variables yields the corresponding mean-field solution and linearizing the equations of motion for small fluctuations around this minimum and subsequently quantizing the classical fields to bosonic fields, gives rise to a quasi-particle theory, living on top of this mean-field solution.

The analogous quantum route was taken in this chapter. Typically, mean-field theories can be formulated either variationally (with the variational state determined by minimizing the energy) or in a self-consistent fashion. In the latter case, one obtains a mean-field Hamiltonian, which being an hermitian operator on the entire many-particle space, possesses a basis of eigenstates. The lowest of these is the mean-field state, being identical to the variational form in the alternative formulation. However, one can now systematically go beyond mean-field theory: the entire original Hamiltonian can always be expressed in terms of the entire set of mean-field eigenstates. The tricky part[4] in deriving the quasi-particle theory on a quantum level consists of defining the appropriate fluctuation

[4]At least to the author before this procedure was clear to him.

operators. These promote transitions between the various mean-field eigenstates and should behave bosonically in some physically meaningful limit. Furthermore, they should be complete in the sense, that an arbitrary operator on the many-body Hilbert space can be expressed in terms of them. If chosen correctly, their time-dependent expectation values in the Heisenberg picture correspond to the scalar fluctuation amplitudes in the time-dependent classical approach.

The quasi-particle Hamiltonian is generally obtained by expressing the entire Hamiltonian in terms of the fluctuation operators and discarding all terms containing more than two. Finding the Jordan normal basis of symplectic norm matrix Σ multiplied by the coefficient matrix yields the quasi-particle eigenenergies and quasi-particle creation and annihilation operators. If the original fluctuation operators approximately obeyed bosonic statistics, this property carries over to the quasi-particle operators. Since a non-normal matrix is diagonalized, spurious modes corresponding to a collective motion and not possessing a bosonic character may also arise.

The art of constructing a suitable and rich quasi-particle theory for a given system substantially depends on the variational state and mean-field theory it is built upon. Restricting the variational state to a low number of parameters may not capture all relevant degrees of freedom and quasi-particle modes. On the other hand, if the number of variational parameters is chosen larger than the number of single-particle modes available to the system, it is fundamentally impossible that the resulting quasi-particles will be true bosons.

Let us exemplify this with an extreme case of the most general variational state: the state consisting of the superposition of all states within a full many-particle basis with the variational parameters being the coefficients. The fluctuation operators would correspond to the quasi-particle creation and annihilation operators and cause transitions between the exact many-body ground state and the excited states. Each quasi-particle state, being an exact eigenstate, would bei infinitely long lived, but not of a bosonic nature at all, as it could contain at maximum one excitation quantum.

There is thus a trade-off between not capturing all physically relevant excitations and obtaining a technically more complicated theory (but richer in physical phenomena), where the bosonic character of the excitations is furthermore reduced if too many degrees of freedom are incorporated. It is generally not guaranteed that a simple quasi-particle theory, capturing all relevant excitations exists. This is for example often encountered in solid state physics, where Fermi liquid theory is known to break down for certain systems.

Constructing the appropriate quasi-particle theory for a given interacting system is thus somewhat of an art and strongly depends on the regime one considers. The theory we have derived within the last two chapters is most likely the simplest systematic quasi-particle beyond Bogoliubov theory, which contains higher excitations, such as the amplitude mode in the condensate.

9. Probing Strongly Interacting Lattice Bosons with Bragg Spectroscopy

9.1 Introduction to Bragg Spectroscopy

With the remarkable control that has been achieved over cold atom systems in recent years, probing techniques to gain insight into the many-body quantum phases play an important role in understanding these systems. In solid state systems, spectroscopic techniques such as angle resolved photoemission spectroscopy and neutron scattering have been established as reference methods for providing energy and momentum resolved insight into the excitational structure of materials. Recently, spectroscopic techniques have also been applied successfully to ultracold atoms, such as radio frequency spectroscopy [156], lattice shaking [157, 140], as well as several experiments using Bragg spectroscopy [46, 31, 47, 155, 120, 87, 154]. Initially, the latter was performed on weakly interacting condensates [155, 154], then extended to strong interactions without a lattice [120]. In more recent experiments, these studies have also been extended to ultracold atoms in optical lattices [46, 31, 47, 137, 166, 129, 133, 98, 177, 79], which opens up the possibility of studying a number of models with strong correlations from condensed matter theory. Up to now, these Bragg spectroscopic experiments have, however, been focused on weakly interacting condensates [46, 31, 47] or the Mott insulating (MI) [31] regime. Here, we investigate the excitational structure of a strongly interacting lattice superfluid (SF) and, for the first time, clearly identify the recently described **amplitude mode** [80, 79, 78, 74, 143, 28, 125, 66, 65, 115, 118].

In the Bogoliubov regime $U/J \ll 1$, the gapless sound mode, corresponding to the excitation of Bogoliubov quasiparticles in a lattice has been investigated experimentally [46, 31, 47]. Intermediate lattice depths allow for the realization of a strongly interacting SF beyond the realm of Bogoliubov theory, exhibiting a rich excitational structure: In addition to the gapless sound mode, the existence of the gapped 'amplitude' mode in the Bose-Hubbard Model (within the lowest band), generated by a physically similar mechanism as the Higgs boson in high energy physics [79, 80, 78], has been a topic of high interest in recent literature [80, 79, 78, 74, 143, 28, 125, 66, 65, 115, 118]. However, linear response calculations in the perturbative limit have suggested that this mode cannot be addressed in a momentum-resolved fashion with Bragg spectroscopy [80] and there has been no clear experimental signature in previous measurements [31]. To bridge the gap between existing idealized theory predictions and our experimental observations, we address a number of important experimental effects in our simulations: 1) the high probing beam intensity; 2) spatial inhomogeneities, such as the harmonic trapping potential breaking the translational symmetry and leading to a broadening in k-space; 3) strong interactions in the SF requiring a treatment beyond Bogoliubov theory; 4) the short probing pulse time leading to a broadened signal in ω-space. Each of these effects can modify the resulting measurement and a comprehensive analysis has not been performed to date.

It is also interesting to note that a fundamental connection exists between Bragg and lattice modulation spectroscopy: the latter can be understood as two coherent Bragg processes, where all Bragg lasers are arranged along the direction of the modulated lattice direction. We elaborate on this connection in chapter (10), and furthermore perform a time-dependent calculation for the experiments [157, 140] in 3D, finding good agreement in the absorption peak frequency at different s.

Within a classical treatment of the laser field and using the correspondence principle, the effect of the time-dependent Bragg field on the atoms is theoretically described by the single particle operator $\mathcal{B}(t) = \frac{V}{2}\left(e^{-i\omega_B t}\rho^\dagger_{\mathbf{p}_\mathrm{B}} + e^{i\omega_B t}\rho_{\mathbf{p}_\mathrm{B}}\right)$, corresponding to a propagating sinusoidal potential with wave vector $|\mathbf{p}_\mathrm{B}|$, where V denotes the Bragg intensity and we use units of $\hbar = 1$. In free space the operator $\rho^\dagger_{\mathbf{p}_\mathrm{B}} = \sum_{\mathbf{p}} a^\dagger_{\mathbf{p}+\mathbf{p}_\mathrm{B}} a_{\mathbf{p}}$ acts as a translation operator in momentum space and simply transfers atoms into higher momentum states $\mathbf{p}_\mathrm{B}$, if energetically allowed, where $a_{\mathbf{p}}$ is the annihilation operator for a momentum state $\mathbf{p}$. However, in the presence of an optical lattice interactions are intensified and the multi-band structure and periodicity of the BZ invalidate this intuitive picture: multiple scattering events are enhanced and may lead to the occupation of a broad distribution of momentum components [Fig. 9.12(c)-(d)]. Moreover, strong interactions require an analysis in terms of a renormalized quasi-particle picture. In this work we focus on the physics within the lowest band, requiring all relevant energy scales to be lower than the band gap.

To incorporate the Bragg operator into our dynamic Gutzwiller calculation, it is transformed into Wannier space via the unitary transformation obtained from a band structure calculation as explicated in section (9.3). This leads to a lowest band representation $\rho^\dagger_{\mathbf{p}_\mathrm{B}} = \sum_{\mathbf{i},\mathbf{j}} \rho_{\mathbf{i},\mathbf{j}} b^\dagger_{\mathbf{i}} b_{\mathbf{j}}$, with the exact intra-band matrix elements $\rho_{\mathbf{i},\mathbf{j}}$ treated beyond the on-site and nearest neighbor approximation (decaying exponentially with $|\mathbf{i}-\mathbf{j}|$), where $\mathbf{i},\mathbf{j}$ denote the site indices. Within bosonic Gutzwiller theory, the variational ansatz for the many-body state consists of a single tensor product of states at each site $|\psi(t)\rangle = \prod_{\otimes\mathbf{i}} |\phi_{\mathbf{i}}(t)\rangle_{\mathbf{i}}$, which correctly recovers both the atomic limit $U/J \to \infty$ and time-dependent Gross-Pitaevskii theory within a coherent state description for weak interactions and it becomes exact in high spatial dimensions. For a strongly interacting condensate in the vicinity of the Mott transition, it furthermore includes the physics of the effective theories by Huber et al. [80, 79]. For a given trap geometry and experimental parameters, the ground state is determined and subsequently time evolved in the presence of the Bragg beam. The equations of motion are determined by minimizing the action (including the time-dependent Bragg operator) and are equivalent to the time evolution generated by a set of effective local Hamiltonians, coupled non-linearly to the states at other sites (see section 3.4).

9.2 Microscopic Derivation of the Bragg Operator

In this section we derive the Wannier representation of the single particle operator associated with the Bragg beam. Bragg spectroscopy is a two-photon process via an intermediate excited state, where the atoms are exposed to two coherent laser beams, as shown in Fig. (9.1). The two laser beams intersect at the position of the atomic cloud at an angle θ and we denote their respective frequencies by $\omega_{1,2}$, their polarization vectors and amplitudes by $\boldsymbol{\mathcal{E}}_{1,2}$ and their wave vectors by $\mathbf{k}_{1,2}$ respectively. This defines the Bragg momentum $\mathbf{k}_B = \mathbf{k}_1 - \mathbf{k}_2$ and and frequency $\omega_B = \omega_1 - \omega_2$, which can be varied independently. The detuning is typically ten orders of magnitude smaller than the absolute frequency, implying $|\mathbf{k}_1| \approx |\mathbf{k}_2|$ and thus, to a very good approximation $|\mathbf{k}_B| \approx 2|\mathbf{k}_1|\sin(\theta/2)$.

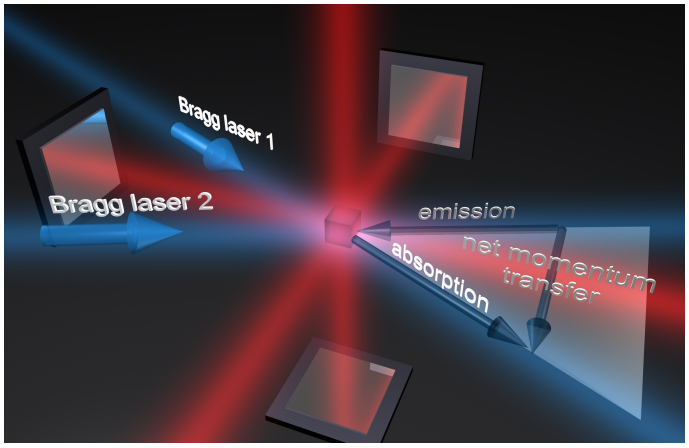

Figure 9.1: The experimental setup to perform momentum-resolved Bragg spectroscopy: in addition to the retro-reflected laser beams creating the optical lattice (shown in red), the atoms are exposed to two Bragg laser beams, shown in blue. One Bragg scattering process may, for example, correspond to to the absorption of a photon from the Bragg laser beam 1 and a stimulated emission process into the Bragg laser beam two, leading to a net momentum transfer in the plane of the two Bragg lasers, which is orthogonal to the bisecting line of the two Bragg lasers.

There are two different pictures to describe the effect of the laser beams on the atoms, which at first seem quite different, but go hand in hand. To derive the operator that describes the effect of the laser beams on the atomic ensemble, we use classical treatment of the electromagnetic field, which is well justified for the typically high laser intensities. The atoms couple to the electromagnetic field via the AC-Stark effect, as derived in chapter (1.3).

For the spatial extent of the atomic cloud, the electric fields of the two laser beams are well described by two plane waves

$$\mathbf{E}_1(\mathbf{r},t) = \boldsymbol{\mathcal{E}}_1 \cos(\mathbf{k}_1 \cdot \mathbf{r} - \omega_1 t), \tag{9.1}$$
$$\mathbf{E}_2(\mathbf{r},t) = \boldsymbol{\mathcal{E}}_2 \cos(\mathbf{k}_2 \cdot \mathbf{r} - \omega_2 t), \tag{9.2}$$

which are not retroreflected. Assuming equal polarization and amplitude, $\boldsymbol{\mathcal{E}} = \boldsymbol{\mathcal{E}}_1 = \boldsymbol{\mathcal{E}}_2$, and since the lasers are coherent, we linearly add the field amplitudes before determining the square modulus for the intensity

$$\begin{aligned} |\mathbf{E}(\mathbf{r},t)|^2 &= |\mathbf{E}_1(\mathbf{r},t) + \mathbf{E}_2(\mathbf{r},t)|^2 \\ &\approx \frac{\boldsymbol{\mathcal{E}}^2}{8}\left[2 + e^{i\mathbf{k}\cdot\mathbf{r}}\, e^{-i\omega_B t} + e^{-i\mathbf{k}\cdot\mathbf{r}}\, e^{i\omega_B t}\right]. \end{aligned} \tag{9.3}$$

To obtain the last line, we have used the rotating wave approximation and neglected fast oscillating terms containing $e^{i(\omega_1+\omega_2)t}$. According to Eq. (1.8), this field acts on the atoms as a spatial potential $V_B(\mathbf{r})$ which, within the formalism of second quantization, couples via the real space density operator $\mathcal{B}(t) \propto \int d^3r\, V_B(\mathbf{r})\, \hat{n}(\mathbf{r})$. The operator, describing the coupling to the two Bragg beams (and henceforth referred to as the *Bragg operator*) can thus be written as

$$\mathcal{B}(t) = \frac{V}{2}(2\hat{N}_{\text{tot}} + e^{-i\omega_B t}\rho^\dagger_{\mathbf{k}_B} + e^{i\omega_B t}\rho_{\mathbf{k}_B}), \tag{9.4}$$

where

$$\rho^\dagger_{\mathbf{q}} = \int d^3r\, e^{i\mathbf{q}\cdot\mathbf{r}}\, \hat{n}(\mathbf{r}) = \int d^3p\, \phi^\dagger_{\mathbf{p}+\mathbf{q}}\, \phi_{\mathbf{p}} \tag{9.5}$$

is the Fourier transform of the spatial density operator $\hat{n}(\mathbf{r}) = \psi^\dagger(\mathbf{r})\,\psi(\mathbf{r})$. The coupling strength V in the operator is related to the microscopic parameters introduced in section (1.3) by

$$V = \frac{|\langle e|\mathbf{d}\cdot\boldsymbol{\mathcal{E}}|g\rangle|^2}{16\delta^2 + 4\Gamma_e^2}. \tag{9.6}$$

The time-averaged intensity of the two coherent laser beams corresponds to a slowly propagating sinusoidal potential, i.e. an additional moving lattice. However, the form of the Bragg operator in Eq. (9.4) suggests an additional, quantum mechanical interpretation: in the momentum basis there is an amplitude $V/2$ that a plane momentum state $|\mathbf{p}\rangle$ gains a momentum kick $\mathbf{k}_B$ and is transferred into the momentum state $|\mathbf{p} + \mathbf{k}_B\rangle$ (the third term in Eq. (9.4) corresponds to the inverse process).

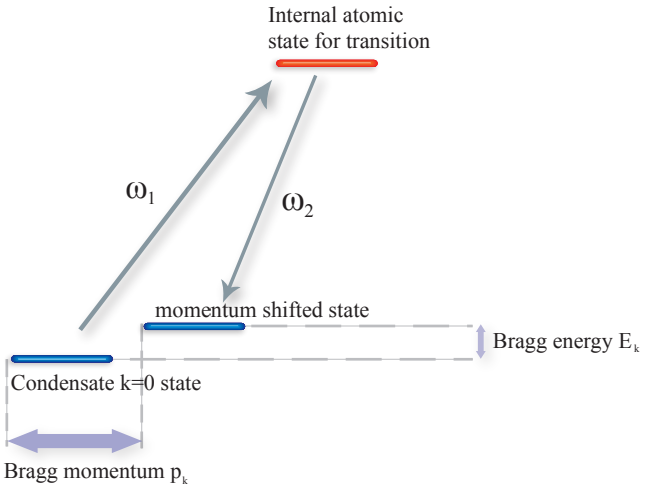

Figure 9.2: Cartoon illustrating the concept of Bragg spectroscopy: the atom is exposed to two coherently coupled laser beams with frequencies ω_1 and ω_2. Via an internal excited state of the atom, two atomic states (same internal state, but different atomic momenta) are effectively coupled.

Microscopically, this corresponds exactly to a second order process where the atom absorbs a photon with momentum $\mathbf{k}_1$ from the first Bragg laser and undergoes a stimulated emission process via the second Bragg laser by the emission of a photon with momentum $\mathbf{k}_2$. Altogether it thus experiences a net momentum kick $\mathbf{k}_B = \mathbf{k}_1 - \mathbf{k}_2$ and gains an energy $\omega_B = \omega_1 - \omega_2$, as shown in Fig. (9.2). The process that the atom emits a photon into the same laser it absorbed it from is also possible, which gives rise to a single particle energy offset and corresponds to the first term in Eq. (9.4). For systems where the particle number is conserved, we can ignore this term. Note that although our treatment of the electromagnetic field was purely classical, this interpretation in terms of photons with the correct momenta and energies emerges naturally.

9.3 The Bragg Operator in the Quasi-Momentum and Wannier Bases

The Bragg operator $\mathcal{B}(t)$, which effectively describes the virtual absorption and stimulated emission of a photon via an intermediate level is most naturally expressed in physical momentum space, where it acts as a superposition of two translation operators $\rho_{\mathbf{p}_\mathrm{B}}$ and $\rho^\dagger_{\mathbf{p}_\mathrm{B}}$ with time-dependent complex phases. For the simulation within the frame of the lowest band Bose-Hubbard model, we seek a representation of this operator, which goes beyond the lowest order description of a moving wave for the local on-site energies. Note that whereas the Bragg operator $\mathcal{B}(t) = \frac{V}{2}\left(e^{-i\omega_B t}\rho^\dagger_{\mathbf{p}_\mathrm{B}} + e^{i\omega_B t}\rho_{\mathbf{p}_\mathrm{B}}\right)$ is not separable within the different spatial dimensions, the two constituents $\rho_{\mathbf{p}_\mathrm{B}}$ and $\rho^\dagger_{\mathbf{p}_\mathrm{B}}$ are very well separable. We therefore first focus on expressing $\rho^\dagger_{\mathbf{p}_\mathrm{B}}$ in the Wannier basis for the 1D case as $\rho^\dagger_{\mathbf{p}_\mathrm{B}} = \sum_{\mathbf{i},\mathbf{j}} \rho_{\mathbf{i},\mathbf{j}} b^\dagger_{\mathbf{i}} b_{\mathbf{j}}$, before composing the Bragg and lattice amplitude modulation operators for the full 3D case in terms of these matrix elements.

One starts with the single particle basis transformation between the Bloch and physical momentum states

$$|k, \alpha\rangle = \sum_{n=-\infty}^{\infty} c_n^{(\alpha,k)} |p = 2nq_l + k\rangle \tag{9.7}$$

where $q_l = \pi/a$ is the lattice momentum and α is the band index. The coefficients $c_n^{(\alpha,k)}$ can be explicitly obtained by diagonalizing the lattice Hamiltonian in quasi-momentum space. Choosing the appropriate normalization, these coefficients constitute a unitary matrix for a parametrically fixed quasi-momentum k,

$$\sum_n c_n^{(\alpha,k)^*} c_n^{(\alpha',k)} = \delta_{\alpha,\alpha'}, \tag{9.8}$$

$$\sum_\alpha c_n^{(\alpha,k)^*} c_m^{(\alpha,k)} = \delta_{n,m}. \tag{9.9}$$

Furthermore it is useful to define the functions $N(p) = \left[\frac{p}{2q_l}\right]$ and $K(p) = p - 2q_l N(p)$ for the transformation from physical momentum to Wannier space, which allows the transformation between Bloch and true momentum states to be expressed as

$$b_{K(p)}^{(\alpha)\ \dagger} = \sum_{m=-\infty}^{\infty} c_{N(p+2q_l m)}^{(\alpha,K(p))}\, a_{p+2q_l m}^\dagger. \tag{9.10}$$

As required by symmetry, this expression is manifestly invariant under $p \mapsto p + 2mq_l$ with $m \in \mathbb{Z}$.

For the basis transformation and subsequent projection onto the lowest band (i.e. considering only terms with $\alpha = 0$) of the lattice along the dimension d with $L^{(d)}$ lattice sites, we define the function

$$M(|\mathbf{i}-\mathbf{j}|, q) = \frac{1}{L^{(d)}} \sum_p e^{iap\,|\mathbf{i}-\mathbf{j}|}\, c_{N(p+q)}^{(\alpha=0,k=K(p+q))^*} c_{N(p)}^{(\alpha=0,k=K(p))}, \tag{9.11}$$

which fulfills the relation $M(-|\mathbf{i}-\mathbf{j}|, q) = M^*(|\mathbf{i}-\mathbf{j}|, q)$. The full 3D operator can then conveniently be expressed in terms of this function as

$$\rho_{\mathbf{i},\mathbf{j}}^\dagger = e^{ia\mathbf{p}_\mathrm{B}\cdot\mathbf{i}} \prod_{d=1}^{3} M((\mathbf{i}-\mathbf{j})\cdot\mathbf{e}_d, \mathbf{p}_\mathrm{B}\cdot\mathbf{e}_d), \tag{9.12}$$

where $\mathbf{i}, \mathbf{j}$ are the 3D lattice site vectors, containing the integer site numbering of the cubic lattice along each dimension and $\mathbf{e}_d$ is the unit vector along the d-th dimension. Note that these matrix elements do not only depend on the Bragg momentum $\mathbf{p}_\mathrm{B}$, but also implicitly on the lattice depth s.

A short calculation explicitly verifies the property $\rho_{\mathbf{i},\mathbf{j}}(p_B = 0) = \delta_{\mathbf{i},\mathbf{j}}$ along one dimension, i.e. different layers are not coupled by the Bragg process if $\mathbf{p}_\mathrm{B}$ lies within a plane parallel to these layers. To first order, the Bragg operator locally corresponds to a sinusoidal potential (shift of effective chemical potential) moving along the direction $\mathbf{p}_\mathrm{B}$, but higher orders also give rise to nearest neighbor and longer range hopping. Usually these higher order terms are neglected, but their significance increases in certain regimes, such as when $\mathbf{p}_\mathrm{B}$ approaches $2q_l$ in the case of lattice modulation spectroscopy, discussed in chapter (10). In Fig. (9.3) the modulus of the matrix elements $\rho_{\mathbf{i},\mathbf{j}}$ is plotted as a function of the discrete lattice distance $|\mathbf{i}-\mathbf{j}|$ for different lattice depths s and Bragg momenta p_B.

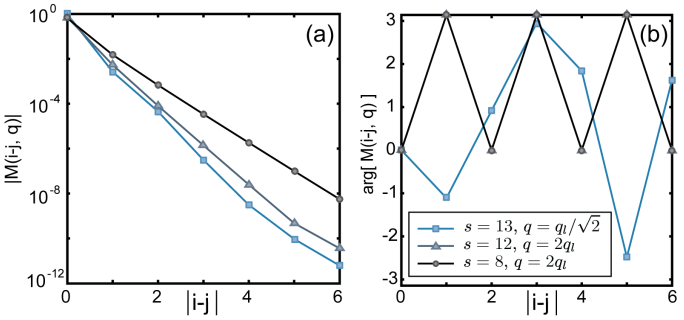

Figure 9.3: Dependence of complex matrix elements on the discrete lattice distance $|\mathbf{i}-\mathbf{j}|$ (subfigure a: modulus, subfigure b: arg). The values for $q = q_l/\sqrt{2}$ and $s = 13$ are relevant for the Bragg experiment addressed in the main text, while the value of $q = 2q_l$ is relevant for lattice modulation spectroscopy, discussed in chapter (10). The behavior of the complex angle of $M(\mathbf{i}-\mathbf{j})$ is determined by q and alternates in a regular fashion for $q = 2q_l$ (here both curves lie on top of one another) in contrast to the case of $q = q_l/\sqrt{2}$. The long-distance exponential decay constant is primarily governed by the lattice depth s.

In Fig. (9.4) the matrix elements of the M-operator, which are time-independent and only a function of the Bragg momentum, amplitude and wavelength of the optical lattice, are plotted. To depict the structure in more clarity, the logarithm of the absolute value of the matrix elements, as well as the complex angle (to illustrate the behavior of the relative phases of the operator) are plotted for two different Bragg momenta: $p_B = 0.1q_l$ and $p_B = 0.7q_l$. (The lattice strength label was not exported correctly. The numbers denote $log_{10}(V_{lat}/E_R)$.)

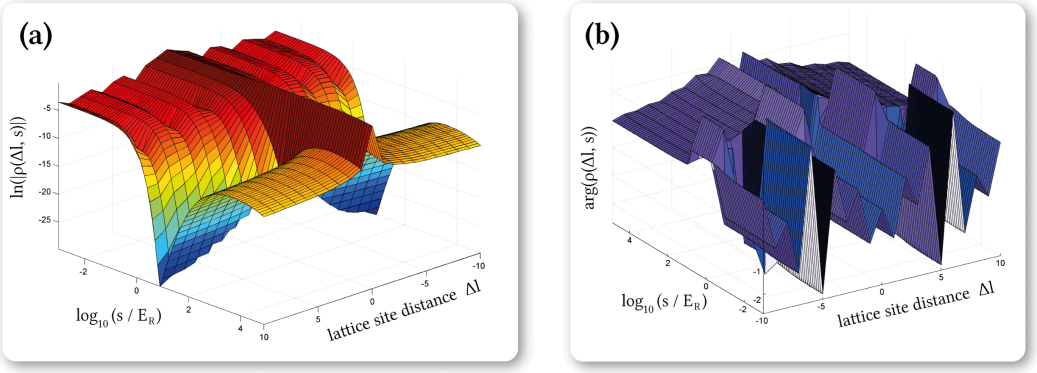

Figure 9.4: Modulus and Arg of the matrix elements of $\rho_{\mathbf{q}}$ in the Wannier basis for $|\mathbf{q}| = 0.7q_l$ along one dimension.

It is interesting to note, that the off-diagonal (hopping) matrix elements decay very strongly in a critical region of the lattice strength, thereafter they increase again with the lattice strength over a large interval. The critical region is also reflected in the behavior of the phase: for weak lattices the phase oscillates with the distance, whereas the phase remains constant for deep lattices.

9.4 Linear Response Theory

In this section, we shortly discuss the response of the system in the long time and low intensity limit along the lines of [153]. Here we can use Fermi's golden rule, as obtained from time-dependent linear response theory in appendix (B). To keep the treatment general, we consider $\mathcal{H}_0$ to describe the interacting bosons with or without a lattice. For the specific form of the eigenstates, one might take $\mathcal{H}_0$ to be the Bogoliubov, or the generalized quasi-particle Hamiltonian in the case of strongly interacting bosons on a lattice. The Bragg operator (9.4) is the weak harmonic perturbation and thus the relation between the density wave operator and the operator F from the perturbative treatment in Eq. (B.14) is $F = \frac{V}{2}\rho_{\mathbf{p}_B}$. Before switching on the perturbing Bragg operator, the system is in the initial many-body ground state $|\psi_i\rangle = |\psi_0\rangle$.

Relation to the Dynamic Structure Factor

Quasi-Particle Excitation Rate

We denote the transfer rate out of the ground state in the linear response regime by Γ, which is simply the sum of transfer rates into all many-body excited states $|\psi_n\rangle$,

$$\Gamma = \sum_n \Gamma_{i\to n} = 2\pi \left(\frac{V}{2}\right)^2 \sum_n |\langle\psi_n|\rho^\dagger_{\mathbf{p}_\mathrm{B}}|\psi_i\rangle|^2\, \delta(E_n - E_i - \omega). \tag{9.13}$$

Note that in the case of deep lattices, where the tunneling energy J and hence the collective sound mode energies are strongly reduced, the associated time scale required in the linear response treatment for the response function to become δ-like grows accordingly.

Energy Transfer Rate

Within the same linear response regime as above, we can also describe the rate at which energy is deposited into the system

$$\frac{d}{dt}\Delta E(t) = \sum_n \Gamma_{i\to n}\,(E_n - E_i) = 2\pi\omega \left(\frac{V}{2}\right)^2 S(\mathbf{p}_\mathrm{B}, \omega). \tag{9.14}$$

Here we introduced the dynamic structure factor, which can be defined as

$$S(\mathbf{q},\omega) = \sum_n |\langle\psi_n|\rho^\dagger_{\mathbf{p}_\mathrm{B}}|\psi_i\rangle|^2\, \delta(E_n - E_i - \omega). \tag{9.15}$$

Its counterpart in the time-domain is the expectation value

$$\tilde{S}(\mathbf{q},t) := \langle\rho_{\mathbf{q}}(t)\,\rho^\dagger_{\mathbf{q}}(0)\rangle, \tag{9.16}$$

where $\rho^\dagger_{\mathbf{q}}(t)$ is the Fourier transform of the spatial density operator at a quasi-momentum $\mathbf{q}$ in the Heisenberg picture, defined in Eq. (9.5). It is related to the frequency-depenent dynamic structure factor by the Fourier transform

$$S(\mathbf{q},\omega) := \frac{1}{2\pi}\int_{-\infty}^{\infty} dt\, e^{i\omega t}\tilde{S}(\mathbf{q},t), \tag{9.17}$$

and is thus the spatio-temporal Fourier transform of the density-density correlations in the gas

$$S(\mathbf{q},\omega) := \frac{1}{2\pi}\int_{-\infty}^{\infty} dt \int d^3r\, d^3r'\, e^{i[\omega t - \mathbf{q}\cdot(\mathbf{r}-\mathbf{r}')]}\langle\hat{n}(\mathbf{r},t)\,\hat{n}(\mathbf{r}',0)\rangle. \tag{9.18}$$

Note that up to this point we made no reference to a lattice. The above results apply both to a system in free space or a lattice. In the low energy limit of the latter case, it is useful to work in the lowest band representation of the lattice. Here, similar relations apply if the continuous density operator is replaced by its discrete Wannier counterpart and the quasi-momentum takes over the role of the momentum.

9.5 Beyond Linear Response: Exact Time Evolution in a Non-Interacting System

Since the single particle eigenstates for fixed quasi-momentum k only contain physical momenta $p = k + 2nq_l$, the lattice Hamiltonian is reducible into blocks with different k (each only coupling the above momenta) and the Bragg operator B only couples momenta separated by p_B, the complete Hamiltonian

$$H = H_{lat} + \theta(t)\, A\, B \tag{9.19}$$

is consequently also reducible into subspaces

$$\mathcal{H} = \bigoplus_k \mathcal{H}_k, \tag{9.20}$$

where $\mathcal{H}_k = \mathrm{span}(\{|p = k + 2nq_l + mp_B\rangle\})$, $m, n \in \mathbb{Z}$. Starting with an eigenstate of the lattice without the Bragg pulse (and thus starting in the subspace $\mathcal{H}_k$ with the initial quasi-momentum k), the state will remain restricted to the respective subspace under time evolution for arbitrary times. For the numerical computation it is thus useful to work in the (truncated) basis of this subspace only.

9.5.1 The Lattice Hamiltonian in the Relevant Subspace

The lattice Hamiltonian in the complete Hilbert space can be written in the basis of momentum eigenstates as

$$\begin{aligned} H_{lat} &= \sum_{\alpha,k} E^{(\alpha,k')} |k', \alpha\rangle\langle k', \alpha| \\ &= \sum_{\alpha,k',j,j'} E^{(\alpha,k')} c_j^{(\alpha,k')} c_{j'}^{(\alpha,k')*} \\ &\quad \times |p = k' + 2jq_l\rangle\langle p = k' + 2j'q_l| \end{aligned} \tag{9.21}$$

To project the Hamiltonian on the restricted subspace, a first step consists of finding the relevant values of k' and j in the sum above. Any state in the subspace can be written as $|m, n\rangle := |p = k + 2nq_l + mp_B\rangle$, where k is the quasi-momentum of the initial eigenstate of H_{lat} (typically $k = 0$). Therefore (k, m, n) can be seen as fixed in the following. A state in the Hamiltonian above is expressed as $|p = k' + 2jq_l\rangle$, where k' is some quasi-momentum in the first Brillouin zone ($|k'| \leq q_l$) and $j \in \mathbb{Z}$ are to be determined. These conditions uniquely fix the values

$$\begin{aligned} j &= n + \left[\frac{k}{2q_l} + m\frac{p_B}{2q_l}\right] \\ k' &= k + mp_B - 2\left[\frac{k}{2q_l} + m\frac{p_B}{2q_l}\right] q_l, \end{aligned} \tag{9.22}$$

where $[\ldots]$ denotes the round function.

To consider only the part of the lattice Hamiltonian on the relevant (physically accessible) subspace, we use the corresponding projection operator

$$\mathbb{1}_k = \sum_{m,n} |m, n\rangle\langle m, n| \tag{9.23}$$

and obtain

$$\begin{aligned} H_{lat,k} &= \sum_{m,n,m',n'} |m, n\rangle\langle m, n|H_{lat}|m', n'\rangle\langle m', n'| \\ &= \sum_{\substack{m,n,m',n' \\ k',\alpha,j,j'}} E^{(k',\alpha)} c_j^{(k',\alpha)} c_{j'}^{(k',\alpha)*} \langle m, n|p = k' + 2jq_l\rangle \\ &\quad \times \langle p = k' + 2j'q_l|m', n'\rangle\ |m, n\rangle\langle m', n'|. \end{aligned} \tag{9.24}$$

Using the orthogonality of momentum states and setting $q_l = 1$ (i.e. the lattice spacing $a = \pi$) yields the identity

$$\langle m, n|p = k' + 2jq_l\rangle = \delta_{k',k+mp_B-2\left[\frac{k}{2}+m\frac{p_B}{2}\right]} \times \delta_{j,n+\left[\frac{k}{2}+m\frac{p_B}{2}\right]}, \tag{9.25}$$

which motivates the definitions

$$\begin{aligned} J(m,n) &:= n + \left[\frac{k}{2q_l} + m\frac{p_B}{2q_l}\right] \\ K(m) &:= k + mp_B - 2\left[\frac{k}{2q_l} + m\frac{p_B}{2q_l}\right] q_l, \end{aligned} \tag{9.26}$$

and the restricted lattice Hamiltonian simplifies to

$$H_{lat,k} = \sum_{m,n,n',\alpha} E^{(K(m),\alpha)} c^{(K(m),\alpha)}_{J(m,n)} c^{(K(m),\alpha)^*}_{J(m,n')} |m,n\rangle\langle m,n'|. \tag{9.27}$$

To numerically integrate the Schrödinger equation in this subspace

$$\frac{\partial}{\partial t}|\psi(t)\rangle = -\frac{i}{\hbar} H_{lat,k}|\psi(t)\rangle, \tag{9.28}$$

the space can be truncated at some maximum (minimum) values M and N ($-M$ and $-N$) that m and n can take on. It has to be verified retrospectively, that during the time evolution the states close to truncation are never occupied significantly. This leads to a set of $(2M+1)(2N+1)$ coupled linear differential equations, which can be solved numerically. A typical time-dependent momentum distribution (not the quasi-momentum) for a one-dimensional system, where the Bragg frequency is chosen on resonance with the transition frequency between the two coupled Bloch eigenstates, is shown in Fig. (9.5).

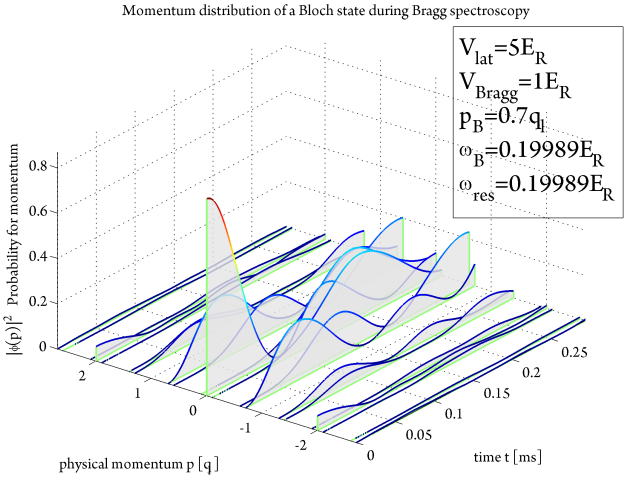

Figure 9.5: 1D momentum distribution (not quasi-momentum) as a function of time for an ideal condensate using exact time evolution.

The system is initially prepared in the ground state, i.e. the $\mathbf{k} = 0$ Bloch state before the Bragg operator is switched on. The initial Bloch state only contains discrete momentum distributions at $p = 2mq_l$, where m is an arbitrary integer. Since the Bragg operator only couples different momentum states which are separated by the Bragg momentum, only a discrete set of momentum states are occupied at any time. For short times and the very strong coupling of the Bragg operator the dominant effect at short times is the transfer of particles out of the $p = 0$ momentum state. In this case the parameters are chosen such that multiple transitions leading to the occupation of higher order momentum states are suppressed, which is not generally the case. In this regime, one can see oscillatory behavior in the occupation of a few involved momentum states, which is analogous to Rabi oscillations in a two level system. The 'Rabi oscillation frequency' is also

inversely related to the Bragg amplitude in this case. Since more than two levels are involved, the scaling of the dynamical behavior with the coupling amplitude is however more complicated in this system than in the two level case. It can be seen that the presence of a lattice significantly complicates the dynamics of the system in comparison to the system in free space.

9.6 Coupling to Quasi-Particles in the Interacting System

We will now additionally consider the effect of particle interactions, where an exact numerical treatment as in the case of a non-interacting condensate is no longer possible in three dimensions. Here we will pursue two different approaches:

9.6.1 Density Wave Operator

Corresponding to a sinusoidal shift of the local chemical potential. Consider translationally invariant case in 1D here: the combined mode index s can be decomposed into two independent quantum numbers k and γ and

$$\begin{aligned} u_{k,\gamma}^{(i,l)} &= \frac{1}{\sqrt{L}} u_{k,\gamma}^{(i)}\, e^{iakl} \\ v_{k,\gamma}^{(i,l)} &= \frac{1}{\sqrt{L}} v_{k,\gamma}^{(i)}\, e^{iakl} \end{aligned} \tag{9.29}$$

$$\begin{aligned} \hat{D} &= \sum_l \cos(aql+\varphi)\, b_l^\dagger b_l \\ &= \sum_l \cos(aql+\varphi)\, {}_l\langle i=0|b_l^\dagger b_l|i=0\rangle_l \\ &\quad + \frac{L}{2}\sum_\gamma \sum_i {}_l\langle i=0|b_l^\dagger b_l|i\rangle_l \Big(e^{-i\omega_{q,\gamma}t}\,(u_{q,\gamma}^{(i)} + v_{q,\gamma}^{(i)})(e^{i\varphi}\,\beta_{-q,\gamma} + e^{-i\varphi}\beta_{q,\gamma}) \\ &\quad + e^{i\omega_{q,\gamma}t}\,({u_{q,\gamma}^{(i)}}^* + {v_{q,\gamma}^{(i)}}^*)(e^{-i\varphi}\,\beta_{-q,\gamma}^\dagger + e^{i\varphi}\beta_{q,\gamma}^\dagger)\Big) + \mathcal{O}(\beta^2). \end{aligned} \tag{9.30}$$

Here we used the fact that ${}_l\langle i=0|b_l^\dagger b_l|i\rangle_l$ can always be chosen real by an appropriate choice of the mean field ground states and that the dispersion relation $\epsilon(k)=\epsilon(-k)$ is symmetric due to reflection symmetry, leading to $\omega_{k,\gamma}=\omega_{-k,\gamma}$, $u_{k,\gamma}^{(i)}=u_{-k,\gamma}^{(i)}$ and $v_{k,\gamma}^{(i)}=v_{-k,\gamma}^{(i)}$. The quasi-particle annihilation and creation operators $\beta_{-k,\gamma}$ and $\beta_{k,\gamma}^\dagger$ are in the Schrödinger representation here. This can be seen when considering the time evolution of a state with a fixed configuration of quasi-particles (i.e. constant $\alpha_s(t)$ in the classical case), where the time evolution of the state under influence of the underlying Hamiltonian was shown to be contained in the ansatz $\prod_{\otimes k}\left(|i=0\rangle_l + \sum_{j=0}^{N_{\max}}\sum_r \left(\alpha_r\, u_r^{(j,l)}\, e^{-i\omega_r t} + \alpha_r^*\, {v_r^{(j,l)}}^*\, e^{i\omega_r t}\right)|j\rangle_l\right)$. In the Heisenberg representation, when using $\beta_{k,\gamma}(t) = e^{-i\omega_{k,\gamma}t}\,\beta_{k,\gamma}$, the expectation value of an arbitrary operator is identical when evaluated in the initial state (i.e. the one above with $t=0$) and the explicit time-dependent exponential factors in the operator vanish.

By defining the coefficients

$$D_\gamma = \frac{1}{2}\sum_i {}_l\langle i=0|b_l^\dagger b_l|i\rangle_l (u_{q,\gamma}^{(i)} + v_{q,\gamma}^{(i)}), \tag{9.31}$$

the operator can then be expressed in the form

$$\begin{aligned} \hat{D} &= \sum_l \cos(aql+\varphi)\, {}_l\langle i=0|b_l^\dagger b_l|i=0\rangle_l \\ &\quad + L\sum_\gamma D_\gamma[e^{i\varphi}\,\beta_{-q,\gamma}(t) + e^{-i\varphi}\beta_{q,\gamma}(t)] + L\sum_\gamma D_\gamma^*[e^{-i\varphi}\,\beta_{-q,\gamma}^\dagger(t) + e^{i\varphi}\beta_{q,\gamma}^\dagger(t)] \\ &\quad + \mathcal{O}(\beta^2) \end{aligned} \tag{9.32}$$

9.6.2 The Bragg Operator in Terms of Quasi-Particle Operators

The density operator above only takes the lowest on-site shift of the potential into account and does not couple to any quasi-particles in the Mott insulator. We now derive a better representation of the Bragg operator in terms of quasi-particle operators by systematically taking all longer-range terms terms (i.e. not only the on-site potential, but all coupling between different sites) into account. Since the Bragg operator is a single particle operator which couples at most two different sites, its representation in terms of quasi-particle operators contains at most four operators $\beta^\dagger$ or β.

The Bragg operator is a superposition of two density wave operators with a different time-dependent complex phase. These are exact conjugates and we consider the term $\rho_{\mathbf{q}}^\dagger$. For clarity, we will consider the 1D case here, which can be directly extended to higher dimensions.The Fourier transformed density operator is the translation operator in physical momentum space

$$\begin{aligned}\rho_{\mathbf{q}}^\dagger &= \int dp\, \phi_{p+q}^\dagger\, \phi_p \\ &= \int dp \sum_{\alpha,\alpha'} c_{N(p+q)}^{(\alpha,K(p+q))^*} c_{N(p)}^{(\alpha',K(p))}\, b_{K(p+q)}^{(\alpha)^\dagger}\, b_{K(p)}^{(\alpha')} \\ &= \sum_{\alpha,\alpha'} \int_{1\mathrm{BZ}} dk\, C_{k,q}^{(\alpha,\alpha')}\, b_{K(k+q)}^{(\alpha)^\dagger}\, b_{K(p)}^{(\alpha')}.\end{aligned} \tag{9.33}$$

Note that in the lowest band projection, this is not necessarily exactly equal or proportional to the (discrete) Fourier transform of the lowest band density operator in the lattice, since the factor

$$C_{k,q}^{(\alpha,\alpha')} = \sum_{n\in\mathbb{Z}} c_{n+N(k+q)}^{(\alpha,K(k+q))^*} c_{n+N(k)}^{(\alpha',K(k))} \tag{9.34}$$

is generally depends on k. We now consider a homogeneous system and project onto the lowest band, i.e. only consider terms with $\alpha = \alpha' = 0$. Using

$$b_k^\dagger b_{k'} = \frac{1}{L}\sum_{l,l'} e^{ia[K(p+q)l - K(p)l']} \sum_{i,j,i',j'} B_{j,i}^* B_{i',j'} |i\rangle_{ll} \langle j|\ |i'\rangle_{l'l'} \langle j'|, \tag{9.35}$$

we express $\rho_{\mathbf{q}}^\dagger$ in the basis of mean-field eigenstates and subsequently in fluctuation operators σ. For $K(q) \neq 0$ the expectation value of the term containing no fluctuation operators vanishes. The lowest non-vanishing term is thus of first order in the fluctuation operators and reads

$$\begin{aligned}\rho_{\mathbf{q}}^\dagger =& \sqrt{L}\sum_{i>0}\left[C_{0,q}^{(0,0)} B_{0,i}^* B_{0,0} + C_{-q,q}^{(0,0)} B_{0,0}^* B_{i,0}\right] \tilde{\sigma}_{K(q)}^{(i)^\dagger} \\ &+\sqrt{L}\sum_{i>0}\left[C_{0,q}^{(0,0)} B_{i,0}^* B_{0,0} + C_{-q,q}^{(0,0)} B_{0,0}^* B_{0,i}\right] \tilde{\sigma}_{-K(q)}^{(i)} + \mathcal{O}(\sigma^2) \\ =& \sum_s \left[R_s \beta_{K(q),s}^\dagger + \tilde{R}_s \beta_{-K(q),s}\right],\end{aligned} \tag{9.36}$$

where the coupling amplitudes R_s and $\tilde{R}_s$ for creating a quasi-particle with quasi-momentum $\mathbf{k}$ or annihilating one with $-\mathbf{k}$ in the mode s respectively, are defined as

$$\begin{aligned}R_s =& \sqrt{L}\sum_{i>0}\left[C_{0,q}^{(0,0)} B_{0,i}^* B_{0,0} + C_{-q,q}^{(0,0)} B_{0,0}^* B_{i,0}\right] u_i^{(K(q),s)^*} \\ &+ \sqrt{L}\sum_{i>0}\left[C_{0,q}^{(0,0)} B_{i,0}^* B_{0,0} + C_{-q,q}^{(0,0)} B_{0,0}^* B_{0,i}\right] v_i^{(K(q),s)^*},\end{aligned} \tag{9.37}$$

$$\begin{aligned}\tilde{R}_s =& \sqrt{L}\sum_{i>0}\left[C_{0,q}^{(0,0)} B_{0,i}^* B_{0,0} + C_{-q,q}^{(0,0)} B_{0,0}^* B_{i,0}\right] v_i^{(-K(q),s)} \\ &+ \sqrt{L}\sum_{i>0}\left[C_{0,q}^{(0,0)} B_{i,0}^* B_{0,0} + C_{-q,q}^{(0,0)} B_{0,0}^* B_{0,i}\right] u_i^{(-K(q),s)}.\end{aligned} \tag{9.38}$$

If the Bragg momentum lies within the first Brillouin zone and $K(\mathbf{q}) = \mathbf{q}$, the full Bragg operator in 3D to first order in the quasi-particle operators is thus

$$\mathcal{B}(t) = \frac{V}{2} \sum_s \left[e^{-i\omega t} R_s \beta^\dagger_{\mathbf{q},s} + e^{-i\omega t} \tilde{R}_s \beta_{-\mathbf{q},s} + e^{i\omega t} R^*_s \beta_{\mathbf{q},s} + e^{i\omega t} \tilde{R}^*_s \beta^\dagger_{-\mathbf{q},s} \right], \tag{9.39}$$

which creates and annihilates quasi-particles at both quasi-momenta $\mathbf{q}$ and $-\mathbf{q}$. For sufficiently long time and within the rotating wave approximation, the last two terms in Eq. (9.39) can be neglected.

9.7 Results for the Homogeneous Interacting System

Within the extended quasi-particle theory, the interacting system of bosons in the lattice is approximately described by a system of non-interacting bosonic quasi-particles (or weakly interacting, if higher terms are taken into account). In the previous section we have expressed the Bragg operator in terms of creation- and annihilation operators of these quasi-particle modes to lowest order (9.39). The advantage of the entire transformation is that we can describe the effect of the Bragg beam onto the interacting system, which is a difficult task, as the effect of a perturbing operator on an effectively non-interacting system, although at the cost of a more complicated coupling.

Linear Response Regime

For short times the population of the quasi-particle modes grows quadratically and proportionally to the square modulus of the coupling $|R_s|^2$ in Eq. (9.37). Taking the long time limit and simultaneously decreasing the intensity V, such that the same number of quasi-particle are excited on average at the Bragg resonance frequency, the sinc^2 shaped absorption peaks become narrower. For very long times, quasi-particles are only excited and energy is only absorbed by the system if the Bragg frequency ω_B of the probing beams exactly matches the quasi-particle energy. For fixed Bragg momentum $\mathbf{p}_\mathrm{B}$, the various quasiparticle energies can be determined from the strongest loss in the momentum component $n(\mathbf{k} = 0)$, gain in $n(\mathbf{k} = \mathbf{p}_\mathrm{B})$, energy absorption or reduction in the condensate fraction as a function of the frequency ω_B, as shown in Fig. (9.6). The occupation of quasi-particle modes at integer multiples of the Bragg momentum also become relevant in the regime where multiple scattering events are likely. These originate from terms of second order in the quasi-particle operators β in the Bragg operator. Depending on the parameters regime, the occupation of higher momentum modes can become significant, as shown in the subfigures (c-h) of Fig. (9.6).

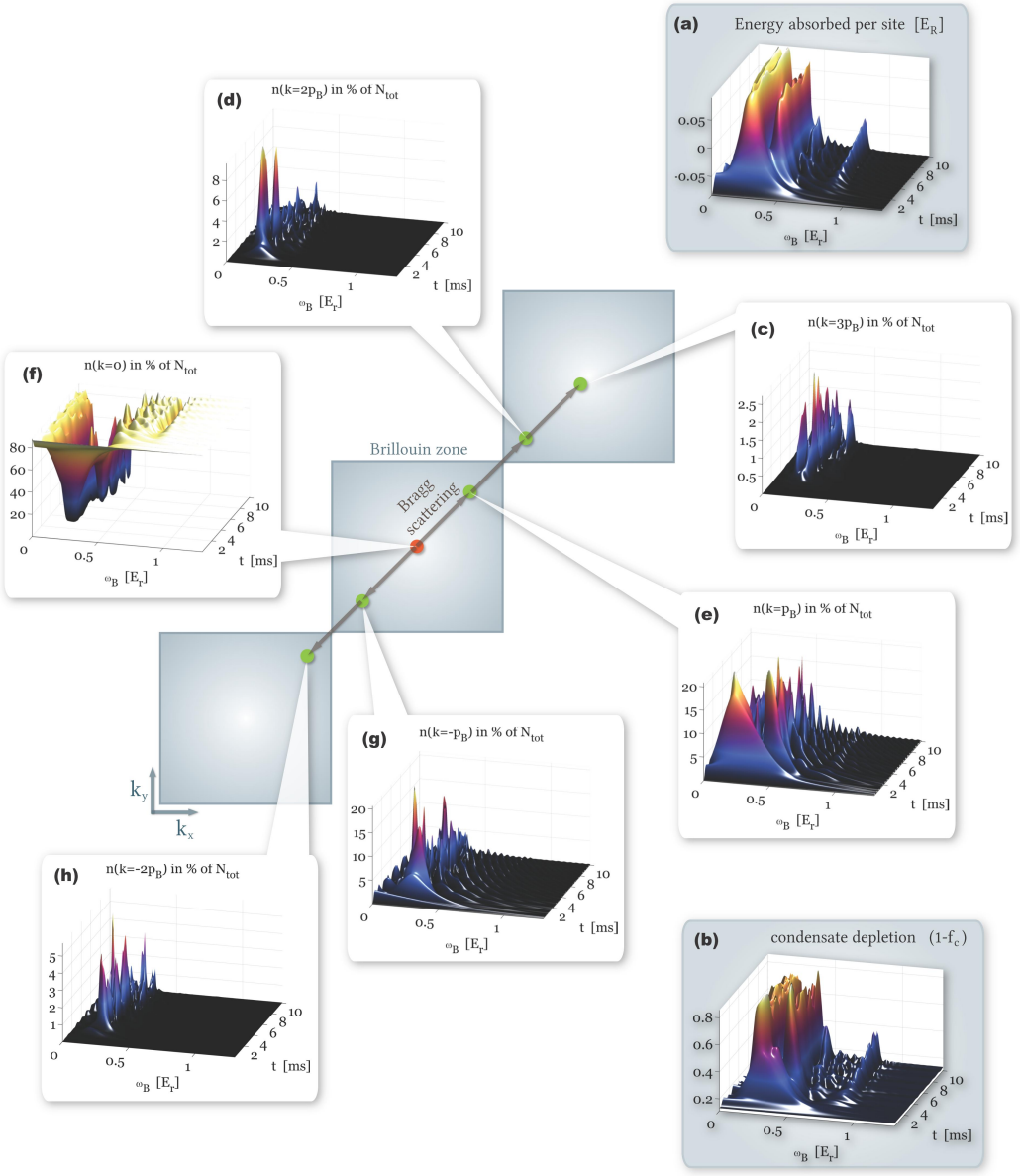

Figure 9.6: Various absorption profiles as a function of the Bragg frequency ω_B and of the exposure time t to a square pulse. The ^{87}Rb gas is in a $s = 9E_r$ homogeneous 3D optical lattice at $\lambda_{lat} = 1030$nm, which is in the regime of intermediate interactions $6J/U \approx 0.7$. It is probed at a Bragg momentum $\mathbf{p}_B = \frac{q_l}{\sqrt{2}}(1,1,0)$ at high intensity of $V = 0.1E_r$, which is beyond the regime described by linear response theory for times $t \gtrapprox 1$ms.

Note that the observed quasi-momentum distributions do not directly correspond to the quasi-particle occupation numbers, except in the non-interacting limit, where all excitations are single-particle like. In the weakly interacting regime, the relevant excitation are Bogoliubov quasi-particles, which are correlated particle-hole excitations at the given quasi-momentum $\mathbf{k}$ and its inverse $-\mathbf{k}$ respectively. Hence, when a quasi-particle at $\mathbf{k} = +\mathbf{p}_B$ is excited this is visible in the quasi-momentum distribution at $\mathbf{k} = -\mathbf{p}_B$. When increasing the interactions further, higher modes such as the amplitude mode also become relevant and the collective excitations deviate from the simple particle-hole Bogoliubov structure. Nevertheless, the excitation of any given quasi-particle mode at $\mathbf{k}$ in a homogeneous system will be reflected in the momentum distribution at $\mathbf{k}$ and $-\mathbf{k}$, whereas the effect at $-\mathbf{k}$ becomes less significant with an increasing mode index (i.e. the *particle-hole* hybridization of the fluctuations is stronger in the energetically low lying modes).

The theoretically predicted quasi-momentum distributions after exciting a strongly interacting condensate in a trap, are shown in subfigures (c-e) in Fig. (9.12) on a logarithmic scale for visual clarity. When choosing the frequency such that mostly amplitude mode quasi-particles are excited (subfigure (e)), this is almost only leads to an occupation of $\mathbf{k} = +\mathbf{p}_\mathrm{B}$ quasi-momentum mode in the non-interacting single-particle basis.

Probing the System Strongly

Coming back to the theoretically calculated absorption spectra for the homogeneous system in Fig. (9.6), we notice that the shown results do not agree with our predictions from linear response theory: in the long time limit the frequency-dependent spectra do not approach the predicted sinc-shape, which becomes narrower for later times. This is due to the strong intensity of the Bragg probing beams, which strongly broadens the peaks and also shifts the positions of their maxima in the long time limit. Although the Bragg intensity $V = 0.1E_r$ used in Fig. (9.6) is weak compared to the lattice depth $s = 9E_r$, it is strong on the relevant energy scale set by the band width. The high intensity of the probing beam leads to a break-down of the non-interacting quasi-particle picture in different respects. Firstly, high intensity V invalidates the approximation of neglecting higher order terms when representing the Bragg operator in terms of quasi-particle operators β. Secondly, the times considered in Fig. (9.6) are far beyond the lowest order perturbative regime and many scattering events induced by the Bragg lasers are likely to occur. Thirdly, already after $\approx$ 2ms a large amount of energy has been deposited in the system and quasi-particle modes are highly excited. In this regime, where the system is no longer close to the ground state, the higher order quasi-particle terms from the original Bose-Hubbard Hamiltonian become relevant and a description in terms of non-interacting quasi-particles (even in the absence of the Bragg probing beam) applies no longer. In fact, the quasi-particles even lose their bosonic character if the system is far away from the ground state. The shift of the peak positions can be understood as a consequence of these higher order terms describing interactions between the quasi-particles, which renormalizes their energy.

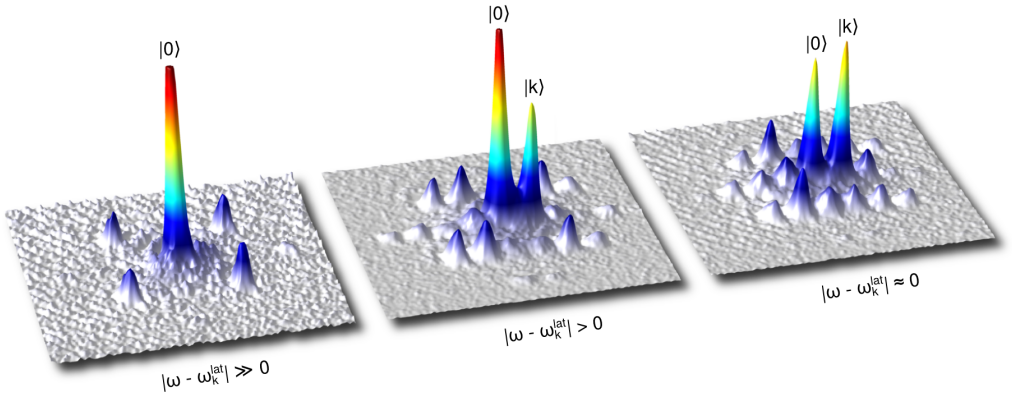

Figure 9.7: Experimentally observed momentum distribution in a 1030nm lattice at $s = 7E_r$ after exposing the system to Bragg probing beams at three different Bragg frequencies ω. If ω is far detuned from the sound mode energy $\omega_\mathbf{k}^\mathrm{lat}$ at the given momentum (here $\mathbf{p}_\mathrm{B} = q_l/\sqrt{2}(1,1,0)$) in the lattice, almost no atoms are transferred in momentum space, as shown in the left figure. As ω approaches the collective mode frequency, an increasing number of particles is transferred into a momentum state shifted by $\mathbf{p}_\mathrm{B}$. Transitions are also induced by the lattice, such that additional peaks appear at momenta related to the Bragg scattered peaks by a reciprocal lattice vector. The image is taken from the thesis by S. Götze [64] and the experiment was performed in the group of K. Sengstock [46].

as shown in Fig. 9.12(a),(b).

The pulse shape investigated theoretically here, is the square pulse where the Bragg intensity V is constant over a fixed time interval t. This leads to the characteristic sinc^2 response in frequency space, as is to be expected from time-dependent perturbation theory and can be seen in Fig. 9.8.

While exposed to the Bragg lasers, atoms are continuously transferred between different quasi-momentum states, with $\mathbf{k} = 0 \rightarrow \mathbf{p}_\mathrm{B}$ initially being the dominant transition at weak interactions. With increasing U/J, backscattering transitions are enhanced and at longer times higher order transitions also become relevant. This can also be seen from the physical momentum distribution $n(\mathbf{p}) = \langle a^\dagger_\mathbf{p} a_\mathbf{p} \rangle$, which is directly related to the quasi-momentum distribution, as shown in Fig. 9.12(c)-(e). In the low intensity and long-time limit, Bragg spectroscopy directly probes the dynamic structure factor. Determining these resonance positions for a range of different momenta $\mathbf{p}_\mathrm{B}$ leads to the dispersion relations with the Bogoliubov, amplitude and higher gapped modes shown in Fig. 9.10 and compared with other theoretical results. A probing beam at resonance with a collective mode frequency induces time- and position-dependent oscillations of the density and the spatial order parameters $\psi_\mathbf{i} = \langle b_\mathbf{i} \rangle$. In a theoretical description, these excitations correspond to coherent states of the respective quasiparticle, i.e. the most classical excitation, and are graphically illustrated in Fig. 9.10(c),(d): a coherent Bogoliubov excitation leads to a dominant spatial and temporal oscillation of the phase of $\psi_\mathbf{i}$ (which becomes pure for $k \rightarrow 0$) and a density wave, whereas an excitation of the amplitude mode leads mainly to an oscillation of the amplitude of $\psi_\mathbf{i}$ and the density modulation is strongly suppressed. The oscillation of $|\psi_\mathbf{i}|$ at constant density can thus be understood as a local periodic transfer of particles between the condensate and the non-condensate.

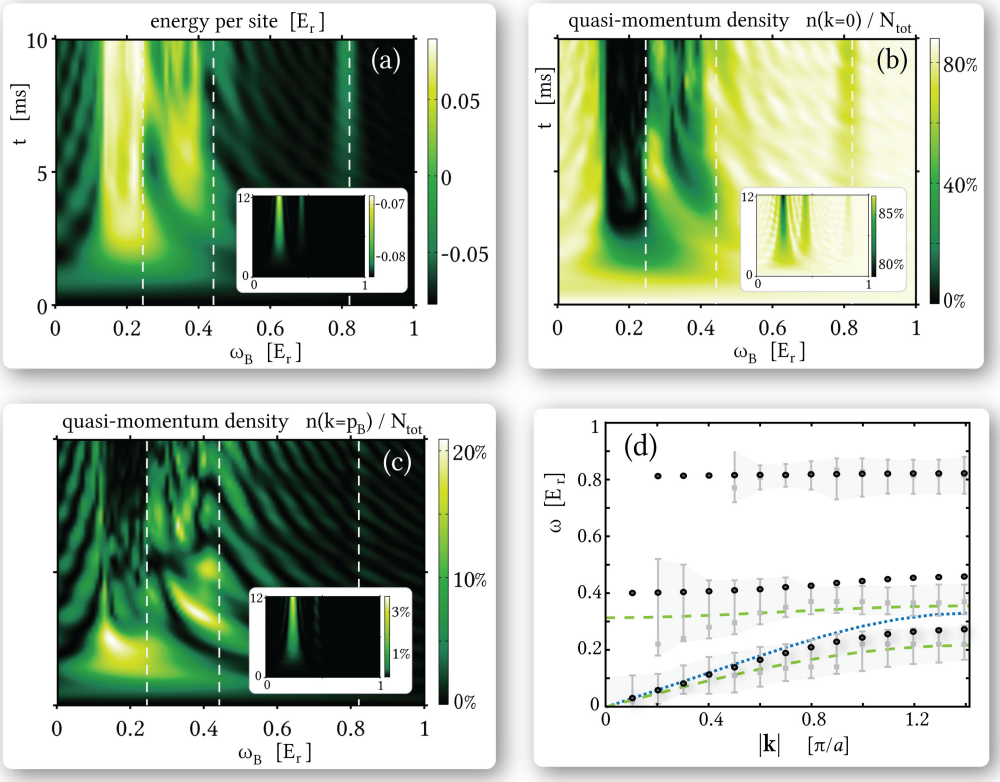

Figure 9.8: Energy absorption (a) and quasi-momentum density (b),(c) spectra for a square pulse at high intensity $V = 0.1E_r$ (insets: weak intensity $V = 0.005E_r$) in the intermediate interaction $s = 9$ regime and for Bragg momentum $|\mathbf{p}_B| = \pi/a$. The resonance frequencies predicted from the maxima of the high intensity energy absorption spectra (plotted as gray squares in (d)) contain a systematic uncertainty quantified by the full width half maximum (FWHM) of the pulse after 10ms $\approx 3.26/J$ indicated by the error bars and shaded region in (d). The comparison with the true quasiparticle energies (dashed white lines in (a-c), black circles in (d)) reveals significant discrepancies. For comparison in (d): the blue dotted line is the Bogoliubov result, the green dashed lines are the results from Ref. [80] for the amplitude and sound modes ($\omega(\mathbf{k}) = \psi_0\sqrt{2Un\epsilon_\mathbf{k}}$ with ψ_0 determined by Gutzwiller).

An essential effect that has to be considered in a realistic modeling of Bragg spectroscopy is the finite intensity of the probing beam. This is particularly important for strong optical lattices, where the typical time scale $1/J$ grows exponentially with s. As the pulse time is restricted by decoherence, an increasing intensity V is required for strong lattices. The analysis of this effect requires a treatment beyond the linear response of the system (i.e. not contained in the dynamic structure factor), as shown in the spectra of the full time-dependent Gutzwiller calculation in Fig. 9.8. Whereas the response in the limit of very small V shown in the insets of Fig. 9.8(a)-(c) is given by δ-shaped peaks as expected, there is a drastic non-trivial broadening of the different peaks for typical experimental intensities $V \approx 0.1E_r$, shown in the respective main figures. This indicates a breakdown of the non-interacting quasiparticle picture of the Bose-Hubbard Model due to the large V. Whereas the amplitude mode's signature is generally stronger in the energy- and $n(\mathbf{k} = 0)$ than in the $n(\mathbf{k} = \mathbf{p}_B)$ profile, the scaling of its spectral weight is nonlinear in V (and thus beyond linear response in this large $V \cdot t$ regime), as shown in comparison of Figs. 9.8(a),(b) and the respective insets.

At high intensity V the spectra are not only broadened, but the supposed resonance frequencies of all modes (gray squares in Fig. 9.8(d)) are systematically shifted to lower frequencies with respect to the true quasiparticle energies (indicated by dashed white lines in Fig. 9.8(a)-(c) and circles in d)), consistent with results obtained within the random phase approximation [115, 118]), i.e. the quasiparticle energies are renormalized by the interaction induced by V. The error bars and shaded areas in Fig. 9.8(d) indicate the FWHM of the energy absorption profile after $t = 10$ms, quantifying the systematic uncertainty in the extracted energies. To the best of our knowledge, this has not been considered in the analysis of experimental data thus far.

9.8 Comparison with Linear Response Theory

According to time-dependent perturbation theory, taking only first order terms into account (i.e. maximally a single scattering process by the perturbing operator), the absorbed energy scales as $E(t) \propto V^2t^2$. The proportionality constant is given by the matrix element (which does not depend on V or t) connecting the initial (ground) state and the final state. Time-dependent perturbation theory does not require a periodic modulation of the perturbing operator in time, although this is exactly the case for Bragg spectroscopy. For a very strong perturbation, it also provides a valid description for a very short time, where the perturbation can be approximated to be constant and where $V \cdot t$ is small. However, this is not the limit, in which Fermi's golden rule applies. Here one furthermore assumes very long times with respect to the inverse modulation frequency, i.e. where the system is exposed to very many cycles and the Fourier width of the $sinc^2$ response becomes very narrow and is well approximated by a δ-distribution. At the same time, the perturbation has to be sufficiently weak over the total temporal interval, that only single scattering processes have to be considered (and for ever longer times, the intensity V has to be reduced accordingly to recover the δ limit). For lowest band physics in cold atomic systems, this long time scale is essentially not within reach (the typical frequencies are below 2kHz and coherence times not much longer than 10's of ms). At the same time, the intensity in experiments has to be adjusted sufficiently high to observe a signal and distinguish it from the background noise (i.e. transfer enough atoms

into higher k states), a requirement which intrinsically contradicts the assumptions of first order temporal perturbation theory.

To demonstrate the deviations from linear response theory, the absorbed energy is shown as a function of time and the Bragg frequency in Fig. (9.9), both on a linear set of axes and on a double logarithmic scale.

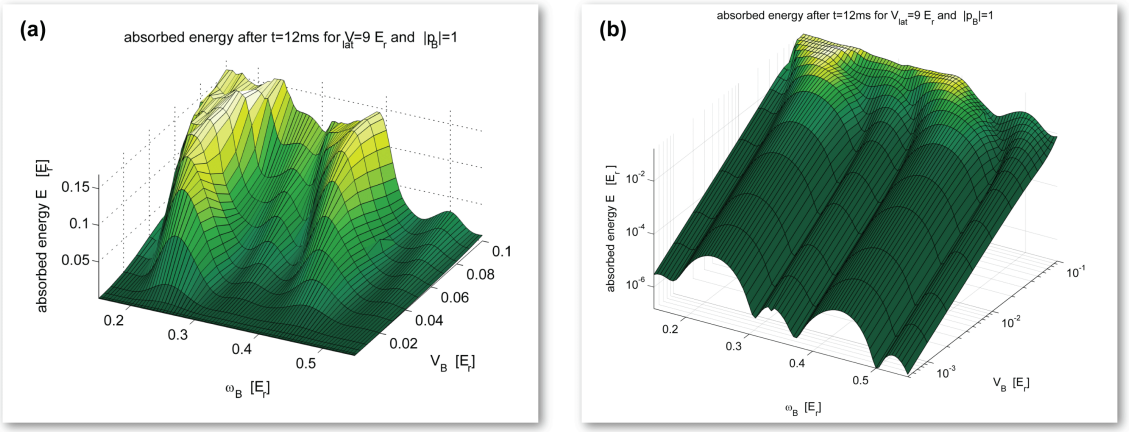

Figure 9.9: Energy absorption at fixed time $t = 12$ms as a function of the Bragg frequency and intensity V, once on a linear scale in (a) and a log-log scale in (b). According to time-dependent perturbation theory, the energy absorption is proportional to t^2, i.e. shows a linear dependence on the log-log scale with a slope of two.

On the log-log plot, the absorbed energy exactly increases with a slope of 2 (i.e. the absorbed energy increases quadratically) in time for all frequencies at short times, which is in accordance with linear response theory. After the system has absorbed a sufficient amount of energy and is no longer close to the initial ground state, the absorbed energy saturates and the absorption peaks are shifted to lower frequencies. This explicitly demonstrates the renormalization of the collective mode frequencies and the intensity broadening of the peaks, which is beyond linear response theory.

9.9 Results for a Realistic Trapped System & Experimental Comparison

Apart from the high intensity of the probing beam required to observe a response in the interacting lattice system, two additional effects have to be considered within a realistic modeling of the experiment: the deviation from a homogeneous system due to the trap, as well as the pulse shape.

Experimental Procedure

In the experiment performed by S. Götze et al. in the Sengstock group at the University of Hamburg [64], ^{87}Rb atoms are cooled in a shallow magnetic trap with $\omega = 2\pi \cdot (16, 16, 11)$ Hz, forming a Bose-Einstein condensate before a 3D cubic optical lattice with a spacing of $a = 515$nm is slowly ramped up to a final intensity of s recoil energies E_r, as described in Ref. [46]. This transfers the atoms into a condensed state in the lowest band of the lattice, where the system is well described by the Bose-Hubbard Model and the s-wave interaction through the background scattering length is parametrized by the interaction constant U. Subsequently, two Bragg laser beams with a slight frequency detuning ω_B but essentially the same wavelength $\lambda = 781.37$nm (i.e. $|\omega_B| \ll c/\lambda$), lying in the x-y-plane of the optical lattice at a coincident angle $\theta_B = 45°$, are applied. This allows the atoms to undergo a two-photon process, in which the momentum kick experienced by an atom is given by $|\mathbf{p}_B| = (4\pi/\lambda)\sin(2\theta_B)$. The specific experimental setup allows the system to be probed along the nodal direction. For brevity, all dispersion relations and results shown in this paper are along this line, connecting the $\Gamma = (0, 0, 0)$ and $M = (1, 1, 0)$ points in the first Brillouin zone.

The Trapping Potential

Every experiment is performed in a finite system and for cold atom experiments the atoms are usually confined by a trapping potential in each dimensional direction. If the spatial extent of the cloud is small compared to the beam width, this is well approximated by a harmonic trap. One may approximately describe the effect of an inhomogeneous system on the energy absorption within the local density approximation, if the spatial potential varies slowly on the scale of the healing length. Within this picture, a small spatial part of the system with an approximately constant potential is approximated by an infinitely large homogeneous system with the corresponding density. The energy transfer rate (or other quantities of interest) in the inhomogeneous system is then obtained by the density-weighted average over the homogeneous systems. However, this approximation fails to describe the collective mode structure in an inhomogeneous system, since the modes may generally still be spatially delocalized. Nevertheless, within the local density approximation (LDA) and the linear response regime, one would expect the δ-like absorption peaks at fixed Bragg-momentum $\mathbf{p}$ to be smeared out over the range of energies corresponding to the densities appearing in the trapped system. The density-dependence of the collective mode energies in the homogeneous system is shown in Fig. (9.10b) for both the weakly and strongly interacting condensate at a fixed quasi-momentum $|\mathbf{k}| = \pi/a$. In contrast to the weakly interacting case, where the quasiparticle energies of the different modes depend approximately linearly on the density (black dotted lines in Fig. 9.10(b)), the dependence in the strongly interacting case is highly non-trivial. The strong dependence can be understood from the excitational particle and hole branches, which may cross each other in the Mott insulator: crossing the phase transition into the SF, the emerging condensate couples the particle/hole branches in the equations of motion, hybridizing these and leading to avoided mode crossings at the previous intersection points, as is shown by the blue squares in Fig. 9.10(b). For all $\mathbf{k}$, U/J and densities in the SF, the sound (amplitude) mode remains the energetically lowest (second lowest) lying mode. Comparing our theoretical results with Bogoliubov theory (black dashed line in Fig. 9.10(a)), excellent agreement is obtained in the weakly interacting limit. At intermediate interactions $s = 9$ ($U/J \approx 8.55$) and density $n = 1$ shown in Fig. 9.8(d)), neither Bogoliubov theory (dotted blue line), nor the theory presented by Huber et al. [80] for strong interactions (dashed green lines) apply and deviate from our results. Here, the dispersion relation obtained by the dynamic Gutzwiller method (black circles in Fig. 9.8(d)) remains valid and continuously connects these two limiting theories.

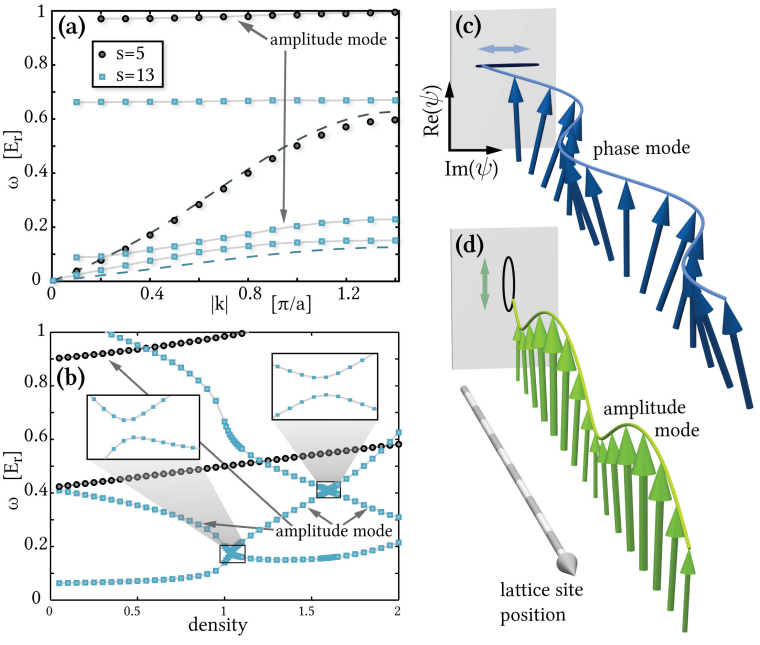

Figure 9.10: (a,b): theoretical dispersion relations for the homogeneous system in the linear response limit at $n = 1$ (a) and density-dependence at $|\mathbf{k}| = \pi/a$ (b) in the SF for weak ($s = 5$, black circles) and strong ($s = 13$, blue squares) interactions. Corresponding Bogoliubov results are shown as black dashed lines in (a). (c,d): Illustration of the order parameter for a coherent excitation of the phase (sound) mode (c) and the amplitude mode (d) in a homogeneous condensate at $\mathbf{k} = (0.8/a, 0, 0)$ and $s = 13$. The projection of all $\psi_\mathbf{i}$'s in the complex plane is shown by the black ellipses: for the sound mode (c), the oscillation is almost exclusively in the tangential, for the amplitude mode (d) mainly in the radial (i.e. in the amplitude) direction.

Here, we go beyond the LDA approximation and simulate the dynamical evolution of the system in a full spatially resolved, time-dependent Gutzwiller calculation. In 3D this contains the full structure of the collective modes in the inhomogeneous system, which can be explicitly obtained as the eigenmodes of the linearized equations of motion as was discussed in chapter (7).

In the experiment, the harmonic trap frequencies in the three dimensions were determined to be $\omega = 2\pi \cdot (26, 26, 21)\,\mathrm{Hz}$ and the total particle number was determined to be $N = 50\,000 \pm 30\%$. The corresponding ground state density distribution for the strongly interacting condensate at $s = 13E_r$ in three dimensions was determined within a static Gutzwiller distribution and is shown in Fig. (9.11). Since the trapping frequency is lower along the z-direction, it is slightly cigar-shaped with a radial width of ≈ 50 lattice sites in the x and y-directions and ≈ 72 sites in the z-direction. The maximum filling (number of atoms per lattice site) at the center is $n_{\mathrm{center}} \approx 1.05$ for this lattice depth. This state is taken as the initial state for the time-dependent Gutzwiller simulation in the presence of the Bragg beam, as discussed in the following paragraph. A shallow trap and low filling $n \lesssim 1.05$, due to the strong density dependence of the mode frequencies, are crucial for an unambiguous identification of the amplitude mode.

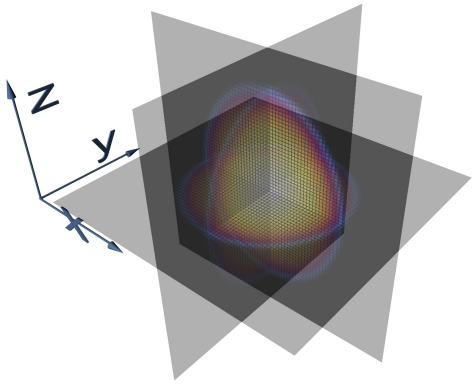

Figure 9.11: Density distribution in the $\omega = 2\pi \cdot (26, 26, 21)\,\mathrm{Hz}$ trap at a lattice depth of $s = 13$. The maximum filling in the center is ≈ 1.05 and at a chemical potential of $\mu = 0.53\mathrm{U}$, there are $N \approx 50\,000$ particles in the system.

The Bragg Pulse

As can be seen from Fig. (9.8) and was mentioned before, a square Bragg pulse leads to the Fourier transformed response in frequency space, i.e. a sinc-function. Only a finite pulse time on the order of 10ms can be used under typical experimental conditions before decoherence sets in. For a square pulse, the resulting wide ringing signal in frequency space would obscure the extraction of a clear peak maximum. To minimize the oscillatory response for a restricted Bragg pulse time, a Blackman-Harris pulse [71] is used to obtain the central results shown in Fig. 9.12, both in experiment and theory. This is essentially a Gaussian (on a compact carrier) envelope function for the modulated Bragg beam, which therefore also leads to an approximately Gaussian response in frequency space. For an equal pulse time, the maximum intensity of such a Blackman-Harris pulse has to be larger than that of a square pulse, if the same number of atoms is to be scattered.

What can be Measured in the Strongly Interacting Condensate

At large s, an additional complication arises in experiments: since the condensate is strongly depleted, the time of flight images are very similar to those of a thermal cloud within the signal to noise ratio and much less information is contained in the time of flight profiles than for the weakly interacting case (where the structure originates from the particle from the condensate).

This is exacerbated by additionally depositing energy into the system, which may partially rethermalize over the run of the experiment. It is therefore not suitable to directly analyze the time of flight profiles in the deep lattice, directly after the system was exposed to the Bragg beams. Rather, one is interested in the amount of energy deposited into the system by the Bragg beams. The total energy of the system is approximately conserved after the Bragg beams have been switched off and the lattice depth is ramped down linearly over 10ms to $s = 10$, bringing the system into a weakly interacting regime. Here it is left to equilibrate and a condensate forms at the lower lattice depth, the condensate fraction of which can be well extracted from the time of flight images. The energy absorbed from the Bragg pulse, leading to an effective temperature in the equilibrated condensate is inversely, but monotonically related to the visibility [20] and it is useful to compare these two quantities.

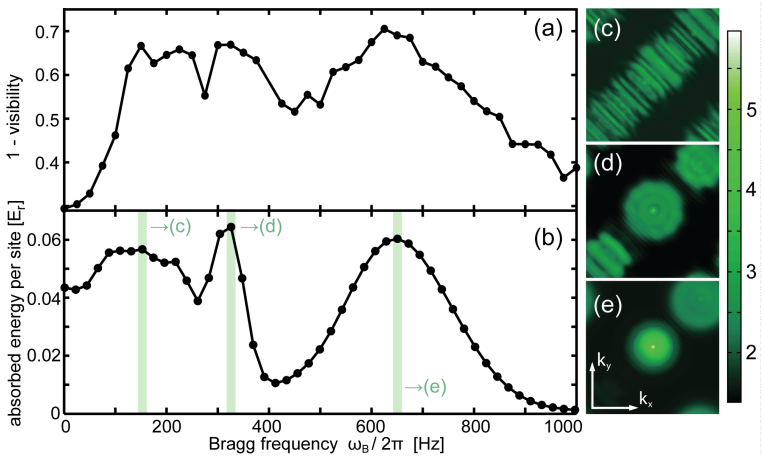

Figure 9.12: Comparison of the experimental visibility (a) and theoretically predicted energy absorption (b) at $|\mathbf{p}_B| = \pi/a$ using a Blackman-Harris pulse of 10ms in an optical lattice with $s = 13$ in a 3D trap. A maximum intensity $V = 0.27E_r$ and the experimentally determined total particle number $N_{\text{tot}} = 5 \cdot 10^4 \pm 33\%$ and $\omega = 2\pi \cdot (26, 26, 21)$ Hz trapping frequency were used for (b), leading to a maximum central density $n = 1.05$. The lower peak is the sound mode, mainly broadened by the high intensity of the Bragg beam to lower frequencies. The upper peak at 650Hz is the gapped amplitude mode, broadened mainly by the trap. Figures (c,d,e) show the theoretically predicted trap broadened logarithmic quasi-momentum distributions in the first Brillouin zone at the frequencies marked by the green lines in (b).

This experimentally measured visibility is shown as a function of the Bragg frequency in Fig. (9.12) and compared to the theoretically predicted energy absorption from a time-dependent Gutzwiller simulation for the trapped system. The lower peak at ~ 200Hz in the spectra is the trap- and intensity-broadened sound mode, whereas the higher peak at ~ 650Hz is the amplitude mode, broadened mainly by the strong density dependence. We stress that only by taking all these effects into account, the good quantitative agreement, shown in Fig. 9.12(b), between theory and experiment in the spectra is achieved.

Dependence on the Lattice Depth

The absorbed energy shown in Fig. (9.12) is for a single value of the lattice depth only. To obtain a clear signal from the amplitude mode, the lattice depth may not be chosen to low, since then the amplitude mode does not have a strong spectral weight and not contribute significantly to the

energy absorption. To be sure that a collective mode in the condensate, and not the particle-hole mode from the Mott insulating state is measured, the lattice depth may also not be chosen too strong, as otherwise some regions in the trap would be in a Mott-insulating like state within an local density approach picture. The chosen lattice depth of $s = 13$ lies within this window.

The dependence of the absorbed energy on the lattice depth is of interest and the experimentally measured signal is shown in Fig. (9.13).

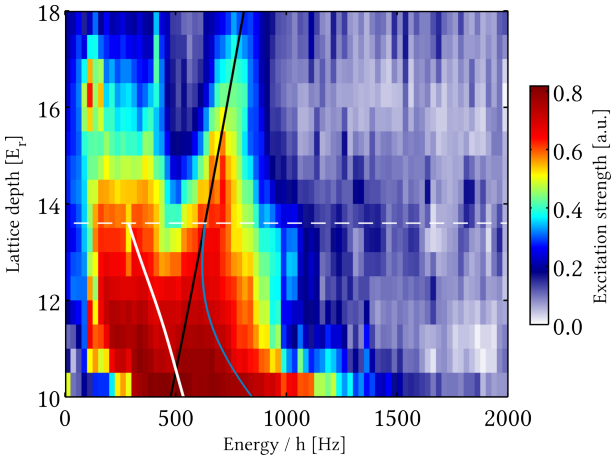

Figure 9.13: The experimentally measured frequency-dependent excitation signal (monotonically related to the absorbed energy) as a function of the lattice depth s at a Bragg momentum of $\mathbf{p}_B = q_l/\sqrt{2}(1,1,0)$. The interaction constant U is shown in black and the dashed white line indicates the mean-field Mott insulator transition in a homogeneous system at density $n = 1$. As a guide to the eye, the blue and white lines indicate the position of the amplitude and sound mode in a homogeneous system at density $n = 1.3$ respectively. It is a coincidence and specific to this filling that the amplitude mode energy seems to approach U at the $n = 1$ mean-field transition. The data is taken from [64].

The blue and white lines in Fig. (9.13), which respectively indicate the energies of the amplitude and the sound mode in the homogeneous system at density $n = 1.3$ only serve as a reference and not as a quantitative comparison. We furthermore point out that it is a matter of coincidence and specific to this density that the amplitude mode energy approaches the interaction energy U, indicated by the black line. For a quantitative comparison, one has to consider that the ground state density distribution of the cloud depends on the lattice depth s. Thus the experimentally measured energy in Fig. (9.13) should not be understood to be at a fixed LDA-averaged density, which significantly complicates the interpretation of the data without further analysis. It should also be noted that beyond the Mott insulator transition point in the homogeneous system at $n = 1$ (indicated by the dashed white line in Fig. (9.13)), the inhomogeneous system in the trap is not in a Mott insulating state. The measured excitation signal in this regime can thus not be uniquely attributed to the collective particle-hole mode in the Mott insulator, but could also be attributed to the superfluid parts of the inhomogeneous cloud within the LDA picture. A more detailed investigation, if possible beyond the scope of time-dependent bosonic Gutzwiller theory (to capture the relevant dynamical effects in the Mott insulator) is of interest to the understanding of these results in the strongly interacting regime beyond the critical interaction strength.

10. Lattice Modulation Spectroscopy

In this chapter, we theoretically describe and discuss lattice modulation spectroscopy, which an alternative spectroscopic technique, with which excitational properties of the gas in the lattice can be measured. In most literature it is claimed, that lattice modulation spectroscopy corresponds to a temporal modulation of the hopping parameter J, which is true to lowest order. It is however commonly overlooked, that there a fundamental connection to Bragg spectroscopy exists. In fact, lattice modulation spectroscopy corresponds to two, simultaneous and coherent Bragg probing processes with a Bragg wavelength corresponding to the wavelength of the lattice. This will be directly seen on the operator level, when comparing the lattice modulation operator with the Bragg operator. Physically this is to be expected, since a slow (compared to the laser frequency) modulation in the intensity of the laser beam could equally well be constructed by using the usual static lattice lasers and additionally, from each of the two sides, superimposing the light of two coherent lasers, which are slightly detuned by the modulation frequency. Each pair of opposing, but frequency detuned lasers can be understood as a Bragg probing laser setup, at a Bragg frequency corresponding to the detuning and a Bragg momentum of $2\pi/a$, i.e. corresponding to quasi-momentum of zero.

To derive the operator corresponding to lattice modulation spectroscopy, we begin with the classical electric fields describing the probing beam. Here, the perturbation is a high frequency reflected wave, as before, but modulated by a low modulation frequency ω_m, leading to a beat signal: The incoming electric field is thus

$$\mathbf{E}_{\text{in}}(x,t) = \mathcal{E}\,\sin(kx+\omega t)\,\sin(\omega_m t) \tag{10.1}$$

and the subsequent derivation is analogous to before, with an outgoing electric field

$$\mathbf{E}_{\text{out}}(x,t) = \mathcal{E}\,\sin(kx-\omega t)\,\sin(\omega_m t) \tag{10.2}$$

eventually leading to the operator in second quantization in k-space

$$\hat{V}_{\text{mod}} = \kappa\mathcal{E}^2\,\sin^2(\omega_m t)\,(\rho^\dagger_{2k}+\rho^\dagger_{-2k}) \tag{10.3}$$

where we furthermore assumed $\omega_m \ll \omega$ and $k = q_l = \frac{\pi}{a}$ corresponds to the lattice vector.

Expressing the operator $\rho^\dagger_{2k}$ (with $k = q_l$) in the Bloch and Wannier bases leads to

$$\begin{aligned}\rho^\dagger_{2q_l} &= \sum_{\alpha,\alpha'=1}^{\infty}\sum_{n\in\mathbb{N}}\sum_{k\in 1\text{stBZ}} {c_{n+1}^{(\alpha,k)}}^{*} c_n^{(\alpha',k)}\, {b_k^{(\alpha)}}^{\dagger} b_k^{(\alpha')} \\ &= \sum_{\alpha,\alpha'=1}^{\infty}\sum_{l,l'=1}^{L} D_{l,l'}^{(\alpha,\alpha')}\, {b_l^{(\alpha)}}^{\dagger} b_{l'}^{(\alpha')}\end{aligned} \tag{10.4}$$

with

$$D_{l,l'}^{(\alpha,\alpha')}(s) \equiv \frac{1}{L}\sum_{n\in\mathbb{N}}\sum_{k\in 1\text{stBZ}} e^{iak(l-l')} c_{n+1}^{(\alpha,k)*} c_n^{(\alpha',k)} \tag{10.5}$$

To see, that the dominant contribution is the coupling of nearest neighboring sites, i.e. that lattice modulation is mainly a modulation of the nearest neighbor hopping J, we evaluate this expression numerically for various lattice intensities s, which is shown in Fig. (10.1). The matrix elements of the operator from the opposite momentum $\rho^{\dagger}_{-2q_l}$ are related by $D_{l,l'}^{(\alpha,\alpha')}(-2q_l) = D_{l,l'}^{(\alpha',\alpha)}(2q_l)$.

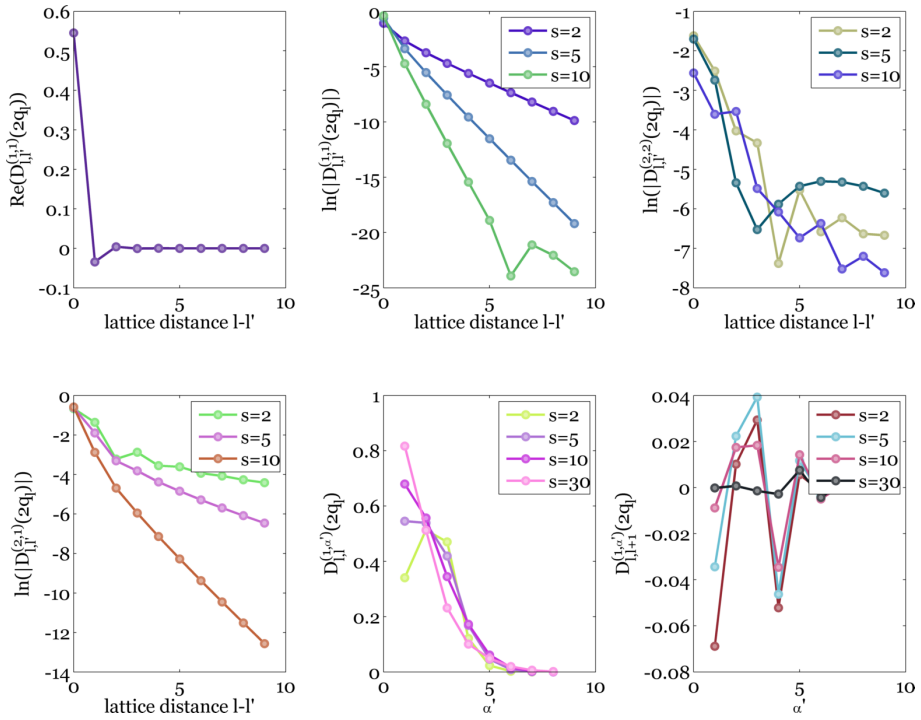

Figure 10.1: The matrix elements $D_{l,l'}^{(\alpha,\alpha')}(s)$ required to express the Bragg operator in the lowest band Wannier basis. The elements describing the coupling between different Wannier states decay exponentially with the distance between these states.

Due to the exponential suppression of the matrix elements with increasing distance, the short ranged terms are generally more important if they lead to a non-trivial coupling. For Bragg spectroscopy, the on-site term, describing a density wave dominates. For lattice modulation spectroscopy, on the other hand, this term simply couples to the overall potential and leads to an irrelevant overall phase. Thus the most important term for lattice modulation spectroscopy is the next highest order, i.e. the nearest neighbor coupling, which is nothing else but an additional time-dependent contribution to the hopping term J.

To draw a connection to the lattice modulation experiments by Stöferle et al. [157, 140], we furthermore performed a time-dependent Gutzwiller calculation based on their experimental parameters. Usually, lattice modulation is understood as a periodic modulation of the nearest neighbor hopping element J, whereas Bragg spectroscopy is thought of as a spatial sinusoidal wave in the on-site energies, moving through the lattice at a velocity $\frac{\omega_B}{p_B}$. Both of these approximations are only true up to lowest order. Here we shortly derive the exact description of these two processes (as used in our numerical implementation) and also point out a fundamental connection between lattice amplitude modulation and Bragg spectroscopy.

It is useful to express the optical lattice potential operator in terms of the momentum shift operator ρ_p (up to a constant) as $V_{\text{lat}} = \frac{sE_r}{4}(\rho^\dagger_{2q_l} + \rho^\dagger_{-2q_l})$. During lattice modulation spectroscopy, the lattice amplitude is temporally modulated with a frequency ω_m and the perturbing operator becomes

$$\hat{V}_{\text{mod}} = \frac{V_m}{4}\cos(\omega_m t)\,(\rho^\dagger_{2q_l} + \rho^\dagger_{-2q_l}). \tag{10.6}$$

Decomposing the cosine into its two complex exponential constituents, this form of the lattice amplitude modulation operator reveals that it corresponds exactly to the sum of two Bragg processes with opposite frequencies $\omega_B = \pm\omega_m$ at fixed momenta $p = \pm 2q_l$ in the direction of the modulated lattice laser beam. However, in contrast to Bragg spectroscopy at $q \neq 2mq_l$ with $m \in \mathbb{Z}$, where the most relevant lowest order term is the offset of the local potential, this term is irrelevant for lattice amplitude modulation (at $q = 2q_l$), where this potential offset is equal for every site and thus only leads to an irrelevant global phase. Hence, the physically relevant lowest order term for lattice amplitude modulation is the temporally modulated coupling to the nearest neighboring sites, i.e. a modulation of J.

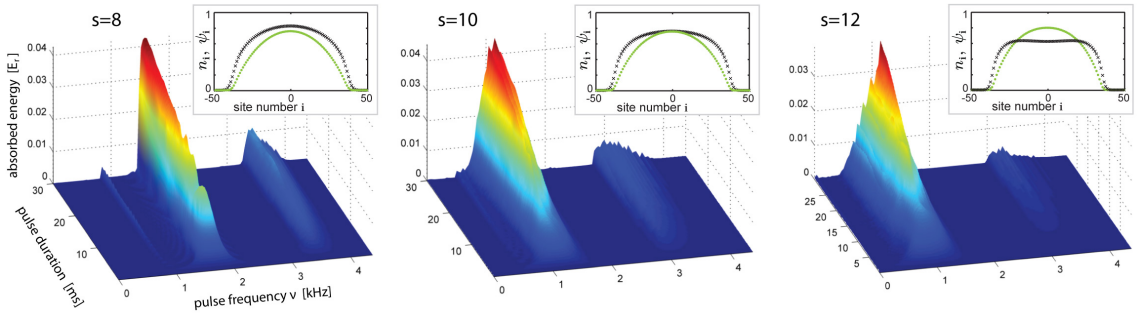

Figure 10.2: Absorbed energy in the condensate during lattice amplitude modulation for different lattice amplitudes $s = 8, 10, 12$. Note that the resonance frequency of the lowest mode (amplitude mode at $k = 0$) decreases with increasing lattice intensity (i.e. increasing interaction strength) in accordance with the experimental observation [157]. The insets show the ground state density profile $n_\mathbf{i}$ (green dots) and the corresponding order parameter distribution $\psi_\mathbf{i}$ (black crosses) along the x-direction through the center of the 3D trap, determined for the respective experimental parameters.

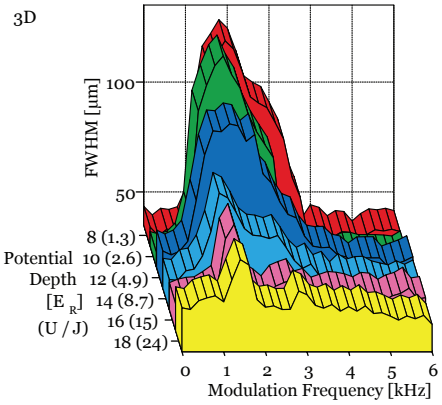

Figure 10.3: The experimentally measured signal at various lattice depths in the experiment by Stöferle et al. in the Esslinger group. The image is taken from [157].

The absorbed energy, calculated within a time-dependent bosonic Gutzwiller calculation, is shown in Fig. 2 as a function of the modulation frequency and the exposure time. The parameters

for this simulation were chosen in accordance with the experiment [157], i.e. ^{87}Rb atoms in a 826nm optical lattice were exposed to a modulation of 20% of the lattice depth and the maximum shown time of 30ms corresponds to the experimental exposure time. We considered three lattice intensities $s = 8, 10, 12$ corresponding to different ratios of U/J, all on the condensate side of the superfluid-Mott insulator transition. The initial density distribution was chosen, such that the central density agreed with the central density calculated for the actual experimental situation (insets in Fig. 2), with a total particle number of $N = 1.5 \times 10^5$ in a lattice with an underlying $\omega = 2\pi \cdot (18, 20, 22)$ Hz harmonic trap and translational invariance was assumed in the z direction. The frequencies of the absorption peaks in our simulation agree well with the position of the observed maxima for the different lattice intensities. The experimentally observed peak widths are, however, considerably larger than in our simulations, an effect which may be attributed to a finite temperature in experiment, as opposed to $T = 0$ in the simulation. Moreover, an increase in the harmonic trapping frequency due to the lattice beams, which was not specified in [157] and accounted for in our simulation, may lead to a higher particle density at the center and hence also a greater inhomogeneity in the density profile, which would lead to a broadening of the absorption peaks. Due to this discrepancy in the peak width, we cannot claim to obtain real quantitative agreement with the experimental data, as for our Bragg experiment. The good correspondence in the peak positions does however indicate, that the lowest peak in the 3D measurement [157] can be associated with the amplitude mode at $k = 0$.

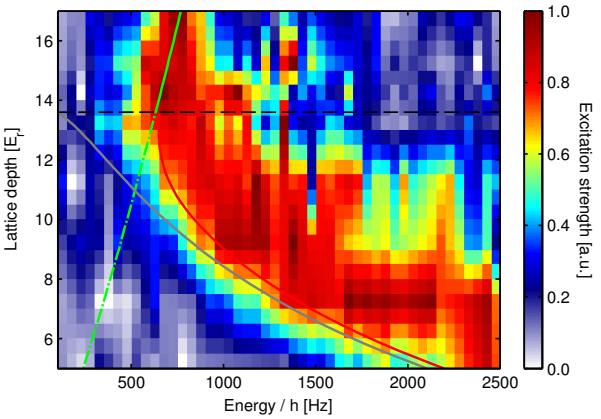

Figure 10.4: The experimentally measured excitation strength from lattice modulation spectroscopy, which is a measure for the absorbed energy, as a function of the lattice depth and the modulation frequency. As for the analogous data from Bragg spectroscopy, it should be kept in mind that the ground state density distribution of the gas depends on the lattice depth. For a rough comparison, the theoretically predicted energy of the amplitude mode at $\mathbf{k} = 0$ in the homogeneous system is indicated by the red line for a density of $n = 1.4$ and by the gray line for $n = 1$. In the homogeneous system, the amplitude mode's energy gap closes when approaching the quantum phase transition. The data was measured by S. Götze et al. [64].

We found that with lattice amplitude modulation spectroscopy the Bogoliubov sound mode cannot be excited, also when going beyond the linear response regime. Thus all peaks observed in the strongly interacting condensate can be attributed to the amplitude and higher gapped modes at $k = 0$ and we furthermore point out that the larger width of the peaks cannot directly be attributed to the condensate phase. This is also in accordance with the experimental data measured by S. Götze et al. in the group of K. Sengstock, shown in Fig. (10.4). The peak ranging from $\nu = 0.9$kHz to 1.9kHz for different lattice intensities in our simulation can be identified with the amplitude mode at $k = 0$, but seems to overlap and merges with the next mode in the experimental data. When crossing the phase transition into the Mott insulator, combined particle-hole modes appear at an energetically similar position as the amplitude mode. However, the quasi-particle structure fundamentally changes when crossing the superfluid-Mott insulator transition and we emphasize that the amplitude mode cannot simply be seen as the U-mode in the condensate. Whereas the phase response of a coherently excited amplitude mode state vanishes when approaching the

transition from the superfluid side, this is large everywhere in the Mott insulator for both the particle and hole branches.

11. Collapse and Revival of a Coherent Matter Field

We now address another intriguing example of dynamics in strongly interacting bosons far from equilibrium: the collapse and revival (CR) of a condensate when the lattice is suddenly ramped up and local interactions dominate [69, 5, 92, 141]. This has been successfully used to observe physics beyond the Bose-Hubbard model, quantifying the density-dependence of the intra- and interspecies interaction energy arising from the admixture of higher band contributions [172, 84, 171, 116]. In recent works [54, 173, 139] the effect of a trapping potential on the $n(\mathbf{k} = 0)$ component during CR, as well as a renormalization of the revival time by a finite J have been considered.

In this chapter we study the full momentum distribution during CR dynamics. We show that after a sudden lattice quench, the dynamics in an inhomogeneous spatial potential can be described by an effective single-particle theory at the discrete times of quantum phase revivals in the limit of negligible J. For the specific case of a harmonic potential, condensate states consisting of coherent superpositions of discrete, equidistantly spaced quasi-momentum states are obtained, forming an intriguing case of non-equilibrium state preparation. The position of the quasi-momentum components in the first Brillouin zone is highly sensitive to a shift of the trapping potential relative to the lattice (see Fig. 11.1) and the appearance of the peaked momentum pattern requires the harmonic trapping time scale to be a rational multiple of the revival time. In an experiment this allows to extract the global trapping potential with high precision. We derive an approximate analytic theory based solely on the dynamical evolution of the single-particle density matrix (SPDM). We verify the applicability under experimental conditions by furthermore performing a numerical analysis based on dynamic bosonic Gutzwiller theory, which includes condensate depletion in the initial state, finite size effects and finite tunneling.

We briefly review the basic CR physics, and proceed by extending the analysis to inhomogeneous systems, including other effects, such as finite tunneling and density-dependent interaction parameters. To observe CR, a bosonic system of atoms in an optical lattice is prepared in a Bose condensed state, before the lattice depth s (expressed in units of the recoil energy E_r) is suddenly ramped up [172, 171, 69] (typically to $s \geq 25$), such that the interaction strength U becomes the dominating energy scale.

11.1 Homogeneous Case

In the case of a homogeneous system, where all lattice sites are equivalent and s is sufficiently high that J/U can be neglected [1], the subsequent time evolution is generated by the Hamiltonian

[1] e.g. for ^{87}Rb in a 738nm $s = 40$ lattice, $J/U \approx 10^{-4}$.

$\mathcal{H} = \frac{U}{2}\hat{n}(\hat{n}-1)$. The evolution of a local annihilation operator can be expressed in the Heisenberg representation as (choosing $\hbar = 1$)

$$b(t) = e^{i\mathcal{H}t} b\, e^{-i\mathcal{H}t} = e^{-iU\hat{n}t}\, b\,. \tag{11.1}$$

We note that the bosonic Gutzwiller method is well justified here, as it assumes a product state of local on-site states. The local number statistics in the superfluid (SF) before the ramp-up, including number squeezing at initially finite U/J is well described and becomes Poissonian in the limit $U/J \to 0$. In this ideal limit, the ground state for a system consisting of N particles on L sites becomes a coherent state in the $\mathbf{k} = 0$ mode $|\psi\rangle = |z\rangle_1 \otimes \ldots \otimes |z\rangle_L$ within a grand-canonical, $U(1)$-symmetry breaking description with a density $n = N/L = |z|^2$. For this state the expectation value of the order parameter (11.1) during CR can then be evaluated exactly [172, 81, 27]

$$\psi(t) = \langle b(t)\rangle = z \exp\left(|z|^2\left(e^{-iUt} - 1\right)\right)\,. \tag{11.2}$$

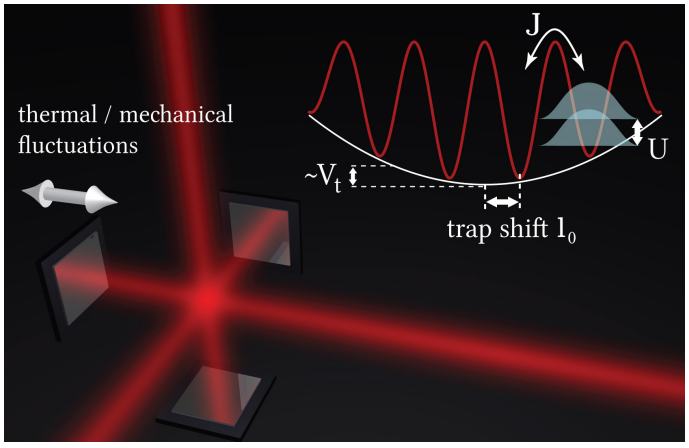

Figure 11.1: The trap shift $\mathbf{l}_0$ is defined as the distance between the minimum of the harmonic potential and the center of the next lattice site (in units of the lattice constant a). As the confinement is created by laser beams different from those creating the lattice in a given direction, thermal and mechanical fluctuations in the experimental setup can lead to a change in $\mathbf{l}_0$.

The condensate fraction is defined as $f_c = \lambda_0/N$, where λ_0 is the largest eigenvalue of the SPDM $\rho_{\mathbf{l},\mathbf{l}'} = \langle b^\dagger_{\mathbf{l}} b_{\mathbf{l}'}\rangle$ and $\mathbf{l}$ is the vectorial site index on the 3D lattice. In the limit of a large homogeneous system, Eq. (11.2) leads to

$$f_c(t) = e^{2|z|^2(\cos(Ut)-1)}, \tag{11.3}$$

which is monotonically related to the visibility measured in experiments [63, 172]. At times $t_m = m\, t_{\mathrm{rev}}$ with the revival time $t_{\mathrm{rev}} = 2\pi/U$ and $m \in \mathbb{N}$, the coefficients $c_n(t)$ in the Fock representation $|\psi(t)\rangle_{\mathbf{l}} = \sum_{n=0}^{\infty} c_n(t)|n\rangle_{\mathbf{l}}$ periodically coincide after having performed $mn(n-1)/2$ rotations in the complex plane, which leads to a revival of the initial condensate. In the case of finite interactions $U/J > 0$ prior to the ramp-up, the phenomenological ansatz

$$f_c(t) = \alpha\, e^{2\beta(\cos(Ut)-1)} - \gamma \tag{11.4}$$

leads to a remarkably good agreement with the exact numerical results for arbitrarily long times. The fitting parameters $\alpha, \beta, \gamma \in \mathbb{R}$ incorporate number squeezing and depletion in the initial condensate.

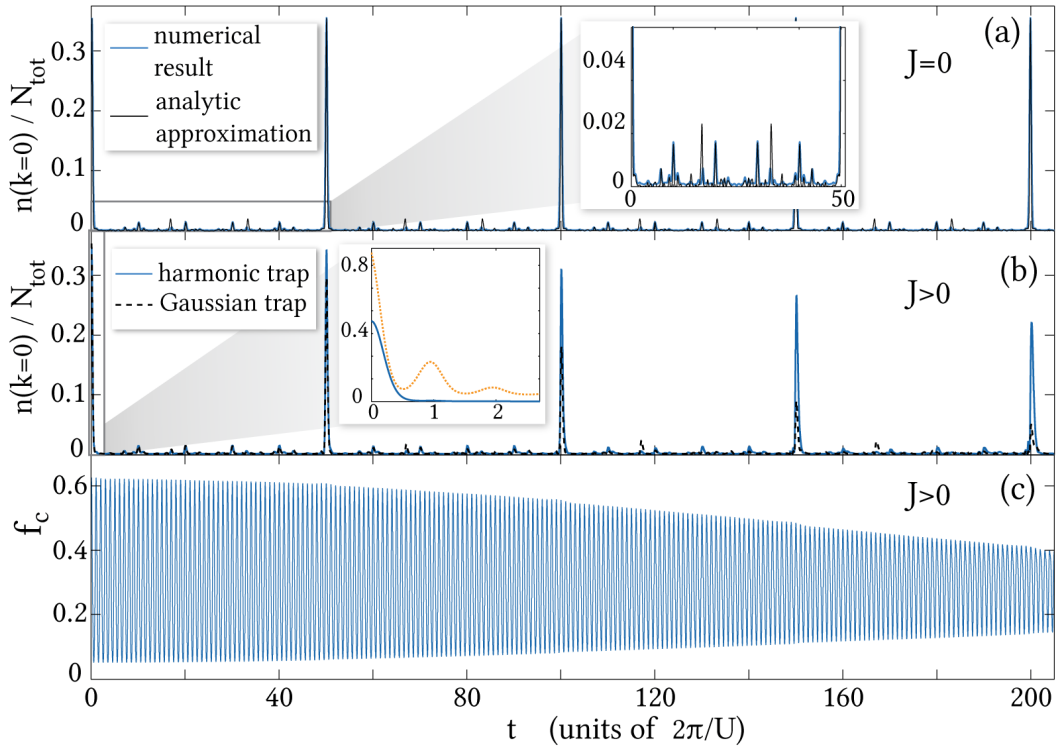

Figure 11.2: Time-dependent occupation of the $\mathbf{k} = 0$ mode (a, b) and condensate fraction (c) for a ^{87}Rb condensate prepared in a 738nm lattice with a central density of $n = 2.6$. The lattice is ramped up from $s = 8$ and a 157.4Hz trap to $s = 26$ and a 346.2Hz trapping frequency with $\mathbf{l}_{0,i} = 0.5$, such that $t_{\mathrm{trap}} = 100 t_{\mathrm{rev}} = 28.29$ms. In subplot (a), J is artificially set to zero after the ramp to compare the numerical results to Eq. 11.9. The inset in (b) shows the initially strong decline in the occupation of the $\mathbf{k} = 0$ mode (blue line) and the central peak $N_p(t)$ (dotted orange line). The particle number in the projected 2D central peak is defined as $N_p(t) = \sum_{k_z} \sum_{\|(k_x,k_y)\|_1 \leq 0.1\frac{\pi}{a}} n(\mathbf{k}, t)$. Additionally, the dashed line in panel (b) shows $n(\mathbf{k} = 0, t)$ for a Gaussian trap, with parameters corresponding to the harmonic potential, and a cloud extension ratio $\frac{R_{cloud}}{w} = 0.1$.

11.2 Inhomogeneous Case

For an inhomogeneous system without translational symmetry, the single site description does not suffice. The time evolution in the atomic limit (neglecting J/U) is generated by the lattice Hamiltonian $\mathcal{H} = \frac{U}{2} \sum_{\mathbf{l}} \hat{n}_{\mathbf{l}}(\hat{n}_{\mathbf{l}} - 1) - \sum_{\mathbf{l}} \mu_{\mathbf{l}} \hat{n}_{\mathbf{l}}$ with the effective chemical potential $\mu_{\mathbf{l}}$ at lattice site $\mathbf{l}$ accounting for the inhomogeneity. Analogously, the time evolution of the local annihilation operators in the Heisenberg picture is

$$b_{\mathbf{l}}(t) = e^{i\mathcal{H}t} b_{\mathbf{l}}\, e^{-i\mathcal{H}t} = e^{-i(U\hat{n}_{\mathbf{l}} - \mu_{\mathbf{l}})t} b_{\mathbf{l}}. \tag{11.5}$$

In case of an initially ideal (but not necessarily homogeneous) condensate, the time- and position-dependent local order parameter can be evaluated exactly

$$\psi_{\mathbf{l}}(t) = \langle b_{\mathbf{l}}(t) \rangle = z_{\mathbf{l}}\, e^{i\mu_{\mathbf{l}} t} e^{|z_{\mathbf{l}}|^2 (e^{-iUt} - 1)}. \tag{11.6}$$

We now turn to the condensate fraction by the convenient decomposition of the SPDM using Eq. (11.5)

$$\rho_{\mathbf{l},\mathbf{l}'}(t) = e^{-i\mu_{\mathbf{l}} t} \langle b_{\mathbf{l}}^\dagger\, e^{iU(b_{\mathbf{l}}^\dagger b_{\mathbf{l}} - b_{\mathbf{l}'}^\dagger b_{\mathbf{l}'})t} b_{\mathbf{l}'} \rangle e^{i\mu_{\mathbf{l}'} t}. \tag{11.7}$$

Remarkably, the time-dependent condensate fraction $f_c(t)$ in an inhomogeneous system is identical to that in the homogeneous system (i.e. $\mu_{\mathbf{l}} = \mu$) for a sufficiently deep lattice (for $J/U \approx 0$ to hold) and identical U. Here, the SPDM $\rho(t) = U(t)\,\tilde{\rho}(t)\,U^\dagger(t)$ is connected to the SPDM of the homogeneous system during CR at the same time $\tilde{\rho}_{\mathbf{l},\mathbf{l}'}(t) = \langle b_{\mathbf{l}}^\dagger\, e^{iU(b_{\mathbf{l}}^\dagger b_{\mathbf{l}} - b_{\mathbf{l}'}^\dagger b_{\mathbf{l}'})t} b_{\mathbf{l}'}\rangle$ through a time dependent unitary transformation by a diagonal matrix with elements $U_{\mathbf{l},\mathbf{l}'}(t) = e^{-i\mu_{\mathbf{l}}t}\delta_{\mathbf{l},\mathbf{l}'}$, thus leaving the eigenvalues and hence the condensate fraction invariant (we emphasize that this does not rely on any approximation). This equivalence means that the revival of the condensate is actually not damped by spatial inhomogeneities. At revival times the condensate state differs from the $\mathbf{k} = 0$ Bloch state, which appears as damping in certain observables such as the visibility [69, 5, 141], but is fundamentally different from a real damping of the condensate. This relation also holds in the case of depleted condensates, where finite interactions are present prior to the ramp up, as also reflected by the numerical results for a harmonic trap shown in Fig. 11.2: whereas $f_c(t)$ (subplot (c)) is only damped by a finite J, $n(\mathbf{k} = 0)$ is almost completely suppressed after a single revival time by the very strong harmonic trap (not considering much longer times, where it may reappear as discussed later).

To calculate the condensate fraction for the specific structure of the SPDM within a Gutzwiller state, a highly efficient method was found to be the iteration of the self-consistency condition for the largest eigenvalue λ_0 in the i-th iteration step

$$\lambda_0^{(i+1)} = \lambda_0^{(i)} \sum_{\mathbf{l}} \frac{|\psi_{\mathbf{l}}|^2}{\lambda_0^{(i)} - n_{\mathbf{l}} + |\psi_{\mathbf{l}}|^2}, \tag{11.8}$$

obtained from a rearrangement of the eigenvalue equation (see appendix (E.3)for detailed discussion). It can be shown that on the interval $[\max_j(n_j - |\psi_j|^2), N_{\text{tot}}]$, the largest eigenvalue is the only attractive fixed point and rapid convergence is achieved. In the case of strong depletion, an adapted Lanczos algorithm is used.

Reverting to the Schrödinger picture of the SPDM, the decomposed form shows that if a condensate state (i.e. a normalized eigenvector $\phi_{\mathbf{l}}^{(0)}(t)$ of $\rho(t)$ corresponding to the macroscopic eigenvalue) is present at time t, its time evolution is exclusively determined by the operator $U^\dagger(t)$, i.e. $\phi_{\mathbf{l}}^{(0)}(t) = \sum_{\mathbf{l}'} U_{\mathbf{l},\mathbf{l}'}^\dagger(t)\phi_{\mathbf{l}'}^{(0)}(0)$. This time evolution is formally also valid during collapse, where the condensate fraction is suppressed. Its observation, however, is only possible at revival times t_m, which can be tuned independently, thus effectively allowing the experimental observation of single particle dynamics in a lattice at arbitrary times. Note that although the effective single particle dynamics may resemble Gross-Pitaevskii theory, its derivation and validity is fundamentally different and relies on the opposite limit $U \gg J$.

Since the true condensate fraction is experimentally not directly accessible in inhomogeneous systems [61, 117], we consider the dynamical evolution of the full quasi-momentum distribution $n(\mathbf{k})$. Under restriction to the lowest lattice band, the physical momentum distribution consists of replicas of the first Brillouin zone, scaled by the Wannier function's respective Fourier coefficient. Using the spectral decomposition of the SPDM $\rho_{\mathbf{l},\mathbf{l}'} = \sum_{i=0}^{L-1} \lambda_i\, \phi_{\mathbf{l}}^{(i)} \phi_{\mathbf{l}'}^{(i)^*}$ in conjunction with the defining property of a BEC, i.e. only a single macroscopic eigenvalue λ_0, $n(\mathbf{k})$ is found to be well approximated by

$$n(\mathbf{k}, t) \approx \frac{N}{L} f_c(t) \left| \sum_{\mathbf{l}} e^{-i\mu_{\mathbf{l}}t - ia\mathbf{k}\mathbf{l}} \phi_{\mathbf{l}}^{(0)}(0) \right|^2 + C(t). \tag{11.9}$$

To a good approximation, the non-condensed atoms lead to a constant incoherent background in $n(\mathbf{k})$ and $f_c(t)$ can be taken from Eq. (11.4), exploiting its independence of spatial inhomogeneities during CR. The background term $C(t) = N(1 - f_c(t))/L$ ensures particle number conservation, $\sum_{\mathbf{k}} n(\mathbf{k}) = N$. We find that all qualitative features arising in a full time-dependent Gutzwiller simulation are captured surprisingly well by Eq. (11.9) at all experimentally relevant time scales.

11.3 Special Case: Harmonically Trapped System

We shall now discuss the characteristics of this time evolution and possible applications. For the case of an underlying harmonic trapping potential $\mu_{\mathbf{l}} = -V_t(\mathbf{l}-\mathbf{l}_0)^2 + \mu_0$, results from a numerical dynamic Gutzwiller calculation for a trapped condensate (diameter $\approx 120a$ in the x-y-plane) are shown in Fig. 11.2 for $n(\mathbf{k}=0,t)$ and the full $n(\mathbf{k},t)$ in Fig. 11.3 for certain times. The essential dynamics of $n(\mathbf{k},t)$ at revivals is well captured within a single particle picture for the condensate state $|\psi(t)\rangle = \sum_{\mathbf{l}} \phi_{\mathbf{l}}^{(0)}(t)|\mathbf{l}\rangle$ (although the condensate vanishes between revivals), where $|\mathbf{l}\rangle$ is the Wannier state at site $\mathbf{l}$. Its time evolution is generated by $U(t)$, since the largest eigenvector of $\tilde{\rho}(t)$ is always identical at revival times.

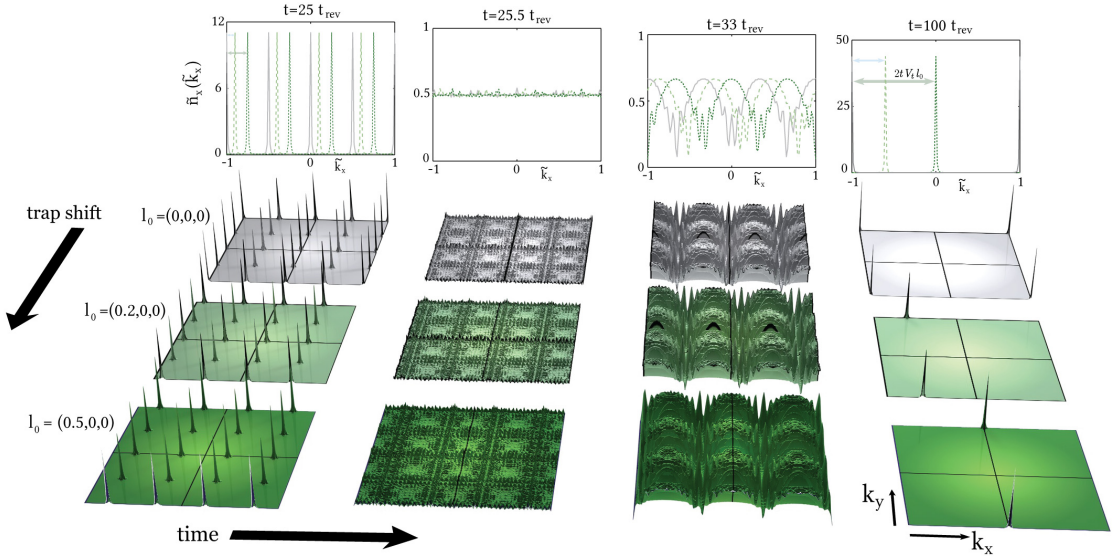

Figure 11.3: Quasi-momentum profile in the first Brillouin zone for different times and lattice shifts $\mathbf{l}_0$ during CR in a harmonic trap, individually scaled on the vertical axis for visual clarity. Parameters as in Fig. 11.2, but initially in a 27.5Hz trap with a central density of $n = 1.67$. Subsequently, this is ramped up to $s = 40$ and a 197.3Hz trapping frequency, such that $t_{\mathrm{trap}} = 200t_{\mathrm{rev}} = 43.88$ms. Each of the plots in the upper row depicts the projected quasi-momentum density $\tilde{n}_x(k_x) \propto \int_{-\pi/a}^{\pi/a} dk_y\, dk_z\, n(\mathbf{k})$ for the three 3D plots (for a given time, but different trap shifts) in the respective column. These projected distributions are all normalized such that $\int_{-1}^{1} d\tilde{k}_x\, \tilde{n}(\tilde{k}_x) = 1$, where $\tilde{k}_x = k_x a/\pi$. A trap shift of l_0 in the x-direction does not change the overall structure of $n(\mathbf{k})$, but leads to a translation of the quasi-momentum profile by exactly $2tV_t l_0$ in the k_x-direction. This shift is indicated by the arrows in the projected quasi-momentum profiles in the upper row.

The condensate's contribution to $n(\mathbf{k},t)$ (relevant during revivals) can then be expressed as

$$n(\mathbf{k},t) = f_c(t)\frac{N}{L}\sum_{\mathbf{l},\mathbf{l}'} A_{\mathbf{l},\mathbf{l}'}\, e^{-i(a\mathbf{k}-2tV_t\mathbf{l}_0)(\mathbf{l}-\mathbf{l}')}\, e^{-itV_t(\mathbf{l}^2-\mathbf{l}'^2)} \tag{11.10}$$

with the amplitudes $A_{\mathbf{l},\mathbf{l}'} = \phi_{\mathbf{l}}^{(0)}(0)\phi_{\mathbf{l}'}^{(0)*}(0)$. The first exponential term shows that a translation of the harmonic trapping potential by $\mathbf{l}_0$ leads to a time-dependent overall translation by $2tV_t\mathbf{l}_0$ of the quasi-momentum profile, which is periodic in the first Brillouin zone. The second term implies a temporal periodicity with a period of the trap time $t_{\mathrm{trap}} = 2\pi/V_t$, up to a translation $4\pi n\mathbf{l}_0$. At most times the last term interferes destructively, but at times $t_n^{(m)} = (n + 1/m)t_{\mathrm{trap}}$ multi-peak structures appear in $n(\mathbf{k})$ and are observable if, additionally, $t_n^{(m)}$ is a multiple of t_{rev}. In the limit of an initially homogeneous condensate, the discrete Fourier transform in Eq. (11.10) can be evaluated explicitly at the times $t_n^{(m)}$ (see appendix (O)) and one obtains

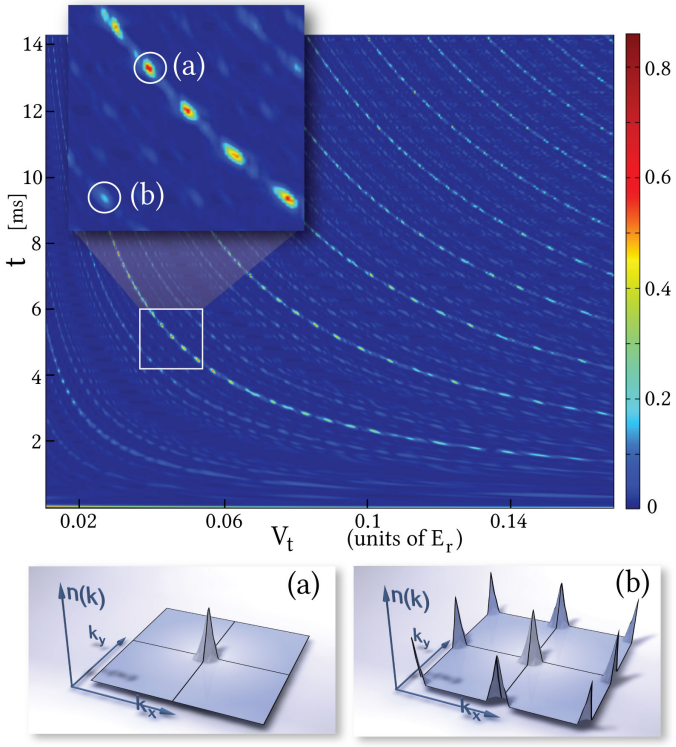

Figure 11.4: Particle number in the central quasi-momentum peak (using the same definition as before) as a function of time and harmonic trapping strength V_t for a trap shift $\mathbf{l}_{0,i} = 0.5$. The position of the maxima allows for a high precision determination of V_t in the presence of the optical lattice. The calculation was performed for ^{87}Rb in a 738nm optical lattice at $s = 32$, including finite J effects and realistic density-dependent interaction parameters U_n [172]. Insets: $n(\mathbf{k})$ at points (a),(b).

$$n(\mathbf{k},t) = N\, f_c(t) \prod_{i=x,y,z} \frac{F(q_i,m)}{m} \tag{11.11}$$

with $F(q_i,m) = \delta_{q_i \bmod 1,\,0}\ \left(1+\delta_{0,m \bmod 2}(-1)^{\frac{m}{2}+q_i}\right)$ and $\mathbf{q} = \frac{am}{2\pi}\mathbf{k} - 2\mathbf{l}_0$. This constitutes the dominant contribution in the outermost left ($t_0^{(8)}$) and right columns ($t_0^{(2)}$) of Fig. 11.3 during revival, whereas the peaks are strongly washed out in the second last column, where the revival time does not fully coincide with ($t_0^{(6)}$). During collapse, shown in the second column of Fig. 11.3, the distribution is essentially flat with little substructure. We stress that at these specific times the condensed atoms collectively occupy one single particle state, consisting of a coherent superposition of quasi-momentum states $(K(m,\nu_x), K(m,\nu_y))$ with equal weight, i.e. for the 2D projected case in a mode

$$a^\dagger_{\mathrm{BEC}} = \frac{1}{m} \sum_{\nu_x,\nu_y=1}^{m} a^\dagger_{k_x=K(m,\nu_x),\,k_y=K(m,\nu_y)} \tag{11.12}$$

with $\frac{a}{\pi}K(m,\nu_i) = \left[\frac{2}{m}(2(\nu_i+l_{0,i})+1+\frac{m}{2})\right] \bmod 1$. This is not to be mistaken as a signature of a fragmented condensate. As the appearance of these patterns is governed not only by the inverse trap time scale, but also by the CR time scale, the temporal discretization is implicitly given by the revival time t_{rev}. A plot of $n(\mathbf{k}=0,t)$ as a function of the trapping frequency is shown in Fig. 11.4: the $1/V_t$ scaling of the time at which a pattern with a significant $n(\mathbf{k}=0,t)$ component appears is in full accordance with Eq. (11.10) and the fainter hyperbolas correspond to momentum profiles with multiple spikes, where, correspondingly, the $k=0$ component is weaker. The non-persistent, dotted intensity of the hyperbolas directly reflects the interplay of the two time scales: only when

a specific trap pattern coincides with a revival of the matter wave field, a significant $n(\mathbf{k} = 0)$ is observed.

A further quantity that can be directly extracted from the distributions in Fig. 11.3 at the revival times, is the position of the trapping potential in a scale smaller than the lattice spacing a. As can be seen from the term $-2tV_t\mathbf{l}_0$ in Eq. (11.10), a microscopic shift $\mathbf{l}_0$ in the harmonic trapping potential leads to a time-dependent translation of the quasi-momentum distribution $n(\mathbf{k})$, as visible in the rows with different $\mathbf{l}_{0,x} = 0, 0.2, 0.5$ in Fig. 11.3. This translation can be experimentally observed on a macroscopic scale after time-of-flight expansion. Thus by comparing the initial $n(\mathbf{k}, t = 0)$ with $n(\mathbf{k}, t_m)$ at revival times, $\mathbf{l}_0$ can directly be determined with high precision.

In turn, this may find application in characterizing the thermal or mechanical stability of the optical setup: as the confining harmonic potential is created by laser beams different from the ones generating the optical lattice in each dimension (see Fig. 11.1), thermal drifts [2] can lead to a shift of $\mathbf{l}_0$, which can be observed in $n(\mathbf{k}, t)$.

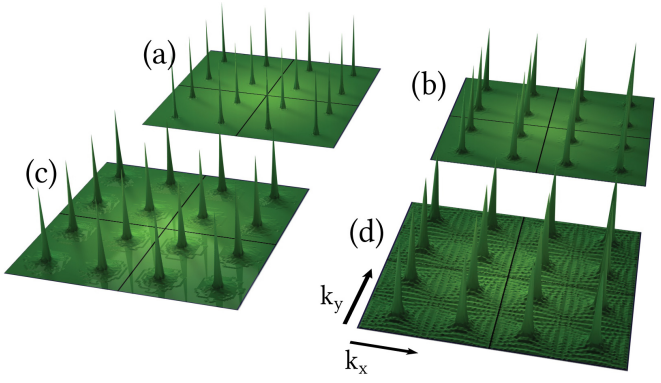

Figure 11.5: Comparison of the quasi-momentum profiles in the first Brillouin zone for quadratic (a) and Gaussian trapping potentials (b,c,d). The relevant parameter quantifying the harmonicity of the Gaussian trap is the ratio between the cloud radius and the width of the Gaussian potential (extension ratio). For subplots (b,c,d) this value was set to (0.1, 0.15, 0.2) respectively, whereas the trap strength and other parameters were set to agree with the strength of the harmonic potential in Fig. 3 in the linear approximation ($t = 25t_{\mathrm{rev}}$ and lattice shift $\mathbf{l}_0 = (0.5, 0.5, 0.5)$). Compared to the harmonic trap, the peaks are successively broadened with an increasing filling factor for a Gaussian potential, but remain clearly visible, even for a large extension factor of 0.2. Due to the scaling of the δ-response of the peaks in $n(\mathbf{k})$ for the harmonic case, the theoretically predicted height of such a peak on a single point of the discrete k-lattice is strongly decreased (cf. black dotted line in Fig. 2b). In the experimental detection, this should be less visible, as the observed quasi-momentum distribution is in any case convolved with the point spread function of the optical imaging system.

11.4 Validity of our predictions

A crucial question is whether our predictions are robust enough to be observable for the harmonic trapping potential in typical experimental setups. As the most important effects we consider the sensitivity towards precise timing as well as deviations from the idealized harmonic trap shape due to the Gaussian intensity profile of the laser beam. For a given trap strength V_t, the required temporal precision (i.e. the time span between lattice ramp and the release of the cloud) is of the order of the revival time, as can be seen in Fig. 2 and Fig. 4. This time scale is precisely controlled in current experiments [172, 171]. The deviations originating from the Gaussian trapping potential require a somewhat more quantitative analysis. The relevant parameter, which quantifies

[2] It is assumed that the time scale of the thermal expansion is large with respect to $1/V_t$.

the quality of the harmonic approximation is the ratio of the cloud radius and the beam radius. In Fig. 2(b) we show the time-dependent occupation $n(\mathbf{k} = 0, t)$ for a true Gaussian trapping potential for the cloud extension ratio $\frac{R_{cloud}}{w} = 0.1$ in comparison to the idealized harmonic case. We find that in this experimentally realistic regime the peaks are somewhat smaller, shorter and broader. However, on the time scale of t_{trap} this effect is weak and should not wash out the structure of $n(\mathbf{k})$ beyond experimental resolution. This can also be seen in Fig. 5, where a comparison of the quasi-momentum profile after $t = 25t_{\mathrm{rev}}$ is given for a harmonic and Gaussian trap with different cloud extension ratios. In a recent experiment [110], exactly these quasi-momentum patterns have been observed in the non-interacting one-dimensional system. In our picture, those data correspond to trap dynamics with an infinite revival time. Since the trapping potential in [110] is not perfectly harmonic, the general feasibility of our predictions has already been experimentally confirmed.

The creation and observation of non-equilibrium condensate states in a non-interacting, one-dimensional system as reported in [110] is contained in our theory as a limiting case and shown in Fig- (11.6). This suggests that the proposed realization in conjunction with collapse and revival dynamics is within experimental reach. With the progress made on the engineering of arbitrary spatial potentials [10, 145, 183], the creation of condensates in an engineered single particle orbital seems very promising.

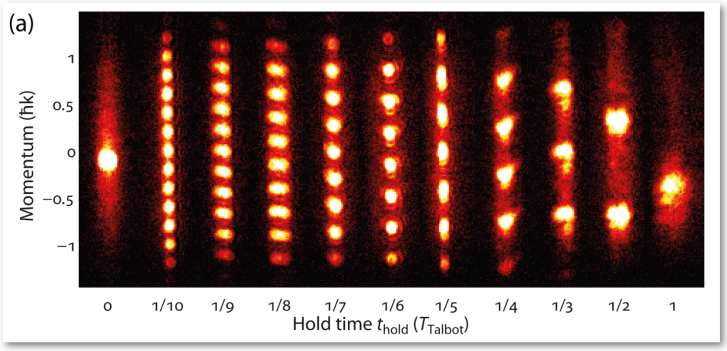

Figure 11.6: Experimentally measured quasi-momentum distributions as a function of the (specifically chosen) hold time t_{hold} in an harmonic trap. The experiment was performed with a non-interacting BEC, corresponding to an infinitely large revival time in our formalism. The discrete multiple peak structure is clearly visible. Furthermore, the position of the single quasi-momentum peak after an entire harmonic oscillator trap time t_{trap} (referred to as T_{Talbot} in the image) is shifted with respect to the initial peak, indicating that the position of the trap minimum does not coincide with the position of a lattice well minimum. It furthermore shows, that this effect on a sublattice scale is experimentally observable. The image is taken from an experiment performed by M. Mark et al. [110].

The quasi-momentum distribution of a corresponding one-dimensional system is nothing but the projection of the two-dimensional distribution on the k_x-axis. The emergent patterns in momentum space can be viewed as the temporal matter-wave analogue of the Talbot effect known from classical optics [161, 131]. From this point of view, one may also see our theory as a generalization of the temporal matter-wave Talbot effect to higher dimensional interacting systems (i.e. two or three dimensions).

12. Stochastic Mean-Field Theory

After having discussed time-dependent phenomena in strongly interaction bosonic lattice systems in various forms in the previous chapters, we now return to time-independent system. The physics of localization in disordered systems in conjunction with interactions has attracted a vast amount of attention over the last decades, and remains one of the most interesting and challenging problems ever since it was initiated by the seminal paper by P. Anderson in 1958 [8]. Anderson essentially considered a single particle in a three-dimensional disordered lattice and found that above a certain critical disorder strength, the particle no longer diffuses through the lattice, i.e. becomes localized. Considering the disorder strength to be a parameter of the system, the system undergoes a quantum phase transition at the critical disorder strength when, in the case of a single particle or non-interacting bosons, the single particle ground state changes from an extended to an exponentially localized[1] state. In the case of non-interacting fermions, the transition occurs when the single-particle states at the Fermi surface become localized, which generally occurs at a different disorder strength than the localization of the single particle ground state. The localization of non-interacting fermions was recently experimentally observed in the DeMarco group [93]. An interesting question to ask is how interactions influence the disorder localization properties and vice versa. The interplay between disorder and interactions in Bose systems has been a vital field of research in condensed matter both in theory and experiment. Clearly, this is a very challenging task in quantum many-particle systems, where even in the absence of interactions many open questions exist and exact solutions are generally not known. For the bosonic case, the line of investigation was mainly initiated by the seminal work of Fisher et al. [55], who first provided a detailed study of localization of interacting bosons in a random potential, which led to the notion of the superfluid-insulator transition and the Bose glass (BG). In the weakly interacting regime, the collective Bogoliubov excitations become localized [59]. While disorder effects in Fermi systems are relevant to a broad range of experimentally accessible scenarios like correlated electron systems, the status was less diverse for Bose systems for a considerable time period, as superfluid ^{4}He situated in random pores of Vycor had been the predominant setup which could be studies with sufficient precision [29]. This changed dramatically when the realization of the superfluid-Mott insulator transition of ultracold bosonic atoms in an optical lattice opened up a new field of investigation [68, 82]. In particular, optical lattices provide a relatively pure and tunable simulation of effective models used to describe solid state systems [75], where effects like disorder can also be realized in a controlled manner. While several alternative realizations of disorder in optical lattices, such as multichromatic lattices with non-commensurate wavelengths [134, 39, 136, 48] or multi-species gases with strongly differing tunneling rates [60, 119] have been proposed recently, speckle laser patterns are probably by now one of the most efficient methods to establish disorder in cold atoms [109, 14, 30, 170, 121, 96]. Therein, it is possible to combine the speckle beam with the remaining apparatus of the optical lattice to simulate disordered lattice systems with a high tuning accuracy and without other side

[1] This means that an envelope function, decaying exponentially in space, exists.

effects. Atoms exposed to a speckle laser potential feature localization effects [99, 100], but speckle laser potentials can also be used in conjunction with optical lattice potentials, in which case the disordered (Bose-) Hubbard model is realized. It was previously debated whether experimental speckle potential setups with a disorder potential autocorrelation lengths of the order of the lattice space are realizable. This was achieved in recent experiments [170, 121] , thus justifying the model of uncorrelated disorder energies at different lattice sites.

The stochastic mean-field theory, which we develop and describe in detail in this chapter, is a very efficient method to capture the relevant phases of the disordered Bose-Hubbard model within a statistical description. As the central quantity is the distribution function for the local order parameters, which are determined self-consistently on a functional level, it does not suffer from finite size effects and describes the system in the thermodynamic limit. This is of special importance for disordered systems, where finite size effects and insufficient sampling of disorder realizations are common problems for numerical methods.

A variety of theoretical approaches [104] has by now been applied to the disordered Bose Hubbard model (BHM), first introduced for ultracold atoms by Jaksch et al. [82], which is described by the Hamiltonian

$$\mathcal{H}_{\text{BH}} = -J \sum_{\langle i,j \rangle} (b_i^\dagger b_j + \text{h.c.}) + \sum_i (\epsilon_i - \mu) n_i + \frac{U}{2} \sum_i n_i (n_i - 1).$$

ϵ_i is an on-site energy shift, which in our case is a spatially uncorrelated random variable drawn from a distribution $p(\epsilon)$ and U is the on-site repulsive interaction. The subscript $\langle i, j \rangle$ indicates the sum over all neighboring pairs of sites. Unless stated otherwise, we use the unit $U = 1$.

Several quantum phases can exist within this model, such as the Mott insulator (MI), the Bose glass, the condensed phase, commonly referred to as the superfluid (SF), as well as the normal phase at finite temperature. The transitions between these phases, which constitute some of the first experimentally feasible quantum phase transitions in bosonic systems, have attracted much attention. Numerically, a powerful approach is Quantum Monte Carlo [95, 88, 144, 138, 128, 36, 127, 70] (QMC). While MI and SF phase can be characterized efficiently [95], the BG phase and the vicinities of the transition lines are significantly more complicated to be adequately described. The main reason is that for finite size calculations in general, it is problematic to capture the correct description of the phase borders, which are essentially dominated by rare events, which is also a problem for QMC methods. In most cases, exact diagonalization studies are simply inadequate due to limited size and number of particles, which often obscures essential physics (however, there may appear aspects that can indeed be suitably captured by small clusters [105]). On the other hand, with a similar range of treatable system sizes as QMC, density matrix renormalization group (DMRG) is an efficient complementary method [130]. However, DMRG is currently only applicable in one spatial dimension and thus does not allow for a description of effects in higher dimensional lattices. Analytically, renormalization group analysis [149, 174, 96], slave boson theory [42], the strong coupling approach [58], and various different kinds of mean field theory descendants have been applied to the BHM with and without disorder [135, 94, 147, 146, 97, 15, 41, 142]. Arithmetically averaged mean-field theories, on the other hand, are incapable of resolving the BG phase at all for $T = 0$ [97], but also for $T > 0$ impose an unphysically strong phase coherence, leading to an overestimation of the SF phase. Other methods like the random phase approximation (RPA) which has successfully been applied to the system without disorder [147, 146] again suffer from finite size effects for the BHM with disorder, as the absence of translational symmetry constrains its applicability to much smaller system sizes.

To circumvent this type of problems in describing the different phases of the disordered BHM, we use the SMFT which has been previously introduced and applied to the disordered BHM at zero temperature [15, 18]. There, it was found that the method efficiently describes localization, is both valid in high dimensions and in the thermodynamic limit, capturing rare events with their respective statistical weight and includes dimensional effects. In particular, it was found that at fixed μ, there exists a critical hopping strength, above which the system remains superfluid for arbitrarily strong disorder.

In this chapter, we present the SMFT in detail and investigate how the results found for the disordered BHM at zero temperature are modified at finite temperature. In addition to prototypical box disorder, we consider exponential speckle disorder to better simulate systems realized in current experiments. Here, the results are qualitatively different in the sense that for any finite disorder strength the MI gives way to the BG.

This chapter is organized as follows: In Sec. 12.1, the SMFT is explained in detail. First the general scope is outlined, followed by the definition of quantities computed within SMFT, such as compressibility, local Greens functions and condensate fraction. In Sec. 12.2, the essential results for the disordered BHM at $T = 0$ are given, followed by the extension of the SMFT calculations to $T \neq 0$. In Sec. 12.3 we extend the results presented for box disorder [15], including finite temperature effects. Alternative types of disorder, in particular disorder induced by speckle lasers are discussed for the BHM in Sec. 12.4. As another possible source of disorder, we discuss the effect of kinetic (hopping) disorder in the BHM in Sec. 12.4.2. However, we find no sensible dependence of the system on this parameter. The applicability of these results to current experiments essentially relies on the estimate of experimental temperature, which is discussed on in Sec. 12.5.1. We find that the experimentally realized temperatures are still far above the regime for which we resolve the previously stated interesting phenomena, such as disorder-induced condensation and reentrant behavior [144]. LDA + SMFT calculations are discussed in Sec. 12.5.2 to provide a closer connection to experimentally measurable quantities. In Sec. 12.6, we conclude that the SMFT is an efficient theoretical approach to disordered Bose systems and promises an adequate description of ongoing experiments.

12.1 Method

As pointed out previously [55, 97], performing a self-consistent disorder average over all local on-site energies is not sufficient to generally describe the insulating Bose-glass phase. From spatially resolved bosonic Gutzwiller calculations, it becomes apparent that this method overestimates long range correlations, predicting the formation of a global condensate into a single particle orbital which consists of the superposition of a large (extensive) number of distinct localized single particle states. In the true Bose glass phase, off-diagonal long range order does not prevail and a large (although not extensive) number of particles may occupy each of these localized modes independently, leading to a condensate fraction $f_c = 0$ in the thermodynamic limit. However, by imposing phase rigidity and averaging over all mean-field parameters $\psi_i = \langle b_i \rangle$ with the same complex phase, the spatially resolved (as well as the arithmetically averaged) Gutzwiller theory leads to a finite average mean-field parameter (MFP) and a finite condensate fraction $f_c = \overline{\langle b \rangle}^2 / \overline{\langle b^\dagger b \rangle}$ in the expected BG regime.

In contrast to the approaches mentioned above, the SMFT is constructed as a single-site theory in the thermodynamic limit, which effectively describes fluctuations in the MFPs using a probability density function (PDF) $P(\psi)$. Set up in this fashion, the SMFT method is not restricted to incorporating disorder fluctuations only, but may also be a powerful approach to treat fluctuations of different origins, such as of thermal or quantum type in a unified framework. The concept of approximating quantum mechanical operators by random variables has been applied previously in a variety of physical scenarios [180, 178, 179]. Here, we will focus on disorder-induced fluctuations at finite temperature. In this section, we will discuss the construction of SMFT in detail, concentrating on the case of including on-site disorder. Extensions of including disorder in the hopping parameter J or thermal fluctuations explicitly are discussed in Sec. 12.4.2 and App. M.6 respectively.

The central quantity, which effectively describes a disordered bosonic lattice gas in the thermodynamic limit is the probability distribution $P(\psi)$. It is assumed to be equal for all sites and in particular independent of the nearest neighbors' on-site energies. The validity of this assumption has been checked using spatially resolved mean-field theory, which is known to become exact in the non-interacting limit, while retaining interaction effects beyond Gross-Pitaevskii theory for finite U/J. It is found that it yields correlation coefficients below 0.05 in all regimes considered [15],

justifying the above assumption. The aim of SMFT is to find a self-consistent solution for $P(\psi)$, which is restricted and uniquely specified by self-consistency equations and minimization of energy.

Consider a cluster of lattice sites composed of a central site i and Z (the coordination number) nearest neighbors, where the corresponding part of the Hamiltonian (12.1) contains the operators on site i within the bosonic Gutzwiller approximation [55, 135, 147, 94]:

$$\mathcal{H}_i^{(\mathrm{MF})} = -J \sum_{\mathrm{n.n.}j} (\psi_j^* b_i + \psi_j b_i^\dagger - \psi_j^* \psi_i) + (\epsilon_i - \mu) b_i^\dagger b_i + \frac{U}{2} b_i^\dagger b_i^\dagger b_i b_i . \tag{12.1}$$

Within this approximation, the site i is coupled to (and the sum extends over) the nearest neighbors via the scalar MFPs $\psi_j = \langle b_j \rangle$, which are random variables within SMFT. Due to global particle number conservation, the MFPs can all be chosen to be real and positive, as any variation in complex phase corresponds to a boost in local kinetic energy. The expectation value $\langle b_j \rangle$ is to be evaluated in the local ground state for $T = 0$ or taking the thermal trace for $T > 0$. Thermal fluctuations can, however, also be incorporated on an explicit stochastic level in the distribution $P(\psi)$ within SMFT, as discussed in App. M.6. Inspecting the Hamiltonian (12.1), it does not depend on the ψ_j's individually, but only on the scaled sum

$$\eta_i = J \sum_{\mathrm{n.n.}j} \psi_j . \tag{12.2}$$

Since the ψ_j's (and in the hopping disorder Sec. 12.4.2 also J) are random variables, the newly defined quantity η_i is also a random variable obeying some distribution $Q(\eta)$. As discussed above, the random variables ψ_j are assumed independent within SMFT, allowing us to express the distribution $Q(\eta)$ by a Z-fold scaled convolution

$$Q(\eta) \;=\; \int_0^\infty d\psi_1 \, P(\psi_1) \ldots \int_0^\infty d\psi_Z \, P(\psi_Z) \times \, \delta\Big(\eta - J \sum_{m=1}^{Z} \psi_m\Big). \tag{12.3}$$

Making use of the convolution theorem, this can be reduced to two one-dimensional Fourier transforms by introducing the characteristic function

$$\varphi(t) = \int d\psi \, P(\psi) \, e^{it\psi}, \tag{12.4}$$

in terms of which the function Q can be expressed as

$$Q(\eta) = \frac{1}{2\pi J} \int dt \, [\varphi(t)]^Z \; e^{-it\eta/J}. \tag{12.5}$$

This can be calculated efficiently for arbitrary coordination numbers Z using the FFT algorithm. The numerical procedure is discussed in App. M.1.

The self-consistency condition can now be formulated in the following way: If the on-site energy ϵ is randomly drawn from $p(\epsilon)$ and ψ_j is randomly drawn from the self-consistently determined distribution $P(\psi)$ for each of the Z nearest neighbors, this defines the single site Hamiltonian (12.1), which can be diagonalized providing the ground state $|\mathrm{g.s.}(\epsilon, \eta)\rangle$. From there, a new MFP $\langle \mathrm{g.s.}(\epsilon, \eta)|b|\mathrm{g.s.}(\epsilon, \eta)\rangle$ can be calculated, with the self-consistency requiring the distribution of this new random variable to be exactly the distribution $P(\psi)$ we initially assumed for the neighboring ψ_j's.

To cast this condition into functional form for a probability distribution in the thermodynamic limit (i.e. for an infinitely large system at fixed density), we first define the function

$$g(\mu - \epsilon, \eta) = \langle \mathrm{g.s.}(\mu - \epsilon, \eta)|b|\mathrm{g.s.}(\mu - \epsilon, \eta)\rangle, \tag{12.6}$$

where $|\mathrm{g.s.}(\mu - \epsilon, \eta)\rangle$ is the ground state of $\mathcal{H}_i^{(\mathrm{MF})}(\mu - \epsilon, \eta)$ given in (12.1).

It is useful to introduce the *conditional* PDF, which is a function of η and ψ, giving the probability density for a specified value ψ if the value of η is fixed and ϵ is distributed according to $p(\epsilon)$. This can be obtained by using the transformation property of a PDF under a variable transform and takes the form

$$\begin{aligned}\tilde{P}(\psi|\eta) &= \sum_{i \,|\, g(\mu-\epsilon_i,\eta)=\psi} \left| \left(\frac{\partial g(\mu',\eta)}{\partial \mu'} \right)_{\mu'=\mu-\epsilon_i} \right|^{-1} p(\epsilon_i) \\ &= \frac{d}{d\psi} \int d\epsilon \, p(\epsilon) \, \Theta\left(\psi - g(\mu-\epsilon,\eta)\right).\end{aligned} \tag{12.7}$$

This function does not obey any self-consistency condition and can be evaluated directly, which is the first step in finding $P(\psi)$. Remembering that the relation between $Q(\eta)$ and $P(\psi)$ is given by (12.3), so that we can express the self-consistency condition as

$$P(\psi) = \int d\eta \, Q(\eta) \, \tilde{P}(\psi|\eta). \tag{12.8}$$

The right hand side can be understood as follows: for every fixed η we have a PDF $P(\psi|\eta)$, which yields a contribution with the respective weight $Q(\eta)$, leading to a marginal distribution for the considered site. If this agrees with the initially assumed distribution $P(\psi)$, a self consistent solution has been found.

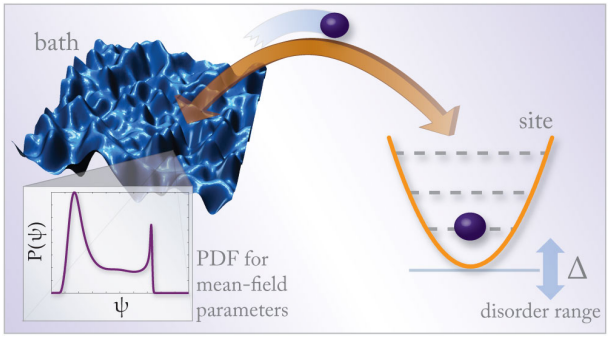

Figure 12.1: Within SMFT, the multiple site lattice model is approximated by an effective single-site problem, where a site is coupled to a bath of mean-field parameters. Disorder-induced fluctuations of the mean-field parameters are accounted for by a statistical distribution $P(\psi)$.

Once this is determined, expectation values of local, self-averaging operators $\hat{A}$ can be directly be determined by

$$\langle \hat{A} \rangle = \mathrm{Tr}\left(\varrho(\beta)\right), \tag{12.9}$$

where

$$\varrho(\beta) = \int d\epsilon \, p(\epsilon) \int d\eta \, Q(\eta) \frac{e^{-\beta \mathcal{H}_i^{(\mathrm{MF})}(\mu-\epsilon,\eta)}}{\mathrm{Tr}\left(e^{-\beta \mathcal{H}_i^{(\mathrm{MF})}(\mu-\epsilon,\eta)}\right)} \tag{12.10}$$

is an effective disorder averaged density operator, incorporating thermal, on-site energy and MFP fluctuations, depending explicitly on $p(\epsilon)$ and the self-consistently determined $Q(\eta)$.

12.1.1 Numerical solution

To solve the SMFT equations numerically, we iterate the self-consistency equations on a discretized grid for ψ, consisting of a superposition of a variable number of equidistantly spaced grids, as explained in App. M.1. For every fixed set of physical parameters, we first numerically determine

the conditional cumulative density distribution function $F(\psi|\eta) = \int_0^\psi d\psi' P(\psi'|\eta)$ for all values of η and ψ which constitute the numerical grids for $Q(\eta)$ and $P(\psi)$ respectively (discussed in App. M.2). Working with the cumulative distribution on a numerical level, as opposed to the PDF itself, is far more controlled and circumvents divergences in the PDF $P(\psi)$, but also in the conditional PDF $P(\psi|\eta)$. The self-consistency condition (12.8) is not influenced by this approach. As can be seen by inspection, the insulating solution $P(\epsilon) = \delta(\epsilon)$ is always a self-consistent solution, equivalent to the $\psi = 0$ solution in the single site theory. However, in the SF regime, there also exists a second, non-trivial self-consistent solution, which corresponds to a lower grand canonical potential and is therefore the physical solution in this case. Furthermore, the physical solution is always found to be the attractive fixed point of the self-consistency mapping in the space of probability distributions, i.e. if the iteration procedure is started at any $P(\psi) \neq \delta(\psi)$, the successive distributions continuously converge towards the physical distribution.

We start the iterative procedure with an initial PDF $P^{(0)}(\psi)$, where all the weight is distributed at small, but non-zero values of ψ, assuring fast convergence in the insulating state and in the vicinity of the phase border. The distribution in the i-th iteration step for the scaled sum of MFPs from the nearest neighboring sites $Q^{(i)}(\eta)$ is calculated from $P^{(i)}(\psi)$ using the convolution theorem for independent random variables and the FFT algorithm (see App. M.1). The new distribution $P^{(i+1)}(\psi)$ is then obtained by integration over η. Numerically this is done by using the trapezoidal rule, as we found that using higher order techniques, such as Simpson's rule, is not robust and lead to incorrect results if δ-peaks appear in the PDF. To verify the validity of the SMFT procedure in the condensed phase, we compare the self-consistently determined SMFT order parameter distribution to a histogram of order parameters from a spatially resolved Gutzwiller calculation for the same physical parameters in Fig. (12.2).

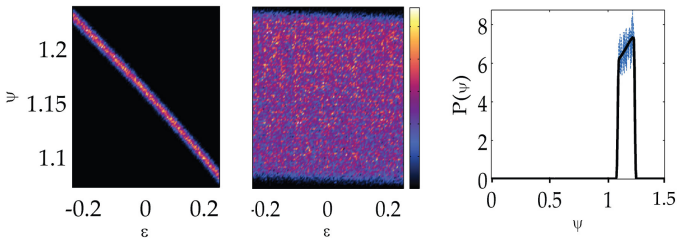

Figure 12.2: Results from a spatially resolved, bosonic Gutzwiller calculation (27 000 sites) in the deep SF regime with box disorder at $J = 0.067$, $Z = 6$, $\mu = 1$, $\Delta = 0.5$, where this method becomes exact (Gross-Pitaevskii regime with depletion). The left figure is a color-coded histogram (corresponding to the 2D probability density function), showing the strong correlation between the on-site energy ϵ and the on-site MFP ψ (correlation coefficient -0.9964), which is not neglected within SMFT. The central figure is a color-coded histogram of the on-site energy and nearest neighbor MFPs, which are only weakly correlated (correlation coefficient -0.0349) and neglected within SMFT. The right figure is a comparison of a self-consistently determined distribution from SMFT for these parameters, compared to a 1D histogram of MFPs from the spatially resolved Gutzwiller calculation (fluctuations originate from the finite system size). Excellent agreement is achieved in this limit.

In the vicinity of the phase border, the computational effort increases due to two effects. Firstly, the convergence is critically slowed down, increasing the required number of iterations. Secondly, the discretization of the ψ-grid plays an ever increasing role and in some parameter regimes directly on the outside of the MI lobes, where the converged distributions are very close to a δ-peak at $\psi = 0$, the numerically determined form of the distributions depends on the discretization (resolution), which is clearly unphysical. In these cases, we have to determine $P(\psi)$ by examining a sequence of converged distributions at ever increasing resolution and define the physical distribution as the limit of this sequence.

12.2 Phases of the disordered BHM

12.2.1 Phases at $T = 0$

For the disordered BHM, three different phases exist at zero temperature: A Mott insulating state, where number fluctuations are suppressed and the particles are localized due to a repulsive interaction. This state exhibits a finite energy gap of order U, thus the single-particle density of states (DOS) at $\omega = 0$ vanishes and the state is incompressible.

If tunneling-induced delocalization dominates, the system is in a condensate (SF) phase, where a macroscopic number of particles can lower their energy by condensing into one single-particle state, thus exhibiting quantum coherence and leading to a finite condensate fraction. Within a grand-canonical mean-field description, this phase breaks the $U(1)$-symmetry of the BH Hamiltonian (12.1) and leads to a non-zero order parameter. The phase border from the SF to any of the insulating phases is thus determined by SMFT, where finite weight in $P(\psi)$ moves to finite values of ψ.

Finally, there is the Bose glass phase, where particles are localized by an interplay of disorder and interactions. However, there exists no single particle state which is occupied macroscopically and thus the BG is not a condensate, i.e. the condensate fraction vanishes ($f_c = 0$). However, there does exist an extensive number of localized single particle states, each of which is occupied by an arbitrarily large, but not macroscopic number of particles. This may be understood as a highly fragmented system of *incoherent* localized 'non-macroscopic quasi-condensates'.

The transition from a BG to a MI is not determined from the self-consistent distribution $P(\psi)$, but by analyzing the compressibility κ or the single particle DOS.

We consider the latter quantity within two frameworks:

1. Considering the purely sing site particle- and hole excitations as specified in [97]. The BG extends over the region where $P(\psi) = \delta(\psi)$ and values of the chemical potential $\mu \in \{m + \epsilon \,|\, m \in \mathbb{N}, \epsilon \in \mathbb{R}, p(\epsilon) > 0\}$, i.e. the borders are independent of J and a direct MI-SF transition is possible.

2. A more detailed analysis presented in [58, 127] relies on the analysis of an effective Hamiltonian in the subspaces of localized single particle- and hole excitations. For finite hopping J in the pure system, these hybridize, lifting the degeneracy and form superpositions with quantum numbers k. Increasing (decreasing) μ/U, the Mott insulating state remains the ground state until the energy difference between the MI state and the $k = 0$ particle (hole) state vanishes, at which point particles delocalize and condense into these states. Now let us return to the disordered case: here the local particle (hole) excitations will not hybridize into fully delocalized states with well-defined quasi-momentum k, but into inhomogeneous states, which depend on the individual disorder configuration. It is however possible to make exact statements about the eigen-energy spectrum for a disordered system in the thermodynamic limit: The lowest kinetic energy is obtained in locally homogeneous regions and approaches the energy of the $k = 0$ particle (hole) state of the pure system, as the size of this locally homogeneous Lifshitz region increases. Furthermore, scaling predicts that the dependence of the kinetic energy on the specific boundaries to the Lifshitz region will reduce, as the size of the region increases. On the other hand, the potential energy of the particle (hole) state is minimized, when the local on-site energy takes on the lowest (highest) possible value over the whole region, i.e. lies at the extrema of $p(\epsilon)$. Therefore, upper (lower) phase boundary of the Mott lobe in the disordered system is obtained by shifting the upper (lower) boundary down (up) by $\max(\{\epsilon | p(\epsilon) > 0\})$ ($\min(\{\epsilon | p(\epsilon) > 0\})$). The MI for box disorder in 3 dimension at $T = 0$ obtained by strong coupling theory using this criterion, is the area enclosed by the orange phase boundaries in Fig. (12.7). The insulating region outside of these lobes, bounded from the SF by the dashed white lines, corresponds to the BG. Using this criterion, the transition from MI to SF always occurs through the BG phase for box disorder within SMFT.

12.2.2 Phases at $T > 0$

At finite temperature $T > 0$, the system is always compressible and the incompressible Mott insulator is replaced by a normal (non-superfluid) phase with a thermally induced compressibility. A central statement in [97] is, that the disorder-averaged single particle DOS calculated by considering purely local excitations only, allows for a clear distinction at $T > 0$ between the BG and the normal phase, as it is zero in the latter. However, when considering delocalized excitations in the particle and hole sector, this statement holds no longer, as there are generally degenerate states in the N-particle particle-hole band and the particle (hole) band in the $N+1$ sector (or the $N-1$ sector for the hole band), which can be seen from the single particle DOS in the Lehmann representation

$$\begin{aligned}\rho(\omega) =& \frac{1}{Z_c} \sum_{l,l',k} e^{-\beta E_l^{(N)}} \left[|\varphi_{l'}^{(l,k)}|^2 \, \delta\left(\omega - (E_{l'}^{(N+1)} - E_l^{(N)})\right) \right. \\ & \left. + |\gamma_{l'}^{(l,k)}|^2 \, \delta\left(\omega - (E_l^{(N)} - E_{l'}^{(N-1)})\right) \right] .\end{aligned} \tag{12.11}$$

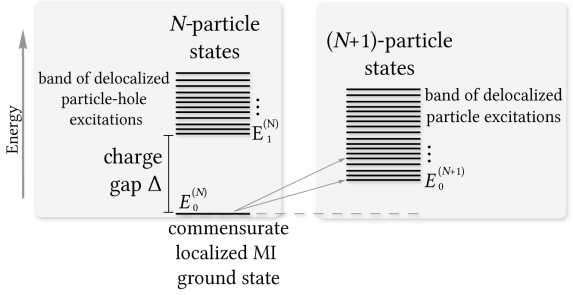

Figure 12.3: Energy structure of the BHM for large U/J without disorder. The levels correspond to the energies of the exact many-particle energy eigenstates of the system with interactions. Due to the $U(1)$-symmetry the energy eigenstates can be chosen to be of well-defined particle number. For commensurate particle number N, the ground state (MI) is separated from a band of particle-hole excitations by a charge gap, while for $N+1$ particles, all eigenstates are delocalized, forming a band of hybridized particle states. At $T = 0$, the single particle DOS has finite weight at frequencies corresponding to energy differences $E_i^{(N+1)} - E_0^{(N)}$ of transitions between N and $N+1$ states. At $T > 0$ transitions between different excited states also contribute, causing the gap to vanish if the two bands overlap and the respective matrix elements do not vanish.

Here, $E_l^{(N)}$ denotes the energy of the l^{th} many-particle eigenstate $|\psi_l^{(N)}\rangle$ of H_{BH}, which can always be chosen to have well-defined particle number N, since $[\mathcal{H}_{\text{BH}}, \hat{N}] = 0$, while l is a label for the eigenstate in this subspace. $\varphi_{l'}^{(l,k)} = \langle \psi_{l'}^{(N+1)} | b_k^\dagger | \psi_l^{(N)} \rangle$ and $\gamma l'^{(l,k)} = \langle \psi_{l'}^{(N+1)} | b_k | \psi_l^{(N)} \rangle$ are the amplitudes for the various possible transitions. If the system is in a Mott insulating state (considering no disorder for the clarification of this argument) as shown in Fig. (12.3), the ground state with N particles is separated from a band of particle-hole excited states by a gap $\delta(J, U)$ (corresponding to the height of the Mott lobe at the respective J/U). As transitions between various excited states can also occur at finite temperature, the SPDOS thus vanishes if the particle-hole band with N particles, overlaps with the particle- or hole band containing $N+1$ or $N-1$ particles, but the weight is suppressed exponentially by δ/T. We thus conjecture, that the BG and the normal phase are not fundamentally distinguishable, and only connected by a crossover.

Following along the lines of [97], we use the disorder averaged local single particle density of states at zero frequency $\overline{\rho}(\omega = 0)$ (see Eq. (M.18, M.19)), to determined the normal phase / BG crossover at finite T. In the presence of disorder the SPDOS containing localized excitations can be calculated explicitly from the local Green's function in this regime (see appendix. (M.5)) and leads to

$$\begin{aligned}\overline{\rho}(\omega, \mu, \Delta, \beta) = & \int d\epsilon \, p(\epsilon) \, \frac{1}{Z(\mu - \epsilon)} \sum_{m=0}^{\infty} e^{-\beta(\frac{U}{2} m(m-1) - \mu m + \epsilon m)} \left[(m+1) \delta(\omega - Um + \mu - \epsilon) \right. \\ & \left. + \, m \, \delta(\omega - U(m-1) + \mu - \epsilon) \right] .\end{aligned} \tag{12.12}$$

$Z(\mu')$ is the local partition function at an effective chemical potential μ' and the two δ-distributions correspond to local particle and hole excitations respectively. Using this criterion leads to an overestimation of the MI / normal phase over the BG and thereby an absence of the BG phase around the tips of the Mott lobes.

12.2.3 Deviations in Finite Size Systems

Although phase transitions are, strictly speaking, only well defined in the thermodynamic limit, crossovers observed in current experiments may indicate phase borders that do not coincide with the borders obtained in systems of infinite size. As discussed above and in [58, 127], the MI/BG phase borders in an infinitely large disordered system simply correspond to the shifted phase borders of the pure system. This argument relies on the existence of arbitrarily large Lifshitz regions, which is clearly no longer given for finite systems. The phase diagram for a finite system therefore strongly depends on the specific disorder realization, with the critical values for the phase borders becoming random variables. Therefore, a better question to ask for a finite system for instance is: For a randomly chosen disorder realization in a system consisting of L sites, what is the probability P_g that the energy gap will be lower than a given value D? In the limit of $J/U \to 0$ this probability is given by

$$P_g(\text{gap} < D) = 1 - (1 - P_D)^L \tag{12.13}$$

with the restriction that $0 < D < U/2$ and

$$P_D = \sum_{m=0}^{\infty} \int_{mU-D}^{mU+D} d\mu'\, p(\mu - \mu'). \tag{12.14}$$

With increasing J/U the MI/BG phase border in the J/U-μ/U-diagram remains a random variable, but with a reduced steepness in the slope for finite systems, as shown in [58, 138]. The BG/SF would also be very likely (in a statistical sense) to move to larger critical values of J in a finite system, as the occurrence probability of 'rare events', favoring a SF, is suppressed.

12.3 Box Disorder

We now consider the Bose-Hubbard model with box disorder, considering both zero and finite temperature. The phase diagrams presented in [15] are extended by taking collective excitations and finite temperature into account. All numerical results presented in the following are for a three-dimensional cubic lattice (Z=6). Box disorder is characterized by a constant probability density for the on-site energies $p(\epsilon) = \frac{1}{\Delta}\Theta(\Delta/2 - |\epsilon|)$ over a bounded interval of width Δ, where $\Theta(x)$ denotes the Heaviside function. Changing the disorder strength may have an influence on the system properties on various levels. Starting in the condensate, where the distribution of order parameters is a δ-distribution if no disorder is present, this distribution is broadened for increasing disorder, as shown in Fig. (12.4). We find that at both constant chemical potential μ, as well as at fixed filling n, there is a critical value of JZ above which the system always remains condensed for arbitrarily strong disorder[2], as becomes clear in Fig. (12.5). For finite interactions this can be physically understood by the formation of a bosonic background, which shields the spatial disordered potential. Within a mean-field picture, the bosons above this background effectively feel a smoothened spatial potential and can condense.

[2]Within this model the disorder is intrinsically assumed that the lowest band approximation holds.

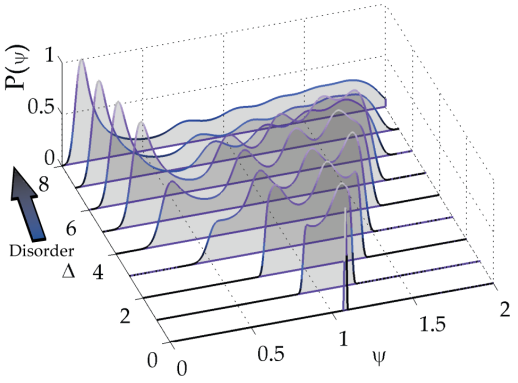

Figure 12.4: Self-consistently determined MFP probability density distributions at fixed $\mu = 1.0$, $J = 0.05$, $Z = 6$ and increasing disorder strength Δ. The distributions are normalized to their maximum value for visual clarity. For $\Delta \to 0$ the PDF converges to a shifted δ-distribution, recovering to the well-known usual MFT for the pure system. With increasing Δ the disorder induces fluctuations in the MFPs, i.e. $P(\psi)$ broadens.

Coming from the insulating state within a local mean-field picture, where the total state of the system is a direct product of local Fock states minimizing the total energy, an increase in disorder reduces the smallest possible particle or hole excitation energy. The local energy gap for a site with an effective chemical potential μ' and a Fock state as ground state $|n = \max(\lceil \mu'/U \rceil, 0)\rangle$ is $E_{\text{particle}} = \max(\lceil \mu'/U \rceil, 0)\, U - \mu'$ for adding a particle and $E_{\text{hole}} = \mu' - (\max(\lceil \mu'/U \rceil, 0) - 1)U$ for creating a hole, if $\mu' > 0$. In the presence of disorder in an infinitely large system, this implies that the energy gap is necessarily reduced by $\Delta/2$ and vanishes in the $J \to 0$ limit as soon as the interval of realizable effective chemical potentials contains a positive integer multiple of U, i.e. $\mathbb{N} \cap [(\mu - \Delta/2)/U, (\mu + \Delta/2)/U] \neq \emptyset$.

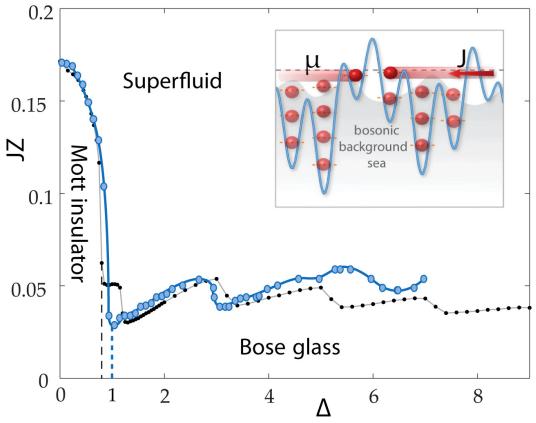

Figure 12.5: SMFT phase diagram in the $JZ - \Delta$-plane for fixed $\mu = 0.4$ (gray line, small black dots) and fixed density $n = 1$ (blue line and larger circles, with error ± 0.003 in JZ). Inset: illustration of the bosonic background screening the strongly disordered spatial potential. The MI/BG phase borders occur at constant Δ, since the mean-field state cannot depend on JZ if all MFPs ψ vanish.

Within the picture of purely local excitations, this argument is independent of temperature and directly reflected by the disorder averaged local DOS

$$\overline{\rho}(\omega, \mu, \Delta, \beta) = \frac{1}{\Delta} \sum_{m=0}^{\infty} (m+1) \frac{\Theta(\frac{\Delta}{2} - |\omega - Um + \mu|)}{Z(Um - \omega)} \left[e^{-\beta E_m (Um - \omega)} + e^{-\beta E_{m+1} (Um - \omega)} \right]. \quad (12.15)$$

In the case of bounded disorder, this directly implies that the system cannot be in a gapped state as soon as the carrier width (Δ for box disorder) equals or exceeds U and that the system is then always in the BG or SF state, i.e. the MI and normal state can only exist at $\Delta < U$ (and not at all for unbounded disorder). When the system is either of these two insulating states at zero temperature, the compressibility $\kappa = \frac{\partial \overline{n}}{\partial \mu}$ is determined by $\overline{\rho}(\omega = 0)$ within a picture of local excitations, where locally degenerate sites change their occupation number by ± 1 if μ is slightly altered. Since for finite temperature thermal particle or hole excitations are also present when the system is gapped, κ is always driven to a finite value. The behavior of κ and $\overline{\rho}(\omega = 0)$ is shown in Fig. (12.6) at the specific chemical potential of $\mu = 1.1U$. Starting at $\Delta = 0$, the system is in a gapped MI / normal state, but increasing Δ, the system undergoes a phase transition at a critical disorder strength of $\Delta = 0.2U$.

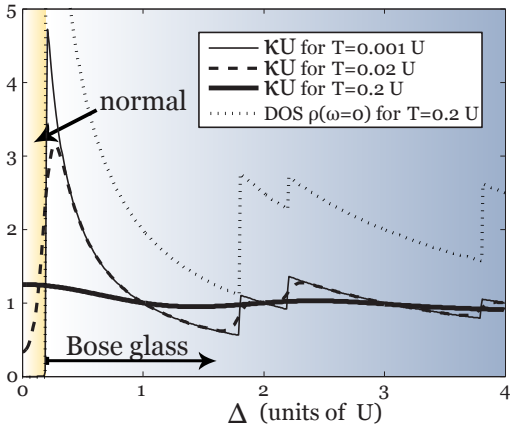

Figure 12.6: Compressibility κ and local single particle DOS in an insulator for box disorder at $\mu = 1.1U$ at various temperatures (in units of U^{-1}). At zero temperature κ vanishes in the MI, but not in the BG and may thus be taken as a quantity to distinguish between them. At finite temperature however, κ becomes non-zero in the normal phase and the sharp features become rounded off by thermal fluctuations. In this case, the disorder averaged DOS of local excitations $\overline{\rho}(\omega = 0)$, which retains all sharp features at $T > 0$, can be used to determine the crossover from a BG to the normal phase, where it remains zero.

At this point the local DOS $\overline{\rho}(\omega = 0)$ takes on a non-zero value, as two different local Fock states can become degenerate at the edge of the box disorder distribution. At low temperatures the compressibility exhibits a significant change from an exponentially small value in T in the normal phase to a large value due to the existence of local configurations of on-site energies which give rise to almost degenerate states with different particle number. There, a small change in the chemical potential leads to a local jump in particle number. In the zero temperature limit the compressibility locally behaves as $\kappa \propto \frac{1}{\Delta}$, since with increasing disorder strength the statistical weight of these events is reduced. When the effective chemical potentials at the borders of the probability distribution enter a region corresponding to a new local particle number $\mu \pm \frac{\Delta}{2}$, the compressibility increases with a jump, corresponding to subsidiary phase transitions between different BG phases at $T = 0$, which turn into less pronounced crossovers with increasing T. Considering the limit of strong disorder $\Delta/U \to \infty$ at fixed μ/U in Fig. (12.6), the system approaches a state in which only half the number of sites are occupied and $\lim_{\Delta \to \infty} \kappa = \frac{1}{2U}$.

However, disorder does not only affect local excitation properties, but leads to an intricate interplay between the hopping and interaction energy scale, influencing the overall coherence properties of the system. Whereas an increase in temperature or interaction energy generally tends to counteract the formation of a condensate, this is true in most, but not all scenarios when increasing the disorder strength. In certain parameter regimes at sufficiently low temperature, an increase in Δ can actually lead to the formation and stabilization of a condensate (i.e. disorder induced condensation), as previously predicted by various methods, including SMFT [15].

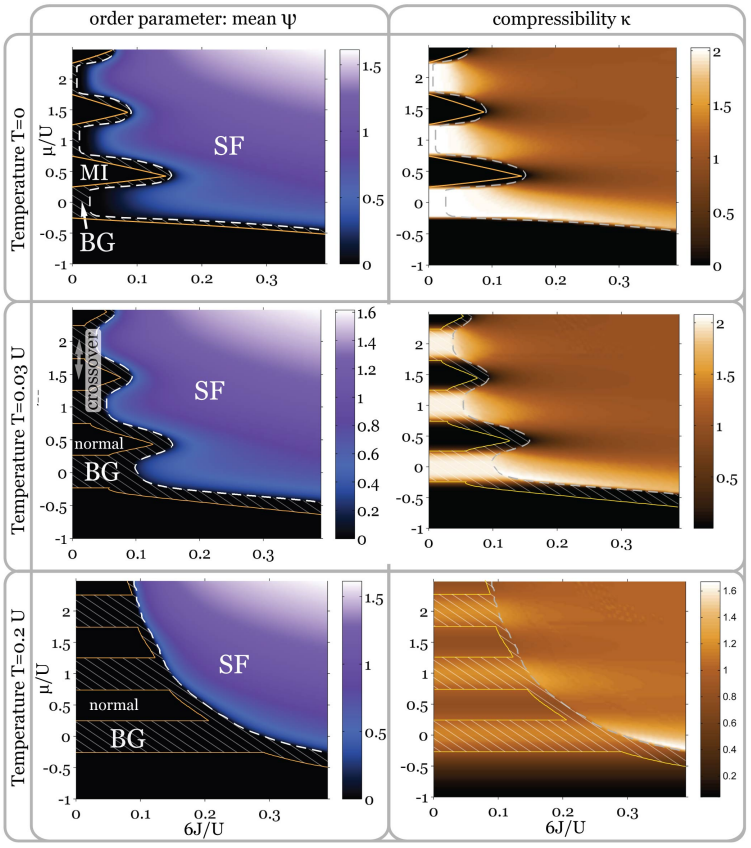

Figure 12.7: Finite temperature phase diagrams for box disorder with $\Delta = 0.5U$ for three temperature regimes: Zero temperature (upper row), intermediate $T = 0.03U$ (middle row) and high temperature regime $T = 0.2U$ (lower row). The left column shows the expectation value of the self-consistently determined distribution, which is the order parameter for the SF-insulator transition. It vanishes in the MI, BG, and the $T > 0$ normal phase. In the $T = 0$ diagrams, the MI/BG phase borders from strong coupling theory are indicated by the orange solid lines. The BG phase is marked by white stripes, at finite $T > 0$ this is determined by a vanishing local DOS only (i.e. not by strong coupling theory). At finite temperature there is only a crossover between the normal and BG phase, and the borders determined by the DOS of purely local excitations is marked by the horizontal white lines. The right column shows the compressibility κ in units of U^{-1}. Whereas this is a suitable quantity to distinguish the MI (incompressible) from the BG at $T = 0$, it is non-zero, but exponentially small in T in the MI in the intermediate regime and of order U^{-1} in the high temperature regime. The white borders indicate the transition to the SF, determined from the respective diagram on the left.

In Fig. (12.7), the effect of increasing temperature is exemplified in three phase diagrams and the compressibility in the three main regimes: the zero, low and high temperature regime at fixed disorder strength. The tips of the MI /normal lobes remain almost unchanged under an increase in T, while the BG region between the initial lobes is strongly enhanced and stabilized, even at a very low temperature of $kT = 0.03U$ (central plots of Fig. (12.7)). Since the SF/insulator phase border still possesses a distinctive lobe structure, but the BG region is strongly enhanced in contrast to the T=0 case (upper plots of Fig. (12.7)), we therefore refer to this situation as the intermediate temperature regime. Furthermore, a large value of compressibility is still a strong indicator for the BG at this temperature, suggesting that it may still useful as an indicator of the transition between the BG and the normal phase in experiment. In the high temperature regime $kT \gtrapprox 0.2U$, on the other hand, (see lower diagrams in Fig. (12.7)) the compressibility is large throughout, approaching the value $\kappa \to U^{-1}$ in the high T limit. The typical temperature of $T \approx 0.2U$ at which the MI and normal phase melts is consistent with previous previous studies [62]. In this temperature regime

the lobe structure of the SF/insulator phase border is totally wiped out and the critical border to the SF follows a $(JZ)_c \propto \mu^{-1}$ decay with increasing filling.

The SF/BG transition is highly sensitive to the system size. When the system approaches the SF phase from the BG phase, the localized single particle orbitals occupied by a large number of bosons increase in size and are occupied by an ever increasing, but never extensive number of particles in the BG phase. At the transition point the localization length, being a measure for the size of these orbitals, diverges and driven by percolation, phase coherence between neighboring orbitals is established, eventually driving the system into the SF phase. In finite size systems, the detection of the transition point thus critically depends on the system size, as the BG phase may be mistaken for the SF phase if the localization length is larger than the system size. SMFT has the advantage that it is constructed in the thermodynamic limit for an infinitely large system in the grand canonical ensemble and takes all possible disorder realizations into account within a functional description for the probability distributions. The numerical error in the discretization performed for the distribution $P(\psi)$ is well controlled and to be distinguished from the finite size deviations made in real space calculations.

In the phase diagram for box disorder Fig. (12.7), SMFT does not give rise to a direct transition from the MI to the SF, if the extended criterion for the MI/BG border, including collective excitations in rare regions is used. This is furthermore demonstrated in the finite temperature phase diagram at constant filling $n = 1$ in Fig. (12.8). Due to the absence of a clear distinction between the normal and BG phase at $T > 0$, the orange border only indicates a crossover between these regimes, but would go over into a MI/BG phase border for $T = 0$. At any $\Delta > 0$ a finite BG region intervenes between the MI and SF phases.

The question whether this transition always occurs via the BG phase has been a highly debated topic since the introduction of the disordered BHM [55], and was established for the one and two dimensional case [130, 160, 128]. In a recent work [127] it was shown that this scenario is true in any finite dimension for bounded disorder, due to the statistical certainty that any possible configuration of on-site energies for a cluster of sites will occur in the limit of an infinitely large system. In the previous work [15] these collective excitations in the BG phase were not considered and within a simpler framework of purely local particle and hole excitations, a direct transition was predicted.

It is known that arithmetically averaged MFT, as well as SMFT providing an improvement in any finite dimension, both become exact in the limit of infinite dimensions, where no BG exists at $T = 0$. However, as argued recently[127] the theorem of inclusions guarantees the existence of an intervening BG phase between the SF and the MI in any arbitrarily high, but finite number of dimensions for bounded disorder. It is instructive to understand the decrease of the BG region, including the collective excitation in the Lifshitz regions in terms of percolation physics: For any finite dimension the outer border between the BG and SF phase specifies the critical value $(J/U)_{\text{crit.1}}$ specifies the lowest energy at which it becomes energetically favorable for the particles to form a global condensate (in SMFT this is the border where $\overline{\psi}$ takes on a finite value). The border between the MI and BG inside the global insulator, specifies the critical value $(J/U)_{\text{crit.2}}$ at which it becomes possible for the system to form large local superfluid patches (locally resembling pure systems) without phase coherence between different patches. With increasing dimensionality of the system, the connectivity between different patches increases (percolation is enhanced) and the required tunneling energy $(J/U)_{\text{crit.1}}$ to form one large percolated patch, i.e. a global condensate, decreases. In the limit of high dimensions, the critical values of J at which these two phenomena occur approach the arithmetically averaged mean-field value [97]

$$JZ_c(\mu) = \Delta \left[n \ln \left(\frac{1 - n + \mu + \Delta/2}{1 - n + \mu - \Delta/2} \right) + (n+1) \ln \left(\frac{n - \mu + \Delta/2}{n - \mu - \Delta/2} \right) \right]^{-1}, \tag{12.16}$$

and the BG disappears, where n is the filling and μ and Δ are given in units of U.

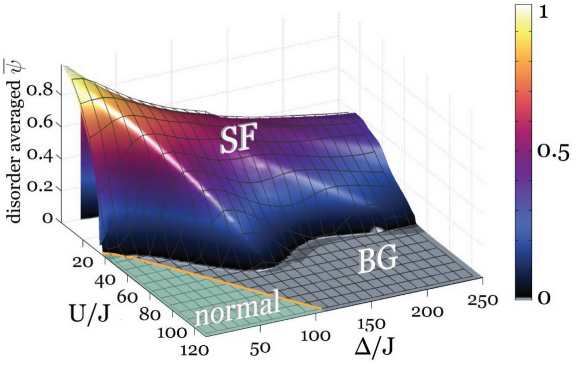

Figure 12.8: Phase diagram for box disorder at fixed density $n = 1$ in the U/J-Δ/J plane at $T = 0.03U$ showing the mean order parameter $\overline{\psi} = \sqrt{f_c}$. Reentrant superfluidity is reflected by the protruding SF lobe (we also find a second less pronounced lobe at higher Δ), where increasing Δ can drive the system through a sequence of SF-insulator transitions. The orange line specifies the crossover from the normal to the BG phase (at $T = 0$ this line becomes the MI-BG phase border) as determined by by shifted mean-field phase borders at this temperature, giving a better approximation than the strong-coupling approach for three dimensions. The simpler criterion of looking at purely local particle and hole excitations Eq. (12.15) would lead to the MI/BG phase border at $U = \Delta$ and predict a direct MI-SF transition at small Δ. Including collective excitations in the BG, as done here, always leads to an intermediate BG phase between the MI and SF in the $T = 0$ limit.

In Fig. (12.8) we present a phase diagram calculated at fixed density $n = 1$ in the low temperature regime $T = 0.03U$. At every point in the diagram, the self-consistent distribution is calculated for a fixed μ, enabling the calculation of the density $\langle n(\mu, \Delta, U, J, T)\rangle$. Thereafter μ is iteratively determined using Ridder's algorithm [1] until the density obtained from SMFT does not deviate more than $\Delta n = 0.005$ from the specified density. In Fig. (12.8), the disorder averaged MFP $\overline{\psi} = \int \psi\, P(\psi) d\psi$ (within SMFT, this is exactly $\sqrt{f_c n}$) clearly shows the usual SF/insulator phase transition (at fixed low temperature) along the line $\Delta = 0$, where the disorder localizes the particles with increasing U/J. Moving outwards into the Δ/J at fixed interaction U/J, the condensed phase is surprisingly robust, surviving local on-site fluctuations Δ several hundred times larger than the hopping energy J, as pointed out in a recent work [70]. This can be understood from the bosons filling up the low-lying sites and forming a 'background sea' via the repulsive interactions, creating an effective smoother potential in which it is energetically favorable for the remaining bosons to delocalize [15]. A remarkable effect at sufficiently low temperature is the appearance of a SF lobe, protruding into the insulating domain at finite Δ. In this regime the interplay between disorder and interactions is non-monotonic in these two effects, and, for the regime $40 \lessapprox U/J \lessapprox 85$, an increase in Δ drives the system into the SF phase, delocalizing the particles. This effect can be understood from the pure BHM μ/U-J/U phase diagram and relies on the existence of a lobe structure, i.e. requires a sufficiently low T. To keep the particle number constant with increasing Δ, μ is required to increase. In certain regimes the majority of sites in the system may enter from an insulating regime between the lobes into a regime inside the lobes, thereby favoring condensation. Qualitatively, the SMFT phase diagram agrees well and shows the disorder induced SF lobe, as found in recent QMC calculation [70] at $T = 0$ on relatively small lattices ($L = 8 \times 8 \times 8$).

At large Δ the order parameter is non-monotonic in U/J, vanishing at sufficiently small U/J which indicates a transition into an Anderson localized state, where the localization almost exclusively disorder-induced. However, the region of extremely small U/J is problematic as Δ/U and μ/U diverge, since very few sites have to contain an ever increasing number of particles to keep the disorder-averaged density fixed, when asymptotically half the number sites (due to the symmetry of the box distribution $p(\epsilon)$) have such a high effective on-site energy, that they contain no particle. Due to the diverging local occupation number, this limit transcends the constraints imposed in the derivation of the BHM in an optical lattice and is, in this sense, unphysical.

12.4 Speckle Disorder

Although a homogeneous box distribution is most commonly used for disorder calculations in theory, it is currently not an experimentally feasible choice. In this section we discuss and compare the results for a realistic disorder distribution created by a speckle laser to those of a box disorder distribution. A laser passing through an inhomogeneous disordered plate leads to a disordered optical potential, which is the Fourier transform of the disordered pattern on the plate. In recent experiments, it has become possible to reduce the autocorrelation length of this disordered potential to the order of the lattice spacing ($\leq 1\mu m$) [170]. With this experimental achievement, the priorly most criticized artifact of a speckle laser for creating uncorrelated disorder has been overcome, thereby making speckle potentials the most promising method for future disorder experiments in optical lattices. The resulting distribution for uncorrelated on-site energies is well approximated by

$$p(\epsilon) = \frac{\Theta(\epsilon)}{\Delta} e^{-\epsilon/\Delta} \tag{12.17}$$

Although it may be argued that an optical speckle potential in experiment is fundamentally bounded by its finite size, it is only essential that the width of the on-site energy distribution exceeds U (which is fulfilled in essentially all experimentally relevant regimes). This justifies the use of (12.17).

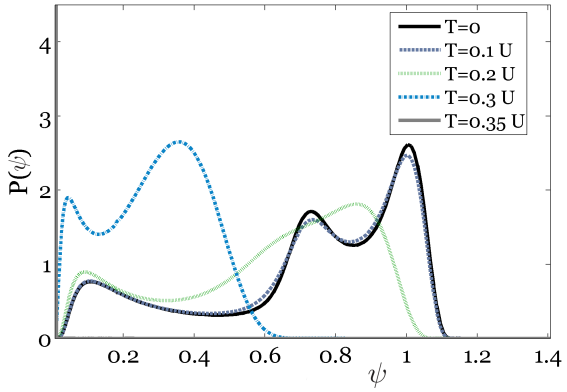

Figure 12.9: Typical self-consistent distributions $P(\psi)$ for speckle disorder for $\Delta = 1U$, $\mu = 1.2U$, $Z = 6$, and $JZ = 0.3U$ at different temperatures. For low temperatures the mean-field parameters in the condensed phase are robust against finite temperature fluctuations, but with increasing temperature the system is eventually driven into an insulating BG phase, as indicated by the distribution at $P(\psi) = \delta(\psi)$ in the at $T = 0.35U$.

To treat this disorder distribution using SMFT, it is useful to perform a transformation of variables $x(\epsilon) = -e^{-\epsilon/\Delta}$, which on a formal level transforms the SMFT conditional probability functions into a form analogous to homogeneous disorder. This step enters only on the level of calculating the conditional cumulative distribution function (CDF),

$$F(\psi|\eta) = \lim_{c\to 0} \int_{c-1}^{0} dx\, \Theta(\psi - g(\mu + \Delta \ln(-x), \eta)). \tag{12.18}$$

Apart from this, the SMFT method remains identical to the homogeneous disorder case. Similarly, arbitrary disorder distributions may also be incorporated into SMFT, although an analytical transformation of the random variable will not exist in general.

In contrast to box disorder, which has been the distribution primarily focused on so far when considering the disordered BHM, speckle disorder is unbounded and arbitrarily high values of ϵ have a finite probability to occur. This leads to the effect (strictly only possible for an infinitely large system) that *turning on* the disorder by an arbitrarily small amount immediately changes a large part of the phase diagram from the MI / normal phase into the BG phase.

In a physical picture, the effective chemical potential μ' can then take on integer multiple values of U (the on-site potential can become arbitrarily high) with a non-zero probability density, where local Fock states with different particle number become degenerate, leading to a finite compressibility and local DOS $\overline{\rho}(\omega = 0)$ at $T = 0$.

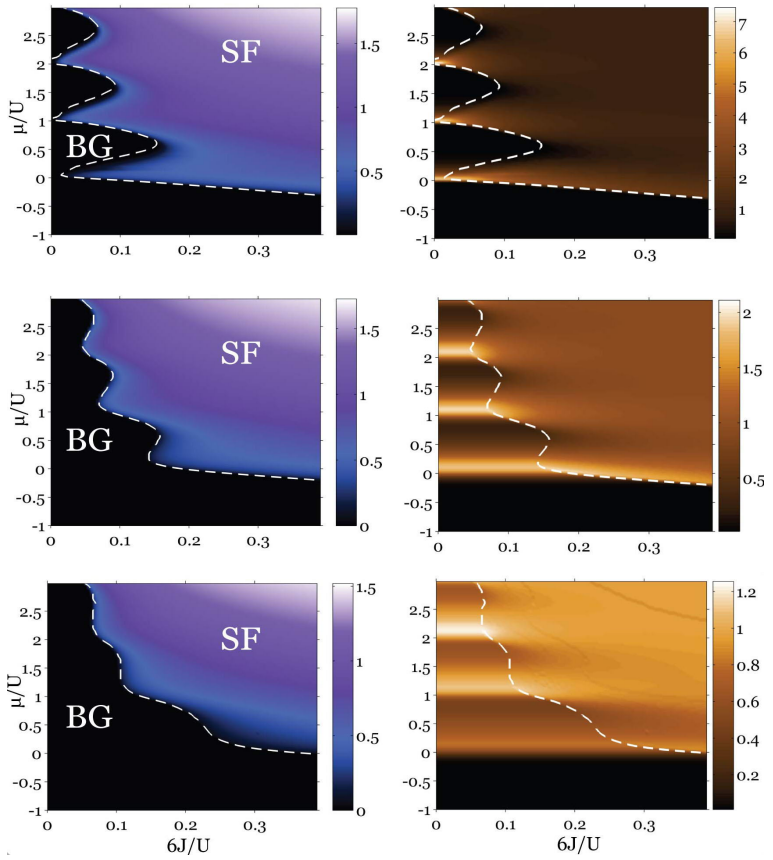

Figure 12.10: Disorder averaged MFP $\overline{\psi} = \int d\psi\, \psi\, P(\psi)$ characterizing the SF-insulator transition (left column), and compressibility (right column, in units of U^{-1}) in the JZ/U-μ/U-plane for **speckle disorder**. Diagrams are shown for increasing disorder strength ($\Delta = 0.1U$, $\Delta = 0.3U$, $\Delta = 1U$) in the zero or low temperature regime ($T = 0$, $T = 0.05U$, $T = 0.05U$) for the (upper, middle, lower) row respectively. In contrast to the behavior for box disorder, the structure of each lobe does not change symmetrically, but rapidly extends in the direction of decreasing μ/U with increasing disorder strength Δ. Since the MI / normal phases do not exist for speckle disorder, the insulating region (black in the left figures) is always a BG. The white lines denote the SF / insulator phase boundaries, indicating where $\overline{\psi}$ takes on a finite value.

In the absence of disorder and at sufficiently high tunneling coupling J, a macroscopic number of particles occupy the $|k = 0\rangle$ Bloch state. Within an effective, symmetry breaking Gutzwiller description the local order parameters $\psi_l = \langle b \rangle_l$ then take on a finite and constant value, reflecting the translational symmetry of the system. Within SMFT this state is characterized by a δ-distribution $P(\psi) = \delta(\psi - \psi_0)$, where ψ_0 is the order parameter of conventional bosonic Gutzwiller theory. Turning on the disorder in such a system in the SF state breaks the translational symmetry of the system, i.e. the condensate state deviates from the $k = 0$ Bloch state, which is reflected by the distribution of MFPs $P(\psi)$ taking on a finite width. Initially for weak disorder, an increase in disorder always leads to a broadening of $P(\psi)$, but for stronger values of Δ the system may eventually be driven toward an insulating state, driving $P(\psi) \to \delta(\psi)$ and thereby decreasing the fluctuations in the MFPs. On the other hand, increasing the temperature suppresses the SF and leads to a decrease of the MFPs above a certain temperature, up to which the SF remains stable, as shown in Fig. (12.9).

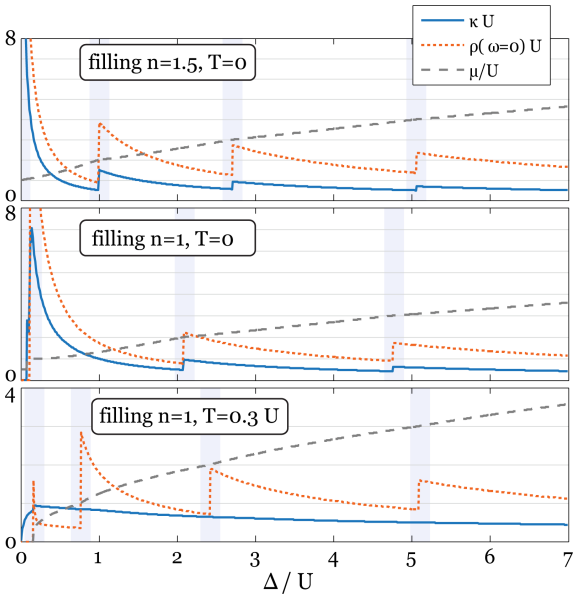

Figure 12.11: The compressibility, local single particle DOS and chemical potential as a function of disorder strength Δ for speckle disorder at constant filling. Comparison of the upper two plots shows a diverging compressibility and local DOS for $\Delta \to 0$ for non-integer filling (the system remains superfluid), while for integer filling it drops to an exponentially small value in Δ at a value of $\Delta \approx 0.1U$ and vanishes in this limit. The lowest figure shows the same quantities at finite temperature $kT = 0.3U$, where thermal fluctuations have totally smeared out the sharp features in the compressibility. However, these persist in the local DOS, although their position is changed due to a temperature induced shift in μ.

The influence which speckle disorder has on the μ/U-J/U-phase diagrams is shown in Fig. (12.10). In contrast to box disorder, where the distribution of on-site energies is symmetric around μ and the insulating lobes give way to the SF in the same way on the upper and the lower side of the lobe, the insulator forms on the lower side of the lobes with increasing Δ for speckle disorder. This can be understood from the fact that only lower values of the effective local chemical potential can occur.

For strong disorder $\Delta \gtrapprox U$, the lobe structure of the insulator / SF phase boundary is washed out, which is similar to the effect of finite temperature. For speckle disorder, κ cannot be used to identify a phase transition, since it is non-zero in both the BG and the SF. A question of interest, regarding the disappearance of the MI /normal phase for an arbitrarily small amount of speckle disorder, is how the compressibility behaves as a function of Δ, as some interpretation is needed, that an 'infinitesimal amount of disorder' can instantaneously convert the whole MI/normal area of the phase diagram into a BG.

In Fig. (12.11), $\kappa(\Delta)$ is shown for different parameters to clarify this dependence. In the insulating state, the compressibility can be calculated explicitly (M.11) and one obtains

$$\kappa = \frac{1}{\Delta}\left[\frac{\sum_m m\, e^{-\beta E_m(\mu)}}{\sum_m e^{-\beta E_m(\mu)}} - \frac{1}{\Delta}\int_0^\infty d\epsilon\, e^{-\frac{\epsilon}{\Delta}} \frac{\sum_m m\, e^{-\beta E_m(\mu-\epsilon)}}{\sum_m e^{-\beta E_m(\mu-\epsilon)}}\right] \tag{12.19}$$

Essentially, two different scenarios have to be considered. First, if μ/U is positive and integer, κ diverges in the limit of vanishing disorder, as is well known from the pure BHM phase diagram, where the density is a step function in μ/U for $J = 0$. This is equivalent to the case for non-integer, fixed particle density n, where the system remains SF for any non-zero J. Second, if μ/U

is non-integer, the compressibility vanishes with decreasing Δ, as the system approaches a point in a Mott lobe away from the border. This corresponds to the case of fixed, integer-valued density n.

We will now discuss the behavior of κ and $\overline{\rho}(\omega = 0)$ at fixed particle density n, shown in Fig. (12.11). Keeping the density constant with rising disorder, requires the chemical potential to be increased, as an ever increasing number of sites shifts to weights with lower occupation numbers. At every point when μ/U passes a positive integer number, a new Fock state becomes potentially occupied, but with an ever decreasing statistical weight as Δ increases. As a result the compressibility experiences a jump at each of these points, as highlighted by the gray regions in Fig. (12.11), where μ/U (dotted gray lines in Fig. (12.11)) passes an integer value. This leads to the characteristic series of ever smaller kinks in $\kappa(\Delta)$. At finite temperature, these features in κ are smeared out over a typical scale of kT, whereas the sharp features in the local single particle DOS survive at $T > 0$ within SMFT (solid blue lines in Fig. (12.11)).

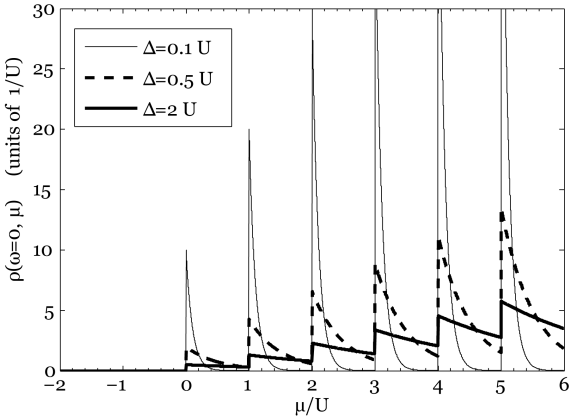

Figure 12.12: The disorder averaged single particle density of states $\rho(\omega = 0, \mu)$ at zero frequency for $T = 0.05U$ for different speckle disorder intensities. For $\Delta = 0$ this consists of a sequence of δ-peaks at positive integer values of μ/U, however for any $\Delta > 0$ this quantity is non-zero for $\mu \geq 0$ and the system is in the BG phase.

To clarify the effect speckle disorder has on $\overline{\rho}(\omega = 0)$ and the immediate disappearance of the MI / normal phase at any $\Delta > 0$, the local DOS is plotted for weak ($\Delta = 0.1U$), intermediate ($\Delta = 0.5U$) and strong ($\Delta = 2U$) in Fig. (12.12) as a function of μ. In the pure system $\overline{\rho}(\omega = 0, \mu)$ consists of a sum of δ-peaks at integer values of μ/U, i.e. at these values of the chemical potential there are two degenerate Fock states $|n = \mu/U\rangle$ and $|n = \mu/U + 1\rangle$ at all sites in the insulator and the local single particle DOS diverges. As soon as speckle disorder is turned on, these δ-peaks are broadened according to the on-site energy distribution (12.17) and $\overline{\rho}(\omega = 0)$ takes on the form of a sequence of superimposed exponential functions, each decaying with the constant Δ. From this it is clear that $\overline{\rho}(\omega = 0)$ takes on a non-zero value as soon as $\Delta > 0$ at any $\mu > 0$, although it is exponentially suppressed for most values of μ at weak disorder $\Delta \ll U$. At zero temperature the different amplitudes of the various peaks in $\overline{\rho}(\omega = 0, \mu)$ at integer μ can be exclusively attributed to the $\sqrt{n}$ factor from the action of the bosonic operators, whereas at $T > 0$ the amplitudes (but not the positions of the sharp features) may also be modified by the Boltzmann factors in (M.18).

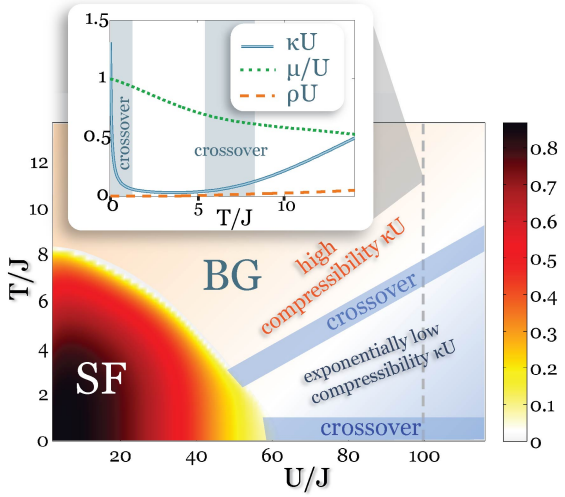

Figure 12.13: Main image: Phase diagram in the T/J-U/J-plane for fixed $\Delta = 10J$ at fixed filling $n = 1$ in three dimensions. For this specific disorder strength the SF region is enlarged by the disorder in comparison to the pure case (i.e. disorder induced condensation, see Sec. 12.4.1).In the lower left corner, the SF exists at sufficiently low T and Δ and the value of disorder-averaged $\overline{\psi}$ is color-coded. Outside the SF region, the system is always in a BG phase, but undergoes two crossovers from a regime with exponentially low compressibility κU for intermediately low $0.02 \lessapprox T/U \lessapprox 0.065$ (for $\Delta/J = 10$) into a strongly compressible BG regime, in the limits of both high and very low T/U. To clarify the quantitative behavior, the compressibility κ, the chemical potential μ and the local single particle DOS $\rho(\omega = 0)$ along the dashed line $U/J = 100$ is shown in the inset.

Fig. (12.13) shows the phase diagram at constant disorder strength $\Delta/J = 1$ and constant density $n = 1$ in units of J. The SF region prevails in the lower left region at low temperature and weak interaction U/J. In this parameter regime the disorder stabilizes the SF phase, actually extending the SF region of the phase diagram in contrast to the pure ($\Delta = 0$) case (disorder-induced condensation, see Sec. 12.4.1). All of the non-SF region in Fig. (12.13) is a BG, since we are dealing with unbounded disorder with $\Delta > 0$, but we can identify a weakly and two strongly compressible regimes in the phase diagram. Since $P(\psi) = \delta(\psi)$ in the BG, the energy scale J cannot influence thermodynamic quantities beyond a scaling relation, implying that the compressibility κU may be a function of T/U only. Therefore the compressibility has a radial structure and it suffices to consider its behavior along a single line (such as $U/J = 100$, depicted in the inset of Fig. (12.13)). This reveals that there are three regimes in this phase diagram: at high temperature $T/U \gtrapprox 0.065$ the system is strongly compressible (κU is of order unity), as thermal fluctuations have wiped out the sharp peaks over a wide range in μ. At intermediately low temperature, the compressibility is exponentially low, as the typical thermal excitation energy scale does not suffice to excite the majority of sites to higher states. Somewhat surprisingly, within a certain parameter regime for Δ and the density n, the system undergoes a further crossover at very low temperature $T/U \approx 0.02$ into a second highly compressible regime. At $T = 0$ and at integer filling, the chemical potential μ/U approaches an integer value from below (green dotted line in the inset of Fig. (12.13)). At these points κ diverges in the pure limit of $\Delta \to 0$, which reveals that the compressibility is grows with the inverse of Δ and only persists in the limit $T \to 0$ if the density n is integer.

12.4.1 Disorder-induced reentrant Superfluidity

At low temperature and fixed density, we find that an increase in Δ can actually drive the system from an insulating into a condensed state within a certain window of U/J, as shown in Fig. (12.14) and Fig. (12.15). Within a very small window of U/J, the system may be driven through an additional sequence of BG and SF phases.

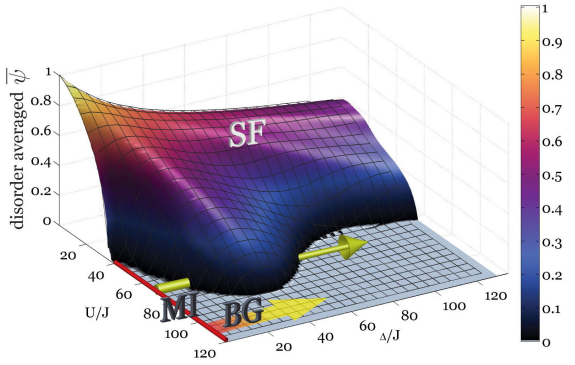

Figure 12.14: Low temperature $kT = 0.03U$ phase diagram showing the disorder-averaged MFP $\overline{\psi}$ for speckle disorder at constant filling $n = 1$ in three dimensions. Multiple reentrant behavior can be seen within a small window of U/J. The red line at $\Delta = 0$ indicates the presence of MI / normal state, for any $\Delta > 0$ the insulator is a BG.

On the $\Delta = 0$ line, the usual SF - insulator transition occurs, whereas along Δ for small values of U, disorder only suppresses the SF slightly up to reasonably large values of Δ/J. For even larger disorder values, the system will eventually undergo the transition into an

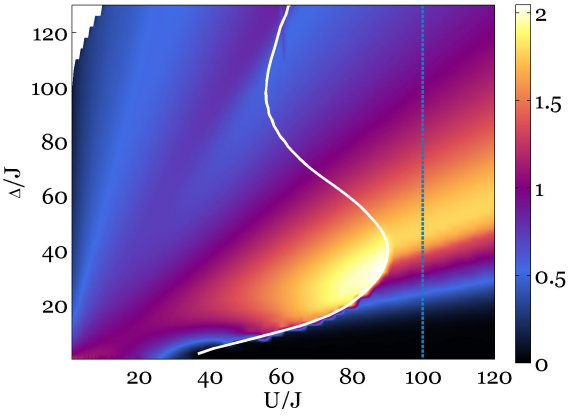

Figure 12.15: Compressibility κ in units of $1/U$ at $kT = 0.03U$ for speckle disorder at constant filling $n = 1$ in three dimensions (same parameters as in Fig. (12.14)). The incompressible normal phase only exists on the line $\Delta/J = 0$, but the region where κ is exponentially small in the insulator extends linearly with U/J. The white line is the SF - insulator phase border, where $\overline{\psi}$ becomes zero. The compressibility along the blue dashed line can be understood as the low temperature case and compared to κ in the lower two plots of Fig. (12.11), where the sharp features have been washed out by temperature, but are still pronounced peaks.

Anderson localized state. In comparison to the corresponding phase diagram for box disorder Fig. (12.8), the extruding superfluid lobe appears at a considerably smaller values of $\Delta \approx 40J$ for speckle disorder ($\Delta \approx 100J$ for box disorder, not the different Δ-axis scale). However, it should be noted that the measure Δ is not the same (in a statistical sense) for the two disorder types: whereas for speckle disorder Δ is also the standard deviation (std), in the case of box disorder the std is only $\frac{\Delta}{2\sqrt{3}} \approx 0.29\Delta$, corresponding to weaker disorder for the same Δ. Examining the position of the superfluid lobe in units of the standard deviation, actually reveals that it appears at slightly smaller disorder strengths for box disorder.

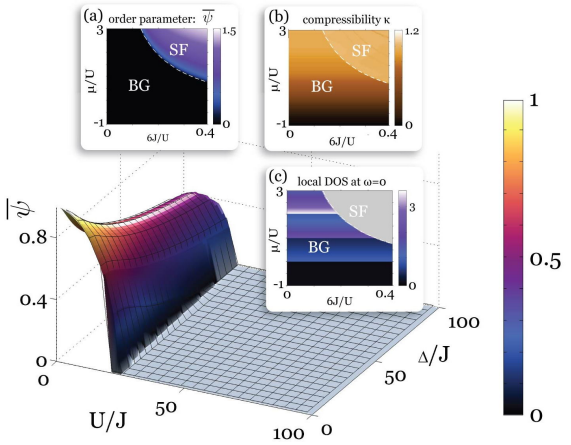

Figure 12.16: Main background image: same $\overline{\psi}$ phase diagram as in Fig. (12.14), but in the experimentally relevant high temperature regime $kT = 0.3U$ at $n = 1$, where disorder cannot induce condensation. Insets: disorder averaged MFP (a), compressibility (b) and local DOS $\overline{\rho}(\omega = 0)$ in the μ/U-JZ/U-plane at the same temperature $T = 0.3U$ for $\Delta = 1U$. In this regime most interesting structure has been washed out by thermal fluctuations and disorder and an increase in either U, Δ or T **always** suppresses condensation.

In the vicinity of the phase border, κ is generally larger in the SF state than in the neighboring insulator, as a shift in μ leads to a locally continuous shift in density. On the lower side of the lobe at disorder strengths $\Delta \lessapprox 40J$, the compressibility jumps across the phase border (i.e. second order transition). At higher values of Δ, κ is almost unaffected by the disappearance of the condensate, i.e. the compressibility is almost exclusively induced by disorder. In the insulating state the ensemble of mean-field states determined by SMFT cannot depend on J (since different sites are only coupled via ψ). Therefore any physical quantity, such as κ, can only be a function of T/U in this regime (reflected in the radial structure of κ in the insulator).

In the high temperature regime relevant for current experiments (see App. 12.5.1 for an approximation of T), the lobe in the $\Delta/J - U/J-$plane at fixed density has vanished completely and an increase in disorder always counteracts the condensate formation. This might explain the recent finding, that no reentrant behavior or disorder-induced condensation was observed in experiments so far [121]. Furthermore, we calculated the $\mu/U - J/U-$phase diagram for this temperature and disorder regime, where the lobe structure is also fully washed out and the system is dominated by thermal fluctuations, as seen in the insets of Fig. (12.16). We therefore conclude that an upper critical temperature, which may depend on the filling, exists for the occurrence of reentrant superfluidity. Our temperature estimation suggests that T is too high in current experiments to observe this effect, which agrees with recent experimental evidence [121].

12.4.2 Hopping Disorder

In addition to diagonal on-site energy disorder, it is possible to incorporate off-diagonal hopping disorder [40] into the SMFT formalism. In this case, the local hopping energy $J_{\langle i,j\rangle}$ between site i and j becomes a random variable, each described by a distribution $p_J(J)$, which we assume to be independent of the on-site energies ϵ_i. This leads to the BH Hamiltonian with on-site, as well as hopping disorder

$$\mathcal{H}_{\text{BH}} = -\sum_{\langle i,j\rangle} J_{\langle i,j\rangle}(b_i^\dagger b_j + \text{h.c.}) + \sum_i (\epsilon_i - \mu) n_i + \frac{U}{2}\sum_i n_i(n_i - 1). \tag{12.20}$$

The PDF $p_J(J)$ has been calculated for a speckle disorder potential [182, 170] using imaginary time evolution.

In contrast to diagonal disorder (on-site energy or interaction), where the fluctuations are incorporated into the conditional PDF (12.7) before the iteration procedure of the SMFT self-consistency equations, the hopping disorder acts as an additional source of fluctuations during this iteration procedure, methodically entering at a different point in the method. The corresponding mean-field Hamiltonian $\mathcal{H}_i^{(\mathrm{MF})}$, (analogous to (12.1)) now depends on the rest of the system only through the new random variable

$$\eta = \sum_{j=1}^{Z} J_j \psi_j, \tag{12.21}$$

where both J_j and ψ_j are random variables, the latter again being assumed to be distributed according to $P(\psi)$. It is therefore convenient to introduce the an intermediate random variable $\phi = J\psi$, distributed according to the PDF $P_\phi(\phi)$. As explained in App. M.3, this new PDF can be expressed explicitly in terms of the PDF's $P(\psi)$ and $p_J(J)$ as

$$P_\phi(\phi) = \int dx\, p_J(e^x)\, P(\phi \cdot e^{-x}), \tag{12.22}$$

numerically allowing the use of the FFT algorithm on a suitable grid. Once $P_\phi(\phi)$ is known, the PDF for the random variable $\eta = \sum_{l=1}^{Z} \phi_l$ can subsequently be calculated by

$$Q(\eta) = \frac{1}{2\pi} \int dt\, [\vartheta(t)]^Z\ e^{-it\eta}, \tag{12.23}$$

where

$$\vartheta(t) = \int d\phi\, P_\phi(\phi)\, e^{it\phi}. \tag{12.24}$$

is the characteristic function of $P_\phi(\phi)$. For the numerical computation of the previous two, the FFT algorithm can be used.

The conditional PDF (12.7) $\tilde{P}(\psi|\eta)$, incorporating the effect of any diagonal (here: on-site) disorder remains unchanged under the inclusion of hopping disorder and is calculated before the SMFT iteration procedure in full analogy to the previous case for the relevant on-site disorder type $p(\epsilon)$. The final self-consistency equation, closing the iteration procedure is also left unchanged to the previous case (12.8)

$$P(\psi) = \int d\eta\, Q(\eta)\, \tilde{P}(\psi|\eta), \tag{12.25}$$

except that the $Q(\eta)$ entering is calculated from (12.23).

Of course the case of pure on-site disorder with a constant hopping energy J_0 can be obtained as a limit of this extension by setting $p_J(J) = \delta(J - J_0)$, causing (12.22) and (12.23) to reduce to (12.3).

The numerical iteration procedure is carried out analogously to Sec. 12.1.1, except that only a single equidistant grid, as restricted by (12.22), can be used. This limits the numerically obtained precision of $P(\psi)$ at small values of ψ.

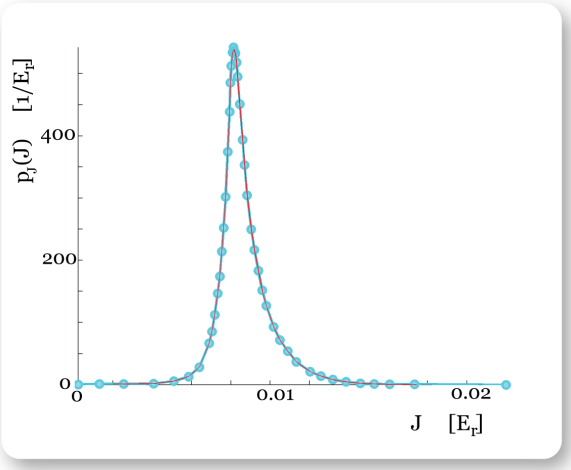

Figure 12.17: Distribution for nearest neighbor J at a lattice strength $s = 14$ and a disorder strength of $s_D = 1E_R$extracted from Zhou & Cerperly [182]. The mean value $\overline{J} = 0.008E_r$ agrees well with the value obtained from a usual band structure calculation for these parameters. The distribution here correspond to a disorder strength of $\Delta = 0.97E_r$ (obtained from a fit of the exponential) and has to be rescaled in the width for our disorder strength of $\Delta = U$. The values shown here were calculated for a 3D $812nm$ cubic lattice, corresponding to an interaction strength of $U = 0.443E_R$ for ^{87}Rb. Furthermore, for the SMFT, a rescaling in the axis for J has to be performed, as we work in units of U. For a given value of J/U, the distribution is shifted, such that the most likely value agrees with this.

In our calculation we use the appropriately scaled distribution $p_J(J)$, matching the on-site disorder strength, as obtained by Zhou and Ceperley [182] for a lattice depth of $s = 14E_R$ and at a speckle disorder strength of $s_D = 1E_R$, where we assume that the standard deviation in $p_J(J)$ is proportional to the disorder intensity s_D (as motivated by their analysis). Since a change in the disorder strength does not change the most probable value of the distribution [182] $p_J(J)$, we model the hopping disorder distribution to have its most likely value at the given value $\overline{J}/U$, with the width being independent thereof. If any weight lies at values of negative J, this is set to zero and the distribution is subsequently renormalized, however this is only relevant for points deep in the insulator and does therefore not influence the results in any way. However, this only occurs at very small values of $\overline{J}/U$ deep in the insulator, making this formal alteration of $p_J(J)$ irrelevant to the result.

As shown in the low temperature phase diagram in the J/U-μ/U-plane in Fig. (12.18), the additional inclusion of hopping disorder leads to a stabilization of the SF phase and a small shift in the phase boundary. For disorder distributions in the typical experimentally relevant parameter regime, the standard deviation of the hopping parameter distribution $p_J(J)$ is three orders of magnitude smaller than the standard deviation of the on-site energy distribution $p(\epsilon)$ (as found in [182], specifically for the distributions used here $\sigma_J/\sigma_\epsilon = 0.0014$). This explains the minor, but clearly resolved modification of the phase boundaries in contrast to the pure on-site disordered case, shown in the upper right inset of Fig. (12.18). As shown in the low temperature phase diagram in the J/U-μ/U-plane in Fig. (12.18), the additional inclusion of hopping disorder leads to a stabilization of the SF phase and a small shift in the phase boundary. For disorder distributions in the typical experimentally relevant parameter regime, the standard deviation of the hopping parameter distribution $p_J(J)$ is three orders of magnitude smaller than the standard deviation of the on-site energy distribution $p(\epsilon)$ (as found in [182], specifically for the distributions used here $\sigma_J/\sigma_\epsilon = 0.0014$). This explains the minor, but clearly resolved modification of the phase boundaries in contrast to the pure on-site disordered case, shown in the upper right inset of Fig. (12.18).

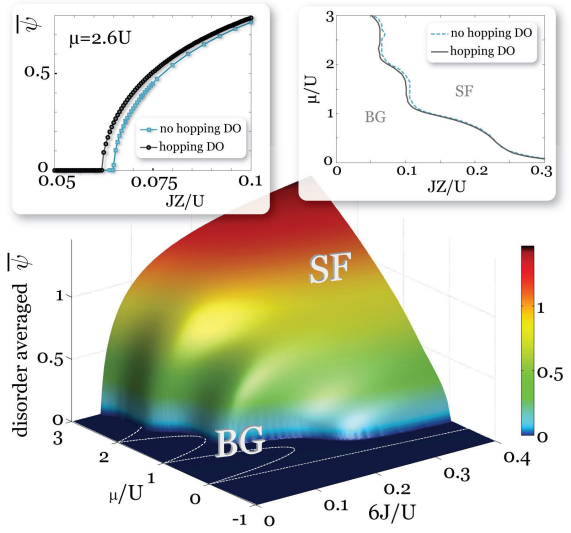

Figure 12.18: Diagrams showing the effect of **hopping disorder** at $T = 0.05U$ and an on-site speckle disorder strength $\Delta = U$. Main 3D figure: disorder-averaged MFP ψ for speckle on-site and experimentally corresponding hopping disorder. For orientation purposes, the MF phase boundary for the pure system is plotted as a thin dashed white line. The value J/U refers to the most likely value of the hopping disorder distribution $p_J(J)$, whereas the width of the distribution $p_J(J)$ is constant. Upper left inset: comparison of the order parameter at fixed $\mu = 2.6U$ with and without hopping disorder, clearly demonstrating that the addition of hopping disorder stabilizes the SF phase and leads to a lower critical value of J in this regime. Upper right inset: Subsequent comparison of phase borders in the μ/U-J/U-plane.

12.5 Incorporating experimental aspects

12.5.1 Temperature estimation in an optical lattice

The initial temperature in the trap, prior to the optical lattice ramp-up, can be determined from the expansion profile of the cloud. If the ramp-up of the optical lattice is performed adiabatically, the entropy of the system is conserved and can actually lead to a cooling of the atoms. The initial entropy of a weakly interacting cloud in the trap using Bogoliubov theory leads to the expression [132]

$$S_{\text{Bog.}}(\beta) = k_B \sum_{\mathbf{p}} \left(\frac{\beta \epsilon_{\mathbf{p}}}{e^{\beta \epsilon_{\mathbf{p}}} - 1} - \ln[1 - e^{\beta \epsilon_{\mathbf{p}}}] \right). \tag{12.26}$$

After ramping the lattice to a sufficiently high intensity, the entropy can be calculate up to first order (neglecting terms containing J) [132]

$$S_{\text{J}=0} = k_B \left[-\beta\mu + \frac{1}{N} \ln(\Xi(M)) + \beta E \right], \tag{12.27}$$

where M is the number of sites and $\Xi(M)$ is the grand canonical partition function. Equating these two expressions for a sufficiently high initial temperature $k_B T_{\text{initial}} > 0.05 E_R$ leads to the relation [132]

$$k_B T_{\text{final}} \approx \frac{U}{3E_R} (k_B T_{\text{initial}} + 0.177 E_R) \tag{12.28}$$

For ^{87}Rb in an optical with a wave length of $\lambda = 812nm$ and intensity $s = 11E_R$, the disorder-averaged interaction constant is $\overline{U}/E_R = 0.355$. As a typical, conservative estimate of the initial temperature before the lattice ramp-up in current experiments [114] we use the value $T_{\text{initial}} = 0.13\mu K$, for which the relation (12.28) predicts a final temperature of $k_B T \approx 0.11 E_R = 0.32U$ after the ramp-up.

12.5.2 LDA incorporating trap effects

To compare the results obtained via SMFT to experimental data on a quantitative level, we performed a LDA+SMFT calculation to incorporate the effect of the trapping potential. Two effects of the lattice laser beams are taken into account: The red-shifted lattice laser beam with a Gaussian profile and beam width w_0 leads to an attractive potential via the ac Stark effect. Furthermore, the local energies of states within a localized Wannier basis are also increased in regions of high intensity, leading to the renormalized effective lower trapping frequency within an harmonic approximation [67].

$$\omega_{\text{eff}}^2 = \frac{4E_R}{mw_0^2}(2s - \sqrt{s}). \tag{12.29}$$

With the addition of an external magnetic trap with trapping frequency ω_{mag}, the total trapping frequency, which the atoms are exposed to is given by

$$\omega_{\text{tot}} = \sqrt{\omega_{\text{eff}}^2 + \omega_{\text{mag}}^2}. \tag{12.30}$$

For every fixed value of the lattice height s, J and U are extracted from the single particle Wannier function (beyond the approximation for deep lattices [67]), the total trapping frequency (12.30) is calculated and the local effective trap energies are assigned on a sufficiently large $3D$ lattice. The chemical potential μ is adjusted using Ridder's method [1] to obtain a specified total particle number. The condensate fraction, depicted in Fig. (12.19), is subsequently averaged over the local values obtained by SMFT, weighted by the respective density.

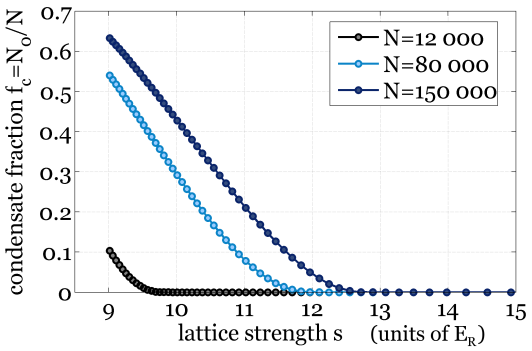

Figure 12.19: The condensate fraction as a function of the lattice strength s for various total particle numbers in a harmonic trap, calculated within LDA and SMFT (connected dotted lines). The calculations were performed at fixed temperature $kT = 0.3U$ and disorder strength $\Delta = 1U$.

We used the following values for the experimental parameters: $w_0 = 110\mu m$, the lattice laser wavelength was set to $\lambda_{\text{lat}} = 812nm$, and the magnetic trapping frequency $\omega_{\text{mag}} = 2\pi\, 40Hz$.

In contrast to the behavior of the order parameter at the transition point, the condensate fraction does not follow a power law decay in the finite trap, but is smeared out a the transition point, as superfluid regions in the trap decay in size with increasing s.

12.6 Conclusion & Outlook

In this chapter we have described the stochastic mean-field theory in detail on a methodological level, and extend it to incorporate finite temperature effects. Subsequently, we have applied it to ultracold atoms in an optical lattice with uncorrelated on-site box disorder distribution and discussed the intricate interplay between interaction, tunneling energy, disorder, filling and finite

temperature effects. Furthermore, we have presented, to the best of our knowledge, the first quantitative theoretical calculations for speckle disorder, which leads to a qualitatively different phase diagram than for box disorder and are of immediate experimental relevance [121]. For this case, we have discussed the characteristic features of the various phases and presented phase diagrams, both at fixed chemical potential and at fixed density. Below a critical temperature, we find disorder-induced condensation and multiple reentrant behavior, both for box and speckle disorder. The temperature in recent experiments [121] is estimated and found to be too high yet to observe disorder-induced condensation. We also find that including hopping disorder in addition to local on-site disorder for a realistic distribution of speckle parameters enhances the insulator and jumps in the order parameter within the SF phase indicate a series of transitions. An LDA+SMFT calculation has been performed to incorporate the effects of an external trap for on-site speckle disorder. Far from all questions have been answered in the field of disordered lattice bosons. For instance, the effect of disorder on the phase diagram of strongly interacting multi-species bosons is unclear. A very challenging further issue, which is beyond the scope of current Monte-Carlo and DMRG methods in three dimensions, is the effect disorder has on the amplitude mode in a disordered condensate. This could for instance be addressed on small clusters within the quasi-particle theory.

Conclusion and Outlook

The development of methods and the theoretical description of ultracold, strongly interacting bosonic atoms in optical lattices lies at the heart of this thesis. A wide range were addressed, from the foundations of the underlying single-particle physics, where a method is devised to efficiently calculate Wannier functions, up to the collective, time-dependent description of interacting many-particle systems in form of the extended quasi-particle theory for strongly interacting bosons.

Embedded into the derivation of the Hubbard model in chapter (2), we derive and present a method to calculate Wannier functions with very high efficiency and, in contrast to other common techniques, without ambiguity. The method relies on the diagonalization of the band-projected real space position operator. In contrast to methods that have existed thus far, this approach can be extended to determine Wannier functions in non-periodic structures, with the only condition that a band gap must be present. Determining the Wannier states constitutes a crucial step in deriving many-particle lattice models from first principles. The procedure we describe also gives the first clear definition of Wannier states in inhomogeneous systems, which have, for example, been approximately determined previously by propagating the unperturbed Wannier state in imaginary time [182]. This opens the door to various interesting applications in future calculations, such as the renormalization of the Wannier states and consequently also the Hubbard parameters in a harmonic trap, a strongly tilted optical lattice and many more possibilities.

In chapter (5) this approach to determine Wannier states is shown to be extendible to higher dimensions for more complicated, non-separable lattices by sequentially diagonalizing appropriately projected position operators. It is demonstrated by constructing the Wannier states for a two-dimensional honeycomb lattice, as was recently realized in the group of T. Esslinger [162], and all Hubbard parameters are calculated. With the development of more complicated optical lattice geometries, as well as in the context of solid state systems, this approach may be valuable for the highly efficient calculation of Wannier states, which thus far have mainly relied on optimized algorithms numerically minimizing the spatial variance [112].

We remain on the microscopic level of deriving a suitable many-particle model Hamiltonian in chapter (4), but include short-ranged interactions. The question we address is the following: given a lattice system, where the single particle Wannier states are known, but a finite inter-particle interaction strength is given, what is the simplest and most accurate model Hamiltonian to effectively describe this many-body system. The interactions leads to transitions into higher bands and would, in principle, require a multi-band treatment when working in the original many-particle Fock basis. On a many-body theoretical level, a multiband treatment is, however, cumbersome and it would be desirable to avoid this if possible. We define the subspaces of dressed bands in the many-particle system and show, that for all typical interaction strengths, an effective single-particle model exists, which gives the optimal low-energy description of the system. Instead of containing all particles in the same local Wannier orbital, as is the case in the usual many-particle occupation number basis, the local basis states of the dressed band basis contain local correlations, originating from the interactions and lowering the local ground state's energy. We define new bosonic ladder operators, which differ from the original Wannier orbital creation and annihilation operators for any finite interaction strength and are the operators appearing in the effective single-band description of the resulting many-body Hamiltonian. We give the exact prescription to transform any given many-particle operator into the dressed band basis. Applying this transformation to the original microscopic Hamiltonian, we show that the resulting effective single-band Hamiltonian can be expressed in either a density-induced fashion on the level of multiple creation and annihilation dressed

band operators or, alternatively, in a density-dependent formulation, where the tunneling and interaction amplitudes depend on the local filling of the respective sites. We calculate the relevant parameters using exact diagonalization and show that the single-particle tunneling induced by the interaction is significant and may even outweigh the usual single-particle hopping term originating from the lattice Hamiltonian. A pair tunneling term and nearest neighbor interaction term are shown to be highly relevant for moderately deep lattices and, again, may even outweigh the single particle tunneling term by an order of magnitude or more for realistically deep lattices. Finally, we investigate the effect of repulsive interactions on the Wannier orbitals and demonstrate that the usual picture of broadened Wannier functions is insufficient to explain the effect on the tunneling. The single-particle orbitals, corresponding to the eigenstates of the single-particle density matrix in the interacting system, are barely affected and negligibly broadened. Rather, the two-particle correlator is significantly affected by the interaction, such that the particles mutually avoid each other, while approximately preserving their combined density profile.

We have developed a quasi-particle theory for strongly interacting bosons in chapter (7) by quantizing the linearized Gutzwiller equations of motion around the mean-field minimum and subsequently quantizing these bosonic degrees of freedom. This can be understood to be the quantized counterpart of, yet going beyond, Gutzwiller theory, just as Bogoliubov theory is the quantized counterpart of, yet goes beyond Gross-Pitaevskii theory.

Alternatively, we have also deduced the extended quasi-particle theory without leaving the quantum domain in chapter (8) by finding the appropriate quantum fluctuation operators corresponding to the classical Gutzwiller fluctuation amplitudes. We have shown that when transformed into quasi-momentum space, these fluctuation operators are of a bosonic nature up to correction terms, which scale with the inverse of the occupation density of the fluctuation modes. Building on the completeness of these operators, in the sense that an arbitrary many-body operator in the lattice can be expressed in terms of these, we express the Bose-Hubbard Hamiltonian in these bosonic fluctuation operators, which directly gives access to the quasi-particle Hamiltonian, as well as the higher order quasi-particle decay and interaction terms. The formalism of generalized unitary transformations is derived in a general context and applied in the diagonalization of the quasi-particle Hamiltonian on the symplectic space of bosonic excitations. This explicitly yields the transformation relations to the new quasi-particle operators, which possess a bosonic character as long as the occupation of the fluctuation modes is low. Henceforth, any given many-particle operator can be explicitly expressed in terms of bosonic quasi-particle operators (and two additional non-bosonic operators in the condensate regime). Working in this new basis yields a more suitable starting point for a further theoretical treatment, since, to the best possible degree, the transformed Hamiltonian is that of an non-interacting system of quasi-particles.

Our quasi-particle theory treats collective excitations in the whole parameter regime of the Bose-Hubbard model on equal footing, in contrast to Bogoliubov theory, which is only valid for condensates in the limit of low depletion. In the Mott insulator, it describes the dispersive particle and hole modes at finite tunneling J/U, which is evidently beyond the realm of Gutzwiller theory. For any given set of parameters, the resulting quasi-particle Hamiltonian describes a set of non-interacting and independent bosonic quasi-particles. Whereas these are the only terms contained in the quasi-particle Hamiltonian in the Mott insulating case, there is an additional term, which is of the form of a kinetic energy of a fictitious particle with a mass $\tilde{m}$ without a restoring force. This does not correspond to any of the bosonic quasi-particles with any effective mass, but has also been found within an extended treatment of Bogoliubov theory [19, 103], where it was associated with the diffusion of the condensate's phase. These degrees of freedom cannot be associated with a bosonic mode and mathematically arise from the fact, that the quasi-particle Hamiltonian cannot be entirely diagonalized on the symplectic space (required to retain the bosonic character of operators under the basis transformation), but only be brought into its Jordan normal form. The two artificial position and momentum operators for the fictitious particle in the condensate are associated with (and required for) total particle number conservation of the entire system when performing dynamics with the entire original Hamiltonian in the quasi-particle basis. As in Bogoliubov theory, if the time evolution were only performed using the non-interacting quasi-particle Hamiltonian, the physical particle number would not be preserved, which implies that the artificial position and momentum operators are associated with the addition and removal of particles to and

from the condensate mode. The artificial mass $\tilde{m}$, which may be related to the *phase rigidity* of the condensate, is calculated and its dependence on various system parameters determined. A further investigation of this degree of freedom, possibly in connection with a particle-number conserving approach to this extended quasi-particle theory, analogous to the approaches that have been devised within the realm of Bogoliubov theory, may be an interesting future direction of investigation.

In the condensate, our quasi-particle theory naturally recovers Bogoliubov theory in the limit of weak interactions, but intrinsically contains condensate depletion effects at any finite interaction strength, which leads to a renormalization of the sound mode energy. Furthermore, it also gives access to the structure of the quasi-particle excitations, and captures the deviation from the pure particle-hole character predicted by Bogoliubov theory. This effect becomes increasingly relevant for stronger interactions. In this case, our quasi-particle theory naturally contains higher excitational modes, such as the amplitude mode (and beyond), which cannot be described within Bogoliubov theory or any renormalized version of it. With a further increase in the interaction strength, the system eventually undergoes a phase transition into the Mott insulator phase at integer filling, where the structure of quasi-particles changes qualitatively: the amplitude and sound modes disappear and the energetically low lying excitations are the particle and hole modes. All the excitational properties are intrinsically contained in our quasi-particle approach.

Furthermore, the quasi-particle ground state differs from the Gutzwiller ground state at any point in the phase diagram if either U or J are non-zero. It contains *fluctuations* in the original fluctuation modes, which lower the energy of this quasi-particle ground state in comparison to the Gutzwiller mean-field state. Analogous to Bogoliubov theory, this quasi-particle ground state can be implicitly defined by the property, that any quasi-particle operator annihilates it – however it can also be calculated and expressed explicitly. The former property, in conjunction with the bosonic commutation relations for the quasi-particle operators, can subsequently be used to calculate arbitrary expectation values of observables beyond the Gutzwiller approximation at arbitrary interaction strength. We analyze a variety of quantities, such as the single particle density of states and the momentum distribution, which also leads in our theory to non-trivial results in the Mott insulator. The case of bosonic species is also shortly discussed, where an instability of the lower hybridized sound mode is observed, indicating the existence of a spatially ordered phase.

In a sense the new quasi-particle modes correspond to a unitary basis transformation on a many-particle level. To lowest order, the interacting lattice Hamiltonian is expressed in terms of non-interacting quasi-particles. However, the higher terms which were neglected before can now also be expressed in this new basis in terms of quasi-particle operators. These processes correspond to different quasi-particle interaction, and decay processes, which we now have explicit access to. The lifetime and decay processes of the amplitude mode quasi-particles, as well as the for the sound mode in the strongly interacting condensate, is an interesting and theoretically unexplored question to date, which will be of interest to investigate in future.

We then proceed by considering probing techniques, experimental accessibility and verification in the following two chapters. In chapter (9) we give an introduction to Bragg spectroscopy and derive the coupling to the many-particle system from first principles. Using a spatially resolved time-dependent Gutzwiller simulation, we simulate the experiment performed in the Sengstock group by S. Götze et al. [17]. When taking the finite pulse time and shape, strong intensity of the Bragg laser beam, as well as the inhomogeneous trapping potential into account, our simulations predict that the amplitude mode should be accessible within Bragg spectroscopy and find good agreement with the experimental data. This is the first experimental observation of the Higgs-type amplitude mode at finite quasi-momentum in a system of strongly interacting lattice bosons. The experimental data in such systems must be interpreted with care: the Bragg beam intensities required to observe a significant signal in the lattice for reasonable probing times are not weak, which invalidates the use of perturbation theory. The high intensity of the probing beam significantly influences the system and shifts the observed peaks to energies lower than the actual quasi-particle energy. It is thus not permitted to interpret the experimentally measured peak positions in these experiments as dispersion relations.

In chapter (10) we consider lattice modulation spectroscopy, which is a further experimental probing technique. In deriving the operator corresponding to this perturbation from first principles,

we point out a close connection to Bragg spectroscopy, which has commonly been overlooked or otherwise not been previously mentioned: Lattice modulation spectroscopy corresponds to two simultaneous and coherent Bragg probing beams. We also perform a full time-dependent Gutzwiller simulation beyond the linear response regime for the experiment performed by Stöferle et al. in the Esslinger group [157] and find agreement in the peak positions. In contrast to the previous interpretation that the sound mode is measured in these experiments, we find that in lattice modulation spectroscopy there is no coupling to the sound mode at all. After all, there is not bosonic sound mode at $\mathbf{k} = 0$, which is associated with the non-diagonalizablity of the quasi-particle Hamiltonian on the symplectic space in the $\mathbf{k} = 0$ subspace. Our simulation strongly suggests, that the observed energy absorption peaks in [157] correspond to the amplitude mode at $\mathbf{k} = 0$ (which is indeed a bosonic mode at $\mathbf{k} = 0$).

In chapter (11) we considered a bosonic system in the limit of strong interactions, far from equilibrium in an external potential. Here, we analyzed the full momentum distribution during collapse and revival of an atomic condensate after a lattice quench, showing that the state at revival times can effectively be described by a single particle theory. We have shown that the true condensate fraction is not damped by the presence of an arbitrary spatial potential, but that the condensate state takes on a different form, such that a damping seems to appear when only looking at $n(\mathbf{k} = 0, t)$. For the specific case of a harmonic trapping potential, condensate states featuring a periodic peak structure in momentum space are created, allowing for high precision determination of the total trapping frequency of the underlying optical and magnetic trap, as well as the position of the trapping potential on a sub-lattice scale. By engineering the spatial potential after the ramp-up, our procedure is suitable for the preparation of exotic non-equilibrium condensate states, as well as transforming different condensate states into each other. These prospects seem realistic in light of recent experimental progress on the engineering of arbitrary spatial potentials [10, 145, 183]. Furthermore, for the first time to the best of the author's knowledge, the exact analytic expression (see appendix (O)) was found for the peak structure appearing in the Talbot effect in quantum optics [161], which also describes the quasi-momentum distribution at the relevant discrete times after a temporal evolution in a harmonically trapped lattice.

In the very last chapter, the focus was shifted to the physics of disordered many-particle systems. A detailed derivation of the stochastic mean-field theory is given and it is extended to finite temperature. The SMFT is found to be a highly efficient method, that can capture the physics of the strongly interacting, disordered Bose-Hubbard model. It is formulated on the level of distribution functions in the thermodynamic limit, inherently circumventing finite size problems ubiquitous to disordered systems. It is capable of predicting the qualitative structure of the phase diagram at a relatively low computational cost and the behavior of the order parameter distribution function gives insight into the underlying physical behavior. The method is applied to homogeneously distributed box disorder, which is the disorder distribution typically assumed by most theoretical investigations. However, with speckle disorder being the best and most promising realization of disordered lattice systems to date, we, for the first time, calculate the phase diagram for this more realistic distribution within SMFT. Due to the unbounded nature of the speckle disorder distribution, the phase diagram is found to be qualitatively different at any finite disorder strength. For this disorder type, we apply the SMFT at both zero and finite temperature. Furthermore, we analyze the effect of additionally adding hopping disorder to the on-site disorder, which is intrinsically relevant for experiments.

An interesting future direction of research would be the application of the quasi-particle theory to strongly interacting disordered systems to analyze non-equilibrium dynamics and the structure of the excitational spectrum in these systems. In weakly interacting systems, the Bogoliubov quasi-particles are predicted to localize at a sufficient disorder strength. Whether this behavior extends to the strongly interacting case and if an analogous localization of amplitude mode quasi-particles occurs in three dimensions is an open question. Furthermore, deviations from the bosonic nature of the quasi-particles may be relevant and possibly even observable if these modes becomes strongly localized in space.

A. Structure and Symmetries of the u-Functions

The u-functions, from which the Bloch functions are obtained with the inclusion of an exponential prefactor, possess the full lattice periodicity

$$u_{\mathbf{k},\alpha}(\mathbf{r}+\mathbf{T}) = u_{\mathbf{k},\alpha}(\mathbf{r}) \tag{A.1}$$

for any lattice vector $\mathbf{T} = m_1\mathbf{a}_1 + m_2\mathbf{a}_2 + m_3\mathbf{a}_3$ which is in accordance with their Fourier decomposition consisting of plane waves with a discrete frequency spectrum at the lattice momenta $\mathbf{G}$ only

$$u_{\mathbf{k},\alpha}(\mathbf{r}) = \sum_{n_1,n_2,n_3} c^{(\mathbf{k},\alpha)}_{n_1,n_2,n_3}\, e^{i(n_1\mathbf{b}_1+n_2\mathbf{b}_2+n_3\mathbf{b}_3)\cdot\mathbf{r}}. \tag{A.2}$$

Transformation under a translation of $\mathbf{k} \mapsto \mathbf{k}+\mathbf{G}$

The uniqueness of the Bloch states (i.e. $|\mathbf{k},\alpha\rangle = |\mathbf{k}+\mathbf{G},\alpha\rangle$) implies the transformation property

$$u_{\mathbf{k}+\mathbf{G},\alpha}(\mathbf{r}) = e^{-i\mathbf{G}\cdot\mathbf{r}}\, u_{\mathbf{k},\alpha}(\mathbf{r}) \tag{A.3}$$

under the shift by an arbitrary reciprocal lattice vector $\mathbf{G}$.

Transformation under a reflection of $\mathbf{k} \mapsto -\mathbf{k}$

Under reflection in $\mathbf{k}$-space the transformation of the state can be inferred from the structure of the Hamiltonian and the consequence for the eigenvectors. When the Hamiltonian is set up in momentum space, only the lattice potential gives rise to non-zero off-diagonal elements[1], whereas the diagonal elements are of the form $(\mathbf{k}+n_1\mathbf{b}_1+n_2\mathbf{b}_2+n_3\mathbf{b}_3)^2/(2m)$. Due to the square, a reflection of $\mathbf{k} \mapsto -\mathbf{k}$ is equivalent to $(n_1,n_2,n_3) \mapsto (-n_1,-n_2,-n_3)$, which leaves the Hamiltonian and its eigenvectors invariant. The resulting u-function for $-\mathbf{k}$ is therefore identical to the one for $+\mathbf{k}$ up to complex conjugation:

$$\begin{aligned} u_{-\mathbf{k},\alpha}(\mathbf{r}) &= \sum_{n_1,n_2,n_3} c^{(\mathbf{k},\alpha)}_{-n_1,-n_2,-n_3}\, e^{i(n_1\mathbf{b}_1+n_2\mathbf{b}_2+n_3\mathbf{b}_3)\cdot\mathbf{r}} \\ &= \sum_{n_1,n_2,n_3} c^{(\mathbf{k},\alpha)}_{n_1,n_2,n_3}\, e^{-i(n_1\mathbf{b}_1+n_2\mathbf{b}_2+n_3\mathbf{b}_3)\cdot\mathbf{r}} \\ &= u^*_{\mathbf{k},\alpha}(\mathbf{r}). \end{aligned} \tag{A.4}$$

[1] Up to a constant energy shift, which can be set to zero.

Realness of Bloch and u-functions at $\mathbf{k} = 0$ at high symmetry points

The high symmetry points in $\mathbf{k}$-space are defined as the set of points, for which a reciprocal lattice vector $\mathbf{G} = n_1\mathbf{b}_1 + n_2\mathbf{b}_2 + n_3\mathbf{b}_3$ exists, such that $-\mathbf{k} = \mathbf{k} + \mathbf{G}$. We can use the properties (A.3) and (A.4) to prove that the Bloch functions can be chosen purely real for these points.

1. $\mathbf{k} = 0$: here $u^*_{0,\alpha}(\mathbf{r}) = u_{0,\alpha}(\mathbf{r})$ directly implies that $u_{0,\alpha}(\mathbf{r})$ is purely real and thus the corresponding Bloch function $\psi_{0,\alpha}(\mathbf{r}) = u_{0,\alpha}(\mathbf{r})$ is also purely real.

2. If $\mathbf{k}$ lies on a high symmetry point on the edge of the Brillouin zone (such as the K or M points for a hexagonal lattice) this implies that $\mathbf{k}$ and $-\mathbf{k}$ are related by a non-zero reciprocal lattice vector $\mathbf{G}$. Using (A.3) and (A.4) this leads to the condition

$$u^*_{\mathbf{k},\alpha}(\mathbf{r}) = e^{-i\mathbf{G}\cdot\mathbf{r}}\, u_{\mathbf{k},\alpha}(\mathbf{r}). \tag{A.5}$$

   In this case we generally have $u_{\mathbf{k},\alpha}(\mathbf{r}) \neq u_{-\mathbf{k},\alpha}(\mathbf{r})$ and these function can generally not be chosen purely real. However, multiplying Eq.(A.5) by $e^{-i\mathbf{k}\cdot\mathbf{r}}$ on both sides and using $-\mathbf{k} = \mathbf{k} + \mathbf{G}$

$$\psi^*_{\mathbf{k},\alpha}(\mathbf{r}) = e^{-i\mathbf{k}\cdot\mathbf{r}}\, u^*_{\mathbf{k},\alpha}(\mathbf{r}) = e^{i\mathbf{k}\cdot\mathbf{r}}\, u_{\mathbf{k},\alpha}(\mathbf{r}) = \psi_{\mathbf{k},\alpha}(\mathbf{r}), \tag{A.6}$$

   it directly becomes clear that this Bloch function is real if the complex phases of the u-functions are chosen appropriately.

B. Time-Dependent Perturbation Theory

To obtain the transition probabilities to different eigenstates of the unperturbed Hamiltonian, we recall the main steps of time dependent perturbation theory. The exact time evolution of an arbitrary state in the Schrödinger picture is given by the Schrödinger equation

$$i\hbar\partial_t|\psi(t)\rangle_I = [\mathcal{H}_0 + V_S(t)]|\psi(t)\rangle_I. \tag{B.1}$$

The splitting of the full Hamiltonian $\mathcal{H}_0 + V(t)$ is arbitrary at this point and generally valid. It is usually done such that the eigenstates and energies of $\mathcal{H}_0$ are explicitly known and $V_S(t)$ is a perturbation, which leads to coupling between the states. Within the interaction picture, the time evolution of a state is determined by the equation of motion

$$i\hbar\partial_t|\psi(t)\rangle_I = V_I|\psi(t)\rangle_I, \tag{B.2}$$

where V_I is the perturbing operator in the interaction picture, which may be time-dependent. The implicit time evolution of any operator is related to the operator in the Schrödinger picture by

$$A_I = e^{i\mathcal{H}_0 t}\, A_S\, e^{-i\mathcal{H}_0 t}. \tag{B.3}$$

By virtue of (Eq. B.2), the equation of motion of the time evolution operator in the interaction picture takes on the form

$$i\hbar\partial_t\, U_I(t) = V_I(t)\, U_I(t), \tag{B.4}$$

which, with the initial boundary condition $U_I(t=0) = \mathbb{1}$, can formally be integrated to give

$$U_I(t) = \mathbb{1} - \frac{i}{\hbar}\int_0^t dt'\, V_I(t')\, U_I(t'). \tag{B.5}$$

By iteratively inserting $U_I(t)$ the Dyson series in different powers of V_I is obtained, with the first terms being

$$U_I(t) = \mathbb{1} - \frac{i}{\hbar}\int_0^t dt'\, V_I(t') + \left(-\frac{i}{\hbar}\right)^2 \int_0^t dt' \int_0^{t'} dt''\, V_I(t')\, V_I(t'') + \dots \tag{B.6}$$

Let us assume that at time $t = 0$ the system is in the eigenstate $|\psi_i\rangle$ of H_0. Using the eigenstates of the unperturbed Hamiltonian $\mathcal{H}_0$ as a basis $|\psi_n\rangle$ with

$$\mathcal{H}_0|\psi_n\rangle = E_n|\psi_n\rangle \tag{B.7}$$

the transition amplitudes,

$$c_n(t) = \langle\psi_n|e^{-i\mathcal{H}t}|\psi_i\rangle, \tag{B.8}$$

i.e. the amplitude that the state of the system is in the state $|\psi_n\rangle$ by a m-th order process (upper index) in V_I is

$$c_n^{(0)}(t) = \delta_{n,i} \tag{B.9}$$

$$c_n^{(1)}(t) = -i \int_0^t dt'\, V_{n,i}(t')\, e^{i(E_n - E_i)t'} \tag{B.10}$$

$$c_n^{(2)}(t) = -\int_0^t dt' \int_0^{t'} dt''\, \sum_m V_{n,m}(t')\, V_{m,i}(t'')\, e^{i(E_n - E_m)t'}\, e^{i(E_m - E_i)t''}, \tag{B.11}$$

where the expressions for the amplitudes of order one or higher $c_n^{(1)}(t)$, $c_n^{(2)}(t)$, ... only apply for states that were initially not occupied $n \neq i$. where the matrix elements of the perturbing operator in the Schrödinger picture were defined as

$$V_{n,m}(t) \equiv \langle \psi_n | V_S(t) | \psi_m \rangle. \tag{B.12}$$

If the series converges, the coefficients of all m-th order processes can be added linearly, leading to the total transition probability

$$|c_n(t)|^2 = |c_n^{(0)}(t) + c_n^{(1)}(t) + c_n^{(2)}(t) + \ldots|^2. \tag{B.13}$$

Note that this is not equivalent to adding the square moduli $|c_n^{(m)}(t)|^2$.

Periodic Perturbation & Fermi's Golden Rule

We now consider the case of a periodic perturbing operator of the form

$$V_S(t) = F^\dagger\, e^{-i\omega t} + F\, e^{i\omega t} \tag{B.14}$$

where F is a time-independent (not necessarily Hermitian) operator. To derive Fermi's golden rule, we are interested in the lowest order only and use the explicit form (B.14) in the first order coefficient (B.9) to obtain

$$c_n^{(1)}(t) = -\langle \psi_n | F^\dagger | \psi_i \rangle \, \frac{e^{i(E_n - E_i - \omega)t} - 1}{E_n - E_i - \omega} - \langle \psi_n | F | \psi_i \rangle \, \frac{e^{i(E_n - E_i + \omega)t} - 1}{E_n - E_i + \omega}. \tag{B.15}$$

We assume that our initial state $|\psi_i\rangle$ is the ground state of $\mathcal{H}_0$ and hence $E_n - E_i$ is always positive. If we restrict the range of the perturbation's frequency ω to be much closer to $E_n - E_i$ than to $E_n + E_i$, the rotating wave approximation of neglecting the second term in (B.15) is justified. We are interested in the probability of finding the state in the excited state $|\psi_n\rangle$ at time t, which is given by

$$|\langle \psi_n | \psi(t) \rangle|^2 = |c_n(t)|^2 = 4 |\langle \psi_n | F^\dagger | \psi_i \rangle|^2 \, \frac{\sin^2([E_n - E_i - \omega]t/2)}{|E_n - E_i - \omega|^2}. \tag{B.16}$$

If the frequency is chosen exactly on resonance, this probability grows exactly quadratic in time. In the limit of large times, this is a representation of the δ-distribution $\lim_{t\to\infty} \frac{\sin^2(wt)}{w^2 t} = \pi\, \delta(w)$ and we can write the occupation probability

$$|c_n(t)|^2 = 2\pi t\, |\langle \psi_n | F^\dagger | \psi_i \rangle|^2\, \delta(E_n - E_i - \omega). \tag{B.17}$$

The factor $1/t$ was absorbed into the δ-distribution, corresponding to a scaling of the sinc-function such that for all times t the integral with respect to the frequency remains constant. Keeping this scaling in mind, we can associate a transition *rate* from the state $|\psi_i\rangle$ into the state $|\psi_n\rangle$

$$\Gamma_{i\to n} = 2\pi\, |\langle \psi_i | F | \psi_n \rangle|^2\, \delta(E_n - E_i - \omega) \tag{B.18}$$

in the long-time limit. This imposes a hierarchy on the ordering of the limits: The sinc-function has a typical width of $4\pi/t$. Approximating this with the δ-distribution requires t to be chosen sufficiently large such that the width is narrow compared to the other relevant energy scales. Then for a fixed t, taking only the first order term along, requires the perturbation strength to be chosen sufficiently weak, that higher order scattering processes can be neglected over this time interval.

C. Wannier State Relations in Double-Welled Unit Cells

To understand the construction of Wannier states if more than a single potential minimum (and hence multiple low energy Wannier states) are present within a single unit cell, we juxtapose the construction of Wannier states in a 1D lattice

1. Choosing the unit cell to contain a single potential minimum, which is the usual procedure. Here we use the site index $\tilde{l}$, the lattice spacing $\tilde{a}$, which is also the spacing between neighboring potential wells on a lattice consisting of $\tilde{L}$ potential minima and Wannier states per energy-separated band. The first BZ consequently extends from $-\frac{\pi}{\tilde{a}}$ to $\frac{\pi}{\tilde{a}}$.
2. Artificially choosing the unit cell to contain two potential minima. Here we use the site (unit cell) index l, which can only take on half as many different values as $\tilde{l}$. The lattice distance here (width of a unit cell) is $a = 2\tilde{a}$ on a lattice consisting of $L = \tilde{L}/2$ unit cells. However, two bands have to be taken into account to construct the physically relevant Wannier states localized to each potential well individually. Here, the BZ is only half as large as in the prior case, extending from $-\frac{\pi}{a} = -\frac{1}{2}\frac{\pi}{\tilde{a}}$ to $\frac{\pi}{a} = \frac{1}{2}\frac{\pi}{\tilde{a}}$, as shown in Fig. C.1.

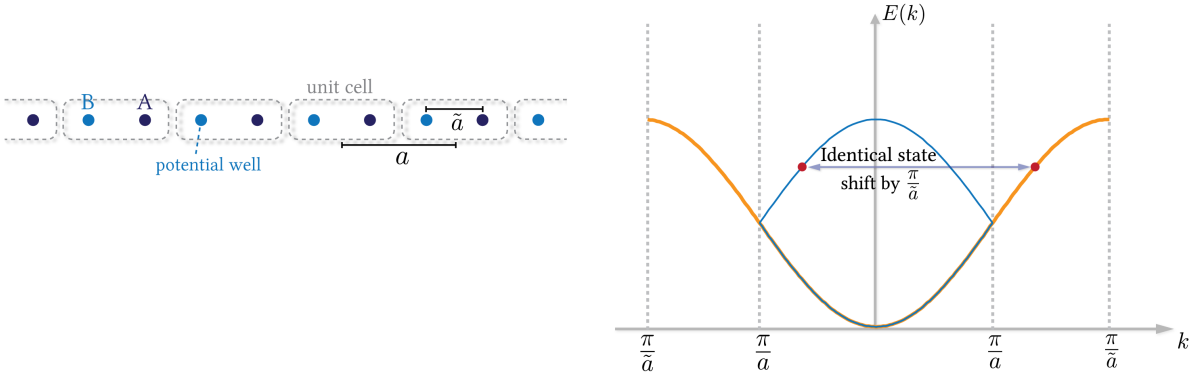

Figure C.1

We will now construct two Wannier states on neighboring potential minima using the two different methods. We first note, that the Bloch states (which are eigenstates of $\mathcal{H}_{\text{lat}}$) are independent of the choice of the unit cell. Since all eigenstates are obtained by both band structure calculations, the

Bloch states in the first excited band obtained within the double-welled unit cell calculation are consequently identical to the states in the quasi-momentum range $[\frac{\pi}{a},\ \frac{\pi}{\tilde{a}}]$ and $[-\frac{\pi}{\tilde{a}},\ -\frac{\pi}{a}]$ obtained from the single-welled band structure calculation. In quasi-momentum space these equivalent states are simply related by a $\frac{\pi}{\tilde{a}}$ translation in k.

We use the convention that the site labeled by $\tilde{l} = 0$ is the right potential minimum (which we refer to as sublattice $\mathcal{A}$) in the unit cell $l = 0$. From the single-welled band structure calculation we choose the phases of the Bloch states $|k\rangle$ in accordance with the usual convention

$$|\tilde{l}\rangle = \frac{1}{\sqrt{\tilde{L}}} \sum_{k}{}' e^{-i\tilde{a}k\tilde{l}} |k\rangle \tag{C.1}$$

i.e. such that a direct superposition leads to a Wannier state which is located at $\tilde{l} = 0$. Here, $\sum_k'$ denotes the sum over all values of k in the larger BZ $\frac{\pi}{a} = \frac{1}{2}\frac{\pi}{\tilde{a}}$.

To obtain the same set of Bloch states from the double-welled band structure calculation, two bands have to be taken into account and we assign an additional band quantum number $|k, \alpha\rangle$. We choose the complex phases of these states such that they are identical to the Bloch states $|k\rangle$ from the single-welled calculation and thus have

$$|k\rangle = \begin{cases} |k, \alpha = 0\rangle & \text{if } |k| < \frac{\pi}{a} \\ |k \pm \pi/\tilde{a}, \alpha = 1\rangle & \text{if } |k| > \frac{\pi}{a} \end{cases} . \tag{C.2}$$

The plus or minus is chosen such that $+ \pm \pi/\tilde{a}$ lies within the first BZ of the double-welled lattice. To construct the Wannier state on sublattice $\mathcal{A}$, one has

$$|l,\, \mathcal{A}\rangle = \frac{1}{\sqrt{2L}} \sum_{k} e^{-iakl} \left[|k, \alpha = 0\rangle + |k, \alpha = 1\rangle \right]. \tag{C.3}$$

This becomes clear for the choice of phases of the state $|\tilde{l} = 0\rangle = |l = 0,\, \mathcal{A}\rangle$ and the translational properties of the Wannier states.

The main intermediate question that arises now, is how the phases are to be chosen for the Wannier states on the sublattice $\mathcal{B}$ in the double-welled band structure calculation. It suffices to determine a single state on sublattice $\mathcal{B}$. We choose the one at $l = 0$, which corresponds to the state $|\tilde{l} = -1\rangle$ when using the convention that sites on sublattice $\mathcal{B}$ are to the left of sites on $\mathcal{A}$ within the unit cell. We thus have

$$\begin{aligned} |\tilde{l} = -1\rangle &= \frac{1}{\sqrt{\tilde{L}}} \sum_{k'}{}' e^{i\tilde{a}k'} |k\rangle' \\ = |l = 0,\, \mathcal{B}\rangle &= \frac{1}{\sqrt{2L}} \sum_{k} \left[e^{i\beta_{k,0}} |k, \alpha = 0\rangle - e^{i\beta_{k,1}} |k, \alpha = 1\rangle \right] \end{aligned} \tag{C.4}$$

Note that the two sums run over different sets of quasi-momenta and that the minus in the second line is a convenient convention, as will be seen. The first sum contains twice as many terms as the second one, however the expression for the state $|\tilde{l} = -1\rangle$ can be rewritten to allow for a direct comparison and to determine the phases $\beta_{k,0}$ and $\beta_{k,1}$.

To rewrite the sum $\sum_{k'}'$ in terms of $\sum_k$, we note that the set of k' which is summed over can be split into two distinct groups, both containing the same number of elements: quasi-momenta $|k| < \frac{\pi}{a}$ lying inside the smaller BZ of the double-welled lattice and quasi-momenta lying outside. Reverting to the double-welled calculation, the latter correspond to Bloch states in the first excited band $\alpha = 1$ of the first Brillouin zone by a translation of the lattice momentum

$$k'_{\text{inside}} = k_{\text{outside}} \pm \frac{\pi}{\tilde{a}}. \tag{C.5}$$

Inserting this into Eq. (C.4), we see that this shift always gives rise to an additional phase shift by $\pm\pi$ in the exponential, i.e. a change of sign. A direct comparison then directly reveals the phases

$$\beta_{k,0} = \beta_{k,1} = ak/2, \tag{C.6}$$

which now allows us to construct all Wannier states on sublattice $\mathcal{B}$

$$|l,\,\mathcal{B}\rangle = \frac{1}{\sqrt{2L}} \sum_k e^{-iak(l-1/2)} \left[|k, \alpha = 0\rangle - |k, \alpha = 1\rangle\right]. \tag{C.7}$$

Extracting the Hopping Elements from the Dispersion Relation

Within the double-welled band structure calculation, the hopping elements J_1 and J_2, shown in Fig. C.2, are calculated differently, although they are physically identical from symmetry arguments.

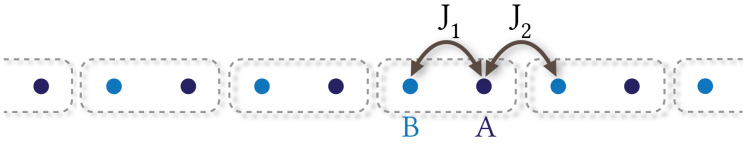

Figure C.2: Two different hopping elements: within and between unit cells.

The intra-cell hopping element between sites within a unit cell is calculated using the eigenvector properties

$$\begin{aligned} J_1 &= \langle l = 0, \mathcal{B}|\mathcal{H}_{\text{lat}}|l = 0, \mathcal{A}\rangle \\ &= \left(\frac{1}{\sqrt{2L}} \sum_k e^{-iak/2}[\langle k, \alpha = 0| - \langle k, \alpha = 1|]\right) \mathcal{H}_{\text{lat}} \left(\frac{1}{\sqrt{2L}} \sum_{k'} [|k', \alpha = 0\rangle + |k', \alpha = 1\rangle]\right) \\ &= \frac{1}{2L} \sum_k e^{-iak/2} \left[E_{k,\alpha=0} - E_{k,\alpha=1}\right]. \end{aligned} \tag{C.8}$$

The inter-cell tunneling element is calculated analogously

$$\begin{aligned} J_2 &= \langle l = 1, \mathcal{B}|\mathcal{H}_{\text{lat}}|l = 0, \mathcal{A}\rangle \\ &= \left(\frac{1}{\sqrt{2L}} \sum_k e^{iak} e^{-iak/2}[\langle k, \alpha = 0| - \langle k, \alpha = 1|]\right) \mathcal{H}_{\text{lat}} \left(\frac{1}{\sqrt{2L}} \sum_{k'} [|k', \alpha = 0\rangle + |k', \alpha = 1\rangle]\right) \\ &= \frac{1}{2L} \sum_k e^{iak/2} \left[E_{k,\alpha=0} - E_{k,\alpha=1}\right]. \end{aligned} \tag{C.9}$$

The equality of these two matrix elements follows from the reflectional symmetry of the dispersion relation $E_{-k,\alpha} = E_{k,\alpha}$ for all bands, which directly reveals $J_1 = J_2$. Furthermore the reflectional symmetry guarantees that the resulting matrix element is purely real. Note that both final expressions in Eq. (C.8) and Eq. (C.9) do not depend on the phases of the Bloch states, i.e. the Wannier states do also not have to be determined explicitly in the case of a double-welled unit cell either.

D. Implementation of the Multiorbital Exact Diagonalization Procedure

Basis Generation

The numerical procedure is implemented in the C++ programming language. The object orientated structure is well suited to efficiently construct a basis in the many-particle subspace at fixed particle number. We work in the Fock number basis M different 3D single particle Wannier orbitals $|n_1, \ldots, n_M\rangle$. Furthermore we sort the orbitals according to their single particle energy in increasing order. A hierarchy can be defined for the set of these Fock space: each such state can be associated with a number $\sum_{j=1}^{M} M^(j-1) n_{M-j+1}$ written in the M-numeral system by writing the occupation numbers in reversed order. A state can then be defined to be *larger, equal or smaller* than another, if its associated number is *larger, equal or smaller* respectively. Implementing such states in a class structure, naturally allows for a definition of larger and lesser operators, where the comparison of two states can be performed within very few comparisons of the integers defining the states. Moreover, the definition of these operators allows for the direct generation of ordered lists of the *map* type from the standard template library. An insertion, as well as the retrieval of a state from such an ordered list can both be performed with $\mathcal{O} \ln L$ efficiency, where L is the length of the list. The algorithm, shown in Fig. (D.1), to construct a uniquely ordered list of $N = \sum_i n_i$ particle basis states is the following:

- We begin with the Fock state, where all particles are in the lowest Wannier orbital $|N, 0, \ldots, 0\rangle$.
- Coming from each state, we define a procedure to generate a set of successive states, by one particle *jumping* from a given orbital to the next higher orbital. There are always between 1 and N such successive states. For example, coming from the state $|2, 1, 0, \ldots, 0\rangle$, we would generate the two states $|2, 0, 1, 0, \ldots, 0\rangle$ and $|1, 2, 0, \ldots, 0\rangle$.
- For each such generated state, it is checked if it already exists in the ordered list. If not it is included and the generation of the successive set of states is called. If it already exists, it is not added and no generation of further states along this path is called, symbolized by the crossed out states in Fig. (D.1).
- The generation of the next set of states can be called recursively. This procedure guarantees that each possible state is generated along some path. If such paths were not truncated, each path would end at the terminal state $|0, \ldots, 0, N\rangle$.
- it can be seen that it is safe to end a branch at the point where a given state already appears in the list, since the tree of branches originating from any given state is unique and will already have been generated if the first state has been reached.

- An energy truncation of the basis can also be naturally implemented within this approach. Since the orbitals are sorted according their single particle energies, the single particle energy contribution along any given path will always increase monotonically. If at any point a generated state lies above the energy threshold, so will all all higher states successively generated from this and it is justified to terminate the path at that point.

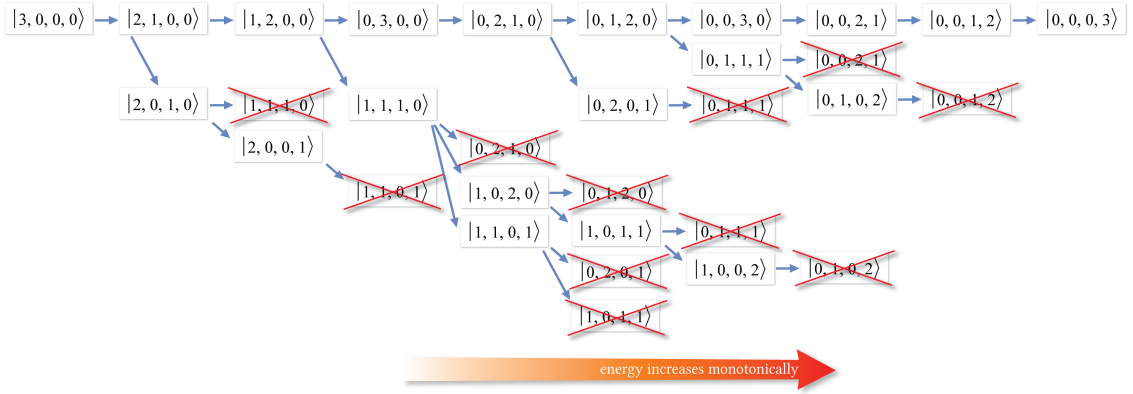

Figure D.1: Procedure to systematically construct all low energy Fock states of the lattice Hamiltonian for $N = 3$ particle in $M = 4$ bosonic modes. Note that the many-particle lattice energy always increases in successive steps, going from left to right. A path (i.e. given sequence of states connected by one particle moving into the next higher orbital) is stopped if the state has been cataloged before, the energy is higher than the cutoff (not shown for this figure, corresponding to a cutoff energy higher than the largest many-particle lattice energy) or the last state has been reached. All subsequent states of such a path can be omitted, since they either have all been cataloged or energetically also lie above the energy cutoff.

Calling the generation of a successive set of states from the initial state, one ends up with a sorted list of N-particle basis states. To furthermore restrict the set to the group of spatially fully symmetric states, one can simply remove the states transforming differently under reflections. Note that it is not permitted to truncate a path as soon as a given state does not belong to the desired symmetry group, since states further along the path may again fulfill the symmetry requirement. The remaining set of sorted states can be directly numbered (defining the matrix index for the numerical representation of the operator) with increasing order (and is accommodated in the *standard template library map* structure). For a given state in the Fock number representation, this structure then allows for the corresponding integer index to be found with $\mathcal{O}(\ln L)$ complexity and vice versa.

Matrix Elements

The calculation of the lattice Hamiltonian matrix elements amounts to the addition of single particle energies. For the calculation of the matrix elements originating from the interaction term, the matrix elements can generally be reduced to a product of three factors, each of which can be evaluated as a one-dimensional integral over Wannier functions[1].

[1] In fact, these spatial integrals don't have to be performed numerically for a further optimization. This is however beyond the scope of this appendix.

E. Aspects of Bosonic Gutzwiller Theory

E.1 Particle Number Conservation within the Dynamic Gutzwiller Approach

The exact particle number is not conserved under time evolution within the time-dependent Gutzwiller approximation, but the average (expectation value) particle number is conserved by the equations of motion, also in the presence of any additional number-conserving perturbing operator $\mathcal{B}$. This can be seen by considering an arbitrary initial Gutzwiller state $|\psi(0)\rangle$ with total particle number expectation value $N(0) = \langle\psi(0)|\hat{N}|\psi(0)\rangle$. Linearizing the time evolution operator, the state after the time step dt

$$|\psi(dt)\rangle = |\psi(0)\rangle - i\,dt\hat{H}|\psi(0)\rangle \tag{E.1}$$

with the particle number expectation value

$$\begin{aligned} N(dt) &= \langle\psi(dt)|\hat{N}|\psi(dt)\rangle \\ &= N(0) + i\,dt\langle\psi(0)|[\hat{H},\hat{N}]|\psi(0)\rangle + O(dt^2). \end{aligned} \tag{E.2}$$

The fact that the particle number is not exactly conserved, but only on average, is expressed by the commutator in the second term not vanishing exactly, but only it's expectation value being zero for an arbitrary state. To see this, we simplify the second term in (E.2) and use the identity $[b, b^\dagger b] = b$

$$\begin{aligned} \langle\psi(0)|[\hat{H},\hat{N}]|\psi(0)\rangle &= \langle\psi(0)|\sum_l [\hat{H}_l, b_l^\dagger b_l]|\psi(0)\rangle \\ &= \langle\psi(0)|\sum_l [\eta_l^* b_l + \eta_l b_l^\dagger, b_l^\dagger b_l]|\psi(0)\rangle \\ &= \sum_l \eta_l^* \langle\psi(0)|b_l|\psi(0)\rangle - \sum_l \eta_l \langle\psi(0)|b_l^\dagger|\psi(0)\rangle \end{aligned} \tag{E.3}$$

Since we only consider terms linear in dt, the mean-field parameters remain constant in time in zeroth order $\psi_l(dt) = \psi_l(0)$. The effect of any single-particle perturbing operator can be described by expressing the operator in the lowest band Wannier representation

$$\mathcal{B} = \sum_{l,l'} B_{l,l'} b_l^\dagger b_{l'}, \tag{E.4}$$

which can be treated within a site-decoupling mean-field approximation for the Gutzwiller time evolution

$$\mathcal{B} \mapsto \sum_{l,l'} B_{l,l'} \left[\langle b_l^\dagger\rangle b_{l'} + b_l^\dagger \langle b_{l'}\rangle - \langle b_l^\dagger\rangle\langle b_{l'}\rangle\right]. \tag{E.5}$$

The diagonal terms of this operator are a multiple of the total unit operator and therefore irrelevant to the time evolution. The off-diagonal number non-conserving terms can be treated on the same footing as the nearest neighbor hopping-term in the Gutzwiller approximation of the Bose-Hubbard model. The local scalar quantity η_l coupling to a local creation operator $b_l^\dagger$ is therefore composed of a term from nearest neighbor tunneling processes and a contribution from the perturbing operator $\mathcal{B}$[1]. Typically, the matrix elements of single particle operators decay exponentially with distance and there is a often a strict hierarchy of on-site terms, nearest neighbor terms, next nearest neighbor terms, etc. To a first approximation, the nearest neighbor terms of the perturbing operator $\mathcal{B}$ are only relevant if the on-site terms become irrelevant by symmmetry, such as in the case of lattice modulation spectroscopy, discussed in chapter (10).

$$\eta_l = J \sum_{\text{n.n. } l' \text{ of } l} \psi_{l'} + \sum_{l'} B_{l,l'} \psi_{l'} \tag{E.6}$$

It was numerically checked that the coupling amplitude between different sites falls of exponentially with the distance between the sites. It should be noted that the exponential coefficient depends on the amplitude of the lattice. The matrix elements $B_{l,l'}$), obey $B_{l',l} = B^*_{l,l'}$ and are, in accordance with restrictions by symmetry translationally invariant in the sense that $B_{l,l'}$ only depends on the distance $(l - l')$. Therefore we can simplify the commutator further and after a short calculation it follows that

$$\begin{aligned} \langle\psi(0)|[\hat{H},\hat{N}]|\psi(0)\rangle =& J \sum_l \sum_{\text{n.n. } l' \text{ of } l} \psi^*_{l'}\psi_l + \sum_l \sum_{l'} B^*_{l,l'}\psi^*_{l'}\psi_l \\ & - J \sum_l \sum_{\text{n.n. } l' \text{ of } l} \psi_{l'}\psi^*_l + \sum_l \sum_{l'} B_{l,l'}\psi_{l'}\psi^*_l \\ =& 0 \end{aligned} \tag{E.7}$$

E.2 Efficient Method of Calculating the Momentum Distribution for Gutzwiller States

The quasi-momentum distribution of a two-dimensional system is given by

$$\frac{1}{L_x L_y} \sum_{l_x,l'_x,l_y,l'_y=0}^{L_x-1,L_y-1} e^{ia([k_x(l_x-l'_x)+k_y(l_y-l'_y)])} \langle b^\dagger_{l_x,l_y}, b_{l'_x,l'_y}\rangle. \tag{E.8}$$

The complexity scales with law L_i^6, which makes it numerically almost impossible to calculate the momentum distributions for system larger than $L_i > 40$. Defining new summation variables $\Delta l_x := l_x - l'_x$ and $s_x := l_x + l'_x$, the two summations can be transformed to

$$\sum_{l_x=0}^{L_x-1} \sum_{l'_x=0}^{L_x-1} \rightarrow \sum_{\Delta l_x=-L_x+1}^{L_x-1} \sum_{s_x=|\Delta l_x|,\ \text{step}=2}^{2L_x-2-|\Delta l_x|} \tag{E.9}$$

E.3 Efficient Calculation of the Condensate Fraction for Gutzwiller States

This method of determining the largest eigenvalue of the SPDM for a bosonic Gutzwiller state was devised by Michael Buchhold [25]. To obtain the condensate fraction f_c in an inhomogeneous system, it is necessary to determine the largest eigenvalue λ_0 of the SPDM $\rho_{l,l'} = \langle b^\dagger_l b_{l'}\rangle$, which is a Hermitian $L \times L$-matrix, L being the number of lattice sites. The condensate fraction is then

[1] In this calculation we only consider processes within the lowest band.

defined as $f_c = \frac{\lambda_0}{N_{\text{tot}}}$, where N_{tot} is the total particle number. Since we determine $f_c(t)$ at many different times, an efficient algorithm to determine the largest eigenvalue is desirable. Here we present a method to determine the largest eigenvalue of the SPDM of a variational state of the bosonic Gutzwiller form, where the computational effort scales proportionally with L. We firstly derive relations holding for all eigenvalues of a SPDM of this form and subsequently use these to formulate a fix point relation for the eigenvalues. The largest eigenvalue can always be found by numerically iterating this fix point relation, as the largest eigenvalue on a large interval around the fix point.

We begin by considering the explicit form of the SPDM for a bosonic Gutzwiller state:

$$\rho_{l,l'} = \langle b_l^\dagger b_{l'} \rangle = \psi_l^* \, \psi_{l'} + \delta_{l,l'} \left(n_l - |\psi_l|^2 \right) \tag{E.10}$$

the off-diagonal part factorizes into products $\psi_l^* \, \psi_{l'}$ of local order parameters $\psi_l = \langle b_l \rangle$, whereas the diagonal part consists of the local densities $n_l = \langle b_l^\dagger b_l \rangle$. Now let $\mathbf{v}$ be an eigenvector of ρ with corresponding eigenvalue λ (i.e. $\rho \mathbf{v} = \lambda \mathbf{v}$). Focusing on a single element j of an eigenvector, we obtain

$$\lambda \, v_j = \sum_l \rho_{j,l} \, v_l = \sum_l \left(\psi_j^* \, \psi_l \, + \delta_{j,l} \left(n_l - |\psi_l|^2 \right) \right) v_l. \tag{E.11}$$

Rearranging this equation and multiplying both sides by ψ_j leads to

$$\left(\lambda - n_j + |\psi_j|^2 \right) \, \psi_j v_j = |\psi_j|^2 \sum_l \psi_l v_l. \tag{E.12}$$

Finally, we divide both sides by $\lambda - n_j + |\psi_j|^2$ and sum over all lattice sites j to obtain

$$1 = \sum_j \frac{|\psi_j|^2}{\lambda - n_j + |\psi_j|^2}. \tag{E.13}$$

This expression no longer contains the eigenvector $\mathbf{v}$ and therefore holds for all eigenvalues λ of ρ. Defining $\alpha = \max_j \{(n_j - |\psi_j|^2)\}$, one can directly infer that ρ cannot have two different eigenvalues λ and λ' in the interval $(\alpha, N_{\text{tot}}]$ both fulfilling Eq. (E.13). In this interval, all the addends in Eq. (E.13) are positive and for $\lambda, \lambda' \in (\alpha, N_{\text{tot}}]$ and $\lambda < \lambda'$ we find that

$$1 = \sum_j \frac{|\psi_j|^2}{\lambda - n_j + |\psi_j|^2} > \sum_j \frac{|\psi_j|^2}{\lambda' - n_j + |\psi_j|^2} = 1 \tag{E.14}$$

leads to a contradiction. This reveals the interesting property, that from the intrinsic form of a bosonic Gutzwiller state, this cannot describe a fragmented BEC.

We now multiply Eq. (E.13) by λ, which can then be seen as a fixed point, which is attractive in the interval $\lambda \in (\alpha, N_{\text{tot}}]$. With this equation one can define the fixed point iteration

$$\lambda^{(i+1)} = \sum_j \frac{\lambda^{(i)} |\psi_j|^2}{\lambda^{(i)} - n_j + |\psi_j|^2}. \tag{E.15}$$

This iteration, restricted to $\lambda^i \in (\alpha, N_{\text{tot}}]$, always converges to the largest eigenvalue of the SPDM with arbitrary precision and directly scales with the number of lattice sites L. In most cases a relative error $\frac{\Delta\lambda}{\lambda} \leq 10^{-6}$ is already obtained after 3-15 iterations.

F. Equations of Motion for the Projection Operator Approach

Here we give the explicit equations of motion for the variational coefficients c_n^j in the projection operator approach. Building on the notation introduced in Sec. (3.5), we use the relations

$$\begin{aligned}
\frac{\delta\varphi_{l',m}(t')}{\delta c_n^{(l)*}(t)} &= \sqrt{m+1}\, c_{m+1}^{(l')}(t')\, \delta_{n,m}\, \delta_{l,l'}\, \delta(t-t') \\
\frac{\delta\varphi_{l',m}^*(t')}{\delta c_n^{(l)*}(t)} &= \sqrt{m+1}\, c_{m}^{(l')}(t')\, \delta_{n,m+1}\, \delta_{l,l'}\, \delta(t-t') \\
\frac{\delta\phi_{l',m}^*(t')}{\delta c_n^{(l)*}(t)} &= \sqrt{(n+1)(n+2)}\, c_{n+2}^{(i)}\, \delta_{n,m}\, \delta_{l,l'}\, \delta(t-t')
\end{aligned} \tag{F.1}$$

leads to the desired equations of motion

$$\begin{aligned}
i\hbar\, \dot{c}_n^{(l)}(t) = {} & (Un(n-1)/2 - \mu n) c_n^{(l)}(t) - J \sum_{l'\in \text{n.n.}(l)} \left[\sqrt{n+1}\varphi_{l'}^*(t) c_{n+1}^{(l)}(t) + \sqrt{n}\varphi_{l'}(t) c_{n-1}^{(l)}(t)\right] \\
& + J \sum_{l'\in \text{n.n.}(l)} \Big[\sqrt{\overline{n}}\varphi_{l',\overline{n}}(t)\, c_{\overline{n}-1}^{(l)}(t)\, \delta_{n,\overline{n}} + \sqrt{\overline{n}}\varphi_{l',\overline{n}}^*(t)\, c_{\overline{n}}^{(l)}(t)\, \delta_{n,\overline{n}-1} \\
& + \sqrt{\overline{n}+1}\, \varphi_{l',\overline{n}-1}^*(t)\, c_{\overline{n}+1}^{(l)}(t)\, \delta_{n,\overline{n}} + \sqrt{\overline{n}+1}\, \varphi_{l',\overline{n}-1}(t)\, c_{\overline{n}}^{(l)}(t)\, \delta_{n,\overline{n}+1}\Big] \\
& + \frac{J^2}{U} \sum_{l'\in \text{n.n.}(l)} \Big[-2\overline{n}(\overline{n}+1)|c_{\overline{n}}^{(l')}|^2\, c_{\overline{n}}^{(l)}\, \delta_{n,\overline{n}} + \overline{n}(\overline{n}+1)|c_{\overline{n}-1}^{(l')}|^2\, c_{\overline{n}+1}^{(l)}\, \delta_{n,\overline{n}+1} \\
& + \overline{n}(\overline{n}+1)|c_{\overline{n}+1}^{(l')}|^2\, c_{\overline{n}-1}^{(l)}\, \delta_{n,\overline{n}-1} + \phi_{l',\overline{n}-1}\sqrt{\overline{n}(\overline{n}+1)}\, c_{\overline{n}-1}^{(l)}\, \delta_{n,\overline{n}+1} \\
& + \phi_{l',\overline{n}-1}^*\sqrt{\overline{n}(\overline{n}+1)}\, c_{\overline{n}+1}^{(l)}\, \delta_{n,\overline{n}-1} - \phi_{l',\overline{n}}\sqrt{\overline{n}(\overline{n}-1)}\, c_{\overline{n}-2}^{(l)}\, \delta_{n,\overline{n}} \\
& - \phi_{l',\overline{n}}^*\sqrt{\overline{n}(\overline{n}-1)}\, c_{\overline{n}}^{(l)}\, \delta_{n,\overline{n}-2} - \phi_{l',\overline{n}-2}^*\sqrt{(\overline{n}+1)(\overline{n}+2)}\, c_{\overline{n}+2}^{(l)}\, \delta_{n,\overline{n}} \\
& - \phi_{l',\overline{n}-2}\sqrt{(\overline{n}+1)(\overline{n}+2)}\, c_{\overline{n}}^{(l)}\, \delta_{n,\overline{n}+2}\Big]
\end{aligned} \tag{F.2}$$

(continued on the following page)

$$
\begin{aligned}
&+\frac{J^2}{U}\sum_{\substack{l',l''\in \text{n.n.}(l)\\ l'\neq l''}}\Big\{2\overline{n}\,\mathrm{Re}(\varphi^*_{l',\overline{n}}\,\varphi_{l''})c^{(l)}_{\overline{n}-1}\delta_{n,\overline{n}-1}+2(\overline{n}+1)\,\mathrm{Re}(\varphi_{l',\overline{n}-1}\,\varphi^*_{l''})c^{(l)}_{\overline{n}+1}\delta_{n,\overline{n}+1}\\
&+\sqrt{\overline{n}(\overline{n}+1)}\,(\varphi_{l',\overline{n}-1}\,\varphi_{l''}+\varphi_{l',\overline{n}}\,\varphi_{l''})c^{(l)}_{\overline{n}-1}\delta_{n,\overline{n}+1}+\sqrt{\overline{n}(\overline{n}+1)}\,(\varphi^*_{l',\overline{n}-1}\,\varphi^*_{l''}+\varphi^*_{l',\overline{n}}\,\varphi^*_{l''})c^{(l)}_{\overline{n}+1}\delta_{n,\overline{n}-1}\\
&-\big[(\overline{n}+1)\,\mathrm{Re}(2\varphi^*_{l',\overline{n}-1}\,\varphi_{l''}-\varphi^*_{l',\overline{n}-1}\,\varphi_{l'',\overline{n}-1})+\overline{n}\,\mathrm{Re}(2\varphi_{l',\overline{n}}\,\varphi^*_{l''}-\varphi_{l',\overline{n}}\,\varphi^*_{l'',\overline{n}})\big]\,c^{(l)}_{\overline{n}}\delta_{n,\overline{n}}\\
&-\sqrt{(\overline{n}+1)(\overline{n}+2)}\varphi^*_{l',\overline{n}-1}\,\varphi^*_{l''}\,c^{(l)}_{\overline{n}+2}\,\delta_{n,\overline{n}}-\sqrt{(\overline{n}+1)(\overline{n}+2)}\varphi_{l',\overline{n}-1}\,\varphi_{l''}\,c^{(l)}_{\overline{n}}\,\delta_{n,\overline{n}}\\
&-\sqrt{\overline{n}(\overline{n}-1)}\,\varphi_{l',\overline{n}}\,\varphi_{l''}\,c^{(l)}_{\overline{n}-2}\,\delta_{n,\overline{n}}-\sqrt{\overline{n}(\overline{n}-1)}\,\varphi^*_{l',\overline{n}}\,\varphi^*_{l''}\,c^{(l)}_{\overline{n}}\,\delta_{n,\overline{n}-2}\\
&-\sqrt{\overline{n}(\overline{n}+1)}\,\varphi^*_{l',\overline{n}}\,\varphi^*_{l'',\overline{n}-1}\,c^{(l)}_{\overline{n}+1}\,\delta_{n,\overline{n}-1}-\sqrt{\overline{n}(\overline{n}+1)}\,\varphi_{l',\overline{n}}\,\varphi_{l'',\overline{n}-1}\,c^{(l)}_{\overline{n}-1}\,\delta_{n,\overline{n}+1}\\
&-\overline{n}\,\mathrm{Re}(\varphi^*_{l',\overline{n}}\,\varphi_{l'',\overline{n}}\,)\,c^{(l)}_{\overline{n}-1}\,\delta_{n,\overline{n}-1}-(\overline{n}+1)\,\mathrm{Re}(\varphi^*_{l',\overline{n}-1}\,\varphi_{l'',\overline{n}-1}\,)\,c^{(l)}_{\overline{n}+1}\,\delta_{n,\overline{n}+1}\Big\}
\end{aligned}
\tag{F.3}
$$

The sum $\sum_{\substack{l',l''\in \text{n.n.}(l)\\ l'\neq l''}}$ extends over the set of all two neighboring sites l' and l'', excluding the terms where the two sites are equal. Here the convention is used, that both terms of the type $(l'=s1,l''=s2)$ $(l'=s2,l''=s1)$ appear in the sum.

$$
\begin{aligned}
\mathcal{C}^{(1)}_{(j,l)}\equiv{}&\overline{n}\,\varphi^*_{l,\overline{n}}\,(|c^{(j)}_{\overline{n}-1}|^2-|c^{(j)}_{\overline{n}}|^2)+(\overline{n}+1)\varphi^*_{l,\overline{n}-1}\,(|c^{(j)}_{\overline{n}+1}|^2-|c^{(j)}_{\overline{n}}|^2)\\
&+\varphi_{l,\overline{n}-1}(\phi^*_{j,\overline{n}-1}-\phi^*_{j,\overline{n}})+\varphi_{l,\overline{n}}(\phi^*_{j,\overline{n}-1}-\phi^*_{j,\overline{n}-2})
\end{aligned}
\tag{F.4}
$$

$$
\mathcal{C}^{(2)}_{(j,l)}\equiv(\overline{n}+1)(\varphi^*_{l,\overline{n}-1}-\varphi^*_l)(|c^{(j)}_{\overline{n}}|^2-|c^{(j)}_{\overline{n}+1}|^2)-\varphi_l\;\phi^*_{j,\overline{n}}-\varphi_{l,\overline{n}}\,\phi^*_{j,\overline{n}-1}
\tag{F.5}
$$

$$
\mathcal{C}^{(3)}_{(j,l)}\equiv\overline{n}(\varphi^*_l-\varphi^*_{l,\overline{n}})(|c^{(j)}_{\overline{n}-1}|^2-|c^{(j)}_{\overline{n}}|^2)+\varphi_l\,(\phi^*_{j,\overline{n}-1}-\phi^*_{j,\overline{n}-2})-\varphi_{l,\overline{n}-1}\phi^*_{j,\overline{n}-1}
\tag{F.6}
$$

The total energy can be divided into terms containing two bonds with the site i being an end point of such a pair of bonds, and other terms. The former term can be expressed as

$$
\begin{aligned}
E_{i,\text{end point}}=\frac{J^2}{U}\sum_{(j,l)\in,\text{n.n.n.}(i)}\Big[&\varphi_i\;C^{(1)}_{(j,l)}+\varphi^*_i\;C^{(1)\;*}_{(j,l)}+\varphi_{i,\overline{n}-1}\,C^{(2)}_{(j,l)}\\
&+\varphi^*_{i,\overline{n}-1}\,C^{(2)\;*}_{(j,l)}+\varphi_{i,\overline{n}}\,C^{(3)}_{(j,l)}+\varphi^*_{i,\overline{n}}\,C^{(3)\;*}_{(j,l)}\Big]
\end{aligned}
\tag{F.7}
$$

and using the functional derivative and subsequent integration leads to the additional term for the equation of motion

$$
\begin{aligned}
\frac{J^2}{U}\sum_{(l',l'')\in,\text{n.n.n.}(l)}\Big[&\sqrt{\overline{n}+1}\,C^{(1)}_{(l',l'')}\,c^{(l)}_{n+1}+\sqrt{\overline{n}}\,C^{(1)\;*}_{(l',l'')}\,c^{(l)}_{n-1}\\
&+\sqrt{\overline{n}}\,C^{(2)}_{(l',l'')}\,c^{(l)}_{\overline{n}}\,\delta_{n,\overline{n}-1}+\sqrt{\overline{n}}\,C^{(2)\;*}_{(l',l'')}\,c^{(l)}_{\overline{n}-1}\,\delta_{n,\overline{n}}\\
&+\sqrt{\overline{n}+1}\,C^{(3)}_{(l',l'')}\,c^{(l)}_{\overline{n}+1}\,\delta_{n,\overline{n}}+\sqrt{\overline{n}+1}\,C^{(3)\;*}_{(l',l'')}\,c^{(l)}_{\overline{n}}\,\delta_{n,\overline{n}+1}\Big]
\end{aligned}
\tag{F.8}
$$

G. Orthogonality Relations for Bogoliubov de Gennes Eigenmodes

G.1 Orthogonality Relations for the GW Fluctuation Coefficients

Consider general inhomogeneous case.

Small fluctuation in MF state for local state at site l expressed in basis of MF stationary ground state

$$|\phi_l(t)\rangle_l = \sum_i \lambda^{(i,l)}(t)\,|i\rangle_l \tag{G.1}$$

with

$$\lambda^{(i,l)}(t) = \delta_{i,1} + \delta\lambda^{(i,l)}(t) \tag{G.2}$$

where $|i\rangle_l$ is the ith excited mean field state in equilibrium.

Define matrix elements (may be different in an inhomogeneous system)

$$B^{(l)}_{i,j} =_l \langle i, |b_l| j\rangle_l \tag{G.3}$$

and the expectation value of the conjugate operator can be expressed as

$${}_l\langle i|b_l^\dagger|j\rangle_l = B^{(l)^*}_{j,i}. \tag{G.4}$$

The linearized equation of motion becomes

$$\begin{aligned} i\partial_t \delta\lambda^{(i,l)}(t) = E_i^{(l)}\delta\lambda^{(i,l)}(t) - J \sum_{l'\in \text{n.n.}(l)} \sum_j \Big[& B^{(l)^*}_{1,i}\Big(B^{(l')}_{1,j}\,\delta\lambda^{(j,l')}(t) + B^{(l')}_{j,1}\,\delta\lambda^{(j,l')^*}(t)\Big) \\ & + B^{(l)}_{i,1}\Big(B^{(l')^*}_{1,j}\,\delta\lambda^{(j,l')^*}(t) + B^{(l')^*}_{j,1}\,\delta\lambda^{(j,l')}(t)\Big)\Big]. \end{aligned} \tag{G.5}$$

For a fixed eigenmode of the whole system s, we make the time-dependent ansatz

$$\delta\lambda^{(j,l)}_s(t) = u^{(j,l)}_s\, e^{-i\omega_s t} + v^{(j,l)^*}_s\, e^{i\omega_s t}. \tag{G.6}$$

Inserting Eq. G.6 into Eq. G.5 and considering that the equality has to be fulfilled for all t, requires the coefficients of the time-dependent factors $e^{\pm i\omega_s t}$ to be equal. This leads to the two time-independent algebraic equations

$$\omega_s\, u_s^{(i,l)} = E_i^{(l)} u_s^{(i,l)} - J \sum_{l'\in \text{n.n.}(l)} \sum_j \left[B_{1,i}^{(l)^*} \left(B_{1,j}^{(l')}\, u_s^{(j,l')} + B_{j,1}^{(l')}\, v_s^{(j,l')} \right) + B_{i,1}^{(l)} \left(B_{1,j}^{(l')^*}\, v_s^{(j,l')} + B_{j,1}^{(l')^*}\, u_s^{(j,l')} \right) \right] \tag{G.7}$$

$$-\omega_s\, v_s^{(i,l)^*} = E_i^{(l)} v_s^{(i,l)^*} - J \sum_{l'\in \text{n.n.}(l)} \sum_j \left[B_{1,i}^{(l)^*} \left(B_{1,j}^{(l')}\, v_s^{(j,l')^*} + B_{j,1}^{(l')}\, u_s^{(j,l')^*} \right) + B_{i,1}^{(l)} \left(B_{1,j}^{(l')^*}\, u_s^{(j,l')^*} + B_{j,1}^{(l')^*}\, v_s^{(j,l')^*} \right) \right]. \tag{G.8}$$

G.1.1 Orthogonality Relation 1 and Realness of Eigenfrequencies

We now multiply Eq. G.7 with the factor $u_r^{(i,l)^*}$ and also consider the complex conjugated equation after an exchange of $s \leftrightarrow r$. The same is done for Eq. G.8 with the factor $v_r^{(i,l)}$

$$\begin{aligned} \omega_s\, u_s^{(i,l)} u_r^{(i,l)^*} = E_i^{(l)} u_s^{(i,l)}\, u_r^{(i,l)^*} - J \sum_{l'\in \text{n.n.}(l)} \sum_j \Bigg[& B_{1,i}^{(l)^*} \left(B_{1,j}^{(l')}\, u_s^{(j,l')}\, u_r^{(i,l)^*} + B_{j,1}^{(l')}\, v_s^{(j,l')}\, u_r^{(i,l)^*} \right) \\ & + B_{i,1}^{(l)} \left(B_{1,j}^{(l')^*}\, v_s^{(j,l')}\, u_r^{(i,l)^*} + B_{j,1}^{(l')^*}\, u_s^{(j,l')}\, u_r^{(i,l)^*} \right) \Bigg] \end{aligned} \tag{G.9}$$

$$\begin{aligned} \omega_r^*\, u_r^{(i,l)^*}\, u_s^{(i,l)} = E_i^{(l)} u_r^{(i,l)^*}\, u_s^{(i,l)} - J \sum_{l'\in \text{n.n.}(l)} \sum_j \Bigg[& B_{1,i}^{(l)} \left(B_{1,j}^{(l')^*}\, u_r^{(j,l')^*}\, u_s^{(i,l)} + B_{j,1}^{(l')^*}\, v_r^{(j,l')^*}\, u_s^{(i,l)} \right) \\ & + B_{i,1}^{(l)^*} \left(B_{1,j}^{(l')}\, v_r^{(j,l')^*}\, u_s^{(i,l)} + B_{j,1}^{(l')}\, u_r^{(j,l')^*}\, u_s^{(i,l)} \right) \Bigg] \end{aligned} \tag{G.10}$$

$$\begin{aligned} -\omega_s^*\, v_s^{(i,l)}\, v_r^{(i,l)^*} = E_i^{(l)} v_s^{(i,l)}\, v_r^{(i,l)^*} - J \sum_{l'\in \text{n.n.}(l)} \sum_j \Bigg[& B_{1,i}^{(l)} \left(B_{1,j}^{(l')^*}\, v_s^{(j,l')}\, v_r^{(i,l)^*} + B_{j,1}^{(l')^*}\, u_s^{(j,l')}\, v_r^{(i,l)^*} \right) \\ & + B_{i,1}^{(l)^*} \left(B_{1,j}^{(l')}\, u_s^{(j,l')}\, v_r^{(i,l)^*} + B_{j,1}^{(l')}\, v_s^{(j,l')}\, v_r^{(i,l)^*} \right) \Bigg] \end{aligned} \tag{G.11}$$

$$\begin{aligned} -\omega_r\, v_r^{(i,l)^*}\, v_s^{(i,l)} = E_i^{(l)} v_r^{(i,l)^*}\, v_s^{(i,l)} - J \sum_{l'\in \text{n.n.}(l)} \sum_j \Bigg[& B_{1,i}^{(l)^*} \left(B_{1,j}^{(l')}\, v_r^{(j,l')^*}\, v_s^{(i,l)} + B_{j,1}^{(l')}\, u_r^{(j,l')^*}\, v_s^{(i,l)} \right) \\ & + B_{i,1}^{(l)} \left(B_{1,j}^{(l')^*}\, u_r^{(j,l')^*}\, v_s^{(i,l)} + B_{j,1}^{(l')^*}\, v_r^{(j,l')^*}\, v_s^{(i,l)} \right) \Bigg] \end{aligned} \tag{G.12}$$

We now take the linear combination (Eq. G.9)-(Eq. G.10) and sum over all sites l and states i:

$$
\begin{aligned}
&(\omega_s - \omega_r^*) \sum_{l,i} u_s^{(i,l)} u_r^{(i,l)^*} \\
&\quad = J \sum_{l} \sum_{l' \in \text{n.n.}(l)} \sum_{i,j} \Big[B_{1,i}^{(l)} B_{1,j}^{(l')^*} u_r^{(j,l')^*} u_s^{(i,l)} + B_{1,i}^{(l)} B_{j,1}^{(l')^*} v_r^{(j,l')^*} u_s^{(i,l)} \\
&\quad + B_{i,1}^{(l)^*} B_{1,j}^{(l')} v_r^{(j,l')^*} u_s^{(i,l)} + B_{i,1}^{(l)^*} B_{j,1}^{(l')} u_r^{(j,l')^*} u_s^{(i,l)} - B_{1,i}^{(l)^*} B_{1,j}^{(l')} u_s^{(j,l')} u_r^{(i,l)^*} \\
&\quad - B_{1,i}^{(l)^*} B_{j,1}^{(l')} v_s^{(j,l')} u_r^{(i,l)^*} - B_{i,1}^{(l)} B_{1,j}^{(l')^*} v_s^{(j,l')} u_r^{(i,l)^*} - B_{i,1}^{(l)} B_{j,1}^{(l')^*} u_s^{(j,l')} u_r^{(i,l)^*} \Big] \\
&\quad = J \sum_{l} \sum_{l' \in \text{n.n.}(l)} \sum_{i,j} \Big[B_{1,i}^{(l)} B_{j,1}^{(l')^*} v_r^{(j,l')^*} u_s^{(i,l)} + B_{i,1}^{(l)^*} B_{1,j}^{(l')} v_r^{(j,l')^*} u_s^{(i,l)} \\
&\quad - B_{1,i}^{(l)^*} B_{j,1}^{(l')} v_s^{(j,l')} u_r^{(i,l)^*} - B_{i,1}^{(l)} B_{1,j}^{(l')^*} v_s^{(j,l')} u_r^{(i,l)^*} \Big]
\end{aligned}
\tag{G.13}
$$

where we used that the summation $\sum_l \sum_{l' \in \text{n.n.}(l)}$ is equivalent to a summation over all pairs of nearest neighbors $2\sum_{\langle l,l' \rangle}$ and we interchanged the indices $i \leftrightarrow j$ and $l \leftrightarrow l'$.

Analogously, we do the same with the combination (Eq. G.11)-(Eq. G.12)

$$
\begin{aligned}
&-(\omega_s^* - \omega_r) \sum_{l,i} v_s^{(i,l)} v_r^{(i,l)^*} \\
&\quad = J \sum_{l} \sum_{l' \in \text{n.n.}(l)} \sum_{i,j} \Big[B_{1,i}^{(l)^*} \Big(B_{1,j}^{(l')} v_r^{(j,l')^*} v_s^{(i,l)} + B_{j,1}^{(l')} u_r^{(j,l')^*} v_s^{(i,l)} \Big) \\
&\quad + B_{i,1}^{(l)} \Big(B_{1,j}^{(l')^*} u_r^{(j,l')^*} v_s^{(i,l)} + B_{j,1}^{(l')^*} v_r^{(j,l')^*} v_s^{(i,l)} \Big) \\
&\quad - B_{1,i}^{(l)} \Big(B_{1,j}^{(l')^*} v_s^{(j,l')} v_r^{(i,l)^*} + B_{j,1}^{(l')^*} u_s^{(j,l')} v_r^{(i,l)^*} \Big) \\
&\quad - B_{i,1}^{(l)^*} \Big(B_{1,j}^{(l')} u_s^{(j,l')} v_r^{(i,l)^*} + B_{j,1}^{(l')} v_s^{(j,l')} v_r^{(i,l)^*} \Big) \Big] \\
&\quad = J \sum_{l} \sum_{l' \in \text{n.n.}(l)} \sum_{i,j} \Big[B_{1,i}^{(l)^*} B_{j,1}^{(l')} u_r^{(j,l')^*} v_s^{(i,l)} + B_{i,1}^{(l)} B_{1,j}^{(l')^*} u_r^{(j,l')^*} v_s^{(i,l)} \\
&\quad - B_{1,i}^{(l)} B_{j,1}^{(l')^*} u_s^{(j,l')} v_r^{(i,l)^*} - B_{i,1}^{(l)^*} B_{1,j}^{(l')} u_s^{(j,l')} v_r^{(i,l)^*} \Big]
\end{aligned}
\tag{G.14}
$$

G.1.1.1 Realness of Eigenfrequencies

Choosing $r = s$ and adding Eq. G.13 and Eq. G.14 one obtains

$$
\begin{aligned}
&(\omega_s - \omega_s^*) \sum_{l,i} \Big(|u_s^{(i,l)}|^2 + |v_s^{(i,l)}|^2 \Big) \\
&\quad = J \sum_{l} \sum_{l' \in \text{n.n.}(l)} \sum_{i,j} \Big[B_{1,i}^{(l)} B_{j,1}^{(l')^*} v_s^{(j,l')^*} u_s^{(i,l)} + B_{i,1}^{(l)^*} B_{1,j}^{(l')} v_s^{(j,l')^*} u_s^{(i,l)} \\
&\quad - B_{1,i}^{(l)^*} B_{j,1}^{(l')} v_s^{(j,l')} u_s^{(i,l)^*} - B_{i,1}^{(l)} B_{1,j}^{(l')^*} v_s^{(j,l')} u_s^{(i,l)^*} \\
&\quad + B_{1,i}^{(l)^*} B_{j,1}^{(l')} u_s^{(j,l')^*} v_s^{(i,l)} + B_{i,1}^{(l)} B_{1,j}^{(l')^*} u_s^{(j,l')^*} v_s^{(i,l)} \\
&\quad - B_{1,i}^{(l)} B_{j,1}^{(l')^*} u_s^{(j,l')} v_s^{(i,l)^*} - B_{i,1}^{(l)^*} B_{1,j}^{(l')} u_s^{(j,l')} v_s^{(i,l)^*} \Big] \\
&\quad = 0
\end{aligned}
\tag{G.15}
$$

where in the last step, we again exchanged $i \leftrightarrow j$ and $l \leftrightarrow l'$ in half of the terms. For a given mode s this implies, that unless all coefficients $|u_s^{(i,l)}|^2$ and $|v_s^{(i,l)}|^2$ are zero, which implies its own vanishing, the eigenfrequency ω_s is real. In the further calculation we do therefore no longer distinguish between ω_s and ω_s^*.

G.1.1.2 Orthogonality Relation 1

We again take the sum Eq. G.13 + Eq. G.14

$$\begin{aligned}
&(\omega_s - \omega_r) \sum_{l,i} \left(u_s^{(i,l)} u_r^{(i,l)^*} - v_s^{(i,l)} v_r^{(i,l)^*} \right) \\
&\quad = J \sum_{l} \sum_{l' \in \text{n.n.}(l)} \sum_{i,j} \Big[B_{1,i}^{(l)} B_{j,1}^{(l')^*} \, v_r^{(j,l')^*} \, u_s^{(i,l)} + B_{i,1}^{(l)^*} B_{1,j}^{(l')} \, v_r^{(j,l')^*} \, u_s^{(i,l)} \\
&\quad - B_{1,i}^{(l)^*} B_{j,1}^{(l')} \, v_s^{(j,l')} \, u_r^{(i,l)^*} - B_{i,1}^{(l)} B_{1,j}^{(l')^*} \, v_s^{(j,l')} \, u_r^{(i,l)^*} \\
&\quad + B_{1,i}^{(l)^*} B_{j,1}^{(l')} \, u_r^{(j,l')^*} \, v_s^{(i,l)} + B_{i,1}^{(l)} B_{1,j}^{(l')^*} \, u_r^{(j,l')^*} \, v_s^{(i,l)} \\
&\quad - B_{1,i}^{(l)} B_{j,1}^{(l')^*} \, u_s^{(j,l')} \, v_r^{(i,l)^*} - B_{i,1}^{(l)^*} B_{1,j}^{(l')} \, u_s^{(j,l')} \, v_r^{(i,l)^*} \Big] \\
&\quad = 0
\end{aligned} \tag{G.16}$$

which implies that the coefficients of any two collective modes r and s with different energy $\omega_s \neq \omega_r$, the coefficients are orthogonal and can otherwise be normalized, such that

$$\sum_{l,i} \left(u_s^{(i,l)} u_r^{(i,l)^*} - v_s^{(i,l)} v_r^{(i,l)^*} \right) = \delta_{s,r}. \tag{G.17}$$

G.1.1.3 Orthogonality Relation 2

We now consider the alternate combination of equations: multiplying Eq. G.7 with the factor $v_r^{(i,l)}$ and the complex conjugate of Eq. G.8 with $u_r^{(i,l)}$ (keeping in mind that $\omega_s^* = \omega_s$), as well as the pair of equations arising by interchanging $r \leftrightarrow s$

$$\begin{aligned}
\omega_s \, u_s^{(i,l)} v_r^{(i,l)} = E_i^{(l)} u_s^{(i,l)} \, v_r^{(i,l)} - J \sum_{l' \in \text{n.n.}(l)} \sum_{j} \Big[& B_{1,i}^{(l)^*} \Big(B_{1,j}^{(l')} \, u_s^{(j,l')} \, v_r^{(i,l)} + B_{j,1}^{(l')} \, v_s^{(j,l')} \, v_r^{(i,l)} \Big) \\
& + B_{i,1}^{(l)} \Big(B_{1,j}^{(l')^*} \, v_s^{(j,l')} \, v_r^{(i,l)} + B_{j,1}^{(l')^*} \, u_s^{(j,l')} \, v_r^{(i,l)} \Big) \Big]
\end{aligned} \tag{G.18}$$

$$\begin{aligned}
-\omega_s \, v_s^{(i,l)} u_r^{(i,l)} = E_i^{(l)} v_s^{(i,l)} u_r^{(i,l)} - J \sum_{l' \in \text{n.n.}(l)} \sum_{j} \Big[& B_{1,i}^{(l)} \Big(B_{1,j}^{(l')^*} \, v_s^{(j,l')} u_r^{(i,l)} + B_{j,1}^{(l')^*} \, u_s^{(j,l')} u_r^{(i,l)} \Big) \\
& + B_{i,1}^{(l)^*} \Big(B_{1,j}^{(l')} \, u_s^{(j,l')} u_r^{(i,l)} + B_{j,1}^{(l')} \, v_s^{(j,l')} u_r^{(i,l)} \Big) \Big]
\end{aligned} \tag{G.19}$$

$$\begin{aligned}
\omega_r \, u_r^{(i,l)} v_s^{(i,l)} = E_i^{(l)} u_r^{(i,l)} \, v_s^{(i,l)} - J \sum_{l' \in \text{n.n.}(l)} \sum_{j} \Big[& B_{1,i}^{(l)^*} \Big(B_{1,j}^{(l')} \, u_r^{(j,l')} \, v_s^{(i,l)} + B_{j,1}^{(l')} \, v_r^{(j,l')} \, v_s^{(i,l)} \Big) \\
& + B_{i,1}^{(l)} \Big(B_{1,j}^{(l')^*} \, v_r^{(j,l')} \, v_s^{(i,l)} + B_{j,1}^{(l')^*} \, u_r^{(j,l')} \, v_s^{(i,l)} \Big) \Big]
\end{aligned} \tag{G.20}$$

$$-\omega_r\, v_r^{(i,l)} u_s^{(i,l)} = E_i^{(l)} v_r^{(i,l)} u_s^{(i,l)} - J \sum_{l' \in \text{n.n.}(l)} \sum_j \Big[B_{1,i}^{(l)} \Big(B_{1,j}^{(l')^*}\, v_r^{(j,l')} u_s^{(i,l)} + B_{j,1}^{(l')^*}\, u_r^{(j,l')} u_s^{(i,l)} \Big) + B_{i,1}^{(l)^*} \Big(B_{1,j}^{(l')}\, u_r^{(j,l')} u_s^{(i,l)} + B_{j,1}^{(l')}\, v_r^{(j,l')} u_s^{(i,l)} \Big) \Big]. \tag{G.21}$$

We now take the combination Eq. G.18+Eq. G.19-Eq. G.20-Eq. G.21 and again sum over all states i and sites l

$$\begin{aligned}
&(\omega_s + \omega_r) \sum_{l,i} (u_s^{(i,l)} v_r^{(i,l)} - u_r^{(i,l)} v_s^{(i,l)}) \\
&\quad = -J \sum_l \sum_{l' \in \text{n.n.}(l)} \sum_{i,j} \Big[B_{1,i}^{(l)^*} \Big(B_{1,j}^{(l')}\, u_s^{(j,l')}\, v_r^{(i,l)} + B_{j,1}^{(l')}\, v_s^{(j,l')}\, v_r^{(i,l)} \Big) \\
&\qquad + B_{i,1}^{(l)} \Big(B_{1,j}^{(l')^*}\, v_s^{(j,l')}\, v_r^{(i,l)} + B_{j,1}^{(l')^*}\, u_s^{(j,l')}\, v_r^{(i,l)} \Big) + B_{1,i}^{(l)} \Big(B_{1,j}^{(l')^*}\, v_s^{(j,l')} u_r^{(i,l)} + B_{j,1}^{(l')^*}\, u_s^{(j,l')} u_r^{(i,l)} \Big) \\
&\qquad + B_{i,1}^{(l)^*} \Big(B_{1,j}^{(l')}\, u_s^{(j,l')} u_r^{(i,l)} + B_{j,1}^{(l')}\, v_s^{(j,l')} u_r^{(i,l)} \Big) - B_{1,i}^{(l)^*} \Big(B_{1,j}^{(l')}\, u_r^{(j,l')}\, v_s^{(i,l)} + B_{j,1}^{(l')}\, v_r^{(j,l')}\, v_s^{(i,l)} \Big) \\
&\qquad - B_{i,1}^{(l)} \Big(B_{1,j}^{(l')^*}\, v_r^{(j,l')}\, v_s^{(i,l)} + B_{j,1}^{(l')^*}\, u_r^{(j,l')}\, v_s^{(i,l)} \Big) - B_{1,i}^{(l)} \Big(B_{1,j}^{(l')^*}\, v_r^{(j,l')} u_s^{(i,l)} + B_{j,1}^{(l')^*}\, u_r^{(j,l')} u_s^{(i,l)} \Big) \\
&\qquad - B_{i,1}^{(l)^*} \Big(B_{1,j}^{(l')}\, u_r^{(j,l')} u_s^{(i,l)} + B_{j,1}^{(l')}\, v_r^{(j,l')} u_s^{(i,l)} \Big) \Big] \\
&\quad = 0
\end{aligned} \tag{G.22}$$

where again we exploited the exchangability of indices $r \leftrightarrow s$ and $l \leftrightarrow l'$ under the sum. For non-degenerate eigenmodes $r \neq s$ in the case when $\omega_r \neq \omega_s$, this leads to the orthogonality relation

$$\sum_{l,i} (u_s^{(i,l)} v_r^{(i,l)} - u_r^{(i,l)} v_s^{(i,l)}) = 0 \tag{G.23}$$

which clearly also holds for the case $r = s$.

H. Action for the Coherent State Bosonic Path Integral

The action, using the bosonic coherent states as variational states is given by

$$\mathcal{S} = \int_{t_i}^{t_f} dt\ \left[-i\langle z(t)|\partial_t|z(t)\rangle + \langle z(t)|H|z(t)\rangle\right], \tag{H.1}$$

with the usual definition of a coherent state

$$|z\rangle = e^{-\frac{|z|^2}{2}} e^{za^\dagger}|0\rangle. \tag{H.2}$$

Here we focus on the term containing the derivative with respect to time, which can be evaluated to be

$$\begin{aligned}\langle z(t)|\partial_t|z(t)\rangle &= e^{-\frac{|z|^2}{2}}\langle 0|e^{z^* a}\left[-\left(\frac{1}{2}\dot{z}(t)z^*(t) + \frac{1}{2}z(t)\dot{z}^*(t)\right)e^{-\frac{|z|^2}{2}}e^{za^\dagger}|0\rangle + e^{-\frac{|z|^2}{2}}\dot{z}(t)\,a^\dagger\,e^{za^\dagger}|0\rangle\right] \\ &= \frac{1}{2}\left[z^*(t)\,\dot{z}(t) - \dot{z}^*(t)\,z(t)\right]\end{aligned} \tag{H.3}$$

in terms of the time-dependent complex fields $z(t)$ and $z^*(t)$. In the action, we would however prefer a form only containing the terms $z^*(t)\,\dot{z}(t)$, such that the functional variation with respect to $z^*(t)$ directly leads to the equations of motion for $\dot{z}(t)$. We therefore use integration by parts $\int dt\,\dot{z}^*(t)\,z(t) = z^*(t)\,z(t) - \int dt\,z^*(t)\,\dot{z}(t)$ to obtain the convenient form

$$\int_{t_i}^{t_f} dt\,\langle z(t)|\partial_t|z(t)\rangle = \int_{t_i}^{t_f} dt\,z^*(t)\,\dot{z}(t) - \left[\frac{1}{2}z^*(t')\,z(t')\right]_{t'=t_i}^{t'=t_f}. \tag{H.4}$$

The last term only leads to a constant contribution, since the two end points of the coherent state parameter are held fixed for the functional variation to determine the equations of motion. They do therefore not affect the resulting equations of motion and this offset is therefore usually neglected already on the level of the action.

I. Formal independence of complex variables and their conjugates

In the context of complex analysis and differential equations, one commonly treats a complex variable z and its complex conjugate z^* as independent variables, i.e. z^* does not change when z is changed. Clearly, this is not true and also not fully analogous to the independence of the real and imaginary parts of a complex variable, since the directions spanned by z and z^* are not orthogonal in the isomorphic $\mathbb{R}^2$ plane.

Here we discuss why this formal procedure works and how it is to be understood. In the context of first order ordinary complex differential equations, as known from the generic form of unitary time evolution in quantum mechanics, a system of the form

$$i\dot{z}_i = \sum_j A_{i,j}\, z_j + \sum_j B_{i,j}\, z_j^* \tag{I.1}$$

is given. It is said that z_i and z_i^* should formally be seen as independent variables, where this form is generic for unitary quantum evolution. For N complex variables z_i, a set of independent $2N$ equations is required for a unique solution, since this would correspond to $2N$ real variables. Decomposing the variables into real and imaginary parts $z_i = a_i + ib_i$, the N complex equations lead to $2N$ equations for the variables $\{a_i, b_i\}$ by equating real and imaginary parts individually:

$$\begin{aligned} \dot{a}_j &= \sum_k (A_{j,k} - B_{j,k}) b_k, \\ \dot{b}_j &= -\sum_k (A_{j,k} + B_{j,k}) a_k, \end{aligned} \tag{I.2}$$

which can be cast into matrix form

$$\begin{pmatrix} \dot{a}_1 \\ \vdots \\ \dot{a}_N \\ \dot{b}_1 \\ \vdots \\ \dot{b}_N \end{pmatrix} = \begin{pmatrix} 0 & (A-B) \\ -(A+B) & 0 \end{pmatrix} \begin{pmatrix} a_1 \\ \vdots \\ a_N \\ b_1 \\ \vdots \\ b_N \end{pmatrix}. \tag{I.3}$$

Since a_j and b_j are independent when purely real, we perform a (non-singular) and invertible variable transform (and its reverse) to complex variables we denote by $c_j = a_j + ib_j$ and $d_j = a_j - ib_j$ given by

$$\begin{pmatrix} c_1 \\ \vdots \\ c_N \\ d_1 \\ \vdots \\ d_N \end{pmatrix} = M \begin{pmatrix} a_1 \\ \vdots \\ a_N \\ b_1 \\ \vdots \\ b_N \end{pmatrix} \tag{I.4}$$

in matrix form, with $M = \begin{pmatrix} \mathbb{1}_N & i\mathbb{1}_N \\ \mathbb{1}_N & -i\mathbb{1}_N \end{pmatrix}$. The original equations of motion then are then transformed into

$$\begin{pmatrix} \dot{c}_1 \\ \vdots \\ \dot{c}_N \\ \dot{d}_1 \\ \vdots \\ \dot{d}_N \end{pmatrix} = \underbrace{M \begin{pmatrix} 0 & (A-B) \\ -(A+B) & 0 \end{pmatrix} M^{-1}}_{-i\begin{pmatrix} A & B \\ -B & -A \end{pmatrix}} \begin{pmatrix} c_1 \\ \vdots \\ c_N \\ d_1 \\ \vdots \\ d_N \end{pmatrix}, \tag{I.5}$$

where the original equations of motion and their conjugates are recovered and $c_i = z_i$ and $d_i = z_i^*$ can be treated as being 'independent', since all applied transformations are well defined and invertible.

J. Unitary Fock Space Transformation Operator for Single-Particle Basis Transformations

When working with two different single particle bases related to the creation operators $\begin{pmatrix} a_1^\dagger \\ \vdots \\ a_L^\dagger \end{pmatrix} \leftrightarrow$ $\begin{pmatrix} b_1^\dagger \\ \vdots \\ b_L^\dagger \end{pmatrix}$ these are related by the single particle unitary transformation, described by a $L \times L$ unitary matrix U, such that

$$b_j^\dagger = \sum_i U_{j,i}\, a_i^\dagger. \tag{J.1}$$

Thus, the creation (and annihilation) operators transform like a vector. However, the matrix U is not an operator acting on the same Hilbert space $\mathcal{H}$ as $a_j^\dagger$ and $b_j^\dagger$ themselves and the question, whether a true unitary operator V on $\mathcal{H}$, describing this 'basis transformation' on an operator level, in the sense of $b_j^\dagger = V^\dagger a_j^\dagger V$, exists?

This can be answered with 'yes' and we will now prove the relation

$$b_j^\dagger = e^{i\sum_{k,l=1}^L G_{lk} a_k^\dagger a_l}\; a_j^\dagger\; e^{-i\sum_{k,l=1}^L G_{lk} a_k^\dagger a_l}\,, \tag{J.2}$$

where G is the Hermitian generating matrix of U, with

$$U = e^{iG}. \tag{J.3}$$

Proof:

Using the Baker-Campbell-Hausdorff (BCH) relation,

$$e^X\, Y e^{-X} = Y + [X,Y] + \frac{1}{2!}[X,[X,Y]] + \frac{1}{3!}[X,[X,[X,Y]]] + \ldots \tag{J.4}$$

with

$$X = i \sum_{k,l=1}^{L} G_{lk}\; a_k^\dagger\, a_l \tag{J.5}$$

and defining

$$\begin{aligned} C^{(1)} &\equiv [X, a_j^\dagger], \\ C^{(m+1)} &\equiv [X, C^{(m)}], \end{aligned} \tag{J.6}$$

the first expression can be evaluated directly

$$C^{(1)} = i \sum_k G_{jk}\ a_k^\dagger. \tag{J.7}$$

This implies that $C^{(m)}$ can be expressed as

$$C^{(m)} = \sum_i C_i^{(m)}\ a_i^\dagger. \tag{J.8}$$

The second relation in Eq.(J.6) leads to the condition for the $C_l^{(m)} \in \mathbb{C}$

$$C_k^{(m+1)} = i \sum_l G_{lk}\ C_l^{(m)}, \tag{J.9}$$

which is satisfied by

$$C_n^{(m)} = i^m\, (G^m)_{jn}, \tag{J.10}$$

and can be proved by induction. Here, G^m denotes the m-th power by matrix multiplication. In this case, the BCH (Eq.J.4) can thus be expressed as

$$\begin{aligned} V^\dagger a_j^\dagger V &= a_j^\dagger + \sum_{m=1}^{\infty} \frac{1}{m!} C^{(m)} \\ &= \sum_{m=0}^{\infty} \sum_{n=1}^{L} \left(\frac{1}{m!} i^m G^m \right)_{jn} a_n^\dagger \\ &= \sum_{n=1}^{L} \left(e^{iG} \right)_{jn} a_n^\dagger \\ &= \sum_{n=1}^{L} U_{jn} a_n^\dagger, \end{aligned} \tag{J.11}$$

thus proving the relation.

K. Properties of Generalized Unitary Transformation Matrices

In this appendix, we derive general properties of generalized unitary transformations, where bosonic creation and annihilation operators can be hybridized, leading to new bosonic operators. This is closely related to canonical transformations on symplectic spaces in classical systems. For the derivation here, we closely follow [19]. Unitary transformations on the level of single particle orbitals are most easily formulated for a many-particle system by the transformation of the creation and annihilation operators for the orbitals. Here the transformation for the creation operators is isomorphic to the transformation of a single particle state.

We refer to a generalized unitary transformation as an extension of such a transformation, but furthermore allowing for a hybridization of creation and annihilation operators. Given the original set of bosonic fluctuation operators to different modes $\delta b_1, \ldots, \delta b_n$, it is convenient to define the column vectors of operators

$$\boldsymbol{\delta}\mathbf{b} = \begin{pmatrix} \delta b_1 \\ \vdots \\ \delta b_{\mathcal{D}} \end{pmatrix}, \qquad \boldsymbol{\delta}\mathbf{b}^\dagger = \begin{pmatrix} \delta b_1^\dagger \\ \vdots \\ \delta b_{\mathcal{D}}^\dagger \end{pmatrix}. \tag{K.1}$$

Defining the $2\mathcal{D} \times 2\mathcal{D}$ matrices

$$\Sigma = \begin{pmatrix} \mathbb{1}_{\mathcal{D}} & 0 \\ 0 & -\mathbb{1}_{\mathcal{D}} \end{pmatrix}, \qquad \gamma = \begin{pmatrix} 0 & \mathbb{1}_{\mathcal{D}} \\ \mathbb{1}_{\mathcal{D}} & 0 \end{pmatrix} \tag{K.2}$$

allows one to express the original bosonic commutation relations $[\delta b_j, \delta b_i^\dagger] = \delta_{i,j}$ in the compact matrix form

$$[\begin{pmatrix} \boldsymbol{\delta}\mathbf{b} \\ \boldsymbol{\delta}\mathbf{b}^\dagger \end{pmatrix}, \begin{pmatrix} \boldsymbol{\delta}\mathbf{b} \\ \boldsymbol{\delta}\mathbf{b}^\dagger \end{pmatrix}^\dagger] = \Sigma. \tag{K.3}$$

Here the matrix elements of Σ are to be understood as the zero and unit operators on the many-particle Fock space.

We can now express any generalized unitary transformation in matrix form as

$$\begin{pmatrix} \boldsymbol{\delta}\mathbf{b} \\ \boldsymbol{\delta}\mathbf{b}^\dagger \end{pmatrix} = W \begin{pmatrix} \boldsymbol{\beta} \\ \boldsymbol{\beta}^\dagger \end{pmatrix}, \tag{K.4}$$

where

$$\boldsymbol{\beta} = \begin{pmatrix} \beta_1 \\ \vdots \\ \beta_{\mathcal{D}} \end{pmatrix}, \qquad \boldsymbol{\beta}^\dagger = \begin{pmatrix} \beta_1^\dagger \\ \vdots \\ \beta_{\mathcal{D}}^\dagger \end{pmatrix} \tag{K.5}$$

are the vectors containing the bosonic quasiparticle annihilation and creation operators, respectively. It will become clear later that it is suitable to write the transformation (K.5) with a product of matrices $W\Sigma$, instead of a single matrix.

These resulting quasi-particle operators are also required to obey bosonic commutation relations $[\beta_j, \beta_i^\dagger] = \delta_{i,j}$, which we can also express in matrix form. We will now derive a general property of the matrix W, by comparing two different expressions for the vector $(\boldsymbol{\beta}^\dagger, \boldsymbol{\beta})^\dagger$. firstly, by directly taking the inverted Hermitian conjugate of Eq. (K.4), we have

$$\begin{pmatrix} \boldsymbol{\beta} \\ \boldsymbol{\beta}^\dagger \end{pmatrix}^\dagger = \begin{pmatrix} \boldsymbol{\delta}\mathbf{b} \\ \boldsymbol{\delta}\mathbf{b}^\dagger \end{pmatrix}^\dagger (W^{-1})^\dagger. \tag{K.6}$$

Secondly, we can first interchange the two sub-vectors $\boldsymbol{\beta}$ and $\boldsymbol{\beta}^\dagger$ with the matrix γ and then consider the inverse

$$\begin{aligned} \begin{pmatrix} \boldsymbol{\beta} \\ \boldsymbol{\beta}^\dagger \end{pmatrix}^\dagger = \begin{pmatrix} \boldsymbol{\beta}^\dagger \\ \boldsymbol{\beta} \end{pmatrix}^t = \left[\gamma \begin{pmatrix} \boldsymbol{\beta} \\ \boldsymbol{\beta}^\dagger \end{pmatrix}\right]^t = \left[W^{-1} \begin{pmatrix} \boldsymbol{\delta}\mathbf{b} \\ \boldsymbol{\delta}\mathbf{b}^\dagger \end{pmatrix}\right]^t \gamma \\ = \left[\gamma \begin{pmatrix} \boldsymbol{\delta}\mathbf{b}^\dagger \\ \boldsymbol{\delta}\mathbf{b} \end{pmatrix}\right]^t (W^{-1})^t \gamma = \begin{pmatrix} \boldsymbol{\delta}\mathbf{b} \\ \boldsymbol{\delta}\mathbf{b}^\dagger \end{pmatrix}^\dagger \gamma (W^{-1})^t \gamma. \end{aligned} \tag{K.7}$$

Comparing Eqns. (K.6) and (K.7) and noting that the equality has to hold for all possible expectation values of the vector operators, the relations

$$\boxed{W^\dagger = \gamma W^t \gamma} \Leftrightarrow \boxed{W^* = \gamma W \gamma} \tag{K.8}$$

are inferred. To obtain further relations for W (such as expressing the inverse as a product of matrices), we use the requirement that the operators β_i also obey bosonic commutation relations. We do this in matrix form and use the original commutation relations (K.3), as well as the property $(W^{-1})^\dagger = \gamma (W^t)^{-1} \gamma$,

$$\begin{aligned} \Sigma &= [\begin{pmatrix} \boldsymbol{\beta} \\ \boldsymbol{\beta}^\dagger \end{pmatrix}, \begin{pmatrix} \boldsymbol{\beta} \\ \boldsymbol{\beta}^\dagger \end{pmatrix}^\dagger] \\ &= [W^{-1} \begin{pmatrix} \boldsymbol{\delta}\mathbf{b} \\ \boldsymbol{\delta}\mathbf{b}^\dagger \end{pmatrix}, \begin{pmatrix} \boldsymbol{\delta}\mathbf{b} \\ \boldsymbol{\delta}\mathbf{b}^\dagger \end{pmatrix}^\dagger \gamma (W^{-1})^t \gamma] \\ &= W^{-1} \Sigma \gamma (W^{-1})^t \gamma. \end{aligned} \tag{K.9}$$

Note that the commutator here does not act on the matrix space, but the space of operators. Inverting this matrix relation and using (K.8) shows that for any transformation of the generalized unitary form, the matrix W must fulfill

$$\mathbb{1} = W^\dagger \Sigma W \Sigma. \tag{K.10}$$

The inverse, which is unique on any finite dimensional space (and both the left and right inverse) is thus

$$W^{-1} = \Sigma W^\dagger \Sigma. \tag{K.11}$$

Note that all of the above properties follow only from the structure of a generalized canonical transformation. No Hamiltonian has appeared so far, on which these properties could depend. These properties and relations will be of use in the following sections.

Mathematically, the set of all generalized unitary transformation matrices W is referred to as the symplectic group $\mathrm{Sp}(2\mathcal{D}, \mathbb{C})$. Analogous to the unitary group leaving the standard euclidean norm of any vector (and standard scalar product between any two vectors) invariant, the symplectic group leaves the norm defined by Σ (and the scalar product defined by Σ between any two vectors) invariant, as can be seen from Eq. (K.10). This is fully equivalent to a transformation of the type (K.4) conserving the bosonic commutation relations. In this sense, bosonic quasi-particle operator spaces are symplectic. In contrast, for fermionic systems the transformation matrices W are unitary and the associated spaces have a simpler, euclidean structure.

K.1 Basis-Transformation for Generic Bosonic Quasi-Particle Hamiltonians

A general Hamiltonian quadratic in the fluctuations is of the form

$$\mathcal{H}^{(2)} = \sum_{i,j} h_{i,j} \delta b_i^\dagger \delta b_j + \frac{1}{2} \sum_{i,j} (\Delta_{i,j}\, \delta b_i^\dagger \delta b_j^\dagger + \Delta_{i,j}^*\, \delta b_i\, \delta b_j), \tag{K.12}$$

where the matrix h is Hermitian and Δ is symmetric. This can also be written in matrix form

$$\mathcal{H}^{(2)} = \frac{1}{2} (\delta b^\dagger,\, \delta b)\, H_{\mathrm{QP}} \begin{pmatrix} \delta b \\ \delta b^\dagger \end{pmatrix} \; - \; \frac{1}{2} \mathrm{Tr}\,(h) \tag{K.13}$$

with the quasi-particle Hamiltonian matrix

$$H_{\mathrm{QP}} = \begin{pmatrix} h & \Delta \\ \Delta^* & h^* \end{pmatrix}. \tag{K.14}$$

Although the matrix H_{QP} is Hermitian (h is Hermitian and Δ is symmetric), a direct diagonalization of H_{QP} does not transform the bilinear form (K.12) into diagonal form, since we saw that the transformation matrix for a generalized unitary transformation is not unitary itself, i.e. $W^{-1} \neq W^\dagger$, but rather satisfies Eq. (K.11). One therefore has to proceed with greater care than in a usual diagonalization problem and we will derive a completeness relation in terms of the existing eigenvectors of ΣH_{QP}, as well as additional vectors, which are mapped onto spurious states by H_{QP}, but are not eigenvectors themselves.

Using Eq. (K.4), we now express the quadratic Hamiltonian in terms of quasi-particle operators

$$\begin{aligned} \mathcal{H}^{(2)} &= \frac{1}{2} (\beta^\dagger,\, \beta)\, W^\dagger H_{\mathrm{QP}} W \begin{pmatrix} \beta \\ \beta^\dagger \end{pmatrix} \; - \; \frac{1}{2} \mathrm{Tr}\,(h) \\ &= \frac{1}{2} (\beta^\dagger,\, \beta)\, \Sigma W^{-1} (\Sigma H_{\mathrm{QP}}) W \begin{pmatrix} \beta \\ \beta^\dagger \end{pmatrix} \; - \; \frac{1}{2} \mathrm{Tr}\,(h)\,. \end{aligned} \tag{K.15}$$

The transformation matrix W is to be chosen, such that the product of matrices is *mostly diagonal* (in a sense to be precisely defined later). The braces in the last line of Eq. (K.15) are placed for visual clarity: if ΣH_{QP} were diagonalizable, choosing the matrix W to contain the eigenvectors of ΣH_{QP} as column vectors, would transform $W^{-1} \Sigma H_{\mathrm{QP}} W$ into a diagonal matrix with the eigenvalues on the diagonal. The subsequent multiplication with the diagonal matrix Σ would not change the diagonal structure, but only transform the negative eigenvalues to their positive counterparts if the eigenvectors in W are chosen in an appropriate order. Note, however, that the matrix ΣH_{QP} is generally not normal (specifically also not Hermitian) and therefore not diagonalizable in the sense that it does not possess a complete basis of eigenstates.

In the following section we will focus on the structure and relations between eigenvectors and eigenvalues of matrices ΣH_{QP}, with H_{QP} of the form in Eq. (K.14). We will see that if a basis of eigenvectors exists, these correspond exactly to the column vectors of the generalized unitary transformation matrix W (if sorted in appropriate order). In this sense the structure of the matrix ΣH_{QP} is such, that the eigenvectors intrinsically correspond to a bosonic quasi-particles.

K.1.1 Eigenvector Properties

Assuming the matrix ΣH_{QP} possess an eigenvector $\mathbf{x}^n = \begin{pmatrix} \mathbf{u}^n \\ \mathbf{v}^n \end{pmatrix}$, such that

$$\Sigma H_{\mathrm{QP}} \begin{pmatrix} \mathbf{u}^n \\ \mathbf{v}^n \end{pmatrix} = \omega_n \begin{pmatrix} \mathbf{u}^n \\ \mathbf{v}^n \end{pmatrix}, \tag{K.16}$$

and recalling the structure (K.14), the eigenvalue equation can also be written as

$$h\mathbf{u}^n + \Delta\mathbf{v}^n = \omega_n \mathbf{u}^n \tag{K.17}$$

$$-\Delta^*\mathbf{u}^n - h^*\mathbf{v}^n = \omega_n \mathbf{v}^n. \tag{K.18}$$

We now derive several properties that follow from this structure.

If $\mathbf{x}^n = \begin{pmatrix}\mathbf{u}^n \\ \mathbf{v}^n\end{pmatrix}$ is a right eigenvector of ΣH_{QP} to ω_n, then $\overline{\mathbf{x}}^n = \mathbf{x}^{n\dagger}\Sigma$ is a left eigenvector of ΣH_{QP} to ω_n^*.

The assumption is $\Sigma H_{\mathrm{QP}}\mathbf{x}^n = \omega_n \mathbf{x}^n$.

We thus have

$$\overline{\mathbf{x}}^n \Sigma H_{\mathrm{QP}} = \mathbf{x}^{n\dagger} H_{\mathrm{QP}} = (\omega_n \mathbf{x}^n)^\dagger \Sigma = \omega_n^* \overline{\mathbf{x}}^n. \tag{K.19}$$

If $\mathbf{x}^n = \begin{pmatrix}\mathbf{u}^n \\ \mathbf{v}^n\end{pmatrix}$ is a right eigenvector of ΣH_{QP} to ω_n, then $\mathbf{y}^n = \gamma\mathbf{x}^{n*} = \begin{pmatrix}\mathbf{v}^{n*} \\ \mathbf{u}^{n*}\end{pmatrix}$ is a right eigenvector of ΣH_{QP} to $-\omega_n^*$.

We first note the relations $\gamma H_{\mathrm{QP}}\gamma = H_{\mathrm{QP}}^*$ and $\Sigma\gamma = -\gamma\Sigma$ to show

$$\omega_n^* \mathbf{x}^{n*} = \Sigma H_{\mathrm{QP}}^* \mathbf{x}^{n*} = \Sigma\gamma H_{\mathrm{QP}}\gamma \mathbf{x}^{n*} = -\gamma\Sigma H_{\mathrm{QP}}\gamma \mathbf{x}^{n*}. \tag{K.20}$$

Multiplying both sides by $-\gamma$ then directly leads to the desired eigenvalue equation.

The matrix Σ can be understood to define a scalar product (or a pseudo-version thereof due to the lack of positive definiteness) on the vector space, which proves to be useful. For any two vectors, we define

$$\langle \mathbf{x}, \mathbf{y}\rangle \equiv \mathbf{x}^\dagger \Sigma \mathbf{y} = \overline{\mathbf{x}}\mathbf{y} \tag{K.21}$$

and the 'square norm' of a vector $\langle \mathbf{x}, \mathbf{x}\rangle$ can be positive, zero or negative.

The properties of the eigenvectors derived above can be seen as a duality between the set of vectors corresponding to a positive and those with a negative norm.

Eigenvectors to non-conjugated eigenvalues are mutually orthogonal with respect to the scalar product (K.21). Let $\Sigma H_{\mathrm{QP}}\mathbf{x}^m = \omega_m \mathbf{x}^m$ and $\Sigma H_{\mathrm{QP}}\mathbf{x}^n = \omega_n \mathbf{x}^n$ be two eigenvectors to eigenvalues not related by complex conjugation $\omega_n \neq \omega_m^*$. Then $\overline{\mathbf{x}}^m \mathbf{x}^n = 0$.

Consider the eigenvalue equation

$$\Sigma H_{\mathrm{QP}}\mathbf{x}^n = \omega_n \mathbf{x}^n \tag{K.22}$$

as well as its Hermitian conjugate

$$\mathbf{x}^{m\dagger} H_{\mathrm{QP}}\Sigma = \omega_m^* \mathbf{x}^{m\dagger} \quad \Leftrightarrow \quad \overline{\mathbf{x}^m}\Sigma H_{\mathrm{QP}} = \omega_m^* \overline{\mathbf{x}^m}. \tag{K.23}$$

Multiplying Eq. (K.22) by $\overline{\mathbf{x}^m}$ from the left and subtracting Eq. (K.23) multiplied by $\mathbf{x}^n$ from the right one obtains

$$0 = (\omega_n - \omega_m^*)\overline{\mathbf{x}^m}\mathbf{x}^n. \tag{K.24}$$

Thus if $(\omega_n - \omega_m^*) \neq 0 \quad \Rightarrow \quad \overline{\mathbf{x}^m}\mathbf{x}^n = 0$.

The previous property also directly implies that as soon as an eigenvalue has a non-zero imaginary part, the corresponding eigenvector has a norm of zero: $\omega_n \neq \omega_n^* \Rightarrow \overline{\mathbf{x}}^n \mathbf{x}^n = \langle \mathbf{x}^n, \mathbf{x}^n \rangle = 0$.

Up to now we saw that non-zero eigenvalues of ΣH_{QP} always appear in pairs and the two respective eigenvectors are also linearly independent. The case of an eigenvalue being zero has to be considered separately though, since there is no guarantee that there are two linearly independent eigenvectors. This also commonly turns out to be the case for bosonic systems, such as in Bogoliubov theory and our extended quasi-particle theory for strong interactions.

In case of eigenvalues zero existing, let us denote one corresponding eigenvectors by P_n, i.e. $\Sigma H_{\mathrm{QP}} P_n = 0$. In case of the eigenvalue zero havening a larger algebraic multiplicity than the geometric multiplicity, one can implicitly define vectors Q_n such that

$$\Sigma H_{\mathrm{QP}} Q_n = -\frac{i}{\mu} P_n \tag{K.25}$$

and μ is a constant that can be chosen a posteriori. This also directly implies that Q_n is linearly independent of P_n: since Q_n is mapped onto a non-zero multiple P_n by ΣH_{QP}, but P_n is mapped onto zero, the two vectors are necessarily different and hence linearly independent. The definition (K.25) can be understood within the context of the Jordan normal for of an endomorphism, where in case of a matrix not being fully diagonalizable, the matrix can always be brought into the generic form

$$\begin{pmatrix} \lambda & 1 & 0 & \\ 0 & \ddots & \ddots & 0 \\ & 0 & \lambda & 1 \\ & & 0 & \lambda \end{pmatrix} \tag{K.26}$$

by an appropriate choice of basis. Applied to our case, this simply amounts to this basis choice, where the non-diagonalizable subblocks are two-dimensional and P_n, Q_n are chosen as the basis vectors of the respective sub-block.

The vectors P_n and Q_n are orthogonal to all other eigenvectors of ΣH_{QP} belonging to non-zero eigenvectors, i.e. $\overline{\mathbf{x}^m} P_n = \overline{\mathbf{x}^m} Q_n = 0 \quad \forall \overline{\mathbf{x}^m}$ corresponding to $\omega_m \neq 0$.

The orthogonality of $P_n$to any $\mathbf{x}^m$ follows from the property, that both are eigenvectors to different eigenvalues.

To show the orthogonality of Q_n to any $\mathbf{x}^m$, we multiply Eq. (K.25) by $\overline{\mathbf{x}^n}$ from the left

$$\begin{aligned} \overline{\mathbf{x}^n} \Sigma H_{\mathrm{QP}} Q_n &= -\frac{i}{\mu} \overline{\mathbf{x}^n} P_n \\ \Rightarrow \omega_n^* \overline{\mathbf{x}^n} Q &= 0. \end{aligned} \tag{K.27}$$

Since by assumption $\omega_n \neq 0$, we have $\overline{\mathbf{x}^n} Q = 0$.

K.2 Construction of a Basis from Eigenvectors of ΣH_{QP} and Supplemental Vectors

Our next goal is to construct a basis in which the quasi-particle Hamiltonian ΣH_{QP} takes on the most diagonal of all possible forms. Since ΣH_{QP} is not Hermitian (not even normal, i.e. generally $\Sigma H_{\mathrm{QP}} (\Sigma H_{\mathrm{QP}})^\dagger - (\Sigma H_{\mathrm{QP}})^\dagger \Sigma H_{\mathrm{QP}} \neq 0$), a complete basis of eigenvectors does always exist. This is

not to say, that there are no eigenvectors. Above we have shown some important properties: due to the structure of a general bosonic quasi-particle Hamiltonian, eigenvectors always appear in pairs to non-zero eigenvalues $\omega_n \leftrightarrow -\omega_n^*$ and eigenvectors to different eigenvalues are mutually orthogonal with respect to the norm (or mathematically more precise: bilinear form) defined by the matrix Σ. Under this norm, any vector $\mathbf{x}$ can have a positive, negative or zero norm $\mathbf{x}^\dagger\Sigma\mathbf{x}$. This property is invariant under any rescaling $\tilde{\mathbf{x}} = \lambda\mathbf{x}$. Also note that a norm of zero $\mathbf{x}^\dagger\Sigma\mathbf{x} = 0$ does not imply that the vector itself is zero. It furthermore follows[1] from the structure of ΣH_{QP}, that eigenvectors to a positive eigenvalue $0 < \omega_n \in \mathbb{R}$ have a positive norm. We denote these positive eigenvectors by $\mathbf{x}^n$ and choose the normalization convention $\mathbf{x}^{n\dagger}\Sigma\mathbf{x}^n = 1$. The conjugate set of eigenvectors to negative eigenvalues we denote by $\mathbf{y}^n$ and normalize these to minus one $\mathbf{y}^{n\dagger}\Sigma\mathbf{y}^n = -1$. For non-zero eigenvalues, these eigenvectors always appear in pairs and are interrelated by

$$\begin{aligned} \mathbf{y}^n &= \gamma\,\mathbf{x}^{n*}, \\ \mathbf{x}^n &= \gamma\,\mathbf{y}^{n*}. \end{aligned} \tag{K.28}$$

We denote the total dimension of the space by $2\mathcal{D}$ (if there are $\mathcal{D}$ complex degrees of freedom and hence twice as many equations), the eigenvector index m runs from 1 to a maximum of $\mathcal{D}$, depending on the number of existing eigenvectors. Since eigenvectors to different eigenvalues are orthogonal, we thus have the relations

$$\mathbf{x}^{n\dagger} H_{\mathrm{QP}} \mathbf{x}^m = \omega_m\,\delta_{n,m}, \tag{K.29}$$

$$\mathbf{y}^{n\dagger} H_{\mathrm{QP}} \mathbf{y}^m = \omega_m^*\,\delta_{n,m}, \tag{K.30}$$

$$\mathbf{x}^{n\dagger} H_{\mathrm{QP}} \mathbf{y}^m = 0. \tag{K.31}$$

K.2.1 Completeness

To derive the explicit form of the completeness relation in terms of eigenvectors $\mathbf{x}^m$ and $\mathbf{y}^m$, we start from Eq. (K.10).For now we assume that a complete basis of eigenvectors of ΣH_{QP} exists. It proves useful to define the canonical basis vectors

$$\mathbf{e}_j \equiv \begin{pmatrix} 0 \\ \vdots \\ 1 \\ \vdots \\ 0 \end{pmatrix}, \tag{K.32}$$

where the one is the j-th element. Then the matrix W and its conjugate can be written as

$$W = \sum_{n=1}^{\mathcal{D}} (\mathbf{x}^n \mathbf{e}_n^\dagger + \mathbf{y}^n \mathbf{e}_{n+\mathcal{D}}^\dagger), \tag{K.33}$$

$$W^\dagger = \sum_{n=1}^{\mathcal{D}} (\mathbf{e}_n \mathbf{x}^{n\dagger} + \mathbf{e}_{n+\mathcal{D}} \mathbf{y}^{n\dagger}), \tag{K.34}$$

i.e. the eigenvectors are the column entries of W, with the $\mathbf{x}$ vectors in the left and the $\mathbf{y}$ vectors in the right half. The inverse matrix $W^{-1} = \Sigma W^\dagger \Sigma$ can also be explicitly constructed from these vectors as

$$W^{-1} = \sum_{n=1}^{\mathcal{D}} (\mathbf{e}_n\,\mathbf{x}^{n\dagger} - \mathbf{e}_{n+\mathcal{D}}\,\mathbf{y}^{n\dagger})\Sigma \tag{K.35}$$

[1] This is not an intrinsic property if the matrices h and Δ were chosen at random, but follows from the structure of the quasi-particle Hamiltonian and the restriction a generalized canonical transformation underlies.

We use these expressions for W and $W^\dagger$ in Eq. (K.10) (or alternatively multiply (K.33) and (K.35)) to obtain

$$\begin{aligned}\mathbb{1} &= W\Sigma W^\dagger\Sigma \\ &= \sum_{m,n=1}^{\mathcal{D}} (\mathbf{x}^m\mathbf{e}_m^\dagger + \mathbf{y}^m\mathbf{e}_{m+\mathcal{D}}^\dagger)\Sigma(\mathbf{e}_n\mathbf{x}^{n\dagger} + \mathbf{e}_{n+\mathcal{D}}\mathbf{y}^{n\dagger})\Sigma \\ &= \sum_{n=1}^{\mathcal{D}} (\mathbf{x}^n\,\mathbf{x}^{n\dagger}\Sigma - \mathbf{y}^n\,\mathbf{y}^{n\dagger}\Sigma).\end{aligned} \tag{K.36}$$

Here we used the relations

$$\begin{aligned}\mathbf{e}_m^\dagger\Sigma\,\mathbf{e}_n &= \delta_{m,n}, \\ \mathbf{e}_{m+\mathcal{D}}^\dagger\Sigma\,\mathbf{e}_{n+\mathcal{D}} &= -\delta_{m,n}, \\ \mathbf{e}_m^\dagger\Sigma\,\mathbf{e}_{n+\mathcal{D}} &= 0,\end{aligned} \tag{K.37}$$

which are valid $\forall m, n \in \{1, \ldots, \mathcal{D}\}$. The completeness relation in Eq. (K.36) shows that any state can be expressed in the basis of eigenvectors $\mathbf{x}^m$ and $\mathbf{y}^m$, but the contributions from the negative eigenvectors have to be added with and additional minus sign. In contrast to the usual canonical scalar product, the Σ on the right can be understood as part of the scalar product, when multiplying an arbitrary vector on the right, to be expanded in terms of eigenvectors.

We now use the completeness relation in Eq. (K.36) twice, on both the left and right side of ΣH_{QP}, and use the eigenvector properties to express this matrix in terms of eigenvectors:

$$\begin{aligned}\Sigma H_{\mathrm{QP}} &= \sum_{m,n=1}^{\mathcal{D}} (\mathbf{x}^m\,\mathbf{x}^{m\dagger}\Sigma - \mathbf{y}^m\,\mathbf{y}^{m\dagger}\Sigma)\Sigma H_{\mathrm{QP}}(\mathbf{x}^n\,\mathbf{x}^{n\dagger}\Sigma - \mathbf{y}^n\,\mathbf{y}^{n\dagger}\Sigma) \\ &= \sum_{n=1}^{\mathcal{D}} (\omega_n\mathbf{x}^n\,\mathbf{x}^{n\dagger}\Sigma + \omega_n^*\mathbf{y}^n\,\mathbf{y}^{n\dagger}\Sigma).\end{aligned} \tag{K.38}$$

Note that by ω_n, we only denote *half* the number of eigenvalues for n ranging from 1 to $\mathcal{D}$, since the eigenvalues always appear in pairs.

Using the representations Eq. (K.33) for W and Eq. (K.34) for $W^\dagger$ explicitly reveals that the matrix $W^\dagger H_{\mathrm{QP}} W$ is diagonal (if a complete basis of eigenvectors exists),

$$W^\dagger H_{\mathrm{QP}} W = \sum_{n=1}^{\mathcal{D}} (\omega_n\mathbf{e}_n\,\mathbf{e}_n^\dagger + \omega_n^*\mathbf{e}_{n+\mathcal{D}}\,\mathbf{e}_{n+\mathcal{D}}^\dagger). \tag{K.39}$$

and that the eigenvalues on the two diagonal subblocks are related by complex conjugation. In the context of matrix diagonalization, where generally the inverse (and not the Hermitian adjoint) matrix is on the left, it is worth pointing out that the left term in Eq. (K.39) can also be written as

$$W^\dagger H_{\mathrm{QP}} W = \Sigma W^{-1}(\Sigma H_{\mathrm{QP}})W, \tag{K.40}$$

i.e. the columns of W are the eigenvectors of ΣH_{QP},

$$\begin{aligned}W &= \left(\begin{pmatrix}\\ \mathbf{x}^1 \\ \\ \end{pmatrix}, \ldots, \begin{pmatrix}\\ \mathbf{x}^n \\ \\ \end{pmatrix}, \begin{pmatrix}\\ \mathbf{y}^1 \\ \\ \end{pmatrix}, \ldots, \begin{pmatrix}\\ \mathbf{y}^n \\ \\ \end{pmatrix}\right) \\ &= \begin{pmatrix} U & V^* \\ V & U^* \end{pmatrix},\end{aligned} \tag{K.41}$$

where U and V are the $(\mathcal{D} \times \mathcal{D})$-dimensional matrices, that contain the vectors $\mathbf{u}^n$ and $\mathbf{v}^n$ respectively as column vectors in increasing order.

For the inverse matrix an additional minus sign has to be multiplied to the lower half

$$\begin{aligned} W^{-1} &= \Sigma W^{\dagger} \Sigma \\ &= \begin{pmatrix} U^{\dagger} & -V^{\dagger} \\ -V^{t} & U^{t} \end{pmatrix}. \end{aligned} \tag{K.42}$$

This form for the inverse follows directly from Eq. (K.36). Note that for finite dimensional matrices, the left inverse is always equal to the right inverse.

L. Green's Functions

L.1 Definition of Green's Functions

In this section we shortly introduce the Green's function formalism, which is extremely useful and widely used, both for linear response analyses and understanding physical phenomena beyond equilibrium. The real time, n-body time ordered lattice Green's function is defined as

$$G^{(n)}(\boldsymbol{\ell}_1, t_1, \ldots, \boldsymbol{\ell}_n, t_n, \boldsymbol{\ell}'_1, t'_1, \ldots, \boldsymbol{\ell}'_n, t'_n) = (-i)^n \langle \mathcal{T}\, b_{\boldsymbol{\ell}_1}(t_1) \ldots b_{\boldsymbol{\ell}_n}(t_n)\, b^\dagger_{\boldsymbol{\ell}'_n}(t'_n) \ldots b^\dagger_{\boldsymbol{\ell}'_1}(t'_1) \rangle. \tag{L.1}$$

The expectation value ist to be evaluated in the ground state when working at $T = 0$ or in the thermal ensemble when working at finite temperature. $b_{\boldsymbol{\ell}}(t)$ is the Wannier annihilation operator on site $\boldsymbol{\ell}$ in second quantization in the Heisenberg representation and $\mathcal{T}$ denotes Wick's time ordering operator, which acts on all Heisenberg operators standing on the right of it in the following fashion: it re-orders the operators, such that the ones with earlier times (lower values of t) stand to the right of the operators at later times. For the fermionic case the whole expression is multiplied with a factor -1^m, where m is the unique number of transpositions required to arrange the operators from the initially given order to the final order.

Henceforth, we will restrict ourselves to the case of bosons, and refer to the single particle Green's function when the index m is omitted. The choice of the single particle basis is arbitrary and the Green's functions simply transform like tensors of the respective order.

The time ordered, retarded and advanced single particle Green's functions are then respectively defined as

$$G_{\boldsymbol{\ell},\boldsymbol{\ell}'}(t, t') = -i\,\theta(t - t')\langle b_{\boldsymbol{\ell}}(t)\, b^\dagger_{\boldsymbol{\ell}'}(t')\rangle - i\,\theta(t' - t)\langle b^\dagger_{\boldsymbol{\ell}'}(t')\, b_{\boldsymbol{\ell}}(t)\rangle \tag{L.2}$$

$$G^r_{\boldsymbol{\ell},\boldsymbol{\ell}'}(t, t') = -i\,\theta(t - t')\langle [b_{\boldsymbol{\ell}}(t),\, b^\dagger_{\boldsymbol{\ell}'}(t')]\rangle \tag{L.3}$$

$$G^a_{\boldsymbol{\ell},\boldsymbol{\ell}'}(t, t') = i\,\theta(t' - t)\langle [b_{\boldsymbol{\ell}}(t),\, b^\dagger_{\boldsymbol{\ell}'}(t')]\rangle. \tag{L.4}$$

The Lehmann representation allows for an explicit expression in frequency space of the temporally Fourier transformed Green's function. This is obtained by inserting the unit operator in the complete many body lattice Hilbert space, expressed as the sum over the complete many particle

basis (although this might not be explicitly known, but its existence is insured), into the expectation value. For the case of the time ordered single particle Greens function, this leads to

$$\begin{aligned} G_{\boldsymbol{\ell},\boldsymbol{\ell}'}(t,t') =& -i\,\theta(t-t')\sum_{\nu}\langle\psi_0|e^{iHt}\,b_{\boldsymbol{\ell}}\,e^{-iHt}|\psi_\nu\rangle\langle\psi_\nu|e^{iHt'}\,b^\dagger_{\boldsymbol{\ell}'}\,e^{-iHt'}|\psi_0\rangle \\ & -i\,\theta(t'-t)\sum_{\nu}\langle\psi_0|e^{iHt'}\,b^\dagger_{\boldsymbol{\ell}'}\,e^{-iHt'}|\psi_\nu\rangle\langle\psi_\nu|e^{iHt}\,b_{\boldsymbol{\ell}}\,e^{-iHt}|\psi_0\rangle \\ =& -i\,\theta(t-t')\sum_{\nu}e^{-i(E_\nu-E_0)(t-t')}\langle\psi_0|b_{\boldsymbol{\ell}}|\psi_\nu\rangle\langle\psi_\nu|b^\dagger_{\boldsymbol{\ell}'}|\psi_0\rangle \\ & -i\,\theta(t'-t)\sum_{\nu}e^{-i(E_0-E_\nu)(t-t')}\langle\psi_0|b^\dagger_{\boldsymbol{\ell}'}|\psi_\nu\rangle\langle\psi_\nu|b_{\boldsymbol{\ell}}|\psi_0\rangle \end{aligned} \tag{L.5}$$

In the special case that the system's Hamiltonian conserves the total particle number $[H,\hat{N}]=0$, the many-body eigenstates can all be chosen to have fixed particle number and the collective quantum number ν can be replaced by a set of two independent quantum numbers $(N,\,\lambda)$: the exact particle number of the many-body state N and the integer excitation number within the N-particle subspace λ.

It is evident from the above expression that the Green's function and thus any expectation values can only depend on the difference in time $t-t'$ if the Hamiltonian is not explicitly time dependent. Thus, the Fourier-transform in frequency space only depends on a single frequency ω and is of the explicit form

$$\begin{aligned} G_{\boldsymbol{\ell},\boldsymbol{\ell}'}(\omega) &= \int_{-\infty}^{\infty} dt\, e^{i\omega t}\, G_{\boldsymbol{\ell},\boldsymbol{\ell}'}(t,t'=0) \\ &= \sum_{\nu}\frac{\langle\psi_0|b_{\boldsymbol{\ell}}|\psi_\nu\rangle\langle\psi_\nu|b^\dagger_{\boldsymbol{\ell}'}|\psi_0\rangle}{\omega-(E_\nu-E_0)+i0^+} - \sum_{\nu}\frac{\langle\psi_0|b^\dagger_{\boldsymbol{\ell}'}|\psi_\nu\rangle\langle\psi_\nu|b_{\boldsymbol{\ell}}|\psi_0\rangle}{\omega-(E_0-E_\nu)-i0^+}. \end{aligned} \tag{L.6}$$

In the particle number conserving case, the matrix elements $\langle\psi^{N'}_\lambda|a^\dagger_{\boldsymbol{\ell}}|\psi^N_0\rangle$ vanish identically unless $N'=N+1$ (analogously for the second term, where the particle number is decreased by one). In this case, the energy difference between two ground states to successive particle numbers is simply the definition of the chemical potential, if the upper and lower discrete derivatives agree, one has

$$E_0^{(N+1)}-E_0^{(N)} = \mu^{(N+1)} \approx \mu \approx \mu^{(N-1)} = E_0^{(N)}-E_0^{(N-1)}. \tag{L.7}$$

The first term in Eq. (L.6) corresponds to particle excitations and has poles at $\omega \geq \mu$, shifted infinitesimally below the real axis. The second term corresponds to hole excitations and has poles at $\omega \leq \mu$, shifted infinitesimally above the real axis.

Performing the same transformations for the retarded and advanced Green's functions, one obtains

$$\begin{aligned} \overset{r}{G^a}_{\boldsymbol{\ell},\boldsymbol{\ell}'}(\omega) &= \int_{-\infty}^{\infty} dt\, e^{i\omega t}\, \overset{r}{G^a}_{\boldsymbol{\ell},\boldsymbol{\ell}'}(t,t'=0) \\ &= \sum_{\nu}\frac{\langle\psi_0|b_{\boldsymbol{\ell}}|\psi_\nu\rangle\langle\psi_\nu|b^\dagger_{\boldsymbol{\ell}'}|\psi_0\rangle}{\omega-(E_\nu-E_0)\pm i0^+} - \sum_{\nu}\frac{\langle\psi_0|b^\dagger_{\boldsymbol{\ell}'}|\psi_\nu\rangle\langle\psi_\nu|b_{\boldsymbol{\ell}}|\psi_0\rangle}{\omega-(E_0-E_\nu)\pm i0^+}. \end{aligned} \tag{L.8}$$

It can be seen directly, that the retarded Green's function only has poles in the lower half of the complex plane, while the advanced Green's function's poles all lie in the upper half.

Transformation properties of the Green's function under a single particle basis change

The denominator in Eq. (L.6) only depends on the energies of the many particle eigenstates and the pole structure is consequently independent of the chosen single particle basis. A unitary single particle basis transformation of the creation and annihilation operators, i.e. $a^\dagger_{\boldsymbol{\ell}} = \sum_m U_{l,m} b^\dagger_m$ leaving the commutation relations invariant, only leads to a redistribution of the different poles' weight. It can 'hide' a pole, if a matrix element in the nominator of Eq. (L.6) vanishes, i.e. the excited state $|\psi_\nu\rangle$ is not connected to the ground state $|\psi_0\rangle$ by the respective creation or annihilation operator.

L.2 Spectral Function

The single particle spectral function is usually defined via the retarded single particle Green's function

$$\mathcal{A}_{\boldsymbol{\ell},\boldsymbol{\ell}'}(\omega) = -\frac{1}{\pi}\,\mathrm{Im}\,G^r_{\boldsymbol{\ell},\boldsymbol{\ell}'}(\omega), \tag{L.9}$$

but can equally well be extracted from the advanced or time ordered Green's functions

$$\begin{aligned}\mathcal{A}_{\boldsymbol{\ell},\boldsymbol{\ell}'}(\omega) &= \frac{1}{\pi}\,\mathrm{Im}\,G^a_{\boldsymbol{\ell},\boldsymbol{\ell}'}(\omega)\\ \mathcal{A}_{\boldsymbol{\ell},\boldsymbol{\ell}'}(\omega) &= -\frac{1}{\pi}\,\mathrm{sgn}(\omega-\mu)\,\mathrm{Im}\,G_{\boldsymbol{\ell},\boldsymbol{\ell}'}(\omega).\end{aligned} \tag{L.10}$$

In the spectral representation it takes on the explicit form

$$\begin{aligned}\mathcal{A}_{\boldsymbol{\ell},\boldsymbol{\ell}'}(\omega) = &\sum_\nu \langle\psi_0|b_{\boldsymbol{\ell}}|\psi_\nu\rangle\langle\psi_\nu|b^\dagger_{\boldsymbol{\ell}'}|\psi_0\rangle\;\delta(\omega-(E_\nu-E_0))\\ &-\sum_\nu \langle\psi_0|b^\dagger_{\boldsymbol{\ell}'}|\psi_\nu\rangle\langle\psi_\nu|b_{\boldsymbol{\ell}}|\psi_0\rangle\;\delta(\omega+(E_\nu-E_0))\end{aligned} \tag{L.11}$$

In a translationally symmetric system, both the Green's function and the spectral function become 'diagonal' in $\mathbf{k}$-space, i.e.

$$G_{\mathbf{k},\mathbf{k}'}(\omega) = G(\mathbf{k},\omega)\,\delta_{\mathbf{k},\mathbf{k}'}. \tag{L.12}$$

At this point it becomes clear that choosing the commutator for bosons (anticommutator for fermions) in the definition of the retarded and advanced Green's functions (Eq. (L.2)) was a suitable choice, as it leads to the sum rule

$$\int_{-\infty}^{\infty} d\omega\,\mathcal{A}_{\boldsymbol{\ell},\boldsymbol{\ell}'}(\omega) = \delta_{\boldsymbol{\ell},\boldsymbol{\ell}'}. \tag{L.13}$$

In the case of bosons, the spectral function can have both very large positive and negative contributions on the positive and negative frequency side respectively, indicating the possibility of a single particle state to be occupied by a large number of bosons. The sum rule expresses that the difference in the area in of the curves is 1 if a particle / hole excitation is created in the same single particle state and is thus fundamentally related to the underlying quantum statistics.

It is useful to define the larger and lesser partial spectral functions

$$\begin{aligned}\mathcal{A}^{>}_{\boldsymbol{\ell},\boldsymbol{\ell}'}(\omega) &= \sum_\nu \langle\psi_0|b_{\boldsymbol{\ell}}|\psi_\nu\rangle\langle\psi_\nu|b^\dagger_{\boldsymbol{\ell}'}|\psi_0\rangle\;\delta(\omega-(E_\nu-E_0))\\ &= \langle\psi_0|b_{\boldsymbol{\ell}}\,\delta(H-E_0-\omega)\,b^\dagger_{\boldsymbol{\ell}'}|\psi_0\rangle\end{aligned} \tag{L.14}$$

$$\begin{aligned}\mathcal{A}^{<}_{\boldsymbol{\ell},\boldsymbol{\ell}'}(\omega) &= \sum_\nu \langle\psi_0|b^\dagger_{\boldsymbol{\ell}'}|\psi_\nu\rangle\langle\psi_\nu|b_{\boldsymbol{\ell}}|\psi_0\rangle\;\delta(\omega+(E_\nu-E_0))\\ &= \langle\psi_0|b^\dagger_{\boldsymbol{\ell}'}\,\delta(H-E_0+\omega)\,b_{\boldsymbol{\ell}}|\psi_0\rangle\end{aligned} \tag{L.15}$$

corresponding to particle and hole excitations respectively. The expression in the last lines can be directly verified by writing the operator function in terms of its eigenvalues and eigenstates

$$\delta(H-E_0-\omega) = \sum_\nu \delta(\omega-(E_\nu-E_0))|\psi_\nu\rangle\langle\psi_\nu| \tag{L.16}$$

$$\delta(H-E_0+\omega) = \sum_\nu \delta(\omega+(E_\nu-E_0))|\psi_\nu\rangle\langle\psi_\nu| \tag{L.17}$$

In terms of these, the full spectral function in Eq. (L.11) can be written as

$$\mathcal{A}_{\boldsymbol{\ell},\boldsymbol{\ell}'}(\omega) = \mathcal{A}^{>}_{\boldsymbol{\ell},\boldsymbol{\ell}'}(\omega) - \mathcal{A}^{<}_{\boldsymbol{\ell},\boldsymbol{\ell}'}(\omega). \tag{L.18}$$

If the ground state energy E_0 is the minimum energy of all many-particle states, such that $E_\nu - E_0 \geq 0$ for all many-particle energies, the weight of the larger and lesser spectral functions is only at positive and negative frequencies respectively, and one can write

$$\mathcal{A}_{\boldsymbol{\ell},\boldsymbol{\ell}'}(\omega) = \theta(\omega)\,\mathcal{A}^{>}_{\boldsymbol{\ell},\boldsymbol{\ell}'}(\omega) - \theta(-\omega)\,\mathcal{A}^{<}_{\boldsymbol{\ell},\boldsymbol{\ell}'}(\omega). \tag{L.19}$$

In the particle number conserving case, where Eq. (L.7) applies and $E_\lambda^{(N+1)} - E_0^{(N)} > \mu$ for all $(N+1)$-particle states λ (and analogously for the $(N-1)$-particle states), one has

$$\mathcal{A}_{\boldsymbol{\ell},\boldsymbol{\ell}'}(\omega) = \theta(\omega-\mu)\,\mathcal{A}^{>}_{\boldsymbol{\ell},\boldsymbol{\ell}'}(\omega) - \theta(\mu-\omega)\,\mathcal{A}^{<}_{\boldsymbol{\ell},\boldsymbol{\ell}'}(\omega). \tag{L.20}$$

The diagonal elements $\mathcal{A}^{>}_{\boldsymbol{\ell},\boldsymbol{\ell}} = |\langle\psi_\nu|b^\dagger_{\boldsymbol{\ell}}|\psi_0\rangle|^2\ \delta(\omega-(E_\nu-E_0))$ of the lesser spectral function have a direct physical interpretation: take the many-particle ground state $|\psi_0\rangle$ and add one particle at site $\boldsymbol{\ell}$. This gives us a different many-particle state, proportional to $b^\dagger_{\boldsymbol{\ell}}|\psi_0\rangle$, which is not necessarily an eigenstate of H, but can nevertheless be expressed in the basis of many-particle eigenstates $|\psi_\nu\rangle$ of H with some expansion coefficients c_ν, i.e.

$$b^\dagger_{\boldsymbol{\ell}}|\psi_0\rangle = \sum_\nu c_\nu|\psi_\nu\rangle. \tag{L.21}$$

We can now ask for the probability that this state is in **any** many-particle eigenstate at energy $(E_\nu - E_0)$. This probability is proportional[1] to $\sum_\nu{}' |c_\nu|^2 = \sum_\nu{}' |\langle\psi_\nu|b^\dagger_{\boldsymbol{\ell}}|\psi_0\rangle|^2$, where the dashed sum $\sum_\nu{}'$ implicitly denotes the summation over all many-particle state with energy $(E_\nu - E_0)$ only. From the representation in Eq. (L.14) it can be seen that this relative probability is exactly the prefactor of the delta-function at this energy. In other words, the greater spectral function is, up to an overall prefactor, nothing but the probability density to measure an energy ω if we perform an energy measurement on the state, where a single particle was added on site $\boldsymbol{\ell}$ to the initial ground state $|\psi_0\rangle$. An analogous interpretation can be found for the diagonal elements of the lesser spectral function, but here a particle is removed at the site $\boldsymbol{\ell}$ and the contribution in the spectral function is at the negative frequency. In the number-conserving case where each eigenstate can be labeled with a fixed particle number, only $(N-1)$-particle states contribute to the lesser spectral function and only $(N+1)$-particle states contribute to the greater spectral function if the initial ground state contains N particles.

If a different single particle basis is used, the interpretation is similar: here one particle is created or annihilated from the ground state in the respective single particle basis orbital. The spectral function becomes particularly simple in the case of a non-interacting system: Here the N-particle ground state is given by the state where all particles occupy the lowest single particle orbital for the bosonic case, or a filled up Fermi sea in the fermionic case. If we consider the diagonal elements of the spectral function in the basis of single particle energy eigenstates, adding or annihilating a single particle in any orbital again leads to a many-particle energy eigenstate (unless the state is annihilated). Thus, for the respective single particle orbital index, the spectral function consists of two δ-peaks above and below the chemical potential $\mu+\epsilon$ and $\mu-\epsilon$, where ϵ is the corresponding single particle energy.

L.3 Reconstructing the Green's Functions from the Spectral Functions

In the previous section it was shown how the full spectral functions can be obtained from any of the Green's functions. Conversely, all the Green's functions can also be constructed from the spectral function through

[1] The overall normalization is easily determined from the sum over all coefficients c_ν, but unimportant here.

$$\begin{aligned} G_{\boldsymbol{\ell},\boldsymbol{\ell}'}(\omega) &= \int_{-\infty}^{\infty} d\omega' \left(\frac{\mathcal{A}^{>}_{\boldsymbol{\ell},\boldsymbol{\ell}'}(\omega')}{\omega - \omega' + i0^+} - \frac{\mathcal{A}^{<}_{\boldsymbol{\ell},\boldsymbol{\ell}'}(\omega')}{\omega - \omega' - i0^+} \right) \\ &= \int_{-\infty}^{\infty} d\omega' \, \frac{\mathcal{A}_{\boldsymbol{\ell},\boldsymbol{\ell}'}(\omega')}{\omega - \omega' + i0^+ \operatorname{sgn}(\omega' - \mu)} \end{aligned} \tag{L.22}$$

$$G^{r/a}_{\boldsymbol{\ell},\boldsymbol{\ell}'}(\omega) = \int_{-\infty}^{\infty} d\omega' \, \frac{\mathcal{A}_{\boldsymbol{\ell},\boldsymbol{\ell}'}(\omega')}{\omega - \omega' \pm i0^+}. \tag{L.23}$$

These relations are valid in any single particle basis and can directly be seen from the structure of the spectral function in Eq. (L.11) and the Green's functions in Eqns. (L.6, L.8). The second line in Eq. (L.22) again applies to the particle number conserving case.

L.4 Single Particle Operator Expectation Values

The expectation values of any single particle operator can be calculated from the single particle spectral functions, which can be seen from the fact that the single particle density matrix can be obtained from the spectral function by integration over all frequencies below μ

$$\begin{aligned} \rho_{\boldsymbol{\ell},\boldsymbol{\ell}'} &= \langle \psi_0 | b^\dagger_{\boldsymbol{\ell}} \, b_{\boldsymbol{\ell}'} | \psi_0 \rangle \\ &= \int_{-\infty}^{\infty} d\omega \; \mathcal{A}^{<}_{\boldsymbol{\ell}',\boldsymbol{\ell}}(\omega) \\ &= -\int_{-\infty}^{\mu} d\omega \; \mathcal{A}_{\boldsymbol{\ell}',\boldsymbol{\ell}}(\omega). \end{aligned} \tag{L.24}$$

For instance the quasi-momentum distribution can directly be extracted from the diagonal part of the spectral function expressed in the basis of Bloch states

$$\begin{aligned} n(\mathbf{k}) &= \langle a^\dagger_{\mathbf{k}} a_{\mathbf{k}} \rangle \\ &= \int_{-\infty}^{\mu} d\omega \, \mathcal{A}_{\mathbf{k},\mathbf{k}}(\omega). \end{aligned} \tag{L.25}$$

L.5 Density of States

The single-particle density of states, which is defined as the trace of the spectral function

$$\mathrm{DOS}(\omega) = \sum_{\boldsymbol{\ell}} \mathcal{A}_{\boldsymbol{\ell},\boldsymbol{\ell}}(\omega). \tag{L.26}$$

Since, for any fixed frequency, it transforms like a single particle operator under a unitary transformation of the single particle basis (under which the trace is invariant), it is independent of the choice of the single particle basis and in this sense a universal, frequency dependent function. It is a measure for the number of many-particle states per energy interval, containing one particle more (for frequencies above the chemical potential) or one particle less (for frequencies below the chemical potential) than the many-particle ground state.

M. Technical Details of the SMFT

M.1 Multi-Grid discretization

To employ the FFT algorithm an equidistant grid is required, which is not compatible with having a very high resolution at small values of ψ ($\sim 10^{-9}$) to capture the behavior in the vicinity of the SF-insulator transition, as well as simultaneously correctly describing the distribution at large values ($\psi \sim 1$). To circumvent this problem, we use a superposition of equidistant grids, which enables us to use the FFT algorithm on each of these grids individually (see Fig. M.1).

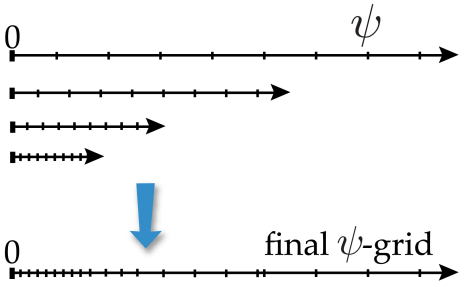

Figure M.1: Illustration of the multi-grid procedure.

This procedure relies on the following property of the convolution (12.3): the Z-fold convolution of the truncated function $P_t(\psi) = \Theta(a-\psi)\,P(\psi)$ with $P(\psi) = 0$ for $\psi < 0$ and $a < \psi_{\max}/Z$ is identical to the Z-fold convolution of $P(\psi)$ up to an easily determinable normalization constant on the interval $[0, a]$. Here $\psi_{\max}$ is the largest value of the grid, if this is finite (as in the discretized numerical case). In our calculations the number of grids used (typically $\approx 1 \ldots 6$) with $200 \ldots 1000$ points per grid is adjusted dynamically within the iteration procedure, depending on the position of the most likely value of $P(\psi)$ and the convergence properties.

M.2 Numerical calculation of the CDF $F(\psi|\eta)$ for box disorder

We found the numerically most efficient method for calculating and tabulating the two-dimensional CDF $F(\psi|\eta)$ to be the following:

For every fixed value of η, consider the function (12.6) $g(\mu', \eta)$ on the interval $\mu' = (\mu - \epsilon) \in [\mu - \Delta/2, \mu + \Delta/2]$. We define the local minima and maxima of this function (including the

end points) in increasing order as $\{\mu_1^{\min}, \mu_2^{\min}, \ldots\}$ and $\{\mu_1^{\max}, \mu_2^{\max}, \ldots\}$. Furthermore the n-th monotonically increasing and decreasing function on the restricted interval, provided that this interval exists, is denoted by

$$g^{(\mathrm{inc},n)}(\mu', \eta) = g(\mu', \eta) \quad \text{for} \quad \mu' \in (\mu_n^{\min}, \tilde{\mu}_n^{\max}) \tag{M.1}$$

$$g^{(\mathrm{dec},n)}(\mu', \eta) = g(\mu', \eta) \quad \text{for} \quad \mu' \in (\mu_n^{\max}, \tilde{\mu}_n^{\min}) \tag{M.2}$$

where

$$\tilde{\mu}_n^{\max} = \min_m \{\mu_m^{\max} | \mu_m^{\max} > \mu_n^{\min}\} \tag{M.3}$$

$$\tilde{\mu}_n^{\min} = \min_m \{\mu_m^{\min} | \mu_m^{\min} > \mu_n^{\max}\} \tag{M.4}$$

By construction, these functions are invertible in μ' within the defined range, allowing us to introduce the functions

$$h^{(\mathrm{inc},n)}(\psi, \eta) = \begin{cases} 0 & \text{if } \psi \leq g(\mu_n^{\min}, \eta) \\ \left(g^{(\mathrm{inc},n)}\right)^{-1}(\psi, \eta) - \mu_n^{\min} & \text{if } \psi \in (g(\mu_n^{\min}, \eta),\ g(\tilde{\mu}_n^{\max}, \eta)) \\ 1 & \text{if } \psi \geq g(\tilde{\mu}_n^{\max}, \eta) \end{cases} \tag{M.5}$$

$$h^{(\mathrm{dec},n)}(\psi, \eta) = \begin{cases} 0 & \text{if } \psi \leq g(\tilde{\mu}_n^{\min}, \eta) \\ \tilde{\mu}_n^{\min} - \left(g^{(\mathrm{dec},n)}\right)^{-1}(\psi, \eta) & \text{if } \psi \in (g(\tilde{\mu}_n^{\min}, \eta),\ g(\mu_n^{\max}, \eta)) \\ 1 & \text{if } \psi \geq g(\mu_n^{\max}, \eta) \end{cases} \tag{M.6}$$

in terms of which the CDF can be written as a superposition

$$F_\eta(\psi) = \frac{1}{\Delta} \sum_n \left(h^{(\mathrm{dec},n)}(\psi, \eta) + h^{(\mathrm{inc},n)}(\psi, \eta) \right) \tag{M.7}$$

M.3 PDF for a product of random variables

Including hopping disorder into the SMFT leads to the task of having to calculate the probability distribution for the newly defined random variable $\phi = J\psi$, if the PDFs for J and ψ are known functions $p_J(J)$ and $P(\psi)$. This can be done by taking the logarithm $s = \ln(\phi) = x + y$ and using the convolution theorem for the PDFs $P_x(x) = e^x\, P_J(e^x)$ (analogously for $P_y(y)$) of the random variables $x = \ln(J)$ and $y = \ln(\psi)$. The resulting distribution for ϕ can be denoted in compact form as

$$P_\phi(\phi) = \int dx\, P_J(e^x)\, P(\phi \cdot e^{-x}). \tag{M.8}$$

Using the FFT-algorithm for the numerical computation of this operation leads to a vast increase in performance, however it requires the functions $P_x(x)$ and $P_y(y)$ to be interpolated on an equidistant grid.

M.4 Compressibility in the insulating phases

In the special case with $P(\psi) = \delta(\psi)$, the disorder integration can be performed explicitly and expressions for the density and the compressibility can be found. Using partial integration and the property $\lim_{\epsilon\to\infty} p(\pm\epsilon) = 0$ for the on-site probability distribution, the disorder averaged density at finite temperature can be expressed as

$$\begin{aligned} \overline{n}(\beta, U, \mu, \Delta) &= \int d\epsilon\, p(\epsilon)\, \frac{\sum_{m=0}^{\infty} m e^{-\beta E_m(U, \mu-\epsilon)}}{\sum_{m=0}^{\infty} e^{-\beta E_m(U, \mu-\epsilon)}} \\ &= -\frac{1}{\beta} \int d\epsilon\, p(\epsilon)\, \frac{\partial}{\partial \epsilon} \left(\ln \sum_m e^{-\beta E_m(\mu-\epsilon)} \right) \\ &= \frac{1}{\beta} \int d\epsilon\, \frac{\partial p(\epsilon)}{\partial \epsilon} \left(\ln \sum_m e^{-\beta E_m(\mu-\epsilon)} \right) \end{aligned} \tag{M.9}$$

with $E_m(U,\mu') = Um(m-1)/2 - \mu' m$.

In the specific case of box disorder with

$$\frac{\partial p(\epsilon)}{\partial \epsilon} = \frac{1}{\Delta}[\delta(\epsilon+\Delta/2) - \delta(\epsilon-\Delta/2)] \tag{M.10}$$

the disorder averaged density takes on the form

$$\overline{n}(\beta,U,\mu,\Delta) = \frac{1}{\Delta\beta}\ln\left[\frac{\sum_m e^{-\beta E_m(\mu+\Delta/2)}}{\sum_m e^{-\beta E_m(\mu-\Delta/2)}}\right] \tag{M.11}$$

and the compressibility $\kappa = \frac{\partial \overline{n}}{\partial \mu}$ can be directly evaluated

$$\kappa = \frac{1}{\beta}\left(\frac{\sum_m m\, e^{-\beta E_m(\mu+\Delta/2)}}{\sum_m e^{-\beta E_m(\mu+\Delta/2)}} - \frac{\sum_m m\, e^{-\beta E_m(\mu-\Delta/2)}}{\sum_m e^{-\beta E_m(\mu-\Delta/2)}}\right). \tag{M.12}$$

For speckle disorder, on the other hand, one has

$$\frac{\partial p(\epsilon)}{\partial \epsilon} = \frac{\delta(\epsilon)}{\Delta} - \frac{\Theta(\epsilon)}{\Delta^2}e^{-\epsilon/\Delta} \tag{M.13}$$

and the compressibility takes on the form

$$\begin{aligned}\kappa = \frac{1}{\Delta}\Bigg[&\frac{\sum_m m\, e^{-\beta E_m(\mu)}}{\sum_m e^{-\beta E_m(\mu)}} \\ &-\frac{1}{\Delta}\int_0^\infty d\epsilon\, e^{-\frac{\epsilon}{\Delta}}\frac{\sum_m m\, e^{-\beta E_m(\mu-\epsilon)}}{\sum_m e^{-\beta E_m(\mu-\epsilon)}}\Bigg].\end{aligned} \tag{M.14}$$

M.5 Local Green's functions and DOS

To obtain the local DOS in an insulating phase, we calculate the single particle Green's functions

$$\begin{aligned} G^{>}(t) &= \langle b(t) b^\dagger(0)\rangle \\ G^{<}(t) &= \langle b^\dagger(0) b(t)\rangle \\ G(t) &= -i[\Theta(t)\, G^{>}(t) + \Theta(-t)\, G^{<}(t)] \end{aligned} \tag{M.15}$$

for local Fock states at finite temperature, where $b(t)$ is the on-site particle annihilation operator in the Heisenberg representation. The Fourier transformed Green's function can be calculated and takes on the form

$$\begin{aligned}\tilde{G}(\omega) &= \int_{-\infty}^{\infty} dt\, e^{i\omega t} G(t) \\ &= \lim_{\gamma\searrow 0}\frac{1}{Z(\mu')}\sum_{m=0}^{\infty} e^{-\beta(\frac{U}{2}m(m-1)-\mu' m)} \\ &\quad\times\left[(m+1)\frac{\omega - Um + \mu' - i\gamma}{(\omega - Um+\mu')^2+\gamma^2}\right. \\ &\quad\left. -m\frac{\omega - U(m-1)+\mu' - i\gamma}{(\omega - U(m-1)+\mu')^2+\gamma^2}\right],\end{aligned} \tag{M.16}$$

where $Z(\mu) = \sum_{m=0}^{\infty} e^{-\beta(\frac{U}{2}m(m-1)-\mu m)}$ is the local partition function. This is related to the single particle DOS by

$$\begin{aligned}\rho(\omega,\mu') &= -\frac{1}{\pi}\mathrm{Im}(\tilde{G}(\omega)) \\ &= \frac{1}{Z(\mu')}\sum_{m=0}^{\infty} e^{-\beta(\frac{U}{2}m(m-1)-\mu' m)}\left[(m+1)\right. \\ &\left.\times\delta(\omega-Um+\mu')+m\delta(\omega-U(m-1)+\mu')\right].\end{aligned} \tag{M.17}$$

Averaging over the on-site energy distribution for speckle disorder leads to the final expression

$$\begin{aligned}\overline{\rho}(\omega,\mu,\Delta,\beta) &= \int d\epsilon\, p(\epsilon)\,\rho(\omega,\mu-\epsilon) \\ &= \frac{1}{\Delta}\sum_{m=0}^{\infty}\frac{(m+1)\,\Theta(\omega-Um+\mu)}{Z(Um-\omega)} \\ &\quad\times e^{-\frac{\omega-Um+\mu}{\Delta}-\beta(m\omega-\frac{U}{2}m(m+1))}[1+e^{-\beta\omega}],\end{aligned} \tag{M.18}$$

whereas for a box disorder distribution one obtains [97]

$$\begin{aligned}\overline{\rho}(\omega,\mu,\Delta,\beta) = \frac{1}{\Delta}\sum_{m=0}^{\infty}(m+1)\frac{\Theta(\frac{\Delta}{2}-|\omega-Um+\mu|)}{Z(Um-\omega)} \\ \times\left[e^{-\beta E_m(Um-\omega)}+e^{-\beta E_{m+1}(Um-\omega)}\right].\end{aligned} \tag{M.19}$$

M.6 Method of incorporating thermal fluctuations explicitly into SMFT

Instead of performing the thermal average before constructing the conditional probability distribution for ψ, the SMFT furthermore also allows to explicitly facilitate the thermal fluctuations of ψ in the probability distribution. We have not yet performed the numerical calculation, but will outline the procedure.

$$P(\psi|\eta) = \frac{d}{d\psi}\int d\epsilon\, p(\epsilon)\,\Theta\left[\psi-\frac{\mathrm{Tr}\left(b\,e^{-\beta H(\eta,\epsilon)}\right)}{\mathrm{Tr}\left(e^{-\beta H(\eta,\epsilon)}\right)}\right], \tag{M.20}$$

where $\Theta(x)$ is the Heaviside step function.

This can be formulated in the following way: for fixed external parameter η (hence **conditional** probability distribution) the on-site energy is randomly drawn from $p(\epsilon)$ and the resulting single site Hamiltonian is diagonalized. For the different eigenstates $|i(\epsilon,\eta)\rangle$ with eigenenergies E_i the respective expectation value $\langle i(\epsilon,\eta)|b|i(\epsilon,\eta)\rangle$ is calculated. Within the grand canonical ensemble, this expectation value has the probability $\left[\mathrm{Tr}\left(e^{-\beta H(\eta,\epsilon)}\right)\right]^{-1} e^{-\beta E_i}$ of occurring. This probability is uncorrelated to the probability of a certain on-site energy ϵ occurring. Expressing this mathematically, we obtain the explicit formula for the conditional probability distribution

$$\begin{aligned}P(\psi|\eta) = &\frac{d}{d\psi}\int d\epsilon\, p(\epsilon)\,\left[\mathrm{Tr}\left(e^{-\beta H(\eta,\epsilon)}\right)\right]^{-1} \\ &\times\sum_{i=1}^{\infty} e^{-\beta E_i(\eta,\epsilon)}\,\Theta\left[\psi-\langle i(\epsilon,\eta)|b|i(\epsilon,\eta)\rangle\right]\end{aligned} \tag{M.21}$$

Equivalently on a formal level, one may work with the cumulative conditional probability function

$$\begin{aligned}F(\psi|\eta) = &\int d\epsilon\, p(\epsilon)\,\left[\mathrm{Tr}\left(e^{-\beta H(\eta,\epsilon)}\right)\right]^{-1} \\ &\times\sum_{i=1}^{\infty} e^{-\beta E_i(\eta,\epsilon)}\,\Theta\left[\psi-g_i(\mu-\epsilon,\eta)\right]\end{aligned} \tag{M.22}$$

with

$$g_i(\mu - \epsilon, \eta) = \langle i(\epsilon, \eta)|b|i(\epsilon, \eta)\rangle. \tag{M.23}$$

To evaluate the expression

$$q_i(\psi) = \int d\epsilon\, f_i(\epsilon)\, \Theta(\psi - g_i(\mu - \epsilon, \eta)) \tag{M.24}$$

we perform a variable substitution

$$\epsilon \mapsto x_i(\epsilon) \tag{M.25}$$

and subsequently

$$dx_i = \underbrace{\frac{dx_i(\epsilon)}{d\epsilon}}_{f_i(\epsilon)} d\epsilon. \tag{M.26}$$

Using the central theorem of calculus one can explicitly construct

$$x_i(\epsilon) = \int_{-\infty}^{\epsilon} d\epsilon'\, f_i(\epsilon'). \tag{M.27}$$

Since

$$f_i(\epsilon) = p(\epsilon)\, \frac{e^{-\beta E_i(\epsilon,\eta)}}{\mathrm{Tr}\left(e^{-\beta H(\epsilon,\eta)}\right)} \tag{M.28}$$

is a non-negative function the monotonously increasing function $x_i(\epsilon) \leftrightarrow \epsilon_i(x)$ is invertible in the relevant range. The conditional cumulative density function can then be explicitly calculated from

$$F(\psi|\eta) = \sum_{i=1}^{\infty} \int dx\, \Theta(\psi - g_i(\mu - \epsilon_i(x)), \eta) \tag{M.29}$$

As in the SMFT for $T = 0$, the self-consistency condition reads

$$P(\psi) = \frac{d}{d\psi} \int_0^{\infty} d\eta\, Q(\eta)\, F(\psi|\eta), \tag{M.30}$$

where $Q(\eta)$ is the $Z-$fold convolved and rescaled function of $P(\psi)$ with the random variable $\eta = J \sum_{i=1}^{Z} \psi_i$. The conditional cumulative density $F(\psi|\eta)$ now also contains the thermal fluctuations explicitly in the distribution (i.e. they are not averaged over within the self-consistency loop), so the subsequent determination of $P(\psi)$ is identical to the previous cases.

N. Dispersion of a Wave Packet for Various Dispersion Relations

Here we shortly discuss the effect the dispersion relation has on the temporal propagation of a wave packet. Let us consider a translationally invariant system, where the momentum k (or analogously the quasi-momentum in case of a lattice) is a quantum number for the energy eigenstates with the respective energy eigenvalue given by the dispersion relation $\epsilon(\mathbf{k})$. The real-space representation of the state we denote by $\psi(x,t) = \langle x|\psi(t)\rangle$ and the momentum representation as $\phi(k,t) = \langle k|\psi(t)\rangle$. The time evolved state can be expressed directly in momentum space, where the Hamiltonian is diagonal and each component of the momentum wave function simply obtains a momentum and time-dependent complex phase shift $e^{-i\epsilon(k)t}$. The real space representation of the time evolved state can also be given explicitly

$$|\psi(t)\rangle = \int dx \int dk\ \phi(k,0)\ e^{i(kx-\epsilon(k)t)}|x\rangle. \tag{N.1}$$

Linear Dispersion - Relativistic Particles

For a linear dispersion relation $\epsilon(k) = ck$ one thus directly finds the real-space wave function at some arbitrary time

$$\psi(x,t) = \int dk\ \phi(k,0)\ e^{ik(x-ct)}, \tag{N.2}$$

i.e. only the position is linearly translated in time $x \mapsto x - ct$. Hence, if only either positive or negative frequency components are present in the initial real space wave packet, it propagates at a constant velocity c without changing its shape otherwise $\psi(x,t) = \psi(x-ct,0)$.

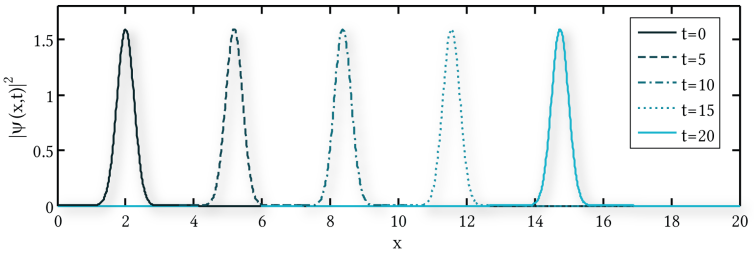

Figure N.1: Temporal evolution of a gaussian wave packet for a particle with a linear dispersion relation.

Note that the real space wave function corresponding to values of k with different sign, propagate in opposite direction. Hence, for a gaussian there is always a second wave packet propagating as $\tilde{\psi}(x,t) = \tilde{\psi}(x+ct,0)$. The weight of this second packet is however suppressed exponentially and usually negligible if the mean momentum k_0, around which the momentum space wave function is centered is much larger than the width of the momentum space wave function.

Quadratic Dispersion - Massive Particles

In contrast, if the dispersion relation is not linear, the different Fourier components (plane or Bloch waves) propagate at different, k-dependent velocities and the real-space wave function changes its shape with time, i.e. disperses. Specifically for a quadratic dispersion relation of a non-relativistic, massive particle $\epsilon(k) = \frac{k^2}{2m}$, one finds

$$\psi(x,t) = \int dk\ \phi(k,0)\ e^{ik(x-\frac{k}{2m}t)}. \tag{N.3}$$

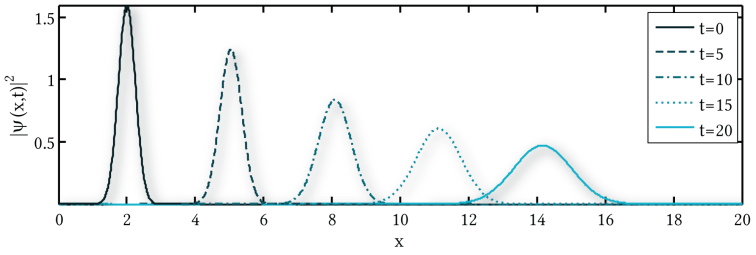

Figure N.2: Temporal evolution of a gaussian wave packet for a massive particle with a quadratic dispersion relation. In this special case, the density profile always remains gaussian, but broadens linearly in time at a rate proportional to the inverse mass.

Bogoliubov Dispersion

We consider the case of the free space Bogoliubov dispersion relation

$$\epsilon(k) = \sqrt{\left(\frac{k^2}{2m}\right)^2 + 2g|\psi|^2\frac{k^2}{2m}}. \tag{N.4}$$

For small momenta (relative to the inverse healing length), the linear term dominates, whereas the quadratic term dominates for large momenta. If the width of the momentum space wave function of the spatially localized wave packet is very narrow compared to the structure of the dispersion relation at wave packet's typical momentum, it is a good approximation to linearize the dispersion relation at that point and propagation of the wave packet will be mainly non-dispersive with a velocity corresponding to the local slope.

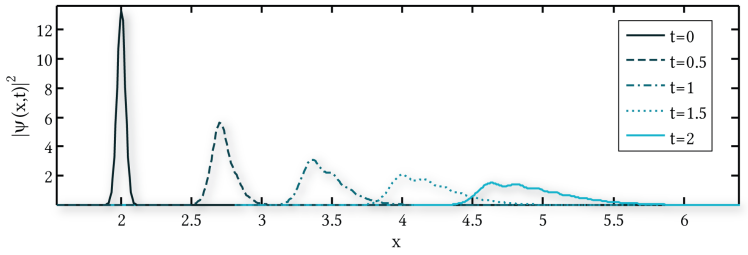

Figure N.3: Propagation of an initial gaussian state for a particle with a Bogoliubov dispersion relation. Not only does the spatial wave function broaden with time, but also looses its reflectional symmetry.

Here we however prepare a spatially narrow wave packet, which has significant frequency components throughout the linear regime of the dispersion relation, but also extends somewhat beyond into the quadratic regime. As shown in Fig. (N.3), the wave packet then disperses and broadens, but also takes on an asymmetric shape with increasing time, in contrast to the case of a purely linear or quadratic dispersion relation. This can be understood from the k-dependence of the sound velocity of each frequency component: due to the admixture of the quadratic term, higher frequency components of the wave packet travel faster than the low frequency components, which all have a constant velocity $c = \sqrt{\frac{g|\psi|^2}{m}}$ in the limit of low momenta.

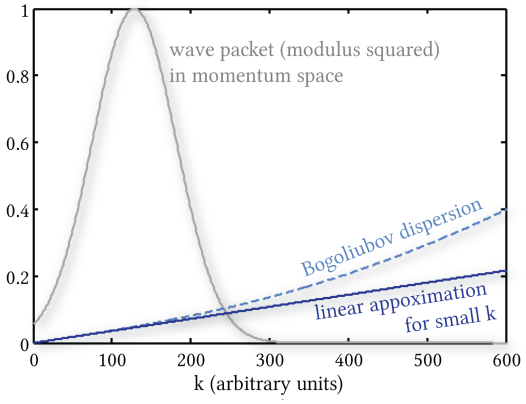

Figure N.4: The specific Bogoliubov dispersion relation used for the propagation in the above figure and the linear approximation for small k are shown as light and dark blue lines respectively. $|\phi(k,t)|^2$, which does not change in time is shown in gray and contains momenta throughout the linear regime, but also components where the energy significantly deviates from the linear behavior and thus lead to dispersive behavior. All quantities are rescaled for visual clarity.

O. Discrete Fourier Transform of a Quadratic Function

The aim of this section is to evaluate $|F(n)|^2$, physically corresponding to the quasi-momentum distribution of the condensate state at certain points in time after evolving in a harmonic confining potential, with

$$F(n) = \sum_{l=0}^{L-1} e^{2\pi i \frac{nl}{L}} \, e^{2\pi i \frac{l^2}{m}}. \tag{O.1}$$

Here $n, L \in \mathbb{N}$ are integers and L is an integer multiple of m, i.e. $L/m \in \mathbb{N}$, to avoid broadening of the peaks in the resulting spectrum. This is a discrete Fourier transform of a quadratic function on a finite interval, but its explicit analytic solution has not been presented to to date to the best of the author's knowledge.

The summation integer l is split into $l = p+qm$, where the newly defined integers can independently take on values in the ranges $p \in \{0, \ldots, m-1\}$ and $q \in \{0, \ldots, \frac{L}{m} - 1\}$. Thus, the previous sum can be written as

$$\begin{aligned} F(n) &= \sum_{p=0}^{m-1} \sum_{q=0}^{\frac{L}{m}-1} e^{2\pi i \frac{n}{L}(p+qm)} \, e^{2\pi i \frac{(p+qm)^2}{m}} \\ &= \sum_{q=0}^{\frac{L}{m}-1} e^{2\pi i \frac{m}{L} nq} \sum_{p=0}^{m-1} e^{2\pi i (\frac{np}{L} + \frac{p^2}{m})} \end{aligned} \tag{O.2}$$

Using the identity

$$\sum_{n=0}^{N-1} e^{2\pi i \frac{k-k'}{N} n} = N \delta_{k,k'}, \tag{O.3}$$

for $N = \frac{L}{m}$, one obtains

$$F(n) = \frac{L}{m} \, \delta_{n \bmod \frac{L}{m}, 0} \sum_{p=0}^{m-1} e^{2\pi i (\frac{np}{L} + \frac{p^2}{m})}. \tag{O.4}$$

This restricts the resulting spectrum to a form with non-zero values only at m periodically spaced positions $n = r\frac{L}{m}$ with $r \in \mathbb{N}$. To determine the value of the sum at these discrete values of n, it is convenient to define the function

$$g(r) = \sum_{p=0}^{m-1} e^{2\pi i (\frac{rp}{m} + \frac{p^2}{m})} \tag{O.5}$$

and it will now be shown that $|g(r)|^2$ is independent of $r \in \mathbb{N}$ for a fixed value of m.

$$\begin{aligned} |g(r)|^2 &= \sum_{p,p'=0}^{m-1} e^{2\pi i (r\frac{p-p'}{m} + \frac{p^2-p'^2}{m})} \\ &= m + \sum_{p=1}^{m-1}\sum_{p'=0}^{p-1} \left[e^{2\pi i (r\frac{p-p'}{m} + \frac{(p+p')(p-p')}{m})} + \text{h.c.} \right]. \end{aligned} \tag{O.6}$$

We now perform a transformation of the summation indices and define $d = p - p'$ and $s = p + p'$. The summation over all terms can be reexpressed in the new variables as

$$\sum_{p=1}^{m-1}\sum_{p'=0}^{p-1} \mapsto \sum_{d=1}^{m-1} \sum_{\substack{s=d \\ \text{step } 2}}^{2(m-1)-d} . \tag{O.7}$$

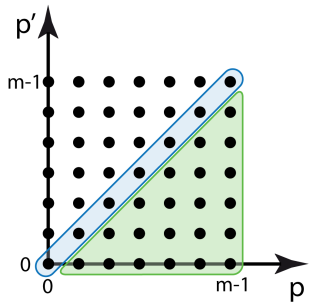

Figure O.1: Illustration of the resummation procedure. The sum of the diagonal values amounts to m, while the values in the lower right triangle correspond to the complex conjugated values in the upper left triangle, mirrored on the diagonal. A summation over $s = p + p'$ at fixed $d = p - p'$ can be understood as sums of the d-th lower off-diagonal, where subsequent values of s are spaced by 2.

Subsequently,

$$\begin{aligned} |g(r)|^2 &= m + \sum_{d=1}^{m-1} \sum_{\substack{s=d \\ \text{step } 2}}^{2(m-1)-d} \left[e^{2\pi i (r\frac{d}{m} + \frac{sd}{m})} + \text{h.c.} \right] \\ &= m + \sum_{d=1}^{m-1} \left[e^{2\pi i r \frac{d}{m}}\, h(d,m) + \text{h.c.} \right], \end{aligned} \tag{O.8}$$

where we defined the function

$$h(d,m) = \sum_{q=\frac{d}{2}}^{m-1-\frac{d}{2}} e^{2\pi i \frac{2qd}{m}} \tag{O.9}$$

with the summation variable $q = s/2$ now running over values with a step size of 1. To evaluate this function for fixed m, the explicitly known expression for the geometric series can be used as long as $d \neq \frac{m}{2}$. In the latter case, it can easily be evaluated and Eq. (O.9) takes on a value $h(d = m/2, m) = (-1)^d\, d$, leading to the generally valid expression

$$
\begin{aligned}
h(d,m) &= (1-\delta_{d,m/2})\left(\frac{1-e^{4\pi i\frac{d}{m}(m-\frac{d}{2})}}{1-e^{4\pi i\frac{d}{m}}}-\frac{1-e^{4\pi i\frac{d}{m}\frac{d}{2}}}{1-e^{4\pi i\frac{d}{m}}}\right)+\delta_{d,m/2}(-1)^d\,d \\
&= (1-\delta_{d,m/2})\left(\frac{2e^{-2\pi i\frac{d}{m}}\sin(2\pi\frac{d^2}{m})\sin(2\pi\frac{d}{m})}{\cos(4\pi\frac{d}{m})-1}\right)+\delta_{d,m/2}(-1)^d\,d.
\end{aligned}
\tag{O.10}
$$

Inserting this result into Eq. (O.8), one obtains

$$
|g(r)|^2 = m+\delta_{0,m \bmod 2}\,(-1)^{\frac{m}{2}}\,m\,\cos(\pi r)+\sum_{d=1}^{m-1}(1-\delta_{d,m/2})\left(\frac{4\cos(2\pi\frac{d}{m}(r-1))\,\sin(2\pi\frac{d^2}{m})\,\sin(2\pi\frac{d}{m})}{\cos(4\pi\frac{d}{m})-1}\right)
\tag{O.11}
$$

The second term only contributes for even m, whereas the sum is identically equal to zero, as will now be shown. The term $(1-\delta_{d,m/2})$ ensures that only an even number of terms may contribute in the sum. This allows for a regrouping of terms and a corresponding resummation, where the terms $d=c$ and $d=m-c$ are considered as pairs, subsequently amounting to zero by using the periodicity and symmetry of the trigonometric functions:

$$
\begin{aligned}
|g(r)|^2 &= m+\delta_{0,m \bmod 2}\,(-1)^{\frac{m}{2}+r}\,m \\
&+\sum_{c=1}^{\lfloor\frac{m-1}{2}\rfloor}\left(\frac{4\cos(2\pi\frac{c}{m}(r-1))\,\sin(2\pi\frac{c^2}{m})\,\sin(2\pi\frac{c}{m})}{\cos(4\pi\frac{c}{m})-1}\right. \\
&\left.+\frac{4\cos(2\pi\frac{m-c}{m}(r-1))\,\sin(2\pi\frac{(m-c)^2}{m})\,\sin(2\pi\frac{m-c}{m})}{\cos(4\pi\frac{m-c}{m})-1}\right) \\
&= m(1+\delta_{0,m \bmod 2}\,(-1)^{\frac{m}{2}+r}).
\end{aligned}
\tag{O.12}
$$

We draw the connection to the quasi-momentum distribution from the condensate state in a harmonic trap at time t

$$
\begin{aligned}
n(\mathbf{k},t) &= \frac{1}{L}\sum_{l,l'}\phi_l(0)\phi_{l'}(0)^*\;e^{-i(ak-2tV_tl_0)(l-l')}\,e^{-itV_t(l^2-l'^2)} \\
&= \left|\frac{1}{\sqrt{L}}\sum_l\phi_l(0)\;e^{-i(ak-2tV_tl_0)l}\,e^{-itV_tl^2}\right|^2,
\end{aligned}
\tag{O.13}
$$

where the initial condensate state is $\phi_l(0)$. Assuming that the condensate is initially in a homogeneous state, i.e. $\phi_l(0)=\phi(0)=e^{i\varphi_0}L^{-\frac{1}{2}}$ with an irrelevant overall phase φ_0, the comparison of Eq. (O.13) with $F(n)$ shows that at the specific times $t=\frac{2\pi}{mV_t}$ by equating

$$
ak-\frac{4\pi}{m}l_0 = 2\pi\frac{n}{L}.
\tag{O.14}
$$

and using $r=\frac{mn}{L}$, one can relate

$$
\begin{aligned}
n(\mathbf{k},t) &= \frac{|\phi(0)|^2}{L}\left|F\left(n=\frac{akl}{2\pi}-\frac{2ll_0}{m}\right)\right|^2 \\
&= \frac{|\phi(0)|^2}{L}\frac{L^2}{m^2}\,\delta_{n \bmod \frac{L}{m},0}\left|g\left(\frac{akm}{2\pi}-2l_0\right)\right|^2.
\end{aligned}
\tag{O.15}
$$

Thus, at the specific time $t = \frac{2\pi}{mV_t}$

$$n(\mathbf{k},t) = \frac{1}{m}\delta_{\left(\frac{akm}{2\pi}-2l_0\right) \bmod 1\,,\,0} \times \left(1+\delta_{0,m \bmod 2}(-1)^{\frac{m}{2}+\frac{akm}{2\pi}-2l_0}\right). \tag{O.16}$$

If the condensate is initially not in a perfectly homogeneous state, but varies slowly in density, the peaks are broadened, but the underlying structure still remains.

For odd integer values of m, the term in brackets always takes on the value one and the momentum profile consists of an equidistant series of peaks at $k = \frac{2\pi}{am}(r + 2l_0)$ and $r \in \mathbb{Z}$. As required from the unitarity of the Fourier transform, the quasi-momentum profile is of course normalized $\sum_k n(\mathbf{k}, t = \frac{2\pi}{mV_t}) = 1$ at these certain times and each peak carries exactly the same weight $1/m$.

For even integer values of m, Eq. (O.16) can be written as

$$n(\mathbf{k},t) = \sqrt{\frac{2}{m}}\delta_{\left(\frac{m}{4}\left[1+\frac{ak}{\pi}\right]-l_0\right) \bmod 1\,,\,0} \tag{O.17}$$

and the quasi-momentum profile consists of only $m/2$ equally strong and equidistantly spaced peaks at $k = \frac{\pi}{a}\left[\frac{4}{m}(s + l_0) - 1\right]$ with $s \in \mathbb{Z}$.

This analytical result agrees perfectly with the results of our numerical simulations. To the best of our knowledge, this analytical expression, which is also of direct relevance for the Talbot effect in quantum optics, has not been obtained so far.

Acknowledgments

First of all, I would like to thank Prof. Dr. Walter Hofstetter for giving me the opportunity to write my thesis is his group. I am grateful for his support, many productive discussions, the possibility to visit numerous conferences and summer schools, as well as for the freedom he gave me in our wide field of research. I am also thankful to Prof. Dr. Roser Valenti, who agreed to referee this thesis despite her exceptionally full schedule.

Special thanks go to various people I had the pleasure of collaborating with on a number of projects. I particularly enjoyed the work with Sören Götze, who, in with his indiminishable enthusiasm, never became tired of answering questions and explaining experimental details to a theorist like me. Furthermore, I very much appreciate and enjoyed the numerous discussions with Andrew Daley, Lincoln Carr, Michael Fleischhauer, James Anglin, Klaus Sengstock, Eugene Demler, Immanuel Bloch. I thank Vincent Liu for not always accepting a diverging zero-point energy, which made me rethink ordering procedures and eventually, out of frustration, directed me towards the quantized version of the extended quasi-particle theory.

I particularly enjoyed the work (as well as many discussion beyond this) with Michael Buchhold with whom I had the pleasure to work together ever since the very beginning of his Bachelor thesis. Deep in my heart, he will always remain one of the greatest and most talented Bachelor students.

I truly enjoyed the great atmosphere and many pleasant experiences in our group over the years: a big thanks goes out to all of you. Special thanks go to David Roosen and Danny Cocks for always lending a helping hand over the years with various programming and network issues. The helping hands of Daniela Wirth-Pagano and Marie Haußels have made often made life somewhat easier, which I appreciate. Denis Semmler deserves a particular mention here: the numerous discussions, thousands of coffees, our collaboration and many hours we spent together in our office will remain a very pleasant memory.

A considerable amount of work was invested in the proof reading of this thesis, which inflicted suffering on Daniel Cocks, Michael Buchhold, Bernd Schmidt, Denis Semmler and Andrii Sotnikov, which I appreciate.

I am also very grateful to my family for their encouragement and helpfulness over the years. My deep gratitude goes to Sara Katrin for supporting and encouraging me over many years. Last but not least, a big thanks you goes to all my friends for the motivation and keeping me on track.

Bibliography

[1] Numerical Recipes 3rd Edition: The Art of Scientific Computing (9780521880688): William H. Press, Saul A. Teukolsky, William T. Vetterling, Brian P. Flannery: Books. URL: http://www.amazon.com/exec/obidos/ISBN=0521880688/numericalrecipesA/.

[2] J. Abo-Shaeer, C. Raman, and W. Ketterle. Formation and Decay of Vortex Lattices in Bose-Einstein Condensates at Finite Temperatures. Physical Review Letters, 88(7):1–4, February 2002. URL: http://link.aps.org/doi/10.1103/PhysRevLett.88.070409, doi:10.1103/PhysRevLett.88.070409.

[3] M. Aidelsburger, M. Atala, S. Nascimbène, S. Trotzky, Y.-a. Chen, and I. Bloch. Experimental Realization of Strong Effective Magnetic Fields in an Optical Lattice. Physical Review Letters, 107(25):1–5, December 2011. URL: http://link.aps.org/doi/10.1103/PhysRevLett.107.255301, doi:10.1103/PhysRevLett.107.255301.

[4] Ehud Altman, Eugene Demler, and Mikhail D. Lukin. Probing many-body states of ultra-cold atoms via noise correlations. PHYS.REV.A, 70:013603, 2004. URL: doi:10.1103/PhysRevA.70.013603.

[5] Marco Anderlini, Jennifer Sebby-Strabley, Jens Kruse, James V Porto, and William D Phillips. Controlled atom dynamics in a double-well optical lattice. Journal of Physics B: Atomic, Molecular and Optical Physics, 39(10):S199–S210, May 2006. URL: http://stacks.iop.org/0953-4075/39/i=10/a=S19.

[6] MH Anderson, JR Ensher, MR Matthews, CE Wieman, and EA Cornell. Observation of Bose-Einstein condensation in a dilute atomic vapor. science, 269(ii):4–7, 1995. URL: http://www.sciencemag.org/content/269/5221/198.short.

[7] P. Anderson. More is different. Science, 177:393, 1972.

[8] P. W. Anderson. Absence of Diffusion in Certain Random Lattices. Phys. Rev., 109(5):1492–1505, Mar 1958. doi:10.1103/PhysRev.109.1492.

[9] Mr Andrews, M Mewes, van Druten NJ, Ds Durfee, Dm Kurn, and W Ketterle. Direct, Nondestructive Observation of a Bose Condensate. Science (New York, N.Y.), 273(5271):84–7, July 1996. URL: http://www.ncbi.nlm.nih.gov/pubmed/8688055.

[10] W S Bakr, A Peng, M E Tai, R Ma, J Simon, J I Gillen, S Fölling, L Pollet, and M Greiner. Probing the superfluid-to-Mott insulator transition at the single-atom level. Science (New York, N.Y.), 329(5991):547–50, July 2010. URL: http://www.sciencemag.org/content/329/5991/547.abstract.

[11] Waseem S. Bakr, Jonathon I. Gillen, Amy Peng, Simon Fölling, and Markus Greiner. A quantum gas microscope for detecting single atoms in a hubbard-regime optical lattice. NATURE, 462:74, 2009. URL: doi:10.1038/nature08482.

[12] Waseem S Bakr, Philipp M Preiss, M Eric Tai, Ruichao Ma, Jonathan Simon, and Markus Greiner. Orbital excitation blockade and algorithmic cooling in quantum gases. Nature, 480(7378):500–3, December 2011. URL: http://dx.doi.org/10.1038/nature10668.

[13] Th. Best, S. Will, U. Schneider, L. Hackermüller, D. van Oosten, I. Bloch, and D.-S. Lühmann. Role of interactions in ^{87}Rb-^{40}**K** bose-fermi mixtures in a 3d optical lattice. Phys. Rev. Lett., 102:030408, Jan 2009. URL: http://link.aps.org/doi/10.1103/PhysRevLett.102.030408, doi:10.1103/PhysRevLett.102.030408.

[14] Juliette Billy, Vincent Josse, Zhanchun Zuo, Alain Bernard, Ben Hambrecht, Pierre Lugan, David Clément, Laurent Sanchez-Palencia, Philippe Bouyer, and Alain Aspect. Direct observation of Anderson localization of matter waves in a controlled disorder. Nature, 453(7197):891–4, June 2008. URL: http://dx.doi.org/10.1038/nature07000, doi:10.1038/nature07000.

[15] U. Bissbort and W. Hofstetter. Stochastic mean-field theory for the disordered Bose-Hubbard model. EPL (Europhysics Letters), 86(5):50007, June 2009. URL: http://stacks.iop.org/0295-5075/86/i=5/a=50007.

[16] Ulf Bissbort. Stochastic mean field theory for the disordered bose-hubbard model. Diploma Thesis, Goethe-Universität Frankfurt am Main, 2007.

[17] Ulf Bissbort, Sören Götze, Yongqiang Li, Jannes Heinze, Jasper Krauser, Malte Weinberg, Christoph Becker, Klaus Sengstock, and Walter Hofstetter. Detecting the Amplitude Mode of Strongly Interacting Lattice Bosons by Bragg Scattering. Physical Review Letters, 106(20), May 2011. URL: http://prl.aps.org/abstract/PRL/v106/i20/e205303, doi:10.1103/PhysRevLett.106.205303.

[18] Ulf Bissbort, Ronny Thomale, and Walter Hofstetter. Stochastic mean-field theory: Method and application to the disordered Bose-Hubbard model at finite temperature and speckle disorder. Physical Review A, 81(6), June 2010. URL: http://pra.aps.org/abstract/PRA/v81/i6/e063643, doi:10.1103/PhysRevA.81.063643.

[19] J.-P. Blaizot and G. Ripka. Quantum Theory of Finite Systems. MIT Press, Cambridge, MA, 1986.

[20] Immanuel Bloch, Jean Dalibard, and Wilhelm Zwerger. Many-body physics with ultracold gases. Rev. Mod. Phys., 80:885–964, Jul 2008. URL: http://link.aps.org/doi/10.1103/RevModPhys.80.885, doi:10.1103/RevModPhys.80.885.

[21] S.N. Bose. Plancks gesetz und lichtquantenhypothese. Zeitschrift für Physik A Hadrons and Nuclei, 26:178–181, 1924. 10.1007/BF01327326. URL: http://dx.doi.org/10.1007/BF01327326.

[22] S F Boys. Construction of Some Molecular Orbitals to Be Approximately Invariant for Changes from One Molecule to Another. Rev. Mod. Phys., 32:296–299, 1960. URL: http://rmp.aps.org/abstract/RMP/v32/i2/p296_1.

[23] Christian Brouder, Gianluca Panati, Matteo Calandra, Christophe Mourougane, and Nicola Marzari. Exponential Localization of Wannier Functions in Insulators. Physical Review Letters, 98(4):1–4, January 2007. URL: http://link.aps.org/doi/10.1103/PhysRevLett.98.046402, doi:10.1103/PhysRevLett.98.046402.

[24] R. Hanbury Brown and R.Q. Twiss. Correlation between photons in two coherent beams of light. NATURE, 177:27, 1956.

[25] Michael Buchhold. Zusammenbruch und neuentstehung makroskopischer kohärenz wechselwirkender bosonen im optischen gitter. Bachelor Thesis, Goethe-Universität Frankfurt am Main, 2010.

[26] B. Capogrosso-Sansone, N. V. Prokof'ev, and B. V. Svistunov. Phase diagram and thermodynamics of the three-dimensional Bose-Hubbard model. Physical Review B (Condensed Matter and Materials Physics), 75(13):134302, 2007. URL: http://link.aps.org/abstract/PRB/v75/e134302, doi:10.1103/PhysRevB.75.134302.

[27] Yvan Castin and Jean Dalibard. Relative phase of two Bose-Einstein condensates. Physical Review A, 55(6):4330–4337, June 1997. URL: http://pra.aps.org/abstract/PRA/v55/i6/p4330_1.

[28] M A Cazalilla, A F Ho, and T Giamarchi. Interacting bose gases in quasi-one-dimensional optical lattices. New Journal of Physics, 8(8):158, 2006. URL: http://stacks.iop.org/1367-2630/8/i=8/a=158.

[29] M. Chan, K. Blum, S. Murphy, G. Wong, and J. Reppy. Disorder and the Superfluid Transition in Liquid ˆ{4}He. Physical Review Letters, 61(17):1950–1953, October 1988. URL: http://prl.aps.org/abstract/PRL/v61/i17/p1950_1.

[30] D. Clément, P. Bouyer, A. Aspect, and L. Sanchez-Palencia. Density modulations in an elongated Bose-Einstein condensate released from a disordered potential. Physical Review A, 77(3), March 2008. URL: http://pra.aps.org/abstract/PRA/v77/i3/e033631.

[31] D. Clément, N. Fabbri, L. Fallani, C. Fort, and M. Inguscio. Exploring correlated 1d bose gases from the superfluid to the mott-insulator state by inelastic light scattering. Phys. Rev. Lett., 102:155301, Apr 2009. URL: http://link.aps.org/doi/10.1103/PhysRevLett.102.155301, doi:10.1103/PhysRevLett.102.155301.

[32] EA Cornell. Nobel Lecture: Bose-Einstein condensation in a dilute gas, the first 70 years and some recent experiments. Reviews of Modern Physics, 74(July), 2002. URL: http://rmp.aps.org/abstract/RMP/v74/i3/p875_1.

[33] M. Cramer. Interaction-Dependent Temperature Effects in Bose-Fermi Mixtures in Optical Lattices. Physical Review Letters, 106(21), May 2011. URL: http://prl.aps.org/abstract/PRL/v106/i21/e215302.

[34] M. Cramer, S. Ospelkaus, C. Ospelkaus, K. Bongs, K. Sengstock, and J. Eisert. Do Mixtures of Bosonic and Fermionic Atoms Adiabatically Heat Up in Optical Lattices? Physical Review Letters, 100(14), April 2008. URL: http://prl.aps.org/abstract/PRL/v100/i14/e140409.

[35] Andrea Damascelli, Zahid Hussain, and Zhi-Xun Shen. Angle-resolved photoemission studies of the cuprate superconductors. Rev. Mod. Phys., 75:473–541, Apr 2003. URL: http://link.aps.org/doi/10.1103/RevModPhys.75.473, doi:10.1103/RevModPhys.75.473.

[36] Long Dang, Massimo Boninsegni, and Lode Pollet. Disorder-induced superfluidity. Physical Review B, 79(21), June 2009. URL: http://prb.aps.org/abstract/PRB/v79/i21/e214529.

[37] Tung-Lam Dao, Antoine Georges, Jean Dalibard, Christophe Salomon, and Iacopo Carusotto. Measuring the one-particle excitations of ultracold fermionic atoms by stimulated raman spectroscopy. Phys. Rev. Lett., 98:240402, Jun 2007. URL: http://link.aps.org/doi/10.1103/PhysRevLett.98.240402, doi:10.1103/PhysRevLett.98.240402.

[38] K B Davis, M R Andrews, N J Van Druten, D S Durfee, D M Kurn, and W Ketterle. P HYSICAL R EVIEW LETTERS. Phys. Rev. Lett., 75(November):3969–3973, 1995.

[39] B. Deissler, M. Zaccanti, G. Roati, C. DŠErrico, M. Fattori, M. Modugno, G. Modugno, and M. Inguscio. Delocalization of a disordered bosonic system by repulsive interactions. Nature Physics, 6(5):354–358, April 2010. URL: http://dx.doi.org/10.1038/nphys1635.

[40] Luca DellŠAnna, Stefano Fantoni, Pasquale Sodano, and Andrea Trombettoni. Critical temperature of non-interacting Bose gases on disordered lattices. Journal of Statistical Mechanics: Theory and Experiment, 2008(11):P11012, November 2008. URL: http://stacks.iop.org/1742-5468/2008/i=11/a=P11012.

[41] B. DeMarco, C. Lannert, S. Vishveshwara, and T.-C. Wei. Structure and stability of Mott-insulator shells of bosons trapped in an optical lattice. Physical Review A, 71(6), June 2005. URL: http://pra.aps.org/abstract/PRA/v71/i6/e063601.

[42] D. Dickerscheid, D. van Oosten, P. Denteneer, and H. Stoof. Ultracold atoms in optical lattices. Physical Review A, 68(4), October 2003. URL: http://pra.aps.org/abstract/PRA/v68/i4/e043623.

[43] O Dutta, A Eckardt, P Hauke, B Malomed, and M Lewenstein. BoseŰHubbard model with occupation-dependent parameters. New Journal of Physics, 13(2):023019, February 2011. URL: http://stacks.iop.org/1367-2630/13/i=2/a=023019.

[44] Clyde Edmiston and Klaus Ruedenberg. Localized atomic and molecular orbitals. Rev. Mod. Phys., 35:457–464, Jul 1963. URL: http://link.aps.org/doi/10.1103/RevModPhys.35.457, doi:10.1103/RevModPhys.35.457.

[45] A. Einstein. Quantentheorie des einatomigen idealen gases. Sitzungsbericht der Preussischen Akademie der Wissenschaften, (22):261, 1925.

[46] P. T. Ernst, S. Götze, J. S. Krauser, K. Pyka, D. S. Lühmann, D. Pfannkuche, and K. Sengstock. Momentum-resolved bragg spectroscopy in optical lattices. NATURE PHYSICS, 6:56, 2009. URL: doi:10.1038/nphys1476.

[47] N. Fabbri, D. Clément, L. Fallani, C. Fort, M. Modugno, K. M. R. van der Stam, and M. Inguscio. Excitations of bose-einstein condensates in a one-dimensional periodic potential. Phys. Rev. A, 79:043623, Apr 2009. URL: http://link.aps.org/doi/10.1103/PhysRevA.79.043623, doi:10.1103/PhysRevA.79.043623.

[48] L. Fallani, J. Lye, V. Guarrera, C. Fort, and M. Inguscio. Ultracold Atoms in a Disordered Crystal of Light: Towards a Bose Glass. Physical Review Letters, 98(13), March 2007. URL: http://prl.aps.org/abstract/PRL/v98/i13/e130404, doi:10.1103/PhysRevLett.98.130404.

[49] PO Fedichev, GV Shlyapnikov, and J. T. M. Walraven. Damping of low-energy excitations of a trapped Bose-Einstein condensate at finite temperatures. Physical review letters, 80(11):2269–2272, 1998. URL: http://link.aps.org/doi/10.1103/PhysRevLett.80.2269.

[50] A.L. Fetter. Nonuniform states of an imperfect Bose gas. Annals of physics, 70(1):67–101, 1972. URL: http://www.sciencedirect.com/science/article/pii/0003491672903302.

[51] AL Fetter and A Svidzinsky. Vortices in a trapped dilute Bose-Einstein condensate. Journal of Physics: Condensed, 135, 2001. URL: http://iopscience.iop.org/0953-8984/13/12/201.

[52] Richard Feynman. Simulating physics with computers. International Journal of Theoretical Physics, 21:467–488, 1982. 10.1007/BF02650179. URL: http://dx.doi.org/10.1007/BF02650179.

[53] Richard P. Feynman. Statistical mechanics. A set of lectures. Advanced Book Classics. 1998. Reprint of the 1972 original.

[54] Uwe Fischer and Ralf Schützhold. Tunneling-induced damping of phase coherence revivals in deep optical lattices. Physical Review A, 78(6), December 2008. URL: http://pra.aps.org/abstract/PRA/v78/i6/e061603.

[55] Matthew P. A. Fisher, G. Grinstein, and Daniel S. Fisher. Boson localization and the superfluid-insulator transition. Physical Review B, 40(1):546–570, July 1989. URL: http://prb.aps.org/abstract/PRB/v40/i1/p546_1, doi:10.1103/PhysRevB.40.546.

[56] Matthew P. A. Fisher, Peter B. Weichman, G. Grinstein, and Daniel S. Fisher. Boson localization and the superfluid-insulator transition. Phys. Rev. B, 40(1):546–570, Jul 1989. doi:10.1103/PhysRevB.40.546.

[57] Simon Foelling, Fabrice Gerbier, Artur Widera, Olaf Mandel, Tatjana Gericke, and Immanuel Bloch. Spatial quantum noise interferometry in expanding ultracold atom clouds. NATURE, 434:481, 2005. URL: doi:10.1038/nature03500.

[58] J. Freericks and H. Monien. Strong-coupling expansions for the pure and disordered Bose-Hubbard model. Physical Review B, 53(5):2691–2700, February 1996. URL: http://prb.aps.org/abstract/PRB/v53/i5/p2691_1.

[59] Christopher Gaul and Cord A. Müller. Bogoliubov excitations of disordered bose-einstein condensates. Phys. Rev. A, 83:063629, Jun 2011. URL: http://link.aps.org/doi/10.1103/PhysRevA.83.063629, doi:10.1103/PhysRevA.83.063629.

[60] Uri Gavish and Yvan Castin. Matter-Wave Localization in Disordered Cold Atom Lattices. Physical Review Letters, 95(2), July 2005. URL: http://prl.aps.org/abstract/PRL/v95/i2/e020401.

[61] F. Gerbier, S. Trotzky, S. Fölling, U. Schnorrberger, J. Thompson, A. Widera, I. Bloch, L. Pollet, M. Troyer, B. Capogrosso-Sansone, N. ProkofŠev, and B. Svistunov. Expansion of a Quantum Gas Released from an Optical Lattice. Physical Review Letters, 101(15), October 2008. URL: http://prl.aps.org/abstract/PRL/v101/i15/e155303.

[62] Fabrice Gerbier. Boson Mott Insulators at Finite Temperatures. Physical Review Letters, 99(12), September 2007. URL: http://prl.aps.org/abstract/PRL/v99/i12/e120405.

[63] Fabrice Gerbier, Artur Widera, Simon Fölling, Olaf Mandel, Tatjana Gericke, and Immanuel Bloch. Phase Coherence of an Atomic Mott Insulator. Physical Review Letters, 95(5), July 2005. URL: http://prl.aps.org/abstract/PRL/v95/i5/e050404.

[64] S. Götze. Momentum-resolved Spectroscopy of Ultracold Bosonic and Fermionic Atoms in Optical Lattices. PhD thesis, Universität Hamburg, 2012.

[65] T. D. Graß, F. E. A. dos Santos, and A. Pelster. Excitation spectra of bosons in optical lattices from the schwinger-keldysh calculation. Phys. Rev. A, 84:013613, Jul 2011. URL: http://link.aps.org/doi/10.1103/PhysRevA.84.013613, doi:10.1103/PhysRevA.84.013613.

[66] T. D. Grass, F. E. A. dos Santos, and A. Pelster. Real-time ginzburg-landau theory for bosons in optical lattices. LASER PHYS., 21:1459, 2011. URL: doi:10.1134/S1054660X11150096.

[67] Markus Greiner. Ultracold quantum gases in three-dimensional optical lattice potentials. PhD Thesis, Ludwig-Maximilians-Universität Mïchen, 2003.

[68] Markus Greiner, Olaf Mandel, Tilman Esslinger, Theodor W Hänsch, and Immanuel Bloch. Quantum phase transition from a superfluid to a Mott insulator in a gas of ultracold atoms. Nature, 415(6867):39–44, January 2002. URL: http://dx.doi.org/10.1038/415039a, doi:10.1038/415039a.

[69] Markus Greiner, Olaf Mandel, Theodor W Hänsch, and Immanuel Bloch. Collapse and revival of the matter wave field of a Bose-Einstein condensate. Nature, 419(6902):51–4, September 2002. URL: http://dx.doi.org/10.1038/nature00968.

[70] V. Gurarie, L. Pollet, N. V. ProkofŠev, B. V. Svistunov, and M. Troyer. Phase diagram of the disordered Bose-Hubbard model. Physical Review B, 80(21), December 2009. URL: http://prb.aps.org/abstract/PRB/v80/i21/e214519.

[71] F. J. Harris78. On the use of windows for harmonic analysis with the discrete fourier transform. Proceedings of the IEEE, 66:51–83, Jan 1978. doi:10.1109/PROC.1978.10837.

[72] Kaden R. A. Hazzard and Erich J. Mueller. On-site correlations in optical lattices: Band mixing to coupled quantum Hall puddles. Physical Review A, 81(3), March 2010. URL: http://pra.aps.org/abstract/PRA/v81/i3/e031602.

[73] J. Heinze, S. Götze, J. Krauser, B. Hundt, N. Fläschner, D.-S. Lühmann, C. Becker, and K. Sengstock. Multiband Spectroscopy of Ultracold Fermions: Observation of Reduced Tunneling in Attractive Bose-Fermi Mixtures. Physical Review Letters, 107(13), September 2011. URL: http://prl.aps.org/abstract/PRL/v107/i13/e135303.

[74] A. F. Ho, M. A. Cazalilla, and T. Giamarchi. Deconfinement in a 2d optical lattice of coupled 1d boson systems. Phys. Rev. Lett., 92:130405, Apr 2004. URL: http://link.aps.org/doi/10.1103/PhysRevLett.92.130405, doi:10.1103/PhysRevLett.92.130405.

[75] W. Hofstetter, J. Cirac, P. Zoller, E. Demler, and M. Lukin. High-Temperature Superfluidity of Fermionic Atoms in Optical Lattices. Physical Review Letters, 89(22), November 2002. URL: http://prl.aps.org/abstract/PRL/v89/i22/e220407, doi:10.1103/PhysRevLett.89.220407.

[76] Chris Hooley and Jorge Quintanilla. Single-Atom Density of States of an Optical Lattice. Physical Review Letters, 93(8):080404, August 2004. URL: http://link.aps.org/doi/10.1103/PhysRevLett.93.080404, doi:10.1103/PhysRevLett.93.080404.

[77] A. Hubener, M. Snoek, and W. Hofstetter. Magnetic phases of two-component ultracold bosons in an optical lattice. Physical Review B, 80(24), December 2009. URL: http://prb.aps.org/abstract/PRB/v80/i24/e245109, doi:10.1103/PhysRevB.80.245109.

[78] S. Huber. Excitations and transport in strongly correlated bosonic matter. PhD thesis, ETH Zürich, 2008.

[79] S. D. Huber, E. Altman, H. P. Buchler, and G. Blatter. Dynamical properties of ultracold bosons in an optical lattice. Physical Review B (Condensed Matter and Materials Physics), 75(8):085106, 2007. URL: http://link.aps.org/abstract/PRB/v75/e085106, doi:10.1103/PhysRevB.75.085106.

[80] S. D. Huber, B. Theiler, E. Altman, and G. Blatter. Amplitude mode in the quantum phase model. Phys. Rev. Lett., 100:050404, Feb 2008. URL: http://link.aps.org/doi/10.1103/PhysRevLett.100.050404, doi:10.1103/PhysRevLett.100.050404.

[81] A. Imamo?lu, M. Lewenstein, and L. You. Inhibition of Coherence in Trapped Bose-Einstein Condensates. Physical Review Letters, 78(13):2511–2514, March 1997. URL: http://prl.aps.org/abstract/PRL/v78/i13/p2511_1.

[82] D. Jaksch, C. Bruder, J. Cirac, C. Gardiner, and P. Zoller. Cold Bosonic Atoms in Optical Lattices. Physical Review Letters, 81(15):3108–3111, October 1998. URL: http://prl.aps.org/abstract/PRL/v81/i15/p3108_1, doi:10.1103/PhysRevLett.81.3108.

[83] Gyu-Boong Jo, Jennie Guzman, Claire Thomas, Pavan Hosur, Ashvin Vishwanath, and Dan Stamper-Kurn. Ultracold Atoms in a Tunable Optical Kagome Lattice. Physical Review Letters, 108(4):1–5, January 2012. URL: http://link.aps.org/doi/10.1103/PhysRevLett.108.045305, doi:10.1103/PhysRevLett.108.045305.

[84] P R Johnson, E Tiesinga, J V Porto, and C J Williams. Effective three-body interactions of neutral bosons in optical lattices. New Journal of Physics, 11(9):093022, September 2009. URL: http://stacks.iop.org/1367-2630/11/i=9/a=093022.

[85] N. Katz, J. Steinhauer, R. Ozeri, and N. Davidson. Beliaev Damping of Quasiparticles in a Bose-Einstein Condensate. Physical Review Letters, 89(22), November 2002. URL: http://prl.aps.org/abstract/PRL/v89/i22/e220401, doi:10.1103/PhysRevLett.89.220401.

[86] Wolfgang Ketterle. Nobel lecture: When atoms behave as waves: Bose-Einstein condensation and the atom laser. Reviews of Modern Physics, 74(October):1131–1151, 2002. URL: http://www.mpipks-dresden.mpg.de/~yast/Articles/MyArt/RMP01131.pdf.

[87] J J Kinnunen and M J Holland. Bragg spectroscopy of a strongly interacting boseŰeinstein condensate. New Journal of Physics, 11(1):013030, 2009. URL: http://stacks.iop.org/1367-2630/11/i=1/a=013030.

[88] Jens Kisker and Heiko Rieger. Bose-glass and Mott-insulator phase in the disordered boson Hubbard model. Physical Review B, 55(18):R11981–R11984, May 1997. URL: http://prb.aps.org/abstract/PRB/v55/i18/pR11981_1.

[89] Steven Kivelson. Wannier functions in one-dimensional disordered systems: Application to fractionally charged solitons. Physical Review, 26(8):4269–4277, 1982. URL: http://prb.aps.org/abstract/PRB/v26/i8/p4269_1.

[90] Walter Kohn. Analytic Properties of Bloch Waves and Wannier Functions. Physical Review, 115(4):809, 1959. URL: http://prola.aps.org/abstract/PR/v115/i4/p809_1.

[91] Walter Kohn. Theory of the Insulating State. Physical Review, 133:A171, 1964. URL: http://prola.aps.org/abstract/PR/v133/i1A/pA171_1.

[92] Corinna Kollath, Andreas Läuchli, and Ehud Altman. Quench Dynamics and Nonequilibrium Phase Diagram of the Bose-Hubbard Model. Physical Review Letters, 98(18), April 2007. URL: http://prl.aps.org/abstract/PRL/v98/i18/e180601.

[93] S. S. Kondov, W. R. McGehee, J. J. Zirbel, and B. DeMarco. Three-dimensional anderson localization of ultracold matter. Science, 334(6052):66–68, 2011. URL: http://www.sciencemag.org/content/334/6052/66.abstract, arXiv:http://www.sciencemag.org/content/334/6052/66.full.pdf, doi:10.1126/science.1209019.

[94] Werner Krauth, Michel Caffarel, and Jean-Philippe Bouchaud. Gutzwiller wave function for a model of strongly interacting bosons. Physical Review B, 45(6):3137–3140, February 1992. URL: http://prb.aps.org/abstract/PRB/v45/i6/p3137_1, doi:10.1103/PhysRevB.45.3137.

[95] Werner Krauth, Nandini Trivedi, and David Ceperley. Superfluid-insulator transition in disordered boson systems. Physical Review Letters, 67(17):2307–2310, October 1991. URL: http://prl.aps.org/abstract/PRL/v67/i17/p2307_1.

[96] Frank Krüger, Jiansheng Wu, and Philip Phillips. Anomalous suppression of the Bose glass at commensurate fillings in the disordered Bose-Hubbard model. Physical Review B, 80(9), September 2009. URL: http://prb.aps.org/abstract/PRB/v80/i9/e094526, doi:10.1103/PhysRevB.80.094526.

[97] K V Krutitsky, A Pelster, and R Graham. Mean-field phase diagram of disordered bosons in a lattice at nonzero temperature. New Journal of Physics, 8(9):187–187, September 2006. URL: http://stacks.iop.org/1367-2630/8/i=9/a=187.

[98] Konstantin V. Krutitsky and Patrick Navez. Excitation dynamics in a lattice bose gas within the time-dependent gutzwiller mean-field approach. Phys. Rev. A, 84:033602, Sep 2011. URL: http://link.aps.org/doi/10.1103/PhysRevA.84.033602, doi:10.1103/PhysRevA.84.033602.

[99] R. C. Kuhn, C. Miniatura, D. Delande, O. Sigwarth, and C. A. Müller. Localization of matter waves in two-dimensional disordered optical potentials. Phys. Rev. Lett., 95:250403, Dec 2005. URL: http://link.aps.org/doi/10.1103/PhysRevLett.95.250403, doi:10.1103/PhysRevLett.95.250403.

[100] R C Kuhn, O Sigwarth, C Miniatura, D Delande, and C A Müller. Coherent matter wave transport in speckle potentials. New Journal of Physics, 9(6):161, 2007. URL: http://stacks.iop.org/1367-2630/9/i=6/a=161.

[101] S. Stringari L. Pitaevskii. Bose-Einstein Condensation. Clarendon Press, Oxford and New York, 2003.

[102] Anthony J. Leggett. Bose-einstein condensation in the alkali gases: Some fundamental concepts. Rev. Mod. Phys., 73(2):307–356, Apr 2001. doi:10.1103/RevModPhys.73.307.

[103] M Lewenstein and L You. PHYSICAL REVIEW LETTERS. Physical Review Letters, (OCTOBER):3489–3493, 1996. URL: http://prl.aps.org/abstract/PRL/v77/i17/p3489_1.

[104] Maciej Lewenstein, Anna Sanpera, Veronica Ahufinger, Bogdan Damski, Aditi Sen De, and Ujjwal Sen. Ultracold atomic gases in optical lattices: mimicking condensed matter physics and beyond. Advances in Physics, 56(2):243–379, 2007. URL: http://www.informaworld.com/10.1080/00018730701223200.

[105] Dirk-Soren Luhmann, Kai Bongs, Klaus Sengstock, and Daniela Pfannkuche. Localisation and Delocalisation of Ultracold Bosonic Atoms in Finite Optical Lattices, 2007. URL: http://www.citebase.org/abstract?id=oai:arXiv.org:0710.0522.

[106] Dirk-Sören Lühmann, Kai Bongs, Klaus Sengstock, and Daniela Pfannkuche. Self-Trapping of Bosons and Fermions in Optical Lattices. Physical Review Letters, 101(5), July 2008. URL: http://prl.aps.org/abstract/PRL/v101/i5/e050402.

[107] Dirk-Sören Lühmann, Ole Jürgensen, and Klaus Sengstock. Multi-orbital and density-induced tunneling of bosons in optical lattices. New Journal of Physics, 14(3):033021, March 2012. URL: http://stacks.iop.org/1367-2630/14/i=3/a=033021.

[108] Roman Lutchyn, Sumanta Tewari, and S. Das Sarma. Loss of superfluidity by fermions in the boson Hubbard model on an optical lattice. Physical Review A, 79(1):1–4, January 2009. URL: http://link.aps.org/doi/10.1103/PhysRevA.79.011606, doi:10.1103/PhysRevA.79.011606.

[109] J. E. Lye, L. Fallani, M. Modugno, D. S. Wiersma, C. Fort, and M. Inguscio. Bose-Einstein Condensate in a Random Potential. Physical Review Letters, 95(7):070401, 2005. URL: http://link.aps.org/abstract/PRL/v95/e070401, doi:10.1103/PhysRevLett.95.070401.

[110] Manfred J Mark, Elmar Haller, Johann G Danzl, Katharina Lauber, Mattias Gustavsson, and Hanns-Christoph Nägerl. Demonstration of the temporal matter-wave talbot effect for trapped matter waves. New Journal of Physics, 13(8):085008, 2011. URL: http://stacks.iop.org/1367-2630/13/i=8/a=085008.

[111] Nicola Marzari, AA Mostofi, JR Yates, Ivo Souza, and David Vanderbilt. Maximally localized Wannier functions: Theory and applications. Arxiv preprint arXiv:1112.5411, 2011. URL: http://arxiv.org/abs/1112.5411, arXiv:arXiv:1112.5411v1.

[112] Nicola Marzari, Ivo Souza, and David Vanderbilt. An Introduction to Maximally-Localized Wannier Functions. Psi-K Scientific Highlight of the Month, 57:129–168, 2003.

[113] Nicola Marzari and David Vanderbilt. Maximally localized generalized Wannier functions for composite energy bands. Physical Review B, 56(20):847–865, 1997. URL: http://prb.aps.org/abstract/PRB/v56/i20/p12847_1.

[114] D McKay, M White, M Pasienski, and B DeMarco. Phase-slip-induced dissipation in an atomic Bose-Hubbard system. Nature, 453(7191):76–9, May 2008. URL: http://dx.doi.org/10.1038/nature06920.

[115] C. Menotti and N. Trivedi. Spectral weight redistribution in strongly correlated bosons in optical lattices. Physical Review B (Condensed Matter and Materials Physics), 77(23):235120, 2008. URL: http://link.aps.org/abstract/PRB/v77/e235120, doi:10.1103/PhysRevB.77.235120.

[116] Alexander Mering and Michael Fleischhauer. Multiband and nonlinear hopping corrections to the three-dimensional Bose-Fermi-Hubbard model. Physical Review A, 063630:1–9, 2011. doi:10.1103/PhysRevA.83.063630.

[117] G. Möller and N. Cooper. Condensed ground states of frustrated Bose-Hubbard models. Physical Review A, 82(6), December 2010. URL: http://pra.aps.org/abstract/PRA/v82/i6/e063625.

[118] Y. Ohashi, M. Kitaura, and H. Matsumoto. Itinerant-localized dual character of a strongly correlated superfluid Bose gas in an optical lattice. Physical Review A (Atomic, Molecular, and Optical Physics), 73(3):033617, 2006. URL: http://link.aps.org/abstract/PRA/v73/e033617, doi:10.1103/PhysRevA.73.033617.

[119] S. Ospelkaus, C. Ospelkaus, O. Wille, M. Succo, P. Ernst, K. Sengstock, and K. Bongs. Localization of Bosonic Atoms by Fermionic Impurities in a Three-Dimensional Optical Lattice. Physical Review Letters, 96(18), May 2006. URL: http://prl.aps.org/abstract/PRL/v96/i18/e180403.

[120] S. B. Papp, J. M. Pino, R. J. Wild, S. Ronen, C. E. Wieman, D. S. Jin, and E. A. Cornell. Bragg spectroscopy of a strongly interacting ^{85}Rb bose-einstein condensate. Phys. Rev. Lett., 101:135301, Sep 2008. URL: http://link.aps.org/doi/10.1103/PhysRevLett.101.135301, doi:10.1103/PhysRevLett.101.135301.

[121] M. Pasienski, D. McKay, M. White, and B. DeMarco. A disordered insulator in an optical lattice. Nature Physics, 6(9):677–680, July 2010. URL: http://dx.doi.org/10.1038/nphys1726.

[122] Oliver Penrose and Lars Onsager. Bose-einstein condensation and liquid helium. Phys. Rev., 104(3):576–584, Nov 1956. doi:10.1103/PhysRev.104.576.

[123] Oliver Penrose and Lars Onsager. Bose-einstein condensation and liquid helium. Phys. Rev., 104(3):576–584, Nov 1956. doi:10.1103/PhysRev.104.576.

[124] C.J. Pethick and H. Smith. Bose-Einstein Condensation in Dilute Gases.

[125] Peter Pippan, Hans Gerd Evertz, and Martin Hohenadler. Excitation spectra of strongly correlated lattice bosons and polaritons. Phys. Rev. A, 80:033612, Sep 2009. URL: http://link.aps.org/doi/10.1103/PhysRevA.80.033612, doi:10.1103/PhysRevA.80.033612.

[126] S. Pitaevskii, LP; Stringari. Landau damping in dilute Bose gases. Physics Letters A, 9601(November):398–402, 1997. URL: http://www.sciencedirect.com/science/article/pii/S037596019700666X.

[127] L. Pollet, N. ProkofŠev, B. Svistunov, and M. Troyer. Absence of a Direct Superfluid to Mott Insulator Transition in Disordered Bose Systems. Physical Review Letters, 103(14), September 2009. URL: http://prl.aps.org/abstract/PRL/v103/i14/e140402.

[128] Nikolay ProkofŠev and Boris Svistunov. Superfluid-Insulator Transition in Commensurate Disordered Bosonic Systems: Large-Scale Worm Algorithm Simulations. Physical Review Letters, 92(1), January 2004. URL: http://prl.aps.org/abstract/PRL/v92/i1/e015703.

[129] Guido Pupillo, Ana Maria Rey, and Ghassan George Batrouni. Bragg spectroscopy of trapped one-dimensional strongly interacting bosons in optical lattices: Probing the cake structure. Phys. Rev. A, 74:013601, Jul 2006. URL: http://link.aps.org/doi/10.1103/PhysRevA.74.013601, doi:10.1103/PhysRevA.74.013601.

[130] S Rapsch, U Schollwöck, and W Zwerger. Density matrix renormalization group for disordered bosons in one dimension. Europhysics Letters (EPL), 46(5):559–564, June 1999. URL: http://stacks.iop.org/0295-5075/46/i=5/a=559.

[131] L Rayleigh. Philos. Mag., (11):1966, 1881.

[132] Ana Rey, Guido Pupillo, and J. Porto. The role of interactions, tunneling, and harmonic confinement on the adiabatic loading of bosons in an optical lattice. Physical Review A, 73(2), February 2006. URL: http://pra.aps.org/abstract/PRA/v73/i2/e023608.

[133] Ana Maria Rey, P. Blair Blakie, Guido Pupillo, Carl J. Williams, and Charles W. Clark. Bragg spectroscopy of ultracold atoms loaded in an optical lattice. Phys. Rev. A, 72:023407, Aug 2005. URL: http://link.aps.org/doi/10.1103/PhysRevA.72.023407, doi:10.1103/PhysRevA.72.023407.

[134] Giacomo Roati, Chiara D'Errico, Leonardo Fallani, Marco Fattori, Chiara Fort, Matteo Zaccanti, Giovanni Modugno, Michele Modugno, and Massimo Inguscio. Anderson localization of a non-interacting Bose-Einstein condensate. Nature, 453(7197):895–8, June 2008. URL: http://dx.doi.org/10.1038/nature07071.

[135] Daniel Rokhsar and B. Kotliar. Gutzwiller projection for bosons. Physical Review B, 44(18):10328–10332, November 1991. URL: http://prb.aps.org/abstract/PRB/v44/i18/p10328_1.

[136] Robert Roth and Keith Burnett. Phase diagram of bosonic atoms in two-color superlattices. Physical Review A, 68(2), August 2003. URL: http://pra.aps.org/abstract/PRA/v68/i2/e023604.

[137] Robert Roth and Keith Burnett. Dynamic structure factor of ultracold bose and fermi gases in optical lattices. Journal of Physics B: Atomic, Molecular and Optical Physics, 37(19):3893, 2004. URL: http://stacks.iop.org/0953-4075/37/i=19/a=009.

[138] Richard Scalettar, Ghassan Batrouni, and Gergely Zimanyi. Localization in interacting, disordered, Bose systems. Physical Review Letters, 66(24):3144–3147, June 1991. URL: http://prl.aps.org/abstract/PRL/v66/i24/p3144_1.

[139] J. Schachenmayer, A. Daley, and P. Zoller. Atomic matter-wave revivals with definite atom number in an optical lattice. Physical Review A, 83(4), April 2011. URL: http://pra.aps.org/abstract/PRA/v83/i4/e043614.

[140] Christian Schori, Thilo Stöferle, Henning Moritz, Michael Köhl, and Tilman Esslinger. Excitations of a Superfluid in a Three-Dimensional Optical Lattice. Physical Review Letters, 93(24):1–4, December 2004. URL: http://link.aps.org/doi/10.1103/PhysRevLett.93.240402, doi:10.1103/PhysRevLett.93.240402.

[141] J. Sebby-Strabley, B. Brown, M. Anderlini, P. Lee, W. Phillips, J. Porto, and P. Johnson. Preparing and Probing Atomic Number States with an Atom Interferometer. Physical Review Letters, 98(20), May 2007. URL: http://prl.aps.org/abstract/PRL/v98/i20/e200405.

[142] Guilhem Semerjian, Marco Tarzia, and Francesco Zamponi. Exact solution of the Bose-Hubbard model on the Bethe lattice. Physical Review B, 80(1), July 2009. URL: http://prb.aps.org/abstract/PRB/v80/i1/e014524.

[143] K. Sengupta and N. Dupuis. Mott-insulator–to–superfluid transition in the bose-hubbard model: A strong-coupling approach. Phys. Rev. A, 71:033629, Mar 2005. URL: http://link.aps.org/doi/10.1103/PhysRevA.71.033629, doi:10.1103/PhysRevA.71.033629.

[144] Pinaki Sengupta, Aditya Raghavan, and Stephan Haas. Disorder-enhanced phase coherence in trapped bosons on optical lattices. New Journal of Physics, 9(4):103–103, April 2007. URL: http://stacks.iop.org/1367-2630/9/i=4/a=103.

[145] Jacob F Sherson, Christof Weitenberg, Manuel Endres, Marc Cheneau, Immanuel Bloch, and Stefan Kuhr. Single-atom-resolved fluorescence imaging of an atomic Mott insulator. Nature, 467(7311):68–72, September 2010. URL: http://dx.doi.org/10.1038/nature09378.

[146] K. Sheshadri, H. Krishnamurthy, Rahul Pandit, and T. Ramakrishnan. Percolation-Enhanced Localization in the Disordered Bosonic Hubbard Model. Physical Review Letters, 75(22):4075–4078, November 1995. URL: http://prl.aps.org/abstract/PRL/v75/i22/p4075_1.

[147] K Sheshadri, H. R Krishnamurthy, R Pandit, and T. V Ramakrishnan. Superfluid and Insulating Phases in an Interacting-Boson Model: Mean-Field Theory and the RPA. Europhysics Letters (EPL), 22(4):257–263, May 1993. URL: http://stacks.iop.org/0295-5075/22/i=4/a=004.

[148] Y. Shin, M. Zwierlein, C. Schunck, a. Schirotzek, and W. Ketterle. Observation of Phase Separation in a Strongly Interacting Imbalanced Fermi Gas. Physical Review Letters, 97(3):5–8, July 2006. URL: http://link.aps.org/doi/10.1103/PhysRevLett.97.030401, doi:10.1103/PhysRevLett.97.030401.

[149] Kanwal Singh and Daniel Rokhsar. Real-space renormalization study of disordered interacting bosons. Physical Review B, 46(5):3002–3008, August 1992. URL: http://prb.aps.org/abstract/PRB/v46/i5/p3002_1.

[150] Michiel Snoek, Irakli Titvinidze, Immanuel Bloch, and Walter Hofstetter. Effect of Interactions on Harmonically Confined Bose-Fermi Mixtures in Optical Lattices. Physical Review Letters, 106(15), April 2011. URL: http://prl.aps.org/abstract/PRL/v106/i15/e155301.

[151] P. Soltan-Panahi, J. Struck, P. Hauke, a. Bick, W. Plenkers, G. Meineke, C. Becker, P. Windpassinger, M. Lewenstein, and K. Sengstock. Multi-component quantum gases in spin-dependent hexagonal lattices. Nature Physics, 7(5):434–440, February 2011. URL: http://www.nature.com/doifinder/10.1038/nphys1916, doi:10.1038/nphys1916.

[152] Parvis Soltan-Panahi, Dirk-Sören Lühmann, Julian Struck, Patrick Windpassinger, and Klaus Sengstock. Quantum phase transition to unconventional multi-orbital superfluidity in optical lattices. Nature Physics, 8(1):71–75, October 2011. URL: http://www.nature.com/doifinder/10.1038/nphys2128, doi:10.1038/nphys2128.

[153] D. Stamper-Kurn and W. Ketterle. Spinor condensates and light scattering from bose-einstein condensates. In R. Kaiser, C. Westbrook, and F. David, editors, Coherent atomic matter waves, volume 72 of Les Houches, pages 139–217. Springer Berlin / Heidelberg, 2001. URL: http://dx.doi.org/10.1007/3-540-45338-5_2.

[154] D. M. Stamper-Kurn, A. P. Chikkatur, A. Görlitz, S. Inouye, S. Gupta, D. E. Pritchard, and W. Ketterle. Excitation of phonons in a bose-einstein condensate by light scattering. Phys. Rev. Lett., 83:2876–2879, Oct 1999. URL: http://link.aps.org/doi/10.1103/PhysRevLett.83.2876, doi:10.1103/PhysRevLett.83.2876.

[155] J. Stenger, S. Inouye, A. P. Chikkatur, D. M. Stamper-Kurn, D. E. Pritchard, and W. Ketterle. Bragg spectroscopy of a bose-einstein condensate. Phys. Rev. Lett., 82:4569–4573, Jun 1999. URL: http://link.aps.org/doi/10.1103/PhysRevLett.82.4569, doi:10.1103/PhysRevLett.82.4569.

[156] J. T. Stewart, J. P. Gaebler, and D. S. Jin. Using photoemission spectroscopy to probe a strongly interacting fermi gas. NATURE, 454:744, 2008. URL: doi:10.1038/nature07172.

[157] Thilo Stöferle, Henning Moritz, Christian Schori, Michael Köhl, and Tilman Esslinger. Transition from a Strongly Interacting 1D Superfluid to a Mott Insulator. Physical Review Letters, 92(13):1–4, March 2004. URL: http://link.aps.org/doi/10.1103/PhysRevLett.92.130403, doi:10.1103/PhysRevLett.92.130403.

[158] J Struck, C Ölschläger, R Le Targat, P Soltan-Panahi, a Eckardt, M Lewenstein, P Windpassinger, and K Sengstock. Quantum simulation of frustrated classical magnetism in triangular optical lattices. Science (New York, N.Y.), 333(6045):996–9, August 2011. URL: http://www.ncbi.nlm.nih.gov/pubmed/21778359, doi:10.1126/science.1207239.

[159] J Struck and M Weinberg. Tunable gauge potential for neutral and spinless particles in driven lattices. Arxiv preprint arXiv:, 1:1–6, 2012. URL: http://arxiv.org/abs/1203.0049, arXiv:arXiv:1203.0049v1.

[160] Boris Svistunov. SuperfluidŰBose-glass transition in weakly disordered commensurate one-dimensional system. Physical Review B, 54(22):16131–16134, December 1996. URL: http://prb.aps.org/abstract/PRB/v54/i22/p16131_1.

[161] H. F. Talbot. Philos. Mag., (9):401, 1836.

[162] Leticia Tarruell, Daniel Greif, Thomas Uehlinger, Gregor Jotzu, and Tilman Esslinger. Creating, moving and merging Dirac points with a Fermi gas in a tunable honeycomb lattice. Arxiv preprint arXiv:, 1, 2011. URL: http://arxiv.org/abs/1111.5020, arXiv:arXiv:1111.5020v1.

[163] C. Trefzger and K. Sengupta. Nonequilibrium Dynamics of the Bose-Hubbard Model: A Projection-Operator Approach. Physical Review Letters, 106(9):1–4, February 2011. URL: http://link.aps.org/doi/10.1103/PhysRevLett.106.095702, doi:10.1103/PhysRevLett.106.095702.

[164] S. Trotzky, L. Pollet, F. Gerbier, U. Schnorrberger, I. Bloch, N. V. ProkofŠev, B. Svistunov, and M. Troyer. Suppression of the critical temperature for superfluidity near the Mott transition. Nature Physics, 6(12):998–1004, October 2010. URL: http://dx.doi.org/10.1038/nphys1799.

[165] Shunji Tsuchiya and Allan Griffin. Damping of Bogoliubov excitations in optical lattices. Physical Review A, 70(2), August 2004. URL: http://pra.aps.org/abstract/PRA/v70/i2/e023611, doi:10.1103/PhysRevA.70.023611.

[166] D. van Oosten, D. B. M. Dickerscheid, B. Farid, P. van der Straten, and H. T. C. Stoof. Inelastic light scattering from a mott insulator. Phys. Rev. A, 71:021601, Feb 2005. URL: http://link.aps.org/doi/10.1103/PhysRevA.71.021601, doi:10.1103/PhysRevA.71.021601.

[167] D. van Oosten, P. van der Straten, and H. T. C. Stoof. Quantum phases in an optical lattice. Phys. Rev. A, 63(5):053601, Apr 2001. doi:10.1103/PhysRevA.63.053601.

[168] G.H. Wannier. The Structure of Electronic Excitation Levels in Insulating Crystals. Phys. Rev., 52(3):191–197, 1937. URL: http://prola.aps.org/abstract/PR/v52/i3/p191_1.

[169] Christof Weitenberg, Manuel Endres, Jacob F. Sherson, Marc Cheneau, Peter SchauSS, Takeshi Fukuhara, Immanuel Bloch, and Stefan Kuhr. Single-spin addressing in an atomic mott insulator. NATURE, 471:319, 2011. URL: doi:10.1038/nature09827.

[170] M. White, M. Pasienski, D. McKay, S. Q. Zhou, D. Ceperley, and B. DeMarco. Strongly Interacting Bosons in a Disordered Optical Lattice. Physical Review Letters, 102(5), February 2009. URL: http://prl.aps.org/abstract/PRL/v102/i5/e055301.

[171] Sebastian Will, Thorsten Best, Simon Braun, Ulrich Schneider, and Immanuel Bloch. Coherent Interaction of a Single Fermion with a Small Bosonic Field. Physical Review Letters, 106(11), March 2011. URL: http://prl.aps.org/abstract/PRL/v106/i11/e115305.

[172] Sebastian Will, Thorsten Best, Ulrich Schneider, Lucia Hackermüller, Dirk-Sören Lühmann, and Immanuel Bloch. Time-resolved observation of coherent multi-body interactions in quantum phase revivals. Nature, 465(7295):197–201, May 2010. URL: http://dx.doi.org/10.1038/nature09036.

[173] F. Wolf, Itay Hen, and Marcos Rigol. Collapse and revival oscillations as a probe for the tunneling amplitude in an ultracold Bose gas. Physical Review A, 82(4), October 2010. URL: http://pra.aps.org/abstract/PRA/v82/i4/e043601.

[174] Jiansheng Wu and Philip Phillips. Minimal model for disorder-induced missing moment of inertia in solid H4e. Physical Review B, 78(1), July 2008. URL: http://prb.aps.org/abstract/PRB/v78/i1/e014515.

[175] Peter Würtz, Tim Langen, Tatjana Gericke, Andreas Koglbauer, and Herwig Ott. Experimental demonstration of single-site addressability in a two-dimensional optical lattice. Phys. Rev. Lett., 103:080404, Aug 2009. URL: http://link.aps.org/doi/10.1103/PhysRevLett.103.080404, doi:10.1103/PhysRevLett.103.080404.

[176] C. N. Yang. Concept of off-diagonal long-range order and the quantum phases of liquid he and of superconductors. Rev. Mod. Phys., 34(4):694–704, Oct 1962. doi:10.1103/RevModPhys.34.694.

[177] Jinwu Ye, J. M. Zhang, W. M. Liu, Keye Zhang, Yan Li, and Weiping Zhang. Light-scattering detection of quantum phases of ultracold atoms in optical lattices. Phys. Rev. A, 83:051604, May 2011. URL: http://link.aps.org/doi/10.1103/PhysRevA.83.051604, doi:10.1103/PhysRevA.83.051604.

[178] V. Yukalov. Nonlinear spin relaxation in strongly nonequilibrium magnets. Physical Review B, 71(18), May 2005. URL: http://prb.aps.org/abstract/PRB/v71/i18/e184432.

[179] V. Yukalov and R. Graham. Bose-Einstein-condensed systems in random potentials. Physical Review A, 75(2), February 2007. URL: http://pra.aps.org/abstract/PRA/v75/i2/e023619.

[180] V. I. Yukalov and E. P. Yukalova. Phys. Part. Nucl., 31, 2000.

[181] S. Q. Zhou and D. M. Ceperley. Construction of localized wave functions for a disordered optical lattice and analysis of the resulting hubbard model parameters, 2009. URL: http://www.citebase.org/abstract?id=oai:arXiv.org:0907.5053.

[182] S. Q. Zhou and D. M. Ceperley. Construction of localized wave functions for a disordered optical lattice and analysis of the resulting Hubbard model parameters. Physical Review A, 81(1), January 2010. URL: http://pra.aps.org/abstract/PRA/v81/i1/e013402.

[183] B Zimmermann, T Müller, J Meineke, T Esslinger, and H Moritz. High-resolution imaging of ultracold fermions in microscopically tailored optical potentials. New Journal of Physics, 13(4):043007, April 2011. URL: http://stacks.iop.org/1367-2630/13/i=4/a=043007.

[184] M W Zwierlein, J R Abo-Shaeer, A Schirotzek, C H Schunck, and W Ketterle. Vortices and superfluidity in a strongly interacting Fermi gas. Nature, 435(7045):1047–51, June 2005. URL: http://www.ncbi.nlm.nih.gov/pubmed/15973400, doi:10.1038/nature03858.